THE JOURNAL OF

# PHYSICAL CHEMISTRY

*Volume 74, Number 10 May 14, 1970*

## NOTES



## COMMUNICATIONS TO THE EDITOR

## AUTHOR INDEX

THE JOURNAL OF
PHYSICAL CHEMISTRY


VOLUME 74, NUMBER 10 MAY 14, 1970

# The Formation and Dissociation of Monochloroiron(III) at High Ionic Strengths: Equilibrium and Kinetic Measurements

**by J. Keith Rowley and Norman Sutin**

*Chemistry Department, Brookhaven National Laboratory, Upton, New York 11973* *(Received December 9, 1969)*

The equilibrium constant for the reaction $Fe^{3+} + Cl^- \rightleftharpoons FeCl^{2+}$ has been measured at 25.0° and various ionic strengths in the range 1.0–6.0 $M$ using spectrophotometric methods. The equilibrium constant is 5.2 ± 0.4, 9.8 ± 0.7, 17.3 ± 1.0, 36.3 ± 1.5, and 110 ± 3 $M^{-1}$ at ionic strengths 1.00, 3.00, 4.00, 5.00, and 6.00 $M$, respectively. The rate of approach to equilibrium was measured by the stopped flow technique at ionic strength 6.00 $M$. Provided the iron(III) concentration is less than about $1 \times 10^{-2}$ $M$, the observed rate constant is given by $k_{obsd} = k_d + k_f[[Fe(III)] + [Cl^-]_T]$ where $k_d = 0.95$ sec$^{-1}$ and $k_f = 102$ $M^{-1}$ sec$^{-1}$ at 25.0° and $[HClO_4] = 6.0$ $M$. The dependence of $k_d$ and $k_f$ on the perchloric acid concentration and on the temperature was measured. It was found that the marked increase in the equilibrium constant for the reaction with increasing ionic strength in the range 1.0–6.0 $M$ is due largely to a more rapid rate of formation of the complex, while the rate of dissociation of the complex as well as the activation parameters for the dissociation are much less sensitive to the ionic strength change. The results are compared with previous investigations, and a model for interpreting the effect of the medium on the equilibrium and kinetic parameters is discussed.

## Introduction

Previous studies of the reaction 1 in perchloric acid

$$Fe^{3+} + Cl^- \rightleftharpoons FeCl^{2+} \qquad (1)$$

solutions have shown that the concentration equilibrium constant

$$K_1 = \frac{[FeCl^{2+}]}{[Fe^{3+}][Cl^-]} = K_1^0 Y \qquad (2)$$

increases dramatically with increasing perchloric acid concentration.[1-3] In the above expression, square brackets denote molar concentrations, $K_1^0$ is the thermodynamic equilibrium constant, and $Y$ is the activity coefficient ratio $y_3y_1:y_2$. Although it is correct to state that the increase in $K_1$ is due to increases in $Y$, this leaves unanswered the question of why $Y$ changes. There can be little doubt that the suggestion[1] that the increase in $Y$ is related to the decreasing availability of solvent water molecules is essentially correct.

In their study of reaction 1 at varying perchloric acid concentrations, Coll, Nauman, and West[1] assumed that the molar absorptivity of $FeCl^{2+}$ is independent of the ionic strength of the medium. Although the determination of the molar absorptivity of $FeCl^{2+}$ at low ionic strengths is difficult and subject to considerable error, there is a good deal of evidence that the molar absorptivity at the lower ionic strengths is not as large as was assumed.[4-6] In order to obtain more information about this system at high perchloric acid concentrations, we have remeasured the concentration equilibrium constant

(1) H. Coll, R. V. Nauman, and P. W. West, *J. Amer. Chem. Soc.*, 81, 1284 (1959).

(2) R. N. Heistand and A. Clearfield, *ibid.*, 85, 2566 (1963).

(3) M. J. M. Woods, P. K. Gallagher, and E. L. King, *Inorg. Chem.*, 1, 55 (1962).

(4) H. Olerup, *Sv. Kem. Tidskr.*, 55, 324 (1943).

(5) R. E. Connick and C. P. Coppel, *J. Amer. Chem. Soc.*, 81, 6389 (1959).

(6) N. Sutin, J. K. Rowley, and R. W. Dodson, *J. Phys. Chem.*, 65, 1248 (1961).

and the molar absorptivity of $FeCl^{2+}$ at several ionic strengths. We have also measured the forward and reverse rates of reaction 1 at an ionic strength of 6.00 $M$. A constant ionic strength medium was chosen for these studies because such a medium is often employed, and its use in this study facilitated comparisons with earlier work. However it should be noted that there is considerable evidence that the use of a constant ionic strength medium does not ensure the constancy of $Y$.[1,7,8]

Reaction 1 may also be written as follows

$$Fe(H_2O)_6^{3+} + Cl^- \rightleftharpoons Fe(H_2O)_5Cl^{2+} + H_2O \quad (3)$$

A good reason for doing so is that reaction 3 indicates that the complex formation involves the replacement of a water molecule coordinated to the ferric ion. On the other hand, it is difficult to discuss the equilibrium constant for the reaction written in this manner because of a lack of information about the water activity and, more important perhaps, because any changes in the hydration shell of the chloride ion as well as possible decreases in the hydration of the $Fe^{3+}$ ion at the higher ionic strengths are ignored in reaction 3. Therefore, unless otherwise specified, we will discuss the system as described by reaction 1. The water activity term in the equilibrium constant for reaction 3 is then included in the activity coefficient ratio for reaction 1.

A question which haunts investigators using aqueous perchlorate solutions is whether perchlorate complexes exist. The arguments against the existence of iron(III) perchlorate complexes in dilute perchlorate solutions have been summarized by Jones, *et al.*[9] We will bypass this issue and consider any perchlorate complex formation as a medium effect. In other words, iron(III) perchlorate complex formation is also included in the $Y$ term.

## Experimental Section

The perchloric acid used was fumed for at least 1 hr to remove any traces of chloride. Density measurements at 25.0° and interpolation of the data of Markham[10] were used to standardize the perchloric acid solutions in the concentration range 3–10 $M$. The density–concentration correlation was extended to 12 $M$ by measuring the density of the concentrated acid solution, then diluting a weighed quantity to approximately 3 $M$ with a weighed quantity of water, and establishing the final concentration by remeasuring the density. By using a 50-ml pycnometer, a standardization could be made which was more accurate than an acid–base titration using volume burets and comparable, at least in principle, to an acid–base titration using weight burets.[11]

An iron(III) perchlorate stock solution was prepared from G. F. Smith ferric perchlorate which had been recrystallized from perchloric acid. The iron(III) concentration in this solution was determined by titrating with standard cerium(IV) solution after reduction to iron(II) with a Jones reductor. The perchloric acid concentration in this stock solution was determined by passing an aliquot through a Dowex 50W ion-exchange column in the hydrogen ion form, titrating the total acid in the effluent with standard base, and correcting for the acid liberated by exchange with ferric ions.

In preparing the solutions, perchloric acid of known density was weighed out carefully except for the equilibrium measurements at ionic strength 5.00 $M$, when a volume buret was used. The stock iron(III) perchlorate solution and the hydrochloric acid solution were pipetted when used in making up solutions.

The rate of approach to equilibrium was studied by measuring the rate of formation of $FeCl^{2+}$ at 340 nm. These measurements were performed by using the stopped flow technique.[12,13] The iron(III) concentration in a given run was always at least five times larger than the total chloride concentration; the maximum concentration of the latter was $4 \times 10^{-4}$ $M$. Perchloric acid as well as perchloric acid–sodium perchlorate mixtures were used to maintain the ionic strength of the solutions at 6.00 $M$. The range of perchloric acid concentrations that could be used in this work was limited by the formation of the iron(III) dimer at lower acidities.

The absorbance measurements at equilibrium were made on a Cary 16 spectrophotometer, except for the measurements at ionic strength 5.00 $M$ and some of the measurements at ionic strength 4.00 $M$ for which a Beckman DU-2 was used. Since the Cary 16 can be read to the nearest 0.0001 absorbance unit over much of the scale, and it has a double monochromator to cut down on scattered light, the data from the Cary 16 are considered to be more accurate than those from the Beckman DU-2.

The procedure for the equilibrium spectrophotometric measurements was essentially as described previ-

(7) (a) J. E. Prue and A. J. Read, *J. Chem. Soc.*, 1812 (1966); (b) A. J. Zielen and J. C. Sullivan, *J. Phys. Chem.*, **66**, 1066 (1962); (c) J. S. Day and P. A. H. Wyatt, *J. Chem. Soc.*, 343 (1966).

(8) (a) T. W. Newton and F. B. Baker, *J. Phys. Chem.*, **67**, 1425 (1963); (b) T. W. Newton and F. B. Baker, *Inorg. Chem.*, **4**, 1166 (1965); (c) J. H. Espenson and D. E. Bineau, *ibid.*, **5**, 1365 (1966); (d) D. W. Carlyle and J. H. Espenson, *J. Amer. Chem. Soc.*, **90**, 2272 (1968).

(9) M. M. Jones, E. A. Jones, D. F. Harmon, and R. T. Semmes, *ibid.*, **83**, 2038 (1961).

(10) A. Markham, *ibid.*, **63**, 874 (1941).

(11) This can be seen from the following calculation. By use of a 50-ml pycnometer the density can be measured with a precision of about 2 parts in 50,000. For a solution of density 1.2 g $cm^{-3}$ this corresponds to an uncertainty in density of about 0.00005 g $cm^{-3}$. Since $\Delta M/\Delta d$ is about 0.017 mol $g^{-1}$ at 3 $M$ perchloric acid, the uncertainty in the molarity is equal to 0.0009 $M$, which corresponds to an uncertainty of 3 parts in 10,000 in the molarity of the 3 $M$ perchloric acid solution.

(12) G. Dulz and N. Sutin, *Inorg. Chem.*, **2**, 917 (1963).

(13) R. J. Campion, T. J. Conocchioli, and N. Sutin, *J. Amer. Chem. Soc.*, **86**, 4591 (1964).

ously.[6] Except at ionic strength 1.00 $M$ the iron(III) concentration was always more than five times larger than the total chloride concentration. The range of iron(III) concentrations used was $2 \times 10^{-3}$ to $3 \times 10^{-2}$ $M$. The ionic strength of the solutions was adjusted with perchloric acid (no sodium perchlorate was added). Measurements were also performed at a constant perchloric acid concentration of 6.00 $M$. At least two different chloride concentrations were used at each ionic strength, and the absorbance of each solution was measured at eight wavelengths, 330, 335, 340, 345, 350, 355, 365, and 380 nm. The spectral band shape was examined closely for evidence of higher chloride complexes.

The absorbance of a solution containing $Fe(ClO_4)_3$, HCl, and $HClO_4$ was first measured, and the absorbance of a solution containing the same concentrations of $Fe(ClO_4)_3$ and $HClO_4$ with the HCl omitted was then subtracted from it.[14] All solutions containing both iron(III) and chloride were protected from light as much as possible to minimize the photochemical reduction of $FeCl^{2+}$ at high perchloric acid concentrations.[1] For the same reason the absorbance was read as soon as possible after mixing and temperature equilibration. All the spectrophotometric measurements were performed at 25.0°.

Isopiestic measurements were performed on three iron(III) perchlorate–perchloric acid mixtures using a perchloric acid solution as a standard. The method used was that described by Robinson and Stokes.[15] Weighed quantities of solutions of known molar concentrations and density were mutually equilibrated at 25.0° for 3 days. The solutions were then reweighed and their densities were remeasured. The isopiestic molar concentrations were calculated from the equilibrium weights and volumes.

In order to check on a hypothesis to be discussed later, an extraction experiment was performed. Forty milliliters of a 1:5 dilution with $n$-heptane of a 36% dinonylnaphthalenesulfonic acid solution in $n$-heptane were shaken for 4 hr with 40 ml of an aqueous phase which was initially 0.85 $M$ in HCl, 0.15 $M$ in $HClO_4$, and 0.0503 $M$ in iron(III) perchlorate. The phases were separated and the chloride concentration in the organic phase and the iron(III) concentration in the aqueous phase were determined. A blank extraction was also performed by shaking 40 ml of the organic phase with 40 ml of an aqueous phase which was 0.85 $M$ in HCl and 0.15 $M$ in $HClO_4$.

## Results

The results of the kinetic measurements are summarized in Table I. At constant perchloric acid concentration the observed rate constants are linearly related to $[Fe(III)] + [Cl^-]_T$, that is, the observed rate constants are given by

$$k_{obsd} = k_d + k_f[[Fe(III)] + [Cl^-]_T] \quad (4)$$

**Table I:** First-Order Rate Constants for the Reaction between Iron(III) and Chloride at Ionic Strength 6.00 $M$

| Temp, °C | $(HClO_4)$, $M$ | $10^3[Fe(III)]$, $M$ | $10^3[Cl^-]_T$, $M$ | $k_{obsd}$, $sec^{-1}$ |
|---|---|---|---|---|
| 2.5 | 5.99 | 2.012 | 0.105 | 0.119 |
| | 5.98 | 4.024 | 0.105 | 0.147 |
| | 5.95 | 8.05 | 0.105 | 0.192 |
| | 5.93 | 12.07 | 0.105 | 0.232 |
| | 5.92 | 14.08 | 0.105 | 0.253 |
| 25.1 | 5.99 | 1.70 | 0.100 | 1.16 |
| | 5.99 | 1.70 | 0.375 | 1.19 |
| | 5.99 | 2.012 | 0.105 | 1.17 |
| | 5.98 | 3.40 | 0.100 | 1.32 |
| | 5.98 | 3.40 | 0.200 | 1.32 |
| | 5.98 | 4.024 | 0.105 | 1.35 |
| | 5.96 | 6.80 | 0.100 | 1.64 |
| | 5.96 | 6.80 | 0.200 | 1.65 |
| | 5.95 | 8.05 | 0.105 | 1.75 |
| | 5.94 | 10.06 | 0.105 | 1.99 |
| | 5.93 | 12.07 | 0.105 | 2.12 |
| | 5.92 | 14.08 | 0.105 | 2.30 |
| | 5.85 | 25.15 | 0.105 | 3.31 |
| | 5.70 | 50.30 | 0.105 | 5.50 |
| | 5.55 | 75.45 | 0.105 | 7.00 |
| | 5.84 | 1.70 | 0.100 | 1.14 |
| | 5.84 | 5.10 | 0.100 | 1.51 |
| | 5.84 | 10.20 | 0.100 | 2.02 |
| | 5.84 | 13.60 | 0.100 | 2.36 |
| | 1.25 | 1.70 | 0.100 | 1.77 |
| | 1.25 | 5.10 | 0.100 | 2.16 |
| | 1.25 | 10.20 | 0.100 | 2.34 |
| | 1.25 | 13.60 | 0.100 | 2.57 |
| | 0.75 | 1.70 | 0.100 | 2.25 |
| | 0.75 | 5.10 | 0.100 | 2.48 |
| | 0.75 | 10.20 | 0.100 | 2.77 |
| | 0.75 | 13.60 | 0.100 | 3.05 |
| 44.6 | 5.99 | 2.012 | 0.105 | 5.6 |
| | 5.98 | 4.024 | 0.105 | 6.7 |
| | 5.95 | 8.05 | 0.105 | 8.8 |
| | 5.93 | 12.07 | 0.105 | 11.0 |
| | 5.92 | 14.08 | 0.105 | 11.5 |

provided the iron(III) concentrations are less than about $1 \times 10^{-2}$ $M$. The values of $k_d$ and $k_f$ calculated from the intercepts and extrapolated initial slopes of plots of $k_{obsd}$ *vs.* $[Fe(III)] + [Cl^-]_T$ at 2.5, 25.1, and 44.6° are 0.099, 0.95, and 4.67 $sec^{-1}$, and 10.9, 102, and 485 $M^{-1}$ $sec^{-1}$, respectively, at $[HClO_4] = 6.0$ $M$, and ionic strength 6.0 $M$. The enthalpies of activation calculated from these rate constants are $\Delta H_d^{\ddagger} = 15.2 \pm 0.6$, and $\Delta H_f^{\ddagger} = 15.2 \pm 0.6$ kcal $mol^{-1}$, leading to an estimate of $0.0 \pm 0.8$ kcal $mol^{-1}$ for $\Delta H_1$, the enthalpy change in reaction 1, at $[HClO_4] = 6.0$ $M$.

The rate constants increase with decreasing perchloric acid concentration at constant ionic strength.

(14) This procedure gives $\epsilon_1 = (\epsilon_{FeCl^{2+}} - \epsilon_{Fe^{3+}})$. Although small contributions to the absorbance from $FeOH^{2+}$ and its dimer are included at ionic strengths 1.00 and 3.00 $M$, these contributions are smaller than the experimental error of the absorbance measurement.

(15) R. A. Robinson and R. H. Stokes, "Electrolyte Solutions," 2nd ed, Academic Press, Inc., New York, N. Y., 1959, p 177.

**Table II:** Summary of the Rate Constants for the Reaction between Iron(III) and Chloride at 25.1°

| $\mu$,[a] $M$ | $a_w$ | $k_{-1}$, $sec^{-1}$ | $k_{-2}$, $M^{-1}$ $sec^{-1}$ | $k_1$, $sec^{-1}$ | $k_2$, $M^{-1}$ $sec^{-1}$ | $k_{-1}/a_w^2$, $sec^{-1}$ | $\Delta H_{-1}^{\ddagger}$, kcal $mol^{-1}$ | $\Delta S_{-1}^{\ddagger}$, cal $deg^{-1}$ $mol^{-1}$ | Ref |
|---|---|---|---|---|---|---|---|---|---|
| 1.00 | 0.961 | 1.61 | 5.63 | 8.4 | 29.8 | 1.68 | 15.6 | −5 | *b* |
| 3.00 | 0.829 | 1.1 | 3.4 | 10.8 | 33.3 | 1.3 | ... | ... | *c* |
| 6.00 | 0.459 | 0.8 | 1.0[e] | 90 | −25[e] | 1.7 | 15.2[f] | −8[f] | *d* |

[a] Ionic strength. [b] Reference 17. [c] Reference 16. [d] This work. [e] The significance of the slope of the plot of $k_{obsd}$ *vs.* $1/[HClO_4]$ is uncertain at 6.00 *M* ionic strength since $K_1$ does not remain constant when $HClO_4$ is replaced by $NaClO_4$. [f] Calculated on the assumption that the acid dependent path can be neglected in 6 *M* $HClO_4$.

For purposes of comparison with previous studies,[5,16,17] values of $k_1$, $k_2$, $k_{-1}$, and $k_{-2}$ defined by

$$k_f = k_1 + k_2/[HClO_4] \quad (5)$$

$$k_d = k_{-1} + k_{-2}/[HClO_4] \quad (6)$$

were calculated from the kinetic data and are presented in Table II. The $k_f$ values presented for the earlier studies were calculated from the $k_d$ values reported there together with the $K_1$ values determined in this study.

Table III presents a sample data set from the equilibrium spectrophotometric measurements at an ionic strength of 1.00 *M*. Since $K_1$ is smallest at this ionic strength, the errors in measuring absorbances should result in the largest errors in $S$ and $I$ at this ionic strength.

**Table III:** Sample Data Set at an Ionic Strength of 1.00 *M*, 25°, and a Wavelength of 335 nm

| $10^3$[Fe(III)], *M* | $10^3[Cl^-]_T$, *M* | $A$[a] | $10^3$[Fe(III)] × $[Cl^-]_T/A$, $M^2$ |
|---|---|---|---|
| 2.514 | 2.628 | 0.0462 | 0.1430 |
| 7.542 | 2.628 | 0.1348 | 0.1470 |
| 12.57 | 2.628 | 0.2190 | 0.1508 |
| 17.60 | 2.628 | 0.2996 | 0.1544 |
| 27.65 | 2.628 | 0.4527 | 0.1605 |
| 2.514 | 5.256 | 0.0909 | 0.1454 |
| 7.542 | 5.256 | 0.2683 | 0.1477 |
| 12.57 | 5.256 | 0.4309 | 0.1533 |
| 17.60 | 5.256 | 0.5911 | 0.1565 |
| 22.63 | 5.256 | 0.7446 | 0.1597 |
| 27.65 | 5.256 | 0.8881 | 0.1636 |

[a] The absorbance per unit path length measured against an iron(III) blank.

The results of the spectrophotometric measurements are summarized in Table IV. The values of the constant parameters, $S/I$ and $1/S$, were calculated from an unweighted linear least-squares analysis of the function

$$\frac{[Fe(III)][Cl^-]_T}{A} = I + S[[Fe(III)] + [Cl^-]_T] \quad (7)$$

**Table IV:** Summary of Equilibrium Spectrophotometric Data at 25.0°

| $\mu$,[a] *M* | $a_w$ | $\lambda_{max}$, nm | $(S/I)$, $M^{-1}$ | $\left(\frac{10^{-3}}{S}\right)_{max}$, $M^{-1}$ $cm^{-1}$ | $10^{-3}$ $Q_{Cl}$[d] | $10^{-3}$ $Q_{Br}$[d] |
|---|---|---|---|---|---|---|
| 1.00 | 0.961 | 335.0 | 5.2 ± 0.4 | 1.42 | 49 | 2.7 |
| 3.00 | 0.829 | 336.0 | 9.8 ± 0.7 | 1.73 | 48 | 3.8 |
| 4.00 | 0.726 | 337.0 | 17.3 ± 1.0 | 2.10 | 41 | 3.5 |
| 5.00 | 0.600 | 339.0 | 36.3 ± 1.5 | 2.52 | 38 | 2.9 |
| 6.00 | 0.459 | 341.5 | 110 ± 3 | 2.72 | 46 | 3.0 |
| 9.00 | 0.093[c] | 352 | | 2.90 | | |
| 6.00[b] | 0.459 | 341.5 | 104 ± 3 | 2.81 | | |

[a] Ionic strength. [b] Medium is 6.00 *M* perchloric acid (the ionic strength was not kept constant). [c] H. Wai and K. Yates, *Can. J. Chem.*, **47**, 2326 (1969). [d] $Q_x$ is the equilibrium constant for the reaction, $Cl^- + CrX^{2+} + Fe^{3+} = FeCl^{2+} + Cr^{3+} + X^-$. The values for the equilibrium constants for the reactions, $Cr^{3+} + X^- = CrX^{2+}$, used in calculating $Q_X$ were obtained from ref 25 ($X^- = Br^-$) and 31 ($X^- = Cl^-$).

where $A$ is the absorbance per unit path length measured against the iron(III) blank. Generally, $1/S$ and $S/I$ are identified with a molar absorptivity, $\epsilon_1$ (which is equal to $(\epsilon_{FeCl^{2+}} - \epsilon_{Fe^{3+}})$), and $K_1$, respectively. This interpretation will be discussed later. The values for the activity of water presented in Table IV are for perchloric acid solutions of the same ionic strength as the solutions used in the spectrophotometric measurements.[18,19] Values of $1/S$ as a function of wavelength at different ionic strengths are presented in Table V.

The isopiestic measurements showed that the following solutions have the same vapor pressures: 5.71 *M* $HClO_4$; (5.56 *M* $HClO_4$ + 0.0491 *M* $Fe(ClO_4)_3$); (5.41 *M* $HClO_4$ + 0.1009 *M* $Fe(ClO_4)_3$); (5.25 *M* $HClO_4$ + 0.1551 *M* $Fe(ClO_4)_3$). The results of the extraction experiment were: chloride concentration in the organic phase in the absence of added iron(III) was $2.3 \times 10^{-3}$ *M*; chloride concentration in the organic

(16) E. G. Moorhead and N. Sutin, *Inorg. Chem.*, **6**, 428 (1967).
(17) H. N. Po and N. Sutin, to be published.
(18) R. M. Rush and J. S. Johnson, *J. Phys. Chem.*, **72**, 767 (1968).
(19) R. A. Robinson and O. J. Baker, *Trans. Proc. Roy. Soc., N. Z.*, **76**, 250 (1946); *Chem. Abstr.*, **41**, 5000d (1947).

**Table V:** Values of $10^{-3}/S^a$ As a Function of Wavelength and Ionic Strength at 25.0°

| λ, nm | μ, M: 1.00 | 3.00 | 4.00[b] | 5.00[b] | 6.00 | 6.00[c] |
|---|---|---|---|---|---|---|
| 380 | 0.33 | 0.47 | 0.64 | 0.85 | 1.02 | 1.05 |
| 365 | 0.70 | 0.94 | 1.25 | | 1.83 | 1.90 |
| 355 | 1.03 | 1.32 | 1.68 | 2.16 | 2.39 | 2.47 |
| 350 | 1.18 | 1.49 | 1.89 | 2.35 | 2.57 | 2.68 |
| 345 | 1.29 | 1.62 | 2.03 | 2.48 | 2.69 | 2.79 |
| 340 | 1.38 | 1.71 | 2.09 | 2.52 | 2.71 | 2.81 |
| 335 | 1.42 | 1.72 | 2.07 | 2.47 | 2.63 | 2.72 |
| 330 | 1.40 | 1.68 | 1.97 | 2.32 | 2.45 | 2.53 |

[a] $1/S$ is usually taken to be the molar absorptivity of $FeCl^{2+}$. The units of $1/S$ are $M^{-1}$ cm$^{-1}$. [b] Measurements made with a Beckman DU-2 spectrophotometer. [c] Medium is 6.00 $M$ perchloric acid (the ionic strength was not kept constant).

phase in the presence of added iron(III) was $3.9 \times 10^{-3}$ $M$; initial iron(III) concentration in the aqueous phase was 0.0503 $M$; iron(III) concentration remaining in the aqueous phase after extraction was 0.0337 $M$.

## Discussion

Before discussing the results two important questions having a bearing on the interpretation of the measurements will be considered. The first question is whether higher chloride complexes exist under the experimental conditions used in this study. This question is crucial in any measurement of the formation equilibrium constant of $FeCl^{2+}$. It is necessary either to correct for the formation of higher complexes, or to use conditions such that $FeCl_2^+$ and higher complexes are not formed to a significant extent.

One criterion often used is to make a plot of variables involving experimental quantities such that if only the first complex is formed, a straight line is obtained, while a curved line is obtained if higher complexes are formed. Using this as the only criterion is risky. Kruh[20] and Baes[21] have pointed out that when spectrophotometric measurements are made in the presence of excess complexing agent, a condition may exist involving $\epsilon_2/\epsilon_1$ and $K_2/K_1$ such that a straight line will be obtained in the plot suggested by eq 7 even when a second complex is formed in significant amounts ($\epsilon_1$ and $\epsilon_2$ are the molar absorptivities of the mono and bis complexes, respectively, and $K_2$ is the formation constant of the bis complex). Significant deviations from the Kruh condition can lead to curvature so slight that it may be masked by experimental scatter. Conditions similar to Kruh's condition may also exist for other kinds of measurements of formation equilibrium constants, for example, for those involving solvent extraction and potentiometric measurements.

Because of the importance of this question, we will summarize the evidence that $FeCl_2^+$ and higher complexes do not form significantly under the experimental conditions used in this study. (a) The concentration of chloride was low. If at a given ionic strength the ratio $K_2/K_1$ is assumed equal to 0.3, then the ratio $[FeCl_2^+]:[FeCl^{2+}]$ under the most unfavorable set of experimental conditions is 0.02. This ratio will be weighted by the ratio $\epsilon_2/\epsilon_1$, which is approximately equal to 2. (b) The experimental points fall on a straight line when plotted according to eq 7. A Kruh-type condition does not exist for the situation in which the formal concentration of iron(III) is large compared to the concentration of chloride unless dimeric iron(III) species are formed. (c) The value of the ratio $S:I$ was determined from data at eight wavelengths, and no trend in this ratio with wavelength was observed. The shape of the absorption band was always the same at a given ionic strength. (d) Although the formal concentration of chloride was varied over a factor of two, no departure from eq 7 was observed. On the basis of these considerations we conclude that only the first chloride complex is formed under the experimental conditions used in this work.

The second question concerns the meaning of an "equilibrium constant" measured at constant ionic strength when the activity coefficient ratio is not constant at constant ionic strength. In other words, can anything be said about this system beyond the statement that $S$ and $I$ represent a description of how the absorbance of $FeCl^{2+}$ changes with changes in the iron(III) and chloride ion concentrations?

An answer to this question can be given if a simple assumption is made concerning ln $Y$. If $N$ is the number of independently variable concentrations, then ln $Y$ may be represented by an $N$-dimensional surface in $(N + 1)$-dimensional space. In the system being considered, the perchloric acid and the iron(III) concentrations will be taken as the only independent variables at constant temperature (in the absence of added sodium perchlorate) since the concentrations of $Cl^-$ and of $FeCl^{2+}$ are very small and are therefore unlikely to have a significant effect on ln $Y$. Thus ln $Y$ will be considered to be a function only of $H$ (= $[HClO_4]$) and $F$ (= [Fe(III)]), in other words, ln $Y = f(H,F)$ at constant temperature. Note that the perchloric acid concentration is always much larger than the iron(III) concentration under the conditions used in these studies, a restriction which should be kept in mind during the following discussion. The assumption will be made that ln $Y$ is a sufficiently slowly varying function of the iron(III) and perchloric acid concentration so that ln $Y$ may be represented by a plane, at least for small changes in $H$ and $F$. This planar region can be defined by three parameters. Once these three parameters are known, then the values of ln $Y$ anywhere in this plane can be calculated using simple geometric considerations. The concentration range over which this assumption is

(20) R. Kruh, *J. Amer. Chem. Soc.*, **76**, 4865 (1954).
(21) C. F. Baes, Jr., *J. Phys. Chem.*, **60**, 878 (1956).

valid will, of course, depend on the system and the conditions being used.

The justification for the planarity assumption rests upon the behavior of mean molal activity coefficients in mixtures of two electrolytes. Above concentrations of about 2 $m$ a plot of ln $\gamma_{\pm}$ for one of the electrolytes *vs.* the molal concentrations of each of the electrolytes is generally a smoothly varying surface which has the greatest curvature along the concentration axes, and, to a good approximation, follows Harned's rule[22] along lines of constant molal ionic strength. The surface often becomes less curved as the concentrations of the electrolytes are increased. The behavior on changing to molar concentrations would not be very different since the density changes are gradual and continuous. In addition, since Harned's rule is a good approximation at constant ionic strength, the planarity assumption will be valid over a large concentration range at conditions close to constant ionic strength.

In general a change in ln $Y$ for a small change in $F$ and $H$ is given by

$$\mathrm{d} \ln Y = \left(\frac{\partial \ln Y}{\partial F}\right)_H \mathrm{d}F + \left(\frac{\partial \ln Y}{\partial H}\right)_F \mathrm{d}H \qquad (8)$$

The planarity assumption states that $(\partial \ln Y/\partial F)_H$ and $(\partial \ln Y/\partial H)_F$ are constants, and consequently the above differential expression can readily be integrated to give

$$\ln Y = \ln Y^0 + \sigma_H F + \sigma_F (H - H^0) \qquad (9)$$

where $(\partial \ln Y/\partial F)_H = \sigma_H$, $(\partial \ln Y/\partial H)_F = \sigma_F$, and the superscript refers to the condition where $F = 0$ and $H = H^0$. The planar region is thus defined by $Y^0$ and the two slopes, $\sigma_H$ and $\sigma_F$. The significance of eq 9 can be seen in terms of the individual activity coefficients. The planarity assumption implies that the natural logarithms of the individual activity coefficients in reaction 1 ($y_1$, $y_2$, and $y_3$), have the following dependence on the two variables

$$\ln y_3 = \ln y_3^0 + a_3 F + b_3 (H - H^0) \qquad (10a)$$

$$\ln y_2 = \ln y_2^0 + a_2 F + b_2 (H - H^0) \qquad (10b)$$

$$\ln y_1 = \ln y_1^0 + a_1 F + b_1 (H - H^0) \qquad (10c)$$

where the $a$'s and $b$'s are constants. Then since

$$\ln Y = \ln y_3 + \ln y_1 - \ln y_2 \qquad (11)$$

it follows that $Y^0 = y_3^0 y_1^0 / y_2^0$, $\sigma_H = (a_3 + a_1 - a_2)$, and $\sigma_F = (b_3 + b_1 - b_2)$. Equation 10 is formally similar to Guggenheim's equation, which has been derived from a model of specific ionic interactions.[23]

It is possible to simplify the above expressions if $H$ and $F$ do not vary independently. Consider a particular perchloric acid concentration, $H^0$. Starting from $H^0$ and $F = 0$ a series of straight lines may be drawn in the $H$–$F$ plane with slopes $(H - H_0)/F = R$. If a particular straight line describes the variation of $H$ and $F$ in the system, then it follows that in such a system ln $Y$ is given by

$$\ln Y = \ln Y^0 + (\sigma_H + R\sigma_F)F \qquad (12)$$

The quantity in parentheses is constant for a given $R$ (that is, when $H^0$ and $(H - H^0)/F$ are kept constant) and will be defined as $\alpha_R$. We thus obtain

$$\ln Y = \ln Y^0 + \alpha_R F \qquad (13)$$

or

$$Y = Y^0 e^{\alpha_R F} \qquad (14)$$

where $\alpha_R = (\sigma_H + R\sigma_F)_R = (\partial \ln Y/\partial F)_R$. The exponential may be expanded to give

$$Y = Y^0\left(1 + \alpha_R F + \frac{(\alpha_R F)^2}{2!} + \ldots\right) \qquad (15)$$

Evidently $Y$ will vary linearly with $F$ when the second-order term in $F$ is negligible.[24,25]

$$Y = Y^0(1 + \alpha_R F) \qquad (16)$$

Substitution for $Y$ in eq 2 gives

$$K_1 = Q_1^0(1 + \alpha_R F) \qquad (17)$$

where $Q_1^0 = K_1^0 Y^0$ is the value of $K_1$ when $F = 0$ and $H = H^0$.

*Application to the Equilibrium Spectrophotometric Measurements.* In a general treatment it is necessary to allow for the formation of an outer-sphere complex between $Fe^{3+}$ and $Cl^-$ in addition to the formation of $FeCl^{2+}$.

$$Fe^{3+} + Cl^- \rightleftharpoons Fe^{3+}||Cl^- \qquad (18)$$

$$K_{out} = \frac{[Fe^{3+}||Cl^-]}{[Fe^{3+}][Cl^-]} \qquad (19)$$

Under these conditions

$$\frac{FC}{A} = \frac{1}{\epsilon_{in}K_{in} + \epsilon_{out}K_{out}} + \frac{K_{in} + K_{out}}{\epsilon_{in}K_{in} + \epsilon_{out}K_{out}}(F + C) - A\left(\frac{K_{in} + K_{out}}{\epsilon_{in}K_{in} + \epsilon_{out}K_{out}}\right)^2 \qquad (20)$$

where $C$ is the total chloride concentration and $K_{in} + K_{out} = K_1$. Since $\epsilon_{in}K_{in} \gg \epsilon_{out}K_{out}$ at the absorbance maximum of the $FeCl^{2+}$ complex, and since the third term in eq 20 may be neglected, we obtain

$$\frac{FC}{A} = \frac{1}{\epsilon_{in}K_{in}} + \frac{K_{in} + K_{out}}{\epsilon_{in}K_{in}}(F + C) \qquad (21)$$

(22) Reference 15, Chapter 15.

(23) E. A. Guggenheim, *Phil. Mag.*, 19, 585 (1935).

(24) An expression analogous to eq 16 has been used at constant ionic strength, for example, in ref 25.

(25) L. O. Spreer, Ph.D. Thesis, University of Colorado, Boulder, Colo., 1969.

Substitution of

$$K_{in} = Q_{in}^0(1 + \alpha_R F) \quad (22)$$

in eq 21 and assuming that at constant ionic strength $\epsilon_{in}$ is medium independent over the variations in concentrations used,[26] and, as has been found in the analogous $CrBr^{2+}$ system,[25] that $K_{out}$ is relatively insensitive to the composition of the medium, gives

$$\frac{FC}{A} = \frac{1}{\epsilon_{in}Q_{in}^0(1 + \alpha_R F)} + \frac{Q_{in}^0(1 + \alpha_R F) + K_{out}}{\epsilon_{in}Q_{in}^0(1 + \alpha_R F)}(F + C) \quad (23)$$

If $\alpha_R F$ is much less than 1, then $1/(1 + \alpha_R F)$ may be expanded, and if terms higher than first power in $F$ and $C$ are neglected in the expansion, we obtain

$$\frac{FC}{A} = \frac{1}{\epsilon_{in}Q_{in}^0} + \frac{(Q_{in}^0 + K_{out} - \alpha_R)}{\epsilon_{in}Q_{in}^0}(F + C) + \frac{\alpha_R C}{\epsilon_{in}Q_{in}^0} \quad (24)$$

Neglecting the third term shows that the intercepts and slopes of plots of $FC/A$ *vs.* $(F + C)$ give

$$\frac{1}{I} = \epsilon_{in}Q_{in}^0 \quad (25a)$$

$$\frac{S}{I} = Q_{in}^0 + K_{out} - \alpha_R \quad (25b)$$

$$\frac{1}{S} = \frac{\epsilon_{in}Q_{in}^0}{Q_{in}^0 + K_{out} - \alpha_R} \quad (25c)$$

The significance of the intercepts and slopes defined by eq 7 and of the quantities listed in Table IV are evident from the above relations. It is also apparent that in order to derive $\epsilon_{in}$ and $Q_{in}^0$ from equilibrium spectrophotometric data, it is necessary to know $K_{out}$ and $\alpha_R$. A reasonable upper limit for $K_{out}$ for this system is 1 $M^{-1}$.[27] Obtaining a value for $\alpha_R$ is more difficult. It might be possible to evaluate $\alpha_R$ by measuring the coefficient of the second-order term in $F$ which has been neglected in deriving eq 22 and 24. This term is approximately equal to $\alpha_R^2F^2/2\epsilon_{in}Q_{in}^3$. If $\alpha_R = 5\ M^{-1}$ and $Q_{in}^0 = 100\ M^{-1}$, then this term is only about 1.5% of the first-order term in $F$ even when $F = 0.2\ M$. Therefore there seems to be little possibility of evaluating $\alpha_R$ by going to sufficiently high iron(III) concentrations so as to obtain curvature of the plot of $FC/A$ *vs.* $(F + C)$ for the reaction at a constant ionic strength of 6 $M$.

Although it is not possible to evaluate any $\alpha_R$ for this system using the equilibrium data presented here, it is possible to calculate $S/I$ $(= Q_1^0 - \alpha_R)$ along any line emanating from $H^0 = 6.0\ M$ from the measured value of $S/I$ along one line and from a measured value of $\sigma_F$. For example, at $H^0 = 6\ M$ the experimental

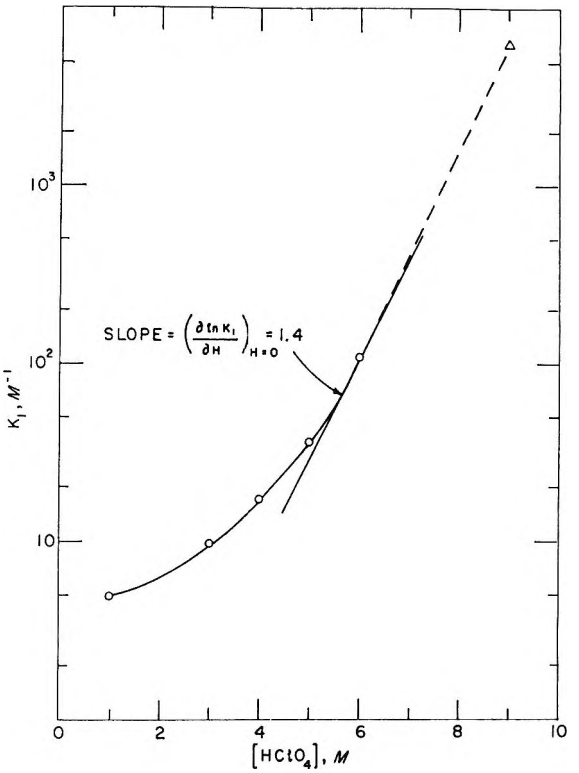


Figure 1. Plot of $K_1$ *vs.* perchloric acid concentration at 25.0°; circles, this work; triangles, ref 1.

value of $(S/I)_\mu = 110\ M^{-1}$, and from the slope of the plot of ln $(S/I)_\mu$ *vs.* $\mu$ (Figure 1) a value of $\sigma_F \approx 1.4\ M^{-1}$ is estimated at $\mu = 6.00\ M$. According to eq 25b, at constant ionic strength ($R = -6$)

$$(S/I)_\mu = Q_{in}^0 + K_{out} - \alpha_\mu \quad (26)$$

It follows from the definition of $\alpha_R = \alpha_H + R\sigma_F$ that

$$(\alpha_H - \alpha_\mu) = 6\sigma_F \quad (27)$$

Therefore at constant perchloric acid concentration ($R = 0$) we calculate a value of 102 $M^{-1}$ for $(S/I)_H$ in

$$(S/I)_H = Q_{in}^0 + K_{out} - \alpha_H = (S/I)_\mu - 6\sigma_F \quad (28)$$

6.0 $M$ perchloric acid using eq 28. This estimate is in good agreement with the experimental value of 104 ± 3 $M^{-1}$.

It is also apparent from eq 25a that a plot of $FC/A$ *vs.* $(F + C)$ made at constant ionic strength should yield the same intercept as the same plot made at a constant perchloric acid concentration equal to that ionic strength. As is evident from Table IV, the data satisfy this requirement rather well. At 340 nm the values of $\epsilon_{in}Q_{in}^0$ are $(2.95 \pm 0.06) \times 10^5\ M^{-2}\ cm^{-1}$ and

(26) This is a reasonable assumption at an ionic strength of 6 $M$, where the molar absorptivity is not very medium dependent (see Figure 2). If, to a first approximation, $\epsilon_{in}$ varies linearly with $F$ with a coefficient $\beta_R$, then $\alpha_R$ should be replaced by $\alpha_R + \beta_R$ in eq 25 and equations derived from it.

(27) This assumption is consistent with measurements of $K_{out}$ for the reaction $Cr^{3+} + Br^- \rightleftharpoons CrBr^{2+}$ reported in ref 25.

$(2.92 \pm 0.06) \times 10^5\ M^{-2}\ cm^{-1}$ for the measurements at $\mu = 6.00\ M$ and $[HClO_4] = 6.00\ M$, respectively.

The conclusions that can be drawn in regard to equilibrium spectrophotometric measurements on a relatively labile system such as the iron(III)–chloride system may now be summarized as follows: (a) The concentration equilibrium constant and the molar absorptivity of the complex cannot be determined unless $\alpha_R$ is known. The quantities obtained are those given by eq 25 when the measurements are performed at constant $R$. (b) There is a possibility of evaluating $\alpha_R$ by measuring the coefficients of higher order terms in $F$ as discussed above. In order to accomplish this, the ratio $\alpha_R:Q_1^0$ should be as large as possible. Unfortunately, if $R$ is chosen so that this ratio is large, the chosen conditions are more likely to be those under which the planarity assumption is invalid. In addition, the effect of the medium changes on both the molar absorptivities and on $K_{out}$ could become important. (c) If any two values for $(Q_1^0 - \alpha_R)$ with a common $H^0$ are known, or, if $\sigma_F$ and one value of $(Q_1^0 - \alpha_R)$ are known, then any other value of $(Q_1^0 - \alpha_R)$ referring to the same $H^0$ may be calculated.

The conclusions regarding nonlabile systems such as the chromium(III)–halide complexes are somewhat different. In these systems $\epsilon_1$ may be determined directly and, consequently, if $K_{out}$ is known, then $\alpha_R$ may be evaluated directly from the changes in the apparent concentration equilibrium constant with changes in medium at constant $R$. Therefore, these systems are more amenable to study than labile systems if evaluating $\alpha_R$ is the objective. Unfortunately, since $\alpha_R$ is probably small compared to the equilibrium constant, data of extremely high accuracy are needed.

*Comparison with Other Studies.* Bearing in mind that the measured quantities are not simply the equilibrium constant and the molar absorptivity, we can still compare the results obtained in this study with those obtained in previous studies under similar experimental conditions. In order to simplify comparison with these studies $S/I$ will be referred to as $K_1$, and $1/S$ as $\epsilon_1$.

It is apparent from Tables IV and V and Figure 2 that the assumption of constant maximum molar absorptivity made in ref 1 is incorrect. The value for this molar absorptivity of $2.90 \times 10^3\ M^{-1}\ cm^{-1}$ in $9\ M\ HClO_4$ measured in this work is in very good agreement with ref 1. The wavelength of maximum absorbance also shifts with increasing ionic strength, in agreement with the findings of Coll, Nauman, and West[1] and in disagreement with the results of Heistand and Clearfield,[2] who ascribed an observed shift to the formation of higher chloride complexes. Although $\epsilon_1$ and $\lambda_{max}$ both change with ionic strength, a plot of $\epsilon_1/\epsilon_{max}$ *vs.* $(\lambda - \lambda_{max})$ gives a single curve for all ionic strengths; in other words, the shape of the absorption band remains unchanged. The observed shifts of $\lambda_{max}$ and $\epsilon_{max}$ for $FeCl^{2+}$ with changes in medium are very similar to the shifts observed by Kosower in the charge transfer spectra of substituted pyridinium iodides in various solvents.[28] It seems very likely that the explanation proposed by Kosower for the shift in $\lambda_{max}$ is also applicable to $FeCl^{2+}$. It is interesting to note that a straight

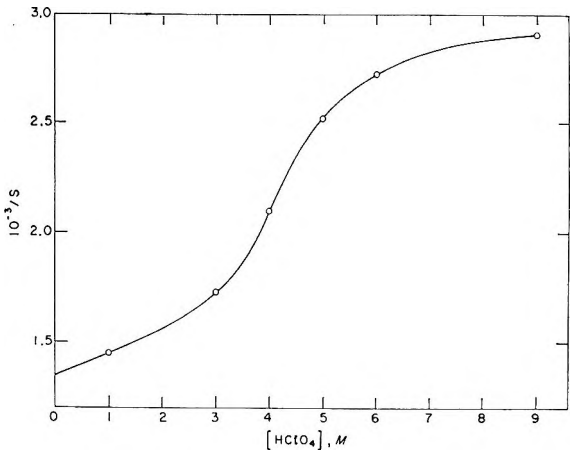


Figure 2. Plot of $\epsilon_{max}$ *vs.* perchloric acid concentration at 25.0°.

line is obtained when the transition energy $hc/\lambda_{max}$ is plotted against $\Delta G^0$ for the reaction. This result suggests that the same medium effect is important in both types of measurement.

A comparison of $K_1$ values is presented in Table VI. The variation of $K_1$ with ionic strength is in fair agreement with the results obtained by Coll, Nauman, and West[1] and in better agreement with the results obtained by Heistand and Clearfield.[2] Because Coll, Nauman, and West assumed a constant value for $\epsilon_1$, good agreement with their data is not to be expected. The low values for $K_1$ obtained spectrophotometrically by Woods, *et al.*,[3] at an ionic strength of 1.00 $M$ are consistent with the presence of $FeCl_2^+$ arising from the high chloride concentrations (up to 0.95 $M$) used in their measurements. If the published values of $K_2$ are approximately correct ($K_2 \approx 1\ M^{-1}$), then there would be significant $FeCl_2^+$ formation at the higher chloride concentrations. This possibility was recognized by Woods, *et al.*, who pointed out that the existence of a Kruh condition was possible, and that a value of $K_1 = 4.35\ M^{-1}$ and $K_2 = 0.9\ M^{-1}$ (or $K_1 = 4.75\ M^{-1}$ and $K_2 = 1.1\ M^{-1}$) would rationalize their observed variation of $K_1$ with wavelength. However, they discounted this possibility because of the general agreement between their electrometric, spectrophotometric, and calorimetric measurements. On the other hand, their spectrophotometric measurements at an ionic strength of 1.00 $M$ are consistent with ours if $K_2 \approx 1\ M^{-1}$. In the presence of excess chloride, the

(28) E. Kosower, *J. Amer. Chem. Soc.*, **80**, 3261 (1958).

**Table VI:** Comparison of $K_1$ Values at 25°

| $\mu$,[a] $M$ | $K_1$, $M^{-1}$ | Ref | $\mu$,[a] $M$ | $K_1$, $M^{-1}$ | Ref |
|---|---|---|---|---|---|
| 0.15 | 9.2 | b | 2.00 | 6.4 | m |
| | 6.3 | c | | 5 | i |
| | 7.6 | d | | 5.3 | c |
| 0.50 | 4.4 | e | | 6.4 | l |
| | 4.1 | c | 3.00 | 6.6 | f |
| | 3.2 | f | | 7.8 | i |
| | 5.6 | g | | 5.8 | n |
| 1.00 | 4.5 | h | | 9.8 | j |
| | 3.9 | c | 4.00 | 20 | i |
| | 2.9 | f | | 12.5 | n |
| | 3.9 | i | | 17.3 | j |
| | 5.2 | j | 5.00 | 48 | i |
| 1.20 | 4.1 | k | | 28 | n |
| | 4.0 | c | | 36.3 | j |
| | 3.0 | f | 6.00 | 92 | n |
| | 5.3 | l | | 110 | j |

[a] $\mu$ = ionic strength. [b] Reference 29. Corrected to 25° using $\Delta H$ = 5.2 kcal/mol. [c] E. Rabinowitch and W. Stockmayer, *J. Amer. Chem. Soc.*, **64**, 335 (1942). Corrected to 25°. [d] Extrapolated from the data obtained in this work and from ref 29. [e] Reference 6. [f] Reference 3. [g] Extrapolated from the data obtained in this work and from ref 6. [h] Reference 28. [i] Reference 2. [j] This work. [k] M. W. Lister and D. E. Rivington, *Can. J. Chem.*, **33**, 1603 (1955). [l] Interpolated from data obtained in this work. [m] Reference 4. Corrected to 25° using $\Delta H$ = 4.0 kcal/mol. [n] Reference 1.

Kruh condition for a linear plot when significant amounts of $FeCl_2^+$ are present is

$$\frac{\epsilon_2}{\epsilon_1} = \frac{1 \pm (1 - 4K_2/K_1)^{1/2}}{2K_2/K_1}$$

If this condition obtains, then the apparent value of $K_1$ changes but a correct value of $\epsilon_1 K_1$ will still be obtained.[20] The values of $\epsilon_1 K_1$ obtained by Woods, *et al.*, are $7.14 \times 10^3\ M^{-2}\ cm^{-1}$ at 335 nm and $1.58 \times 10^3\ M^{-2}\ cm^{-1}$ at 380 nm. The values obtained in this study at the same wavelengths are $7.11 \times 10^3$ and $1.69 \times 10^3\ M^{-2}\ cm^{-1}$, respectively. As expected, the agreement of the $\epsilon_1 K_1$ values is satisfactory. In addition, a value of "$K_1$," may be estimated for the experimental conditions used in ref 3. If $\epsilon_2/\epsilon_1$ is assumed to be equal to 2.0, then $K_2/K_1 = 0.25$ would satisfy the Kruh condition. Small deviations from the Kruh condition lead to curvature so slight that it may be masked by the experimental error. By assuming $K_1 = 5\ M^{-1}$, $K_2 = 1\ M^{-1}$, and $\epsilon_2 = 2\epsilon_1$, calculating the absorbance, and plotting the results as done in ref 3, a line is obtained with no curvature within the experimental error of the measurements. When the best straight line is drawn, a value of "$K_1$" $\approx 2.5\ M^{-1}$ is obtained. This may be compared with the value of "$K_1$" $= 2.9\ M^{-1}$ obtained in ref 3. The similarity of the calculated and observed "$K_1$" values supports the interpretation that the value of $K_1$ reported in ref 3 is in error because of the presence of higher chloride complexes.

If the experimental conditions used by Woods, *et al.*, result in significant $FeCl_2^+$ formation, then it is puzzling that the result of White, Kelly, and Li[29] at $\mu = 1.00\ M$ is in relatively good agreement with the result obtained in this study since they used the same range of chloride concentrations as Woods, *et al.* White, *et al.*, studied the effect of chloride concentration on the extraction of $Fe^{3+}$ with a liquid cation exchanger, dinonylnaphthalenesulfonic acid. They plotted $1/K_d$ *vs.* $[Cl^-]$, where

$$K_d = \frac{\sum [Fe^{III}]_{org}}{\sum [Fe^{III}]_{aq}}$$

and obtained a straight line. The formation of higher complexes can lead to a slight curvature which might be masked by experimental scatter, but the apparent value of $K_1$ based on drawing the best straight line through the experimental points should be higher than the true value.

A possible explanation consistent with their data and ours is that $FeCl^{2+}$ is also extracted. If this is true, then at constant acidity in the aqueous phase, and constant concentration of dinonylnaphthalenesulfonic acid in the organic phase, the formal distribution ratio is given by

$$K_d = \frac{K_3^d[Fe^{3+}]_{aq} + K_2^d[FeCl^{2+}]_{aq}}{[Fe^{3+}]_{aq} + [FeCl^{2+}]_{aq} + [FeCl_2^+]_{aq}} \quad (29)$$

$$\frac{1}{K_d} = \frac{1 + K_1C + K_1K_2C^2}{K_3^d[1 + K_2^dK_1C/K_3^d]} \quad (30)$$

where $K_3^d$ and $K_2^d$ are the distribution ratios for $Fe^{3+}$ and $FeCl^{2+}$, respectively. This relation is formally similar to the one considered by Kruh for spectrophotometric measurements. A Kruh condition can also obtain here in which case a linear plot of $1/K_d$ *vs.* $C$ results. This condition is

$$\frac{K_2^d}{K_3^d} = \frac{1 \pm (1 - 4K_2/K_1)^{1/2}}{2} \quad (31)$$

Therefore, if $FeCl^{2+}$ is extracted, and if the Kruh condition is approximately satisfied, then a nearly linear plot of $1/K_d$ *vs.* $C$ will be obtained. If $K_1 = 5\ M^{-1}$ and $K_2 = 1\ M^{-1}$, then the Kruh condition is $K_2^d/K_3^d = 0.28$ or 0.72. In order to test this hypothesis the extraction experiment was performed. Again assuming the values of $K_1 = 5\ M^{-1}$ and $K_2 = 1\ M^{-1}$, a value of $K_2^d/K_3^d = 0.03$ is calculated from the extraction data. This is considerably smaller than the Kruh condition values of 0.28 or 0.72. Therefore, $FeCl^{2+}$ is extracted, but not to an extent large enough to account for the results of White, *et al.* The fact that chloride is ex-

(29) J. M. White, P. Kelly, and N. C. Li, *J. Inorg. Nucl. Chem.*, **16**, 337 (1961).

tracted in the blank suggests that additional equilibria obtain in the organic phase and that the situation is more complicated than has been assumed.

The value of $K_1 = 4.4\ M^{-1}$ at ionic strength 0.50 obtained by Sutin, Rowley, and Dodson[6] is very likely too low. Although the product $\epsilon_1 K_1$ can readily be determined, it becomes increasingly difficult to obtain a value for $\epsilon_1$ or $K_1$ as $K_1$ decreases. Extrapolation of the results obtained in the present study (in which an improved spectrophotometer was used) gives $\epsilon_1 = 1.38 \times 10^3\ M^{-1}\ cm^{-1}$ at 335 nm and ionic strength 0.50 $M$. This value together with the value of $7.61 \times 10^3\ M^{-2}\ cm^{-1}$ for $\epsilon_1 K_1$ obtained by Sutin, *et al.*, gives $K_1 = 5.6\ M^{-1}$ at ionic strength 0.50 $M$ and 25°.

Fordham[30] has recently measured $K_1$ at ionic strength of 0.15 $M$ and 20°. He obtained a value of $K_1 = 7.9 \pm 4.4\ M^{-1}$ at constant perchlorate concentration and a value of $K_1 = 4.0 \pm 0.11\ M^{-1}$ at variable perchlorate concentration and constant ionic strength. The first value was obtained at low chloride concentrations (0-7.5 $\times 10^{-3}$ $M$), but the latter value was obtained using chloride concentrations as high as 0.127 $M$. Therefore, it seems highly probable that this value of $4.0\ M^{-1}$ is too low because of the formation of the second complex $FeCl_2^+$ and the existence of a Kruh-type condition as previously discussed in connection with the results of Woods, *et al.* This is reflected in the high apparent molar absorptivity of $2334\ M^{-1}\ cm^{-1}$ at 340 nm which is very similar to that reported in ref 3. Using Fordham's value for $\epsilon_1 K_1$ at the low chloride concentrations and a value of $\epsilon_1 = 1.36 \times 10^3\ M^{-1}\ cm^{-1}$ at 25° extrapolated from our data to $\mu = 0.15$ $M$ gives a value for $K_1 = 6.5\ M^{-1}$ at $\mu = 0.15$ $M$ and 20°.

Finally, measurements have been made of the inner-sphere chromium(III)–halide equilibria at different ionic strengths.[25,31] These studies can be compared with this work by calculating an equilibrium constant, $Q_X$, at 25° for the reaction

$$Cl^- + CrX^{2+} + Fe^{3+} = FeCl^{2+} + Cr^{3+} + X^- \qquad Q_X$$

at various water activities. In order to calculate $Q_X$ it is necessary to extrapolate the equilibrium constants for the chromium(III)–halide reactions to 25° and then to interpolate to a given water activity. The values obtained are shown in Table IV. Within the uncertainties resulting from the extrapolations and interpolations both of the calculated equilibrium constants are independent of the water activity. This comparison therefore suggests that the equilibrium constants of related reactions behave similarly with changes in water activity.

*Application to the Kinetic Measurements.* In common with other complex-formation reactions, it will be assumed that the formation of $FeCl^{2+}$ proceeds in two steps. The first step is the rapid formation of the outer-sphere complex (reaction 18), and the second step is the rate-determining conversion of the outer sphere into the inner-sphere complex.

$$Fe^{3+}||Cl^- \underset{k_{-x}}{\overset{k_x}{\rightleftharpoons}} FeCl^{2+} \qquad (32)$$

Note that $k_x$ and $k_{-x}$ are, in general, functions of the acidity. In terms of this mechanism the rate of formation of $FeCl^{2+}$ is given by

$$\begin{aligned}\frac{d(FeCl^{2+})}{dt} &= k_x[Fe^{3+}||Cl^-] - k_{-x}[FeCl^{2+}] \\ &= k_x K_{out}[Fe^{3+}][Cl^-] - k_{-x}[FeCl^{2+}] \\ &= k_{obsd}([FeCl^{2+}]_{eq} - [FeCl^{2+}])\end{aligned} \qquad (33)$$

where

$$\begin{aligned}k_{obsd} &= \frac{k_{-x}[1 + (K_{out} + K_{in})(F + C)]}{1 + K_{out}(F + C)} \\ &= k_{-x} + \frac{K_{out}k_x(F + C)}{1 + K_{out}(F + C)}\end{aligned} \qquad (34)$$

If $[1 + K_{out}(F + C)]^{-1}$ is expanded in a series we obtain

$$k_{obsd} = k_{-x} + k_x K_{out}(F + C) - k_x K_{out}^2(F + C)^2 + \ldots \qquad (35)$$

Evidently $k_d = k_{-x}$ and $k_f = k_x K_{out}$. By analogy with the equilibrium considerations we will assume that

$$k_{-x} = k_{-x}^0(1 + \alpha_{-x}F + \alpha_{-x}^2F^2/2! + \ldots) \qquad (36)$$

$$k_x = k_x^0(1 + \alpha_x F + \alpha_x^2F^2/2! + \ldots) \qquad (37)$$

where $k_x^0$ and $k_{-x}^0$ refer to the conditions $H = H^0$ and $F = 0$. On substituting eq 36 and 37 into eq 35 and neglecting terms in $(F + C)$ or $F$ of higher order than two, we obtain[32]

$$\begin{aligned}k_{obsd} = k_{-x}^0 + k_x^0 K_{out}\left(1 + \frac{\alpha_{-x}}{Q_{in}^0}\right)(F + C) + \\ \left[k_x^0 K_{out}\left(\alpha_x - K_{out} + \frac{\alpha_{-x}^2}{2Q_{in}^0}\right)\right](F + C)^2 - \\ \frac{k_x^0 K_{out}\alpha_{-x}C}{Q_{in}^0} - k_x^0 K_{out}\alpha_x(F + C)C\end{aligned}$$

The last two terms are negligible since the maximum $C$ is equal to $4 \times 10^{-4}$ $M$. Also since $\alpha_{-x}$, $\alpha_x$, and

(30) A. W. Fordham, *Aust. J. Chem.*, **22**, 1111 (1969).

(31) C. F. Hale and E. L. King, *J. Phys. Chem.*, **71**, 1779 (1967).

(32) We have assumed that in 6.00 $M$ $HClO_4$ the acid-dependent kinetic term is negligibly small. If it is not, a second-order term in $F$ with a positive coefficient is obtained due to the changing acidity at constant ionic strength and, as a result, the value of $\alpha_x - K_{out}$ derived from the data would represent an upper limit.

$K_{out}$ are all small compared to $K_{in}$, $\alpha_{-x}^2/2Q_{in}^0$ is negligible compared to $(\alpha_x - K_{out})$. Therefore

$$k_{obsd} = A + B(F + C) + C(F + C)^2 \quad (38)$$

where

$$A = k_{-x}^0$$

$$B = k_x^0 K_{out}\left(1 + \frac{\alpha_{-x}}{Q_{in}^0}\right)$$

$$C = k_x^0 K_{out}(\alpha_x - K_{out})$$

Note that since $B \approx k_x^0 K_{out}$, it follows that $C/B \approx (\alpha_x - K_{out})$. Also since $K_{in} = k_x K_{out}/k_{-x}$ and $Q_{in}^0 = k_x^0 K_{out}/k_{-x}^0$, the following relations obtain

$$\alpha_\mu = (\alpha_x - \alpha_{-x}) \quad (39)$$

$$\left(\frac{S}{I}\right)_\mu = Q_{in}^0 - \alpha_\mu + K_{out}$$

$$\approx \frac{B}{A} + \frac{C}{B} \quad (40)$$

The coefficients, $A$, $B$, and $C$, were evaluated by fitting all of the kinetic data at 25° (with sodium perchlorate absent) using the method of averages. The following values were obtained: $A = 0.97$ sec$^{-1}$, $B = 98\ M^{-1}$ sec$^{-1}$, $C = -220\ M^{-2}$ sec$^{-1}$. These numbers are sensitive to the data used and to the grouping of the data. If the additional requirement is made that these coefficients must be consistent with the equilibrium value of $(S/I)_\mu = 110\ M^{-1}$, then a slightly different set of coefficients is obtained: $A = 0.95$ sec$^{-1}$, $B = 102\ M^{-1}$ sec$^{-1}$, $C = -270\ M^{-2}$ sec$^{-1}$. Since these are consistent with $(S/I)_\mu$ and fit the kinetic data well, they were used to calculate the following parameters at constant $\mu = 6.00\ M$

$$k_{-x}^0 = 0.95 \pm 0.02 \text{ sec}^{-1}$$

$$(Q_{in}^0 + \alpha_{-x}) = 107 \pm 3\ M^{-1}$$

$$(\alpha_x - K_{out}) = -2.7 \pm 0.4\ M^{-1}$$

In order to proceed further it is necessary to make some additional assumptions. The first is that transition state theory may be applied. In terms of transition state theory $\alpha_x$ and $\alpha_{-x}$ have the following significance

$$Y_x = \frac{y_3 y_1}{y_\pm} = Y_x^0 e^{\alpha_x F} \quad (41a)$$

$$Y_{-x} = \frac{y_2}{y_\pm} = Y_{-x}^0 e^{\alpha_{-x} F} \quad (41b)$$

in which the subscript, $\pm$, refers to the transition state. Note that in eq 41a the activity coefficient for the outer-sphere complex has been put equal to $y_3 y_1$. This is a consequence of the assumption that $K_{out}$ is medium independent. Therefore

$$\alpha_x = \alpha_3 + \alpha_1 - \alpha_\pm \quad (42a)$$

$$\alpha_{-x} = \alpha_2 - \alpha_\pm \quad (42b)$$

Although $K_1$, $\Delta H_1$, and $\Delta S_1$ vary markedly with ionic strength, it is apparent from the data presented in Table II that $k_{-1}$, $\Delta H_{-1}^\pm$, and $\Delta S_{-1}^\pm$ are rather insensitive to the composition of the medium. In other words, the variations in the thermodynamic parameters with the composition of the medium result mainly from variations in the parameters for the formation rather than for the dissociation reaction. The insensitivity of the dissociation parameters indicates that there is a strong resemblance between the inner-sphere complex and the transition state for the reaction, at least insofar as the sensitivity of these two states to changes in the composition of the medium is concerned. Since $k_{-1}$ is insensitive to the perchloric acid concentration in the range 1.0 to 6.0 $M$, it is very likely that $k_{-1}$ is independent also of the iron(III) concentration. Put somewhat differently, it does not seem very reasonable that relatively small changes in the iron(III) concentration would have an effect on $k_{-1}$ when much larger changes in the perchloric acid concentration do not. In other words, these considerations suggest that $\alpha_{-x} \approx 0$, or $\alpha_2 \approx \alpha^\pm$. However this estimate of $\alpha_{-x}$ is uncertain because of our lack of knowledge concerning the role of water in the reaction. If the reaction is considered as reaction 3, then it becomes of interest to examine the values of $k_{-1}/a_w$ rather than $k_{-1}$. It can be seen from Table II that $k_{-1}/a_w$ is slightly more constant than $k_{-1}$ with respect to changes in the perchloric acid concentration. However, the magnitude of the experimental error does not permit any conclusions to be drawn about the role of water in the transition state for the reaction. If, in fact, $k_{-1}/a_w$ is constant rather than $k_{-1}$ with changes in the medium, then $\alpha_{-x}$ is not equal to zero, but is instead equal to $(\partial \ln a_w/\partial F)_\mu$. Since

$$\left(\frac{\partial \ln a_w}{\partial F}\right)_\mu = \left(\frac{\partial \ln a_w}{\partial \mu}\right)_F \left(\frac{\partial \mu}{\partial F}\right)_{a_w}$$

and since

$$\left(\frac{\partial \mu}{\partial F}\right)_{a_w} = \left[6 + \left(\frac{\partial H}{\partial F}\right)_{a_w}\right]$$

it is apparent that $(\partial \ln a_w/\partial F)_\mu$ can be estimated from the value of $(\partial H/\partial F)_{a_w} = -3.0$ from our isopiestic data, and from the value of $(\partial \ln a_w/\partial \mu)_{F=0} = -0.31\ M^{-1}$ at $H^0 = 6.00\ M$ from the data in ref 18 and 19. The resulting value is $(\partial \ln a_w/\partial F)_\mu \approx 0.9\ M^{-1}$ at $H^0 = 6.00\ M$. Using zero and $0.9\ M^{-1}$ as approximate values of the limits of $\alpha_{-x}$ we estimate that $\alpha_{-x} = 0.5 \pm 1.0\ M^{-1}$. If it is further assumed that $K_{out}$ is equal to $0.2\ M^{-1}$ and is medium independent as has

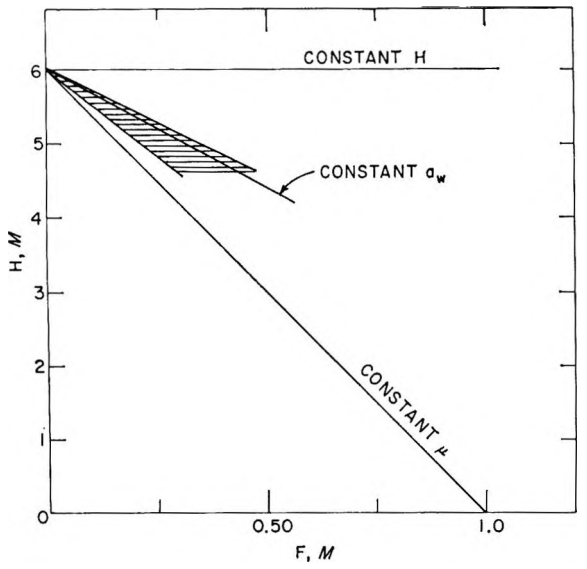


Figure 3. Plot of perchloric acid concentration *vs.* iron(III) concentration showing the position of the constant water activity line in the *H–F* plane. The constant *Y* line lies within the shaded area.

been found for $Cr^{3+}||Br^-$,[25] then the following estimates are obtained for the medium effect parameters

$$\alpha_x = -2.5 \pm 0.5\ M^{-1}$$

$$\alpha_\mu = -3.0 \pm 1.1\ M^{-1}$$

$$\sigma_H = \alpha_H = 5 \pm 1\ M^{-1}$$

The value of $\sigma_H$ was calculated from the definition of $\alpha_R = R\sigma_F + \sigma_H$ using the above value of $\alpha_\mu$ and $\sigma_F = 1.4\ M^{-1}$ at $H^0 = 6.00\ M$. It should be noted that it was not possible to obtain estimates of the above parameters solely from the equilibrium measurements.

The above estimate of $\alpha_\mu$ enables us to locate the position of the constant *Y* line in the *H–F* plane. This can be done using the above values of $\sigma_F$ and $\sigma_H$ and calculating from the definition of $\alpha_R$ a value for *R* when $\alpha_R$ is equal to zero. Because of the large uncertainty in $\alpha_\mu$, a shaded area is used in Figure 3 to show the position of the constant *Y* line within the stated uncertainty. The position of the constant $a_w$ line is also shown. That the constant $a_w$ line lies within the shaded area is consistent with the contention of Coll, Nauman, and West[1] that the water activity is of primary importance in determining $K_1$ for this reaction in solutions of concentrated electrolytes. That this should be so is somewhat surprising since mean molal ionic activity coefficients in binary mixtures of electrolytes are not generally constant at constant water activity. The problem of controlling the medium when determining equilibrium constants in solutions of concentrated electrolytes remains a difficult one even for reactions in which constant water activity is of primary importance since working at constant water activity is awkward.

In conclusion, it has been found that the variation of $K_1$, $\Delta H_1$, and $\Delta S_1$ with perchloric acid concentration arises almost entirely from changes in the kinetics of formation of $FeCl^{2+}$ rather than from changes in the dissociation kinetics. This increased rate of formation of $FeCl^{2+}$ with decreasing water activity indicates that chloride ion is entering the inner coordination shell of the hydrated $Fe^{3+}$ more easily. This may be rationalized, in part, in terms of a decrease in the hydration number of the $Fe^{3+}$ (and perhaps also of the $Cl^-$ ion) with decreasing water activity. In this case reaction 3 would not accurately describe the complex formation. Studies at even lower water activities should further elucidate the important role of water in this system.

*Acknowledgment.* This work was performed under the auspices of the U. S. Atomic Energy Commission. We also wish to thank the R. T. Vanderbilt Co. Inc., New York, for their generous gift of dinonylnaphthalenesulfonic acid.

# Energy Transfer in Thermal Methyl Isocyanide Isomerization. Dependence of Relative Efficiency of Helium on Temperature[1a]

by S. C. Chan,[1b] J. T. Bryant, and B. S. Rabinovitch

*Department of Chemistry, University of Washington, Seattle, Washington 98105* *(Received January 5, 1970)*

The thermal methyl isocyanide isomerization system was studied with helium as the added inert bath gas at five different temperatures over a range of 115°. A lowering of the apparent activation energy by 1.5 kcal $mol^{-1}$ was observed. The dependence of observed activation energy on cross-sectional changes with temperature is discussed. While the direction of change is in accordance with predictions from theoretical calculations, the actual variation is small and a much wider variation of temperature is required for appreciable effects.

## Introduction

Vibrational energy transfer at the high levels of excitation in thermal reaction systems has now been extensively documented in the methyl isocyanide isomerization system at 280.5°.[2] What is still little studied in thermal systems is the variation of the relative collisional efficiency $\beta_c$ with temperature. The literature does afford an interesting difference. In the thermal decomposition of hydrogen peroxide, a large decrease in activation energy upon the addition of helium to a substrate system was observed;[3] on the other hand, in the thermal decomposition of nitrous oxide, a significant activation energy increase upon adding $CF_4$, $CO_2$, or $SO_2$, respectively, was found.[4]

Based on some theoretical assumptions which accord with much of the data on the temperature dependence of vibrational energy transfer in chemical activation systems,[5] it is expected that in thermal systems the observed activation energy should decrease on the introduction of weak collider bath molecules.[6]

In the present paper, a study of the variation of $\beta_c$ with temperature in the thermal methyl isocyanide isomerization system is reported for helium as the inert bath molecule. Helium has been shown to be the weakest activation–deactivation collider in the system[2] and is expected to demonstrate a maximum temperature variation. The reaction rate was studied over a variation of 115° at temperatures from 210 to 326°.

## Experimental Section

The sources and purification of methyl isocyanide and helium have been described elsewhere.[7,8]

The apparatus, procedure, and chemica lanalysis have been discussed in detail elsewhere. A static method was used; a 12-l. Pyrex flask served as the reactor and a salt bath as thermostat.

In each run, a roughly constant amount ($8 \times 10^{-3}$ mm) of methyl isocyanide was expanded into the reactor together with a known amount of He. Reaction was carried to 2–50% conversion; the lower percentage was used for low temperature runs, while the upper amount was convenient for high temperature.

The product of the reaction was analysed by gas chromatography with a 14-ft column of 1% tetraglyme on Fluoropak-80.

## Results

Measurements of the pumping rate of He at 315° were made, and it was found that the pumping-down correction to the reaction time was negligible.

The measured unimolecular rate constants ($k_0$) at 210, 220, 315, and 326° are summarized in Table I; those at 280.5° are given elsewhere.[2]

The second-order activation rate constants, $k^a$, were evaluated from the slope of the plots of $k_0$ *vs.* $p$, the pressure of added helium. These quantities are also listed in Table I. The Arrhenius activation energy, $E_a$, was obtained from these (Figure 1) and is 35.2 kcal $mol^{-1}$.

(1) (a) This work was supported by the National Science Foundation; (b) Ph.D. Thesis, 1970.

(2) S. C. Chan, B. S. Rabinovitch, J. T. Bryant, L. D. Spicer, T. Fujimoto, Y. N. Lin, and S. Pavlou, submitted for publication.

(3) W. Forst, *Can. J. Chem.*, **36**, 1308 (1958).

(4) T. N. Bell, P. L. Robinson, and A. B. Trenwith, *J. Chem. Soc.*, 1440 (1955); 1474 (1957).

(5) (a) G. H. Kohlmaier and B. S. Rabinovitch, *J. Chem. Phys.*, **38**, 1692, 1709 (1963); (b) D. W. Setser, B. S. Rabinovitch, and J. W. Simons, *ibid.*, **40**, 1751 (1964); **41**, 800 (1965).

(6) D. C. Tardy and B. S. Rabinovitch, *ibid.*, **45**, 3720 (1966); **48**, 1282 (1962).

(7) F. J. Fletcher, B. S. Rabinovitch, K. W. Watkins, and D. J. Locker, *J. Phys. Chem.*, **70**, 2823 (1966).

(8) S. C. Chan, J. T. Bryant, L. D. Spicer, and B. S. Rabinovitch, *ibid.*, **74**, 2058 (1970).

**Table I:** Measured Rates of Isomerization at Different Temperatures

| Temp, °C | $k_0$, $10^{-5}$ sec$^{-1}$ | $p$, $10^{-2}$ mm | $k_M$,[a] $10^{-5}$ sec$^{-1}$ mm$^{-1}$ |
|---|---|---|---|
| 210 | 0.0396 | 16.5 | |
| | 0.0548 | 27.9 | |
| | 0.0735 | 43.1 | |
| | 0.0844 | 53.9 | |
| | 0.106 | 61.6 | 0.138 ± 0.012[a] |
| 220 | 0.0544 | 12.9 | |
| | 0.0819 | 20.0 | |
| | 0.134 | 35.9 | |
| | 0.131 | 46.7 | |
| | 0.187 | 62.5 | |
| | 0.236 | 75.2 | |
| | 0.220 | 79.5 | 0.257 ± 0.021 |
| 280.5[b] | | | 16.4 ± 0.2 |
| 315 | 39.7 | 25.6 | |
| | 66.0 | 51.4 | |
| | 89.3 | 73.6 | |
| | 121 | 110 | |
| | 147 | 136 | 96.3 ± 1.8 |
| 326 | 57.9 | 25.9 | |
| | 108 | 53.9 | |
| | 141 | 78.9 | |
| | 170 | 98.9 | |
| | 190 | 114 | 148 ± 5 |

[a] Standard deviation of the slope of the least-squares line. [b] Rate data given in ref 2.

## Discussion

Now $\beta_c$ is given by the expression

$$\beta_c = \frac{k_M^a}{k_A^a}\left(\frac{\mu_{AM}}{\mu_{AA}}\right)^{1/2}\left(\frac{\sigma_{AA}}{\sigma_{AM}}\right)^2 \xi \qquad (1)$$

where the $\mu$'s and $\sigma$'s are reduced masses and Lennard-Jones force constants, respectively, for the appropriate collision pairs (A ≡ isocyanide, M ≡ helium). Here $\xi = \langle\Omega_{AA}^{(2,2)*}\rangle/\Omega_{AM}^{(2,2)*}$, where the numerator is a tabulated function[9] of $T^*(kT/\epsilon_A)$ and of $\delta_{max} = \mu_A^2/2\epsilon_A\sigma_A^3$; $\epsilon_A$ is the force constant and $\mu_A$ is the dipole moment of A; the denominator is a tabulated function of $T^*(kT/\epsilon_{AM})$. Equation 1 is simply the ratio of $k^a$ values corrected for collision frequency.

On differentiation of the logarithm of $\beta_c$ with respect tc $1/T$, eq 1 becomes

$$\frac{d \ln \beta_c}{d(1/T)} = \frac{1}{R}(E_a^A - E_a^M) + \frac{d \ln \xi}{d(1/T)} \qquad (2)$$

This affords an estimate of the temperature variation of $\beta_c$.

The fall-off behavior of the pure substrate system has already been studied.[7,10] The Arrhenius activation energy $E_a^A = 36.3$ kcal was measured for the low pressure region. It remains to evaluate the differential $d \ln \xi/d(1/T)$ in eq 2 in order to estimate the change of $\beta_c$. There is no simple functional relationship between $\Omega'^{(2,2)*}$ and $T$, and this differential cannot be evaluated analytically.[11] A plot of $\ln \xi$ *vs.* $1/T$, however, reveals

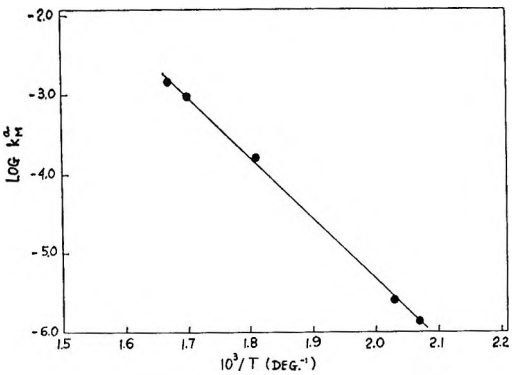


Figure 1. Arrhenius plot for the thermal $CH_3NC$–He system.

the existence of a linear relationship in this temperature range. $d \ln \xi/d(1/T)$ was estimated from the slope of this straight line and is assumed to be independent of temperature. The quantity is equal to 222°K and produces a decrease of 0.44 kcal mol$^{-1}$ in the observed activation energy in the $CH_3NC$–He system. The significance of eq 2 is thus the following. The observed variation with temperature of the relative rate at constant pressure is not the true variation of $\beta_c$ which should be based on a constant ratio of collision cross sections. Accompanying the change in temperature is a relative variation of collision cross sections of the substrate and the bath molecules in the form of the dependence of $\xi$ on $T$. The observed change in activation energy must be corrected by this in order to find the true temperature dependence of $\beta_c$. In general, this correction will tend to be larger when $\epsilon_A/k$ and $\epsilon_M/k$ differ widely or when the collisional behavior of pure A and of A with M follow different potential laws.

Thus $d \ln \beta_c/d(1/T)$ is equal to $1000(1.1 + 0.4)/R$ for this system, where $R$ is in cal mol$^{-1}$ deg$^{-1}$. Equation 2 can then be easily integrated. The value $\beta_c = 0.24$ has already been measured for helium at 280.5°;[2] then $\beta_c$ can be estimated for other temperatures (Table II).

It has been previously shown[6] that $\beta_c$ is a function of $E'$, *i.e.*, $\beta_c = \beta_c(E')$, where $E'$ is a dimensionless parameter defined as, $E' = \langle\Delta E\rangle/\langle E^+\rangle$; $\langle\Delta E\rangle$ is the average amount of energy removed per collision from the excited species by a bath molecule, and $\langle E^+\rangle$ is the equilibrium value of the average excess energy of the substrate molecules above the critical threshold. The differential in eq 2 can formally be expressed as

$$\frac{d \ln \beta_c}{d(1/T)} = \frac{\partial \ln \beta_c}{\partial\langle\Delta E\rangle}\frac{\partial\langle\Delta E\rangle}{\partial(1/T)} + \frac{\partial \ln \beta_c}{\partial\langle E^+\rangle}\frac{\partial\langle E^+\rangle}{\partial(1/T)} = (E_a^A - E_a^M)/R \qquad (3)$$

(9) L. Monchick and E. A. Mason, *J. Chem. Phys.*, **36**, 2746 (1961).

(10) F. W. Schneider and B. S. Rabinovitch, *J. Amer. Chem. Soc.*, **84**, 4215 (1962).

(11) J. O. Hirschfelder, C. F. Curtiss, and R. B. Bird, "Molecular Theory of Gases and Liquids," John Wiley and Sons, Inc., New York, N. Y., 1934, p 1126.

**Table II:** Summary Values of $\beta_c$, $\langle E^+ \rangle$, and $\langle \Delta E \rangle$ at Different Temperatures

| Temp, °C | $\beta_c$(He) | $\langle E^+ \rangle$, cm$^{-1}$ | $\langle \Delta E \rangle$,[a] cm$^{-1}$ |
|---|---|---|---|
| 210 | 0.29 | 400 | 460 |
| 220 | 0.28 | 410 | 460 |
| 280.5 | 0.24 | 470 | 450 |
| 315 | 0.22 | 510 | 450 |
| 326 | 0.21 | 500 | 447 |

[a] Values are based on the exponential form for the collisional transition probability distribution (ref 6); the change with temperature has only qualitative significance.

if $\xi$ is independent of temperature. Based on a particular statistical model for the collisional transition probability distribution, it has been shown that both terms on the right-hand side of eq 3 are either greater than or equal to zero, depending on whether the bath molecule is a weak collider or a strong collider, respectively. Universal plots of $\beta_c$ *vs.* $E'$ have been given.[6] For weak colliders, it appears that the exponential model is more appropriate.[6,12] The variation of $\langle E^+ \rangle$ with temperature for the thermal methyl isocyanide system may be readily evaluated, and the value of $\langle \Delta E \rangle$ for helium inert gas at different temperatures can thus be estimated (Table II).

The observed activation energy in the present system decreases in the presence of a weak collider bath molecule. This change is in the opposite direction to that found in the work of Trenwith, *et al.*[4] Over a temperature range from 650 to 750°, they observed an increase in the activation energy for pure substrate ($\sim$55 kcal mol$^{-1}$) of 14, 3.6, and 2.3 kcal mol$^{-1}$ upon adding $SO_2$, $CF_4$, and $CO_2$, respectively. The first increase is suspiciously large as the authors themselves have suggested. The data are suspect for the two remaining smaller activation energies, also, since the system is complex and, in addition, substrate—inert gas dilution effects[6] may be prominent. But if the direction of the change is correct in general, this suggests that the thermal decomposition of nitrous oxide, which is a small molecule, cannot be described by a quasistatistical model of vibrational energy transfer which seems appropriate for large molecules at high levels of excitation and which predicts a decrease in activation energy.[6] A qualitative criterion of the expected behavior is the relative collisional efficiencies of noble gases in this system; helium was found to be the most efficient of these. This is in accord with experimental findings[13] at low energy levels for small molecules and also with general predictions derived from the Landau–Teller theory.[14] Indeed, Nikitin claimed to find a good fit[15] between the experimental rate constant and that calculated *via* the Schwartz–Herzfeld equation[14] for the pure substrate system. We hope that further experimental confirmation will be sought.

In the hydrogen peroxide system[3] an ostensible lowering of 5.6 kcal mol$^{-1}$ (48.1 to 42.5 kcal mol$^{-1}$) in activation energy upon adding helium was found, which is surprisingly large. The temperature was only varied over a range of 40° (431–470°), and the Arrhenius plots show very bad scatter; we believe that this alleged activation energy decrease is not reliable.

In the methyl isocyanide system, the true activation energy decrease is only 1.1 + 0.4 = 1.5 kcal mol$^{-1}$ in the presence of helium over a 115° range. The activation energy estimated from the Arrhenius plot is very sensitive to experimental error in rate constants, and our results should be considered as only qualitative; they give an indication that collisional efficiency may decrease slowly with rise in temperature for this system. But no marked effects are to be expected for small temperature changes in thermal systems on the basis of the present results at not very highly elevated temperatures.

(12) Y. N. Lin and B. S. Rabinovitch, *J. Phys. Chem.*, 72, 1726 (1968).

(13) R. A. Walker, T. D. Lossing, and S. Legvold, National Advisory Committee Aeronautical Technical Notes, 1954, p 3210.

(14) For comprehensive reviews, see (a) T. L. Cottrell and J. C. McCoubrey, "Molecular Energy Transfer in Gases," Butterworth and Co. (Publishers) Ltd., London, 1969; (b) K. F. Herzfeld and T. A. Litovitz, "Absorption and Dispersion of Ultrasonic Waves," Academic Press, Inc., New York, N. Y., 1959.

(15) E. E. Nikitin, *Dokl. Phys. Chem.*, 129, 921 (1959).

# Energy Transfer in Thermal Methyl Isocyanide Isomerization. Relative Cross Sections of Fluoroalkanes and Nitriles[1a]

by S. C. Chan,[1b] J. T. Bryant, L. D. Spicer, and B. S. Rabinovitch

*Department of Chemistry, University of Washington, Seattle, Washington 98105* *(Received January 5, 1970)*

The inert gas effect on the thermal isomerization of methyl isocyanide at 280.5° by the members of the homologous series of *n*-perfluoroalkanes and *n*-nitriles has been studied up to $C_6$ in both cases. Relative collision diameters of these molecules, appropriate for the phenomenon of vibrational energy transfer involved, were obtained. $\Delta\sigma_{CF_2} = 0.54$ Å is close to the value for $\Delta\sigma_{CH_2}$; higher perfluoroalkanes and alkanes are closely comparable in effective size. A dipolar orientation effect on the collision diameter of nitriles was observed. Some corrections and additions to earlier published values for hydrocarbons are described.

## Introduction

It has been a general practice in chemical kinetics to resort to transport properties or second virial coefficient data for values of the collision diameters of various molecules. In addition to the fact that these properties frequently do not offer a consistent set of collision diameters,[2] it was not clearly established that these collision diameters are appropriate for interpreting intermolecular vibrational energy transfer efficiencies.

It has been pointed out previously[3] that by studying energy transfer efficiencies of a series of different inert molecules (M) in a thermal unimolecular reaction (the isomerization of methyl isocyanide (A) was the vehicle used),[4] it is possible to deduce a self-consistent set of collision diameters appropriate for this phenomenon. The results for homologous series of *n*-alkanes, 1-alkenes, and 1-alkynes were reported. The postulate was made[3] that, starting at some critical molecular size, higher members in each homologous series should display a constant relative activation–deactivation efficiency on a collision-for-collision basis, $\beta_c$, which is believed to be unity. (The quantity $\beta_c$ is more exactly designated as $^5\beta_0(D)$, where the subscript signifies the second-order region and $D$ is the dilution, which is here $\infty$.)

A relation was given of the form

$$R_{ni} = [\beta_{\mu(n+i)}/\beta_{\mu n}]^{1/2} - 1 = i\Delta s_{AM}/s_{AM_n} \qquad (1)$$

where $i$ is an increment to $n$, the number of carbons in the critical member. In eq 1, $\beta_\mu$ is the pressure-for-pressure relative inert gas efficiency, $\beta_p$, corrected for reduced mass differences, *i.e.*

$$\beta_\mu = \beta_p(\mu_{AM}/\mu_{AA})^{1/2} = (k_M{}^a/k_A{}^a)(\mu_{AM}/\mu_{AA})^{1/2} \qquad (2)$$

$$\beta_c = \beta_\mu(s_{AA}{}^2/s_{AM}{}^2) \qquad (3)$$

the $\mu$ quantities are the reduced masses, the $k^a$ are bimolecular collisional activation rate constants, and the $s$ are effective collision diameters; finally, $\Delta s_{AM}$ is the average increment in collision diameter per structural unit increment in the homologous series. A plot of $R_{ni}$ *vs.* $i$ is linear.

The slope provides a value of the relative incremental collision diameter. By adoption of a single value of the collision diameter for any one molecule, most logically the isocyanide (substrate) molecule, a consistent set of relative collision diameters derived from the phenomenon in question may be obtained for all other bath molecules which are at or above the critical size. Detailed discussion may be found in paper I.[3b]

In the present paper, the work has been pursued further and the results for homologous series of *n*-perfluoroalkanes and *n*-nitriles are reported, together with some additional data for hydrocarbons.

## Experimental Section

*Materials.* The sources and purity of methyl isocyanide, hydrogen cyanide, propionitrile, butyronitrile, hydrocarbons, and tetrafluoromethane were the same as described previously.[3,4] Other compounds ($C_2F_6$, $C_3F_8$, $C_4F_{10}$, $C_5F_{12}$, and $C_6F_{14}$; $CD_3CN$, $C_4H_{11}CN$, $C_5H_{11}CN$) were the best commercial grades available. The purity of each compound was checked by gas chromatography; impurities were removed by distillation. All gases were deoxygenated by the freeze–pump–melt method.

(1) (a) This work was supported by the National Science Foundation; (b) Graduate School Predoctoral Fellow whose Ph.D. thesis may be consulted for further details.

(2) See, for example, (a) J. O. Hirschfelder, C. F. Curtiss, and R. B. Bird, "Molecular Theory of Gases and Liquids," John Wiley and Sons, New York, N. Y., 1954, p 1110; also (b) R. A. Svehla, NASA Technical Report R-132, 1962, p 34.

(3) (a) B. S. Rabinovitch, Y. N. Lin, S. C. Chan, and K. W. Watkins, *J. Phys. Chem.*, **71**, 3715 (1967); (b) Y. N. Lin, S. C. Chan, and B. S. Rabinovitch, *ibid.*, **72**, 1932 (1968), called I.

(4) F. J. Fletcher, B. S. Rabinovitch, K. W. Watkins, and D. J. Locker, *ibid.*, **70**, 2823 (1966), called II.

(5) D. C. Tardy and B. S. Rabinovitch, *J. Chem. Phys.*, **48**, 1282 (1968); Y. N. Lin and B. S. Rabinovitch, *J. Phys. Chem.*, **72**, 1726 (1968).

*Apparatus and Procedure.* A 12-l. Pyrex flask fitted with a Delmar Teflon stopcock was used as the reactor. The reactor was heated in a molten nitrate–nitrite salt bath maintained at a temperature of 280.5° and regulated by a proportional controller. Three chromel–alumel thermocouples located at three different points in the salt bath were used to measure the temperature. Temperature variation over the salt bath was ±0.2° and did not vary during a run.

The seasoning of the reactor and handling of gases were essentially the same as described in I and II. Low-boiling inert gases were measured in a gas buret; the gas was frozen into a U-tube next to the reactor and was then expanded into the reactor together with a known amount of methyl isocyanide, previously measured out. Higher boiling gases were measured by weighing; a small amount of liquid was weighed in a melting point capillary tube, the tube was then introduced into the vacuum system next to the reactor, the liquid was degassed and was then flashed into the reactor.

A parent gas pressure of ~0.012 mm was used in each run, and the inert gas was added in from 5- to 60-fold excess over the parent. The higher end of the range was used for less efficient gases, and the lower end was used for those whose efficiencies were comparable to the parent. Approximately 12% of propionitrile, relative to methyl isocyanide was present in most gas mixtures in the role of an internal standard for the chemical analysis. A carrier gas was sometimes employed in transporting reaction gases in order to eliminate losses.

In all other respects the procedure followed those in I. Isomerization was carried to 10–25% reaction. The reaction rate of each gas was measured at a minimum of five different concentrations of the inert gas.

*Analysis.* Because of the small initial amount of isocyanide ($4.0 \times 10^{-6}$ mol), the whole sample was analyzed. A 14-ft length of 1% tetraglyme on Fluoropak-80 column was used for analysis. Known mixtures were analysed from time to time to check the calibration; calibration mixtures included the inert gas and carrier gas when necessary. It was customary to analyze the runs on both an absolute and relative internal basis, based on the admixed propionitrile in the reaction mixture. The propionitrile was unaffected by the reaction or by subsequent passage through a silver cyanide solid column which removed unreacted isocyanide.

For the runs with $CD_3CN$ as inert gas, products were analyzed with a Consolidated MS-103 mass spectrometer. The peaks corresponding to mass numbers 41 and 39 were monitored. The mass spectrometer was calibrated with a known mixture of $CH_3CN$–$CD_3CN$.

## Results

Rate constants calculated by the internal method showed more fluctuation than the absolute rate constants; hence, in the computation of $k_M{}^a$ only the latter are used. The internal rate constants were still useful in signalling the occurrence of systematic errors.

The rate constants for activation were found by the method of least squares from the relation, $k_0 = b + k_M{}^a C_M$, where $k_M{}^a$ is the second-order rate constant for collisional activation of A by species M, and $b$ is an extrapolated intercept constant which should be equal to the rate constant for pure methyl isocyanide at the standard pressure of 0.012 mm, but tended to be higher than that value. It has been shown[5] that $k_M{}^a$ may vary with pressure, *i.e.*, with parent gas dilution; the present data correspond to the high dilution case, and in the manner described earlier, this explains in part the observed increase in $b$.

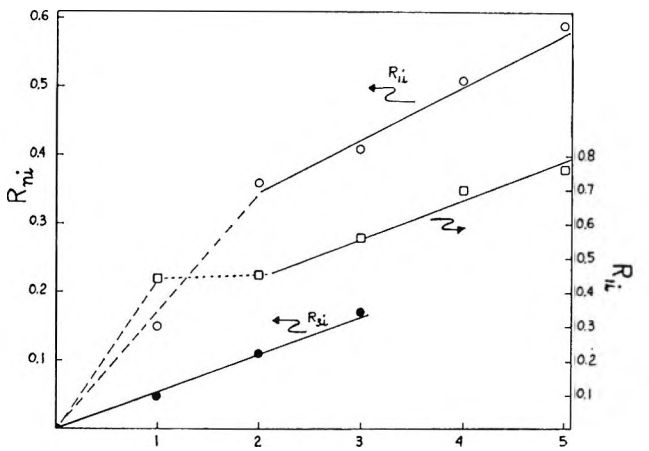


Figure 1. Plots of $R_{1i}$ *vs.* $i$ for perfluoroalkanes (○), and nitriles (□); and $R_{3i}$ *vs.* $i$ (●) for perfluoroalkanes.

The efficiencies, $\beta_p$ and $\beta_\mu$, for perfluoroalkanes and nitriles are summarized in Table I. Plots of $R_{ni}$ *vs.* $i$ are shown in Figure 1. Detailed kinetic data are given in the Appendix.

**Table I:** Measured Efficiency of Perfluoroalkanes and Nitriles

| | $CF_4$ | $C_2F_6$ | $C_3F_8$ | $C_4F_{10}$ | $C_5F_{12}$ | $C_6F_{14}$ |
|---|---|---|---|---|---|---|
| $\beta_p{}^a$ | 0.34 | 0.43 | 0.58 | 0.62 | 0.69 | 0.75 |
| $(\mu_{AM}/\mu_{AA})^{1/2}$ | 1.17 | 1.24 | 1.28 | 1.31 | 1.32 | 1.34 |
| $\beta_\mu$ | 0.40 | 0.53 | 0.74 | 0.81 | 0.91 | 1.01 |
| | HCN | $CD_3CN$ | $C_2H_5CN$ | $C_3H_7CN$ | $C_4H_9CN$ | $C_5H_{11}CN$ |
| $\beta_p$ | 0.57[b] | 0.92 | 0.88 | 0.97 | 1.12 | 1.17 |
| $(\mu_{AM}/\mu_{AA})^{1/2}$ | 0.89 | 1.02 | 1.07 | 1.12 | 1.16 | 1.19 |
| $\beta_\mu$ | 0.50 | 0.93 | 0.94 | 1.09 | 1.30 | 1.39 |

[a] $k_A{}^a = 96.0 \times 10^{-6}$ mm$^{-1}$ sec$^{-1}$. [b] New value, from data of ref 12.

## Discussion

*Collision Diameters. A Correction.* The quantities $s_{AM}$ are approximated by the relation, $s_{AM}^2 = \sigma_{AM}^2\Omega_{AM}^{(2,2)*}$, where $\Omega_{AM}^{(2,2)*}$, the reduced collision integral, is a tabulated function[6] of the reduced temperature $T^* = kT/\epsilon_{AM}$. The empirical combining rules, $\sigma_{AM} = (\sigma_A + \sigma_M)/2$ and $\epsilon_{AM} = (\epsilon_A\epsilon_M)^{1/2}$ were used.

Some remarks on this relation and a correction to the treatment given earlier (papers I and II) are appropriate here. As noted in II the values of $\sigma$ for polar molecules deduced from transport data by use of the Stockmayer potential differ little from the values obtained from the Lennard–Jones potential; values of $\sigma_{AM}$ based on the latter potential were used for both polar and nonpolar M molecules. However, an error was made inasmuch as collision integrals based on the Lennard–Jones potential were also used for all molecules, and when the collision partners are both polar, as in the pure substrate system, appropriate quantities are the angle-averaged reduced collision integrals $\langle\Omega^{(2,2)*}\rangle$, based on the Stockmayer potential.[7] This integral is a function of $T^*$ and $\delta_{max}$, where $\delta_{max} = \mu^2/2\epsilon\sigma^3$, $\mu$ being the dipole moment. An empirical combining rule was used,[8] $(\delta_{max})_{AM} = \mu_A\mu_M/2\epsilon_{AM}\sigma_{AM}^3$. Based on these integrals, $s_{AA}$ assumes the value 5.90 Å rather than the earlier value of 5.15 Å. All the $\beta_c$ values presented in previous work are raised correspondingly. In particular, for the alkane homologous series the constant efficiency $\beta_c$ reached by larger alkanes becomes 0.85, instead of 0.70 as reported in I (with use of the constants[3] $\sigma_{C_4H_{10}} = 5.20$ Å, and $(\epsilon/k)_{C_4H_{10}} = 325$°K). This increase places the constant efficiency much closer to unity. The remaining discrepancy of $\beta_c$ from unity can be attributed to a systematic experimental error, which will be clarified in the Appendix. A higher value of $\sigma_A$ of 6.76 Å, which had previously been invoked in I, is unnecessary. A number of the hydrocarbon gases have been remeasured, and the data are listed in the Appendix.

*Perfluoroalkanes.* From the plot of $R_{nt}$ *vs.* $i$ in Figure 1 with $n = 1$ as a "trial" value, it is seen that at $M_3$ the curve turns and becomes a straight line. It is concluded that $C_3F_8$ is the critical member of this series; a plot of $R_{3t}$ *vs.* $i$ gives a straight line (Figure 1).

With the postulate of unit efficiency of $\beta_c$ for $C_3F_8$ and higher perfluoroalkanes, $s_{AM}$ for the collision pair A–M of these molecules can be calculated relative to $s_{AA}$ which has been evaluated with use of the force constants, $\sigma_A = 4.47$ Å and $\epsilon_A/k = 380$°K, given in papers I and II. The slope of the $R$ plot provides smoothed values of these quantities. It is also of interest to calculate $\sigma_M$ for the various molecules; for this calculation, additional knowledge of $\epsilon/k$ is needed. The literature values are incomplete and inconsistent, and one might hope that $\epsilon_M/k$ could be estimated from an expression which is applicable for spherical nonpolar molecules

$$\epsilon/k = 0.77T_c = 1.15T_b \qquad (4)$$

where $T_c$ and $T_b$ are the critical temperature and the boiling point, respectively. The calculated values of $\sigma_M$ are listed in Table II, case a. It is noted that on this basis $\sigma_M$ for the perfluoroalkanes appear smaller than those for the corresponding hydrocarbons (Table III). Since on several grounds there is no reason to believe that smaller alkanes are larger than their perfluoro analogs, the use of eq 4 must be reconsidered.

**Table II:** Calculated Collision Constants of Perfluoroalkanes

| | | $C_3F_8$ | $C_4F_{10}$ | $C_5F_{12}$ | $C_6F_{14}$ |
|---|---|---|---|---|---|
| | | ←——$\Delta s_{AM}/s_{AM_3} = 0.057 \pm 0.003$——→ | | | |
| $\epsilon_M/k$, °K | a | 270 | 305 | 335 | 360 |
| | b | 160 | 160 | 160 | 160 |
| $s_{AM}$, Å[a] | a | 5.04 | 5.33 | 5.62 | 5.91 |
| | b | **5.04** | **5.33** | **5.62** | **5.91** |
| $\Omega_{AM}^{(2,2)*}$ | a | 1.24 | 1.27 | 1.30 | 1.31 |
| | b | 1.13 | 1.13 | 1.13 | 1.13 |
| $\sigma_{AM}$, Å | a | 4.54 | 4.72 | 4.93 | 5.18 |
| | b | 4.75 | 5.02 | 5.29 | 5.56 |
| $\sigma_M$, Å | a | 4.61 | 4.97 | 5.39 | 5.89 |
| | b | **5.03** | **5.57** | **6.1** | **6.65** |
| $\Delta\sigma_M$, Å | | | 0.54 | | |

[a] $\sigma_A = 4.47$ Å, $\epsilon_A/k = 380$°K.

Viscosity data[2b,9,10] yield values for $\epsilon/k$ of 134, 163, 195, and 160°K for $CF_4$, $C_2F_6$, $C_5F_{12}$, and $C_6F_{14}$, respectively (values for $\sigma$ of 4.66, 5.56, 7.36, and 8.05 Å, respectively, are paired with these). Second virial coefficients[10] give 153, 162, and 163°K for $CF_4$, $C_5F_{12}$, and $C_6F_{14}$ (together with $\sigma$ of 4.70, 11.4, and 12.9 Å, respectively). There is no apparent trend in the variation of $\epsilon/k$ with molecular complexity. If $\epsilon/k = 160$°K is uniformly assigned for $C_3F_8$ and higher members of the series, this plausibly represents a lower limit of $\epsilon/k$ and an upper limit of $\sigma_M$. These values are listed in Table II, case b. On this basis, the $\sigma_M$ for fluorocarbons are larger than for the corresponding hydrocarbons; $\Delta\sigma_M$ per $CF_2$ unit is 0.54 Å and is similar to that per $CH_2$ unit (Table III).

(6) See ref 2a, p 1126.

(7) L. Monchick and E. A. Mason, *J. Chem. Phys.*, 35, 1676 (1961).

(8) E. A. Mason and L. Monchick, *ibid.*, 36, 2746 (1962).

(9) See ref 2a, p 245.

(10) T. M. Reed, III, "Fluorine Chemistry," Vol. 5, J. H. Simons, Ed., Academic Press, New York, N. Y., 1964, p 150.

**Table III:** Efficiency and Collision Constants of Hydrocarbons[a]

| | $C_1$ | $C_2$ | $C_3$ | $C_4$ | $C_5$ | $C_6$ | $C_7$ | $C_8$ | $C_9$ | $C_{10}$ |
|---|---|---|---|---|---|---|---|---|---|---|
| | | | | | *n*-Alkanes | | | | | |
| $\beta\mu$[a] | 0.33* | 0.52* | 0.67 | 0.89* | 0.99* | 1.08* | 1.23 | 1.27 | 1.49* | 1.59 |
| $\sigma_M$, Å | | | | 5.23 | 5.77 | 6.31 | 6.85 | 7.39 | 7.93 | 8.47 |
| $\Delta\sigma_M$, Å | | | | | | 0.54 | | | | |
| | | | | | *n*-1-Alkenes | | | | | |
| $\beta\mu$ | | 0.38* | 0.61 | 0.78 | 0.91* | 1.09* | 1.30* | 1.23* | 1.38 | 1.46* |
| $\sigma_M$, Å | | | | 5.09 | 5.65 | 6.21 | 6.77 | 7.33 | 7.89 | 8.45 |
| $\Delta\sigma_M$, Å | | | | | | 0.56 | | | | |
| | | | | | *n*-1-Alkynes | | | | | |
| $\beta\mu$ | | 0.33* | 0.54 | 0.80 | 0.98* | 1.08 | 1.24* | 1.36* | ... | 1.66 |
| $\sigma_M$, Å | | | | | 5.81 | 6.43 | 7.05 | 7.67 | 8.29 | 8.91 |
| $\Delta\sigma_M$, Å | | | | | | 0.62 | | | | |

[a] Asterisk signifies new data which supersedes older determination, or a corrected value which includes additional previously unreported data; unasterisked quantities are corrected values based on the old data.

*Nitriles.*[11] Since $CH_3CN$ is the product of the isomerization under investigation, its inert gas effect cannot be conveniently studied; instead, $CD_3CN$ was used and is expected to have similar efficiency to $CH_3CN$ inasmuch as other results[12] have shown that isotopic substitution of H does not alter efficiency. Because of the similarity in structure, $CD_3CN$ is also expected to have the same efficiency as the parent $CH_3NC$ and, indeed, near-unit efficiency was found (Table I). Higher nitriles should also display unit efficiency on a collision-for-collision basis, since these molecules are the more complex members of the same series. On this basis, $CD_3CN$ is the critical member of this series; an $R$ plot with HCN as the "trial" critical member is expected to demonstrate a straight line behavior from $C_2$, *i.e.*, $CD_3CN$ onward. However, the $R$ plot displays a peculiar shape (Figure 1): the curve levels off from $C_2$ to $C_3$ and then increases.

The flattened part of the curve may be explained qualitatively in terms of the electrostatic interaction between the polar groups of the inert and substrate molecules. All the nitriles studied, except HCN, have about the same dipole moment as the substrate molecule, ~4 D. The term in the Stockmayer potential for the dipolar electrostatic interaction is $(-\mu_A\mu_M)(2\cos\theta_1\cos\theta_2 - \sin\theta_1\sin\theta_2\cos\phi)/r^3$, where $\theta_1$ and $\theta_2$ are the angles of inclination of the axes of the two dipoles to the line of centers of the molecules, $\phi$ is their azimuthal angle, and $r$ is the separation of the dipoles of strength $\mu_A$ and $\mu_M$, respectively. At 5.5 Å, the interaction energy for the antiparallel configuration of the two polar groups in the nitrile and the cyanide exceeds $1.5RT$ at the reaction temperature 280°. The average dipolar interaction energy $V(r)_{es} = (-2\mu_A^2)\mu_M^2/3kTr^6$ at this separation is around $RT$ and is less than $RT$ when $r$ is larger. One can conceive of a range near the substrate molecule within which dipolar interaction is important; nitrile molecules that enter this range will be oriented on collision. The magnitude of this range (~5.5 Å) is about that of the collision diameter of the propionitrile molecule. This explains, at least qualitatively, why the effective collision diameter of propionitrile is not much greater than that of $CD_3CN$, as reflected in their nearly equal $R$ values, despite its additional $CH_2$ group. Higher nitriles with longer chains have larger diameters; $V(r)_{es}$ is decreased at the enhanced collision distance and dipolar interaction effect becomes less important. Recently, elastic scattering of homologous series of strongly polar nitriles and weakly polar *n*-alkynes by acetonitrile and propane, respectively, have been studied at 25° in some crossed molecular beam experiments;[13] these results also demonstrate some dipolar peculiarities of the lower members in the nitrile–acetonitrile series.

**Table IV:** Calculated Collision Constants of Nitriles

| | $C_3H_7CN$ | $C_4H_9CN$ | $C_5H_{11}CN$ |
|---|---|---|---|
| | $\Delta s_{AM}/s_{AM4} = 0.065 \pm 0.016$ | | |
| $\epsilon_M/k$, °K | 400 | 400 | 400 |
| $\mu$, D | 4.07[a] | 4.12[a] | 4.16[b] |
| $s_{AM}$, Å | 6.22 | 6.62 | 7.02 |
| $\langle\Omega_{AM}^{(2,2)*}\rangle$ | 1.56 | 1.51 | 1.46 |
| $\sigma_{AM}$, Å | 4.98 | 5.38 | 5.80 |
| $\sigma_M$, Å | 5.49 | 6.29 | 7.13 |

[a] A. L. McClellan, "Tables of Experimental Dipole Moments," W. H. Freeman and Co., San Francisco, Calif., and London, 1963. [b] Extrapolated value.

(11) For a preliminary report, see S. C. Chan, B. S. Rabinovitch, L. D. Spicer, and J. T. Bryant, *J. Phys. Chem.*, **73**, 2464 (1969).

(12) S. C. Chan, B. S. Rabinovitch, J. T. Bryant, L. D. Spicer, T. Fujimoto, Y. N. Lin, and S. Pavlou, submitted for publication.

(13) W. H. Duewer, Ph.D. Thesis, University of Washington, 1970.

From a sufficiently large member onward, $R$ values in the nitrile series should increase in a more normal fashion, as for the alkanes, and $\sigma_M$ can be estimated for the larger nitriles. But for polar bath gases, the calculation is complicated by the need for an *a priori* knowledge of $\sigma_M$ in order to evaluate $\delta_{max}$ and the $\Omega$ integral. $\sigma_M$ was estimated by iteration from a trial value. Based on $\beta_c = 1$ for $C_3H_7CN$ (*i.e.*, $M_4$) and with all $\epsilon/k = 400°K$ as in III, values of $\sigma_M = 5.49$, 6.29, and 7.13 Å for $C_3H_7CN$, $C_4H_9CN$, and $C_5H_{11}CN$, respectively, were found (Table IV). An average $\Delta\sigma_M$ per $CH_2$ unit of 0.82 Å is estimated (this quantity is not constant from member to member); this is big compared to the value of 0.54 Å obtained from the *n*-alkane series (Table III) and is uncertain due to the scatter of the abbreviated $R$ plot for the nitriles.

*General Remarks.* It should be noted that the potentail constant $\sigma_M$ assigned from these kinetic experiments are all relative to the assigned values $\sigma_A = 4.47$ Å and $\epsilon_A/k = 380°K$, and the former values depend on the assignment of $\epsilon_M/k$. On the other hand, the relative effective collision diameters $s_{AM}$ for members of a series at, or above the critical size are given directly by the rate data ($\beta_\mu$), and do not depend on force constant assignments for M. The kinetics-based values of $s_{AM}$ obtained for hydrocarbons and fluorocarbons are compared with viscosity-based parameters in Table V; the comparison is as extensive as is allowed by the availability of values of the latter. The agreement between the two sets of values is reasonably good and provides further confirmation that viscosity-based potential parameters may be used in the interpretation of this energy transfer phenomenon. The modest discrepancy for the fluorocarbons may reflect possible error in the viscosity measurements.

**Table V:** Comparison of Some Collision Diameters Based on Kinetics and Viscosity Measurements

| | $s_{AM}$, Å | | | | | | | |
|---|---|---|---|---|---|---|---|---|
| | *n*-$C_4H_{10}$ | *n*-$C_5H_{12}$ | *n*-$C_6H_{14}$ | *n*-$C_8H_{18}$ | *n*-$C_9H_{20}$ | $C_4H_8$-1 | *n*-$C_5F_{12}$ | *n*-$C_6F_{14}$ |
| Kinetics[a] | 5.53 | 5.84 | 6.15 | 6.77 | 7.08 | 5.38 | 5.62 | 5.91 |
| Viscosity[b] | 5.50 | 6.01 | 6.02 | 6.73 | 7.11 | 5.52 | 6.39 | 6.64 |

[a] Based on $s_{AA} = 5.90$ Å. [b] Based on potential parameters given in ref 2a and 10.

## Appendix A

It was found that previously reported rate constants (I and II) for the bath molecules were systematically low; over two dozen—although not all—gases were repeated, and an average systematic discrepancy ~17% was found. This is believed to be due in part to a temperature discrepancy and in part to analytical error. Measurements for the *n*-alkanes $CH_4$, $C_2H_6$, $C_4H_{10}$, $C_5H_{12}$, $C_6H_{14}$ were repeated, and for $C_9H_{20}$ were extended (Appendix B). The efficiency $\beta_c$ of the larger hydrocarbons is close to unity. The efficiencies for those gases which were not reexamined have been raised uniformly by 17%; since the absolute measurements have been proved more reliable, only these are included in the recalculation of the older data. The new data and the corrected values for other alkanes were used to construct a new $R$ plot which is not given here because it is quantitatively virtually identical with that reported in I. $R$ plots involve rate ratios and are insensitive to systematic error. The collision diameters of the *n*-alkanes have been calculated (Table III) on the assumption that $\beta_c = 1$ for all alkanes from $C_4H_{10}$ onwards; $\epsilon/k = 325°K$ was uniformly assumed as in I.

New measurements have also been made for some *n*-alkene-1 compounds, $C_5H_{10}$-1 and $C_{10}H_{20}$-1; in addition, previously unreported or modified data for $C_5H_{10}$-1, $C_6H_{12}$-1, and $C_7H_{14}$-1, and for the *n*-alkyne-1 compounds $C_5H_8$-1, $C_7H_{12}$-1, and $C_8H_{14}$-1 are given in Appendix B. Corrected values of other old rate data for the remaining *n*-alkenes and *n*-alkynes were also used to construct new $R$ plots. These plots are again closely similar to those reported in I and need not be redrawn. The collision diameters derived for larger members of these hydrocarbon series are tabulated in Table III. Since the polarity of these molecules is small, the variation in the $\Omega$-integral due to dipolar interaction is negligible even for butene-1 and pentyne-1, the critical members of the respective series. A uniform value, $\epsilon/k = 315°K$, was used along the series, as in I, with $\Omega^{*1/2} = 1.13$.

## Appendix B

The new and the supplemented values for several hydrocarbons and the present values for the *n*-fluoroalkanes and nitriles are given in Table VI.

**Table VI:** Summary of Some Rate Data for Methyl Is ocyanide (280.5°)

| Bath[a] gas | $k_0$, $10^{-1}$ sec$^{-1}$ | $p$, $10^{-2}$ mm | $k_M$,[a] $10^{-3}$ mm$^{-1}$ sec$^{-1}$ | Bath[a] gas | $k_0$, $10^{-1}$ sec$^{-1}$ | $p$, $10^{-2}$ mm | $k_M$,[a] $10^{-3}$ mm$^{-1}$ sec$^{-1}$ |
|---|---|---|---|---|---|---|---|
| $CH_4$ | 11.5 | 22.4 | | $n$-$C_5H_{10}$-1* | 21.4 | 25.8 | |
| | 15.3 | 31.1 | | | 24.8 | 29.9 | 0.76 ± 0.02 |
| | 17.8 | 36.7 | | $n$-$C_6H_{12}$-1* | 10.8 | 8.21 | |
| | 21.8 | 42.9 | | | 12.8 | 10.8 | |
| | 26.2 | 57.5 | 0.43 ± 0.03[b] | | 12.9 | 12.0 | |
| $C_3H_6$ | 8.64 | 10.2 | | | 17.8 | 16.8 | |
| | 13.8 | 21.9 | | | 21.4 | 17.1 | |
| | 16.3 | 24.5 | | | 21.4 | 17.5 | |
| | 17.3 | 27.2 | | | 19.6 | 19.2 | |
| | 18.4 | 28.6 | | | 24.0 | 19.9 | |
| | 18.1 | 28.7 | | | 28.1 | 26.4 | |
| | 20.3 | 31.7 | 0.54 ± 0.03 | | 28.8 | 30.3 | |
| $n$-$C_4H_{10}$ | 7.95 | 6.39 | | | 32.1 | 31.2 | 0.88 ± 0.07 |
| | 9.38 | 8.76 | | $n$-$C_7H_{14}$-1* | 12.5 | 8.4 | |
| | 12.5 | 11.9 | | | 10.3 | 8.5 | |
| | 13.3 | 13.5 | | | 13.6 | 11.6 | |
| | 17.6 | 18.8 | 0.79 ± 0.03 | | 19.6 | 14.0 | |
| $n$-$C_5H_{12}$ | 9.48 | 7.42 | | | 17.3 | 17.0 | |
| | 13.0 | 11.6 | | | 23.8 | 18.0 | |
| | 17.2 | 16.9 | | | 21.5 | 21.4 | |
| | 22.3 | 22.3 | | | 26.0 | 21.5 | |
| | 24.4 | 25.4 | 0.84 ± 0.02 | | 33.8 | 26.7 | |
| $n$-$C_6H_{14}$ | 11.2 | 7.74 | | | 33.0 | 30.7 | 1.02 ± 0.11 |
| | 12.2 | 9.74 | | $n$-$C_{10}H_{20}$-1 | 12.4 | 7.05 | |
| | 17.0 | 14.0 | | | 18.1 | 12.0 | |
| | 17.9 | 15.6 | | | 19.4 | 13.3 | |
| | 21.3 | 19.7 | | | 26.6 | 18.1 | |
| | 24.8 | 23.3 | 0.89 ± 0.02 | | 29.0 | 22.4 | 1.13 ± 0.09 |
| $n$-$C_9H_{20}$* | 6.66 | 1.77 | | $n$-$C_5H_8$-1* | 9.52 | 7.08 | |
| | 9.62 | 3.98 | | | 10.8 | 9.10 | |
| | 9.23 | 5.08 | | | 11.6 | 10.1 | |
| | 8.22 | 5.95 | | | 13.9 | 11.8 | |
| | 13.1 | 5.96 | | | 15.0 | 12.3 | |
| | 13.5 | 6.17 | | | 15.8 | 12.4 | |
| | 11.6 | 6.85 | | | 16.1 | 15.5 | |
| | 14.0 | 8.39 | | | 17.6 | 17.6 | |
| | 17.1 | 8.40 | | | 17.0 | 18.9 | |
| | 14.2 | 8.84 | | | 23.6 | 21.8 | |
| | 13.2 | 9.06 | | | 24.2 | 24.3 | |
| | 18.8 | 10.6 | | | 25.1 | 25.0 | |
| | 19.3 | 11.1 | | | 25.8 | 26.6 | |
| | 16.8 | 12.6 | | | 30.6 | 31.8 | |
| | 21.0 | 13.5 | | | 31.1 | 32.4 | 0.83 ± 0.04 |
| | 17.8 | 14.1 | | $n$-$C_7H_{12}$-1* | 8.89 | 3.89 | |
| | 20.8 | 16.4 | | | 11.9 | 6.35 | |
| | 23.2 | 17.9 | | | 16.6 | 10.5 | |
| | 26.3 | 18.6 | | | 18.5 | 12.7 | |
| | 32.1 | 20.3 | 1.13 ± 0.09 | | 24.7 | 17.1 | |
| $n$-$C_5H_{10}$-1 | 12.0 | 10.7 | | | 20.5 | 17.6 | |
| | 18.0 | 18.4 | | | 28.1 | 21.4 | |
| | 20.2 | 21.2 | 0.78 ± 0.01 | | 33.8 | 25.4 | |
| $n$-$C_5H_{10}$-1* | 3.84 | 3.40 | | | 29.5 | 26.7 | 1.00 ± 0.09 |
| | 5.42 | 3.98 | | $n$-$C_8H_{14}$-1* | 6.42 | 2.80 | |
| | 8.57 | 7.38 | | | 7.72 | 5.72 | |
| | 8.48 | 8.38 | | | 11.1 | 6.64 | |
| | 10.1 | 9.82 | | | 12.6 | 9.20 | |
| | 12.5 | 14.5 | | | 14.3 | 9.92 | |
| | 14.6 | 16.1 | | | 16.9 | 11.7 | |
| | 16.9 | 18.8 | | | 18.7 | 11.9 | |
| | 17.6 | 19.6 | | | 20.2 | 13.2 | |
| | 19.2 | 22.1 | | | 16.6 | 14.8 | |
| | 19.6 | 22.5 | | | 20.1 | 16.3 | |
| | 22.4 | 25.2 | | | 21.8 | 16.4 | |
| | 22.4 | 25.3 | | | 25.0 | 18.7 | |

**Table VI** (*Continued*)

| Bath[a] gas | $k_0$, $10^{-1}$ sec$^{-1}$ | $p$, $10^{-2}$ mm | $k_M$,[a] $10^{-1}$ mm$^{-1}$ sec$^{-1}$ | Bath[a] gas | $k_0$, $10^{-1}$ sec$^{-1}$ | $p$, $10^{-2}$ mm | $k_M$,[a] $10^{-2}$ mm$^{-1}$ sec$^{-1}$ |
|---|---|---|---|---|---|---|---|
| $n$-$C_6H_{14}$-1* | 25.4 | 21.5 | | $CD_3CN$ | 6.08 | 5.42 | |
| | 24.0 | 21.8 | | | 8.70 | 8.37 | |
| | 32.8 | 26.1 | | | 14.2 | 13.4 | |
| | 35.4 | 29.3 | 1.05 ± 0.06 | | 12.5 | 14.3 | |
| $CF_4$ | 9.20 | 17.9 | | | 16.3 | 16.3 | |
| | 9.06 | 18.9 | | | 6.58 | 5.42 | |
| | 11.1 | 25.2 | | | 8.96 | 8.37 | |
| | 13.2 | 30.0 | | | 13.3 | 13.4 | |
| | 14.9 | 36.3 | 0.33 ± 0.02 | | 13.0 | 14.3 | |
| $C_2F_6$ | 8.67 | 13.6 | | | 16.7 | 16.3 | 0.88 ± 0.06 |
| | 9.38 | 16.4 | | $C_2H_5CN$ | 6.74 | 4.69 | |
| | 12.2 | 21.1 | | | 10.7 | 10.1 | |
| | 15.2 | 29.7 | | | 12.2 | 11.8 | |
| | 20.5 | 42.5 | 0.41 ± 0.02 | | 13.3 | 13.1 | |
| $C_3F_8$ | 6.36 | 7.69 | | | 14.7 | 14.2 | |
| | 7.00 | 9.40 | | | 16.1 | 16.3 | |
| | 9.05 | 13.5 | | | 16.7 | 17.1 | |
| | 12.2 | 18.7 | | | 17.9 | 19.0 | |
| | 12.0 | 19.5 | | | 20.7 | 21.1 | |
| | 14.1 | 21.8 | | | 23.0 | 24.4 | 0.84 ± 0.02 |
| | 18.5 | 29.8 | 0.55 ± 0.02 | $n$-$C_3H_7CN$ | 11.8 | 8.44 | |
| $n$-$C_4F_{10}$ | 6.38 | 5.69 | | | 15.4 | 11.7 | |
| | 8.61 | 9.39 | | | 16.1 | 13.6 | |
| | 10.8 | 13.3 | | | 19.8 | 17.7 | |
| | 13.4 | 18.3 | | | 26.9 | 24.4 | 0.93 ± 0.05 |
| | 15.5 | 20.6 | 0.59 ± 0.02 | $n$-$C_4H_9CN$ | 10.5 | 6.39 | |
| $n$-$C_5F_{12}$ | 4.21 | 3.76 | | | 13.1 | 8.87 | |
| | 5.60 | 4.38 | | | 17.9 | 12.5 | |
| | 5.25 | 4.50 | | | 20.3 | 15.7 | |
| | 5.53 | 5.57 | | | 23.4 | 17.8 | 1.10 ± 0.06 |
| | 7.36 | 6.63 | | | 6.25 | 2.90 | |
| | 8.18 | 8.73 | | | 6.65 | 4.16 | |
| | 9.83 | 11.1 | | | 15.1 | 11.4 | |
| | 12.8 | 14.9 | | | 21.3 | 17.9 | 1.04 ± 0.04 |
| | 15.1 | 19.6 | | | | | |
| | 17.1 | 22.9 | 0.66 ± 0.02 | $n$-$C_5H_{11}CN$ | 8.40 | 4.40 | |
| $n$-$C_6F_{14}$ | 4.90 | 3.24 | | | 11.6 | 7.38 | |
| | 6.44 | 5.38 | | | 14.8 | 9.40 | |
| | 8.44 | 8.05 | | | 18.8 | 12.1 | |
| | 8.61 | 8.36 | | | 22.4 | 16.8 | |
| | 10.1 | 9.52 | | | 25.1 | 19.2 | 1.13 ± 0.07 |
| | 9.73 | 9.78 | | | | | |
| | 13.4 | 15.1 | 0.72 ± 0.03 | | | | |

[a] Asterisk denotes old data whose rate constants were corrected uniformly by 17%. [b] Error limit is provided by the standard deviation of the slope of the least squares line.

# The Addition and Abstraction Reaction of Thermal Hydrogen Atoms with Fluorinated Ethylenes

by R. D. Penzhorn and H. L. Sandoval

*Chemistry Department, Faculty of Physical and Mathematical Sciences, University of Chile, Santiago, Chile*
*(Received September 15, 1969)*

The photolysis of HBr was studied in the presence of ethylene and of each of the six fluoroethylenes, with overall conversions below 0.1%. The results were interpreted in terms of a thermal hydrogen atom addition and abstraction reaction from these compounds. The increasing relative rates of addition are *cis*-$C_2F_2H_2$:$C_2FH_3$:$C_2H_4$:*trans*-$C_2F_2H_2$:1,1-$C_2F_2H_2$:$C_2F_3H$:$C_2F_4$ = 1.00:1.12:1.43:1.67:2.08:2.36:2.42, respectively, and those of abstraction are $C_2FH_3$:$C_2F_3H$:*cis*-$C_2F_2H_2$:*trans*-$C_2F_2H_2$:1,1-$C_2F_2H_2$ = 1.00:1.78:1.94:3.61:6.60, respectively.

## Introduction

A review of the literature reveals that, whereas the hydrogen atom addition to ethylene has been extensively investigated, little attention has been paid to the study of the reaction of these atoms with halogen-substituted ethylenes. In an early investigation, Allen, Melville, and Robb[1] obtained for the reaction of hydrogen atoms with tetrafluoroethylene a collision efficiency of $0.3 \times 10^{-4}$. More recently,[2] thereact ion between H atoms and vinyl chloride was investigated by photolyzing HI in the presence of $C_2H_3Cl$. The following reactions were suggested

$$H + HI \longrightarrow H_2 + I \qquad (a)$$

$$H + C_2H_3Cl \longrightarrow C_2H_4Cl \qquad (b)$$

$$H + C_2H_3Cl \longrightarrow C_2H_2Cl + H_2 \qquad (c)$$

$$H + C_2H_3Cl \longrightarrow C_2H_3 + HCl \qquad (d)$$

A chlorine atom abstraction from an olefinic bond had not been reported previously. Further, gas chromatographic evidence strongly suggested that (c), a hydrogen atom abstraction reaction, took place and, moreover, was faster than (b), the corresponding addition to the double bond. This is interesting in view of the generally accepted fact that abstraction by hydrogen atoms from even the higher olefins is usually quite small when compared with the addition reaction, at least at room temperature.

In view of the scarcity of quantitative data for the reaction of H atoms with halogenated olefins and of the fact that substitution of hydrogen by halogens in olefins seems to have a great effect on the reaction mechanism, it seemed of interest to examine the relative rates of addition and, if occurring, abstraction of hydrogen atoms with the complete series of fluoroethylenes.

## Experimental Section

*Apparatus.* The apparatus employed for this investigation was essentially the same as one described elsewhere.[3] Reaction took place in a 195-$cm^3$ cell provided with a Vycor window, attached to a 3501 $cm^3$ volume. The gases were mixed and circulated with an approximately 7 $cm^3 \times sec^{-1}$ unidirectional circulating pump. Only greaseless Viton A diaphragm valves were used in the reaction and gas measuring section of the apparatus. Hydrogen bromide and the fluoroethylenes were measured with a very sensitive dibutyl phthalate differential pressure manometer, which had the mercury side covered with a dibutyl phthalate film to avoid the mercury contamination of the system. The manometer was capable of detecting a pressure differential greater than 1/200 mm of mercury and was not temperature sensitive at our experimental conditions. During the later stages of this work, this manometer was replaced by a more convenient to operate and of similar sensitivity Kern-Springham glass spiral manometer. The overall reproducibility was not affected by this change. $CO_2$ was measured with a Wallace and Tiernan absolute pressure gauge. As a light source, a Hanovia SH type medium pressure mercury lamp was employed, operated at 1.2 A with the help of a voltage stabilizer.

*Reagents.* Hydrogen bromide, carbon dioxide, vinyl fluoride and 1,1-difluoroethylene were from the Matheson Co. and *cis*- and *trans*-difluoroethylene were from Penninsular Chem Research. Trifluoroethylene was prepared by alcoholic zinc dehalogenation of 1-chloro-2-bromo-1,2,2-trifluoroethane (kindly supplied by ICI).

(1) P. E. M. Allen, H. W. Melville, and J. C. Robb, *Proc. Roy. Soc.*, **A218**, 311 (1953).

(2) A. M. Rennert and M. H. J. Wijnen, *Ber. Bunsenges. Phys. Chem.*, **72**, 222 (1968).

(3) R. D. Penzhorn and B. deB. Darwent, *J. Phys. Chem.*, **72**, 1639 (1968).

Thirty-six grams of the starting material was added dropwise to a vigorously stirred mixture of 20 g of zinc powder and 50 cm³ of ethanol at 60° over a period of 4 hr. The product was removed *via* a condenser and a vacuum-jacketed column packed with Fenske helices and condensed into two traps, the first one in Dry Ice and the second in liquid nitrogen. The trap with Dry Ice retained most of the trifluoroethylene plus some alcohol and starting material, while the second trap retained a small amount of pure product. The first fraction was distilled with a vacuum-jacketed column to separate the unchanged starting material and the alcohol from the trifluoroethylene. The product obtained was purified by gas chromatography on a 20-ft column of 30% dibutyl phthalate on firebrick (30–80 mesh). Tetrafluoroethylene was obtained by thermal decomposition of Teflon, following a technique suggested in the literature.[4]

All gases were repeatedly purified by trap to trap distillations and their purity controlled on a gas chromatograph and with an AEI MS2 mass spectrometer. Total impurities never exceeded 0.5%.

*Procedure.* The gases were successively expanded and condensed into the reaction system, isolated by a stopcock, again expanded, mixed for at least 30 min, and finally photolyzed for periods between 5 and 30 min. The time of photolysis was varied in order to obtain a quantity of hydrogen measurable in a gas buret, never below 15 and usually of about 40 μmol. This was possible because the rate of hydrogen formation for a certain HBr pressure proved to be directly proportional to the time.

After photolysis the gases were condensed and the resulting molecular hydrogen measured by *PVT* procedures on a gas buret. A special precaution was necessary with ethylene because of the relatively high vapor pressure of this gas at liquid nitrogen temperatures. For ethylene, the Toepler-collected total noncondensables were compressed into a U-shaped capillary and frozen down with liquid nitrogen. The remaining noncondensables were then expanded into the comparatively large volume of the Toepler pump, isolated from the U tube by a stopcock, and measured as in previous experiments. Mass spectrometric analysis of the noncondensables separated by this method showed that they were about 99% $H_2$. The ethylene remaining in the U tube contained less than 0.5% $H_2$. A large number of experiments were carried out using a solid nitrogen trap between the reaction system and the Toepler pump. Both techniques gave consistent experimental results.

In most experiments the $CO_2$ pressure was kept between 250 and 300 mm. This gas was used to facilitate the operation of the circulating pump, improve the gas mixing, and assure proper thermalization.

Mercury was kept away from the reaction system at all times with the help of at least two liquid nitrogen traps per entrance. Total conversion for a series of runs was always below 0.1%.

All fluoroolefins could be photolyzed without producing any measurable noncondensables, an indication that no hydrogen producing impurities were present.

When the uv absorption spectrum above 2000 Å of 1 atm of $C_2FH_3$ and 1 atm of 1,1-$C_2F_2H_2$ in a 5-cm cell was taken, no absorption was detected with vinyl fluoride and only a very slight absorption, starting at 2300 Å, was observed with 1,1-$C_2F_2H_2$. When the HBr absorption coefficients (in good agreement with those of Rommand[5]) determined between 2000 and 2300 Å were compared with those of 1,1-$C_2F_2H_2$, it was found that the former were larger by an average factor of about $10^3$. The uv absorption of $C_2F_4$ was studied by Lacher, *et al.*,[6] and can also be considered negligible in comparison to HBr. It was felt that this observation can be extended to the rest of the fluoroolefins. No signs of polymerization were detected.

## Results

Experimentally this investigation was based upon measurements of hydrogen quantum yields, Φ, of $H_2$. These were determined by comparison of the hydrogen yield obtained by photolysis of HBr ($\Phi_{H_2} = 1$ for conversions below 1%) in the presence of $CO_2$, with the hydrogen yield from the same mixture but with added fluoroolefin. Since in all experiments the conversion was kept very low, it was possible to carry out several photolyses with the same mixture by only adding increasing amounts of either fluoroethylenes or HBr. The validity of this procedure was verified by two types of experiments: (a) repeated photolysis of the same mixture which gave comparable results within the experimental error; (b) addition of HBr to a certain mixture which reproduced the results expected for the new ratio, from previous experiments with the same mixture; see, for example, experiments 122 and 125. The latter results suggest, furthermore, that no important secondary reactions interfered in the photolyses of HBr–fluoroethylene mixtures. Several calibration photolyses with the pertinent HBr–$CO_2$ mixtures as well as frequent calibration curves of the HBr pressure *vs.* hydrogen yield were carried out before and after each series of runs to take care of small variations in the lamp intensity and so reduce the experimental error.

When a mixture of 10 mm of $C_2F_4$ with 1.5 mm of HBr ($C_2F_4$:HBr ratio 6.67) or a mixture of 8.05 mm of $C_2FH_3$ with 4 of mm HBr ($C_2FH_3$:HBr ratio 2.01) were repeatedly photolyzed at room temperature, adding

(4) J. Heicklen, V. Knight, and S. A. Greene, *J. Chem. Phys.*, **42**, 221 (1965).

(5) J. Rommand, *Ann. Phys.* (Paris), **4**, 527 (1949).

(6) J. R. Lacher, L. E. Hummel, E. F. Bohmfalk, and J. D. Park, *J. Amer. Chem. Soc.*, **72**, 5486 (1950).

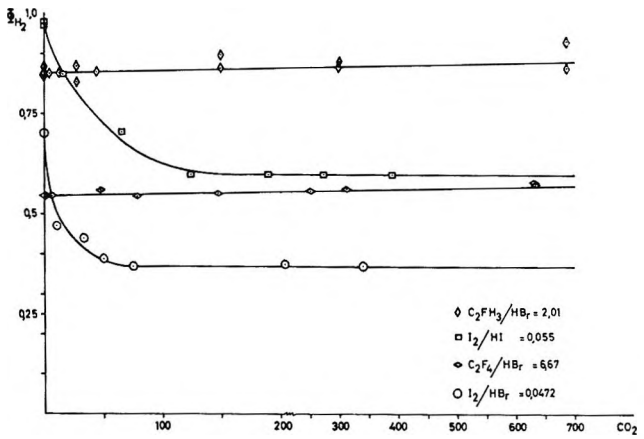


Figure 1. $CO_2$ pressure effect on the hydrogen quantum yield from: ⊡, 0.167 mm of $I_2$ with 3.02 mm of HBr; ⊙, 0.175 mm of $I_2$ with 4.00 mm of HBr; ◊, 8.05 mm of $C_2FH_3$ with 4.00 mm of HBr; and ◇, 10.0 mm of $C_2F_4$ with 1.5 mm of HBr mixtures.

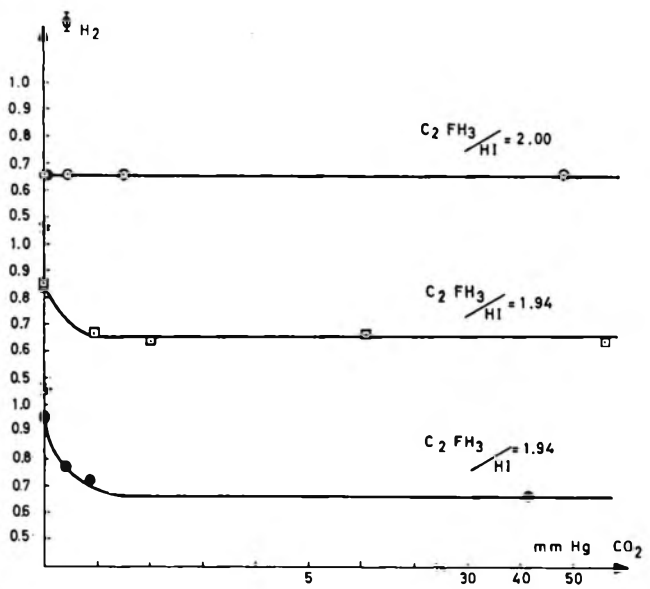


Figure 2. Effect of $CO_2$ pressure, at room temperature, on the hydrogen quantum yield $\Phi$ of $H_2$ from the photolysis of ⊙, 2.08 with 4.16; ⊡, 1.10 with 2.14; and ●, 0.61 with 1.17 mm of HI–$C_2FH_3$ mixtures.

each time increasing amounts of $CO_2$ as an inert diluent, no pressure effect on the hydrogen quantum yield up to a pressure of about 700 mm could be observed (see Figure 1). This is in marked contrast with two series of experiments in which a mixture of 0.167 mm of $I_2$ with 3.02 mm of HI ($I_2$:HI ratio 0.055) and 0.175 mm of $I_2$ with 4.00 mm of HBr ($I_2$:HBr ratio 0.044) were photolyzed, also at room temperature and again with increasing addition of $CO_2$. This time, a pronounced initial decrease of the quantum yield was found, which leveled off after a pressure of approximately 50 and 100 mm of $CO_2$, respectively (see Figure 1). When HBr was replaced by HI and a 2.08 mm of HI with 4.16 mm of $C_2FH_3$ mixture was photolyzed, again no pressure effect was observed, but when the ratio of HI:$C_2FH_3$ was kept constant and the total pressure of the reactants reduced to about 3 mm the quantum yield decreased with pressure. This decrease was even larger when the reactants pressure was further lowered (see Figure 2).

A study of the effect of the partial pressure variation of the fluoroethylenes ($C_2F_xH_y$ where $x + y = 4$) and hydrogen bromide upon $\Phi_{H_2}$ gave a straight line relationship between the HBr:$C_2F_xH_y$ ratios and $(1/\Phi_{H_2} - 1)^{-1}$. This type of investigation was carried out for $C_2H_4$, $C_2FH_3$, 1,1-$C_2F_2H_2$, *cis*-$C_2F_2H_2$, *trans*-$C_2F_2H_2$, $C_2F_3H$, and $C_2F_4$. All experiments were performed at room temperature and in the presence of $CO_2$ at pressures generally above 250 mm. The data of these experiments are listed in Table I and plotted in Figures 3 and 4. As can be observed, most compounds show an intercept appreciably higher than zero when the HBr:$C_2F_xH_y$ ratio approaches this same number. The only exceptions are ethylene and perfluoroethylene, whose intercepts were found to be −0.056 and 0.074, respectively, by the least-squares method. The slopes were found to be only a function of the HBr:$C_2F_xH_y$ ratio, as can be observed from some experiments in which only one reagent ($C_2F_xH_y$ or HBr) was varied and the other kept constant (see, for example, experiments 217–225 or 150–153), and from some others in which the ratio was maintained constant but the partial pressures of HBr and $C_2F_xH_y$ about quadrupled (experiments 147 and 153). In addition, the slope was found completely pressure independent as is apparent from some experiments with *trans*-$C_2F_2H_2$ (experiments 191–192 and 205–206) where the $CO_2$ pressure was increased from about 250 to 550 mm. Photolysis repeated under constant conditions gave satisfactory reproducibility. The following slopes and intercepts were calculated by the least-squares method with an IBM 360 computer: $C_2H_4$, 11.87 ± 0.11 and −0.056 ± 0.035; $C_2FH_3$, 15.12 ± 0.60 and 0.447 ± 0.273; *trans*-$C_2F_2H_2$, 10.18 ± 0.28 and 1.088 ± 0.068; *cis*-$C_2F_2H_2$, 16.96 ± 0.40 and 0.977 ± 0.197; 1,1-$C_2F_2H_2$, 8.18 ± 0.60 and 1.603 ± 0.329; $C_2F_3H$, 7.19 ± 0.19 and 0.379 ± 0.0831; and $C_2F_4$, 7.02 ± 0.18 and 0.074 ± 0.072.

## Discussion

The photochemistry of HBr has been discussed recently.[7] Upon photolysis with a medium pressure arc the HBr molecule will dissociate giving essentially a normal electronic state ($^2P_{3/2}$) bromine atom and a ground state ($^2S_{1/2}$) hot hydrogen atom, according to

$$HBr + h\nu \longrightarrow H^* + Br \qquad (e)$$

(asterisk denotes a hot radical). The produced hydrogen atoms may possess energies from 23 up to 39.5 kcal/mol, considering the bond energy of HBr as 88 kcal/mol, the HBr absorption onset as 2650 Å, and the

(7) R. M. Martin and J. E. Willard, *J. Chem. Phys.*, **40**, 3007 (1964).

**Table I**

| Expt no. | HBr, mm | $C_2F_xH_y$, mm | $\frac{[HBr]}{[C_2F_xH_y]}$ | $R_{H_2}^{\circ}$ [a] | $R_{H_2}$ | $\left(\frac{1}{\Phi_{H_2}} - 1\right)^{-1}$ | $CO_2$, mm |
|---|---|---|---|---|---|---|---|
| | | | $C_2H_4$ | | | | |
| 158 | 2.10 | 2.75 | 0.763 | 30.0 | 27.0 | 9.00 | 277.5 |
| 159 | 2.10 | 10.07 | 0.208 | 30.0 | 21.0 | 2.34 | 277.5 |
| 160 | 2.10 | 10.07 | 0.208 | 30.0 | 21.0 | 2.34 | 277.5 |
| 161 | 2.10 | 16.39 | 0.128 | 30.0 | 18.0 | 1.50 | 277.5 |
| 229 | 1.51 | 4.52 | 0.334 | 22.5 | 18.0 | 4.00 | 265.0 |
| 230 | 1.51 | 9.10 | 0.166 | 22.5 | 15.0 | 2.00 | 265.0 |
| 232 | 1.51 | 24.16 | 0.0625 | 22.5 | 9.25 | 0.70 | 265.0 |
| 297 | 1.53 | 10.20 | 0.150 | 15.33 | 9.67 | 1.71 | 227.5 |
| 298 | 1.53 | 18.30 | 0.0837 | 15.33 | 7.33 | 0.917 | 227.5 |
| | | | $C_2FH_3$ | | | | |
| 145 | 2.00 | 2.12 | 0.944 | 31.0 | 29.0 | 14.50 | 257.5 |
| 146 | 2.00 | 2.12 | 0.944 | 31.0 | 29.0 | 14.50 | 257.5 |
| 147 | 2.00 | 4.32 | 0.463 | 31.0 | 28.0 | 9.34 | 257.5 |
| 148 | 2.00 | 6.62 | 0.302 | 31.0 | 26.0 | 5.20 | 257.5 |
| 149 | 2.00 | 9.02 | 0.222 | 31.0 | 24.5 | 3.75 | 257.5 |
| 150 | 2.00 | 15.35 | 0.130 | 31.0 | 21.0 | 2.10 | 257.5 |
| 151 | 3.30 | 15.35 | 0.215 | 38.5 | 30.0 | 3.53 | 257.5 |
| 152 | 5.30 | 15.35 | 0.345 | 51.0 | 43.0 | 5.37 | 257.5 |
| 153 | 8.50 | 15.35 | 0.554 | 67.0 | 60.0 | 8.58 | 257.5 |
| 279 | 1.50 | 12.85 | 0.117 | 15.17 | 10.33 | 2.14 | 153.0 |
| 280 | 1.50 | 15.96 | 0.094 | 15.17 | 9.33 | 1.60 | 153.0 |
| 281 | 1.50 | 19.46 | 0.077 | 15.17 | 9.0 | 1.46 | 153.0 |
| 282 | 1.50 | 22.58 | 0.067 | 15.17 | 9.0 | 1.46 | 153.0 |
| | | | *cis*-$C_2F_2H_2$ | | | | |
| 217 | 1.03 | 1.08 | 0.952 | 18.0 | 17.0 | 17.0 | 272.5 |
| 218 | 1.03 | 1.08 | 0.952 | 18.0 | 17.0 | 17.0 | 272.5 |
| 219 | 1.03 | 2.58 | 0.400 | 18.0 | 16.0 | 8.0 | 272.5 |
| 220 | 1.03 | 4.10 | 0.251 | 18.0 | 15.0 | 5.0 | 272.5 |
| 221 | 1.03 | 5.60 | 0.184 | 18.0 | 14.0 | 3.5 | 272.5 |
| 222 | 1.03 | 7.12 | 0.145 | 18.0 | 13.5 | 3.0 | 272.5 |
| 223 | 1.03 | 8.62 | 0.120 | 18.0 | 13.5 | 3.0 | 272.5 |
| 224 | 1.03 | 10.24 | 0.101 | 18.0 | 13.5 | 3.0 | 272.5 |
| 225 | 1.03 | 12.54 | 0.0822 | 18.0 | 13.5 | 3.0 | 272.5 |
| | | | *trans*-$C_2F_2H_2$ | | | | |
| 211 | 1.60 | 3.30 | 0.483 | 23.3 | 20.0 | 6.07 | 255 |
| 212 | 1.60 | 5.70 | 0.281 | 23.3 | 19.0 | 4.42 | 255 |
| 213 | 1.60 | 7.32 | 0.218 | 23.3 | 18.0 | 3.40 | 255 |
| 214 | 1.60 | 7.32 | 0.218 | 23.3 | 18.0 | 3.40 | 255 |
| 199 | 1.60 | 7.60 | 0.211 | 24.0 | 18.5 | 3.36 | 262.5 |
| 200 | 1.60 | 10.70 | 0.150 | 24.0 | 17.0 | 2.43 | 262.5 |
| 201 | 1.60 | 10.70 | 0.150 | 24.0 | 17.1 | 2.48 | 262.5 |
| 203 | 1.60 | 12.70 | 0.126 | 24.0 | 16.5 | 2.20 | 262.5 |
| 204 | 1.60 | 15.10 | 0.106 | 24.0 | 16.0 | 2.00 | 262.5 |
| 205 | 1.60 | 16.50 | 0.097 | 24.0 | 16.0 | 2.00 | 262.5 |
| 206 | 1.60 | 16.50 | 0.097 | 24.0 | 16.0 | 2.00 | 525 |
| 182 | 1.90 | 3.00 | 0.633 | 29.0 | 25.5 | 7.29 | 255 |
| 183 | 1.90 | 5.20 | 0.368 | 29.0 | 24.0 | 4.80 | 255 |
| 184 | 1.90 | 7.20 | 0.264 | 29.0 | 23.0 | 3.83 | 255 |
| 185 | 1.90 | 9.20 | 0.207 | 29.0 | 22.0 | 3.14 | 255 |
| 186 | 1.90 | 12.00 | 0.158 | 29.0 | 21.0 | 2.62 | 255 |
| 187 | 1.90 | 15.00 | 0.127 | 29.0 | 20.0 | 2.22 | 255 |
| 188 | 1.90 | 15.00 | 0.127 | 29.0 | 20.0 | 2.22 | 255 |
| 189 | 1.90 | 18.00 | 0.106 | 29.0 | 20.0 | 2.22 | 255 |
| 190 | 1.90 | 18.00 | 0.106 | 29.0 | 19.5 | 2.05 | 255 |
| 191 | 1.90 | 22.70 | 0.084 | 29.0 | 20.0 | 2.22 | 255 |
| 192 | 1.90 | 22.70 | 0.084 | 29.0 | 20.0 | 2.22 | 547 |

**Table I** (*Continued*)

| Expt no. | HBr, mm | $C_2F_xH_y$, mm | $\frac{[HBr]}{[C_2F_xH_y]}$ | $R_{H_2}{}^{\circ a}$ | $R_{H_2}$ | $\left(\frac{1}{\Phi_{H_2}} - 1\right)^{-1}$ | $CO_2$, mm |
|---|---|---|---|---|---|---|---|
| | | | | $1,1\text{-}C_2F_2H_2$ | | | |
| 134 | 2.10 | 4.25 | 0.495 | 36.0 | 31.0 | 6.20 | 265 |
| 136 | 2.10 | 6.40 | 0.329 | 36.0 | 30.0 | 5.00 | 265 |
| 137 | 2.10 | 8.50 | 0.247 | 36.0 | 28.0 | 4.00 | 265 |
| 138 | 2.10 | 11.60 | 0.181 | 36.0 | 27.0 | 3.00 | 265 |
| 139 | 3.20 | 11.60 | 0.275 | 44.0 | 35.0 | 3.89 | 265 |
| 140 | 4.30 | 11.60 | 0.370 | 51.0 | 43.0 | 5.38 | 265 |
| 141 | 4.30 | 34.10 | 0.126 | 51.0 | 38.0 | 2.92 | 265 |
| 142 | 4.30 | 34.10 | 0.126 | 51.0 | 35.0 | 2.19 | 265 |
| 334 | 2.18 | 1.20 | 1.817 | 33.625 | 31.86 | 18.10 | 253 |
| 335 | 2.18 | 2.34 | 0.932 | 33.625 | 30.75 | 10.69 | 253 |
| 336 | 2.18 | 3.44 | 0.634 | 33.625 | 29.50 | 7.151 | 253 |
| 337 | 2.18 | 10.33 | 0.212 | 33.625 | 26.37 | 3.635 | 253 |
| 338 | 2.18 | 42.33 | 0.052 | 33.625 | 18.36 | 1.20 | 253 |
| 339 | 2.18 | 42.33 | 0.052 | 33.625 | 18.36 | 1.20 | 253 |
| 329 | 1.59 | 6.15 | 0.259 | 33.20 | 27.30 | 4.63 | 270 |
| 330 | 1.59 | 6.15 | 0.259 | 33.20 | 27.30 | 4.63 | 270 |
| 422 | 1.43 | 4.03 | 0.355 | 31.00 | 25.50 | 4.63 | 255 |
| 423 | 1.43 | 14.02 | 0.102 | 31.00 | 21.50 | 2.26 | 255 |
| 424 | 1.43 | 43.09 | 0.033 | 31.00 | 19.10 | 1.60 | 255 |
| | | | | $C_2F_3H$ | | | |
| 167 | 2.10 | 2.10 | 1.000 | 30.50 | 27.00 | 7.70 | 252.5 |
| 168 | 2.10 | 4.10 | 0.513 | 30.50 | 24.00 | 3.70 | 252.5 |
| 169 | 2.10 | 6.50 | 0.322 | 30.50 | 22.50 | 2.81 | 252.5 |
| 171 | 2.10 | 9.10 | 0.231 | 30.50 | 21.00 | 2.21 | 252.5 |
| 172 | 2.10 | 9.10 | 0.231 | 30.50 | 21.00 | 2.21 | 252.5 |
| 173*a* | 2.10 | 12.40 | 0.169 | 30.50 | 19.00 | 1.65 | 252.5 |
| 173*b* | 2.10 | 12.40 | 0.169 | 30.50 | 19.00 | 1.65 | 252.5 |
| 174*a* | 2.10 | 15.70 | 0.133 | 30.50 | 17.00 | 1.26 | 252.5 |
| 174*b* | 2.10 | 15.70 | 0.133 | 30.50 | 17.00 | 1.26 | 252.5 |
| 175 | 7.00 | 15.70 | 0.447 | 57.50 | 45.00 | 3.60 | 252.5 |
| 176 | 7.00 | 15.70 | 0.447 | 57.50 | 45.00 | 3.60 | 252.5 |
| | | | | $C_2F_4$ | | | |
| 119 | 2.10 | 2.10 | 1.000 | 38.00 | 33.25 | 7.00 | 147.5 |
| 120 | 2.10 | 4.50 | 0.468 | 38.00 | 30.00 | 3.75 | 147.5 |
| 122 | 2.10 | 6.65 | 0.317 | 38.00 | 27.00 | 2.45 | 250.0 |
| 123 | 2.10 | 8.80 | 0.238 | 38.00 | 25.00 | 1.92 | 250.0 |
| 124 | 2.10 | 11.10 | 0.189 | 38.00 | 23.00 | 1.53 | 250.0 |
| 125 | 3.25 | 11.10 | 0.301 | 48.00 | 32.00 | 2.00 | 250.0 |
| 126 | 4.45 | 11.10 | 0.400 | 50.00 | 36.00 | 2.58 | 250.0 |
| 127 | 7.50 | 11.10 | 0.676 | 65.00 | 54.00 | 4.90 | 250.0 |
| 271 | 1.50 | 10.00 | 0.150 | 16.50 | 9.00 | 1.20 | 312.0 |
| 272 | 1.50 | 12.10 | 0.124 | 16.50 | 7.66 | 0.87 | 312.0 |
| 273 | 1.50 | 14.25 | 0.105 | 16.50 | 7.33 | 0.80 | 312.0 |
| 274 | 1.50 | 18.15 | 0.083 | 16.50 | 6.60 | 0.67 | 312.0 |
| 275 | 1.50 | 23.25 | 0.065 | 16.50 | 5.56 | 0.51 | 312.0 |
| 276 | 1.50 | 23.25 | 0.065 | 16.50 | 5.53 | 0.51 | 312.0 |

[a] $R_{H_2}{}^{\circ}$ expressed in units of mm/5-min photolysis × 0.126 $cm^3$.

spectral energy distribution of the radiated mercury lines of the lamp employed in this work. No clear statement can be made with regard to the relative importance of the various possible hydrogen atom energies.

When a mixture of a fluoroethylene and HBr is photolyzed, only the HBr molecule will decompose. The fate of the produced hot hydrogen atom is to react either with HBr or else with the existing fluoroolefin, by one of the following reactions

$$H^* + HBr \longrightarrow H_2 + Br \quad (1)$$

$$H^* + C_2F_xH_y \longrightarrow C_2F_xH_{y+1} \quad (2)$$

$$H^* + C_2F_xH_y \longrightarrow C_2F_xH_{y-1} + H_2 \quad (3)$$

$$H^* + C_2F_xH_y \longrightarrow C_2F_{x-1}H_y + HF \quad (4)$$

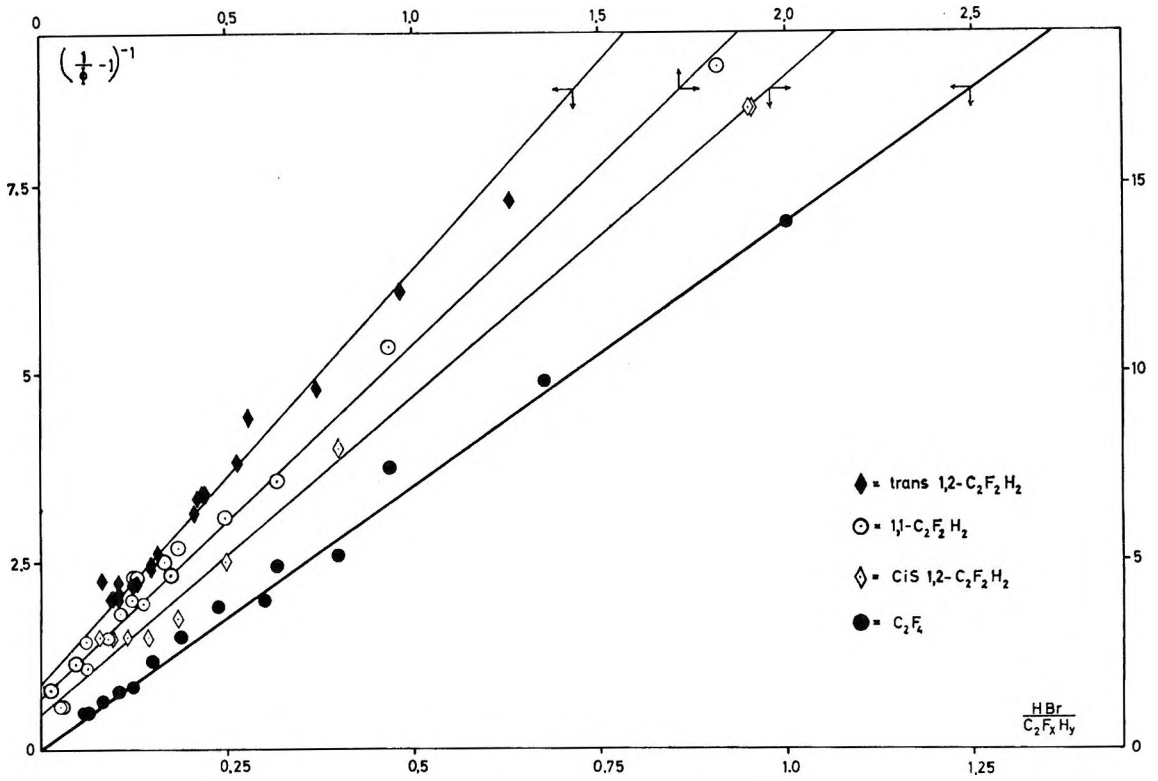


Figure 3. Graphical representation of the data from Table I according to eq II for *trans*-1,2-$C_2F_2H_2$, 1,1-$C_2F_2H_2$, *cis*-1,2-$C_2F_2H_2$, and $C_2F_4$.

or to be thermalized by collisions

$$H^* + M \longrightarrow H + M \qquad (5)$$

with an inert diluent M ($CO_2$ or any of the other reagents).

The thermal hydrogen atoms can then undergo a set of reactions, similar to those of the corresponding hot atoms

$$H + HBr \longrightarrow H_2 + Br \qquad (6)$$

$$H + C_2F_xH_y \longrightarrow C_2F_xH_{y+1} \qquad (7)$$

$$H + C_2F_xH_y \longrightarrow C_2F_xH_{y-1} + H_2 \qquad (8)$$

$$H + C_2F_xH_y \longrightarrow C_2F_{x-1}H_y + HF \qquad (9)$$

All possible fluoroethylene radical reactions were neglected in view of the low conversions employed in this work.

Applying the usual steady-state considerations, the following relation can be derived

$$\frac{R_{H_2}^\circ}{R_{H_2}} = \frac{1}{\Phi_{H_2}} = 1 + \frac{(k_9 + k_7)C_2F_xH_y}{k_6HBr + k_8C_2F_xH_y} \qquad (I)$$

where $R_{H2}^\circ$ corresponds to the hydrogen produced from HBr alone or with $CO_2$, and $R_{H2}$ is the hydrogen produced when the same pressure of HBr is photolyzed in the presence of fluoroolefin.

Only one important assumption was made in the derivation of eq I. It was considered that under the prevailing conditions all of the reactions were thermal, *i.e.*, $k_5M \gg k_3\,HBr + (k_2 + k_3 + k_4)C_2F_xH_y$. Clearly the hydrogen atoms produced during the primary photolytical act are hot as can be deduced from some experiments of the pressure effect of $CO_2$ on $\Phi_{H_2}$ for HX–$I_2$ mixtures. Initially small and increasing amounts of $CO_2$ will reduce the $\Phi_{H_2}$ up to a certain pressure, after which the hydrogen production becomes pressure independent. It is interesting to note that it takes about half the $CO_2$ pressure to moderate equal ratios of $I_2$:HX when X is Br as when it is I. This indicates that, with the same incident λ 2537 Å light, the energy of the H atoms produced from HI is about double that from HBr which, considering the bond energy of 70 kcal/mol of HI and 88 kcal/mol of HBr, is in agreement with expectations (see Figure 1), provided little energy goes into excitation of the X atom. It is then reasonable to infer that HBr alone, at least at pressures of 1.5 mm, will not completely moderate the hot H atoms. When the same type of experiments were carried out with $C_2FH_3$ or $C_2F_4$ and HBr no such pressure effect on the hydrogen quantum yield could be detected, which seems to suggest that the fluoroethylenes play an important role in the moderation process and that these binary systems are in thermal conditions at least at total fluoroethylene pressures above 4 mm. Some experiments were carried out using HI. The H atoms produced from this hydrogen halide at 2537 Å will have essentially 41 kcal/mol,[8] about 16 kcal/mol

(8) L. E. Compton and R. M. Martin, *J. Phys. Chem.*, **73**, 3474 (1969).

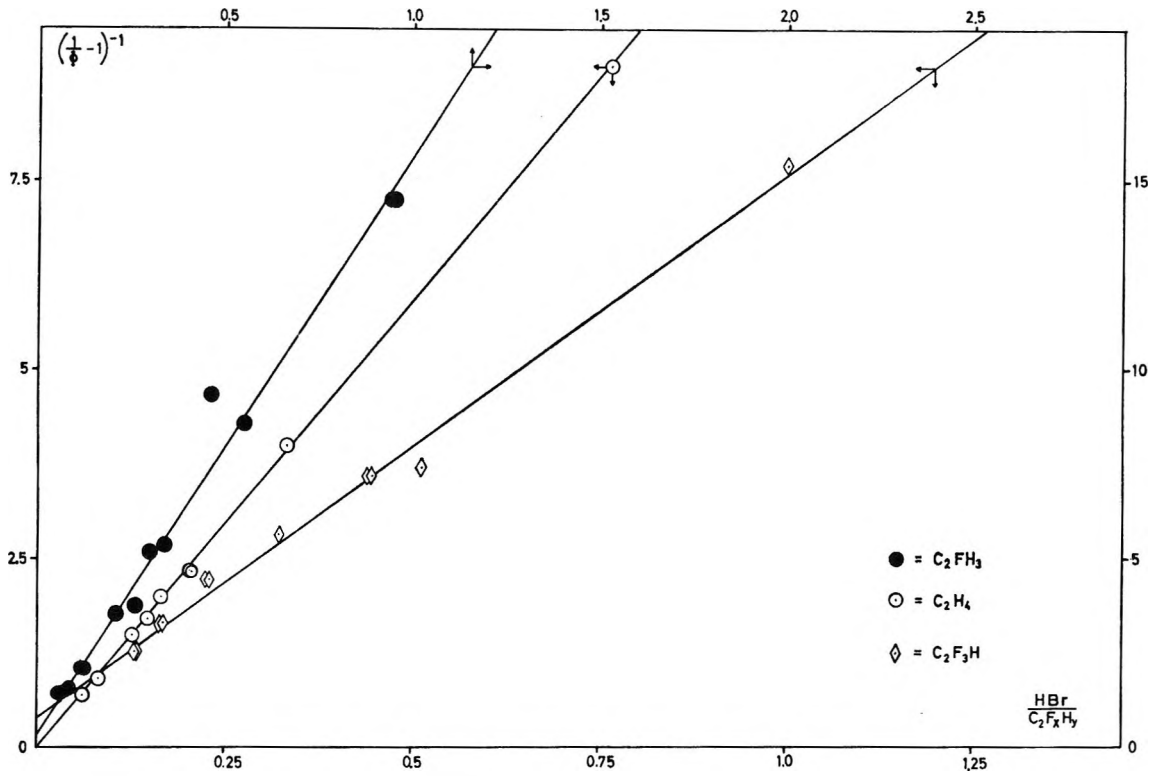


Figure 4. Graphical representation of the data from Table I according to eq II for $C_2FH_3$, $C_2H_4$, and $C_2F_3H$.

higher than those produced from HBr at the same wavelength. With HI a $CO_2$ pressure effect on $\Phi_{H_2}$ was noticed, but only at very low reactant pressure (see Figure 2). The extent of the reduction increased as the total pressure was lowered. This is in contrast with a study of the photolysis of a 9:1 and a 5.5:1 mixture of $C_2D_4$ with about 1 mm of HI, where a plateau was reached only after a total pressure of the order of 200 mm.[9] A similar observation was made recently by Wooley and Cvetanović,[10] who used $H_2S$ as the H atom source. These results clearly indicate that the fluoroolefins are more effective H* atom moderators than ethylene or iodine and that therefore the collisions of these compounds with the hot hydrogen atoms are quite inelastic. The higher efficiency of the fluorinated olefins can be attributed to the greater density of vibrational levels of the C–F bonds and the related increase in the number of effective oscillators of these molecules. Furthermore, considering that a hydrogen abstraction occurs with the fluoroolefins, it can be suggested that the average reaction probability per hot collision is low because no structure was observed in the moderation curves of Figures 1 and 2.

When a hot H atom collides with a fluoroolefin molecule, a superhot alkyl radical will be formed with an ex-

$$H^* + C_2F_xH_y \longrightarrow C_2F_xH_{y+1}^{**}$$

cess energy given by the sum of the exothermicity of the reaction and the energy carried by the H atom. This radical may decompose according to

$$C_2F_xH_{y+1}^{**} \longrightarrow C_2F_xH_y + H$$

even at total pressures of a few hundred millimeters. A thermalized H atom, on the contrary, will either abstract or otherwise give rise to a much longer-lived fluoroalkyl radical

$$H + C_2F_xH_y \longrightarrow C_2F_xH_{y+1}^*$$

whose fate will be to disappear by reaction with HX or $C_2F_xH_y$.

Upon rearrangement, eq I becomes

$$\left(\frac{1}{\Phi_{H_2}} - 1\right)^{-1} = \frac{k_8}{k_7 + k_9} + \frac{k_6}{k_7 + k_9}\frac{(HBr)}{(C_2F_xH_y)} \qquad (II)$$

which can be seen plotted for the various fluoroethylenes in Figures 3 and 4. The slopes of the straight lines can be identified with $k_6/(k_7 + k_9)$ and the intercepts with $k_8/(k_7 + k_9)$. The behavior predicted by eq II was observed for all fluoroolefins with the exception of $C_2H_4$ and $C_2F_4$ which show only a negligible intercept, attributable to the experimental error. From the previous treatment it is expected that perfluoroethylene should not show an intercept, because this compound has no hydrogen and therefore reaction 8 cannot take place. With ethylene, on the other hand, only reaction 9 can be *a priori* disregarded and therefore an intercept is possible, but it is a well established fact that hydrogen abstraction from ethylene does not occur at room temper-

(9) R. D. Penzhorn, *Diss. Abstr. B*, **28**, 2379 (1967).

(10) G. R. Wooley and R. J. Cvetanović, *J. Chem. Phys.*, **50**, 4697 (1969).

**Table II:** Ratios of Rate Constants

| Compd | $k_7/k_6$ | $k_8/k_7$ | $k_8/k_6$ |
|---|---|---|---|
| $C_2H_4$ | 0.0843 ± 0.0008 | −0.056 ± 0.035 | ... |
| $C_2FH_3$ | 0.0662 ± 0.0026 | 0.45 ± 0.27 | 0.0297 ± 0.0178 |
| 1,1-$C_2F_2H_2$ | 0.1223 ± 0.0091 | 1.60 ± 0.32 | 0.196 ± 0.0540 |
| *cis*-$C_2F_2H_2$ | 0.0589 ± 0.0014 | 0.98 ± 0.20 | 0.0577 ± 0.0132 |
| *trans*-$C_2F_2H_2$ | 0.0983 ± 0.0027 | 1.09 ± 0.07 | 0.1070 ± 0.0077 |
| $C_2F_3H$ | 0.1390 ± 0.0039 | 0.38 ± 0.08 | 0.0528 ± 0.0128 |
| $C_2F_4$ | 0.1425 ± 0.0037 | 0.074 ± 0.072 | ... |

ature and is of negligible importance even for the higher olefin.[11]

Up to now, with the sole exception of some very hot hydrogen atom studies,[12] no conclusive evidence for fluorine abstraction reactions has been reported, not even for the fluoroalkanes.[13,14] Scott and Jennings[15] suggested that a reaction for fluorine abstraction

$$H + CH_3—CH_2F \longrightarrow CH_3—CH_2 + HF$$

takes place during the Hg-photosensitized decomposition of ethyl fluoride. The presence of ethyl radicals explained the formation of such products as $n$-$C_4H_{10}$, $C_2H_6$, and $C_2H_4$. Nevertheless, the evidence given is not conclusive. The possibility that hydrogen atoms, generated by the interaction between mercury and the substrate, could react with the other radical produced in the primary process, $CH_3$–CHF, cannot be ruled out. In that event the following sequence of reactions would also explain the observed products

$$CH_3—CHF + H \longrightarrow CH_3—CH_2F^*$$

$$CH_3—CH_2F^* \longrightarrow CH_2{=}CH_2 + HF$$

$$CH_2{=}CH_2 + H \longrightarrow CH_3—CH_2, \text{ etc}$$

Ethylene could also come from a primary unimolecular decomposition of an exited ethyl fluoride molecule. Finally, Wijnen, *et al.*,[2] could not detect fluorine atom abstraction from $CH_2{=}CHF$ by H atoms. In view of all the previous considerations, it seems reasonable to assume that $k_7$ and $k_8 \gg k_9$. Table II summarizes the $k_7/k_6$, $k_8/k_7$, and $k_8/k_6$ ratios for all fluoroethylenes. From the data it is apparent that hydrogen abstraction is of considerable importance for the fluoroethylenes and that for 1,1-$C_2H_2F_2$ and for *trans*-$C_2F_2H_2$ it is even faster than the corresponding addition, indicating that replacement of hydrogen by halogen atoms weakens the C–H bond strength of the corresponding olefins.

Although there is a very regular variation in the fluoroethylene structures, there seems to be no obvious correlation with any trend in the addition and abstraction reaction. With the exception of *cis*-$C_2F_2H_2$ and ethylene, it can be observed that there is an increase in the rate of addition with increasing fluorine substitution.

The relative rate of addition of methyl radicals to ethylene and tetrafluoroethylene has been investigated in the gas phase.[16] It was found that the reactivity of the fluorinated compound is about ten times faster than that of ethylene. It is a well established fact that hydrogen atoms and the methyl group, both electroneutral radicals, show great similarities in their trends and chemical behavior. Accordingly, we find that tetrafluoroethylene has a 1.69 times affinity for hydrogen atoms than ethylene. Robb, *et al.*, found that tetrafluoroethylene reacts with H atoms about 25 times slower than ethylene. This surprisingly different result could be explained by a mercury-photosensitized decomposition of the reagents, which takes place quite readily.[17,18] It is interesting to notice that both the H and the $CH_3$ radical were found to be unreactive toward $C_2Cl_4$.

Some studies of the addition of electrophilic radicals like $CCl_3$[19] and $CF_3$,[20] collected in Table III, have been compared with the data for H and $CH_3$ addition. These radicals will also add preferably to the less halogen substituted side of the olefin but, being electrophilic, will add increasingly slower with fluorine substitution. However, to explain all the observed trends, more data on activation energies and preexponential factors are needed, as well as information with respect to the site of the abstraction.

Table II shows the $k_8/k_6$ ratios for the fluoroethylene series. Again, no regular trend is observed. The abstraction rate increases in the order $C_2FH_3$, $C_2F_3H$, *cis*-$C_2F_2H_2$, *trans*-$C_2F_2H_2$, and 1,1-$C_2F_2H_2$. Evidently, the most favorable molecule will be the highly polarized 1,1-$C_2F_2H_2$. The surprisingly low $C_2F_3H$ rate can

(11) R. J. Cvetanović, *Advan. Photochem.*, **1**, 149 (1963).

(12) R. Odum and R. Wolfgang, *J. Amer. Chem. Soc.*, **85**, 1050 (1963).

(13) H. N. Chadwell and T. Titani, *ibid.*, **55**, 1363 (1933).

(14) J. R. Dacey and J. W. Hodgins, *Can. J. Res. Sect. B*, **28**, 173 (1950).

(15) P. M. Scott and K. R. Jennings, *Chem. Commun.*, 700 (1967).

(16) R. P. Buckley and M. Szwarc, *J. Amer. Chem. Soc.*, **78**, 5696 (1956).

(17) J. Heicklen, V. Knight, and S. A. Greene, *J. Chem. Phys.*, **42**, 221 (1965).

(18) A. B. Callear and R. J. Cvetanović, *ibid.*, **24**, 873 (1956).

(19) J. M. Tedder and J. C. Walton, *Trans. Faraday Soc.*, **62**, 1859 (1966).

(20) A. P. Stefani, L. Herk, and M. Szwarc, *J. Amer. Chem. Soc.*, **83**, 4732 (1961).

**Table III:** Relative Rate Constants for Different Addition Reactions to Fluoroolefins[a]

| Compd | $CF_3$[b] | $CCl_3$[c] | $CH_3$[d] | H[e] |
|---|---|---|---|---|
| $C_2H_4$ | 1.000 | 1.0000 | 1.0 | 1.00 |
| $C_2FH_3$ | ... | 0.8610 | ... | 0.79 |
| 1,1-$C_2F_2H_2$ | ... | 0.0998 | ... | 1.45 |
| *cis*-$C_2F_2H_2$ | ... | ... | ... | 0.70 |
| *trans*-$C_2F_2H_2$ | ... | ... | ... | 1.16 |
| $C_2F_3H$ | ... | 0.0108 | ... | 1.65 |
| $C_2F_4$ | 0.151 | 0.0010 | 10.0 | 1.69 |

[a] Data expressed relative to ethylene. [b] See ref 20. [c] See ref 19. [d] See ref 16. [e] Present work.

partly be attributed to the decrease in the number of available C–H bonds.

As mentioned before, Wijnen found that a hydrogen abstraction reaction occurs between H atoms and vinyl chloride. In a earlier study of the photolysis of HI–$C_2H_4$ mixtures,[9] the ratio of rate constants $k(H + C_2H_4)/k_a$ was found to be 0.0593 at room temperature. When this result is combined with the $k(H + C_2H_4)/k_6$ ratio found in the present investigation, a value of 1.43 can be calculated for $k_a/k_6$. With these values, the rates of addition and abstraction of H atoms with vinyl chloride and fluoride with respect to $k_6$, can be calculated as in the following table.

| | $k_7$ or $k_b/k_6$ | $k_8$ or $k_c/k_6$ |
|---|---|---|
| $C_2H_3Cl$ | 0.0508 | 0.109 |
| $C_2H_3F$ | 0.0662 | 0.0297 |

It seems reasonable to suggest that the inductive effect of electron attraction, which is greater for fluorine than for chlorine,[21] will favor addition of H atoms to $C_2FH_3$. Nevertheless, the experimental rate difference would have been expected to be greater.

The existence of a resonance effect between the $\pi$ electrons of the double bond and the nonbonding electrons of the halogens[22,23] could explain the hydrogen abstraction. However, contrary to observation, the rate with $C_2FH_3$ would have been expected to be faster than that with $C_2ClH_3$ considering that, from chemical properties of the ground states of halogenated molecules, the mesomeric effect (electron release) is greater for fluorine than for chlorine.

*Acknowledgment.* The financial support from FORGE (The Funds for Overseas Research Grants and Education) and from the Comisión Nacional de Investigaciones Científicas y Tecnológicas de Chile is gratefully acknowledged.

(21) D. T. Clark. J. N. Murrell, and J. M. Tedder, *J. Chem. Soc.*, 1250 (1963).

(22) L. Pauling, "Nature of the Chemical Bond," Cornell University Press, Ithaca, N. Y., 1945.

(23) J. R. Majer, *Advan. Fluorine Chem.*, 2 (1961).

# Free Radical Chain Reactions in the Radiolysis and Photolysis of Isobutyl Bromide[1]

by Donna Kutsko Bakale[2] and Hugh A. Gillis[3]

*Department of Chemistry, Case Western Reserve University, Cleveland, Ohio 44106 and Division of Physics, National Research Council, Ottawa 7, Canada* *(Received November 12, 1969)*

The radiolysis or photolysis of isobutyl bromide results in isomerization to *t*-butyl bromide and decomposition to isobutylene and hydrogen bromide with initial yields which are characteristic of chain processes. These decomposition products reach equal plateau concentrations of about 0.05 mol % at low doses for pure isobutyl bromide. The effects of dose rate and of adding isobutylene, hydrogen bromide, or ethylene on the major products have been studied. All of the observations are consistent with a free radical chain mechanism in which the following are important reactions: $Br\cdot + (CH_3)_2CHCH_2Br \rightleftharpoons HBr + (CH_3)_2\dot{C}CH_2Br$ (5), $Br\cdot + (CH_3)_2C{=}CH_2 \rightleftharpoons (CH_3)_2\dot{C}CH_2Br$ (6), $Br\cdot + (CH_3)_2C{=}CH_2 \rightleftharpoons (CH_3)_2CBrCH_2\cdot$ (7). From the data equilibrium constants are calculated for these reactions: $K_5 = (7.9 \pm 2.2) \times 10^{-4}$; $K_6 = 323 \pm 60$ l. mol$^{-1}$; $K_7 = 4 \pm 2$ l. mol$^{-1}$. The activation energy for reaction 6 is estimated at 8.5 kcal mol$^{-1}$. The production of *t*-butyl bromide could also be explained by an intraradical bromine atom shift or by the formation of a bridged bromoalkyl radical, instead of by reaction 7.

## Introduction

During the past few years several reports on the radiation-induced isomerization of alkyl bromides and chlorides have been published. The radiation-induced isomerization of *n*-propyl chloride to isopropyl chloride has been particularly thoroughly studied by Willard and coworkers.[4,5] It was shown that the results can be explained by an HCl-catalyzed chain mechanism involving an intraradical chlorine atom shift which is presumably reversible

$$CH_3\dot{C}HCH_2Cl \rightleftharpoons CH_3CHClCH_2\cdot$$

*n*-Butyl chloride and isobutyl chloride undergo similar reactions.[5] In contrast to these results with the chlorides, the radiation-induced isomerization of *n*-propyl bromide to isopropyl bromide proceeds with a $G$ of only about 2.1,[5,6] which suggests that a chain mechanism is not operative, and the reaction is not catalyzed by HCl.[5] Since the present investigation was begun, experiments have been reported on the radiation-induced isomerization of *n*-butyl bromide to *sec*-butyl bromide which proceeds with quite large $G$'s.[7] However, a one-step intraradical shift is not invoked. Rather it is proposed that a bromoalkyl radical rearranges through steps involving elimination of a bromine atom, olefin isomerization, and readdition of a bromine atom.

In an investigation carried out in collaboration with one of us (H. A. G.), Gallivan found that upon irradiation at low dose rates, isobutyl bromide gives large initial yields of isobutylene ($G \simeq 110$), and *t*-butyl bromide ($G \simeq 120$).[8] These yields, unfortunately rather irreproducible, are very much larger than those reported earlier by Wilcox[9] at much higher doses. The present work was carried out with the hope of obtaining further information on the mechanism of the radiation-induced chain decomposition and isomerization of isobutyl bromide.

## Experimental Section

*Materials.* Isobutyl bromide from Matheson Coleman and Bell was washed repeatedly with distilled water to remove *t*-butyl bromide (by preferential hydrolysis) and isobutylene (by hydration), dried, and further purified by distillation at 8–10 mm through a 3-ft column packed with glass helices. The average mole percentages of impurities in material used in experiments were determined by gas chromatography to be as follows: isobutane, $<5 \times 10^{-5}$; 1,2-dibromo-2-methylpropane, $<10^{-4}$; hydrogen bromide, $<10^{-3}$; isobutylene, $\sim 10^{-4}$; *t*-butyl bromide, $\sim 10^{-3}$; *n*-butyl bromide plus $C_8$ hydrocarbons, 1–2.

Isobutylene (J. T. Baker) and ethylene (Philips Research Grade) were distilled on the vacuum line, with retention of the first two-thirds, and degassed thoroughly. Hydrogen bromide (J. T. Baker) was dried by passing it

(1) Supported in part by the U. S. Atomic Energy Commission.

(2) Based in part on the Ph.D. thesis submitted by D. K. Bakale to Case Western Reserve University, 1969.

(3) To whom correspondence should be addressed at the National Research Council.

(4) H. L. Benson, Jr., and J. E. Willard, *J. Amer. Chem. Soc.*, **83**, 4672 (1961).

(5) M. Takehisa, G. Levey, and J. E. Willard, *ibid.*, **88**, 5694 (1966).

(6) R. J. Neddenriep and J. E. Willard, *J. Phys. Chem.*, **65**, 1206 (1961).

(7) D. H. Martin and F. Williams, *J. Amer. Chem. Soc.*, **92**, 769 (1970).

(8) J. B. Gallivan, M.A. Thesis, St. Francis Xavier, Antigonish, Nova Scotia, 1962.

(9) W. S. Wilcox, *Radiat. Res.*, **10**, 112 (1959).

twice through a spiral column packed with glass beads and submerged in a bath at −78° and then degassed.

*Preparation of Samples.* Several common drying agents were found to be unsatisfactory as their addition to liquid isobutyl bromide at room temperature led to the formation of isobutylene and *t*-butyl bromide. The only substance tried which did not cause such reactions was Linde Molecular Sieve 4A powder, and it was used for all the experiments reported here. Distilled isobutyl bromide was made to pass in the vapor phase through a column (6 mm i.d., 18 cm long) containing alternate layers of glass wool and the Molecular Sieve 4A powder. A new column was used for each 8–10 ml of sample and degassed by heating under vacuum for several days prior to use. Degassing of samples was effected by refluxing under vacuum at a cold finger at −78°. Samples of about 0.6 ml of liquid were condensed on the vacuum line into cells prepared from 6-mm i.d. Pyrex tubing and with each fitted with a break-seal and septum holder. In the preparation of solutions, calibrated volumes on the vacuum line were used to measure out known amounts of isobutyl bromide and additives. Unirradiated samples of pure isobutyl bromide and of solutions that had been subjected to the normal drying and degassing procedures were analyzed frequently to determine concentrations of significant impurities (especially *t*-butyl bromide) and to check on the accuracy of the procedures for preparing solutions. After having been sealed off, all samples were stored at −196° until used.

Cells for photolyses were prepared from 6-mm i.d. quartz tubing connected by way of graded seals to the usual Pyrex break-seals and septum holders.

*Irradiations and Photolyses.* Most irradiations were carried out in a Nuclear Systems Hot Rodder $^{60}Co$ source at room temperature. Fricke dosimetry was used to determined the normal dose rate, used for the majority of runs. Corrections were applied for differences in electron density between the dosimeter solution and isobutyl bromide. The normal dose rate in isobutyl bromide varied from $0.97 \times 10^{17}$ to $0.67 \times 10^{17}$ eV $g^{-1}$ $min^{-1}$ over the course of this research. Lower dose rates were obtained by placing samples further away than normal from the $^{60}Co$. Irradiations at a higher dose rate ($0.80 \times 10^{18}$ eV $g^{-1}$ $min^{-1}$) were performed with a $^{60}Co$ source in the Department of Radiation Biology at Case Western Reserve University. The dose rate taken for this source was that given by the manufacturer, corrected for source decay and electron density differences.

Photolyses were performed in a Rayonet Srinivasan–Griffin photochemical reactor with one low-pressure mercury lamp. According to the manufacturer 85% of its light was at 253.7 nm. Actinometry was performed by photolyzing oxygen-saturated ethyl iodide, for which the quantum yield for formation of molecular iodine is 0.5.[10] Iodine was measured spectrophotometrically at 478 nm, and a molar extinction coefficient of $1.28 \times 10^3$ $M^{-1}$ $cm^{-1}$ was used.[11] The intensity was determined to be $0.119 \pm 0.014 \times 10^{18}$ quanta $g^{-1}$ $min^{-1}$. It was established that the extinction coefficient of isobutyl bromide at 253.7 nm is high enough to ensure absorption of all the incident light under our conditions.

*Analyses.* Products other than hydrogen bromide were analyzed for on a column of DC-200 silicone oil on Chromosorb on a chromatograph equipped with a flame ionization detector; 10 μl of irradiated liquid was injected within 1 min of the end of irradiation. Ethylene, isobutane, and isobutylene were separated with a flow rate of 7 ml $min^{-1}$ of nitrogen carrier gas. At 14 min after injection the flow rate was increased to 92 ml $min^{-1}$ for the separation of ethyl bromide, *t*-butyl bromide, isobutyl bromide, and 1,2-dibromo-2-methylpropane in that order. Temperature programming was begun from room temperature at 48 min, and a maximum of 120° was reached at 64 min. Peaks were qualitatively identified by comparison of their retention times with those of known samples. Simultaneous injections of a standard and irradiated sample were used to further verify the identification of the 1,2-dibromo-2-methylpropane peak. Calibration factors relating detector response to quantity of product were determined for all products at frequent intervals.

Hydrogen bromide could not be separated conveniently from the irradiated sample by extraction with water because of hydrolysis of the isobutyl and *t*-butyl bromides. Instead analysis for hydrogen bromide was based on the production of carbon dioxide from the reaction of hydrogen bromide with sodium bicarbonate.[12] Prior to each analysis a 6-mm i.d. column was filled to a depth of 4.5 cm with sodium bicarbonate and attached to the entrance of a gas chromatograph equipped with a thermal conductivity detector. An injection of 350 μl of sample was made onto the bicarbonate column within 2 min of the end of irradiation, and the resulting carbon dioxide was separated on a 2-ft column of silica gel at 50°. It was found that the efficiency of conversion of hydrogen bromide to carbon dioxide was not 100%. Therefore, many solutions of known amounts of hydrogen bromide in isobutyl bromide were used to carefully establish a calibration curve over the entire concentration range used in this work. This curve was found to be a good straight line described by: molecules of $CO_2$ = 0.77 (molecules of HBr − $0.3 \times 10^{18}$). It was established that this relationship did not change during this work. The quantitative relationship between instrumental response and quantity of carbon dioxide was established just before or after each analysis for hydrogen bromide.

(10) S. Hacobian and T. Iredale, *Nature*, **166**, 156 (1950).

(11) E. O. Hornig and J. E. Willard, *J. Amer. Chem. Soc.*, **79**, 2429 (1957).

(12) G. F. Harrison, "Vapour Phase Chromatography," D. H. Desty, Ed., Academic Press, Inc., New York, N. Y., 1957, p 332.

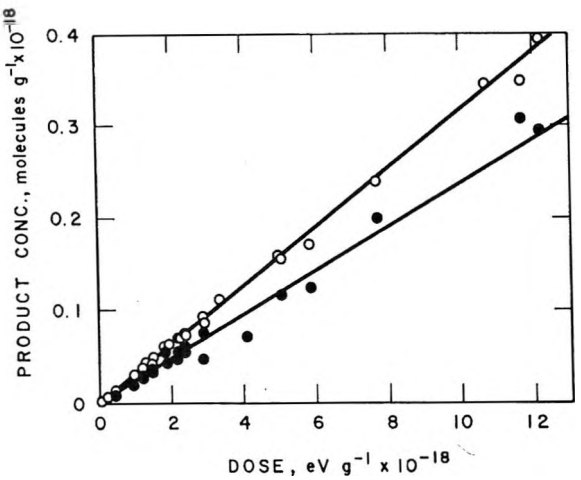


Figure 1. Production of isobutane and 1,2-dibromo-2-methylpropane as functions of dose during the radiolysis of pure isobutyl bromide: O, isobutane; ●, 1,2-dibromo-2-methylpropane.

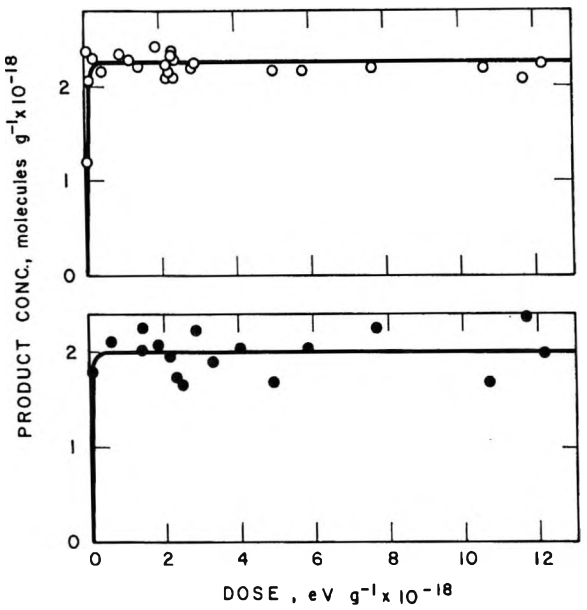


Figure 2. Production of isobutylene and hydrogen bromide as functions of dose during the radiolysis of pure isobutyl bromide: O, isobutylene; ●, hydrogen bromide.

A more complete description of experimental details is available.[2]

## Results

*Product Yields in the Radiolysis of Pure Isobutyl Bromide.* Product yields were studied at doses up to $12.2 \times 10^{18}$ eV g$^{-1}$. The concentrations of isobutane and 1,2-dibromo-2-methylpropane increase linearly with dose with $G$'s of 3.2 ± 0.2 and 2.4 ± 0.4, respectively, as shown in Figure 1. The effect of dose on the yields of isobutylene and hydrogen bromide, shown in Figure 2, is much different in that plateau concentrations of $2.28 \pm 0.12 \times 10^{18}$ molecules g$^{-1}$ (0.052 mol %) and $2.0 \pm 0.3 \times 10^{18}$ molecules g$^{-1}$, respectively, were reached after less than $0.1 \times 10^{18}$ eV g$^{-1}$ and these concentrations did not change significantly with further irradiation. The shortest irradiation gives $G$ (isobutylene) = 17,600 which must be a lower limit for the initial $G$. Since isobutylene and hydrogen bromide are the major nonisomeric products, stoichiometry requires that their yields be equal within experimental error, and this requirement is satisfied.

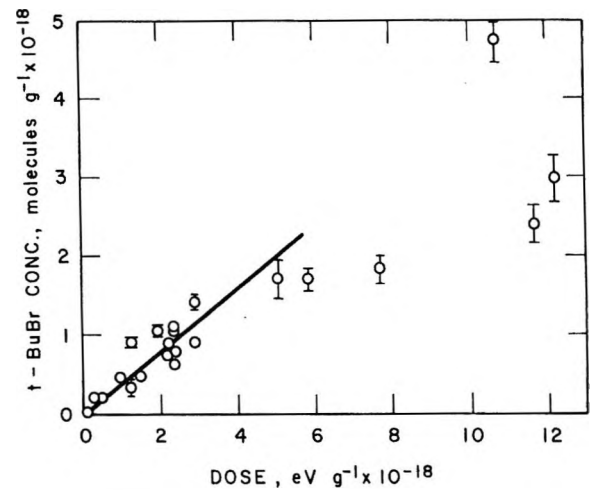


Figure 3. Production of $t$-butyl bromide as a function of dose during the radiolysis of pure isobutyl bromide.

The yields of $t$-butyl bromide, shown in Figure 3, had to be corrected for a thermal reaction occurring during irradiation and the subsequent short interval before analysis. This is a reaction between product isobutylene and hydrogen bromide

$$HBr + (CH_3)_2C{=}CH_2 \longrightarrow (CH_3)_3CBr \qquad (1)$$

In order to investigate this reaction, 9 samples of pure isobutyl bromide were each given the same dose of $\sim 1.2 \times 10^{18}$ eV g$^{-1}$ and kept unopened in the dark at room temperature for various lengths of time (up to 20 hr) prior to analysis. The data for isobutylene concentration as a function of time from the end of irradiation fit a good second-order plot, as expected if reaction 1 occurs in one step with equal initial concentrations of hydrogen bromide and isobutylene. Also there is a good correspondence between the decrease in isobutylene and the increase in $t$-butyl bromide. From the second-order plot we calculate $k_1$ as $6.7 \pm 1.2 \times 10^{-22}$ g molecule$^{-1}$ min$^{-1}$. This value was used to correct all measured $t$-butyl bromide yields for this thermal reaction. For pure isobutyl bromide and the normal dose rate this correction was about 12%.

The $t$-butyl bromide yields also had to be corrected for the change in dose rate due to decay of the source. These corrections were made on the assumption that $G$ is inversely proportional to the square root of the dose rate; experimental support for this assumption is given below. The maximum correction of this sort was 15%.

The error bars associated with a point in Figure 3 and

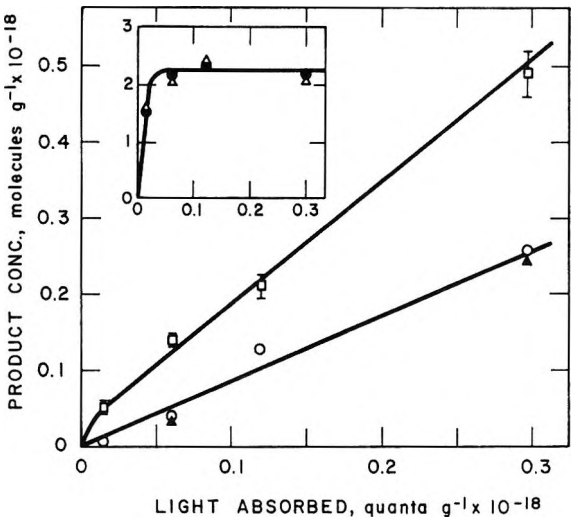


Figure 4. Product yields as functions of light absorbed during the photolysis of pure isobutyl bromide: □, *t*-butyl bromide; ○, isobutane; ▲, 1,2-dibromo-2-methylpropane; △, hydrogen bromide; ●, isobutylene.

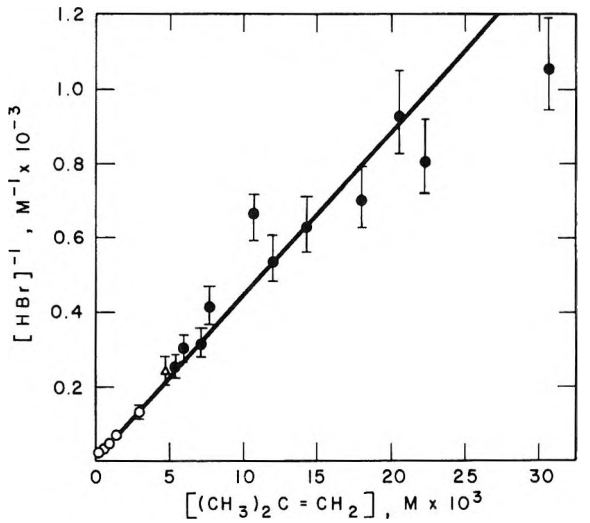


Figure 5. Recripocal of plateau hydrogen bromide concentration as a function of plateau isobutylene concentration for irradiated pure isobutyl bromide or solutions of hydrogen bromide or isobutylene: ○, solutions with added hydrogen bromide; △, pure isobutyl bromide; ●, solutions with added isobutylene.

subsequent figures indicate the estimated uncertainty in a single measurement. The data in Figure 3 show more scatter than can be accounted for by analytical errors and by uncertainties in corrections. $G$(*t*-butyl bromide) is probably constant at 40 ± 10 at doses up to about $4 \times 10^{18}$ eV g$^{-1}$ but appears to decrease at higher doses.

Two other fairly large products were detected in the chromatograms; these were not positively identified but their retention times indicate that they are probably branched monobromooctanes. Their ratio of yields varies between 2 and 8 with no trend as a function of dose. They are produced with a total initial $G$ of 7.5 and then reach a constant concentration of $\sim 0.16 \times 10^{18}$ molecules g$^{-1}$ at a dose of $\sim 3 \times 10^{18}$ eV g$^{-1}$.

Several attempts to find $C_8$ dibromides as products were unsuccessful. Only 1,8-dibromooctane and 2,5-dibromo-2,5-dimethylhexane were available for determination of chromatographic retention times; the former was obtained commercially and the latter was prepared. From the absence of peaks with retention times around those of these two dibromides it is concluded that $G < 0.15$ for any $C_8$ dibromide.

*Photolysis of Pure Isobutyl Bromide.* The behavior of the five major products with time of photolysis is shown in Figure 4. The quantum yields are: isobutane, 0.85 ± 0.18; *t*-butyl bromide, 1.58 ± 0.34 (for the linear portion of the curve); 1,2-dibromo-2-methylpropane, 0.85 ± 0.18. The plateau concentrations of isobutylene and hydrogen bromide are $2.2 \pm 0.1 \times 10^{18}$ and $2.3 \pm 0.2 \times 10^{18}$ molecules g$^{-1}$, respectively; these are the same, within experimental error, as the plateau concentrations observed in the radiolysis of pure isobutyl bromide. The concentrations of isobutylene and hydrogen bromide at the shortest photolysis time (7 sec) represent minimum initial quantum yields of 114. The two products suspected of being monobromooctanes which were found in radiolysis were also found in photolysis and appeared to reach the same plateau concentration of $\sim 0.16 \times 10^{18}$ molecules g$^{-1}$.

*Radiolysis with Added Isobutylene and Hydrogen Bromide.* The concentrations of isobutylene added were 0.63 to $15.2 \times 10^{18}$ molecules g$^{-1}$, or 0.014 to 0.34 mol %. These concentrations include values much less than and much greater than the plateau concentration produced in pure isobutyl bromide. The dose dependence of the five major products was studied at 0.052 and 0.204 mol % isobutylene. It is similar to that in pure isobutyl bromide in that concentrations of isobutane, 1,2-dibromo-2-methylpropane, and *t*-butyl bromide are linear with dose, and concentrations of isobutylene and hydrogen bromide are constant from $0.1 \times 10^{18}$ to the highest dose studied, $3.1 \times 10^{18}$ eV g$^{-1}$. These plateau concentrations of isobutylene and hydrogen bromide in general are different from the initial concentrations.

The minimum and maximum amounts of hydrogen bromide added prior to irradiation were 2.5 and $23 \times 10^{18}$ molecules g$^{-1}$, or 0.056 and 0.52 mol %. The effects of dose were investigated at three of the five additive concentrations used, and again these effects were qualitatively the same as for pure isobutyl bromide.

Because plateau concentrations of isobutylene and hydrogen bromide are reached at very low doses, these should be more significant quantities than the concentrations added before irradiation. Therefore product yields are presented in Figures 5, 6, and 7 as functions of the plateau concentrations of isobutylene for all the experiments with initially added hydrogen bromide or iso-

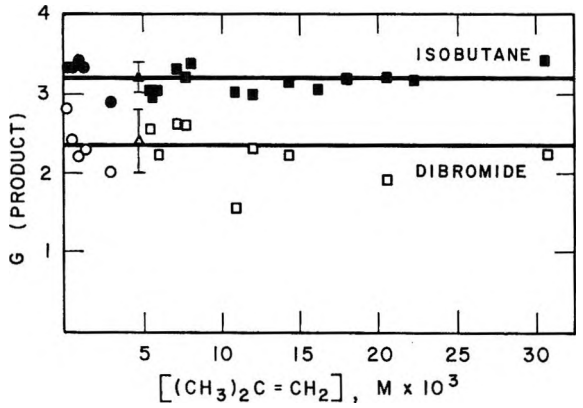


Figure 6. Yields of isobutane and 1,2-dibromo-2-methylpropane as functions of plateau isobutylene concentration for irradiated pure isobutyl bromide or solutions of hydrogen bromide or isobutylene: O●, solutions with added hydrogen bromide; △▲, pure isobutyl bromide; □■, solutions with added isobutylene.

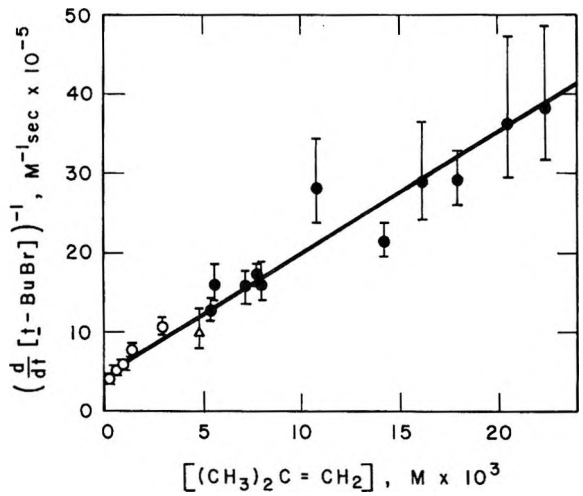


Figure 7. Recipocal of the rate of production of *t*-butyl bromide as a function of plateau isobutylene concentration for irradiated pure isobutyl bromide or solutions of hydrogen bromide or isobutylene: O, solutions with added hydrogen bromide; △, pure isobutyl bromide; ●, solutions with added isobutylene.

butylene, and the points for initially pure isobutyl bromide are included as well. In all cases the net yields of hydrogen bromide and isobutylene are found to be equal within experimental error. In these experiments doses were below the value at which $G$(*t*-butyl bromide) appears to decrease. Figure 5 shows that $[HBr]^{-1}$ is linear in $[(CH_3)_2C{=}CH_2]$ or that the product $[HBr][(CH_3)_2C{=}CH_2]$ is a constant equal to $2.25 \times 10^{-5}$ mol$^2$ l.$^{-2}$. Figure 6 shows that the yields of isobutane and 1,2-dibromo-2-methylpropane are not affected by the addition of isobutylene or hydrogen bromide. Figure 7 is a plot of the reciprocal of the rate of production of *t*-butyl bromide against the plateau concentration of isobutylene, and it gives a straight line with a positive intercept.

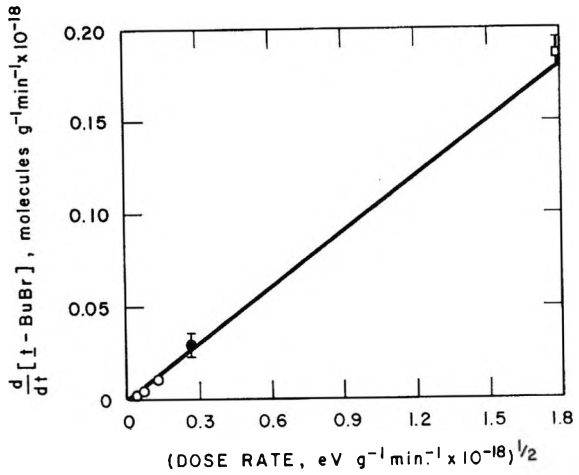


Figure 8. Rate of production of *t*-butyl bromide as a function of the square root of dose rate during the radiolysis or photolysis of pure isobutyl bromide: O, radiolysis at lower dose rates; ●, radiolysis at the normal dose rate; □, photolysis.

*Dose Rate Effects.* The dependence of product yields on dose rate is shown in Table I and Figure 8. Dose rates were measured directly only at the normal dose rate, $0.073 \times 10^{18}$ eV g$^{-1}$ min$^{-1}$, and at $0.80 \times 10^{18}$ eV g$^{-1}$ min$^{-1}$. At both dose rates $G$ (isobutane) = 3.2. It is concluded that $G$ (isobutane) is independent of dose rate, and the rate of isobutane production was used to estimate the dose rate at the other positions used. The rate of formation of isobutane with time during the photolysis experiments corresponds to an effective irradiation dose rate of $3.16 \times 10^{18}$ eV g$^{-1}$ min$^{-1}$, and the photolysis yields are included in the table on this basis. This assumes that the formation of isobutane is a measure of total initiation in both radiolysis and photolysis.

**Table I:** Product Formation as a Function of Dose Rate in Pure Isobutyl Bromide

| $10^{-18}$ Dose rate, eV g$^{-1}$ min$^{-1}$ | $10^{-18}$ Plateau concn, molecules g$^{-1}$ | | |
|---|---|---|---|
| | Isobutylene | Hydrogen bromide | $G$ (dibromide) |
| 0.0018 ± 0.0002 | 2.41 ± 0.13 | 2.0 ± 0.2 | *c* |
| 0.0056 ± 0.0006 | 2.36 ± 0.12 | 2.0 ± 0.2 | *c* |
| 0.016 ± 0.001 | 2.29 ± 0.12 | 2.05 ± 0.2 | c |
| 0.073 ± 0.004[a] | 2.28 ± 0.12 | 2.0 ± 0.3 | 2.4 ± 0.4 |
| 0.80 ± 0.06 | 2.36 ± 0.12 | 2.4 ± 0.2 | 2.0 ± 0.4 |
| 3.16 ± 0.32[b] | 2.2 ± 0.12 | 2.3 ± 0.2 | 3.2 ± 0.3 |

[a] Normal dose rate. [b] Photolysis experiment. [c] Not determined.

Table I shows that the plateau concentrations of isobutylene and hydrogen bromide are independent of dose rate. It shows that $G$ of 1,2-dibromo-2-methylpropane is also dose rate independent; the high value at the

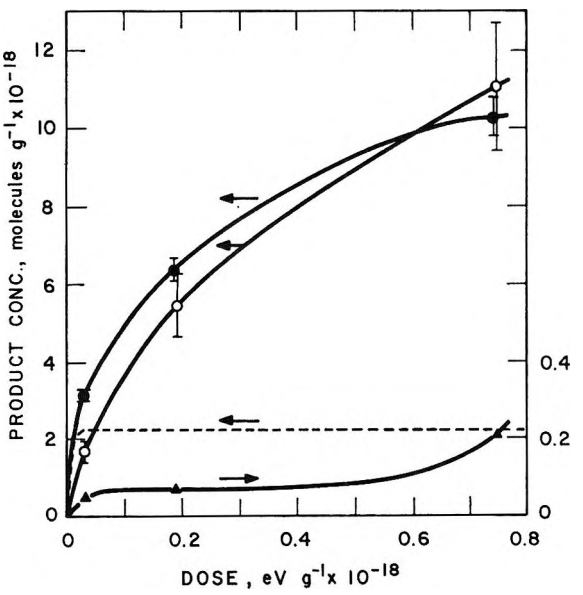


Figure 9. Product yields as functions of dose during the radiolysis of solutions of 1.04 mol % ethylene in isobutyl bromide. Dotted line indicates isobutylene yields during the radiolysis of pure isobutyl bromide: ●, isobutylene; ○, ethyl bromide; ▲, *t*-butyl bromide.

photolysis "dose rate" is related to the fact that dibromide production is equal to isobutane production in photolysis but lower in radiolysis.

Figure 8 shows that the rate of formation of *t*-butyl bromide is approximately proportional to the square root of the dose rate. This conclusion is based almost entirely on the results from the photolysis experiment and the radiolysis experiment at the normal dose rate. At the lower dose rates the measurements of yields due to radiation-induced formation of *t*-butyl bromide are quite imprecise because of the more significant contributions from reaction 1. The behavior shown in Figure 8 is that expected of the product of a radical chain process involving radical–radical termination.

*Radiolysis and Photolysis with Added Ethylene.* Product formation as a function of dose in the radiolysis of solutions containing 1.04 mol % ethylene is shown in Figure 9. Ethyl bromide and isobutylene are produced with comparable yields, and the concentrations of isobutylene achieved are much higher than the plateau concentration reached with pure isobutyl bromide. The yields of *t*-butyl bromide show a complicated behavior with dose. The concentrations present at the lowest dose of $0.03 \times 10^{18}$ eV $g^{-1}$ give the following minimum initial $G$'s: ethyl bromide, 10,000; isobutylene, 5500; *t*-butyl bromide, 155. The $G$'s of isobutane and 1,2-dibromo-2-methypropane are the same as for pure isobutyl bromide.

In one experiment a solution of 1.05% ethylene in isobutyl bromide was photolyzed to a dose of $0.12 \times 10^{18}$ quanta $g^{-1}$. Quantum yields for the principal products are: ethyl bromide, 51; isobutylene, 46; *t*-butyl bromide, 0.7; isobutane, 0.7; 1,2-dibromo-2-methylpropane, 0.7.

*Thermal Addition of Bromine to Isobutylene.* Two experiments were done in which an excess of liquid bromine was injected into a dilute solution of isobutylene in isobutyl bromide that was neither dried nor degassed. 1,2-Dibromo-2-methylpropane, the only product detected, was produced in amounts comparable to the original amounts of isobutylene, and the reaction was complete within 25 sec.

## Discussion

The general nature of a mechanism which will account for the experimental results obtained in the radiolysis and photolysis of isobutyl bromide is dictated by three pieces of evidence from this study. (a) Initial $G$'s and quantum yields are very large. (b) Radiolysis and photolysis of pure isobutyl bromide are very similar in that they result in the same plateau concentrations of isobutylene and hydrogen bromide, and the effects of adding ethylene are similar with both methods of inducing reaction. (c) The dependence of the rate of *t*-butyl bromide formation on the square root of the dose rate is the behavior expected of the product of a chain process with second-order termination. Also significant is the finding by Gallivan that the presence of $5 \times 10^{-3}$ $M$ iodine in isobutyl bromide virtually eliminates the production of isobutylene ($G = 0.15$) and *t*-butyl bromide ($G = 0.22$).[8] These results indicate that a free-radical chain mechanism is operative.

We propose that the following are the important reactions in the radiolysis and photolysis of isobutyl bromide, either pure or with added isobutylene or hydrogen bromide.

$$(CH_3)_2CHCH_2Br \xrightarrow[\text{or } \gamma]{h\nu} (CH_3)_2CHCH_2\cdot + Br\cdot \quad (2)$$

$$(CH_3)_2CHCH_2\cdot + (CH_3)_2CHCH_2Br \longrightarrow (CH_3)_3CH + (CH_3)_2\dot{C}CH_2Br \quad (3)$$

$$(CH_3)_2CHCH_2\cdot + HBr \longrightarrow (CH_3)_3CH + Br\cdot \quad (4)$$

$$Br\cdot + (CH_3)_2CHCH_2Br \rightleftharpoons HBr + (CH_3)_2\dot{C}CH_2Br \quad (5)$$

$$Br\cdot + (CH_3)_2C{=}CH_2 \rightleftharpoons (CH_3)_2\dot{C}CH_2Br \quad (6)$$

$$Br\cdot + (CH_3)_2C{=}CH_2 \rightleftharpoons (CH_3)_2CBrCH_2\cdot \quad (7)$$

$$(CH_3)_2CBrCH_2\cdot + HBr \longrightarrow (CH_3)_3CBr + Br\cdot \quad (8)$$

Termination reactions will be considered below.

In photolysis, reaction 2 is expected to be the only initiation reaction. In radiolysis, primary products are electrons, ions, and excited molecules. Probable subsequent processes include dissociative electron capture, ion–molecule reactions, and decomposition of excited molecules to free radicals. Neutralization processes will give additional free radicals. The net effect of these processes that is of importance for this study is ex-

pected to be the predominant rupture of the C–Br bond, as was found in the radiolysis of *n*-propyl bromide.[6] Therefore the rate of production of isobutane in radiolysis should be a fairly good measure of the rate of initiation. Abstraction of the tertiary hydrogen atom, as in reactions 3 and 5, is very much favored over abstraction of one of the primary hydrogens.[13,14]

The addition of bromine atoms to olefins, as in reactions 6 and 7, is considered to have a very low activation energy.[15] The reversibility of the reaction is important in the mechanism of catalysis of *cis–trans* isomerization.[16] Also, the reverse of reaction 7 has been shown to be important in the radical chain chlorination of *t*-butyl bromide.[17]

Reactions 4, 8, and the reverse of reaction 5 should occur readily since the activation energy of the reaction of methyl radicals with hydrogen bromide in the gas phase has been estimated as 1.5 ± 0.9 kcal mol$^{-1}$.[18] Another possible reaction of $(CH_3)_2CBrCH_2\cdot$ is abstraction from isobutyl bromide

$$(CH_3)_2CBrCH_2\cdot + (CH_3)_2CHCH_2Br \longrightarrow (CH_3)_3CBr + (CH_3)_2\dot{C}CH_2Br \quad (9)$$

However, this reaction should not be important once a plateau concentration of hydrogen bromide is reached, since at the lowest plateau concentration of hydrogen bromide in this work (0.01 mol %) the rate of reaction 8 is calculated to be 20 times that of reaction 9 by taking $k_8 = 5.4 \times 10^6$ mol$^{-1}$ sec$^{-1}$ (as deduced for the reaction of the bromoethyl radical with hydrogen bromide[19]) and $k_9 = 10^8 \exp -(8900/RT)$.[20]

The mechanism will be considered under the following conditions: (a) hydrogen bromide and isobutylene as well as the three chain carriers $(CH_3)_2\dot{C}CH_2Br$, $(CH_3)_2CBrCH_2\cdot$, and Br· have attained steady-state concentrations; (b) the rates of initiation and termination reactions are small by comparison with those of the propagation reactions such as (5); (c) the rate of reaction 8 is much less than that of the reverse of reaction 7. Justification for this last assumption will be given below. In the mechanistic expressions which follow, the symbols A· and B· will be used to designate the radicals $(CH_3)_2\dot{C}CH_2Br$ and $(CH_3)_2CBrCH_2\cdot$, respectively.

Under these conditions the ratios of concentrations of radicals are given by the expressions

$$\frac{[A\cdot]}{[Br\cdot]} = K_6[(CH_3)_2C{=}CH_2] = K_5\frac{[i\text{-BuBr}]}{[HBr]} \quad (I)$$

$$\frac{[A\cdot]}{[B\cdot]} = \frac{K_6}{K_7} \quad (II)$$

$K_5$ ( $= k_5/k_{-5}$), $K_6$, and $K_7$ are equilibrium constants. Equation I leads to the prediction that the product of the plateau concentrations of hydrogen bromide and of isobutylene is a constant ($C$).

$$[(CH_3)_2C{=}CH_2][HBr] = K_5[i\text{-BuBr}]/K_6 = C \quad (III)$$

The behavior predicted by expression III is shown in Figure 5 to be true for all the experiments, which involve a large range of concentrations of isobutylene and hydrogen bromide. The value of $C$ is $2.25 \times 10^{-5}$ mol$^2$ l.$^{-2}$. The observation that the plateau concentrations are the same in photolysis and radiolysis, despite the great difference in rates of initiation, is also in accord with expression III.

The rate of production of *t*-butyl bromide is given simply by eq IV. Since the concentrations of both B· and hydrogen bromide are constant, the rate of production of *t*-butyl bromide should be constant at constant dose rate, as observed. The effect of dose rate on production of *t*-butyl bromide is found by finding the dose rate effect on [B·]. We assume that all termination reactions are diffusion controlled and therefore have approximately the same rate constant, $k_t$. Then setting the rate of initiation, $R_i$, equal to the rate of termination results in the expression

$$\frac{d}{dt}[t\text{-BuBr}] = k_8[B\cdot][HBr] \quad (IV)$$

$$\left(\frac{R_i}{2k_t}\right)^{1/2} = [A\cdot] + [B\cdot] + [Br\cdot] \quad (V)$$

Expressions I, II, IV, and V may be combined to give

$$\left(\frac{d}{dt}[t\text{-BuBr}]\right)^{-1} = \frac{(K_6/K_7) + 1}{k_8C}\left(\frac{2k_t}{R_i}\right)^{1/2} \times [(CH_3)_2C{=}CH_2] + \frac{1}{K_7k_8C}\left(\frac{2k_t}{R_i}\right)^{1/2} \quad (VI)$$

Equation VI requires that the rate of *t*-butyl bromide production vary with the square root of the dose rate at constant isobutylene concentration and that the inverse of the rate of *t*-butyl bromide production vary linearly with the plateau isobutylene concentration at constant dose rate. Figure 8 shows that the former requirement is obeyed within the large experimental error, and Figure 7 shows that the latter requirement is followed over the considerable range of plateau concentrations achieved in this study by initially adding var-

(13) B. A. Thrush, *Progr. React. Kinet.*, **3**, 65 (1965).

(14) G. C. Fettis, J. H. Knox, and A. F. Trotman-Dickenson, *Can. J. Chem.*, **38**, 1643 (1960).

(15) (a) R. J. Cvetanovic, *Advan. Photochem.*, **1**, 115 (1963); (b) F. W. Mitchell, B. C. Green, and J. W. T. Spinks, *Can. J. Chem.*, **38**, 689 (1960); (c) H. Steinmetz and R. M. Noyes, *J. Amer. Chem. Soc.*, **74**, 4141 (1952).

(16) R. B. Cundall, *Progr. React. Kinet.*, **2**, 167 (1964).

(17) W. O. Haag and E. I. Heiba, *Tetrahedron Lett.*, 3683 (1965).

(18) N. A. Gac, D. M. Golden, and S. W. Benson, *J. Amer. Chem. Soc.*, **91**, 3091 (1969).

(19) K. T. Wong and D. A. Armstrong, *Can. J. Chem.*, **47**, 4183 (1969).

(20) P. J. Boddy and E. W. R. Steacie, *ibid.*, **38**, 1576 (1960).

ious amounts of hydrogen bromide or isobutylene. From the slope we obtain

$$\frac{(K_6/K_7) + 1}{k_8 C}\left(\frac{2k_t}{R_i}\right)^{1/2} = 1.52 \times 10^8 \text{ sec l.}^2 \text{ mol}^{-2} \quad \text{(VII)}$$

$K_6/K_7$ may be estimated from expression VII by estimating the other terms. $C$ has been determined experimentally, $R_i$ is estimated from $G$ (isobutane) and the dose rate, and the value chosen for $k_8$ has been given above. The rate constant for termination, $k_t$, is calculated from the Smoluchowski equation[21] as $5.3 \times 10^9$ l. mol$^{-1}$ sec$^{-1}$ by using the measured self-diffusion coefficient of isobutyl bromide[22] and by taking the encounter diameter as 3.5 Å. $K_6/K_7$ is thus calculated to be 74. This estimate is probably only good within a factor of 2, but it may be concluded safely that $K_6/K_7$ is much larger than 1. Then from expression VI and Figure 7 slope/intercept = 323/60 l. mol$^{-1}$ =

$$[(K_6/K_7) + 1]K_7 = K_6 \quad \text{(VIII)}$$

The combination of this value with the experimental $C$ gives an experimental value for $K_5 = (7.9 \pm 2.2) \times 10^{-4}$. It may also be combined with the estimated $K_6/K_7$ to give an approximate value of $K_7$ of 4 l. mol$^{-1}$. $K_6$ is certainly expected to be greater than $K_7$ both because Br·, like H·, adds to isobutylene to preferentially form the tertiary radical,[15a] and because $k_{-7}$ is probably larger than $k_{-6}$ because a weaker tertiary carbon–bromine bond rather than a primary one is broken in the decomposition.

An estimate of $E_{-6}$, the activation energy for decomposition of $(CH_3)_2\dot{C}CH_2Br$, can be obtained from the above value of the equilibrium constant $K_6$. The forward reaction should be diffusion controlled and hence should have about the same rate constant as the termination reaction, $5.3 \times 10^9$ $M^{-1}$ sec$^{-1}$. By further taking $A_{-6} = 10^{13.5}$ sec$^{-1}$, $E_{-6}$ is calculated as 8.5 kcal mol$^{-1}$. This agrees well with the value of 7.7 kcal mol$^{-1}$ estimated by Wong and Armstrong[19] for the activation energy of decomposition of the bromoethyl radical.

An estimate of the validity of the assumption that $k_8[B\cdot][HBr] \ll k_{-7}[B\cdot]$ can now be made. $E_{-7}$ should be less than $E_{-6}$ for the reason discussed above. However, assumptions that $E_{-7} = E_{-6} = 8.5$ kcal mol$^{-1}$, $A_{-7} = 10^{13}$ sec$^{-1}$ and $k_8 = 5.4 \times 10^6$ l. mol$^{-1}$ sec$^{-1}$ lead to the conclusion that at the highest hydrogen bromide concentration used in this work (0.52 mol %), reaction 8 and the reverse of reaction 7 proceed at the same rate. A more realistic (smaller) choice for $E_{-7}$ makes $k_8[B\cdot][HBr] \ll k_{-7}[B\cdot]$.

Thus far we have considered only one mechanism, and this seems to be in accord with the experimental observations. However, there are at least two other reaction paths which could lead to the formation of $(CH_3)_2CBrCH_2\cdot$ and thence to *t*-butyl bromide. (1) Bromine atoms may add to isobutylene to give exclusively the tertiary radical $(CH_3)_2\dot{C}CH_2Br$, and an equilibrium may exist between $(CH_3)_2\dot{C}CH_2Br$ and $(CH_3)_2CBrCH_2\cdot$ involving an intraradical shift

$$(CH_3)_2\dot{C}CH_2Br \rightleftharpoons (CH_3)_2CBrCH_2\cdot \quad (7')$$

Such a reaction has been proposed in the photoinitiated radical chain chlorination of propyl and butyl bromides at −78°,[23] though later work on the same systems favors a bromine atom elimination–readdition sequence.[17] (2) The abstraction of hydrogen from isobutyl bromide and the addition of bromine atoms to isobutylene may result in a single radical R· which is either a bridged bromoalkyl radical or a rapidly resonating bromoalkyl radical. With this mechanism, reactions 6 and 7 would be replaced by 6′ and 8 by 8′

$$Br\cdot + (CH_3)_2CH_2CH_2Br \longrightarrow HBr + R\cdot \quad (6')$$

$$R\cdot + HBr \longrightarrow Br\cdot + \alpha(CH_3)_2CHCH_2Br + (1 - \alpha)(CH_3)_3CBr \quad (8')$$

Evidence for the existence of such bridged haloalkyl radicals has come from studies of free radical halogenations.[24]

It is easily shown that both of these mechanisms lead to expressions that are quite analogous to III, VI, and VII.[2] That is, our data cannot differentiate between elimination–readdition, intraradical transfer, or bridged radical mechanisms. If the intraradical shift mechanism is assumed, then the slope of Figure 7 should be given by

$$\frac{K_7' + 1}{k_8 C}\left(\frac{2k_t}{R_i}\right)^{1/2}$$

from which we estimate $K_7' = 74$. This is quite different from the conclusion by Takehisa, Levey, and Willard that the equilibrium constant for the interconversion $CH_3\dot{C}HCH_2Cl \rightleftharpoons CH_3CHClCH_2\cdot$ is approximately 0.4.[5] However, as the authors point out, this conclusion is based on the questionable assumption that both radicals react with HCl at the same rate.

*Radiolysis and Photolysis of Ethylene Solutions.* The additional reactions expected because of the added ethylene are

$$Br\cdot + C_2H_4 \rightleftharpoons C_2H_4Br\cdot \quad (10)$$

$$C_2H_4Br\cdot + (CH_3)_2CHCH_2Br \longrightarrow C_2H_5Br + (CH_3)_2\dot{C}CH_2Br \quad (11)$$

$$C_2H_4Br\cdot + HBr \longrightarrow C_2H_5Br + Br\cdot \quad (12)$$

These additional reactions complicate considerably the

(21) A. M. North, "The Collision Theory of Chemical Reactions in Liquids," John Wiley and Sons, New York, N. Y., 1964, p 68.

(22) L. H. Stein and P. C. Carman, *J. S. Afr. Chem. Inst.*, **9**, 55 (1956).

(23) P. S. Skell, R. G. Allen, and N. D. Gilmour, *J. Amer. Chem. Soc.*, **83**, 504 (1951).

(24) (a) W. Thaler, *ibid.*, **85**, 2607 (1963); (b) P. S. Skell, D. L. Tuleen, and P. D. Readio, *ibid.*, **85**, 2849 (1963).

mechanistic expressions. We have not been able to simplify them, and thus can make only a qualitative comparison between the results and the behavior predicted by the mechanism. The presence of ethylene is expected to result in an increase in isobutylene yields because of the protective effect of the ethylene, and in a chain production of ethyl bromide. As the dose and therefore isobutylene concentration increase, the differential $G$'s for isobutylene and ethyl bromide should both decrease. The results shown in Figure 9 for the radiolysis and given in Results for the photolysis are in agreement with these mechanistic conclusions. They also indicate that ethylene is less reactive than isobutylene toward bromine by the fact that in Figure 9 the isobutylene concentration is near a plateau at the highest dose even though the concentration of ethylene is still about 3 times that of isobutylene. In a study of the photolytic addition of hydrogen bromide to a number of olefins, Abell also found isobutylene more reactive than ethylene toward bromine atoms.[25]

*Termination.* The only measured product that is almost certainly exclusively a termination product is 1,2-dibromo-2-methylpropane. If this is the only termination product and the isobutane yield is truly a measure of initiation, then the yields of 1,2-dibromo-2-methylpropane and of isobutane should always be equal, within experimental error. In fact the yields of isobutane are always larger, but only slightly so. Further, there is no change (within the experimental error of 15–20%) in $G$ of 1,2-dibromo-2-methylpropane over the entire range of hydrogen bromide and isobutylene concentrations in this work. These facts pose a difficulty. The ratio $[A\cdot]/[Br\cdot]$ at steady state can be calculated from eq I for all experiments except those with added ethylene. By using our experimental value for $K_5$ we calculate that this ratio varies from 10 to 0.15 in going from minimum to maximum hydrogen bromide concentration. The ratio $[A\cdot]/[B\cdot]$ should remain constant at 74 ± 40. Therefore, by assuming that all termination reactions have about the same rate constant, we conclude that termination should vary from predominantly A–A at low hydrogen bromide concentrations to predominantly Br–Br at high concentrations with A–Br termination being most important at intermediate concentrations. These reactions are

$$2Br\cdot \longrightarrow Br_2 \quad (13)$$

$$2(CH_3)_2\dot{C}CH_2Br \longrightarrow \text{dimer} \quad (14)$$

$$\longrightarrow \text{1,2-dibromo-2-methylpropane} + (CH_3)_2C{=}CH_2 \quad (15)$$

$$\longrightarrow (CH_3)_2CHCH_2Br + CH_2BrC(CH_3){=}CH_2 \quad (16)$$

$$\longrightarrow (CH_3)_2CHCH_2Br + (CH_3)_2C{=}CHBr \quad (17)$$

$$(CH_3)_2\dot{C}CH_2Br + Br\cdot \longrightarrow (CH_3)_2CBrCH_2Br \quad (18)$$

The difficulty is resolved if two assumptions are true. (a) Any molecular bromine formed by reaction 13 reacts quickly and completely with isobutylene to give 1,2-dibromo-2-methylpropane. That this assumption is substantially true is indicated by our experiments and by a report that bromine adds in the dark to isobutylene dissolved in carbon tetrachloride to produce 1,2-dibromo-2-methylpropane (85%) and methallyl bromine (15%).[26a] The reaction may be accelerated by hydrogen bromide.[26b] (b) In the majority of reactive A–A encounters, disproportionation involving bromine atom transfer occurs—*i.e.*, reaction 15 is much more important than reactions 14, 16, and 17. There is little information available in the literature on ratios of disproportionation to combination of haloalkyl radicals. A recent gas-phase value for this ratio for *t*-butyl radicals, to which $(CH_3)_2\dot{C}CH_2Br$ is analogous, is 2.32.[27] For unsubstituted alkyl radicals these ratios are higher in the liquid than in the gas phase.[28] Further, Heicklen has shown that chlorine substitution can increase the ratios substantially, and chlorine atom transfer can be much more favorable than hydrogen atom transfer in the disproportionation.[29] Thus, he found that in the reaction of a chloroethyl with a chlorobutyl radical in the gas phase, disproportionation with chlorine atom transfer is 4.5 times faster than combination and 9.6 times faster than disproportionation with hydrogen atom transfer. This effect might be even greater with bromoalkyl radicals since C–Br bonds are weaker than C–Cl bonds. Therefore it is entirely possible that reactions 14, 16, and 17 are unimportant by comparison with reaction 15.

*Acknowledgment.* The authors are very grateful to Dr. G. R. McMillan for many helpful discussions of this work.

(25) P. I. Abell, *Trans. Faraday Soc.*, **60**, 2214 (1964).

(26) (a) P. S. Juneja and E. M. Hodnett, *J. Amer. Chem. Soc.*, **89**, 5685 (1967); (b) S. V. Anantakrishnan and C. K. Ingold, *J. Chem. Soc.*, 984 (1935).

(27) J. O. Terry and J. H. Futrell, *Can. J. Chem.*, **46**, 664 (1968).

(28) (a) P. S. Dixon, A. P. Stefani, and M. Swarz, *J. Amer. Chem. Soc.*, **85**, 2551 (1963); (b) H. A. Gillis, *J. Phys. Chem.*, **71**, 1089 (1967).

(29) J. Heicklen, *J. Amer. Chem. Soc.*, **87**, 445 (1965).

# Electron Spin Resonance Study of Elementary Reactions of Fluorine Atoms[1]

by Edward L. Cochran, Frank J. Adrian, and Vernon A. Bowers

*Applied Physics Laboratory, The Johns Hopkins University, Silver Spring, Maryland 20910* *(Received December 4, 1969)*

Electron spin resonance (esr) spectroscopy is used to detect the free radical products of the reactions of fluorine atoms with various simple molecules in dilute solid solutions of the reactants in argon at 4°K. The fluorine atoms are produced by photolytic decomposition of $F_2$, and the reactant molecules include some of the simplest saturated and unsaturated hydrocarbons. In these systems a fluorine atom tends to abstract a hydrogen atom from a saturated molecule (such as $CH_4$, $C_2H_6$, $n$-$C_3H_8$, and $CH_3OH$) and to add to a double bond in an unsaturated molecule (such as CO, $C_2H_2$, and $C_6H_6$); however, hydrogen abstraction may compete with double-bond addition in the cases of $C_6H_6$ and $C_2H_2$. Reaction of F atoms with $n$-propane yields the methyl and isopropyl radicals, suggesting that the expected $n$-propyl radical is formed in an excited state which decomposes to give the methyl radical. The *trans*-fluorovinyl and fluorocyclohexadienyl radicals are observed for the first time and values of their fluorine hyperfine structure constants are determined.

## I. Introduction

Elementary reactions of fluorine atoms have not been extensively studied, due in part to their very great reactivity with most substrates and in part to the lack of suitable atom precursors for photochemical work. These reactions are of considerable chemical interest, however, and the free radical products of such reactions are of interest as subjects for molecular structure investigations. For this reason we have explored the utility of the matrix isolation technique for such studies.[2]

In this method the reaction of interest is carried out in a dilute solid solution of the reactants in an inert matrix at low temperatures. Under suitable conditions very reactive fluorine atom precursors such as $F_2$ can be used without complicating molecular reactions, fluorine atoms can be generated photochemically, and the initial product(s) of the reaction between the atom and a second molecule can be stabilized before undergoing further reaction.

In this paper we shall discuss the results of electron spin resonance (esr) studies of the free radical products of the reactions of F atoms with a variety of molecules including some of the simplest saturated and unsaturated hydrocarbons. In favorable cases, esr spectroscopy permitted the free radical products to be identified and the values of some of their fluorine and proton hyperfine splitting constants to be determined. Identification of the free radical products of various reactions verified the existence of some elementary reactions which are probably important steps in complex gas-phase reactions of fluorine and its compounds.

## II. Experimental Section

The general procedure in these experiments was to deposit on a sapphire rod at 4°K a mixture of argon, the reactant gas, and a small amount of $F_2$ or, occasionally, $OF_2$. The concentrations of reactant gas used ranged from 1 to 10%, and the $F_2$ concentration varied from 0.1 to 1%. When $F_2$ was used, it was deposited on the rod simultaneously with the other components, but through an independent stainless steel inlet line to avoid premature mixing and gas-phase reactions (as discussed in the next section, thermal gas-phase reactions sometimes occurred despite this precaution). The sample was then photolyzed for varying periods of time, usually of the order of a few hours, using a 100 W medium pressure mercury lamp with a Pyrex envelope. Other general features of these experiments such as the cryostat, the sample deposition system, and the esr spectrometer have been described previously.[3]

## III. Results and Discussion

The fluorine atom reactions studied, together with those free radical products which could be identified from their esr spectra, are listed in Table I. It is likely, of course, that this list of radical products is incomplete since some reaction products contain esr lines which could not be assigned to a specific radical, and there is always the possibility of radical products whose esr spectra are too broad and weak to be detected.

In addition to their free radical products, nearly all the photolytic systems listed in Table I gave an anomalous esr line which probably is not due to a simple molecular free radical. The general appearance of this line, which is shown in Figure 1 as it appears with the FCO radical in the photolysis products of $F_2$ in a 20% CO, 80% Ar matrix,[4] is the same in all systems. However, the separation between its high-and low-field peaks

(1) Work supported by the Naval Ordnance Systems Command, U. S. Department of the Navy, under Contract NOw 62-0604-c.

(2) Previous studies of fluorine atom reactions using the matrix isolation technique include: F. J. Adrian, E. L. Cochran, and V. A. Bowers, *J. Chem. Phys.*, **43**, 462 (1965); M. E. Jacox and D. E. Milligan, *ibid.*, **46**, 184 (1967).

(3) (a) C. K. Jen, S. N. Foner, E. L. Cochran, and V. A. Bowers, *Phys. Rev.*, **112**, 1169 (1958); (b) S. N. Foner, E. L. Cochran, V. A. Bowers, and C. K. Jen, *J. Chem. Phys.*, **32**, 963 (1960).

(4) E. L. Cochran, F. J. Adrian, and V. A. Bowers, *ibid.*, **44**, 4626 (1966).

**Table I:** Fluorine Atom Reactions Studied[a]

| Reaction | Free radical products |
|---|---|
| $F + O_2$ | $FO_2$ |
| $F + CO$ | FCO |
| $F + CH_4$ | $CH_3$ |
| $F + C_2H_6$ | $C_2H_5$ |
| $F + n\text{-}C_3H_8$ | $CH_3$, $i\text{-}C_3H_7$ (?) |
| $F + CH_3OH$ | $CH_2OH$ |
| $F + C_2H_4$ | Unidentified radical(s) present |
| $F + C_2D_2$ | *trans*-CD=CDF, C≡CD (?) |
| $F + C_6D_6$ | $C_6D_6F$, $C_6D_5$ |

[a] (?) Denotes a product whose identification is somewhat tentative.

varies somewhat and the resolution of these peaks varies a great deal from one system to another.

The ease of formation of this anomalous paramagnetic species also varies considerably from one system to another. Generally this resonance is more readily observed in matrices containing unsaturated molecules (CO, $C_6H_6$, $C_2H_4$, but not $O_2$[5]) than it is in matrices containing alkanes. The strength and ease of appearance of this line is greater the greater the concentration for any given reactant. At very low concentrations of $F_2$ and reactant, the line forms only on warm-up following photolysis of the sample. At the higher concentrations of the more reactive molecules, the sample exhibits this resonance even prior to photolysis, apparently as a result of a thermal reaction occurring during deposition. Table II illustrates these relationships. The tendency for samples containing $F_2$ to undergo thermal reactions during deposition, or to give the broad anomalous resonance on photolysis, severely limited the concentrations of reactants that could be used. Consequently, the esr spectra of the free radical products of some of these reactions were relatively weak.

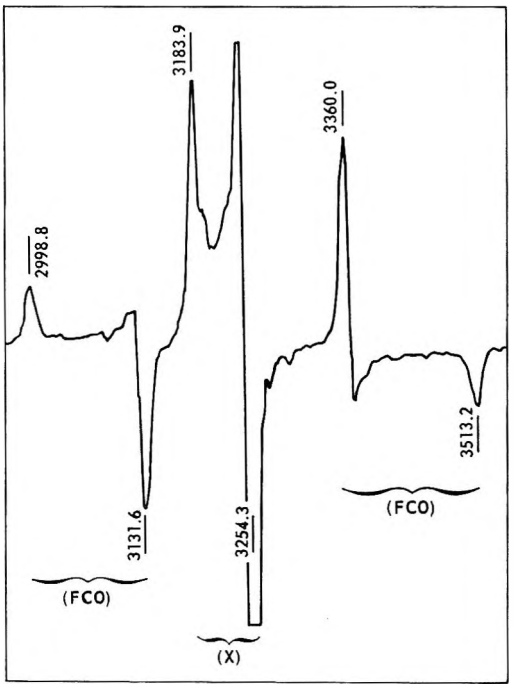


Figure 1. Esr spectrum of the products of the photolysis of $F_2$ in a 20% CO–80% Ar matrix. The anomalous complex line (×) appears along with the FCO radical in this spectrum.

**Table II:** Effect of Concentration of Reactants on Observed Reaction Products in Argon Matrix

| Reactant | Concn, % | $F_2$ concn, % | Product observed: Prior to photolysis | Product observed: After photolysis | Product observed: After warming |
|---|---|---|---|---|---|
| $C_2H_6$ | 1 | 0.1 | None | $C_2H_5$ | AL[a] |
| $C_2H_6$ | 1 | 1.0 | None | Initial: $C_2H_5$ Ultimate: AL | AL |
| $C_2H_6$ | 10 | 1.0 | $C_2H_5$ | AL | AL |
| $C_2H_4$ | 1 | 0.1 | None | AL | AL |
| $C_2H_4$ | 10 | 1.0 | AL | AL | AL |

[a] AL indicates the broad, usually very strong, unidentified line described in the text.

The absence of hyperfine structure (hfs) in the anomalous spectrum despite the fact that it is formed in systems which usually contain both fluorine and hydrogen nuclei strongly suggests that it cannot be due to a simple paramagnetic molecule. This conclusion is supported by the fact that this spectrum appears in such a wide variety of chemical systems. It seems likely that the anomalous esr spectrum is due to an aggregate of paramagnetic species in which the unpaired electrons are sufficiently delocalized to average out the individual nuclear hfs (exchange narrowing[6]). Further study will be required, however, to verify this hypothesis.

Of the free radical products listed in Table I, both FCO[4] and $O_2F$[7] have been discussed in detail previously. The other reactions and their products will be discussed in this paper.

*A. Saturated Molecules.* Inspection of Table I shows that the reaction of an F atom with a saturated hydrocarbon or similar molecule generally results in abstraction of an H atom from the saturated hydrocarbon. This general principle is illustrated by the following discussion of specific reactions.

*1. $F + CH_4$.* The esr spectrum of the products of the photolysis of $F_2$ (0.1%)–$CH_4$ (10%)–Ar (90%) is

(5) The reaction of F with $O_2$ to form $O_2F$ is apparently very efficient judging from the fact that this is the only radical observed in systems which contain even a trace of $O_2$, *cf.* R. W. Fessenden and R. H. Schuler, *J. Chem. Phys.*, **44**, 434 (1966).

(6) G. E. Pake, "Paramagnetic Resonance," W. A. Benjamin, Inc., New York, N. Y., 1962, pp 93–95.

(7) F. J. Adrian, *J. Chem. Phys.*, **46**, 1543 (1967).

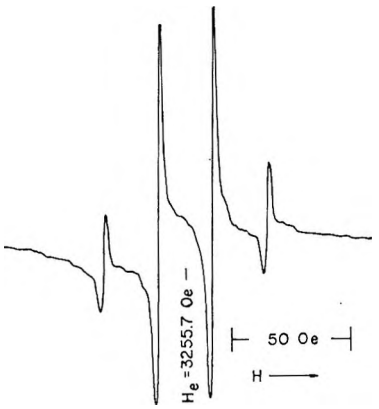


Figure 2. Esr spectrum at 4°K of the products of the photolysis of $F_2$ in $CH_4$–Ar. In this and subsequent figures, $H_e$ denotes the magnetic field strength for resonance of the free electron.

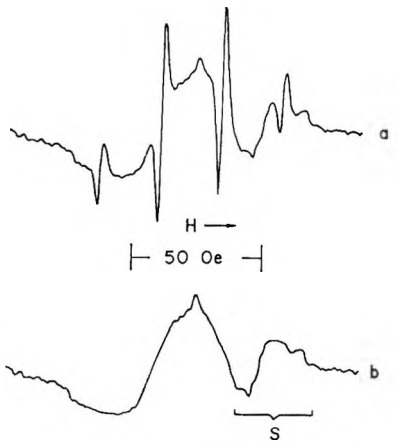


Figure 3. (a) Esr spectrum at 40°K of the products of the photolysis of $F_2$ in $CH_4$–Ar. (b) Spectrum remaining after the sharp line $CH_3$ spectrum is subtracted out of (a). S denotes a resonance in the sapphire rod on which the samples are deposited.

shown in Figure 2. The sharp-line quartet is the methyl radical[3a] whose production is attributed to the reaction

$$F + CH_4 = CH_3 + HF$$

The $CH_3$ spectrum is superimposed on a broad line, but we cannot tell whether this broad line is due to clustered $CH_3$ radicals whose lines are broadened by dipolar interactions, to another free radical, or is the precursor of the anomalous esr line which appeared when the sample was warmed.

Upon warming this sample to 35°K, the anomalous esr line appeared, *cf.* Figure 3, and at 45°K it is the only line in the system. (The line marked S in Figure 3 is a resonance in the sapphire rod which is saturation broadened at 4°K and which, therefore, appears only at low microwave power or high temperature. Since it is not part of the photolytic system, it will not be discussed further, and in most cases it has been subtracted out of other spectra in which it appeared.) It will be seen that this line is somewhat narrower in terms of separation between the high-and low-field peaks, is less well resolved, and is very much weaker than the anomalous esr line shown in Figure 1.

*2.* $F + C_2H_6$. The esr spectrum of the products of the photolysis of $F_2(0.1\%)$–$C_2H_6(1\%)$–Ar(99%) is shown in Figure 4. Comparison with the spectrum obtained by the photolysis of ethyl iodide in argon showed that this spectrum is due to the ethyl radical.[8] The formation of this radical is attributed to the reaction

$$F + C_2H_6 = C_2H_5 + HF$$

It is noteworthy in connection with the reaction of F atoms with *n*-propane, which will be discussed next, that no hydrogen atoms or $CH_3$ radicals were found in this photolytic system.

The broad background line is considerably weaker in this case than it was in the previous case where $F_2$ was photolyzed in $CH_4$–Ar. Possibly this is because the al-

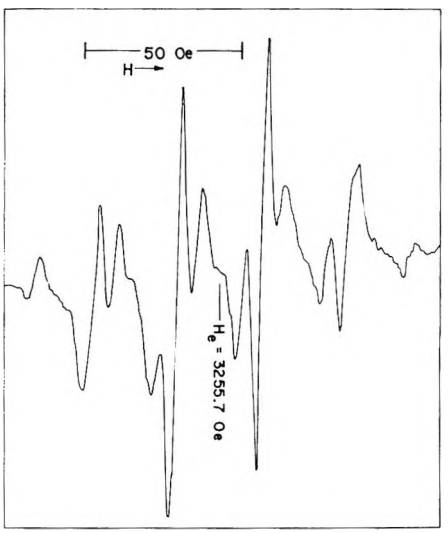


Figure 4. Esr spectrum at 4°K of the products of the photolysis of $F_2$ in $C_2H_6$–Ar.

kane concentration was ten times lower in this system. On warm-up, however, the anomalous esr line, very similar in appearance to that shown in Figure 3, began to grow in at 20°K, and at 40°K it was the only line in the spectrum.

*3.* $F + n\text{-}C_3H_8$. The reaction of fluorine atoms with *n*-propane has interesting complications not observed in the reactions of F atoms with methane and ethane. The esr spectrum of the products of the photolysis of $OF_2(1\%)C_3H_8$–(25%)–Ar(74%) is shown in Figure 5. (An identical spectrum was produced by the photolysis of $F_2$ in $n$-$C_3H_8$–Ar except that in this system, the spectrum was complicated by the presence of the anomalous esr line immediately after photolysis.) This spectrum consists of four sharp lines with a spacing of

(8) E. L. Cochran, F. J. Adrian, and V. A. Bowers, *J. Chem. Phys.*, **34**, 1161 (1961).

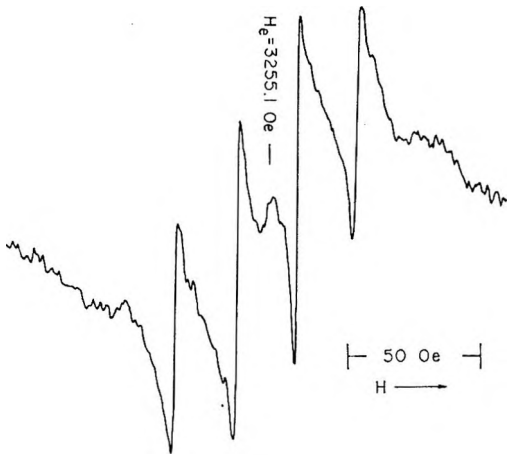


Figure 5. Esr spectrum at 4°K of the products of the photolysis of $OF_2$ in $n$-$C_3H_8$–Ar.

23 Oe, which are due to the methyl radical, superimposed on a broad symmetrical spectrum which possesses a certain amount of structure. Comparison of this spectrum with the spectrum of the $n$-propyl radical produced by the photolysis of $n$-propyl iodide in argon[8] shows that little if any $n$-propyl radical is present in this spectrum. That part of the spectrum which remains after the sharp-line $CH_3$ spectrum has been subtracted out is shown in Figure 6a. It will be shown momentarily that part of this spectrum may be due to the isopropyl radical.

We considered the following three reactions for the production of $CH_3$ in the reaction of F atoms with $n$-$C_3H_8$

$$F + n\text{-}C_3H_8 \longrightarrow HF + [n\text{-}C_3H_7^*] \longrightarrow [CH_3 + C_2H_4] \quad (1)$$

$$F + n\text{-}C_3H_8 \longrightarrow HF + [i\text{-}C_3H_7^*] \longrightarrow [CH_3 + C_2H_4] \quad (2)$$

$$F + n\text{-}C_3H_8 \longrightarrow CH_3 + CH_2FCH_3 \quad (3)$$

Here, an asterisk denotes a species in an excited electronic state. We believe that the first mechanism is the most likely. The second mechanism requires that migration of a hydrogen atom from one carbon to another accompany or follow the splitting off of a $CH_3$ radical from the excited isopropyl radical. The activation energy for this process should be considerably greater than the activation energy for the decomposition of an excited $n$-propyl radical into a methyl radical and ethylene. The third mechanism is considered unlikely because the corresponding reaction was not observed in the reaction of F atoms with ethane.

That part of the esr spectrum which remains after the $CH_3$ lines have been subtracted out, *cf.* Figure 6a, consists of six rather broad lines plus a weak line in the center, all of which are superimposed on a very broad approximately symmetric line. This broad line is

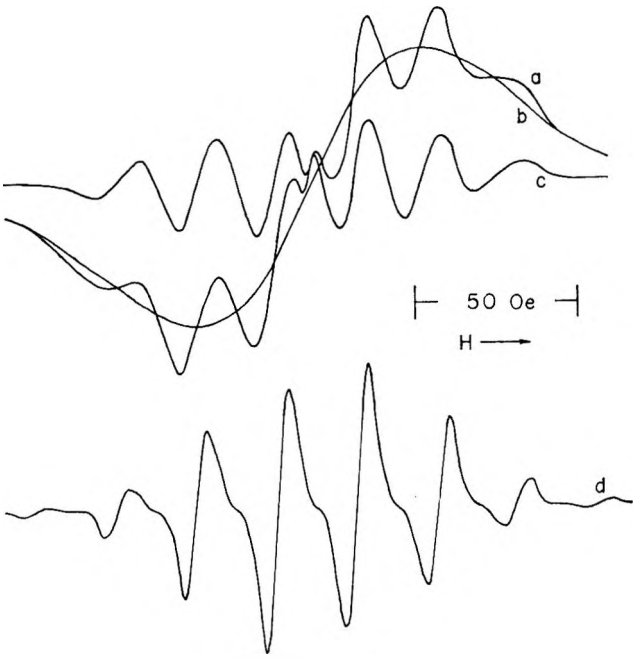


Figure 6. (a) Esr spectrum remaining after the sharp line $CH_3$ spectrum is subtracted out of the spectrum in Figure 5. (b) Estimate of the broad unresolved component of spectrum (a). (c) Spectrum which remains after the broad line (b) is subtracted from the spectrum (a). (d) Computed spectrum of the isopropyl radical rigidly trapped in a polycrystalline medium. For simplicity, the noise has been artificially deleted from these spectra.

shown in Figure 6b and the spectrum which remains after both the sharp $CH_3$ lines and the broad line have been subtracted out is shown in Figure 6c. We may interpret the spectrum shown in Figure 6a in at least two different ways. Since the strongest four of the resolved lines in this spectrum are at the positions of the $CH_3$ lines, it is possible that they are due to $CH_3$ radicals whose lines are broadened in some way, such as by dipolar interactions. The broad structureless line, *cf.* Figure 6b, is perhaps similar in origin to the broad line observed in the (F + $CH_4$) system, *cf.* Figure 2. This interpretation has the disadvantage that it does not account for the two resolved lines at the high- and low-field ends of the spectrum. It does not account for the weak center line either but this could be due to a trace of some other paramagnetic substance. Alternatively, we may regard the six resolved lines (neglecting the weak center line) as belonging to the same radical, in which case we note that the positions and relative intensities of these six lines are compatible with the spectrum of the isopropyl radical observed by Fessenden and Schuler,[9] provided that in the solid matrix allowance is made for line broadening by the anisotropic part of the $\alpha$ proton hfs splitting. A calculation of the esr spectrum expected for $i$-$C_3H_7$ in a rigid matrix gave the result shown in Figure 6d;[10] the agreement between this calculated

(9) R. W. Fessenden and R. H. Schuler, *J. Chem. Phys.*, **39**, 2147 (1963).

spectrum and the six-line spectrum shown in Figure 6c is quite good. Thus, it is strongly indicated that the isopropyl radical is a product of the reaction of F atoms with *n*-propane.

*4. F + $CH_3OH$.* Photolysis of $F_2$(0.1%)–$CH_3OH$ (1%)–Ar(99%) gave the spectrum shown in Figure 7. The high-field portion of this spectrum is obscured by the presence of the sapphire rod resonance, denoted as S in Figure 7; otherwise, the spectrum is a triplet in which the center line is strong and sharp and the outer lines are weak and complex. This triplet is the characteristic hfs multiplet of the $\alpha$ protons in radicals of the form R–$CH_2$ when trapped in a polycrystalline matrix provided that some rotation or reorientation of these $\alpha$ protons makes them magnetically equivalent.[8] Since the work of Livingston and Zeldes[11] on the isotropic esr spectrum of $CH_2OH$ has shown that the hfs splitting due to the OH proton is very small, we conclude that our spectrum is due to this radical. We cannot tell from our results, however, whether the motion of the $\alpha$ protons which renders them magnetically equivalent is an internal rotation or reorientation about the CO bond or a rotation of the entire molecule about the CO bond.

Production of the $CH_2OH$ radical is, of course, attributed to the reaction

$$F + CH_3OH \longrightarrow CH_2OH + HF$$

The absence from our spectrum of lines attributable to $CH_3O$ does not, however, prove that the reaction does

$$F + CH_3OH \longrightarrow CH_3O + HF$$

not occur in this system. If we neglect momentarily the possibility of Jahn–Teller distortion of the trigonally symmetric $CH_3$ group, the $CH_3O$ radical has a degenerate electronic ground state, and consequently, a nonvanishing component of the electronic orbital angular momentum along the CO bond. Attempts to observe the esr spectra of electronically degenerate radicals in polycrystalline inert gas matrices have failed, presumably because the extremely anisotropic electronic $g$ factor of such radicals causes extreme line broadening.[3a] Although Jahn–Teller distortions of the $CH_3$ group and/or interactions of the radical with its surroundings may lift the ground-state degeneracy, the esr lines are still likely to be unobservably broad.[12]

From the complex low-field line of the triplet spectrum in Figure 7 we get the following values for the "averaged" $\alpha$ proton hfs tensors: $|A_{\parallel}| = 25$ and $|A_{\perp}| = 16$ Oe where the parallel direction is the axis of rotational averaging of the $\alpha$ proton hfs tensors. (The low-field edge of this complex line corresponds to the magnetic field oriented along the symmetry axis of the "averaged" hfs tensor whereas its high-field peak corresponds to the magnetic field perpendicular to this symmetry axis.)[8] If we assume that $A_{\parallel}$ and $A_{\perp}$ have the same sign, then we get 19 Oe for the isotropic $\alpha$ proton hfs constant which is in good agreement with the value of 19.2 Oe, which is obtained by extrapolating to 4°K the accurate temperature-dependent values obtained for this radical by Livingston and Zeldes.[11] The anisotropic part of the "averaged" tensor is in good agreement with the values calculated[8] using the components of the $\alpha$ proton hfs tensor measured in the CH(COOH)$_2$ radical.[13] The structure on the center line of the spectrum could be due to an OH proton hfs splitting of about 2 Oe, but there are other possible explanations for this structure such as a slight anisotropy in the electronic $g$ factor of this radical.

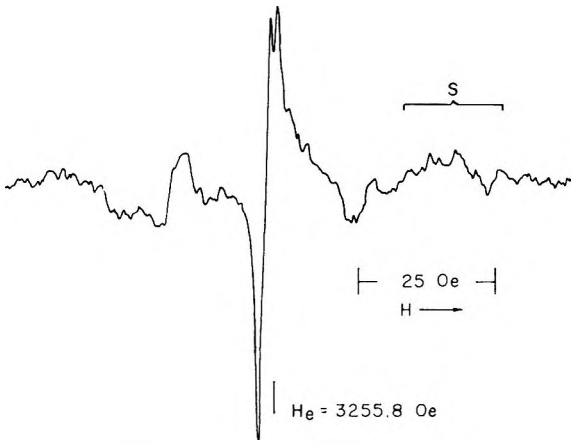


Figure 7. Esr spectrum at 4°K of the products of the photolysis of $F_2$ in $CH_3OH$–Ar. S denotes a resonance in the sapphire rod.

*B. Unsaturated Molecules.* The previous results indicated that the reaction of an F atom with a saturated molecule is likely to result in abstraction of an H atom to form HF and a free radical. When an F atom reacts with an unsaturated molecule, however, it is likely that the F atom will add to a multiple bond. Our results indicate that such addition reactions do occur, but that hydrogen abstraction also may occur in some cases. Of course, in reactions involving unsaturated diatomic molecules, such as the previously studied CO and $O_2$, addition to the double bond is the only possibility.

*1. F + $C_2H_4$.* Although this system was studied under a wide range of experimental conditions, such as concentration of $F_2$ and $C_2H_4$ in the matrix, deposition rate, and photolysis time, no radical products of this reaction could be positively identified. The $F_2$–$C_2H_4$ system was more prone to undergo thermal reaction during deposition than any other system studied. When such thermal reactions occurred, the broad anomalous esr line was present immediately after deposition

(10) This calculation is the same as that described in ref 8 except that the $\beta$ proton hfs constant is taken to be 24.7 Oe following ref 9 instead of 32 Oe.

(11) R. Livingston and H. Zeldes, *J. Chem. Phys.*, **44**, 1245 (1966).

(12) M. G. Townsend and S. I. Weissman, *ibid.*, **32**, 309 (1960); J. H. Freed, *ibid.*, **43**, 1427 (1965).

(13) H. M. McConnell, C. Heller, T. Cole, and R. W. Fessenden, *J. Amer. Chem. Soc.*, **82**, 766 (1960).

of the sample, and subsequent photolysis did not produce any observable changes in the spectrum, *cf.* Table II. At low $F_2$–$C_2H_4$ concentrations, when the anomalous line appeared only after photolysis it was the only line present. In a few cases, however, a broad but symmetric esr line appeared upon photolysis of the sample, and the belief that this line was due to a free radical product was strengthened by the fact that a line of the same overall width but with a certain amount of structure was observed when deuterioethylene was used in place of ethylene, *cf.* Figure 8. It is possible that this spectrum is due to the $CD_2FCD_2$ radical, the lines of which are badly broadened by the modulating effect of some internal or external rotation of the radical on the highly anisotropic fluorine hfs splitting. This, however, is only a possible explanation of a negative result and no definite conclusions can be made in this case.

*2.* $F + C_2H_2$. Since the experience with ethylene suggested that deuteration of the reactants simplified the esr spectrum and made it more interpretable, this reaction was studied by photolyzing $F_2(0.1\%)$–$C_2D_2$-(1%)–Ar(99%). We believe that the resulting spectrum, which is shown in Figure 9, is due to two different radicals which are denoted as A and B in Figure 9.

The main feature of the esr spectrum of A is a pair of complex lines characteristic of the highly anisotropic but axially symmetric hfs splitting of a fluorine nucleus.[4] The components of the fluorine hfs tensor as determined from the positions of the individual peaks of the complex lines (the outer pair of peaks correspond to the magnetic field parallel to the symmetry axis of the fluorine hfs tensor whereas the other pair of peaks correspond to the field perpendicular to this symmetry axis)[4,8] are as follows: $|A_{\parallel}| = 110$ and $|A_{\perp}| = 49$ Oe. It is probable that both $A_{\parallel}$ and $A_{\perp}$ have the same sign (otherwise the isotropic fluorine hfs constant would be nearly zero) but this cannot be definitely established from our experimental data. Superimposed on this complex doublet is a certain amount of deuterium hfs which gives the perpendicular components of the lines a triplet substructure and which broadens the parallel components. If we assume that the triplet splitting of the perpendicular peaks is due to a single deuterium (the justification for this will be clearer momentarily) then the observed splitting corresponds to a deuteron hfs constant of 5.8 ± 0.5 Oe or, equivalently, a proton hfs constant of 38 Oe.

From these results we believe that spectrum A is due to one of the two possible isomers of the radical CD=CDF, formed from the reaction

$$F + C_2D_2 \longrightarrow CD{=}CDF$$

Judging from the results obtained from the vinyl radical,[9,14] the $\alpha$ deuterium hfs will be very small in this radical which is in agreement with the observation of a triplet splitting due to a single deuterium nucleus in the esr spectrum. Moreover, a combination of the experimental results for the vinyl radical[9,14] together with theoretical considerations[15] led to the conclusion that the proton hfs constants of the *cis* and *trans* $\beta$ protons in the vinyl radical are 34 and 68 Oe, respectively. The deuterium splitting which we observed is equivalent to a *cis* proton splitting; thus, we conclude that the fluorovinyl radical formed in this system has the fluorine atom *trans* to the unpaired electron orbital.

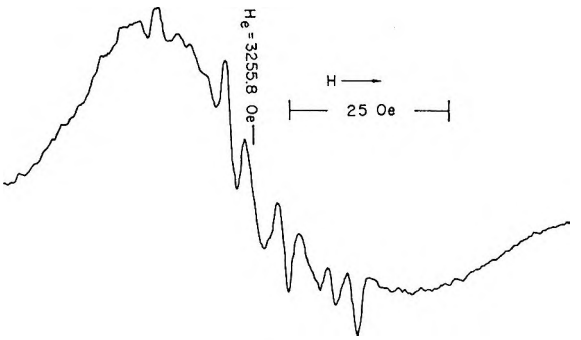


Figure 8. Esr spectrum at 4°K of the products of the photolysis of 0.1% $F_2$ in a matrix containing 1% $C_2D_4$ and 99% Ar.

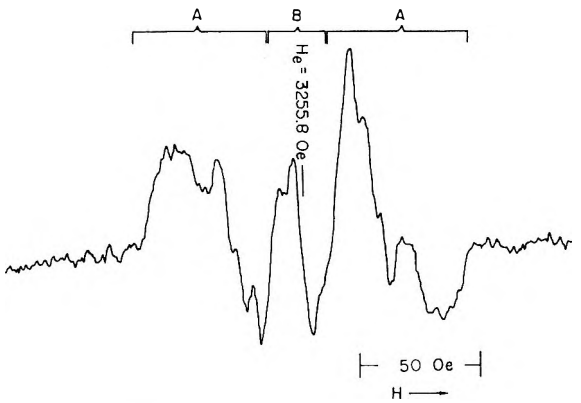


Figure 9. Esr spectrum at 4°K of the products of the photolysis of $F_2$ in $C_2D_2$–Ar.

The esr spectrum attributed to B consists of a line in the center of the spectrum, which line has partially resolved structure characteristic but not conclusive of a 5-Oe hfs triplet. It is believed that this line is due to a separate radical rather than a part of the spectrum attributed to radical A because the large anisotropic fluorine hfs splitting which accounts for the pair of complex lines precludes a line in the center of the spectrum.

The following two possible assignments for the radical B were considered. The first was a substituted vinyl radical produced by the reaction of the primary fluorovinyl radical with another acetylene molecule. Such a radical is consistent with the apparent absence of a large fluorine hfs in the spectrum of B, but the formation of such a secondary radical at the low $C_2D_2$ concentration

(14) E. L. Cochran, F. J. Adrian, and V. A. Bowers, *J. Chem. Phys.*, **40**, 213 (1964).

(15) F. J. Adrian and M. Karplus *ibid.*, **41**, 56 (1964).

(1%) used here is doubtful. Also the results obtained for the vinyl radical suggest that this substituted vinyl radical should have *cis* and *trans* $\beta$ deuteron hfs splittings of 5 and 10 Oe, respectively, which splittings should give a broader and/or more highly structured esr line than is actually observed. The second possibility considered was the formation of the deuterioethynyl radical (C≡CD) by the hydrogen abstraction reaction

$$F + C_2D_2 \longrightarrow CCD + DF$$

or, alternatively, by secondary photolysis of the primary fluorovinyl radical.[16] Although the spectrum attributed to a radical B in Figure 9 is very different from the isotropic 2.6 Oe triplet observed when $C_2D$ was prepared by the photolysis of $C_2D_2$ in argon,[14] it is possible that the radical is unable to rotate in the present system. If this were the case, the observed deuterium hfs splitting could be a combination of isotropic and anisotropic hfs which produces a spectrum which is markedly different from the isotropic spectrum. Although for these reasons and the fact that the phenyl radical is formed in the reaction of F atoms with benzene (*cf.* the next section) we tentatively identify radical B as the deuterioethynyl radical; definite identification of this radical will require further work.

*3.* $F + C_6H_6$. Photolysis of $F_2$ in $C_6H_6$–Ar gave a very complex many-line esr spectrum. Photolysis of $F_2$(0.2%) in $C_6D_6$(2%)–Ar(98%) gave the greatly simplified spectrum shown in Figure 10. This spectrum and that produced by photolysis of $F_2$ in $C_2D_2$–Ar (*cf.* Figure 9) are similar in that they both contain a pair of complex lines and a center line, although the relative intensities of the lines and their spacings are different in the two spectra. Accordingly, the interpretation of this spectrum is similar to that of the $F_2$–$C_2D_2$ spectrum, that is, the pair of complex lines is attributed to the fluorocyclohexadienyl radical produced by the reaction

$$F + C_6D_6 \longrightarrow C_6D_6F$$

and the center line is attributed to the phenyl radical which is produced either by the reaction

$$F + C_6D_6 \longrightarrow C_6D_5 + DF$$

or by secondary photolysis of the $C_6D_6F$ radical.[16]

From the positions of the parallel and perpendicular peaks in the pair of complex lines assigned to the $C_6D_6F$ radical we obtained the following results for the components of the fluorine hfs tensor: $|A_{||}| = 173$ and $|A_{\perp}| = 82$ Oe.[4,8] Again it is probable that $A_{||}$ and $A_{\perp}$ have the same sign but this cannot be established definitely from the experimental results. The width of the individual peaks of the complex lines (*ca.* 15 Oe) and the absence of any resolved deuterium hfs for these peaks is consistent with the fact that, judging from the hfs of the cyclohexadienyl radical,[9] the $C_6D_6F$ radical should have a number of deuteron hfs splittings ranging in magnitude from 1.4 to 7 Oe.

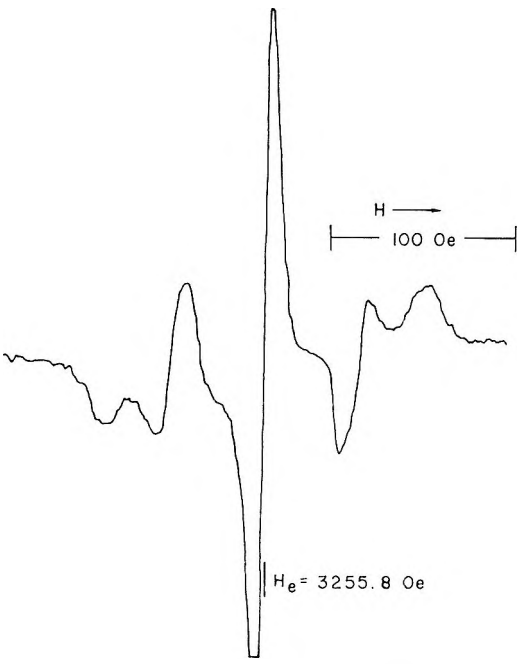


Figure 10. Esr spectrum at 4°K of the products of the photolysis of $F_2$ in $C_6D_6$–Ar.

The assignment of the center line of the spectrum to the phenyl radical is based on the excellent agreement between the shape of this line and the computed spectrum of an unresolved hfs multiplet due to a pair of 2.9-Oe deuteron hfs splittings where the individual hfs lines are gaussian with an rms width of 2.3 Oe. This deuteron hfs splitting corresponds to a proton hfs splitting of 18.7 Oe which is in good agreement with experimental values of the *ortho* proton splitting in the phenyl radical.[17] The 2.3 Oe gaussian shape of the individual lines of the hfs multiplet is in good agreement with the shape of the fully resolved hfs lines in the spectrum produced by photolysis of $F_2$ in $C_6H_6$–Ar. (The proton hfs splittings of these radicals are large enough so that many of the lines are individual hfs lines and not composites of several unresolved hfs lines. There are, however, so many of these lines and some of the lines of the two radicals overlap so extensively that a detailed analysis of this spectrum was not attempted.)

*C. Summary.* The foregoing studies of the reactions of fluorine atoms with various simple organic molecules suggest that in the case of a saturated molecule the initial step is a hydrogen abstraction reaction, whereas in the case of an unsaturated molecule, addition of the F atom to a double bond predominates but hydrogen abstraction also may occur in some cases. In one case, *i.e.*, the reaction of F and $n$-$C_3H_8$, a product

(16) The possibility of secondary photolysis was suggested by P. H. Kasai in a private communication.

(17) J. E. Bennett, B. Mile, and A. Thomas, *Proc. Roy. Soc.*, **A293**, 246 (1966); P. H. Kasai, E. Hedaya, and E. B. Whipple, *J. Amer. Chem. Soc.*, **91**, 4364 (1969).

of the primary reaction ($n$-$C_3H_7$) is left in an excited state which immediately undergoes secondary decomposition.

It is believed that two of the radicals produced in these reactions, namely, the *trans*-fluorovinyl radical and the fluorocyclohexadienyl radical, have not been observed previously. The observed values of the hfs constants of these molecules are given in Table III. Also given in Table III are the "averaged" components of the $\alpha$ proton hfs tensor of the $CH_2OH$ radical which average is the result of a rotation or reorientation of the $CH_2$ group about the CO bond.

**Table III:** Free Radical Hyperfine Splitting Constants which have not been Previously Determined. All hfs Constants in Oersteds

| Radical | Nucleus | $\lvert A_{\parallel}\rvert$ | $\lvert A_{\perp}\rvert$ | $\lvert A_{iso}\rvert$ |
|---|---|---|---|---|
| $CH_2OH$ | $\alpha$-H[a] | 25 | 16 | 19 |
| *trans*-CH=CHF | F | 110 | 49 | 69[b] |
| *trans*-CH=CHF | *cis*-$\beta$-H | ... | ... | 38 |
| $C_6H_6F$ | F | 173 | 82 | 112[b] |

[a] Average values produced by rotation or reorientation of the $CH_2$ group about the CO bond. [b] Computed from $A_{\parallel}$ and $A_{\perp}$ by assuming that these two quantities have the same sign.

# Reaction Rate of Trifluoromethyl Radicals by Rapid Scan Infrared Spectroscopy

**by Teiichiro Ogawa, Gary A. Carlson, and George C. Pimentel**

*Chemistry Department, University of California, Berkeley, California 94720* *(Received November 10, 1969)*

The rate of reaction of trifluoromethyl radicals, $CF_3$, to form hexafluoroethane, $C_2F_6$, has been measured through the flash photolysis of trifluoromethyl iodide coupled with rapid scan infrared spectroscopy. The percentage of the $CF_3$ formed that appears as $C_2F_6$ (the quantum yield) depends upon the pressure of added gases: for 100 mm Ar, $\phi = 0.68$; 50 mm $N_2$, $\phi = 0.55$; 400 mm $N_2$, $\phi = 0.45$; 50 mm $CO_2$, $\phi = 0.54$; 400 mm $CO_2$, $\phi = 0.43$. The rate constant was also found to be dependent upon the added gas, presumably due to vibrational deactivation processes. $2CF_3 \rightarrow C_2F_6$: 25° Ar, 100 mm, $k = (5.9 \pm 0.7)10^{12}$ cm³/mol sec; 60° Ar, 100 mm, $k = (7.1 \pm 1.0)10^{12}$ cm³/mol sec; 25° $N_2$, 400 mm, $k = (9.2 \pm 0.9)10^{12}$ cm³/mol sec; 25° $CO_2$, 400 mm, $k = (8.8 \pm 0.9)10^{12}$ cm³/mol sec. The slight temperature dependence corresponds to an activation energy between 0.3 and 2.5 kcal/mol. The argon results, corrected to 127°, are about a factor of 2 below the rate constant value obtained by Ayscough using the sector method. Possible explanations of this small discrepancy are considered.

## Introduction

Ayscough[1] measured the rate of combination of $CF_3$ radicals to form $C_2F_6$ using sectored photolysis of $(CF_3)_2CO$ at a single temperature. Pritchard and Dacey[2] estimated that the reaction might have an activation energy as high as 2.1 kcal/mol, but Giles and Whittle[3] concluded that it was more likely to be near zero. In view of the fundamental kinetic importance of this prototype reaction, further study is warranted.

Flash photolysis techniques, coupled with uv-visible spectroscopy, have been used for the characterization of many transient species but in rather few cases for direct kinetic studies. Presumably, this is because of inherent difficulties in the control of transient molecule concentration, temperature, and side reactions. Nevertheless, the method permits direct observation of transient intermediates and their kinetic behavior. This opportunity is particularly beneficial when flash methods are coupled with infrared detection because of its general applicability. Kinetic spectra are likely to provide at once photometric information about reactant loss, product growth, intermediate species growth and loss, and side reactions, whether expected or not. A prototype infrared study of a first-order decomposition, that of chloroformic acid, has been reported from this laboratory.[4] In the present work, we have investigated the rate of second-order reaction of two $CF_3$ radicals to give $C_2F_6$, another important prototype.

(1) P. B. Ayscough, *J. Chem. Phys.*, **24**, 944 (1956).

(2) G. O. Pritchard and J. R. Dacey, *Can. J. Chem.*, **38**, 182 (1960).

(3) R. D. Giles and E. Whittle, *Trans. Faraday Soc.*, **61**, 1425 (1965).

(4) R. J. Jensen and G. C. Pimentel, *J. Phys. Chem.*, **71**, 1803 (1967).

## Experimental Section

Infrared spectra were recorded on a 200 μsec time scale using the rapid scanning spectrometer developed by Herr and Pimentel.[5,6] Both the spectrometer and associated photolysis apparatus were modified from the original design in some details.[7,8] A rotating grating blazed at 1500 $cm^{-1}$ in first order was used instead of the prism and Littrow mirror. A Kodak 240 filter eliminated higher-order energy. A copper-doped germanium detector (Santa Barbara Instruments Co.) was cooled with liquid helium. A modified Beckman multiple reflection cell (up to 1-m path) served as the flash photolysis cell. Light from an external flash photolysis lamp, discharging 1400–1700 J at 10–11 kV, entered the cell through a 6.3 × 28 cm quartz window in the cell top. The flash had a half-intensity duration of 16 μsec. The temperature of the multiple reflection cell was controlled over the range 25–70° by placing the entire cell in an insulated enclosure and heating it with a heating tape.

The concentration of $CF_3$ radical was determined from a spectral scan taken immediately following photolysis by measuring the optical density of the 2166 $cm^{-1}$ $CF_3$ band ($\nu_3$, R branch).[9] Kinetic information was gained in a series of experiments with various time delays between flash peak and spectral scan ranging from 44 to 489 μsec. The Tektronix 535A oscilloscope sweep speed and time delays were checked within ±2% with a calibrated time-mark generator. The detector was used under linear response conditions. Normally a 200-$cm^{-1}$ region centered on the band of interest was scanned in 200 μsec. The 100% transmission line was determined in each experiment from a spectrum recorded a few seconds before the flash. The base line was determined by reference to totally absorbing parent bands and from the base line at the end of an extended scan recorded shortly after photolysis.

Quantum yield measurements were based upon spectra recorded on a Beckman IR-9 spectrophotometer and compared to appropriate reference gas spectra recorded at measured concentrations.

Samples of $C_2F_6$ (Columbia Organic Chemicals Co.), $CF_3I$ (Peninsular Chem Research), $CF_3NO$ (Peninsular Chem Research), and NO (Matheson) were each frozen and melted several times under vacuum prior to use. Argon (Matheson, 99.999%) was used without purification, as were nitrogen (Matheson, 99.997%) and carbon dioxide (Matheson, 99.95%).

Argon, nitrogen, or carbon dioxide was added to every photolysis sample to moderate the temperature rise due to flash heating to only a few degrees. The gases, a few tenths of a mm of $CF_3I$ and 100 mm of Ar, 400 mm of $N_2$, or 400 mm of $CO_2$, were allowed to mix overnight in a blackened 25-l. glass flask prior to transfer into the multiple reflection cell.[10]

## Results

The rate constant for $C_2F_6$ formation was measured with $CF_3I$ as precursor. In earlier work[7] $C_6H_5COCF_3$ was also used, and both the 1266-and the 1087-$cm^{-1}$ bands of $CF_3$ were measured. The side reactions encountered with $C_6H_5COCF_3$, which differ markedly from those to be considered for $CF_3I$, were fully identified. These studies will not be reported here because of gas mixing difficulties,[10] but since they gave results in good agreement with $CF_3I$ experiments conducted under identical experimental conditions, they tend to corroborate the $CF_3I$ results to be described.

*Reactions.* The primary $CF_3I$ photolysis mechanism gives $CF_3$ and electronically excited, $^2P_{1/2}$, iodine atoms (hereafter, I*).[11]

$$CF_3I \xrightarrow{h\nu} CF_3 + I^* \qquad (1)$$

No $CF_4$ (or $C_2F_4$) product was found unless the inert gas diluent was omitted. Hence the diluent (Ar, $N_2$, or $CO_2$) prevents an undesired side reaction, that of $CF_3$ with $CF_3I$ to form $CF_4$. Clearly, the added gas moderates the $CF_3$ translational energy and so eliminates fluorine abstraction because of a substantial activation energy (the activation energy for H abstraction from $CH_4$ by $CF_3$ is 11 kcal/mol).[12] We believe the abstraction of $CF_3$ from $CF_3I$ to form $C_2F_6$, another undesired side reaction, is eliminated in the same manner. The following reactions remain to be considered.

$$CF_3 + CF_3 \xrightarrow{k_{2a}} C_2F_6 \qquad (2a)$$

$$CF_3 + CF_3 + M \xrightarrow{k_{2b}} C_2F_6 + M \qquad (2b)$$

$$CF_3 + I^* \xrightarrow{k_{3a}} CF_3I \qquad (3a)$$

$$CF_3 + I^* + M \xrightarrow{k_{3b}} CF_3I + M \qquad (3b)$$

$$CF_3 + I^* \xrightarrow{k_{3c}} CF_3 + I \qquad (3c)$$

$$CF_3 + I \xrightarrow{k_4} CF_3I \qquad (4)$$

$$I^* + M \xrightarrow{k_5} I + M \qquad (5)$$

(5) G. C. Pimentel and K. C. Herr, *J. Chim. Phys.*, 61, 1509 (1964).

(6) K. C. Herr and G. C. Pimentel, *Appl. Opt.*, 4, 25 (1965).

(7) G. A. Carlson, Ph.D. Dissertation, University of California, Berkeley, Calif., 1966.

(8) K. C. Herr, G. A. Carlson, and G. C. Pimentel, *Kagaku no Ryoiki*, 21, 12 (1967).

(9) G. A. Carlson and G. C. Pimentel, *J. Chem. Phys.*, 44, 4053 (1966).

(10) In earlier work (see ref 7), the gas constituents were added sequentially to the multiple reflection cell and a 5-min period was allowed for mixing. Subsequently, it was discovered that uniform mixing requires at least 20 min. This mixing difficulty makes the quantitative kinetic measurements in ref 7 suspect.

(11) R. J. Donovan and D. Husain, *Trans. Faraday Soc.*, 62, 11 (1966).

(12) H. Carmichael and H. S. Johnston, *J. Chem. Phys.*, 41, 1975 (1964).

The reactions of I* deactivation by argon and $CF_3I$ (reaction 5) and the combination of iodine atoms to form $I_2$ are all slow enough to ignore in the present work.[13,14] Deactivation of I* by nitrogen or by carbon dioxide may not be entirely negligible and will be discussed. Reaction 3a probably occurs only to a limited extent because of the large amount of energy to be removed (21.7 kcal) before the molecule is stabilized. Reaction 3b probably occurs in the presence of the higher pressures used with $N_2$ and $CO_2$, acting to lower somewhat the quantum yield of $C_2F_6$ formation through reaction 2. Reaction 3c probably has a rate constant comparable to the I* deactivation rate constants observed with other molecules with unpaired spins, $O_2$ and NO, respectively, $10^{12}$ and $2.8 \times 10^{12}$ $cm^3$/mol sec.[15] The rate constant $k_4$ could be quite large, in analogy to the rate constant for the reaction between $CH_3$ and Cl, which is $4 \times 10^{14}$ $cm^3$/mol sec at 400°K.[16] The deduction of the actual relative magnitudes of these rate constants is an important part of the interpretation of our data. For M = argon, it seems clear that $k_5$ can be neglected, and that reaction 4 is rapid compared to 3c. If so, every reaction 3c results in formation of $CF_3I$. Then the rate of disappearance of $CF_3$ will be for argon

$$\frac{-\mathrm{d}(CF_3)}{\mathrm{d}t} = 2k_2(CF_3)^2 + k_3(CF_3)(I^*) \qquad (6)$$

The constant $k_2$ includes contributions by reactions 2a and 2b, so $k_2 = k_{2a} + (M)k_{2b}$. Similarly, the constant $k_3$ includes contributions by 3a, 3b, and 3c, so $k_3 = k_{3a} + k_{3b}(M) + k_{3c}$. Equation 6 will not be applicable to the $N_2$ and $CO_2$ data, where reactions 3b and 5 become quite important.

*$C_2F_6$ Quantum Yield.* The relative yields of $C_2F_6$ and $CF_3I$ products contain information about the ratio of $k_2$ to $k_3$. To measure these yields, we compared the total $C_2F_6$ obtained under typical flash conditions to the total $CF_3$ formed in the flash. The latter was determined by adding NO as a radical scavenger. This addition eliminated $C_2F_6$ formation, presumably through quantitative formation of $CF_3NO$. The quantum yield for $C_2F_6$, the per cent conversion of $CF_3$ to $C_2F_6$, is, then, the quotient of twice the $C_2F_6$ product obtained without NO divided by the total $CF_3NO$ produced in the presence of excess NO.

Experiments were performed with 1700 J flash energy, ~0.35 mm $CF_3I$ and with excess inert gas, argon (100 mm), nitrogen (50 and 400 mm), or carbon dioxide (50 and 400 mm). The amount of product was monitored with two $CF_3NO$ bands, one at 1272 $cm^{-1}$ (which gave optical densities near 0.1) and another at 1598 $cm^{-1}$ (which gave optical densities near 0.03). The amount of $CF_3NO$ did not depend upon which inert gas was present but it did increase by about 25% as the NO pressure was increased over the range 0.7–4.8 mm. This is undoubtedly due to the direct reaction between $CF_3I$ and NO. The effect is small, however, and Figure 1 shows that the data permit an accurate extrapolation to the $CF_3NO$ product yield at zero NO pressure to give $(5.9 \pm 0.2) \times 10^{-3}$ mm $CF_3NO$.

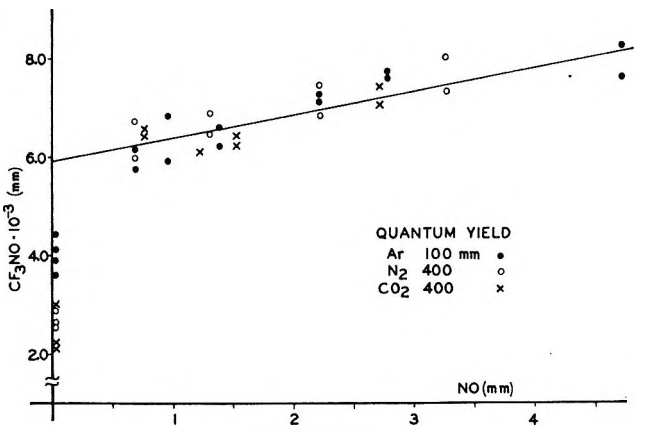


Figure 1. The effect of NO pressure on $CF_3NO$ product yield: 0.35 mm $CF_3I$, 1700 J.

With no nitric oxide present, the $C_2F_6$ product was measured through the $C_2F_6$ band at 1251 $cm^{-1}$. Optical densities fell in the range 0.15–0.30. Table I summarizes the results. Argon, the least efficient collisional deactivator, displays the highest quantum yield and no detectable temperature dependence up to 60°. In contrast, there is no doubt that $\phi$ is pressure dependent with either $N_2$ or $CO_2$ present. This could be due to reaction 3b or to a significant contribution by reaction 5 followed by reaction 4.

**Table I:** $C_2F_6$ Quantum Yield. $CF_3I$ with Various Inert Gases. $p(CF_3I) = 0.25$ mm, $T = 25°$, 1700 J

| Inert gas | Inert gas, mm | No. of expts | $\phi$ | $k_3/k_2$[b] |
|---|---|---|---|---|
| Ar[a] | 100 | 4 | $0.68 \pm 0.06$ | 0.38 |
| $N_2$ | 50 | 4 | $0.55 \pm 0.06$ | 0.77 |
| | 400 | 3 | $0.45 \pm 0.04$ | 1.30 |
| $CO_2$ | 50 | 5 | $0.54 \pm 0.08$ | 0.80 |
| | 400 | 3 | $0.43 \pm 0.07$ | 1.44 |

[a] Two experiments carried out at 60° indicated no effect of temperature upon $\phi$ within experimental uncertainty. [b] Based upon the assumption that reactions 5 and 4 can be neglected.

For the argon data, the quantum yield suffices to determine the ratio $k_3/k_2$ without knowledge of the

(13) R. J. Donovan and D. Husain, *Nature*, **206**, 171 (1965); *Trans. Faraday Soc.*, **63**, 2023 (1967).

(14) R. L. Strong, J. C. W. Chien, P. E. Graf, and J. E. Willard, *J. Chem. Phys.*, **26**, 1287 (1956).

(15) R. J. Donovan and D. Husain, *Trans. Faraday Soc.*, **62**, 2023 (1966).

(16) J. H. Know, *ibid.*, **58**, 275 (1962).

initial $CF_3$ concentration. The flash period is short compared to the effective $CF_3$ half-life (~400 μsec), so the flash can be acceptably approximated as a δ function. Then eq 6 can be solved numerically using the initial conditions, at $t = 0$, $(CF_3)_0 = (I^*)_0$ and adjusting the ratio $k_3/k_2$ parametrically to fit the measured quantum yield. For the argon experiments, the quantum yield 0.68 is obtained with $k_3/k_2 = 0.38$.

For comparison, Table I also lists the values of $k_3/k_2$ that result from the $N_2$ and $CO_2$ measurements if eq 6 is used. These numbers would be significant if the pressure effect arises from an increase in the rates of reactions 2b and 3b, but not if it is associated with the sequence of reactions 5 and 4.

*Kinetics of $CF_3$ Loss: Argon Moderator.* For kinetic interpretation of the argon data, eq 6 is more convenient in the form

$$-\frac{d(CF_3)}{dt} = 2k_2(CF_3)^2\left[1 + \frac{k_3(I^*)}{2k_2(CF_3)}\right] = 2k_2(CF_3)^2(\alpha) \quad (7)$$

In our experiments, during the time intervals over which our measurements extend, the $CF_3$ pressure approximately halves. Numerical calculations, based upon a reasonable estimate of $k_3/k_2$, show that $(I^*)/(CF_3)$ is relatively constant, so that the parenthetical quantity $\alpha$ changes by less than 20%. If $\alpha$ is assumed to be constant, and equal to its average value in the time interval studied, $\bar{\alpha}$, eq 7 is readily solved

$$\frac{(CF_3)_0}{(CF_3)} = 2\bar{\alpha}k_2(CF_3)_0 t + 1 \quad (8)$$

For a δ function flash, the value of $(CF_3)_0$ is indicated by the $C_2F_6$ yield at $t = \infty$ and the $C_2F_6$ quantum yield

$$(CF_3)_0 = \frac{2(C_2F_6)_\infty}{\phi} \quad (9)$$

With the final assumption of Beer's law, eq 8 becomes

$$\frac{(OD_{C_2F_6})_\infty}{OD_{CF_3}} = \frac{2\bar{\alpha}k_2}{b\epsilon_{CF_3}} t(OD_{C_2F_6})_\infty + \frac{\epsilon_{C_2F_6}}{\epsilon_{CF_3}}\frac{\phi}{2} \quad (10)$$

$(OD_{C_2F_6})_\infty$ is the optical density of $C_2F_6$ at 1251 $cm^{-1}$ at $t = \infty$; $\epsilon_{C_2F_6}$ is the extinction coefficient of $C_2F_6$ at 1251 $cm^{-1}$; $OD_{CF_3}$ is the optical density of $CF_3$ at 1266 $cm^{-1}$ at time $= t$ (corrected for $C_2F_6$ overlap absorption at 1266 $cm^{-1}$ at time $= t$); $\epsilon_{CF_3}$ is the extinction coefficient of $CF_3$ at 1266 $cm^{-1}$; $b$ = path length = 1000 cm.

Experimentally, the 1251-$cm^{-1}$ band of $C_2F_6$ gives a linear Beer's law plot under our optical conditions up to OD = 0.7, which encompasses the optical density range used. The band widths and rotational spacings of $CF_3$ are sufficiently close to those of $C_2F_6$ that it, too, undoubtedly obeys Beer's law amply well for the purposes of this study.

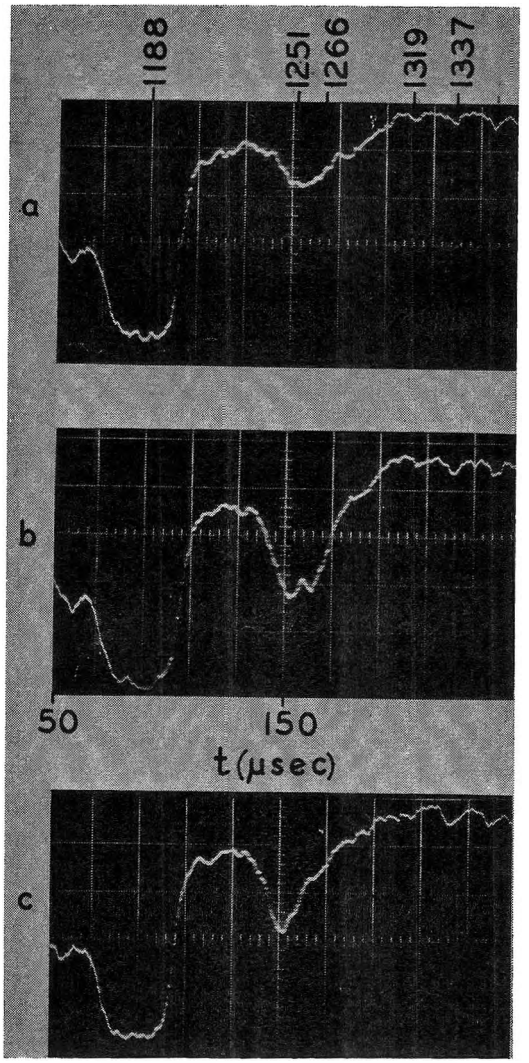


Figure 2. A typical experiment: 0.35 mm $CF_3I$, 100 mm Ar, 25°, 20 μsec/div: (a) before flash; strong band at 1188 $cm^{-1}$ is due to $CF_3I$; (b) 50 μsec after 1700-J flash; (c) several seconds after flash; band at 1251 $cm^{-1}$ is due to $C_2F_6$.

Spectra from a typical kinetics experiment are seen in Figure 2. Spectrum a was recorded several seconds before flash photolysis. A strong $CF_3I$ absorption is seen at 1188 $cm^{-1}$ and two atmospheric $H_2O$ features appear above 1300 $cm^{-1}$. The broad absorption near 1265 $cm^{-1}$ is in part due to a weak $CF_3I$ absorption at 1275 $cm^{-1}$ and in part due to the spectrometer optics. Spectrum b was recorded beginning 50 μsec after flash initiation. It shows a $CF_3$ absorption as 1266 $cm^{-1}$ partly overlapped by a $C_2F_6$ product band at 1251 $cm^{-1}$. Spectrum c, recordedse veral seconds after photolysis, shows the final $C_2F_6$ product band.

Optical densities are estimated from spectrum a, which indicated the 100% transmission curve appropriate for spectrum b. The 0% transmission base line is indicated accurately by the absorption at the center of the intense 1188 $cm^{-1}$ $CF_3I$ band, as corroborated in separate experiments in which $C_2F_6$ was added until the gas became optically thick at 1266 $cm^{-1}$.

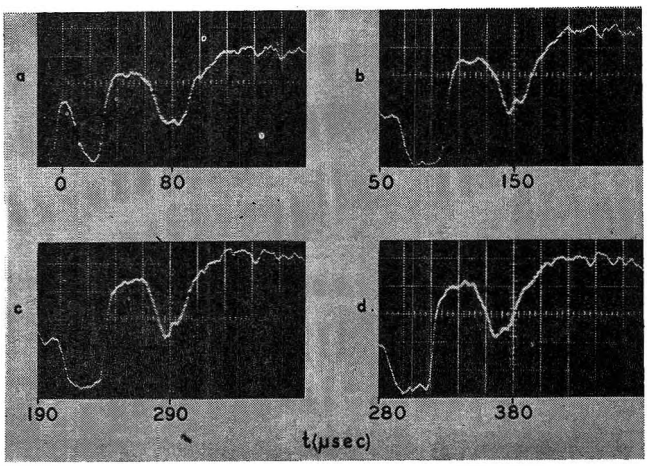


Figure 3. The effect of time after flash on $CF_3$ intensity: 0.35 mm $CF_3I$, 100 mm Ar, 25°, 1700 J, time from flash peak to scanning of 1266 $cm^{-1}$ band; (a) 85 μsec; (b) 155 μsec; (c) 295 μsec; (d) 377 μsec.

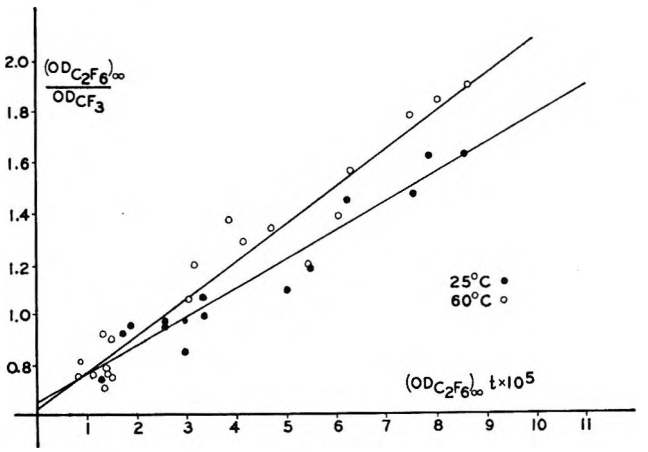


Figure 4. Second-order kinetics plot: $CF_3$ in argon (100 mm) at 25 and 60°.

Figure 3 shows spectra taken in four separate experiments with varying time delay between flash initiation and spectral scan. The delay periods, measured from flash peak to the time of scan through 1266 $cm^{-1}$, vary from 85 to 377 μsec. The loss of the $CF_3$ band is clearly evident. Not so evident is the contribution of the $CF_3$ band to the 1251 $cm^{-1}$ $C_2F_6$ absorption. A plot of the ratio of intensities at 1251 and 1266 $cm^{-1}$ extrapolated to zero time delay shows[7] that the 1266-$cm^{-1}$ $CF_3$ absorption is the R branch of a doublet, and that the P branch is centered at 1254 $cm^{-1}$, overlapping the $C_2F_6$ absorption. Hence the $C_2F_6$ corrections at 1266 $cm^{-1}$ are much smaller than suggested by the intensity of the 1251 $cm^{-1}$ feature (always less than 10%).

The experimental data from 15 distinct $CF_3I$–Ar experiments at room temperature are plotted in Figure 4 (dots), using the coordinates appropriate to eq 10. For these argon experiments, $\bar{\alpha} = 1.42$. The initial $CF_3I$ pressure was 0.30 mm. The data reasonably fit a straight line with intercept 0.65 ± 0.05 and slope (11.2 ± 1.0) × $10^3$ $sec^{-1}$. Also shown in Figure 4 are data recorded at 60° (open circles) which fit a straight line with intercept 0.63 ± 0.05 and slope (14.6 ± 1.0) × $10^3$ $sec^{-1}$.

The value of $\epsilon_{C_2F_6}$ under the photolysis optical conditions was found to be (2.87 ± 0.09) × $10^6$ $cm^2$/mol at 25° and (2.56 ± 0.18) × $10^6$ $cm^2$/mol at 60° in separate measurements made with known pressures of $C_2F_6$. Hence the intercept provides a value of $\epsilon_{CF_3}$ = (1.50 ± 0.12) × $10^6$ and (1.38 ± 0.24) × $10^6$ at 25 and 60°, respectively. These values of $\epsilon_{CF_3}$ and the slopes found in Figure 4 lead to the values $k_2$ = (5.9 ± 0.7) × $10^{12}$ $cm^3$/mol sec at 25° and $k_2$ = (7.1 ± 1.0) × $10^{12}$ $cm^3$/mol sec at 60°. These values of $k_2$, coupled with the $k_3/k_2$ ratio of 0.38, lead to $k_3$ estimates of (2.2 ± 0.3) × $10^{12}$ and (2.7 ± 0.5) × $10^{12}$ $cm^3$/mol sec at 25 and 60°, respectively.

Although this graphical presentation affords a convincing view of the data in support of the use of eq 10, the assumption that $(I^*)/(CF_3)$ is constant introduces a small error. Consequently, eq 7 was numerically integrated without this assumption using the graphical estimate of $\epsilon_{CF_3}$ and a least-squares parametric determination of the quantity $k_2$. The value of $k_2$ so obtained was 10% larger, a correction we will ignore.

*Kinetics of $CF_3$ Loss: Nitrogen or Carbon Dioxide Moderator.* The experiments with $N_2$ and $CO_2$ buffer gases are less readily interpreted because of the possible effect of reactions 4 and 5. Since our data are not sufficient to warrant introducing $k_4$ and $k_5$ parametrically, we have treated the data just as described for the argon experiments. This procedure attributes the entire pressure effect to reactions 2b and 3b. There is some evidence that this is a valid interpretation. If reactions 4 and 5 contribute significantly, then the data should not be well represented by the second-order kinetics of equations 7 and 10. They can be fitted by eq 10, however, within experimental uncertainties.

Table II summarizes the $N_2$ and $CO_2$ results, along with those discussed earlier for argon. The values of $\epsilon_R$ obtained are in substantial agreement with each other and with the argon figure, so an average value of 1.5 × $10^6$ $cm^2$/mol was used in the calculations of $k_2$ and $k_3$.

**Table II:** Rate Constants and $CF_3$ Absorption Coefficients

| Inert gas | P, mm | Temp, °C | $10^{-6}\epsilon_{CF_3}$, $cm^2$/mol | $10^{-12}k_2$, $cm^3$/mol sec | $10^{-12}k_3$, $cm^3$/mol sec |
|---|---|---|---|---|---|
| Ar | 100 | 25 | 1.50 ± 0.12 | 5.9 ± 0.7 | 2.2 ± 0.3 |
| | 100 | 60 | 1.38 ± 0.24 | 7.1 ± 1.0 | 2.7 ± 0.5 |
| $N_2$ | 400 | 25 | 1.4 ± 0.1 | 9.2 ± 0.9 | 12.0 ± 1.2 |
| $CO_2$ | 400 | 25 | 1.6 ± 0.1 | 8.8 ± 0.9 | 12.6 ± 1.3 |

## Discussion

The rate constants presented in Table II display differences well outside our estimated experimental uncertainty. It is reassuring, though, that the values of $\epsilon_{CF_3}$ are all in reasonable agreement. We believe that the rate constant differences are not spurious, that both $k_2$ and $k_3$ ($k_{3b}$) are higher in the presence of 400 mm of $N_2$ or of $CO_2$ than in the presence of 100 mm of Ar. We also believe that the temperature effect with argon is real, though the change is marginally close to the experimental uncertainty. This temperature effect corresponds to an activation energy of 1.0 kcal/mol for both reactions 2 and 3 but the experimental uncertainty defines a rather broad range between 0.3 and 2.5 kcal/mol.

Accepting this estimate of $E_A$, the rate constant in Table II can be extrapolated to 127°, the temperature at which Ayscough made his measurements.[1] The results are, for Ar (100 mm), $N_2$ (400 mm), and $CO_2$ (400 mm), respectively, 9.1, 14.1, and 13.1 $\times$ $10^{12}$ $cm^3$/mol sec. These values are all about a factor of 2 below the result obtained by Ayscough, 23 $\times$ $10^{12}$ $cm^3$/mol sec, with 40 mm of his precursor present, hexafluoracetone. Speculation about the cause of this discrepancy is surely presumptive, since Ayscough's value has its own uncertainty (unspecified). In fact one can take some pleasure from the factor of 2 agreement between these two measurements based upon entirely different techniques. Nevertheless, it is tempting to consider the possible causes of the observed differences.

A difficulty in Ayscough's study has come to light since his work was published. Gordon[17] has shown that $CF_3$ adds to the carbonyl oxygen of hexafluoroacetone to give a $(CF_3)_2COCF_3$ radical that is quite stable with respect to decomposition ($E_A \sim 31$ kcal). This radical reacts with $CF_3$ to give the stable ether, $(CF_3)_3COCF_3$. From Gordon's data, we calculate that 7 $\pm$ 2% of the $CF_3$ radicals in Ayscough's experiments will be so consumed. Taking this reaction into account will tend to lower Ayscough's value, though probably not as much as a factor of 2.

The more likely explanation of the discrepancy is suggested by our own observation of significant pressure effects. These can be likened to the significant changes in the rate constant for combination of methyl radicals as parent pressure is varied. Kistiakowsky and Roberts[18] have reported a fourfold increase in $k_2$ for ($CH_3$ + $CH_3$) in acetone photolyses when the acetone pressure was raised from 1 to 10 mm. The effect is attributed, of course, to the counterpart of reaction 2b, to vibrational deactivation of the excited $C_2H_6$ combination product. To attribute all of the $k_2$ variation to such a pressure effect would imply that the deactivating efficiency of hexafluoroacetone exceeds those of $N_2$ and $CO_2$ which, in turn, exceed that of argon. This is undoubtedly a correct conclusion, so the argument is quite creditable.

Perhaps the most important conclusion of this work is the estimate of $E_A$ for reaction 2. Despite the large range of uncertainty in this estimate, we feel that the internal consistency of our data and the comparison to Ayscough's high-temperature value suggest that the activation energy, though small, is indeed nonzero, a qualitatively interesting conclusion.

Giles and Whittle[3] have measured the activation energy difference, $E_A(CH_3CF_3) - {}^1/_2[E_A(C_2H_6) + E_A(C_2F_6)] = -170 \pm 80$. If $E_A(C_2F_6) = 1.0$ kcal and if $E_A(C_2H_6) = 0$, then their difference implies that $E_A(CH_3CF_3)$ is roughly half-way between (330 $\pm$ 80), not an implausible result.

Another view can be based upon the interpretation that the nonzero activation energy for the $CF_3$–$CF_3$ reaction is due to the dipole moment of the nonplanar $CF_3$ radical. If $CF_3$ has a dipole moment of 1.6 D (the dipole moment of $HCF_3$), the energy of repulsion between two $CF_3$ molecules would reach 1 kcal at a carbon–carbon separation near 3 Å. This is reasonable since, at shorter distances, bonding interactions would become dominant. Since $CH_3$ is planar, this repulsion would not be present, so this argument leads to the conclusion that the $CF_3$–$CH_3$ and $CH_3$–$CH_3$ activation energies would both be zero. If we place $E_A(CF_3CH_3) = E_A(C_2H_6) = 0$, the Giles and Whittle measurement implies that $E_A(C_2F_6)$ lies between 180 and 500 cal, a range that overlaps the lower end of the range defined in the present work (0.3 to 2.5 kcal).

*Acknowledgments.* We wish to thank the Office of Naval Research and the Air Force Office of Scientific Research for support of this research and the National Science Foundation for fellowship aid (to G. A. C.).

(17) A. S. Gordon, *J. Chem. Phys.*, **36**, 1330 (1962).

(18) G. B. Kistiakowsky and E. K. Roberts, *ibid.*, **21**, 1637 (1953).

# Radicals Formed by the Reaction of Electrons with Amino Acids in an Alkaline Glass[1,2]

by Michael D. Sevilla

*Atomics International Division, North American Rockwell Corporation, Canoga Park, California 91304*
*(Received November 4, 1969)*

The reactions of electrons with a number of amino acids in an alkaline $D_2O$ glass have been investigated by use of electron spin resonance spectroscopy. The electron initiates a series of reactions upon attachment to glycine and alkyl-substituted amino acids. Electron attachment at 77°K first produces the dianion which deaminates upon warming to produce a second radical species. Further warming to the softening point of the glass results in the appearance of a third radical species. The esr spectra of this species are consistent with the structure, $ND_2-\dot{C}(R)-CO_2^-$, which indicates that the deaminated species is abstracting from the $\alpha$ carbon of the parent amino acid. Reactions of electrons with other amino acids depend on the nature of the side group. For example, electron attachment to methionine produces methyl radicals by cleavage of the S–$CH_3$ bond, and electron attachment to asparagine produces an anion of the amide group. The radical intermediates identified are found to be in agreement with those proposed from investigations of the radiolysis of aqueous solutions of amino acids. A comparison of results of this work with those found in esr investigations of irradiated single crystals shows that the subsequent reactions of the deaminated radical species of amino acids with alkyl side groups are different in aqueous media than in crystalline amino acids.

## Introduction

Investigations of the radiolysis of the amino acids glycine and L-alanine in dilute aqueous solution have given evidence that the hydrated electron adds to the carboxyl group.[3] Results of the analysis of products of the radiolysis of these systems are consistent with the interpretation that the amino acid anion formed subsequently deaminates to produce a ·CH(R)COOH radical and that this species reacts by abstraction from the parent molecule[3]

$$NH_3^+CH(R)COO^- + \cdot CH(R)COOH \longrightarrow NH_2\dot{C}(R)COOH + CH_2(R)COOH \quad (1)$$

Electron spin resonance studies of irradiated solid amino acids (usually single crystals) at 77°K have also shown that electrons formed in the radiolysis add to the carboxyl group and that deamination subsequently occurs upon warming.[4-13] These esr studies show that the abstraction step as in reaction 1 does not occur in solid amino acids with alkyl side groups.[5,11,12] No abstraction reaction is found to occur in L-alanine.[5] For valine, deamination is followed by abstraction of a hydrogen atom from the tertiary carbon of the alkyl side group.[11,12] Results found for irradiated solid leucine and isoleucine also indicate that abstraction occurs from the tertiary carbon of the alkyl group.[11] Results found for solid glycine (R = H) may suggest partial abstraction of one of the $\alpha$ protons;[13] however this is uncertain.[14]

In this work an esr study of the reactions of photolytically produced electrons with a number of amino acids in an aqueous medium has been performed to further elucidate the role of the electron in the radiolysis of these systems. In the course of this investigation it was found that several reactions occurred after electron attachment to an amino acid and that the free radical intermediates in these reactions could be

(1) This work was supported by the Division of Biology and Medicine of the U. S. Atomic Energy Commission.

(2) The work was presented in part at the 158th National Meeting of the American Chemical Society, New York, N. Y., Sept 9, 1969.

(3) See D. B. Peterson, J. Holian, and W. M. Garrison, *J. Phys. Chem.*, **73**, 1568 (1969), and references therein.

(4) J. Sinclair and M. W. Hanna, *J. Chem. Phys.*, **50**, 2125 (1969).

(5) J. Sinclair and M. W. Hanna, *J. Phys. Chem.*, **71**, 84 (1967).

(6) H. C. Box, E. E. Budzinski, and H. G. Freund, *J. Chem. Phys.*, **50**, 2880 (1969).

(7) H. C. Box, H. G. Freund, and E. E. Budzinski, *J. Amer. Chem. Soc.*, **88**, 658 (1966).

(8) P. B. Ayscough and A. K. Roy, *Trans. Faraday Soc.*, **64**, 582 (1968).

(9) Y. A. Kruglyak, M. L. Pulatova, Y. V. Mozdor, Y. N. Sud'bina, V. G. Pasoyan, and L. P. Kayushin, *Biofizika*, **13**, 401 (1968).

(10) Electron attachment to carboxyl groups has been found to occur in irradiated carboxylic acids as well. See J. E. Bennett and L. H. Gale, *Trans. Faraday Soc.*, **64**, 1174 (1968).

(11) F. Patten and W. Gordy, *Radiat. Res.*, **14**, 573 (1961).

(12) H. C. Box, H. G. Freund, and E. E. Budzinski, *J. Chem. Phys.*, **46**, 4470 (1967).

(13) M. A. Collins and D. H. Whiffen, *Mol. Phys.*, **10**, 317 (1966).

(14) The uncertainty is not whether a radical of the form $NH_3^+-CH-CO_2^-$ is present as this is adequately proven. It is whether this species arises from abstraction as in reaction 1 or is the product of a series of reactions initiated by the positive ion which is formed in the radiolysis. See ref 5 and 9 for a discussion of this question.

stabilized and observed by esr spectroscopy. From this study, information confirming the reaction scheme proposed through radiolysis studies in aqueous solution is found. Results are found for alkyl-substituted amino acids which confirm the difference in the abstraction step between aqueous solution and the crystalline state. In addition, results for several amino acids with reactive side groups show these groups to be the site of electron attack.

One previous study of the reaction of radiolytically produced electrons with several amino acids in an alkaline glass has been reported.[8] The amino acids common to both studies are glycine and alanine. These workers find that a deaminated radical species is the product of electron attachment, as is found here. However, they did not observe the first radical species, the dianion. In this work it is found that the dianions are relatively stable. In addition, a third radical species which was not previously reported is found in this work.

## Experimental Section

The amino acids used in this study were obtained from Calbiochem (Grade A) and were used without further purification.

The experimental procedure employed was essentially that of Ayscough, Collins, and Dainton[15] as modified by Holroyd and Glass.[16] In this method a deoxygenated 8 *N* NaOD (92% $D_2O$) solution containing 5 m*M* $K_4Fe(CN)_6$ and 1 to 50 m*M* solute (amino acid) is cooled to 77°K to form a glass. The concentration of amino acid used is dependent upon its absorbance at 2537Å. Amino acids such as glycine and those with alkyl side groups do not absorb appreciably at this wavelength and therefore the higher concentrations were used.

The glass formed is photolyzed with 2537-Å uv light at 77°K for approximately 1 min. The photolysis produces a dark blue color due to the electron. At this point, an esr spectrum is taken of the sample to ensure that photolysis of the organic solute is minimal. The sample is then photobleached at 77°K with light from an infrared lamp for approximately 4 min. The electrons become mobile and react with the solute.

A Varian V4510 esr spectrometer equipped with a dual-cavity Fieldial magnetic field regulator and variable temperature accessory was employed in this work. Measurements of hyperfine splittings and $g$ values were made *vs.* potassium peroxylamine disulfonate ($A_N$ = 13.0 G, $g$ = 2.0056).

## Results and Discussion

*1. Glycine and Amino Acids with Alkyl Side Groups.* At 77°K electron attachment to glycine and the amino acids with alkyl side groups, *i.e.*, alanine, leucine, isoleucine, and valine, results in esr spectra at ($g \cong 2.003$ (Figures 1–3) which show good resolution

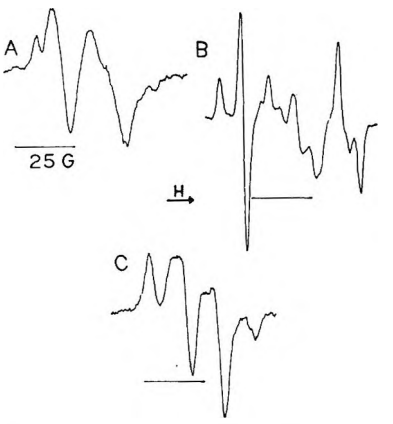


Figure 1. Electron spin resonance (esr) spectra of radical species produced by reaction of electrons with glycine in a deuterated alkaline glass. A, First species the dianion at 90°K. B, Second species $\cdot CH_2CO_2^-$ after warming to 180°K. C, Third species $\cdot CH(ND_2)CO_2^-$ at 190°K. The magnetic field increases from left to right for each spectrum in this figure and subsequent figures.

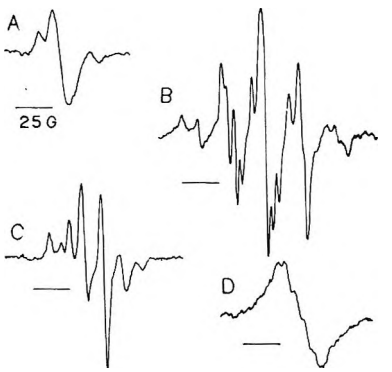


Figure 2. Esr spectra of radical species produced by reaction of electrons with L-alanine in a deuterated alkaline glass. A, First species the dianion at 90°K. B, Second species $\cdot CH(CH_3)CO_2^-$ at 180°K. C, Third species $ND_2\dot{C}(CH_3)CO_2^-$ at 195° K. D. Third species $NH_2\dot{C}(CH_3)CO_2^-$ at 190°K in alkaline $H_2O$, Note loss of resolution due to the proton splittings on nitrogen and increased dipole–dipole interactions.

only for glycine (Figure 1a).[17] The remaining amino acids generally show only broad singlet spectra 10–12 G wide (see Figures 2a and 3a). These spectra can be associated with the dianion radicals of the amino acids formed through reaction 2. The dianions are rela-

$$\begin{array}{l} \mathrm{ND_2} \\ | \\ \mathrm{R{-}CH{-}CO_2^-} \end{array} + \mathrm{e^-} \longrightarrow \begin{array}{l} \mathrm{ND_2} \\ | \\ \mathrm{R{-}CH{-}CO_2^{2-}} \end{array} \qquad (2)$$

(15) P. B. Ayscough, R. G. Collins, and F. S. Dainton, *Nature*, **205**, 965 (1965).

(16) R. A. Holroyd and J. W. Glass, *Int. J. Radiat. Biol.*, **14**, 445 (1968).

(17) The $g$ values found for the various dianions did not differ significantly. The $g$ values for the subsequent radical species found in this work were also approximately 2.003. Thus it was not possible to distinguish the various radical species on the basis of the $g$ value.

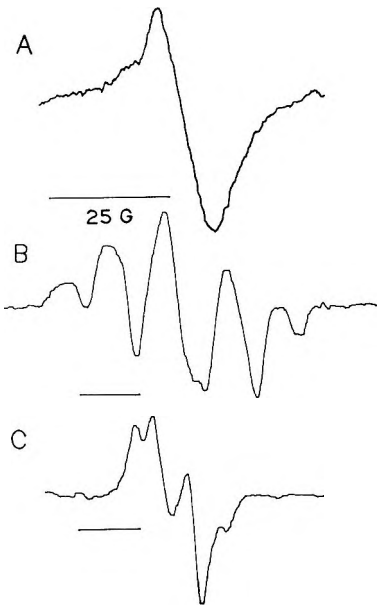


Figure 3. Esr spectra of radical species produced by reaction of electrons with L-leucine. A, First species the dianion at 90°K. B, Second species $\cdot CHRCO_2^-$ at 180°K. Another radical species, possibly unreacted dianion, increases the intensity of the central component. C, Third species $ND_2\dot{C}RCO_2^-$ at 195°K.

tively stable at 77°K although for glycine there was evidence for partial deamination even at this temperature.

The glycine dianion spectrum consists of a *ca.* 23-G doublet (the small components at the ends of the spectrum arise from the deaminated species).[18] The 23-G splitting can only arise from one of the protons $\beta$ to the carboxyl carbon. Its magnitude can be used to determine the spatial configuration of the $\beta$ protons. The relation between the isotropic $\beta$-proton splitting, $A_\beta^H$, and spatial configuration is given by

$$A_\beta^H = B_0\rho^\pi + B_2\rho^\pi \cos^2\theta \qquad (I)$$

This relation has been previously described in detail[19] and shown applicable to anions in an alkaline glass in work on the acetate dianion.[20] The acetate dianion should have a $\pi$-electron structure similar to glycine. Work on this species has given values of $B_0\rho^\pi = -3.2$ and $B_2\rho^\pi \cong 30$.[20] Using these values we find that $\theta \cong 20°$ for the $\beta$ proton of 23-G splitting. The lack of resolution of the second proton indicates that $\theta$ is near $-100°$ for this proton.

The dianions of L-alanine, L-leucine, L-isoleucine, and L-valine have one $\beta$ proton but their spectra do not show resolution of a proton splitting.[21] This suggests that the $\beta$ proton is in an orientation ($\theta$) which produces a small coupling ($50 \leq \theta \leq 130°$).

When the dianions of glycine and the alkyl amino acids are warmed to $T \leq 180°$K, a second radical species is formed. The esr spectra for these radicals (which are discussed in detail below) can only be interpreted on the basis that the dianions have undergone reductive deamination (reaction 3).

$$R{-}\overset{ND_2}{\overset{|}{C}}H{-}CO_2^{2-} \longrightarrow R{-}\dot{C}H{-}CO_2^- + ND_2^- \qquad (3)$$

For glycine a polycrystalline anisotropic spectrum (Figure 1b) due to the 2 $\alpha$ protons of the $\cdot CH_2CO_2^-$ radical is observed. At high modulation amplitudes in an $H_2O$ glass the spectrum becomes more nearly a 1:2:1 intensity ratio with a *ca.* 21-G splitting expected from other work on this species.[7-9,11] The structure of this radical has been verified by the reaction of electrons with $\alpha$ chloroacetic acid. This species is known to react by loss of chlorine to form the $\cdot CH_2CO_2^-$ radical.[15] An *identical* spectrum to that found in Figure 1b is observed. For L-alanine a spectrum (Figure 2b) expected from the $\cdot CH(CH_3)CO_2^-$ radical is observed. The spectrum arises from three equivalent methyl protons and one anisotropic $\alpha$ proton. The end multiplets of this spectrum clearly show the anisotropy of the $\alpha$ proton. The structure of the radical is further verified due to the fact that an identical spectrum is found by the reaction of electrons with $\alpha$-chloropropionic acid. Previously reported isotropic couplings of 24 G (methyl) and 21.4 G ($\alpha$ proton) adequately reproduce the spectrum when resolution of the anisotropic structure is lost in $H_2O$ glass.[5,8]

The spectra found for the second radical species of leucine, isoleucine, and valine can also be interpreted in terms of a deaminated radical, although in each case an interfering radical signal (probably unreacted dianion or electron) is apparent in the central portion of the spectra.[22] The spectrum for L-leucine (Figure 3b) can be interpreted in terms of a large 48-G splitting due to a single proton and a 20-G splitting due to two approximately equivalent protons. Owing to its magnitude the large 48-G splitting must arise from a $\beta$ proton. Thus the $\alpha$ proton and the remaining $\beta$ proton in the leucine $\alpha$ carbon radical structure have a splitting of approximately 20 G.[23] The intensity ratio expected from this interpretation is 1:2: ~2:2:1. The agreement with the experimental ratio is only fair. However, the interpretation presented here is considered the most likely since the total spread in the spectrum of 88

(18) Similar $\beta$-proton splittings have been found for glycine anion in single crystals (see ref 4, 8, and 9).

(19) M. D. Sevilla and G. Vincow, *J. Phys. Chem.*, **72**, 3647 (1968).

(20) M. D. Sevilla, *ibid.*, **74**, 669 (1970).

(21) The L-alanine dianion does show some resolution (Figure 2A). The line shape is suggestive of an anisotropic nitrogen hyperfine splitting.

(22) The deamination step for these species occurs at slightly higher temperature and is slower than for alanine or glycine. Thus it is difficult to prevent some mixture of the three radical species in this step.

(23) Due to the large line width in this radical, *ca.* 12 G, the hyperfine splittings for the $\alpha$ and $\beta$ proton may differ significantly and still average to 20 G.

G must arise from the interaction of $\beta$ protons. The spatial configuration of the $\beta$ protons in the deaminated species necessary to produce the observed splittings can be estimated by use of eq 1. For radicals of this type $B_0\rho^\pi$ and $B_2\rho^\pi$ are typically 0–4 G and 45 G, respectively.[19] The observed splittings would then arise for $\theta_1 \sim 0°$ and $\theta_2 \sim 120°$. This interpretation is supported by the fact that similar splittings are found for the deaminated species of $\alpha$ aminobutyric acid,[8] a radical whose steric interactions should place the $\beta$ protons in a configuration similar to the protons in leucine.

The esr spectrum of the second radical of L-isoleucine (Figure 4a) shows only a 22-G doublet presumably due to the $\alpha$ proton and no further splitting. Since the radical species expected has a single $\beta$ proton

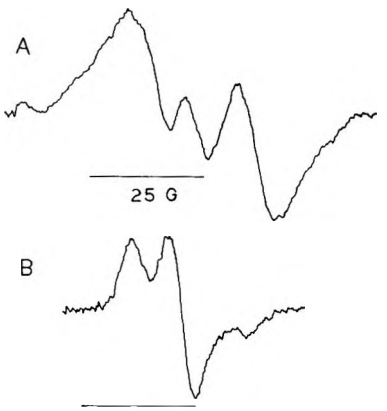


Figure 4. Esr spectra of radical species produced by reaction of electrons with L-isoleucine. A. Second species $\cdot CHRCO_2^-$ at 180°K. The central component arises from another radical species, most likely the unreacted dianion. B. Third species $ND_2\dot{C}RCO_2^-$ at 185°K. The dianion radical spectrum consists of a 10 G wide singlet.

as well as an $\alpha$ proton, this indicates that the $\beta$ proton is less than the line width in magnitude (10 G). A configuration ($75° < \theta < 105°$) which corresponds to a small $\beta$ proton splitting is reasonable from considerations of the steric interactions of the alkyl substituent in the radical.

The valine second species has a structure similar to that of isoleucine, *i.e.*, one $\beta$ proton and one $\alpha$ proton. The observed spectrum shows a 34 G total spread but little resolution. The 34-G spread is 12 G wider than expected for only an $\alpha$ proton. This suggests a 12-G $\beta$ proton splitting for the only $\beta$ proton.

Further warming of the alkaline glass containing the second radical species and the parent amino acid to *ca.* 190°K causes the glass to soften and results in an early complete conversion of the second radical species to a third ($g_{\text{isotropic}} \cong 2.003$). Interpretation of the esr spectra of the third species for each amino acid provides strong evidence for an abstraction reaction (reaction 4).

$$\begin{array}{l} \quad ND_2 \\ \quad | \\ R{-}CH{-}CO_2^- + R{-}\dot{C}H{-}CO_2^- \longrightarrow \\ \qquad\qquad\qquad ND_2 \\ \qquad\qquad\qquad | \\ \qquad\qquad\qquad R{-}\dot{C}{-}CO_2^- + RCH_2CO_2^- \end{array} \quad (4)$$

The esr spectrum observed for the third species of glycine consists of a 13.5-G doublet with small line components on either side of the doublet (Figure 1c). This spectrum can be interpreted on the basis of a radical of the structure $ND_2\dot{C}HCO_2^-$. The 13.5-G doublet must then arise from the $\alpha$ proton and the smaller line components from an anisotropic nitrogen with $A_{||} \cong 14.5$ G, $A_\perp < 3.5$ G ($^1/_2$ line width) and $g_\perp \leqq g_{||}$.

By analogy to glycine the spectrum observed for the third species of alanine (Figure 2c) would be expected to arise from the radical $ND_2\dot{C}(CH_3)CO_2^-$. For this radical a quartet splitting due to the methyl group would be expected which should be approximately equal to the $\alpha$-proton splitting in the third radical species of glycine. In addition, an anisotropic nitrogen splitting with parameters similar to those for the glycine radical should be found. Analysis of the spectrum yields a 13-G splitting due to three equivalent protons, an anisotropic nitrogen splitting with the parameters $A_{||} \cong 12$ G and $A_\perp < 2.5$ G, and $g_\perp - g_{||} \cong 0.0014$.[24] The results therefore provide convincing evidence for the identity of the radical species and consequently for the abstraction reaction, reaction 4.

The third spectra found for leucine (Figure 3c), isoleucine (Figure 4b) and valine are also interpretable on the basis of a radical of the structure $ND_2\dot{C}RCO_2^-$. Leucine shows a 13-G doublet and the anisotropic splittings of the nitrogen, $A_{||} \cong 12$ G, $A_\perp < 3.5$ G with $g_\perp - g_{||} \cong 0.0012$. The doublet must arise from one of the $\beta$ protons. The other $\beta$ proton must have a splitting less than the line width in magnitude. The values $\theta_1 = 45°$ and $\theta_2 = -75°$ would produce such proton splittings.[25,26] Isoleucine and valine show nearly identical third spectra. $\beta$-Proton splittings are not observable; only spectra which are characteristic of an anisotropic nitrogen are observed.[27] The nitrogen splittings are $A_{||} \cong 12$ G and $A_\perp < 3$ G with $g_\perp -$

(24) Owing to the large line widths and the consequent overlapping of components, the differences in values of the molecular $g$ values, $g_\perp$ and $g_{||}$, must be considered as estimates.

(25) The $\alpha$-carbon splitting for the third species of glycine suggests a spin density of *ca.* 0.5. A value of $B_2\rho^\pi$ equal to 25 G was therefore employed in this calculation.

(26) In polyleucine the analogous radical ($-NH\dot{C}(R)C(O)-$, with R) is formed after radiolysis (R. C. Drew and W. Gordy, *Radiat. Res.*, 18, 552 (1963)). To explain the hyperfine splittings found for the $\beta$-protons values of $\theta = 40°$ and $-80°$ were suggested. These values are in good agreement with those found here for the third radical species of leucine.

(27) N. Edelstein, A. Kwok, and A. H. Maki, *J. Chem. Phys.*, **41**, 179 (1964).

$g_{||} \cong 0.0013$ for both radicals. The lack of observation of a $\beta$-proton splitting suggests a spatial configuration ($\theta$) for the $\beta$ proton near 90°. This orientation is in excellent agreement with that expected from the steric interactions of the alkyl groups in these radicals.

It should be noted that the other possible site of hydrogen abstraction for leucine, isoleucine, and valine, *i.e.*, abstraction from the tertiary carbon of the alkyl group, would produce spectra totally inconsistent with those found in this work.[11,12]

The identification of the third radical species of the amino acids with the $ND_2$–$\dot{C}$(R)–$CO_2^-$ radical is further confirmed by the work of Taniguchi, *et al.*[28] They produced the $NH_2$-$\dot{C}$(H)$CO_2H$ radical in an aqueous flow system by the reaction of glycine and "hydroxyl" radicals. They find the $\alpha$-proton splitting to be 12.4 G in good agreement with that found here (13.5 G) for the third radical species of glycine. In addition, they find an isotropic nitrogen coupling of 6.6 G. From this value, the nitrogen spin density of 0.26 found by Taniguchi, *et al.*, to give good agreement with experiment, and the anisotropic hyperfine tensor for an axially symmetric aromatic nitrogen,[29] $A_{||}^N$ and $A_{\perp}^N$ are calculated to be 14.4 G and 2.7 G, respectively. These values are in excellent agreement with the experimental results of 14.5 G and < 3.5 G found for glycine. The values of $A_{||}^N$ and $A_{\perp}^N$ found for alanine, leucine, isoleucine, and valine are also in good agreement with the calculated values. This is expected because an $\alpha$-alkyl group should affect the spin density distribution only slightly.

*2.* L-*Asparagine and* $\beta$-*Alanine.* The amino acids discussed below were not found to conform to a general mechanism. In most cases they reacted in a unique manner depending on their side group. Thus they are discussed individually.

L-*Asparagine.* Reaction of the electron with asparagine at 77°K produces a radical whose esr spectrum shows a well resolved 24-G doublet (Figure 5a). Upon warming to 180°K the doublet splitting increases slightly to 26 G; however deamination does not occur. Upon further warming to 190°K the doublet converts directly to a spectrum (Figure 5b) characteristic of a third radical species showing a 13.5-G doublet splitting further split by an anisotropic nitrogen with $A_{||}^N \cong 14.5$, $A_{\perp}^N < 3.5$ G, and $g_{\perp} \cong g_{||}$.

Since doublet splittings were not found for carboxylic dianions with side groups such as alanine, leucine, isoleucine, and valine, and since the amide group of acetamide has been found to be quite reactive to electrons,[20] the first radical species is most likely the anion of the amide group of asparagine. The magnitude of the doublet splitting is that expected for a $\beta$ proton adjacent to the amide carbon at an angle of approximately 25° (this calculation assumes that the values of $B_0\rho^\pi$ and $B_2\rho^\pi$ for acetamide and the asparagine amide group

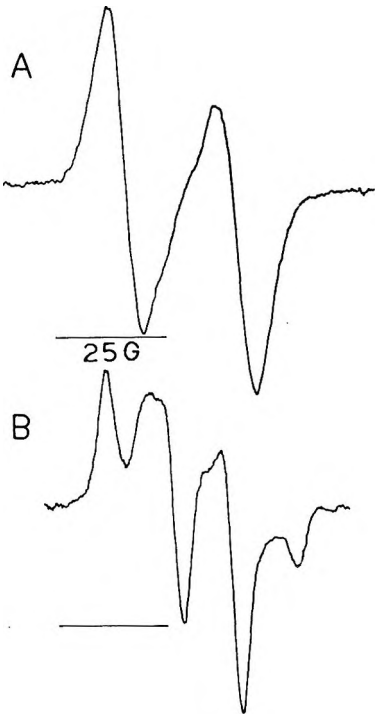


Figure 5. Esr spectra of radical species produced by reaction of electrons with L-asparagine. A, First species, the amide anion, at 175°K. B, Second radical species at 190°K. The second species resulted directly from the first. A radical species of the form $H\dot{C}RCO_2^-$ was not observed.

are the same).[20] The remaining $\beta$ proton which is unresolved must then be at an angle ($\theta$) near −95°.

The final species observed upon warming to 190°K may be the species associated with abstraction of the $\alpha$ proton. However, the fact that identical hyperfine parameters are found for this species and the glycine third species may point to a unique reaction resulting in $ND_2$–$\dot{C}H$–$CO_2^-$.

$\beta$-*Alanine.* Reaction of the electron with $\beta$-alanine at 77°K produces the dianion whose esr spectrum consists essentially of a 24-G doublet with a further splitting on the up-field line. Upon warming to 180°K the spectrum changes to a more nearly symmetric doublet (Figure 6), possibly due to a reorientation of the $\beta$ protons but deamination does not occur. Further warming to 190°K results in a loss of signal without observance of a second or third radical species. These results are in agreement with those of product analysis which show $\beta$-alanine does not undergo reductive deamination in aqueous solution.[30]

Reactions of electrons with the amino acids lysine, glutamic acid, phenylalanine, threonine, and serine were also investigated. All formed anion radicals, al-

(28) H. Taniguchi, K. Fukui, S. Ohnishi, H. Hatano, H. Hasegawa, and T. Maruyama, *J. Phys. Chem.*, **72**, 1926 (1969).

(29) J. N. Herack and W. Gordy, *Proc. Natl. Acad. Sci.*, **54**, 1287 (1965).

(30) R. L. Willin and W. M. Garrison, *Radiat. Res.*, **32**, 452 (1967).

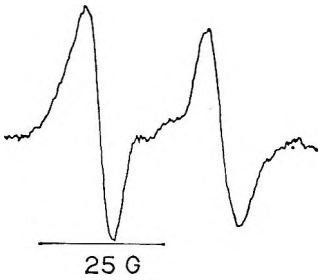


Figure 6. Esr spectrum of the β-alanine dianion at 180°K produced by reaction of electrons with β-alanine. No further reaction was observed for the dianion.

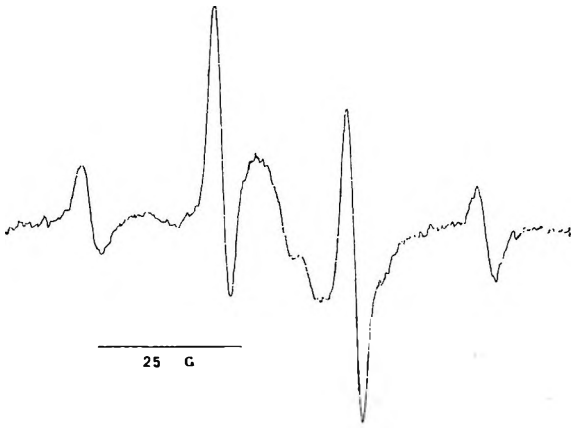


Figure 7. Esr spectrum of radical species produced by reaction of electrons with L-methionine at 77°K. The sharp four-line spectrum is due to the methyl radical. The broad signal in the central portion of the spectrum is most likely the carboxylic dianion.

though threonine and serine produced very little anion radical, perhaps due to the fact that the parent compound is in the alkoxyl ion form ($RO^-$) before reaction with the electron. Upon warming to 170°K lysine and glutamic acid showed evidence of deamination and eventually upon further warming produced spectra characteristic of the third radical species found for the alkyl amino acids. The dianion of phenylalanine did not give evidence of any further reaction.

*3. Sulfur-Containing Amino Acids. L-Methionine.* Reaction of the electron with methionine at 77°K results in the spectrum in Figure 7. The sharp 1:3:3:1 quartet of 22.5-G separation is undoubtedly due to the methyl radical. A second singlet species ($g \cong 2.003$), which is probably the carboxylic dianion, is also present in the spectrum.

The production of methyl radicals must occur by carbon–sulfur bond cleavage

$$\begin{array}{l} ND_2—\underset{\displaystyle CO_2^-}{\underset{|}{CH}}—CH_2—CH_2—S—CH_3 + e^- \longrightarrow \\ \qquad ND_2—\underset{\displaystyle CO_2^-}{\underset{|}{CH}}—CH_2—CH_2—S^- + CH_3\cdot \end{array} \quad (5)$$

To ensure that the methyl radical did not arise from photolysis, samples were photolyzed in the absence of $K_4Fe(CN)_6$. The results showed no signal due to the methyl radical. Thus it is certain that the methyl radicals are produced by reaction of the electron with methionine.

Upon warming the sample the methyl radical and the carboxylic dianion signals disappear and a new spectrum appears which could and probably does arise from several species formed by reactions of the methyl radicals and the dianion. No assignment is therefore attempted.

*L-Cystine.* Cystine proved to be very reactive toward the electron. Photobleaching a solution of cystine (1 m*M*) and the electron at 77°K produced a bright yellow color associated with the disulfide anion. The esr spectrum shows a single broad (30 G wide) resonance at $g \cong 2.012$. The high $g$ value is indicative of a sulfur anion. During warming, the signal decays without the growth of a second species.

## Summary and Conclusions

*1. Amino Acids with Reactive Side Groups.* The reaction of electrons with the amino acids asparagine, methionine, and cystine shows that the reactive side group in these molecules is a point of electron localization or attack. For asparagine, electron attachment to the amide group is indicated. Reactions of electrons with methionine produce methyl radicals by C–S bond cleavage. Cystine is found to produce the disulfide anion.

It is felt the results found here for methionine and cystine may be of significance in the interpretation of the results of previous electron spin resonance studies of irradiated single crystals of methionine[31–33] and cystine.[34,35]

*2. Glycine and Amino Acids with Alkyl Side Groups.* Radical intermediates observed in this work after electron attachment to glycine and L-alanine in an alkaline medium are in agreement with those proposed previously to account for the results of radiolysis experiments in aqueous solution at pH 7; that is, the electron is found to add to the carboxyl group, the amino acid dianion formed subsequently deaminates to produce a $\cdot CHRCO_2^-$ radical, and this species abstracts from the α carbon of the parent amino acid to form the $ND_2\dot{C}(R)CO_2^-$ radical. Results found here for the amino acids leucine, isoleucine, and valine are also in agreement with this mechanism.

(31) D. G. Cadena and J. R. Rowlands, *J. Chem. Soc., B*, 488 (1968).

(32) E. Cipollini and W. Gordy, *J. Chem. Phys.*, **37**, 13 (1962).

(33) J. H. Hadley, *Bull. Amer. Phys. Soc.*, **13**, 1695 (1968).

(34) K. Akasaka, S. Ohnishi, T. Suita, and I. Nitta, *J. Chem. Phys.*, **40**, 3110 (1964).

(35) H. C. Box and H. G. Freund, *ibid.*, **40**, 817 (1964).

The difference in pH between this work and previous work results in certain differences in the radical species solely due to protonation. For example, the parent compound at pH 7 is the zwitterion, $NH_3^+CHRCO_2^-$. The anion, deaminated, and final radical species most likely have the structure $NH_3^+CHRCO_2H^-$, $\cdot CHRCO_2H$, and $NH_2\dot{C}RCO_2H$, respectively. The amine group of the third species is not considered to be protonated at pH 7, since esr results in aqueous solution have shown that the amine group of $NH_2\dot{C}HCO_2H$ is unprotonated even at acid pH.[28] This differs from results in the solid state which show the amine group is protonated.[13]

As was discussed previously, electron spin resonance investigations of irradiated single crystals of amino acids with alkyl side groups have shown that the electron attachment and deamination steps occur but abstraction from the $\alpha$-carbon position does not occur. Instead, abstraction occurs from the tertiary carbon of the alkyl group. If no tertiary carbon proton is available, as in the case of alanine, abstraction does not occur. The difference in results between the crystalline and aqueous media is considered significant. It suggests that the environment largely determines the most stable final radical species.

Finally, the fact that the radical intermediates stabilized in an alkaline glass correspond to those proposed from studies of the radiolysis of amino acids in aqueous solution (taking into account differences in protonation) suggests the techniques used in this work may be employed in other systems to yield results applicable to the solution chemistry of these systems.[36]

(36) A study of the reactions of electives and peptides is in progress.

# Pulse Radiolysis Studies of Deaerated Alcoholic Solutions of Alkali Halides and Potassium Hydroxide

by Shigeyoshi Arai, Akira Kira, and Masashi Imamura

*The Institute of Physical and Chemical Research, Yamato-machi, Saitama, Japan* *(Received December 1, 1969)*

The pulse radiolysis of alcoholic solutions of alkali halides and potassium hydroxide has been studied in the concentration range from $10^{-2}$ to 3 *M*. Absorption bands due to $Cl_2^-$, $Br_2^-$, and $I_2^-$ were observed in irradiated solutions of alkali halides. On the other hand, the light-absorbing species in irradiated solutions of potassium hydroxide may be assigned to the $CH_2O^-$ radical and the $CH_3CHO^-$ radical. Further, the intense absorption due to the solvated electron was observed in all cases. Yields of the solvated electron increase with increase in concentration of the solutes. This may be attributed to the reaction $ROH^+ + X^- \rightarrow ROH + X$ leading to a decrease of the charge neutralization between the solvated electron and the positive ion in the spur region. A halogen atom produced by this reaction combines with a halogen ion.

## Introduction

A number of papers[1-6] have been published concerning the pulse radiolysis of aqueous solutions of alkali halides at various pH's. The transient species absorbing light in the uv region were identified as $Cl_2^-$, $Br_2^-$, and $I_2^-$ in these works. The following mechanism has been considered to account for the formation of $Br_2^-$ and $I_2^-$ at neutral pH.

$$X^- + OH \longrightarrow X + OH^- \quad (1)$$

$$X + X^- \longrightarrow X_2^- \quad (2)$$

In the case of the chloride ion reaction 1 is not believed to occur at neutral pH since the reaction appears to be endothermic.[7] However, Anbar and Thomas[1] observed the formation of $Cl_2^-$ at chloride concentrations of 0.1 *M* or greater. Recently, Hamill[8] proposed that X could

(1) M. Anbar and J. K. Thomas, *J. Phys. Chem.*, **68**, 3829 (1964).

(2) B. Cercek, M. Ebert, C. W. Gilbert, and A. J. Swallow, "Pulse Radiolysis," Pergamon Press, Inc., Elmsford, N. Y., 1965, p 83.

(3) H. C. Sutton, G. E. Adams, J. W. Boag, and B. D. Michael, "Pulse Radiolysis," Pergamon Press, Inc., Elmsford, N. Y., 1965, p 61.

(4) M. S. Matheson, W. A. Mulac, J. L. Weeks, and J. Rabani, *J. Phys. Chem.*, **70**, 2092 (1966).

(5) J. K. Thomas, *Trans. Faraday Soc.*, **61**, 702 (1965).

(6) J. H. Baxendale, P. L. T. Bevan, and D. A. Scott, *ibid.*, **64**, 2398 (1968).

(7) A. O. Allen, "The Radiation Chemistry of Water and Aqueous Solution," Van Nostrand-Reinhold Co., Inc., Princeton, N. J., 1961, p 63.

(8) W. H. Hamill, *J. Phys. Chem.*, **73**, 1341 (1969).

be formed at high concentrations of halide ions by the reaction

$$H_2O^+ + X^- \longrightarrow H_2O + X \qquad (3)$$

The action of ionizing radiation on alcohols is in many ways similar to that on water. However, little attention has been paid to alcoholic solutions of alkali halides. Theard and Burton[9] investigated $^{60}Co$ $\gamma$ radiolysis of methanol solutions of potassium iodides and several other salts. They suggested that the methoxy radical oxidized the iodide ion in a manner similar to reaction 1. This process was supported by the pulse radiolysis study of the same system.[10]

In the present paper transient species in irradiated alcoholic solutions of alkali halides at relatively high concentrations have been studied by the pulse radiolysis technique. The observed results can be explained by a reaction analogous to reaction 3.

## Experimental Section

The pulsed electron source was a 3-MeV Mitsubishi Van de Graaff accelerator. Pulse lengths were 0.3, 0.7, 1.4, and 3.5 $\mu$sec. In most of the experiments the shortest pulse length was used. The upper limit of the current was approximately 200 mA. A 0.7-$\mu$sec pulse at 160 mA delivers a dose of $9.6 \times 10^3$ rads. Solutions were irradiated in box-shape cells with the high-purity silica windows on both sides. The inside dimensions of the cell were 1.3 cm × 2.2 cm × 2.2 cm. A glass bulb was provided with the cell for the purpose of degassing solutions.

The spectrophotometric observation technique is essentially identical with those commonly employed in pulse radiolysis studies.[11] An "Ushio" 150-W xenon lamp was used as the continuous light source. The light beam passed twice through the reaction cell at right angles to the direction of the electron beam. The optical path length was 4.4 cm. The monochromator used was a "Nalumi RM 23." Two photomultipliers, HTV R-106 and R-136, were set behind the monochromator so that light at two different wavelengths can be measured at the same time. When a spectrum was plotted, one photomultiplier was used at the fixed wavelength to monitor the pulse intensity.

Methanol and ethanol were purified by a method similar to that described in an earlier paper.[12] Alkali halides and potassium hydroxide were of analytical reagent grade and were used without further purification. The samples were degassed on a vacuum line by shaking while pumping. Solutions of sodium iodide were prepared in a different manner, since they turned yellow in the presence of air. A certain amount of sodium iodide was loaded and degassed in the irradiation cell before methanol was distilled into the cell *in vacuo*.

Further details of the apparatus will be reported elsewhere. A part of the present work has been carried out at Ohio State University. The apparatus used there has been described in an earlier paper.[13]

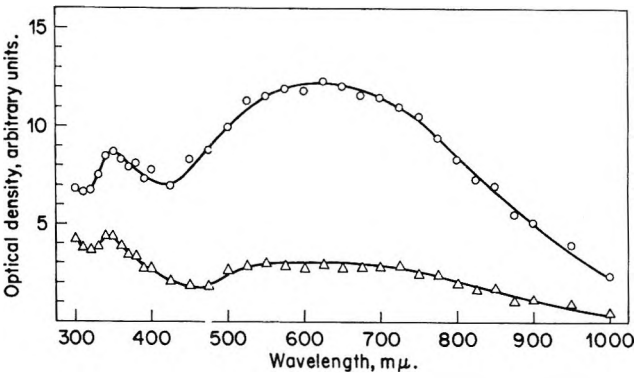


Figure 1. Absorption spectra of irradiated ethanol solution of lithium chloride. The concentration of lithium chloride is 3.31 *M*: ○, 1.7 $\mu$sec after pulse; △, 4.7 $\mu$sec after pulse.

## Results

*Chloride Ion.* Figure 1 shows the absorption spectra obtained by irradiating an ethanol solution of lithium chloride at 3.31 *M*. The spectrum exhibits two peaks with $\lambda_{max}$ at 625 m$\mu$ and $\lambda_{max}$ at 350 m$\mu$. The light-absorbing species in the wavelength region longer than 500 m$\mu$ decays by the first-order rate law with $\tau_{1/2}$ of 1.8 $\mu$sec. It can be assigned confidently to the solvated electron, although $\lambda_{max}$ shifts from 700 m$\mu$ for pure ethanol.[14,15] Anbar and Hart[16] have reported that various electrolytes affect the absorption spectrum of the hydrated electron by a shift to shorter wavelength. The same effect may also be expected in the case of alcoholic solutions. Furthermore, the absorption spectra of the solvated electron seem to be broader in these solutions. Decay curves in the wavelength region shorter than 400 m$\mu$ show a large contribution due to a species longer-lived than the solvated electron. The wavelength of the maximum absorption of this species agrees well with that of $Cl_2^-$.[1,17,18] Although the $CH_3CHOH$ radical absorbs light below about 400 m$\mu$, its spectrum[15,19] increases smoothly as

(9) L. M. Theard and M. Burton, *J. Phys. Chem.*, **67**, 59 (1963).

(10) F. S. Dainton, I. V. Janovsky, and G. A. Salmon, *Chem. Commun.*, 335 (1969).

(11) L. M. Dorfman and M. S. Matheson, *Progr. React. Kinet.*, **3**, 237 (1965).

(12) I. A. Taub, D. A. Harter, M. C. Sauer, Jr., and L. M. Dorfman, *J. Chem. Phys.*, **41**, 979 (1964).

(13) S. Arai, D. A. Grev, and L. M. Dorfman, *ibid.*, **46**, 2572 (1967).

(14) M. C. Sauer, Jr., S. Arai, and L. M. Dorfman, *ibid.*, **42**, 708 (1965).

(15) S. Arai and M. C. Sauer, Jr., *ibid.*, **44**, 2297 (1966).

(16) M. Anbar and E. J. Hart, *J. Phys. Chem.*, **69**, 1244 (1965).

(17) M. S. Matheson, W. A. Mulac, and J. Rabani, *ibid.*, **67**, 2613 (1963).

(18) R. Devonshire and J. J. Weiss, *ibid.*, **72**, 3815 (1968).

(19) I. A. Taub and L. M. Dorfman, *J. Amer. Chem. Soc.*, **84**, 4053 (1962).

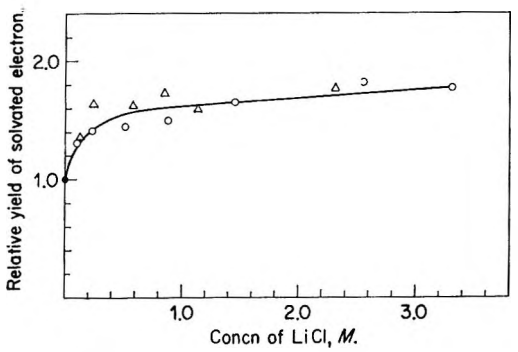


Figure 2. Relative yields (initial optical densities) of the solvated electron as a function of lithium chloride concentration: O, ethanol solutions of LiCl; △, methanol solutions of LiCl; ●, pure alcohols.

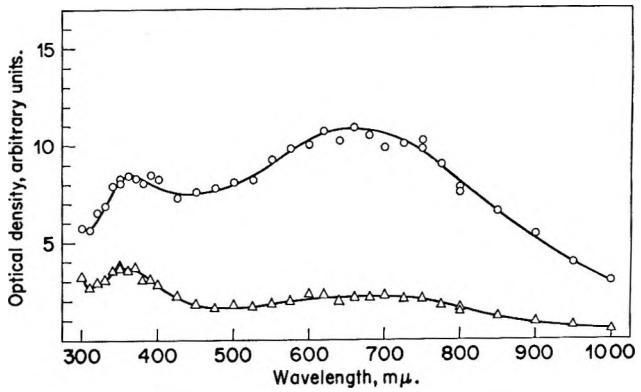


Figure 3. Absorption spectra of irradiated ethanol solution of lithium bromide. The concentration of lithium bromide is 0.45 *M*: O, 1.5 μsec after pulse; △, 5.3 μsec after pulse.

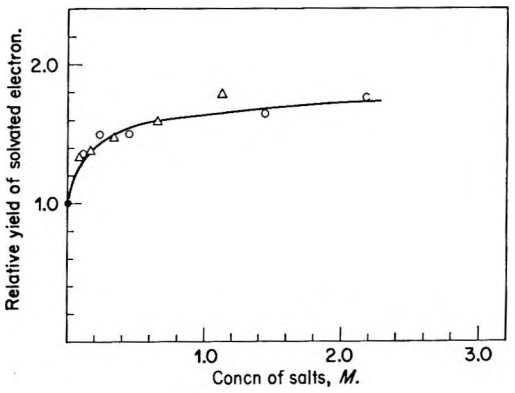


Figure 4. Relative yields (initial optical densities) of the solvated electron as a function of salt concentration: O, ethanol solutions of LiBr; △, methanol solutions of NaBr; ●, pure alcohols.

the wavelength decreases and the absorption intensity is relatively weak, even at 300 mμ.

Similar spectra have been obtained for irradiated methanol solutions of lithium chloride.

In Figure 2 initial optical densities of the solvated electron are shown as a function of salt concentration. Since the solvated electron decays by the first-order rate law, initial optical densities were estimated by the extrapolation of the linear log $D$ *vs.* $t$ plot to the middle point of the pulse. On the other hand, the decay curve of the solvated electron in pure ethanol and methanol is not first order, and probably includes the second-order reaction with the counterion. Therefore, assuming the occurrences of both the first-order reaction and the second-order reaction, an empirical equation which expresses the decay behavior was determined in a manner similar to that in a previous paper.[20] The decay curve then was extrapolated to find the initial optical density. As shown in Figure 2, addition of lithium chloride to alcohols results in greater yields of the solvated electron. Values are almost constant above 1 *M* of the solute. This fact indicates that additional formation of the solvated electron does not arise from the direct effect of ionizing radiation on the solute. The $^{60}Co$ γ radiolysis of methanol solution of 1 *M* lithium chloride also has been carried out in the presence of $1 \times 10^{-2}$ *M* nitrous oxide,[21] which converts $e_{sol}^-$ into nitrogen by the following reaction.

$$e_{sol}^- + N_2O \longrightarrow N_2 + O^-$$

The yield of nitrogen was $G(N_2) = 2.7$. There is still a lack of agreement among various investigators on the yield of the solvated electron in the radiolysis of pure methanol. $G$ values have been reported from 1.1 to 2.0.[14,22-24] Suryanarayanan and Lichtin have recently reported $1.45 \pm 0.30$.[25] $G(N_2) = 2.7$, which is apparently higher than any of these reported values, indicates an increase of the yield of the solvated electron in the presence of lithium chloride.

Half-lives of the solvated electron in solution are almost independent of the concentration of lithium chloride. Average values are 1.8 μsec for ethanol solutions and 1.7 μsec for methanol solutions. $Cl_2^-$ was observed only at chloride ion concentrations greater than 1 *M*. The time necessary for $Cl_2^-$ to disappear is several tens of μsec.

*Bromide Ion.* Figure 3 shows the absorption spectra obtained by irradiating an ethanol solution of lithium bromide at 0.45 *M*. The peak at 660 mμ is due to the solvated electron,[14] while the peak at 360 mμ agrees well with the absorption maximum of $Br_2^-$.[2-4,17,18] Similar spectra have been observed in irradiated methanol solutions of lithium bromide and sodium bromide.

In Figure 4 initial optical densities of the solvated electron are shown as a function of salt concentration. The solvated electron in these solutions decays by the first-order rate law. Average half-lives are 2.0 μsec

(20) S. Arai and L. M. Dorfman, *J. Chem. Phys.*, **41**, 2190 (1964).
(21) H. Seki, S. Arai, and M. Imamura, to be published.
(22) H. Seki and M. Imamura, *J. Phys. Chem.*, **71**, 870 (1967).
(23) E. Hayon and M. Moreau, *ibid.*, **69**, 4053 (1965).
(24) K. N. Jha and G. R. Freeman, *J. Chem. Phys.*, **48**, 5480 (1968).
(25) K. Suryanarayanan and N. N. Lichtin, *J. Phys. Chem.*, **73**, 1384 (1969).

for ethanol solutions of lithium bromide, and 1.5 μsec for methanol solutions of sodium bromide. $Br_2^-$ was observed at salt concentrations greater than 0.3 *M*, and the approximate time of its disappearance is 100 μsec.

*Iodide Ion.* Figure 5 shows the absorption spectra obtained by irradiating methanol solutions of sodium iodide. The peak at 380 mμ agrees well with the absorption maximum of $I_2^-$ in the uv region.[5,6,17,18] Furthermore, another peak of the spectrum observed at 20 μsec after pulse is in good agreement with the absorption maximum of the additional band of $I_2^-$ in the longer wavelength region.[18] The spectrum observed at 1 μsec after the pulse shows a shoulder at about 600 mμ. The light-absorbing species at this wavelength decays by the first-order rate law with a half-life of 1.9 μsec regardless of the concentration of sodium iodide. This species can be identified as the solvated electron. The absorption due to $I_2^-$ or other longer-lived species is almost negligible at this wavelength.

In Figure 6 initial optical densities of the solvated electron are shown as a function of salt concentration. The absorption at 740 mμ which fits the absorption maximum of $I_2^-$ decays by the second-order rate law except for the initial rapid portion due to the solvated electron. The time necessary for the disappearance is about several hundred μsec. In the shorter wavelength region a highly stable species is observed after $I_2^-$ disappears almost completely. Although the absorption spectrum of this species is similar to $I_2^-$, the absorption maximum is at about 360 mμ and there is no band in the longer wavelength region. These characteristics fit the absorption spectrum of $I_3^-$.[26] $I_2^-$ is formed efficiently at concentrations of sodium iodide as low as $10^{-2}$ *M*.

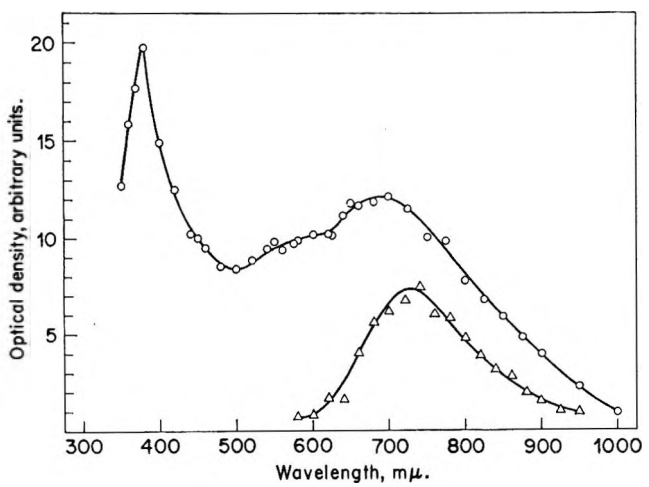


Figure 5. Absorption spectra of irradiated methanol solutions of sodium iodide. Optical density scale for the lower spectrum is expanded fivefold. However, absolute intensities of both spectra cannot be compared to each other because of the difference in the irradiation condition: ○, 1.0 μsec after pulse, the concentration of NaI is 0.56 *M*; △, 20.0 μsec after pulse, the concentration of NaI is 0.68 *M*.

*Potassium Hydroxide.* Figure 7 shows the absorption spectra obtained for irradiated alcoholic solutions of potassium hydroxide and an ethanol solution of sodium metal observed 30 μsec after the pulse. The latter solution was prepared by dissolving sodium metal in ethanol, and then degassing by the freezing and pumping method. In these solutions the initial intense absorption due to the solvated electron is observed in the visible region. Yields and half-lives of the solvated electron are shown in the Table I. These yields were determined in a manner similar to that described in the case of lithium chloride solution. After decay of the solvated electron the absorption due to the longer-lived species which decays by the second-order rate law is observed in the uv region as shown in Figure 7. Their absorption spectra which are different from those of the $CH_2OH$ radical and the $CH_3CHOH$ radical in intensity may be attributed to the $CH_2O^-$ radical and the $CH_3CHO^-$ radical. Sherman[27] reported evidence for the existence of the $CH_2O^-$ radical in irradiated methanol solutions of potassium hydroxide.

**Table I:** Relative Yields and Half-Lives of the Solvated Electron in Irradiated Alcoholic Solutions of Potassium Hydroxide and Ethanol Solution of Sodium Metal

| Solvent | Solute | Conc, *M* | Relative yield | Half-life, μsec |
|---|---|---|---|---|
| Methanol | KOH | 0.15 | 1.7 | 3.5 |
| Methanol | KOH | 0.27 | 1.8 | 3.6 |
| Methanol | KOH | 0.37 | 1.9 | 3.8 |
| Methanol | KOH | 0.58 | 1.9 | 3.7 |
| Methanol | KOH | 1.65 | 1.9 | 4.1 |
| Methanol | KOH | 2.00 | 1.9 | 4.3 |
| Methanol | KOH | 2.65 | 1.9 | 5.2 |
| Ethanol | KOH | 0.14 | 1.7 | 4.5 |
| Ethanol | KOH | 0.29 | 1.7 | 5.1 |
| Ethanol | KOH | 0.60 | 1.8 | 6.8 |
| Ethanol | Na | 0.27 | 2.1 | 5.5 |

## Discussion

Addition of alkali halides to methanol and ethanol results in increased yield of the solvated electron, along with the formation of $X_2^-$.

Freeman and Fayadh[28] have concluded that the *G* value of the solvated electron is roughly proportional to the static dielectric constant of the solvent. In their model the coulombic attraction between the electron and the parent positive ion draws them back together, while diffusive forces drive them apart. However, the measurements made with alcoholic solutions

(26) D. Meyerstein and A. Treinin, *Trans. Faraday Soc.*, **59**, 1114 (1963).

(27) W. V. Sherman, *Chem. Commun.*, 790 (1966).

(28) G. R. Freeman and J. M. Fayadh, *J. Chem. Phys.*, **43**, 86 (1965).

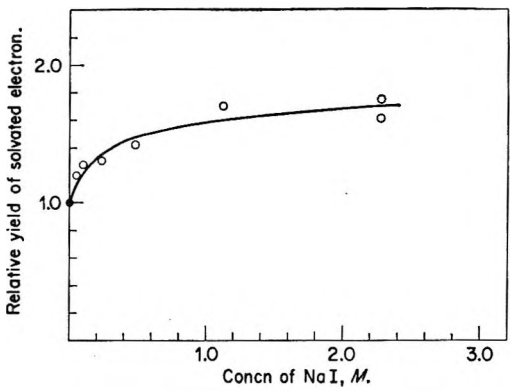


Figure 6. Relative yields (initial optical densities) of the solvated electron as a function of sodium iodide concentration: O, methanol solutions; ●, pure methanol.

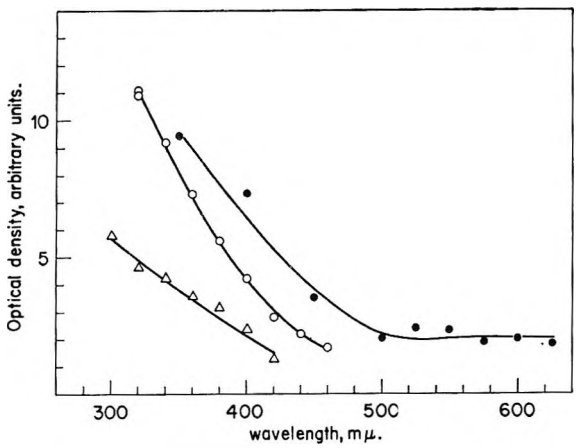


Figure 7. Absorption spectra of irradiated alcoholic solutions of potassium hydroxide and ethanol solution of sodium metal: O, 30.0 μsec after pulse, ethanol solution of KOH (0.29 *M*); ●, 30.0 μsec after pulse, ethanol solution of Na (0.27 *M*); △, 30.0 μsec after pulse, methanol solution of KOH (3.28 *M*).

of various electrolytes[29] show that the static dielectric constant decreases as the concentration of electrolytes increases. This result predicts the reduction of the yield of the solvated electron, if the above-mentioned model is applied to the present systems.

Generally speaking, reactions in the spur region occur at solute concentrations greater than $10^{-2}$ *M* in aqueous solutions. Hayon and Moreau[23] have investigated the $^{60}$Co γ radiolysis of alcoholic solutions of lithium nitrate and chloroacetic acid over a wide concentration range. These compounds are considered to react efficiently with reducing species such as the solvated electron and the hydrogen atom. They have found that above a certain solute concentration ($\simeq 10^{-2}$ *M*) the yield of the reducing species increases with further increase in the solute concentration. This result has been attributed to electron capture by solutes in the spur region leading to a decrease of the neutralization reaction.

$$e_{sol}^- + \text{solute} \longrightarrow \text{product}$$

$$e_{sol}^- + ROH^+ \longrightarrow ROH$$

Thomas and Bensasson[30] have observed directly the decay behavior of the solvated electron in both water and ethanol using the nanosecond pulse radiolysis apparatus. A certain portion of the solvated electron has been found to disappear over an initial period of 70 ∼ 80 nsec in both cases. The addition of 0.1 *M* sodium hydroxide to ethanol inhibits the fast decay and gives only the slower decay. They suggest that the rapid decay is due to the reaction of the solvated electron with the positive ion in the spur region, and the addition of sodium hydroxide removes the positive ion.

Our observations only follow the solvated electron decay on a microsecond time scale. The initial yields obtained from decay curves should correspond to the yields of the solvated electron which escapes geminate recombination. If the addition of potassium hydroxide removes the positive ion in irradiated solutions, the yield of the freely diffusing solvated electron will increase. It is the case as shown in Table I. The results obtained from irradiated alcoholic solutions of alkali halides may also be explained by the removal of the positive ion in the spur region. The primary positive ion in irradiated alcohols should be mainly $ROH^+$. $ROH^+$ is generally believed to change into the $ROH_2^+$ ion as the result of an ion-molecule reaction within $10^{-14}$ sec, based on rate constants determined from results in the mass spectrometer. Halogen ions are considered not to react with $ROH_2^+$ in alcohols. Therefore, we conclude that halogen ions react with $ROH^+$ to prevent its ion–molecule reaction, as suggested by Hamill[8] for aqueous solutions of alkali halides. A probable mechanism may be as follows. Reaction 6

$$ROH \xrightarrow{\sim\sim} ROH^+, e_{sol}^-, + \ldots \quad (4)$$

$$ROH^+ + ROH \longrightarrow ROH_2^+ + RO$$

$$\text{or other radical} \quad (5)$$

$$e_{sol}^- + ROH_2^+ \longrightarrow ROH + H \quad (6)$$

$$ROH^+ + X^- \longrightarrow ROH + X \quad (7)$$

$$X + X^- \longrightarrow X_2^- \quad (8)$$

$$X + ROH \longrightarrow ROH_2^+ + X^- + \text{radical} \quad (9)$$

occurs in the spur region. In dilute solutions of potassium hydroxide the positive ion may be removed by reaction 10 and in the concentrated solutions by

$$ROH_2^+ + RO^- \longrightarrow 2ROH \quad (10)$$

reaction 11. The fact that reaction 7 competes with

$$ROH^+ + RO^- \longrightarrow ROH + RO \quad (11)$$

reaction 5 at the concentration of 0.1 *M* indicates $k_7 \cong 100\ k_5$. It appears that either rate constants of

(29) J. A. Lane and J. A. Saxton, *Proc. Roy. Soc.*, **A214**, 531 (1952).
(30) J. K. Thomas and R. V. Bensasson, *J. Chem. Phys.*, **46**, 4147 (1967).

reaction 7 are extraordinarily large because of the rapid intermolecular transfer of the positive charge, or rate constants of ion–molecule reaction 5 are much lower in liquids than under conditions of mass spectrometric studies.

The formation of $I_2^-$ at concentrations of sodium iodide as low as $10^{-2}$ $M$ can be explained by the following mechanism. At least in the case of the chloride

$$CH_3O + I^- \longrightarrow CH_3O^- + I \qquad (12)$$

$$I + I^- \longrightarrow I_2^-$$

ion, the reaction similar to reaction 12 is considered thermodynamically impossible at room temperature since the electron affinities of the $CH_3O$ radical or the $CH_3CH_2O$ radical may be equal to or more likely less than that of the OH radical.

The absorption due to the solvated electron decays by the first-order rate law in all solutions of alkali halides, indicating the reaction with an alcohol molecule

$$e_{sol}^- + ROH \longrightarrow RO^- + H \qquad (13)$$

The solvated electron decays by the first-order rate law in solutions of potassium hydroxide. However, the half-life increases with concentration of potassium hydroxide, which has not been observed for all alkali halide solutions. It seems likely that the hydrogen atom produced by reaction 13 reproduces the solvated electron at high concentrations of potassium hydroxide in competition with the abstraction reaction from the solvent molecule. If reaction 14 takes place, one might expect

$$H + RO^- \longrightarrow e_{sol}^- + ROH \qquad (14)$$

$$H + ROH \longrightarrow H_2 + \text{radical} \qquad (15)$$

such a variation of the half-life of the solvated electron with concentration of potassium hydroxide. Another possibility is that the solvated electron forms an ion pair ($e_{sol}^-$, $K^+$) at high concentrations of potassium ion. This ion pair might react with solvent alcohol at much lower rate than the free solvated electron. Further investigation of alkaline solutions is in progress.

*Acknowledgment.* The authors wish to thank Mr. S. Wako for technical assistance in operation of the Van de Graaff accelerator. The present work was initiated by S. A. during his stay at Ohio State University. The authors also wish to thank Prof. L. M. Dorfman and the Radiation Chemistry Group at Ohio State University.

# Chemiluminescent Reactions after Pulse Radiolysis of Aqueous Solutions of Acriflavin. Effects of Halides and Pseudo Halides

**by W. A. Prütz**

*Radiologisches Institut der Universität Freiburg, 7800 Freiburg im Breisgau, Germany*

**and E. J. Land**

*Paterson Laboratories, Christie Hospital and Holt Radium Institute, Manchester M20 9BX, England*

*(Received January 20, 1970)*

Chemiluminescent emissions occurring after pulse radiolysis of aqueous solutions of acriflavin can be enhanced up to three times in the presence of $X^-$ (halides or pseudo halides). Reactions of $e_{aq}^-$ with the products of X atom or $X_2^-$ attack upon the dye are believed to be the cause of the enhanced emissions.

## Introduction

Several dyes of the xanthene and acridine type have been found to exhibit chemiluminescence after reaction with the products of water radiolysis, OH radicals and $e_{aq}^-$.[1-4] Application of pulse radiolysis has made it possible to study the kinetics of this chemiluminescence, which was found to build up and decay during tens of microseconds after a pulse. Various tests using $e_{aq}^-$ scavengers and OH scavengers showed that the reaction of $e_{aq}^-$ with an OH adduct of the dye (DOH) or

(1) W. Prütz, K. Sommermeyer, and E. J. Land, *Nature*, 212, 1043 (1966).

(2) W. Prütz and E. J. Land, *Biophysik*, 3, 349 (1967).

(3) L. I. Grossweiner and A. F. Rodde, Jr., *J. Phys. Chem.*, 72, 756 (1968).

(4) W. Prütz and K. Sommermeyer, *Biophysik*, 4, 48 (1967).

with semioxidized dye ($D^+$) was the most probable main emission-forming process.[2] The efficiency of this process was found to be about $10^{-2}$ quanta per reaction[2] for the dye rhodamine B. Evidence in the case of fluorescein and eosin for the involvement of an OH adduct, rather than semioxidized dye, has been deduced by Grossweiner and Rodde[3] using sequential light flash and electron pulse irradiation. Low-energy X-irradiation of aqueous dyes leads to chemiluminescent emission, which is again strongly quenched by $e_{aq}^-$ scavengers and some OH scavengers.[4]

Previous investigations showed that addition of small amounts of iodide to dye solutions leads to a considerable increase in the emission induced by electron pulse irradiation[2] or low-energy X-irradiation.[4] This effect was attributed to a chemiluminescent reaction involving iodine atoms and semireduced dye ($D^-$).[2] In the present pulse radiolysis experiments the iodide effect and also similar effects due to other halides and pseudo halides have been systematically studied. The dye acriflavin was selected for this study although other dyes, *e.g.*, eosin, fluorescein,[2] and β-naphthylamine,[5] also yield enhanced emissions on adding iodide.

## Experimental Section

The acriflavin (3,6-diamino-10-methyl acridinium chloride) used was of analytical reagent grade and was supplied by Fluka A.G., Switzerland. The solutions for all emission experiments were deaerated by bubbling with argon for at least 1 hr. The water used was redistilled from alkaline permanganate in an atmosphere of nitrogen. Solutions were irradiated in spectrosil cells with 8–14-MeV electrons from a Vickers linear accelerator using the pulse radiolysis apparatus of Keene.[6] Pulses of 2 μsec or less were used, the dose per pulse varying from 150 to 250 rads. With pure water a very weak and short-lived emission was observed, probably arising from the irradiation cell itself. This emission was subtracted in the results reported below. The time characteristics of the observed dye emission were reproducible to within ±15%. The calculations of emission time characteristics were carried out using the IBM-7040 digital computer of the University of Freiburg Computer Center. Doses were measured either by modified ferrous sulfate (Fricke) dosimetry or using the absorption of $e_{aq}^-$, taking $\epsilon(720\text{ nm}) = 1.8 \times 10^4\ M^{-1}\ cm^{-1}$,[7] together with a $G(e_{aq}^-)$ value of 2.6.[8]

## Results

*(1) Acriflavin Alone.* The time dependencies of the pulse-radiolysis-induced chemiluminescence of neutral solutions of acriflavin for various dye concentrations can be seen in Figure 1a–c (curves with no $I^-$). All time characteristics were measured at 505 nm, the maximum of the emission spectrum which corresponded to the spectrum of the uv-induced fluorescence.

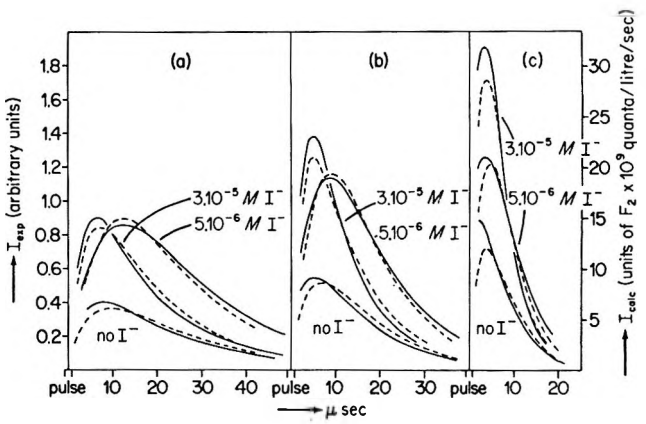


Figure 1. Time dependence of the emission from deaerated aqueous solutions of acriflavin in the presence of various concentrations of sodium iodide, after irradiation with 2-μsec pulses of ~180 rads; (a) $10^{-6}$ *M* acriflavin; (b) $2 \times 10^{-6}$ *M* acriflavin; (c) $5 \times 10^{-6}$ *M* acriflavin. ——, experimental, - - - -, calculated. Ordinate: lhs, experimental emission intensity (arbitrary units); rhs, calculated emission intensity (units of $F_2 \times 10^9$ quanta/l. sec). Abscissa: time after the pulse (μsec).

The reactivity of acriflavin toward $e_{aq}^-$ and OH radicals was obtained from light absorption measurements. The half-life of $e_{aq}^-$ in water alone was ~20 μsec for the doses used. A rate constant of $3.7 \times 10^{10}\ M^{-1}\ sec^{-1}$ ±10% for the reaction of $e_{aq}^-$ with acriflavin was obtained from the decay of electron absorption at 650 nm for various dye concentrations in the range $5 \times 10^{-6}$ *M* to $2 \times 10^{-5}$ *M*. A value of $3.3 \times 10^{10}\ M^{-1}\ sec^{-1}$ was reported earlier.[2] In the presence of $10^{-1}$ *M* HCOONa, acriflavin is bleached by way of concurrent fast and slow first-order processes. Both processes lead to the formation of a relatively long-lived product, lasting milliseconds, which has a narrow peak at 387 nm (Figure 2a). The rate of the fast process matched well the rate constant for the reaction of $e_{aq}^-$ with acriflavin. The slow process is most probably due to the reaction of acriflavin with $COO^-$, formed from the reaction of OH with formate. A rate constant of $3.7 \times 10^8\ M^{-1}\ sec^{-1}$ ±10% was thus obtained for the reaction acriflavin + $COO^-$.

For the reaction of OH radicals with acriflavin a rate constant of $1.2 \times 10^{10}\ M^{-1}\ sec^{-1}$ ±20% was obtained from the bleaching of dye absorption at 450 nm, using nitrous oxide-saturated solutions. This reaction leads to new intermediate species absorbing in the range 300–400 nm with a peak at ~350 nm and also, more weakly, above 500 nm (Figure 2b). The buildup of this absorption was wavelength independent and agreed

(5) K. Sommermeyer, V. Birkwald, and W. Prütz, *Strahlenther.*, 116, 354 (1961).

(6) J. P. Keene, *J. Sci. Instrum.*, 41, 493 (1964).

(7) E. M. Fielden and E. J. Hart, *Trans. Faraday Soc.*, 63, 2975 (1967).

(8) L. M. Dorfman and M. S. Matheson, *Progr. React. Kinet.*, III, 237 (1965).

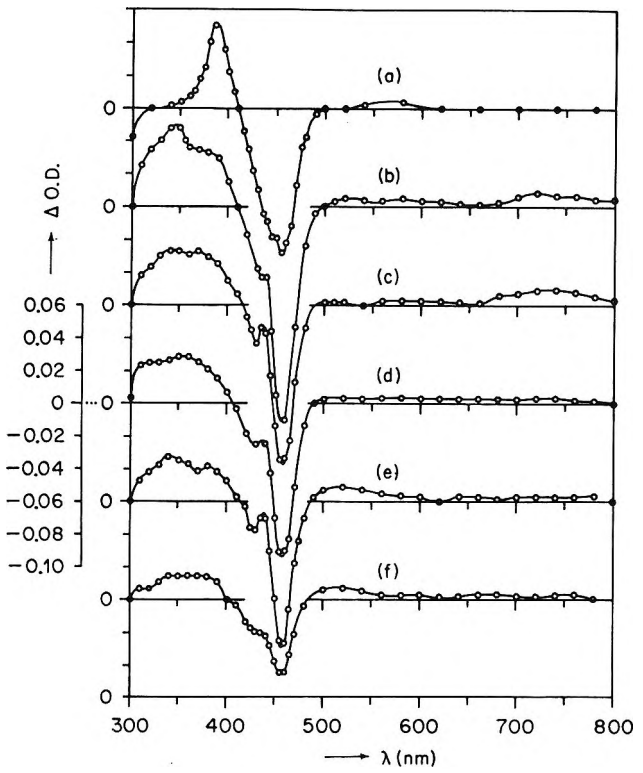


Figure 2. Absorption changes after irradiation of aqueous solutions of $10^{-5}$ $M$ acriflavin with 1-$\mu$sec pulses of ~180 rads. (a) Argon-flushed solution containing $10^{-1}$ $M$ HCOONa, 15 $\mu$sec after the pulse; (b) $N_2O$-saturated solution of dye alone, 20 $\mu$sec after the pulse; (c) $N_2O$-saturated solution containing $10^{-5}$ $M$ KI, 20 $\mu$sec after the pulse; (d) $N_2O$-saturated solution containing $10^{-3}$ $M$ KBr, 150 $\mu$sec after the pulse; (e) $N_2O$-saturated solution containing $10^{-5}$ $M$ KCNS, 15 $\mu$sec after the pulse; (f) $N_2O$-saturated solution containing $10^{-3}$ $M$ KCNS, 400 $\mu$sec after the pulse. Ordinate: Change in optical density. Abscissa: wavelength (nm).

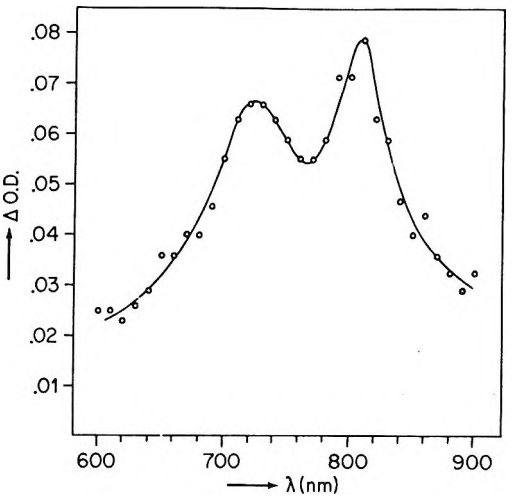


Figure 3. Spectrum of the transient red absorption occurring after pulse radiolysis of $N_2O$-saturated aqueous $10^{-4}$ $M$ acriflavin using pulses of ~2000 rads. Ordinate: Change in optical density. Abscissa: wavelength (nm).

well with the bleaching rate. The decay was wavelength dependent, suggesting that more than one product results from the attack of acriflavin by OH radicals. At 400 nm the decay followed first-order kinetics ($k_I \sim 4.7 \times 10^3$ sec$^{-1}$) whereas below this wavelength and above 500 nm the absorption became much longer lived and decayed by second-order kinetics ($k_{II}/\epsilon$(320 nm) $\sim 3 \times 10^4$ cm sec$^{-1}$). Cordier and Grossweiner[9] have suggested that in the case of eosin and fluorescein both OH adducts and semioxidized dye are formed by the action of OH radicals. A similar situation might explain the observed wavelength-dependent decay of oxidized acriflavin products. Lim, *et al.*,[10] have studied the photoionization of acriflavin in rigid glass at 77°K and reported that semioxidized acriflavin has a peak around 790 nm. After irradiation of $10^{-4}$ $M$ acriflavin with ~2000-rad pulses an absorption in the range 600–900 nm could be observed (Figure 3). The decay of the absorption at 720 nm and 810 nm was slightly different, indicating that both semioxidized dye and OH adducts may absorb in this range.

(2) *Effect of Iodide.* Figure 1 shows the time dependencies of the emission from pulse-radiolyzed acriflavin in the presence of various concentrations of sodium iodide. The spectrum of the emission was not affected when iodide was added. The enhancing effect is most remarkable at low iodide concentrations where the total emission intensity ($\int_0^\infty I(t)\,dt$) is increased up to a factor of 2.5 (Figure 4). At concentrations of $[I^-] > 10^{-5}$ $M$ a progressive decrease of total light output and emission lifetime is observed. The decrease of emission intensity between $10^{-5}$ $M$ and $10^{-4}$ $M$ iodide is not due to physical fluorescence quenching *via* perturbation of spin–orbit coupling,[11] which only becomes apparent at $[I^-] > 10^{-3}$ $M$. The lifetime and initial optical density of $e_{aq}^-$ was unaltered when iodide was added up to $10^{-4}$ $M$.

Absorption changes following pulse radiolysis were studied in order to get an estimate of the reactivity of iodide intermediates toward acriflavin. A nitrous oxide saturated solution of $10^{-5}$ $M$ acriflavin containing $10^{-5}$ $M$ KI showed a very rapid bleaching of dye absorption ($t_{1/2} \sim 3$ $\mu$sec) at 450 nm and a corresponding product formation at 300–400 nm. The rate of these absorption changes was about twice as fast as of the corresponding changes in the absence of iodide. At $10^{-5}$ $M$ iodide the formation of OH products of the dye is strongly suppressed by the fast reaction of $I^-$ with OH radicals, which according to Baxendale, *et al.*,[12] has a rate constant of $3.4 \times 10^{10}$ $M^{-1}$ sec$^{-1}$. The iodine

(9) P. Cordier and L. I. Grossweiner, *J. Phys. Chem.*, **72**, 2018 (1968).

(10) E. C. Lim, C. P. Lazzara, M. Y. Yang, and G. W. Swenson, *J. Chem. Phys.*, **43**, 970 (1965).

(11) M. Kasha, *ibid.*, **20**, 71 (1952).

(12) J. H. Baxendale, P. L. T. Bevan, and D. A. Stott, *Trans. Faraday Soc.*, **64**, 2389 (1968).

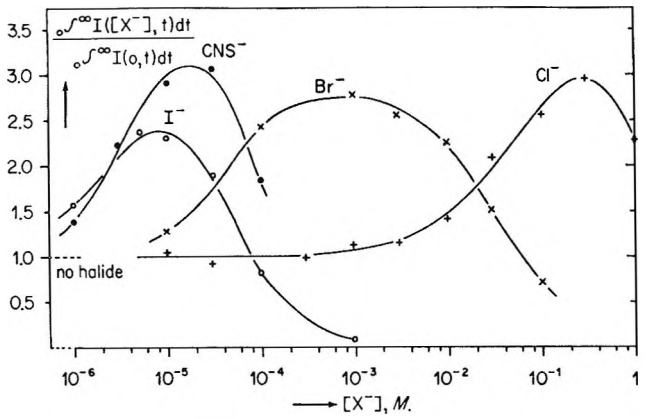


Figure 4. Plot of the relative total emission from aqueous solutions of $2 \times 10^{-6}$ $M$ acriflavin *vs.* the concentration of halide or $CNS^-$ added. The dose was ~180 rads/pulse except for $CNS^-$ where the dose was ~250 rads/pulse. Ordinate: relative emission: $\int_0^\infty I([X^-], t)\, dt / \int_0^\infty I(0, t)\, dt$. Abscissa: molar halide concentration: $[X^-]$ (log scale).

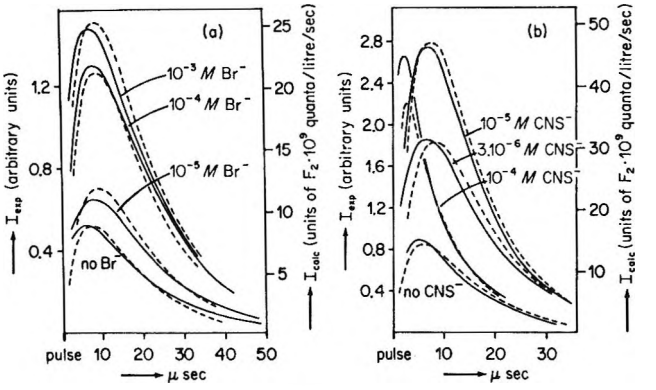


Figure 5. Time dependence of the emission from deaerated solutions of $2 \times 10^{-6}$ $M$ acriflavin in the presence of various concentrations of (a) potassium bromide and (b) potassium thiocyanate, after irradiation with 0.2-μsec pulses of ~180 and ~250 rads, respectively. ——, experimental, - - - -, calculated. Ordinate: lhs, Experimental emission intensity (arbitrary units); rhs, calculated emission intensity (units of $F_2 \times 10^9$ quanta/l. sec). Abscissa: time after the pulse (μsec).

atoms thus formed react too slowly with $I^-$ ($k(I + I^-) = 7.6 \times 10^9$ $M^{-1}$ $sec^{-1}$)[12] to identify the fast increase in absorption around 360 nm with formation of $I_2^-$ which also absorbs at this wavelength. The very fast dye bleaching and product formation seems therefore to be due to a rapid reaction of acriflavin with iodine atoms. Only a limiting value of $\geq 2 \times 10^{10}$ $M^{-1}$ $sec^{-1}$ can be obtained for the rate constant of this reaction since OH products of the dye and $I_2^-$ may give minor contributions to the absorption changes observed. The change in absorption in the range 300–800 nm for nitrous oxide saturated $10^{-5}$ $M$ acriflavin $10^{-5}$ $M$ iodide 20 μsec after the pulse is shown in Figure 2c. When the iodide concentration was increased to $10^{-1}$ $M$, iodine atoms were completely converted to $I_2^-$ before reaction with $10^{-5}$ $M$ dye could occur. The slow decay of $I_2^-$ obtained from $10^{-1}$ $M$ iodide alone was only slightly increased by the presence of $10^{-5}$ $M$ acriflavin. These results indicate that the rate of reaction of $I_2^-$ with acriflavin is $< 2 \times 10^8$ $M^{-1}$ $sec^{-1}$.

(3) *Effect of Bromide.* When potassium bromide was added to acriflavin solutions a similar increase in emission on pulse radiolysis was obtained (Figure 5a). The main difference between the two halides was in the effect of concentration on the total emission intensity (Figure 4). A more than ten times higher bromide concentration had to be added before a similar increase in emission intensity occurred. The total intensity was enhanced by a factor of ~2.7 at $10^{-3}$ $M$ bromide but progressively fell again in the range $10^{-3}$ $M$ to $10^{-1}$ $M$ bromide. This falloff is probably mainly due to physical quenching.[11] It was not possible to get an estimate of the rate constant for the reaction of acriflavin with bromine atoms since in this case $Br^-$ itself reacts much faster with bromine atoms than with OH radicals (Table I[13–17]). The reaction of acriflavin with $Br_2^-$, however, could be observed when absorption changes of nitrous oxide-saturated solutions of $10^{-3}$ $M$ bromide in presence and absence of acriflavin were compared. The rate constant of $k(D + Br_2^-) = 3.7 \times 10^9$ $M^{-1}$ $sec^{-1}$ ±15% thus obtained from $Br_2^-$ removal (360 nm) and simultaneous dye bleaching (450

**Table I:** Rate Constants for Various Reactions of Halide and Thiocyanate Species with Acriflavin in Neutral Aqueous Solution[a]

| X⁻ | I⁻ | Br⁻ | CNS⁻ |
|---|---|---|---|
| $k(X^- + OH)$ | 3.4[b] | 0.12[c] | 2.8[b] |
| $k(X^- + X \rightleftharpoons X_2^-)$ | | | |
| Forward | 0.76[b] | 0.54[d,e] | 0.7[b] |
| Backward (*) | 6.0[b] | 0.064[d] | 3.4[b] |
| $2k(X_2^- + X_2^-)$ | 0.77[f] | 0.33[c] | 0.29[g] |
| $k(D + X)$ | ≥2.0[h] (4.5) | (3.0) | ≥2.0[h] (4.5) |
| $k(D + X_2^-)$ | ≤0.02[h] | 0.37[h] | 0.1[h] |
| $k(e_{aq}^- + X)$ | (2.0) | (2.0) | (2.0) |
| $k(e_{aq}^- + X_2^-)$ | (2.0) | 1.3[b] | (2.0) |

[a] In units of $10^{10}$ $M^{-1}$ $sec^{-1}$, except (*) in $10^4$ $sec^{-1}$. The rate constants in brackets are assumed values used for the calculations of emission time characteristics. [b] Reference 12. [c] Reference 13. [d] Reference 14. [e] Reference 15. [f] Reference 16. [g] Reference 17. [h] This paper.

(13) M. S. Matheson, W. A. Mulac, J. L. Weeks, and J. Rabani, *J. Phys. Chem.*, **70**, 2092 (1966).

(14) H. C. Sutton, G. E. Adams, J. W. Boag, and B. D. Michael in "Pulse Radiolysis," M. Ebert, J. P. Keene, A. J. Swallow, and J. H. Baxendale, Ed., Academic Press, London, 1965, p 61.

(15) B. Cercek, M. Ebert, C. W. Gilbert, and A. J. Swallow in "Pulse Radiolysis," M. Ebert, J. P. Keene, A. J. Swallow, and J. H. Baxendale, Ed., Academic Press, London, 1965, p 83.

(16) L. I. Grossweiner and M. S. Matheson, *J. Phys. Chem.*, **61**, 1089 (1957).

(17) G. E. Adams, J. W. Boag, J. Currant, and B. D. Michael in "Pulse Radiolysis," M. Ebert, J. P. Keene, A. J. Swallow, and J. H. Baxendale, Ed., Academic Press, London, 1965, p 117.

nm) using $10^{-5}$ $M$ acriflavin is very much higher than the corresponding $I_2^-$ rate constant. The $Br_2^-$ product, like the OH product, has a broad absorption between 300 nm and 400 nm (Figure 2d). The $Br_2^-$ product absorbing around 350 nm lasted much longer than the OH products of the dye.

(4) *Effect of Chloride.* The addition of $\leqslant 10^{-3}$ $M$ potassium chloride did not affect the chemiluminescence emission from $2 \times 10^{-6}$ $M$ acriflavin. Between $10^{-2}$ $M$ and $3 \times 10^{-1}$ $M$ chloride a continuous increase in total emission up to a factor of 3 was observed (Figure 4). At the same time the intensity maximum shifted from $\sim$5 $\mu$sec after the pulse in chloride-free solutions to $\sim$10 $\mu$sec in $3 \times 10^{-1}$ $M$ chloride. In all cases the emission had completely decayed after $\sim$50 $\mu$sec. Above $3 \times 10^{-1}$ $M$ chloride the total emission began to fall again, probably due to physical quenching by $Cl^-$. No emission was observed from $10^{-1}$ $M$ chloride alone in water in the range 300 nm to 600 nm. The reaction of $Cl_2^-$ with acriflavin was investigated by studying the absorption of nitrous oxide saturated 1 $M$ KCl in presence and absence of $10^{-5}$ $M$ acriflavin. The slow rate of formation of $Cl_2^-$ and overlap of its absorption with that of dye intermediates made it difficult to estimate the rate constant $k(Cl_2^- + \text{acriflavin})$. A very tentative value of $\sim 4 \times 10^9$ $M^{-1}$ sec$^{-1}$ was obtained from the rate of dye removal at 450 nm.

(5) *Effect of $CNS^-$ and Other Pseudo Halides.* On Figure 5b is shown the effect of adding various amounts of potassium thiocyanate to $2 \times 10^{-6}$ $M$ acriflavin. The effect appears to be quite similar to that obtained on adding iodide. Thus the total emission increased to a maximum at about $10^{-5}$ $M$ to $3 \times 10^{-5}$ $M$ $CNS^-$ (Figure 4). Above $3 \times 10^{-5}$ $M$ $CNS^-$ the total emission became progressively reduced and the lifetime decreased rapidly. Absorption measurements carried out on acriflavin in the presence of $CNS^-$ likewise strongly resembled the results obtained with the acriflavin–iodide system (Figure 2e). Using $10^{-5}$ $M$ acriflavin containing $10^{-5}$ $M$ KCNS in nitrous oxide saturated solution a fast bleaching of dye at 450 nm was observed, together with an equally fast buildup of product absorbing at 360 nm. These results indicated a rate constant for the reaction CNS + acriflavin of $\geqslant 2 \times 10^{10}$ $M^{-1}$ sec$^{-1}$. The situation was more complicated here than in the iodide system in that the $(CNS)_2^-$ formed to a minor extent under these conditions also reacts with the dye. By comparing the rate of decay of $(CNS)_2^-$ absorption at 500 nm in $10^{-3}$ $M$ KCNS solution alone with the decay obtained in the presence of $10^{-5}$ $M$ acriflavin, a rate constant of $1.0 \times 10^9$ $M^{-1}$ sec$^{-1}$ $\pm$ 15% was obtained for the reaction $(CNS)_2^-$ + acriflavin.

Sodium azide at a concentration of $5 \times 10^{-5}$ $M$ strongly enhanced (by a factor of $\sim$3) the emission of $2 \times 10^{-6}$ $M$ acriflavin although the lifetime of the emission was slightly less than for dye alone. Increasing the azide concentration to $3 \times 10^{-4}$ $M$ caused a further reduction in emission lifetime and also total light output. Potassium cyanide strongly quenched the emission from acriflavin ($2 \times 10^{-6}$ $M$) when present at $5 \times 10^{-5}$ $M$ and $3 \times 10^{-4}$ $M$.

## Discussion

(1) *Acriflavin Alone.* The buildup and decay of the pulse radiolysis induced emission has been interpreted[2] in terms of the following reactions

$$\mathrm{D-OH} \longrightarrow \mathrm{DOH} \qquad (1a)$$

$$\searrow \mathrm{D^+ + OH^-} \qquad (1b)$$

$$\mathrm{DOH} + e_{aq}^- \longrightarrow \mathrm{D^*} + \mathrm{OH^-} \qquad (2a)$$

and/or

$$\mathrm{D^+} + e_{aq}^- \longrightarrow \mathrm{D^*} \qquad (2b)$$

If OH adducts (DOH) and semioxidized dye ($D^+$) are formed equally fast then the build-up rate of the emission will be the same for both processes 2a and 2b. The decay of the emission formed *via* 2a and 2b is determined by the decay of $e_{aq}^-$, the shortest-lived participant. The lifetime of the lowest excited singlet state of acriflavin is $4 \times 10^{-9}$ sec,[18] which is short compared with the microsecond time characteristics under discussion. An increase in dye concentration shortens the lifetime of the emission by way of the fast $e_{aq}^-$ removing reaction

$$\mathrm{D} + e_{aq}^- \longrightarrow \mathrm{D^-} \qquad (3)$$

The time dependence of the emission from the reactions 2a and 2b, in quanta/l. sec at a time $t$ after the pulse, is given by

$$I(t) = N[e_{aq}^-](t)(A_2[\mathrm{DOH}](t) + B_2[\mathrm{D^+}](t))$$

where $N$ is Avogadro's number. $A_2$ and $B_2$ are the products of quantum efficiency $\eta$ (quanta/reaction) and rate constant $k$ of the chemiluminescent reactions 2a and 2b, respectively, both of which are unknown. The time characteristics thus calculated do not help to distinguish between DOH and/or $D^+$ as chemiluminescence participants since the DOH/$D^+$ ratio is unknown. Although the results of Grossweiner and Rodde[3] using fluorescein and eosin favor reaction 2a, it is difficult to understand why recombination between electrons and $D^+$, if it is formed, should be less efficient than reaction 2b in forming excited states. The dotted lines in Figure 1 (curves with no iodide) were calculated assuming that either OH adducts or semioxidized dye, or both, are involved in the chemiluminescence. The expression $(A_2 f_a + B_2 f_b) = F_2$, where $f_a$ and $f_b$ represent the fraction of DOH and $D^+$ formed, remains an unknown factor which was adjusted to obtain the best fit with the experimental set of curves. The measured rate constants $k_2$ ($k_{2a}$

(18) A. Schmillen, *Z. Physik*, **135**, 294 (1953).

$= k_{2b}$) and $k_3$ were used for these calculations and the following contributions for the decay of $e_{aq}^-$ and OH radicals in pure water

$$\frac{d[e_{aq}^-]}{dt} = -k_0 - k[e_{aq}^-](t)[OH](t)$$

$$\frac{d[OH]}{dt} = -k_{00} - k[e_{aq}^-](t)[OH](t)$$

The constant $k$ is the second-order rate of the reaction of $e_{aq}^-$ with OH ($3.0 \times 10^{10}$ $M^{-1}$ $sec^{-1}$ [19]) and $k_0$ is a first-order rate constant chosen to give the best fit with the experimental decay of $e_{aq}^-$ in pure water ($k_0 \sim 3.5 \times 10^4$ $sec^{-1}$ for 180 rads/pulse). A corresponding $k_{00}$ value for OH of $\sim 8 \times 10^3$ $sec^{-1}$ was assumed for the same dose. Reasonable agreement with the experimental curves was obtained (see Figure 1). The discrepancies occurring were probably partly due to errors in dosimetry, since the chemiluminescence from reaction 2 is proportional to $(dose)^2$ at low doses.

*(2) Effect of Iodide.* The fast reaction of OH with iodide, or more generally with halide $X^-$, appears

$$X^- + OH \longrightarrow X + OH^- \qquad (4)$$

to interfere with the chemiluminescent process 1–2. Published rate constants for reaction 4 for various halides are collected in Table I. To explain the enhancing effect of iodide it seems reasonable to assume that iodine atoms formed *via* reaction 4 participate in new chemiluminescent reactions. In our earlier description of the iodide effect,[1,2] the following process was suggested where $D^-$ is the product of reaction 3.

$$D^- + X \longrightarrow D^* + X^- \qquad (5)$$

It was postulated that the quantum efficiency of 5 was higher than that of reaction 2.

Equilibrium 6 has recently been studied for iodide

$$X^- + X \rightleftharpoons X_2^- \qquad (6)$$

solutions by Baxendale, *et al.*,[12] who found an equilibrium constant of $\sim 10^5$ $M^{-1}$ and a fast rate constant for the forward reaction (see Table I). Thus at $[I^-] \geq 10^{-5}$ $M$, the forward reaction 6 rapidly removes the iodine atoms which could be involved in the possible luminescence enhancing process 5, thus explaining qualitatively the observed quenching of emission at $[I^-] \geq 10^{-5}$ $M$. More quantitative considerations, however, seem to rule out reaction 5. At $3 \times 10^{-5}$ $M$ iodide the half-life of iodine atoms is $\sim 3$ $\mu$sec according to the rate constant for reaction 6 given by Baxendale, *et al.*,[12] and our own observations, whereas the emission from $10^{-6}$ $M$ acriflavin containing $3 \times 10^{-5}$ $M$ iodide lasts over 30 $\mu$sec (see Figure 1a).

The very rapid reaction of acriflavin with iodine atoms ($k \geq 2 \times 10^{10}$ $M^{-1}$ $sec^{-1}$) could lead to iodine adducts of the dye and/or semioxidized dye

$$D + X \longrightarrow DX \qquad (7a)$$

$$\searrow D^+ + X^- \qquad (7b)$$

This could lead to the following possible emission forming processes

$$DX + e_{aq}^- \longrightarrow D^* + X^- \qquad (8a)$$

$$D^+ + e_{aq}^- \longrightarrow D^* \qquad (8b) = (2b)$$

Reaction 3 of dye with $e_{aq}^-$ would again explain the observed decrease of emission lifetime at constant $[I^-]$ and increasing dye concentration. Since formation of DI and/or $D^+$ *via* (7a) or (7b) is faster than formation of DOH and/or $D^+$ in aqueous acriflavin alone an enhancement of emission might be expected. An important factor in the relative emissions in the presence and absence of iodide could be a variation of the adduct:semioxidized dye ratio in going from OH attack to I attack. In the case of adducts the positions of attachment may also alter in going from OH to I attack. Comparison of the absorption curves in Figure 2 suggests that the degree of emission enhancement could be related to the transient absorption having an apparent peak at 435 nm. This peak underlies the absorption of acriflavin itself, which has a peak at 450 nm but no pronounced shoulder around 435 nm. Since this shoulder appears when the transient is formed from OH, I, $Br_2^-$ or CNS, it is likely to be due to the same species in each case, *i.e.*, more consistent with semioxidized acriflavin than an adduct. Lim, *et al.*,[10] reported only a red absorption of semioxidized acriflavin in rigid glass but no data below 500 nm were given. This previous and the present results would be consistent if semioxidized acriflavin has two peaks—a weak one around 790 nm and a much stronger one around 435 nm. The proposed emission-forming process 8a might have been expected to be less efficient than the corresponding process with OH adducts, since the iodide involved is known to quench efficiently the fluorescence of dyes by perturbation of the spin–orbit coupling.[11]

A further process which could be involved in the enhancement of emission is

$$D + X_2^- \longrightarrow DX_2^- \qquad (9a)$$

$$\searrow D^+ + 2X^- \qquad (9b)$$

$$DX_2^- + e_{aq}^- \longrightarrow D^* + 2X^- \qquad (10a)$$

$$D^+ + e_{aq}^- \longrightarrow D^* \qquad (10b) = (2b)$$

In the case of iodide the rate constants of the reaction 9a and/or 9b are much too slow (Table I) to yield a significant amount of $DI_2^-$ and/or $D^+$ during the lifetime of $e_{aq}^-$.

(19) M. S. Matheson and J. Rabani, *J. Phys. Chem.*, 69, 1324 (1965).

The time dependence of the total emission expected when in general semioxidized dye and adducts (DR) of OH, X and $X_2^-$ are involved is given by

$$I(t) = N[e_{aq}^-](t)\sum_i (A_i[DR_{(i)}](t) + B_2[D_{(i)}^+](t))$$

$i = 2, 8, 10$. The dye products are numbered according to the chemiluminescent reaction in which they participate. $A_i = k_{ia}\eta_{ia}$ and $B_2 = k_{2b}\eta_{2b}$ are unknown factors. Since no experimental evidence for a difference in the rates of adduct and semioxidized dye formation by the attack of any oxidizing radical could be obtained, this formula can be written

$$I(t) = N[e_{aq}^-](t)\sum_i F_i[D_{(i)}^{ox}](t)$$

where

$$[D_{(i)}^{ox}] = [DR_{(i)}] + [D_{(i)}^+]$$

$$F_i = A_i f_{a(i)} + B_2 f_{b(i)}$$

Calculations were carried out to test if this expression gave a quantitative description of the observed time characteristics at various dye and iodide concentrations. Reactions 1–4 and 6–10, contributions for the decay of $e_{aq}^-$ and OH in pure water, and the following additional reactions were taken into account. For the unknown

$$X_2^- + X_2^- \longrightarrow X_3^- + X^- \quad (11)$$

$$X + e_{aq}^- \longrightarrow X^- \quad (12)$$

$$X_2^- + e_{aq}^- \longrightarrow 2X^- \quad (13)$$

reactions 12 and 13 rate constants of $2 \times 10^{10}$ $M^{-1}$ $sec^{-1}$ were assumed. These reactions in fact had only a very minor influence upon the calculated time characteristics. When the rate constant $k_7(D + I)$, for which only a limiting value of $\geq 2 \times 10^{10}$ $M^{-1}$ $sec^{-1}$ had been obtained, was increased to $4.5 \times 10^{10}$ $M^{-1}$ $sec^{-1}$, better agreement with the observed buildup of the emission was obtained. The dotted curves in Figure 1 show the calculated emission time characteristics which best fit the experimental data, obtained using the relative values for $F_2$, $F_8$, and $F_{10}$ given in Table II, and the rate constants collected in Table I. The factors $F_i$ may be interpreted in various ways depending upon the mechanism. If $D^+$ were the only participant, *i.e.*, $\eta_{2a} = \eta_{8a} = \eta_{10a} = 0$, these factors would be directly proportional to the fractions of $D^+$ formed by attack of the different radicals. In fact there seems to be a qualitative relationship between these factors and the intensity of the transient absorption at 435 nm (see Figure 2) for the various halides. On the other hand, adducts may contribute toward the emission and could even be the only participants, *i.e.*, $\eta_{2b} = 0$. In this case the factors $F_i$ would represent the net relative efficiencies of the different $e_{aq}^- +$ adduct reactions in giving emission. An increase of the assumed values of $k_7(D + X)$ would lead to smaller values of $F_8$.

**Table II:** Relative Values for $F_i = k_{ia}\eta_{ia}f_{a(i)} + k_{2b}\eta_{2b}f_{b(i)}$ for the Various Possible Chemiluminescent $e_{aq}^- +$ Oxidized Dye Reactions in the Presence of Various Halides

| $X^-$ | $F_2$ | $F_8$ | $F_{10}$ |
|---|---|---|---|
| $I^-$ | 1 | 1.25 | $\leq 2.0$ |
| $Br^-$ | 1 | 4.00 | 8.2 |
| $CNS^-$ | 1 | 1.89 | 0.0 |

*(3) Effect of Bromide.* The experimental observation that over ten times higher bromide concentrations are required to give the same increase as found in the case of iodide, is consistent with Br or $Br_2^-$ being the precursor of the enhanced emission. According to the rate constants quoted in Table I, the formation of Br in neutral solutions *via* reaction 4 is more than ten times slower than the corresponding formation of I. The emission was seen to increase up to $10^{-3}$ $M$ bromide although the rate of Br removal *via* reaction 6 is of the same order as for iodide (Table I). Thus $Br_2^-$ rather than Br is likely to be involved in the chemiluminescence observed, at least above $10^{-3}$ $M$ bromide where Br atoms are converted to $Br_2^-$ in less than 1 $\mu$sec. The relatively fast rate constant $k(D + Br_2^-)$, if compared with the corresponding $D + I_2^-$ rate, gives support to this suggestion.

The dotted curves in Figure 5 were again calculated using the reaction mechanism 1–4 and 6–13 and the appropriate rate constants quoted in Table I. The relative values of $F_2$, $F_8$, and $F_{10}$ which gave the best fit of the experimental data are given in Table II.

*(4) Effect of Chloride.* The apparently slow rate of reaction 4 of chloride with OH radicals in neutral solution ($<10^{-3}$ $M^{-1}$ $sec^{-1}$)[20] could explain why very high chloride concentrations are needed to see an effect. Few data about the formation and stability of chlorine atoms are available to help decide to what extent Cl atoms are involved in the present luminescence. Anbar and Thomas[21] found on pulse radiolysis of neutral NaCl solutions that significant amounts of $Cl_2^-$ could only be detected when the chloride concentration was $\geq 0.1$ $M$. This might suggest that $Cl_2^-$ is involved in the increase in emission at $[Cl^-] > 10^{-1}$ $M$. Species of the type $XOH^-$ have also been proposed in the chloride[21] and bromide[13] systems and could be involved in the chemiluminescences.

Ahnström[22] proposed a mechanism to explain the light emission observed during dissolution of irradiated NaCl crystals in aqueous solutions of fluorescing dyes. This mechanism involved the formation and recombination of Cl atoms and $e_{aq}^-$ to give $Cl^{*-}$ which then transferred energy to a fluorescent molecule. For

(20) J. F. Ward and L. S. Myers, Jr., *Radiat. Res.*, **26**, 483 (1965).
(21) M. Anbar and J. K. Thomas, *J. Phys. Chem.*, **68**, 3829 (1964).
(22) G. Ahnström, *Acta Chem Scand.*, **19**, 300 (1965).

the doses of 150 to 200 rads used in the present experiments a concentration of $\leqslant 5 \times 10^{-7}$ $M$ Cl would be formed if all OH were converted into Cl atoms. At $2 \times 10^{-6}$ $M$ dye and $10^{-1}$ $M$ $Cl^-$ the lifetime of Cl atoms would be very short due to its reactions with $Cl^-$ and dye, leaving little chance for formation of $Cl^{*-}$ *via* reaction of Cl atoms with $e_{aq}^-$. Therefore energy transfer from $Cl^{*-}$ to the dye cannot be involved in the present emission enhancement. In fact irradiated NaCl crystals on dissolution probably give rise to the same species as obtained on irradiating NaCl solutions. Therefore the emissions obtained on dissolving irradiated NaCl in dye solutions are probably formed *via* a similar mechanism to the one now proposed.

(5) *Effect of $CNS^-$.* From the experimental results it could be deduced that, like iodide, the corresponding reactions of CNS–dye products with $e_{aq}^-$ would explain the enhanced emissions. The dotted lines of Figure 5b thus calculated using the appropriate rate constants given in Table I lead to the optimum relative values $F_2$, $F_8$, and $F_{10}$ given in Table II.

(6) *Conclusions.* The enhancement of the emission from irradiated acriflavin solutions by addition of various halides or pseudo halides seems in all cases to be associated with the formation of dye products, *via* attack of halide intermediates X and $X_2^-$, which then react with $e_{aq}^-$ in chemiluminescent reactions. Neither the emission nor the absorption measurements carried out led to a definite decision as to whether the semioxidized dye and/or the OH, X, and $X_2^-$ adducts of the dye participate in the emission-forming step. The relative reactivities of the various X and $X_2^-$ intermediates toward acriflavin follow the order $I \sim CNS > OH > Cl_2^- \sim Br_2^- > (CNS)_2^- \gg I_2^-$. This is similar to the order of oxidizing power: $OH > Cl_2^- > Br_2^- \gg I_2^-$ found by Langmuir and Hayon[23] from the measured reactivities of these species with various solutes, mainly alcohols.

Advances in this system are possible by measurements of the absolute yields of emissions and by further absorption studies using both pulse radiolysis and flash photolysis in order to identify the spectrum of semioxidized acriflavin.

*Acknowledgments.* The authors wish to thank the late Professor K. Sommermeyer for stimulating this work, Dr. L. G. Lajtha and Dr. M. Ebert for encouragement and support, and Dr. J. P. Keene and Mr. B. W. Hodgson for constant supervision of the accelerator and pulse radiolysis apparatus. Financial support to W. P. was given by the Deutsche Forschungsgemeinschaft.

(23) M. E. Langmuir and E. Hayon, *J. Phys. Chem.*, **71**, 3808 (1967).

# Quenching of Lucigenin Fluorescence

**by Kenneth D. Legg**[1a]

*Department of Chemistry and Laboratory for Nuclear Science, Massachusetts Institute of Technology, Cambridge, Massachusetts*

**and David M. Hercules**[1b]

*Department of Chemistry, University of Georgia, Athens, Georgia 30601* *(Received December 9, 1969)*

A study is reported for the quenching of lucigenin (dimethylbis(acridinium) nitrate) fluorescence by various anions and amines. A linear relationship is found between quenching efficiency and ionization potential. Efficient quenchers such as chloride, cyanide, sulfite, thiocyanate, and sulfide ions have diffusion-controlled rate constants. The quenching of lucigenin fluorescence has been shown to proceed by formation of a transient charge-transfer complex. In the absence of quenchers, lucigenin undergoes a photochemical reaction which probably occurs from the lowest excited singlet state.

## Introduction

Weber[2] has reported the quenching of lucigenin (dimethylbis(acridinium) nitrate) fluorescence by chloride, bromide, iodide, and thiocyanate ions. He noted that the quenching by iodide and bromide appeared to be due to the "heavy-atom" effect,[3] while quenching by chloride and thiocyanate appeared to be related to their oxidation potentials. Leonhardt

(1) (a) NIH Predoctoral Fellow, 1965–1968. (b) Address all correspondence to this author.

(2) K. Weber, *Z. Phys. Chem.*, **B50**, 100 (1941).

(3) J. G. Calvert and J. W. Pitts, Jr., "Photochemistry," John Wiley and Sons, Inc., New York, N. Y., 1967.

and Weller[4] observed charge-transfer quenching of perylene fluorescence by electron donors, notably amines. They confirmed what others[5] surmised, namely, that quenching proceeds through a charge-transfer intermediate

$$F^* + Q \longrightarrow (F^-Q^+) \longrightarrow F + Q$$

In the case of perylene quenching by amines, they were able to observe the monoanion radical of perylene in polar solvents. They were also able to show a relationship between the ionization potential of the amine and its quenching efficiency. These observations were in accord with the mechanism

$$P^* + Q \longrightarrow (P\cdot^-Q\cdot^+) \quad (1)$$

$$(P\cdot^-Q\cdot^+) \longrightarrow P\cdot^-_{solv}Q\cdot^+_{solv} \quad (2)$$

$$(P\cdot^-Q\cdot^+) \longrightarrow P + Q \quad (3)$$

They were not able to observe the charge-transfer complex ($P^-Q^+$) due to its short lifetime ($<10^{-7}$ sec).

As a part of our studies[6] on the chemiluminescence of lucigenin, we felt it important to study the quenching of lucigenin fluoresence as well as the nature of the excited state responsible for its photochemical reaction. The results of these studies are reported here.

## Experimental Section

*Chemicals.* Lucigenin (dimethylbis(acridinium) nitrate) was obtained from Columbia Organic Chemicals and was recrystallized twice from 1:1 methanol–ethanol. All other organic and inorganic chemicals were reagent grade and were used without purification.

*Solvents.* Absolute ethanol (U. S. Industrial Chemicals Co.), dimethyl sulfoxide (DMSO), dimethylformamide (DMF) (Matheson Coleman and Bell, spectroscopic grade), and acetonitrile (AN) (Eastman, spectroscopic grade) were used as obtained.

*Apparatus.* Absorption spectra were obtained on a Cary Model 14 spectrophotometer. Fluorescence studies used a Turner Model 210 absolute spectrofluorometer. Fluorescence lifetimes were measured using a TRW Model 31A nanosecond fluorometry system.[7] The flash photolysis system was constructed from components manufactured by Xenon Corp. (Medford, Mass.) and has been described in detail by Bailey, *et al.*[8]

## Results and Discussion

The effect of a series of anions on the fluorescence intensity of lucigenin is shown in Table I. Iodide and bromide were excluded from this study because of the possibility of quenching by the "heavy-atom" effect. The rate constants for quenching, $k_q$, were calculated from the Stern–Volmer relationship

$$\frac{I_0}{I_Q} = 1 + k_q\tau(Q) \quad (I)$$

where $I_0$ is the fluorescence intensity with no quencher added, $\tau$ the lifetime of the excited state in this absence of quenching, and $I_Q$ the intensity at quencher concentration, (Q). These rate constants give a good indication of relative quenching efficiencies of the various ions. To a first approximation the quenching efficiency appears to be related to the ionization potential, although this is far from an exact correlation. In certain cases a general correlation is complicated by rapid photoreaction between lucigenin and the anion. Fluorescence lifetime measurements gave quenching constants comparable to those in Table I.

**Table I:** Effect of Anions on Lucigenin Fluorescence in Water

| Added salt[a] | Fluorescence intens[b] | Quenching const, $M^{-1}$ sec$^{-1}$ | Ionization potential of anion,[c] eV |
|---|---|---|---|
| None | 100 | ... | 17.4 |
| KF | 100 | ... | |
| $NaClO_4$ | 100 | ... | |
| $Na_2SO_4$ | 60 | $7.1 \times 10^8$ | |
| $NaC_2H_3O_2$ | 31 | $2.3 \times 10^9$ | 10.35 |
| $NaHSO_3$ | 8.5 | $1.1 \times 10^{10}$ | |
| NaOH | ... | $1.1 \times 10^{10}$[d] | 13.2 |
| KCN | 5.5 | $1.8 \times 10^{10}$ | 13.7 |
| KCl | 5.1 | $1.9 \times 10^{10}$ | 13.0 |
| | | $4.4 \times 10^{10}$[d] | 13.0 |
| $Na_2SO_3$ | 3.4 | $3.0 \times 10^{10}$ | |
| NaSCN | 1.4 | $7.4 \times 10^{10}$ | |
| $Na_2S$ | 0.3 | *e* | 10.5 |

[a] Concentration of all quenchers $5.00 \times 10^{-2}$ *M*. [b] Measured relative to a value of 100 with no quencher added. Concentration of lucigenin in all solutions was $1.00 \times 10^{-4}$ *M*. [c] R. W. Kiser, U. S. Atomic Energy Commission Report TID-6142, 1960, Washington, D. C. [d] From fluorescence lifetime measurements. [e] Photoreacts. A calculated *k* gave $3.2 \times 10^{11}$ $M^{-1}$ sec$^{-1}$.

Qualitatively, the results of Table I are quite interesting. It is not surprising that ions like fluoride and perchlorate do not show a quenching effect, nor is it surprising that strong reducers such as sulfide, sulfite, or bisulfite are quenchers. What is interesting, though, is that mild reducing agents such as thiocyanate, chloride, cyanide, and acetate have very large quenching constants. Even sulfate ions show a quenching effect.

(4) H. Leonhardt and A. Weller in "Luminescence of Organic and Inorganic Materials," H. D. Kallmann and G. M. Spruch, Ed., John Wiley and Sons, Inc., New York, N. Y., 1962.

(5) (a) E. Bauer, *Z. Phys. Chem.*, **B16**, 465 (1932); (b) J. Weiss and H. Fischgold, *ibid.*, **B32**, 135 (1936).

(6) K. D. Legg and D. M. Hercules, *J. Amer. Chem. Soc.*, **91**, 1902 (1969).

(7) "TRW Fluorometry Handbook," TRW Instruments, El Segundo, Calif., 1968.

(8) (a) D. N. Bailey, Ph.D. Thesis, Massachusetts Institute of Technology, Cambridge, Mass., 1968; (b) D. N. Bailey, D. K. Roe, and D. M. Hercules, *J. Amer. Chem. Soc.*, **90**, 6291 (1968).

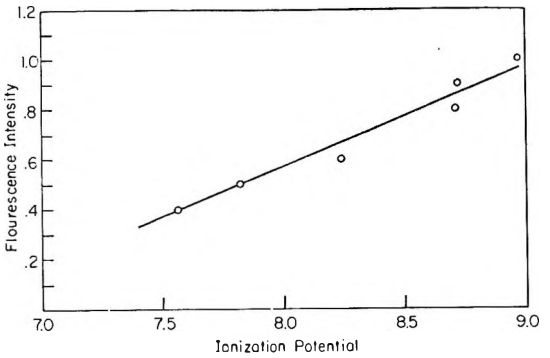


Figure 1. Relationship between the ionization potentials of amines and their efficiency of quenching lucigenin fluorescence. $I_f$ is the measured fluorescence intensity of a solution containing $10^{-4}$ $M$ lucigenin and $2 \times 10^{-2}$ $M$ amine in water. With no amine added, the relative fluorescence intensity was 10.0. Amines used and their ionization potentials:[7,8] methylamine (8.97), isopropylamine (8.72), *n*-butylamine (8.71), dimethylamine (8.24), triethylamine (7.82), and triethylamine (7.56).

Because amines were shown to be efficient charge-transfer quenchers of aromatic hydrocarbons[4] and because ionization potential data are readily available for amines,[9,10] a study was performed of the quenching of lucigenin by a series of aliphatic amines. A plot of relative fluorescence intensities with quencher present *vs.* ionization potential of the quencher is shown in Figure 1. The linear dependence of fluorescence quenching efficiency on the ionization potential of the quencher is good evidence that electron transfer is involved in the quenching step.

That ionization potential alone is not the only factor important in lucigenin fluorescence quenching can be seen by reference to Figure 1. Quenching by chloride gives an $I_f$ value of 1.2 on the scale of the figure, even though the ionization potential of chloride is 13.0 eV. This indicates that chloride is a more efficient quencher than any of the amines studied. It is doubtful if these results are due to collisional frequency factors, since chloride and the amines all have essentially diffusion-controlled rate constants. Rather, the increased efficiency of chloride quenching probably reflects better bonding between the positively and negatively charged species, resulting in greater orbital overlap and a more efficient pathway for electron transfer.

Leonhardt and Weller were able to observe an effect of solvent polarity on the quenching efficiency of amines on perylene fluorescence.[4] This was ascribed to solvent stabilization of the radical ions formed by the charge-transfer step, more polar solvents showing greater efficiency. Similar studies were run for the chloride quenching of lucigenin as shown in Table II. From these data it is evident there is no solvent effect on the quenching efficiency.

The studies described above clearly indicate that quenching of lucigenin fluorescence occurs by a charge-transfer mechanism similar to that proposed by Leonhardt and Weller for quenching of perylene fluorescence by amines.[4] On this basis the mechanism of quenching of lucigenin fluorescence by chloride ion may be written

**Table II:** Chloride Quenching of Lucigenin Fluorescence as a Function of Solvent

| Solvent | $I_0/I_Q$[a] | Solvent | $I_0/I_Q$[a] |
|---|---|---|---|
| Water | 5.4 | Dimethyl sulfoxide | 5.5 |
| Ethanol | 5.1 | Acetonitrile | 5.3 |

[a] $I_0$ is the fluorescence intensity measured from a $10^{-4}$ $M$ solution of lucigenin in the appropriate solvent. $I_Q$ is the fluorescence intensity in the same solvent containing $10^{-2}$ $M$ tetramethylammonium chloride. Relative precision of the rates is $\pm 0.15$.

$$L^{2+} + h\nu \longrightarrow (L^{2+})^*$$

$$(L^{2+})^* + Cl^- \longrightarrow (L\cdot^+Cl\cdot)$$

$$(L\cdot^+Cl\cdot) \longrightarrow L^{2+} + Cl^-$$

It was not possible to detect the presence of the $L\cdot^+$ radical or to determine if the lucigenin triplet is produced by the second electron-transfer step. Lucigenin was found to show serious photodecomposition under flash excitation which would be necessary for such studies. The mechanism is also consistent with the lack of a solvent effect on the efficiency of the charge-transfer reaction. Because the charge-transfer complex $(L\cdot^+Cl\cdot)$ has essentially the same net charge whether the electron is on the chlorine or the lucigenin, solvent reorientation effects on electron transfer would be expected to be small. One would expect a larger solvent effect on amine quenching, because of the charge separation produced in the complex $(L\cdot^+A\cdot^-)$. However the presence of amines caused serious photodecomposition of lucigenin in nonaqueous solvents, complicating such studies.

That anions generally are more efficient quenchers of lucigenin fluorescence than are amines is consistent with the proposed mechanism. A doubly charged cation would have a stronger attraction for an anion than for an amine. This would result in a lower activation energy for formation of the charge-transfer complex and an overall increase in quenching efficiency.

The proposed mechanism for dissipation of energy from the excited singlet state of lucigenin is shown in Figure 2. Although the absolute ground- and excited-state energies of $L^{2+}$, $L\cdot^+$, and $Cl^-$ are not known, because chloride does not reduce lucigenin, its highest occupied orbital must lie below the lowest unfilled orbital of lucigenin. In Figure 2, part 1 is the state dia-

(9) K. Watanabe, *J. Chem. Phys.*, 26, 542 (1957).
(10) K. Watanabe, *ibid.*, 26, 1773 (1957).

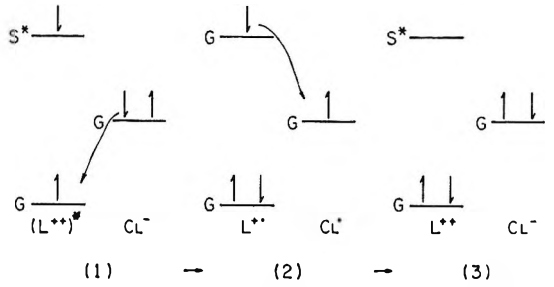


Figure 2. Energy-level diagrams showing the proposed mechanism of energy dissipation in the fluorescence quenching of lucigenin by chloride.

gram for excited singlet-state lucigenin $(L^{2+})^*$ and for chloride ion. When the charge-transfer complex with chloride is formed, the situation depicted in part 2 of Figure 2 results. Energetically the electron from the chloride will preferably go into the lowest possible level in lucigenin as shown by the arrow in part 1 of Figure 2. When the charge-transfer complex breaks up, the electron transferred back to the chlorine atom will be that from the highest energy level of $L^{\cdot+}$ which then leaves lucigenin and chloride both in the ground state (Figure 2, part 3).

It was observed that oxygen showed little or no quenching effect on lucigenin fluorescence. Although this may seem strange because of the extensive fluorescence quenching by oxygen in many systems, when forming charge-transfer complexes, oxygen acts as an electron *acceptor*,[11] while the effective quenchers reported here act as electron *donors*.

During the course of flash photolysis studies, it was noted that lucigenin photoreacts in water but that when chloride was present, no photoreaction occurred. Figure 3 shows the absorption spectra before and after 10 flashes. When chloride was present at $10^{-1}$ $M$, no absorption change was noted.

Three experiments were run to determine the nature of the photoreaction. A solution of lucigenin in water was vacuum degassed by six freeze–pump–thaw cycles and irradiated in a photoreactor for 1 hr using 365-nm radiation. Significant photoreaction occurred. Next, a solution of lucigenin in water was saturated with oxygen and irradiated under the same conditions. Photoreaction was observed amounting to 90% of that of the degassed sample. Third, a solution of lucigenin in water containing 0.1 $M$ KCl was irradiated under the same conditions after being vacuum degassed. No evidence of photoreaction was seen. These three experiments are consistent with photoreaction occurring from the lowest excited singlet state of lucigenin. The small amount of quenching observed for a solution saturated with oxygen is inconsistent with the behavior of most known triplets.[3] Assuming that oxygen would quench the lucigenin triplet by a reaction that is nearly diffusion controlled, one can calculate by eq 1 that the triplet lifetime in the

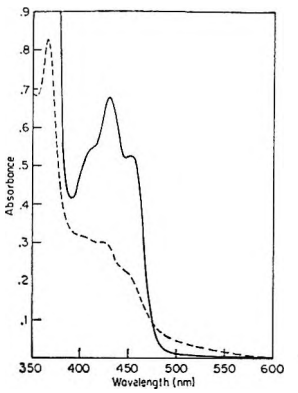


Figure 3. Absorption spectra of lucigenin in water before and after flashing: ——, before flashing; - - - - - -, after 10 flashes, 500 J per flash.

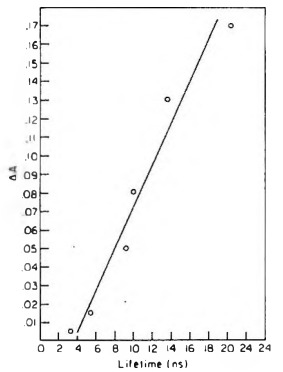


Figure 4. Absorbance changes *vs.* fluorescence lifetime for lucigenin solutions containing chloride. $\Delta A$ is the change in absorbance observed after 1 hr of irradiation at 365 nm on a carrousel reactor. Measurements were performed at 450 nm. Solutions had sufficient chloride added to adjust the fluorescence lifetime of lucigenin in the range of 3–20 nsec.

absence of quenching would be *ca.* $10^{-7}$ to $10^{-8}$ sec. Because there is no readily apparent source of extensive spin–orbit coupling in the lucigenin molecule, a triplet having such a short lifetime seems unlikely. Furthermore, a triplet state having such a short lifetime would probably be radiative.[12] The slight decrease in photoreactivity when oxygen was present probably resulted from an enhancement of the intersystem-crossing rate by oxygen perturbation.[3]

To identify the photoreactive state further as the singlet, solutions of lucigenin containing varying amounts of chloride were photolyzed. This provided a series of solutions of lucigenin with varying quantum efficiencies of fluorescence and fluorescent lifetimes. The lifetimes were measured and the solutions were placed in a carrousel photoreactor for 1 hr. At the end of this time the decrease in absorbance at 450 nm was measured. The change in absorbance, $\Delta A$, at

(11) H. Tsubomura and R. S. Mulliken, *J. Amer. Chem. Soc.*, 82, 5966 (1960).

(12) F. E. Lytle and D. M. Hercules, *ibid.*, 91, 253 (1969).

450 nm is a measure of the amount of photoreaction. When the lifetime of lucigenin is plotted *vs.* $\Delta A$, a straight line should result if the reaction proceeds from the singlet state, since chloride quenches the singlet state of lucigenin. Figure 4 shows the plot of $\Delta A$ *vs.* the lifetime which indicates that the photoreaction proceeds through the first excited singlet state of lucigenin. It might be argued that chloride quenching of the lowest singlet and triplet states of lucigenin could account for the results of Figure 4. Although this is possible, to have the slope of Figure 4 so close to unity and the reaction proceed mainly from the triplet would require a rather fortuitous combination of excited-state lifetimes and quenching rate constants. Long-term photolysis of lucigenin has yielded a product of yet undetermined structure. Traces of N-methylacridone are present, and it has been shown that the reaction product is not dimethylbiacridine.

*Acknowledgments.* The work was supported in part through funds provided for by the U. S. Atomic Energy Commission under Contract AT(30-1)-905. We wish to thank Anthony Vaudo for his assistance in the flash photolysis work. We also thank a reviewer for suggesting the explanation for the lack of oxygen quenching.

# Halogen-Sensitized Photoionization of N,N,N′,N′-Tetramethyl-*p*-phenylenediamine in Liquid Halogenomethanes

**by W. C. Meyer**

*Physical Research Laboratory, The Dow Chemical Company, Midland, Michigan 48640* *(Received October 3, 1969)*

Production of Wurster's Blue is shown to be a one-photon process independent of the solvent dielectric constant. Sensitization is confined to halogenated electron acceptors. The constancy of quantum yields with excitation energy excludes vibronic photochemistry. Yields in chlorinated solvents are distinctly less than in brominated solvents, which lends credence to the contention that the organic halide undergoes dissociative reduction to stabilize the transient ion pair of the excited donor–acceptor entity.

## Introduction

Photoionizations of aromatic molecules isolated in rigid solutions have been found to be biphotonic phenomena,[1,2] with evidence that the triplet state is an intermediate which absorbs the second quantum to complete the ionization step.[2] In fluid solution the two-photon requirement is sustained, but a partially ionized state replaces the triplet state as intermediate, and a single quantum path emerges in solvents of low polarity, thought to be due to the trace presence of oxidizers.[3] When certain electron-accepting solutes are deliberately added to aromatic amines in hydrocarbon glasses, photoionization is promoted; in fact in some cases no ionization occurs in their absence.[4] (The reaction also assumes a linear dependence on light intensity.) Donor–acceptor complexes, a type of association expected in these systems, can dissociate into ion radicals in polar solvents[5] or upon light absorption.[6] The single quantum ionization path has received less attention with regard to ionization efficiency, excitation wavelength dependence, etc. Because there was a variability in the efficiency of organic halides to enhance photoionization and possible mechanisms other than dissociative reduction of the halide were not considered,[4] a more thorough study of the role of the organic halide in the process was undertaken.

How then is sensitization promoted by organic halides? Charge-transfer complexes between aromatic amines and halogenomethanes have been reported.[7] What relation, if any, does complex formation have with sensitized photoionization? Is complex formation

(1) J. P. Ray and T. D. S. Hamilton, *Nature*, **206**, 1040 (1965).

(2) K. D. Cadogan and A. C. Albrecht, *J. Phys. Chem.*, **72**, 929 (1968).

(3) R. Potashnik, M. Ottolenghi, and R. Bensasson, *ibid.*, **73**, 1912 (1969).

(4) M. Kondo, M. R. Ronayne, J. P. Guarino, and W. H. Hamill, *J. Amer. Chem. Soc.*, **86**, 1297 (1964).

(5) R. Foster and T. J. Thomson, *Trans. Faraday Soc.*, **58**, 860 (1962).

(6) C. Lagercrantz and M. Yhland, *Acta Chem. Scand.*, **16**, 1043. (1962).

(7) K. M. C. Davis and M. F. Farmer, *J. Chem. Soc., B*, 28 (1967)

a necessary but perhaps not sufficient requirement for sensitization? Do halogenomethanes act as separate entities, such as energy reservoirs for photoejected electrons, or do they intimately partake in the initial step of ionization? Heavy-atom effects, which must be present to some degree, are one source of perturbation for the process. In short, by what pathway does a single photon of 3.1 eV cause ionization in rigid solutions? Experimental evidence is amassed to answer these questions.

First, photoionization of the aromatic amine N,N,N′,N′-tetramethyl-*p*-phenylenediamine (TMPD) is studied in liquid solution to determine the dependence of quantum yield with halogenation of the solvent and the effect of solvent dielectric constant and other variables on the process. The light intensity dependence is stringently tested.

The phenomenon is extended to polymer films in the following paper. Conditions for photoionization of aromatic amines are outlined and the donor–acceptor association between the amine and halogenomethane is verified. Luminescence and ionization thresholds are compared to provide information about the nature of association and its relation to photoionization.

Advantage is taken of polymer rigidity to study the nature of trapping sites from a comparison of thermal- and light-induced detrapping of charged species at room temperature and 77°K.

Polymer films lend themselves nicely to luminescence studies, and the third paper treats halogen perturbation of the fluorescence and phosphorescence polarization of TMPD in polystyrene films. When results are correlated to the oriented photoproduct (Wurster's Blue), the overall pathway of photoionization becomes evident.

## Experimental Section

TMPD, obtained as the dihydrochloride salt from Eastman Kodak, was precipitated as the free amine from aqueous KOH, dried, and sublimed. Liquid halogenomethanes were all used immediately after being freshly distilled. All other materials were used as received.

Room temperature absorption spectra were run on the Cary 15 spectrophotometer.

Photoionization experiments were followed using an HB200 superpressure mercury light source and a uv Bausch & Lomb monochromator with a dispersion of 3.2 nm/mm for excitation. Slit widths of 2 mm gave sufficient light intensity for photoionization and allowed experiments to be realistically conducted at 10-nm intervals. The solution was continuously stirred during the experiment to ensure a homogeneous concentration of product throughout the cell. A tungsten light source and visible monochromator set at right angles to the uv light source provided the means for monitoring blue color formation. The monochromator was set to pass 570-nm light, a wavelength where Wurster's Blue alone absorbs. Light transmitted through the sample was detected with a 1P-28 photocell. An interference filter in front of the photocell eliminated uv and other stray light. Light transmission with time of irradiation of uv light was recorded on a Sargent Model SR recorder. The cell was quartz with the dimensions 1.9 × 1.9 × 6 cm; an extended tubing served as a holder. The cell conveniently held 25 ml of solution. For determining the light intensity dependence, neutral-density filters consisting of calibrated wire screens were used. The exciting light could be varied an order of magnitude.

Concentrations of $10^{-3}$ *M* TMPD in various solvents were prepared in the dark with some precaution taken to exclude oxygen; nitrogen was bubbled through the solutions for 10 min. TMPD was irradiated in its first electronic absorption band at 10-nm intervals. The rate of production of Wurster's Blue was linear with time for 30 sec or more. To simplify calculations and eliminate effects of photoproduct light absorption in the uv region, the rate was calculated at time $t = 0$ from the slope of the 570-nm optical density–time curve. Fresh solutions were substituted when 10% conversion of TMPD to Wurster's Blue had taken place. Relative lamp intensities were determined using an integrating screen of esculin.[8] The absolute intensity was found for one wavelength using a ferrioxalate actinometer,[9] and the remainder was converted to absolute values.

## Results

An influence of solvent dielectric constant on photoionization of certain organic dyes has been reported by Holmes.[10] A general increase in ionization efficiency with increasing solvent dielectric constant was seen, with the onset occurring at a value greater than 4.7. Hence the possibility of change of solvent dielectric constant through addition of solutes must be probed.

Solvents were chosen to cover a range of dielectric constants. The results are presented in Table I. Included is the observation of whether TMPD fluorescence was present or absent when irradiated.

Several important facts emerge from the data. The first is that the dielectric constant *per se* does not assume dominance until high values are reached. This parallels the results of Kainer and Überle,[11] who found the complete transfer of an electron from TMPD to chloranil did not take place in solvents of low dielectric constant, but it did occur in acetonitrile; the transfer was not photoinduced, however. In the present work photoionization took place only in halogenated solvents irrespective of their dielectric constants. A correla-

(8) E. J. Bowen, *Proc. Roy. Soc.*, **A154**, 349 (1936).
(9) C. G. Hatchard and C. A. Parker, *ibid.*, **A235**, 518 (1956).
(10) E. O. Holmes, Jr., *J. Phys. Chem.*, **70**, 1037 (1966).
(11) H. Kainer and A. Überle, *Chem. Ber.*, **88**, 1147 (1955).

**Table I:** Solvent Effect on Wurster's Blue Production and TMPD Fluorescence

| Solvent | Dielec const | TMPD fluorescence | TMPD photoionizn |
|---|---|---|---|
| Acetonitrile | 37.5 | Slight | Slight |
| Cyclohexanone | 18.3 | Slight | Slight |
| Pyridine | 12.3 | No | No |
| $CH_2Cl_2$ | 9.1 | No | Yes |
| $CH_2Br_2$ | 7.2 | No | Yes |
| $CH_3I$ | 7.0 | TMPD insoluble | |
| Methyl ether | 5.0 | Yes | No |
| $CHCl_3$ | 4.8 | No | Yes |
| $CHBr_3$ | 4.4 | No | Yes |
| Ethyl ether | 4.3 | Yes | No |
| *o*-Xylene | 2.6 | Yes | No |
| Toluene | 2.4 | Yes | No |
| $CCl_4$ | 2.2 | No | Ppt formed |

tion between Wurster's Blue formation and the absence of TMPD fluorescence is evident. (The well-known quenching action of halogen-containing compounds toward luminescence of emitting molecules accounts for the lack of fluorescence in these solvents apart from any competitive photochemistry, and any correlation may be coincidental. Further experiments are needed to clear up this point.)

Photoionization of TMPD (and other aromatic amines) in these solvents has several directions from which it might proceed. Enhanced singlet–triplet transitions induced by a heavy-atom effect could both quench fluorescence and promote ionization, the latter either through a triplet–triplet annihilation mechanism[12] or through the absorption of a second photon directly.[2] A nonlinear dependence on exciting light is predicted for either mechanism. Another mechanism is a donor–acceptor type of association wherein the quenching mechanism involves charge-transfer interaction similar to that witnessed for substituted naphthalenes,[13] and ionization arises from the complete transfer of an electron when light absorption occurs within the complex. In fact an analogous path similar to the above mechanisms is possible if low-lying triplet charge-transfer energy levels are thermally populated, since then a single photon could conceivably effect ionization in the manner of intramolecular triplet-state participation. Fluorescence might be quenched because of competing photochemistry from the amine-excited singlet state, an ionization pathway advanced by Meyer and Albrecht[14] but erroneously based on a one-photon absorption process.

If, in addition to or in spite of the aforementioned possible roles of organic halides in sensitized photoionizations, dissociative reduction of the halide is an essential ingredient, and thus in the final sense the halide acts as a separate entity to stabilize the transient ion pair by removing excess electronic energy, then

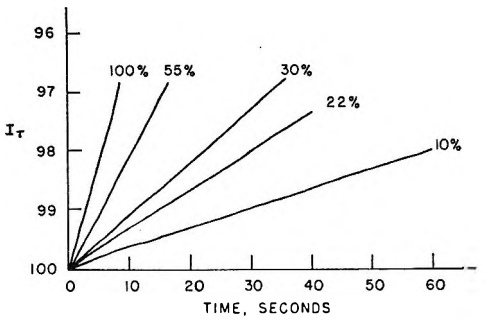


Figure 1. Variation of rate of TMPD photoionization with change in intensity of 310-nm excitation in steps from 100% intensity to 10% intensity. The ordinate is the intensity of 575-nm light transmitted by Wurster's Blue (cell path 1.9 cm; solvent $CHCl_3$).

sensitizer efficiency should to some extent depend on the strength of the C–X bond (X = halogen), greater efficiency occurring in compounds having weaker bonds.

One crucial test of many of the potential mechanisms is the dependence of the rate of photoionization on exciting light intensity. The light intensity dependence was carefully measured for all excitation wavelengths studied in the quantum yield determinations. Figure 1 reproduces the experimental rate curves generated for one set of conditions. The linearity of the initial rise permits slopes to be easily resolved. The results for Wurster's Blue production in various halogenomethanes are summarized in Table II. The rate was assumed to take the form

$$(dC/dt)_{t=0} = \phi I_0^n = k(dD/dt)_{t=0} = -(k/I_{av})(\Delta I/\Delta t)_{t=0} \quad (1)$$

Wurster's Blue concentration, $C$, at time $t$ is related to its optical density, $D$, through the proportionality constant $k$ using Beer's law. The quantum yield, $\phi$, and incident light intensity, $I_0$, are determined in the normal manner. The slope of decreasing transmitted visible light with time of uv irradiation, divided by the average transmitted light in the time interval, $\Delta t$, is thus proportional to the rate of Wurster's Blue production (the right-hand side of eq 1). The cell path length and TMPD concentration were chosen such that all incident uv light was absorbed. The light exponent of 1 accords with results of other systems in rigid glasses.[4,15] Triplet–triplet annihilation or absorption of a second photon by the triplet state or other biphotonic mechanisms are eliminated as possibilities.

(12) L. P. Gary, K. de Groot, and R. C. Jarnagin, *J. Chem. Phys.*, **49**, 1577 (1968).

(13) S. Ander, H. Blume, G. Heinrich, and D. Schulte-Frohlinde, *Chem. Commun.*, 745 (1968).

(14) W. C. Meyer and A. C. Albrecht, *J. Phys. Chem.*, **66**, 1168 (1962).

(15) J. P. Simons and P. E. R. Tatham, *J. Chem. Soc.*, *A*, 854 (1966).

**Table II:** Light Intensity Dependence of Photoionization Rate in Different Halogenomethanes[a]

| Solvent | $n$ (light exponent) |
|---|---|
| $CHCl_3$ | $1.12 \pm 0.17$ |
| $CHBr_3$ | $1.10 \pm 0.04$ |
| $CHCl_2$ | $0.91 \pm 0.03$ |
| $CH_2Br_2$ | $0.94 \pm 0.05$ |
| Av | $1.02 \pm 0.07$ |

[a] Values for 360-nm excitation.

The extent to which fluorescence may be quenched through competition of photochemistry from the excited singlet state, and if any vibronic effects in the photochemistry are manifested,[16] are investigated from the magnitude and wavelength dependence of the quantum yield. Quantum yields of Wurster's Blue production as a function of excitation wavelength and solvent are presented in Table III. Yields for brominated methane derivatives do not extend to shorter wavelengths because of light absorption complications of the solvent. The extinction coefficient of the photoproduct in the visible region was determined for each solvent using the procedure outlined by Meyer and Albrecht.[14]

**Table III:** Quantum Yields of TMPD Photoionization as a Function of Excitation Wavelength and Solvent

| λ, nm | $10^3\phi$ | | | |
|---|---|---|---|---|
| | $CHCl_3$ | $CH_2Cl_2$ | $CH_2Br_2$ | $CHBr_3$ |
| 280 | 5.2 | 5.9 | ... | ... |
| 290 | 4.9 | 5.9 | ... | ... |
| 300 | 5.3 | 3.5 | ... | ... |
| 310 | 5.0 | 3.4 | ... | ... |
| 320 | 4.7 | 3.4 | 8.7 | ... |
| 330 | 3.7 | 3.9 | 6.9 | 7.2 |
| 340 | 4.1 | 4.4 | 7.4 | 7.5 |
| 350 | 3.5 | 4.6 | 7.2 | 6.8 |
| 360 | 4.6 | 3.9 | 8.2 | 8.0 |
| 370 | 4.5 | 2.8 | 7.7 | 7.8 |
| 380 | ... | ... | ... | 6.9 |
| 390 | ... | ... | ... | 6.8 |

The constancy of $\phi$ with excitation energy excludes vibronic photochemistry of the excited singlet state of TMPD. The almost random variation of $\phi$ is taken as a measure of experimental accuracy, albeit the downward trend at longer wavelengths is probably not an experimental artifact. The low values of $\phi$ definitely eliminate fluorescence quenching based on competitive photoionization; instead the formation of either charge-transfer complexes or enhanced singlet–triplet intersystem crossing can explain this quenching. Quantum yields in chlorinated solvents are distinctly less than in brominated solvents, a trend not quantitatively established by Hamill and coworkers[4] in hydrocarbon glasses. This result supports the contention that organic halide dissociation, where a C–X bond is broken, governs the efficiency of the sensitizer.

An interesting observation, which also lends credence to halide dissociation, arose when *p*-chloranil was added to form a 1:1 ratio of TMPD to chloranil in $CHCl_3$. TMPD failed to ionize when irradiated. Chloranil forms a strong 1:1 complex with TMPD,[11] and apparently the proximity of the strong electron acceptor shielded TMPD from the near-neighbor presence of halogenomethane solvent molecules, thus preventing stabilization of any transient electron transfer through reductive dissociation of the more unstable solvent halide. (A complex of TMPD–chloranil in the polycrystalline state has a threshold energy of 5.0 eV for photoemission of electrons,[17] an energy requirement not met in this work.) When added to a photolyzed sample, chloranil increased the rate of fading of Wurster's Blue. The acceptor either must have complexed with $TMPD^+$ and then abstracted the ejected electron (from whatever its environment) or may first have formed an anionic species before migrating to the cation (and in a sense desolvated the electron).

The overwhelming concentration of heavy-atom solvent molecules undoubtedly masked any oxygen effect on the rate of photoionization. Oxygenated and degassed samples showed no change in photoactivity.

The critical and specific presence of halogenated electron acceptors which undergo dissociative reduction easily, in contradistinction to acceptors merely having differing electron affinities, is indicated but has not been thoroughly pursued. The influence of temperature and viscosity on the rate of ionization also have not been ascertained. These and other considerations, such as the extent of heavy-atom effects as a source of perturbation and the relative orientation of any donor–acceptor complexes (whether TMPD is a $\pi$- or n-type donor), are taken up in subsequent papers where a rigid environment is employed.

(16) R. S. Becker, E. Dolan, and D. E. Balke, *J. Chem. Phys.*, **50**, 239 (1969).

(17) T. Hibma, J. G. Vegter, and J. K. Kommandeur, *ibid.*, **49**, 4755 (1968).

# Halogen-Sensitized Photoionization of Aromatic Amines in Molded Polymer Films

by W. C. Meyer

*Physical Research Laboratory, The Dow Chemical Company, Midland, Michigan 48640* *(Received October 3, 1969)*

The one-photon ionization of N,N,N′,N′-tetramethyl-*p*-phenylenediamine (TMPD), N,N′-diphenyl-*p*-phenylenediamine, and *m*-phenylenediamine sensitized primarily with halogenomethane electron acceptors at room temperature and 77°K in molded polymer films are independent of polymer composition, matrix viscosity, or temperature. The existence of donor–acceptor complexes in polymer matrices is shown from optical absorption spectra, where the appearance or intensification of long-wavelength bands increases monotonously with degree of halogenation of the acceptor. The remarkable coincidence of ionization and luminescence thresholds of TMPD in the presence of a given halogenomethane and among all acceptors (1) implicates $\pi$ electrons of the donor in the photoionization process, (2) eliminates contributions of direct singlet–triplet absorption to the process or long-wavelength absorption, and (3) suggests the induced long-wavelength bands contain little $\pi$-electron character. The rates at which photolyzed fragments recombine in the dark and under constant visible light at room temperature and 77°K indicate *all* anionic species produced at 77° occupy shallow traps which are not filled during a room-temperature ionization. Light-sensitive traps exist at both temperatures with an energy depth of 2.15 eV.

## Introduction

The one-photon halogen-sensitized ionization of N,N,N′,N′-tetramethyl-*p*-phenylenediamine (TMPD) in liquid halogenomethanes revealed that the organic halide probably undergoes dissociative reduction to stabilize transient ion-pair formation.[1] Solvent dielectric constants were not of concern until high values were reached. What other criteria might be necessary prior to the dissociation step were not established. Thus complex formation between donor amines and acceptor halogenomethanes is known,[2] but whether ionization proceeds from light absorption within a charge-transfer band or more correctly from TMPD absorption slightly perturbed by the proximity of the heavy-atom molecule was not decided. Singlet- or triplet-state involvement of the amine is always of concern, and partition, if any, between the two was not examined. The underlying nature of sensitized photoionization prior to dissociation of the halogenomethane is of interest in the present work.

Isolation of the photochemical event in a rigid environment allows effects of certain variables to be more readily evaluated. Examples included here are change in macroscopic viscosity, a broader selection of electron acceptors with no interference of solvent interaction, comparison of threshold energies of ionization and luminescence, and sensitivity of recombination of fragments to light. Use of polymer matrices in the past was concentrated on emission properties of embedded molecules.[3,4] Most polymer matrices have been formed by *in situ* polymerization of the monomer containing the dissolved phosphor. This technique suffers from lack of versatility: no residual monomer can be tolerated; no real change in viscosity is possible; the procedure is tedious if a gamut of variation is desired. A second approach is to melt a mixture of the phosphor and thermoplastic under pressure. The experience has been that concentration gradients exist in the final matrix even when extreme care is taken in the initial mixing step. Films cast from a solvent containing the plastic and dopant also give inhomogeneous rigid solutions, and the film thickness is normally too thin to sustain less sensitive photochemical studies. A modification of these techniques is used in this work which eliminates most of their shortcomings.

The necessary presence of halogenated electron acceptors in order for amine photoionization to occur is verified in molded polymer films. The role of the polymer as a binder, aromatic amines other than TMPD, electron acceptors of differing affinities, viscosity changes, and the nature and energetics of trapping sites in the polymer are treated. Comparison of ionization and phosphorescence thresholds affords several conclusions about the photoionization pathway.

## Experimental Section

Purification of materials and photoionization apparatus were essentially the same as described elsewhere.[1] Polymer films containing 0.10 *m* TMPD and an electron acceptor were prepared by dissolving 5 g of poly-

(1) W. C. Meyer, *J. Phys. Chem.*, **74**, 2118 (1970).

(2) K. M. C. Davis and M. F. Farmer, *J. Chem. Soc., B*, 28 (1967).

(3) G. Oster, N. Geacintov, and A. U. Khan, *Nature*, **196**, 1089 (1962).

(4) N. Trublin, R. Santus, and M. Ptak, *Compt. Rend.*, **260**, 1134 (1965).

mer in 50 ml of solvent and adding 0.082 mg of TMPD and an equimolar amount of other solutes if desired. The solution was evaporated to dryness in the absence of light. Trace quantities of solvent remained (and in certain cases this was essential to observe photoeffects). The material was then compression molded into a uniform transparent sheet of *ca.* 10-mil thickness under a pressure of 5000 psi and 120°. Uniform concentrations and film thicknesses were obtained.

To follow photoionization rates, a section of film was mounted at an angle such that the sample could be simultaneously excited with uv light and viewed with visible light at a wavelength which the photoproduct alone absorbed. Low-temperature experiments required the film to be positioned in the lower part of an unsilvered dewar filled with liquid nitrogen. Nitrogen bubbles were channeled out of the light path.

## Results and Discussion

Molded polymer films containing residual traces of solvent have an intermediate viscosity between liquid solutions and matrices prepared from *in situ* polymerizations or hydrocarbon rigid glasses. Hence it was necessary to confirm that (1) no intramolecular biphotonic ionization occurred, (2) the character of halogen-sensitized photoionization was not altered, and (3) the polymer acted solely as a binder for the reactants, with perhaps some influence on the trapping properties or recombination of photolyzed fragments.

Toluene was chosen as a common solvent to detect unsensitized photoionization of TMPD since it itself is a poor donor when complexed. A film of polystyrene containing TMPD and residual toluene exhibited no photoactivity. When $CHCl_3$ replaced toluene, a molded sheet produced Wurster's Blue from TMPD when irradiated, as confirmed by the visible absorption spectrum. Biphotonic ionizations leading to stable products are prohibited, perhaps because of rapid recombination rates. Identical results are found at 77°K; little change in matrix rigidity must occur not to have a biphotonic mechanism emerge at the lower temperature.

Halogen-sensitized ionizations of TMPD in polymer films at room temperature and 77°K obviously retain the character which was demonstrated in liquid solution.[1] Table I presents comparisons of quantum yields and light intensity exponents for these situations. Essentially identical yields are found and a linear dependence of light intensity is evident in all media and temperatures for each halogenomethane.

If the polymer acts as a binder for donor–acceptor molecules without taking part in the ionization event, then color formation should be independent of polymer composition. Recombination of the photoejected electron (or anionic component) with the ionized donor would more likely be subject to viscosity differences, functional group differences, etc. Indeed poly(methyl methacrylate) and polystyrene display identical rates of Wurster's Blue formation and fading rates (Table I), as does a 65:35 copolymer composition by weight. When the halogen is attached to the polymer chain, some degree of sensitization is possible. Films of poly(vinyl chloride) and poly(2,5-dichlorostyrene) exhibit photochromism when no other halogen-containing compound is introduced (Table I). Other qualitative observations point to no active role of the polymer in photoionization providing it contains no halogen.

**Table I:** Light Intensity Dependence and Quantum Yields of TMPD Photoionization

| Medium | Halogenomethane | Temp, °K | Light exponent[a] | Quantum yield $\times 10^3$ [a] |
|---|---|---|---|---|
| $CHCl_3$[b] | $CHCl_3$ | 298 | 1.12 | 4.6 |
| $CH_2Cl_2$[b] | $CH_2Cl_2$ | 298 | 0.91 | 4.2 |
| $CHBr_3$[b] | $CHBr_3$ | 298 | 1.10 | 7.3 |
| PMM[c] | $CH_2Cl_2$ | 298 | 1.27 | 6.6 |
| PS[c] | $CH_2Cl_2$ | 298 | 0.94 | 6.6 |
| PS | $CHCl_3$ | 298 | 1.09 | 7.8 |
| PS | $CHCl_3$ | 77 | 1.10 | 8.6 |
| PS | $CHBr_3$ | 298 | 0.97 | 8.0 |
| PS | $CHBr_3$ | 77 | 1.20 | 8.4 |
| PS | $CCl_4$ | 298 | 0.97 | 3.3 |
| PS | $CCl_4$ | 77 | 1.00 | 7.0 |
| PVC[c] | PVC | 298 | 1.18 | 2.8 |
| DiClPS[c] | DiClPS | 298 | ... | ~0.2 |

[a] Average over first electronic absorption band. [b] Liquid solution results taken from ref 1. [c] PMM = poly(methyl methacrylate); PS = polystyrene; PVC = poly(vinyl chloride); DiClPS = poly(2,5-dichlorostyrene).

One advantage of molded polymer films is the matrix viscosity may be varied by including varying amounts of a particular polymer plasticizer to the solution prior to evaporation of the solvent. A polystyrene film plasticized with dioctyl phthalate showed intermediate behavior; it appeared slightly less sensitive to actinic radiation than an unplasticized sample. Poly(vinyl chloride) plasticized with glycerin and poly(methyl methacrylate) plasticized with dibutyl phthalate also showed little change in sensitivity. Indications are a viscosity decrease reduces photoionization efficiencies. Thus the consistently larger quantum yields given in Table I at 77°K compared to room temperature values for a given acceptor could reflect the difference in matrix rigidity.

The generality of the phenomenon was briefly examined using other aromatic amines: N,N′-diphenyl-*p*-phenylenediamine generated a green product and *m*-phenylenediamine a yellow product in polystyrene. Their behavior contrasts to that of TMPD in that no fading of color occurs, and in fact a long-term *increase* in optical density in the dark is noted. Again the

presence of an organic halide is mandatory for color formation. Relative yields of photoionization of N,N′-diphenyl-*p*-phenylenediamine are wavelength independent. The thermal reaction is consistent with a free-radical mechanism initiated by decomposition of the halogenated hydrocarbon.[5] Electron donors which failed to effect photoionization in the presence of an organic halide were triphenylamine, *o*-aminophenol, and N,N-dimethyl-*m*-toluidine. Triphenylamine will yield a green product when a film, cast from a halogenomethane solvent, is not completely dry.

Acceptors of differing electron affinities were incorporated in films in a 1:1 molar ratio to TMPD. Those surveyed were *p*-dinitrobenzene, biphenyl, $CBr_4$, *p*-benzoquinone, phthalic anhydride, chlorobenzene, *o*-dichlorobenzene, and $CClF_2CCl_3$. Many of these acceptors associate strongly with TMPD. In fact the sample containing TMPD and phthalic anhydride dried to a blue tint, implying complete transfer of an electron took place without the intervention of light. Only films with the acceptors $CBr_4$ and, to a lesser extent, $CClF_2CCl_3$ were photosensitive. Chlorobenzene when used as a solvent promoted slight TMPD photoionization in molded films. Chloride analyses of polystyrene films containing TMPD and residual halogenomethanes presented in Table II indicate that 1:1 molar ratios of donor–acceptor solutes should be sufficient to impart sensitization if such were to ensue. At one-third the TMPD concentration, $CH_2Cl_2$ demonstrates excellent sensitization.

**Table II:** Chloride Analysis by Polystyrene Films[a]

| Halogenomethane | % Cl (total) | Method | Solvent molality |
|---|---|---|---|
| $CCl_4$ | 15.8 | Parr bomb-Volhard method | 1.11 |
| $CHCl_3$ | 3.56 | Parr bomb-Volhard method | 0.334 |
| $CH_2Cl_2$ | 0.25 | Activation analysis | 0.035 |

[a] TMPD is 0.10 *m*.

Electron affinities of 1,4-dinitrobenzene, $CCl_4$, *p*-benzoquinone, $CHCl_3$, and chlorobenzene are all comparable (0.4–0.7 eV).[6] Since, of the above, only $CCl_4$ and $CHCl_3$ act as sensitizers, dissociative reduction of the halogenomethane is one requisite for sensitization, a conclusion reached previously.[1] Association quotients of these acceptors (excluding chlorobenzene) with TMPD in *n*-hexane are as large as those for association with hexamethylbenzene,[7] a classical electron donor. Any obvious difference in complexing ability or nature of complexing of these acceptors is not apparent.

The existence of complexes in polymer films is shown from the optical absorption spectra presented in Figures 1 and 2. Curve A in Figure 1 represents TMPD absorption in polystyrene unperturbed by complex formation. Toluene was used as solvent. A solution of TMPD in *n*-hexane at a concentration $5.07 \times 10^{-3}$ *m* in a 1-cm cell to give the same absorbance as in the polymer film possessed an absorption spectrum only slightly displaced to shorter wavelengths. The dis-

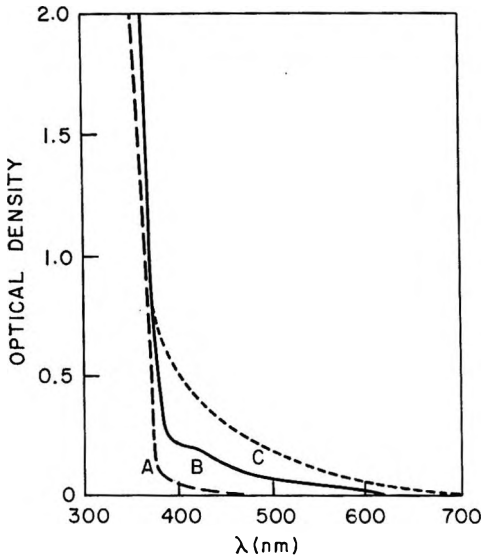


Figure 1. Absorption spectra of TMPD–halogenomethane complexes in polystyrene films (film thickness): A, TMPD–toluene (8.5 mil); B, TMPD–$CHCl_3$ (10.3 mil); C, TMPD–$CCl_4$ (10.7 mil).

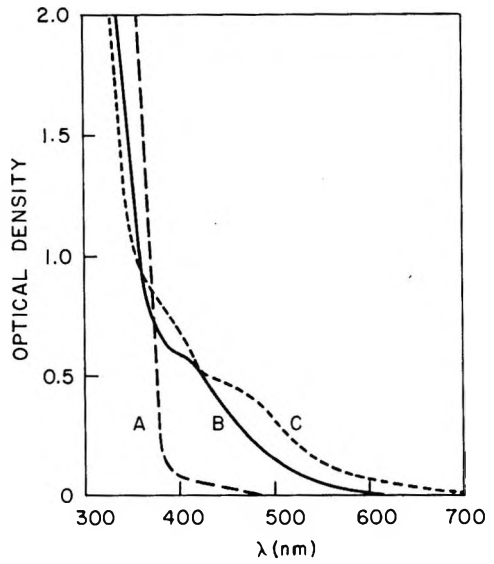


Figure 2. Absorption spectra of TMPD–halogenomethane complexes in polystyrene films (film thickness): A, TMPD–$CH_2Cl_2$ (11.6 mil); B, TMPD–$CHBr_3$ (6.0 mil); C, TMPD–$CBr_4$ (7.2 mil).

(5) R. H. Sprague, H. L. Fichter, Jr., and E. Wainer, *Phot. Sci. Eng.*, 5, 98 (1961).

(6) G. Briegleb, *Angew. Chem.*, 76, 326 (1964).

(7) W. C. Meyer, unpublished work.

crepancy is presumed to be a normal solvent shift. Results of luminescence studies[8] prove major TMPD dimer formation is absent and substrate effects are negligible for 0.10 *m* TMPD in these matrices. All halogenomethanes are transparent above 310 nm except $CBr_4$, which absorbs below 350 nm. $CCl_4$, curve C in Figure 1, shows a more pronounced deviation than $CHCl_3$, curve B, from the toluene spectrum, thus suggesting stronger interaction of $CCl_4$ with TMPD and in agreement with solution results.[2] Figure 2 continues with additional acceptors. $CH_2Cl_2$ is barely distinguishable from the toluene reference. $CBr_4$ and $CHBr_3$ deviate the most from the standard. This progressive distortion with increasing halogenation signifies the shift to longer wavelengths is not impurity absorption or TMPD dimer absorption. Films containing traces of halogenomethanes but no TMPD disclose no strong absorption above 310 nm. Complex formation of TMPD with halogenomethanes in polystyrene films is thus reasonably established.

Threshold energies of TMPD photoionization and phosphorescence emission are given in Table III. The

**Table III:** Threshold Energies of TMPD in Polystyrene

| Halogenomethane | Temp, °K | Ionization threshold, nm | Phosphorescence threshold, nm |
|---|---|---|---|
| Toluene, as blank | 77 | ... | 390 |
| $CH_2Cl_2$ | 298 | 385 | ... |
| $CH_2Cl_2$ | 77 | 380 | 380 |
| $CHCl_3$ | 298 | 400 | ... |
| $CHCl_3$ | 77 | 390 | 390 |
| $CCl_4$ | 77 | 390 | NA |
| $CHBr_3$ | 298 | 390 | ... |

remarkable coincidence of ionization and phosphorescence thresholds in a given sample and among each other signifies the following points.

(1) Absorption to wavelengths longer than 400 nm cannot be singlet–triplet TMPD absorption induced by a heavy-atom effect. Otherwise phosphorescence excitation would occur.[9] There is no reason to suppose this spectral region is not a charge-transfer type of band with totally quenched luminescence.[10]

(2) It follows from statement (1) that direct absorption into the long-wavelength band provides insufficient energy to ionize TMPD. Secondly the $\pi$-electron system must be of prime importance in the ionization process (where singlet and triplet emissions originate).

(3) Despite the above considerations, TMPD cannot photoionize as an isolated unperturbed molecule. A biphotonic dependence would be evident.[11]

(4) The failure of ionization thresholds to reflect C–X halogenomethane bond dissociation energies, when dissociative reduction is a requisite for sensitization, and the near-neighbor presence of donor and acceptor in the matrix together suggest the stability of the complex derives from contributions other than $\pi$ donation; *i.e.*, the appearance or intensification of long-wavelength bands has little TMPD $\pi$-electron character and does not lead to photoionization because of this reason.

It turns out the threshold for the second photon step from the triplet state in the biphotonic ionization of TMPD in rigid 3-methylpentane is ~390 nm.[11] If a low-lying charge-transfer triplet level was thermally populated in the present work, then concurrent thresholds for one- and two-photon ionizations is not unexpected. Energy requirements for a one-photon event are also then explained in the same framework. However, quantum yields of the one-photon-sensitized ionization do not display the wavelength variation found in the two-photon study. No esr signals are detectable in the dark in polymer matrices, indicating there is no triplet complex ground state or population of such a level. The sensitized ionization threshold simply coincides with the edge of the (mostly) unperturbed TMPD absorption band.

Thus the premise that three types of complexes might exist—stable CT complexes in the ground state which exhibit absorption but no emission or photochemistry, contact interaction that slightly perturbs TMPD emission, and a third variety that is photosensitive and may or may not luminesce—is discounted for several reasons. Suppose an arbitrary critical distance of approach is necessary for a stable complex to exist. Beyond this boundary a distribution of distances typify the degree of interaction for luminescent (and possibly nonluminescent) species that may photoionize. In this setting the efficiency of ionization should increase with increasing excitation energy, since higher energy barriers can be surmounted in the transfer of charge; *i.e.*, those looser complexes separated by larger distances should have higher threshold energies compared to acceptors situated closer to TMPD. In fact for very loose complexes, perhaps as noted for $CH_2Cl_2$ complexing, a biphotonic mechanism should prevail in the manner of methyl halides.[12] Also, less photoionization should be observed as a greater proportion of stable complexes is formed, since depletion of photosensitive complexes must ensue. This leads to an inverse rela-

(8) W. C. Meyer, *J. Phys. Chem.*, **74**, 2127 (1970).

(9) W. Rothman, A. Case, and D. R. Kearns, *J. Chem. Phys.*, **43**, 1067 (1965).

(10) S. Ander, H. Blume, G. Heinrich, and D. Schulte-Frohlinde, *Chem. Commun.*, 745 (1968).

(11) K. D. Cadogan and A. C Albrecht, *J. Phys. Chem.*, **72**, 929 (1968).

(12) W. G. French and J. E. Willard, *ibid.*, **74**, 240 (1970).

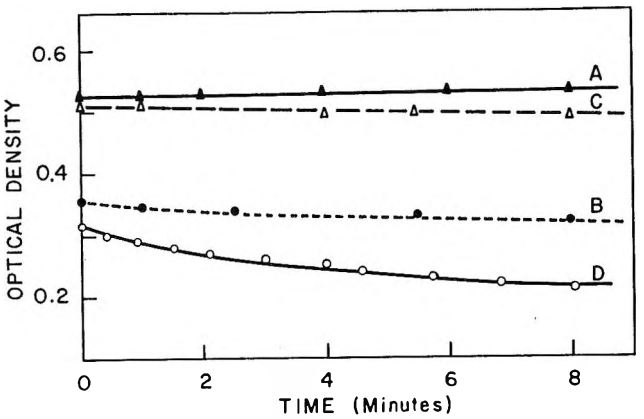


Figure 3. Fading rates of Wurster's Blue in polystyrene films under various conditions: A, room temperature dark decay; B, dark decay at 77°K; C, room temperature decay with constant 575-nm irradiation; D, decay at 77°K with constant 575-nm irradiation.

tionship between ionization quantum yield and association constant, a conclusion contrary to the results. Differing threshold levels of ionization for each acceptor, if direct CT absorption was the sole precursor of ionization, would be expected, as suggested earlier. Finally, it would be difficult to explain the correlation between quenching of luminescence and ionization efficiency in the framework without invoking separate mechanisms, an artifice not needed in the present interpretation.[8]

The extent to which photolyzed fragments recombine and the rate of recombination were determined from monitoring the fading rate of Wurster's Blue under appropriate conditions. Disappearance of Wurster's Blue may proceed along the normal route of recombination of charged species; it may undergo more complicated chemistry with the matrix to give a product (transparent) other than original TMPD; reaction of the anion fragment with the polymer substrate to give a product which does regenerate TMPD but alters the chemical constitution of the surroundings is another possibility. Any secondary reactions should be retarded at lower temperatures from the standpoint of energy of activation. The "negligible" change in polymer rigidity with change of temperature precludes any cage-effect advantage. A plausible explanation based on charge recombination is advanced.

Figure 3 illustrates the decay of Wurster's Blue at room temperature and 77°K for dark (thermal) recombination and under constant radiation of the monitoring light, 575 nm. There is no fading of color at room temperature in the dark (curve A) during a 10-min interval. A noticeable decrease is seen at 77°K during this time interval in the dark (curve B). This contrast is accounted for by invoking different energy levels of trapping in the matrix for the anionic species. Lowering the temperature may create strains or other local imperfections which act as shallow traps in close proximity to the cation. These traps when filled may be emptied thermally to precipitate the recombination step. At room temperature no such traps are filled if they exist (curve A). An interesting observation on the distribution of filled traps is made when it is noted that on warming a film irradiated at 77°K to room temperature, all color disappears. Clearly at 77° *all* fragments were in shallow traps and none occupied the sites filled during a room temperature ionization.

Enhanced rates of recombination result when constant 575-nm light floods the sample (curves C and D). The effect is greatest for the low-temperature experiment. Thus there exist light-sensitive traps of 2.15-eV depth (and probably less) at room temperature with apparently a greater number occupied at 77°K. One source of greater light-sensitive traps at the lower temperature may be the shallow traps which can be thermally emptied as well (see above). Photobleaching is reminiscent of the recombination course of electrons witnessed in hydrocarbon glasses.[13] Difficulties appear in this type of scheme for a one-photon TMPD ionization. Formation of $D^{+}\cdot A + e^{-}$ demands an energy comparable to the biphotonic path outlined in rigid solutions. A more suitable choice is $D^{+}\cdot X + Y^{-}$ or $D^{+}\cdot X^{-} + Y$ where Y is a fragment dissociated from a halogenomethane. If light absorption is more a property of a filled trap than of the species occupying the trap, then synonymous light sensitivity for $e^{-}$ and $Y^{-}$ is reasonable. Only differences in mobility would be seen. Photoconductivity experiments to measure mobilities would be helpful. The sluggish response to light eliminates electronic motion, at least in the same context as in rigid hydrocarbon glasses.[14]

Long-term thermal decay of Wurster's Blue at room temperature over a period of 15–20 hr leads to a permanent yellow discoloration which increases in intensity as more photochromic cycles are performed. On the other hand, if a low-temperature photolyzed sample is warmed, no discoloration develops and all Wurster's Blue disappears. It follows that photobleaching deals with direct charge recombination rather than degradation.

(13) W. M. McClain and A. C. Albrecht, *J. Chem. Phys.*, **43**, 465 (1965).

(14) G. E. Johnson and A. C. Albrecht, *ibid.*, **44**, 3162 (1966).

# Correlation of the Luminescence Perturbation of N,N,N′,N′-Tetramethyl-*p*-phenylenediamine with the Path of Halogen-Sensitized Photoionization

by W. C. Meyer

*Physical Research Laboratory, The Dow Chemical Company, Midland, Michigan 48640* *(Received October 3, 1969)*

Quenching of title compound (TMPD) luminescence by halogenomethanes is consistent with charge-transfer (CT) interaction rather than normal heavy-atom perturbation. With the exception of $CBr_4$, those quenchers that caused the largest deviation from exponential TMPD phosphorescence decay also shortened the lifetime the most, with greater quenching efficiency following the degree of acceptor halogenation: $CHBr_3 > CBr_4 > CCl_4 > CHCl_3 > CH_2Cl_2$. A stable CT complex is postulated for $CBr_4$ association and contact interaction for the remainder. Polarized emission and photoionization results reveal changing polarization of TMPD transition moments in the presence of $CHCl_3$. The TMPD–$CHCl_3$ complex has the halomethane adjoint to the TMPD lone-pair nitrogen electrons (l-type donor) rather than above the plane of the benzene ring as in typical $\pi$ donors. Thus, luminescence quenching and changing polarization of transitions are due to intramolecular CT mixing of (l, $a_\pi$) states with ($\pi$, $\pi^*$) states, the interaction of which is intensified by *intermolecular* CT complexing (l $\rightarrow$ $\sigma^*$ transitions of the complex). Because photoionization commences when the TMPD intramolecular absorption band is entered, thereby implicating the $\pi$-electron system and barring direct absorption into a CT continuum, the electron in essence transfers from a benzene-like $\pi$ molecular orbital to a halogenomethane $\sigma^*$ orbital (prior to acceptor dissociative reduction) but by an indirect coupling scheme. The lack of direct overlap is compensated by coupling of the states through (l, $a_\pi$) state mixing involving the lone-pair electrons in TMPD.

## Introduction

The aromatic amine N,N,N′,N′-tetramethyl-*p*-phenylenediamine (TMPD) may photoionize with a single quantum of 3.1 eV only if a halogen-containing electron acceptor is present.[1] In particular, halogenomethanes are most effective, the reason being one of stabilization of transient ion-pair formation through dissociative reduction of the halogenomethane.[2,3] Although the appearance of charge-transfer absorption bands confirms the near-neighbor presence of halide sensitizer to amine, coincident luminescence and photoionization thresholds, located near the high-energy side of the bands, signify ionization proceeds from light absorption within the (mostly) unperturbed TMPD $\pi$-electron manifold.[1] Since a biphotonic mechanism is ruled out, the models of Cadogan and Albrecht[4] and Lim, *et al.*,[5] do not apply. The threshold results also eliminate the possibility of singlet–triplet absorption, induced by heavy-atom perturbations, from contributing to the long-wavelength bands.

The present work accents the quenching aspects of the organic halide with respect to donor luminescence and phosphorescence lifetimes in molded polymer films. The relative magnitude of heavy-atom perturbation of both singlet–singlet and triplet–singlet transitions are established and compared from total luminescence spectra. Phosphorescence decay characteristics are used to compare quenching efficiencies with degree of halogenation of the acceptor. Photoselection experiments seek to detect changing polarization of transitions perturbed *via* the presence of the external halogen atom. The relative orientation of donor to acceptor in the complex is also surmised from the polarized emission results. Correlation of luminescence results with the one-photon ionization act conjures a definite electronic path for the latter.

An aside permeating the study is the search for significant donor dimer formation, impurity artifacts, or substrate interaction attendant with concentrated solutions. Luminescence quenching or emission altered from that of isolated molecules, differences in phosphorescence lifetimes, and changing fractional transition moments along selected coordinate axes will register their presence.

## Experimental Section

Purification of materials and preparation of polymer films containing uniform concentrations of donor and acceptor throughout the matrix are described elsewhere.[1,2] Polystyrene films containing 0.10 *m* TMPD

(1) W. C. Meyer, *J. Phys. Chem.*, **74**, 2122 (1970).

(2) W. C. Meyer, *ibid.*, **74**, 2118 (1970).

(3) M. Kondo, M. R. Ronayne, J. P. Guarino, and W. H. Hamill, *J. Amer. Chem. Soc.*, **86**, 1297 (1964).

(4) K. D. Cadogan and A. C. Albrecht, *J. Phys. Chem.*, **72**, 929 (1968).

(5) E. C. Lim and G. W Swenson, *J. Chem. Phys.*, **39**, 2768 (1963).

and residual amounts ($10^{-1}$–$10^{-2}$ $M$) of either $CH_2Cl_2$, $CHCl_3$, $CCl_4$, $CHBr_3$, $CBr_4$, or toluene were used. All films were approximately 10 mils thick.

Studies were carried out at 77°K. Excitation of the sample was achieved using an HB-200 superpressure Hg lamp and a Bausch & Lomb grating monochromator blazed for 250 nm. A Corning 9863 uv filter at the monochromator exit removed stray light. The condensing lens system of the monochromator focused actinic radiation onto the film. The film was immersed in liquid nitrogen in a Pyrex dewar with the lower portion unsilvered. A brass platform located on the bottom channeled nitrogen bubbles out of the light path.

Luminescence spectra were recorded using a second monochromator, blazed for 500 nm, set at an angle from the primary source. A 1P-28 photocell situated at the exit slit detected light emission from the sample. Its intensity was recorded on a Sargent SN recorder. A Corning 7380 filter at the monochromator entrance eliminated unwanted uv stray light.

Phosphorescence lifetimes were obtained from the decay curve of the afterglow when excitation was interrupted. All filters and the monochromator were removed from in front of the detector to view the entire phosphorescence band, thus improving the signal-to-noise ratio of the partially quenched luminescence. After uv excitation for 5–10 sec, the primary light source was cut off and the photocell simultaneously exposed to the phosphorescence. The radiative lifetime was sufficiently long and the detector sensitive enough such that the decay curve extended full-scale on the recorder.

Polarized emission studies required a modified geometrical arrangement of equipment. Polarized exciting light was provided by a stack of quartz plates set at the Brewster's angle for light of 365 nm. Monochromatic uv light, after passing through the monochromator and Corning 9863 filter, was partially reflected from the surface of the plates. The linearly polarized reflected light was focused on the sample. At right angles to the incident light was situated a condensing lens, an analyzer (Polaroid disk), a nonluminescent filter solution to remove unwanted light, and finally a 1P-21 phototube to measure relative emission intensities. The apparatus is represented schematically in Figure 1. Fluorescence emission ($\lambda_{max}$ 395 nm) was isolated from phosphorescence emission ($\lambda_{max}$ 475 nm) by inserting an aqueous solution of acridine orange, which absorbs all light of wavelengths 440–505 nm, between the analyzer and detector. Phosphorescence detection with no fluorescence contamination was accomplished using auramine O in water (it absorbs all radiation less than 470 nm). To correct for the inherent polarization preference of the apparatus, crumpled tissue paper was used as a blank in place of the film in the dewar. Totally reflected light from a metal mirror placed in front of the quartz plates made possible a source of unpolarized light. Incident light of 395 and 546 nm simulated conditions of isotropic sample emission. The apparatus prevented the normal procedure of rotating a polarizer to correct for instrumental bias from being followed.[6]

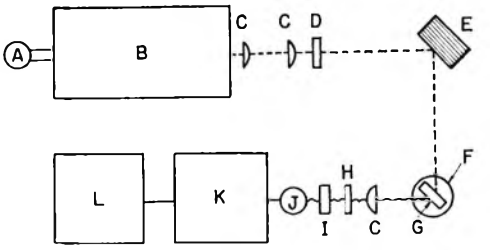


Figure 1. Geometric arrangement of polarized light experiment: A, uv light source; B, monochromator; C, lenses; D, Corning 9863 filter; E, stack of quartz plates; F, dewar; G, sample film; H, analyzer; I, aqueous filter solution; J, photocell; K, photocell power source; L, recorder.

## Results

*A. Luminescence Spectra.* When dealing with concentrated solutions, such as in the present work, emissions characteristic of solute–solute interactions or extraneous impurity luminescence are of concern. The formation of dimers or excimers, for example, would lead to either luminescence quenching or emission altered from that of individual molecules. Self-quenching is more properly determined from reduced luminescence lifetimes and depolarization of emission. Luminescence quenching *via* a foreign molecule (a halogenomethane in this case) can be examined from the nature of the quantum yield ratio of phosphorescence to fluorescence.

Figure 2 illustrates the uncorrected total emission from a 0.10 $m$ TMPD polystyrene film at 77°K, where toluene was used as a solvent. This film was shown previously to undergo no photochemistry when irradiated.[1] Its luminescence spectrum should indicate the extent and nature of any TMPD–TMPD interplay or substrate perturbation. (Weak polystyrene phosphorescence[7] is not detected when a film is doped with TMPD. A typical energy transfer from host-to-guest acceptor probably occurs. Absorption of light by the polymer is minor in any case for the excitation wavelengths used.) The trace amounts of toluene residing in the film are not considered to be of consequence. Resolution of the emission in Figure 2 into fluorescence and phosphorescence components was accomplished by recording the phosphorescence with the exciting light cut off. The total-emission spectrum is virtually identical with that of TMPD emission in hydrocarbon glasses.[8] The fluorescent peak at 397

(6) A. H. Kalantar and A. C. Albrecht, *Ber. Bunsenges. Phys. Chem.*, **68**, 361 (1964).

(7) M. T. Vala, Jr., J. Haebig, and S. A. Rice, *J. Chem. Phys.*, **43**, 886 (1965).

(8) W. M. McClain and A. C. Albrecht, *ibid.*, **43**, 465 (1965).

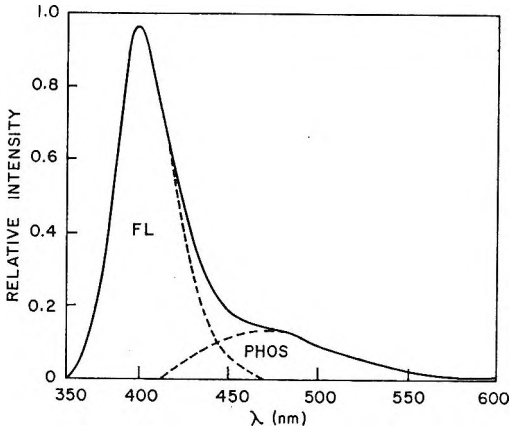


Figure 2. Fluorescence (FL) and phosphorescence (PHOS) of 0.10 *m* TMPD in polystyrene film with traces of toluene at 77°K and 365-nm excitation.

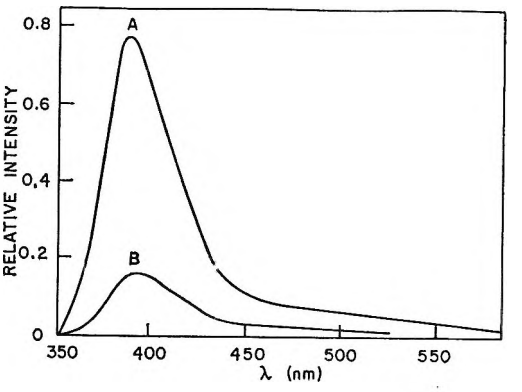


Figure 3. Total luminescence of TMPD in polystyrene films containing traces of $CH_2Cl_2$ (curve A) and $CHCl_3$ (curve B) at 77°K and 365-nm excitation.

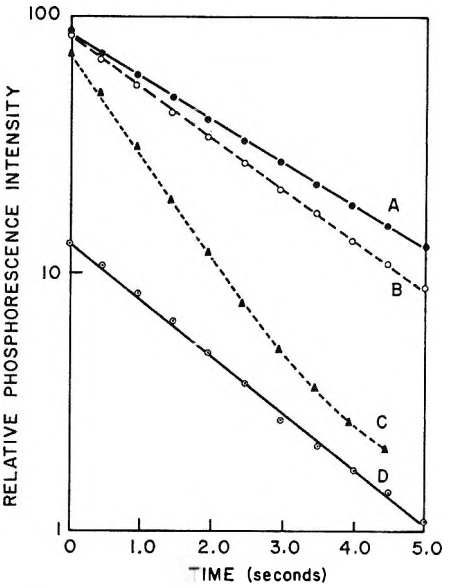


Figure 4. Phosphorescence decay of 0.10 *m* TMPD in polystyrene at 77°K containing (A) toluene (blank), (B) $CH_2Cl_2$, (C) $CHBr_3$, and (D) $CBr_4$. Initial intensities are not to scale.

nm in the present study is displaced somewhat from the peak found at 386 nm in rigid 3-methylpentane. The phosphorescence maximum lies at 473 nm and is in excellent agreement with the peak in 3-methylpentane at 474 nm. The results reveal no extraneous emission; thus no major intermolecular perturbation is indicated.

If $CH_2Cl_2$ or $CHCl_3$ replaces the residual amounts of toluene, quenching of TMPD luminescence results. Figure 3 presents spectra with these quenching agents. A halogenomethane quenches both fluorescence and phosphorescence. In addition, $CHCl_3$ is the better quencher. No quantitative spectra were possible with other halogenomethanes since sample emission was too feeble to be monochromatically recorded. Area integration of the luminescent components in Figure 3 establishes that the quantum yield ratio of phosphorescence to fluorescence remains constant, independent of the halogenomethane.

If the quenching mechanism was a normal heavy-atom effect, enhanced singlet–triplet intersystem crossing would lead to a reduced fluorescence yield and an increase in the aforementioned quantum yield ratio.[9] Similar quenching effects on *both* states suggests instead an influence of charge-transfer interaction, an effect consistent with the triplet and singlet quenching of naphthalenes in solution.[10]

*B. Phosphorescence Lifetimes.* The less intense phosphorescent samples lend themselves to lifetime studies because the entire phosphorescence band can be viewed. Relative quenching strengths and perturbation effects can be determined for halogenomethanes from their influence on lifetime shortening of TMPD phosphorescence and its deviation from exponential decay.[11] In Figure 4 is shown the phosphorescence decay behavior for various sample compositions. It is interesting that TMPD with toluene, $CH_2Cl_2$, and $CBr_4$ give first-order decay, $CHCl_3$ gives almost first-order, and $CHBr_3$ and $CCl_4$ give the largest deviation from exponential decay. Examination of lifetimes reveals that $CH_2Cl_2$ perturbs TMPD phosphorescence only slightly. Lifetimes follow the order $CH_2Cl_2$ (2.2) > $CHCl_3$ (2.0) > $CCl_4$ (1.4) > $CBr_4$ (1.3) > $CHBr_3$ (~1.0), where the values in parentheses refer to the phosphorescence lifetimes in seconds. With the exception of $CBr_4$, those compounds that cause the largest deviation from exponential decay also shorten the lifetime the most. The trend of shorter lifetimes with increasing halogen atomic number follows that of other systems.[9,11]

With toluene used in place of halogenomethanes, TMPD has a phosphorescence lifetime of 2.45 sec in polystyrene films. This value agrees within experi-

(9) S. P. McGlynn, *et al.*, *J. Chem. Phys.*, 39, 675 (1963).

(10) S. Ander, H. Blume, G. Heinrich, and D. Schulte-Frohlinde, *Chem. Commun.*, 745 (1968).

(11) S. Siegel and H. S. Judeikis, *J. Chem. Phys.*, 42, 3060 (1965).

mental error precisely with the dark triplet-state decay of TMPD in rigid 3-methylpentane (2.47 sec).[4] Bimolecular or other quenching effects are not evident in the polymer films. In view of a viscosity influence on the radiative and nonradiative decay processes from the triplet state,[12] the agreement is surprising. A logical explanation is that the mixing scheme of singlet–triplet states for the radiative process is uninfluenced in either medium by the environment; *i.e.*, spin–orbit coupling or any other factors that affect the radiative transition probability derive solely from intramolecular properties. Nonradiative dissipation of energy would then require equal TMPD coupling with the different surroundings, providing radiationless decay contributes significantly to the triplet-state lifetime.

The heavy-atom effect accounted for the variation in the decay processes in the other compounds. Complexing of the amine donor with a halogenomethane may increase the singlet–triplet mixing already present in the uncomplexed molecule without introducing any new coupling path, or enhanced intersystem crossing might include charge-transfer (CT) contributions.[13] For an aromatic amine, intermolecular and intramolecular CT contributions must be considered. A new coupling scheme will of course result in changing polarization of transition moments; polarized emission experiments reported next amplify these deliberations. The enhancement of singlet–triplet transitions for complexed TMPD by way of a particular coupling scheme is reserved for later.

The anomalous exponential decay of TMPD phosphorescence when complexed with $CBr_4$ suggests a stable complex may be formed and the remaining acceptors may interact with TMPD in a more random manner (contact CT complexes). $CBr_4$ has a relatively large association quotient with TMPD in *n*-hexane (5.28),[14] as calculated using the Benesi–Hildebrand approach.[15] There is some wavelength dependence, however. Thus, although a 1:1 complex is the dominant species, other higher order complexes and perhaps contact interactions also contribute to the spectrum.[16] If a stable complex is formed or a specific geometrical arrangement is preferred, the radiative decay should be exponential with a lifetime characteristic of the complex. If, on the other hand, the perturbation involves a distance factor, such as in a heavy-atom effect or contact CT interaction, the decay will be nonexponential because of the distribution of separations likely to be found in the matrix. Weak association between TMPD and chlorinated methane derivatives is known.[17] Thus, perturbation of TMPD phosphorescence lifetimes is entirely consistent with CT complex formation as the source, in agreement with luminescence quenching results. The appropriate mixing scheme leading to CT quenching and its relation to sensitized photoionization remain to be found.

*C. Polarized Emission and Photoionization.* Relative polarization of transition moments derived from a photoselection experiment may be qualitatively compared through the degree of polarization, $P$. Theoretically $P$ varies from $+1/2$ for absorption and emission along the same molecular axis to $-1/3$ for emission perpendicular to the absorption axis, but since the theoretical limits are rarely observed, Albrecht[18] has introduced a correction term to account for intrinsic depolarizing effects, such as concentration depolarization, readsorption, unparallel light, and irregularities in the sample. The calibration factor is above and beyond the normal practice of correcting for instrument bias of polarized light and represents all other randomizing effects. Use is made of this factor here, and it is denoted by $\Delta$.

Table I summarizes the polarization data. The long axis of TMPD is taken along the line joining the *para* substituents in the plane of the ring, and the short axis is perpendicular to the long axis, also in the plane of the ring.

Fortunately, the absolute transition probabilities of TMPD have been determined (in rigid 3-methylpentane).[6] Short-axis absorption and fluorescence of TMPD in polystyrene (with traces of toluene) is first assumed, as was shown to be true in the hydrocarbon glass; this assumption determines what randomization factor ($\Delta = 0.034$) is needed to correct for intrinsic depolarization, *i.e.*, to adjust the observed degree of polarization of 0.486 to the theoretical value of 0.50 for transitions along the same axis. If concentration depolarization and substrate perturbation is absent, this $\Delta$ must be a constant and hold for phosphorescence data also. The fraction of long-axis phosphorescence emission, using the above $\Delta$, agrees very well with that in 3-methylpentane glasses. Thus, not only is the use of a constant $\Delta$ supported for both types of emission, but its low value indicates the absence of randomizing effects. TMPD in polystyrene behaves emission-wise like an isolated molecule embedded in a hydrocarbon glass, even though its concentration is 0.10 *m*. Films of *ca.* 10-mil thickness must be sufficiently thin to eliminate the reabsorption problem inherent in samples of this concentration.

If TMPD retains all short-axis fluorescence in polymer films containing residual $CHCl_3$, a larger $\Delta$ (0.127) is necessary. An inconsistency enters when polarized photoionization results are taken into account, however. The photoproduct Wurster's Blue absorbs along its long axis in the 500-nm region.[19] No evidence exists

(12) S. J. Ladner and R. S. Becker, *J. Chem. Phys.*, **43**, 3344 (1965).
(13) K. B. Eisenthal, *ibid.*, **45**, 1850 (1966).
(14) W. C. Meyer, unpublished work.
(15) H. A. Benesi and J. H. Hildebrand, *J. Amer. Chem. Soc.*, **71**, 2703 (1949).
(16) G. D. Johnson and R. E. Bowen, *ibid.*, **87**, 1655 (1965).
(17) K. M. C. Davis and M. F. Farmer, *J. Chem. Soc., B*, 28 (1967).
(18) A. C. Albrecht, *J. Amer. Chem. Soc.*, **82**, 3813 (1960).
(19) A. C. Albrecht and W. T. Simpson, *ibid.*, **77**, 4454 (1955).

**Table I:** Polarized Emission and Photoionization of TMPD

| Matrix | Fractional transition probability: Absorption (365 nm) | Fluorescence (400 nm) | Phosphorescence (480 nm) | Wurster's Blue absorption (575 nm) | Intrinsic corr factor, Δ[a] |
|---|---|---|---|---|---|
| 3-Methylpentane | All short axis[b] | All short axis[b] | 0.16, long axis[b] | All long axis[c] | ... |
| Polystyrene (PS) + toluene | Assumed short axis | Assumed short axis | 0.14, long axis | ... | 0.034 |
| PS + $CHCl_3$ | Assumed short axis | Assumed short axis | 0.20, long axis | ... | 0.127 |
| PS + $CHCl_3$ | Assumed short axis | ... | ... | Assumed long | 0.47 |
| Or if No More Randomization Than PS–Toluene Sample | | | | | |
| PS + $CHCl_3$ | 0.09, long | ... | ... | Assumed long | 0.034 |

[a] Δ = randomization factor to correct for intrinsic depolarization. See text. [b] Taken from Figure 8 of ref 6. [c] Reference 19.

to claim that Wurster's Blue generated from TMPD sensitized by a halomethane is spectrally different from chemically produced $TMPD^+$. The function of the sensitizer does not seem to concern the cation. Also the same Δ must apply to emission and photoionization experiments in the $CHCl_3$-containing sample, since the correction factor pertains to depolarizing effects of light *absorption*. Yet a completely different and abnormal Δ (0.47) obtains when all short-axis TMPD absorption at 365 nm is accepted in the photoionization experiment; hence either all short-axis absorption is in error and/or all short-axis fluorescence also is incorrect when TMPD is perturbed by a halogen. Regardless of whether depolarization effects increase when $CHCl_3$ replaces toluene (a larger Δ), the oriented Wurster's Blue and polarized emission results verify that molecular properties change. Indeed, if no depolarization effects intrude beyond those of the reference (Δ = 0.034), 9% long-axis absorption occurs at 365 nm. Likewise, the Δ calculated for all short-axis fluorescence does not recover the same long-axis probability for phosphorescence as found in the toluene-containing standard (see Table I).

## Discussion

The changing polarizations of transition probabilities, expressed as degree of polarization, allow the relative orientation of donor to acceptor in the complex to be surmised. TMPD–halomethane complexes can exist in two isomeric configurations. $CHCl_3$ is known to complex with benzene, a π-electron donor, in an orientation in which the chloroform proton is directed approximately at right angles to the plane of the ring and in the vicinity of the hexagonal axis.[20] On the other hand, a linear structure has been demonstrated for CT complexes between a tertiary nitrogen atom and a halogen molecule.[21] The nitrogen acts as an n donor in this case. Neither orientation can be excluded for TMPD. What are the consequences of the polarization results on each configuration?

*Case I. Halogenomethane Directly above the Plane of the Ring.* The transition moment for CT absorption will lie approximately along the line joining the centers of donor and acceptor. Since the transfer of charge is from the benzene-like π orbital of TMPD to the $\sigma^*$ antibonding orbital of $CHCl_3$ and is thus polarized out of plane, all out-of-plane intramolecular transitions may be enhanced directly *via* coupling with CT states (singlet or triplet where allowed). Because some loss of symmetry is to be expected through random contact and, hence, orientation of donor and acceptor to each other, slight in-plane mixing is also likely. TMPD phosphorescence is the only intramolecular transition which has a component perpendicular to the plane of the ring. Intensity stealing by this component would make phosphorescence more negatively polarized when TMPD is complexed and excitation occurs in the normal intramolecular absorption band. The opposite trend is predicted when absorption occurs in the CT band, as phosphorescence and absorption now lie along the same axis. The toluene–TMPD blank, in conjunction with luminescence threshold results, however, affirms that phosphorescence originates from absorption within the intramolecular band—perturbed slightly by any halogen in the vicinity—for all samples.[1] Furthermore, CT absorption for this sandwich configuration should not contribute directly to in-plane intensities to the extent of 9% long-axis absorption in complexed TMPD. From this standpoint Wurster's Blue yields an equivocal result, since its long-axis absorption is perpendicular to both out-of-plane CT absorption and intramolecular short-axis absorption. The more positive polarization of TMPD phosphorescence (−0.18 in PS–toluene *vs.* −0.11 in PS–$CHCl_3$) excludes having the acceptor above the plane of the ring.

*Case II. Halogenomethane Adjoint to Nitrogen Atom.*

(20) L. W. Reeves and W. G. Schneider, *Can. J. Chem.*, 35, 251 (1957).

(21) O. Hassel, *J. Mol. Phys.*, 1, 241 (1958).

The CT transition moment now extends from the lone-pair orbital on the nitrogen atom to the center of the halogenomethane, an $l,\sigma^*$ transition. Mixing with ($\pi$, $\pi^*$) states must be by indirect means to quench luminescence. Because overlap of $\pi$ and $\sigma^*$ orbitals should be small or nonexistent in this configuration, $\pi \rightarrow \sigma^*$ transfer of charge directly is excluded, and a mixing scheme must be introduced also for photoionization. The obvious coupling scheme involves the ($l$, $a_\pi$)[22] state of the lone-pair electrons. Complexing will raise the energy levels of these states, in analogy with (n, $\pi^*$) states. Displacement to higher energies favors stronger coupling between ($l$, $a_\pi$) and ($\pi$, $\pi^*$) states because a higher density of vibronic states is available for interaction.[23] Thus, enhanced intersystem crossing, luminescence quenching, and reduced luminescence lifetimes are due to *intramolecular* charge-transfer mixing of ($l$, $a_\pi$) states with ($\pi$, $\pi^*$) states, the interaction of which is aided by *intermolecular* CT complexing. The polarization results are consistent with this hypothesis. $l \rightarrow a_\pi$ transitions are not polarized entirely in plane, as in $\pi \rightarrow \pi^*$ transition, nor are they polarized entirely out of plane, as in $n \rightarrow \pi^*$ transitions. Perturbation of all transition probability axes would be effected.

Threshold studies have shown that photoionization of TMPD commences when the intramolecular absorption band is entered, thereby implicating $\pi$ electrons in the process and barring direct absorption into a CT continuum.[1] The path of ionization is thus understood and explained within the context of the $l,a_\pi$ mixing scheme. Electron transfer might possibly be described as a tunneling mechanism. In fact, photoionization efficiencies are relatively temperature independent.[2] A tunneling barrier of course stabilizes the transient ion pair, allowing degradation of the halomethane to ensue. Sandwich-oriented complexes, where a recombination barrier does not exist but strong overlap is possible, apparently do not form stable ion radicals except in polar media.[24] Similarly, rapid recombination and the brief lifetime of excited halomethane would prevent $l \rightarrow \sigma^*$ transitions from leading to TMPD ionization.

In the photolysis of halogenomethanes alone in rigid hydrocarbon solutions, Simons and Tatham[25] attributed the one-photon process of 4.9-eV energy to the crowding of outlying Rydberg orbitals. In favorable cases an electron is thought to transfer to adjacent halomethane molecules and become trapped. A crowding effect is invoked to modify Rydberg levels such that the excited $n,\sigma^*$ transitions may reach and overlap them. This view is untenable with the present work. Direct electron ejection in nonpolar solvents commands an energy requirement not far below gaseous ionization potentials in the absence of sensitizers. Population of Rydberg orbitals, in the absence of sensitizers, requires 2 quanta of uv light.[4] Rydberg orbitals of TMPD undoubtedly overlap acceptor $\sigma^*$ orbitals, but no apparent means is available to populate them in a 1-quantum step of 3.1 eV without also construing an enormous lowering of their energy from halogen perturbation ($\sim$2.8 eV). Thus, the perturbation envisioned to produce electron transfer by neighboring like molecules is without experimental basis. An acceptable mechanism of color formation is a one-photon-induced dissociation of the halomethane, where a C–X bond is broken. Light-sensitive traps of halomethane fragments exist in polymer matrices.[1]

(22) M. Kasha in "Light and Life," W. D. McElroy and B. Glass, Ed., Johns Hopkins University Press, Baltimore, Md., 1961, p 31.

(23) R. M. Hochstrasser, *Accounts Chem. Res.*, 1, 266 (1968).

(24) C. Lagercrantz and M. Yhland, *Acta Chem. Scand.*, 16, 1043 (1962).

(25) J. P. Simons and P. E. R. Tatham, *J. Chem. Soc., A*, 854 (1966).

# Low-Temperature Matrix Isolation Study of Hydrogen-Bonded, High-Boiling Organic Compounds. I. The Sampling Device and the Infrared Spectra of Pyrazole, Imidazole, and Dimethyl Phosphinic Acid

by S. T. King

*Chemical Physics Research Laboratory, The Dow Chemical Company, Midland, Michigan 48640*
*(Received December 8, 1969)*

A matrix isolation device has been developed to study the hydrogen-bonded, high-boiling organic compounds by infrared spectroscopy. This device can isolate the monomeric species of hydrogen-bonded samples in an inert gas matrix within a reasonably short time and can be conveniently used for routine analysis. Infrared spectra of pyrazole, imidazole, and dimethyl phosphinic acid isolated in argon matrix are discussed.

## Introduction

The low-temperature matrix isolation technique has been used by infrared spectroscopists for more than fifteen years in the study of unstable molecular species,[1] high-boiling inorganic compounds[2] and low-boiling hydrogen-bonded compounds.[3] Several review papers in this field have been published recently by Barnes and Hallam,[4] and by Hermann and Harvey.[5] As was pointed out by these authors, little information can be found in the literature about matrix isolation of large organic molecules. We have directed our attention to matrix isolation of large organic molecules, especially the hydrogen-bonded compounds, for some time. Our results show that the matrix isolation technique is applicable to some problems regarding hydrogen-bonded organic solids. In this first paper we report a matrix isolation device which can be used to isolate the monomeric species of strongly hydrogen-bonded organic compounds in a reasonably short time and which can be used for routine analysis. The infrared spectra of argon matrix isolated pyrazole, imidazole, and dimethyl phosphinic acid are discussed.

It is well known that molecules with OH or NH groups are usually intermolecularly bonded in the liquid or solid phases. Under these conditions, the O–H or N–H stretching absorption band is broad in the infrared spectrum, and it is often difficult to interpret this broad band into useful chemical information. On the other hand, the unassociated OH group shows a sharp absorption in the region 3800–3500 $cm^{-1}$, which the unassociated NH group shows a sharp absorption in the region 3600–3300 $cm^{-1}$, and the frequency at which this band absorbs enables specific identification of the particular group present in the molecule. Infrared spectra of unassociated species of molecules containing the NH or OH group can be obtained in dilute solution, but the molecule must be soluble in a suitable solvent which does not mask the $\nu_{NH}$ or $\nu_{OH}$ absorption bands or other bands. Moreover, many compounds are not soluble in a suitable solvent, and the spectra of their unassociated species cannot be studied in this manner. In some cases, the infrared spectrum of the monomeric species can be obtained in vapor phase at high temperature. However, for solid samples with very low vapor pressure, a good vapor spectrum is often very difficult to obtain. In addition, the overlapping of the broad bands in a gas phase spectrum often makes it difficult to distinguish them. The spectrum of the monomeric species isolated in a low-temperature matrix can avoid all the problems discussed above.

The hydrogen bonding of some low-boiling compounds such as $NH_3$, $HN_3$, $CH_3OH$, $H_2O$, was first studied by Pimentel's group in their early matrix iso-

(1) For example: M. E. Jaeox and D. E. Milligan, *J. Chem. Phys.*, **48**, 4040 (1968); L. Andrews, *ibid.*, **47**, 4834 (1967); N. G. Moll and W. E. Thompson. *ibid.*, **44**, 2684 (1966); R. P. Spratley, J. J. Turner, and G. C. Pimentel, *ibid.*, **44**, 2063 (1966).

(2) For example: W. Weltner, Jr., and D. McLeod, Jr., *ibid.*, **45**, 3096 (1966); R. L. Redington, *ibid.*, **44**, 1238 (1966); S. Schlick and O. Schnepp, *ibid.*, **41**, 463 (1964); A. Snelson, *ibid.*, **46**, 3652 (1967).

(3) M. VanThiel, E. D. Becker, and G. C. Pimentel, *ibid.*, **27**, 486 (1957); E. D. Becker and G. C. Pimentel, *ibid.*, **25**, 224 (1956); G. C. Pimentel, *ibid.*, **44**, 3641 (1966); E. Catalano, R. H. Sanborn, and J. W. Frazer, *ibid.*, **38**, 2265 (1963); R. L. Redington and D. E. Milligan, *ibid.*, **37**, 2162 (1962); D. E. Milligan, R. M. Hexter, and K. Dressler, *ibid.*, **34**, 1009 (1961).

(4) A. J. Barnes and H. E. Hallam, *Quant. Rev., Chem. Soc.*, **23**, 392 (1969).

(5) T. S. Hermann and S. R. Harvey, *Appl. Spectrosc.*, **23**, 435 (1969); T. S. Hermann, S. R. Harvey, and C. N. Honts, *ibid.*, **23**, 451 (1969); T. S. Hermann, *ibid.*, **23**, 461 (1969); T. S. Hermann, *ibid.*, **23**, 473 (1969).

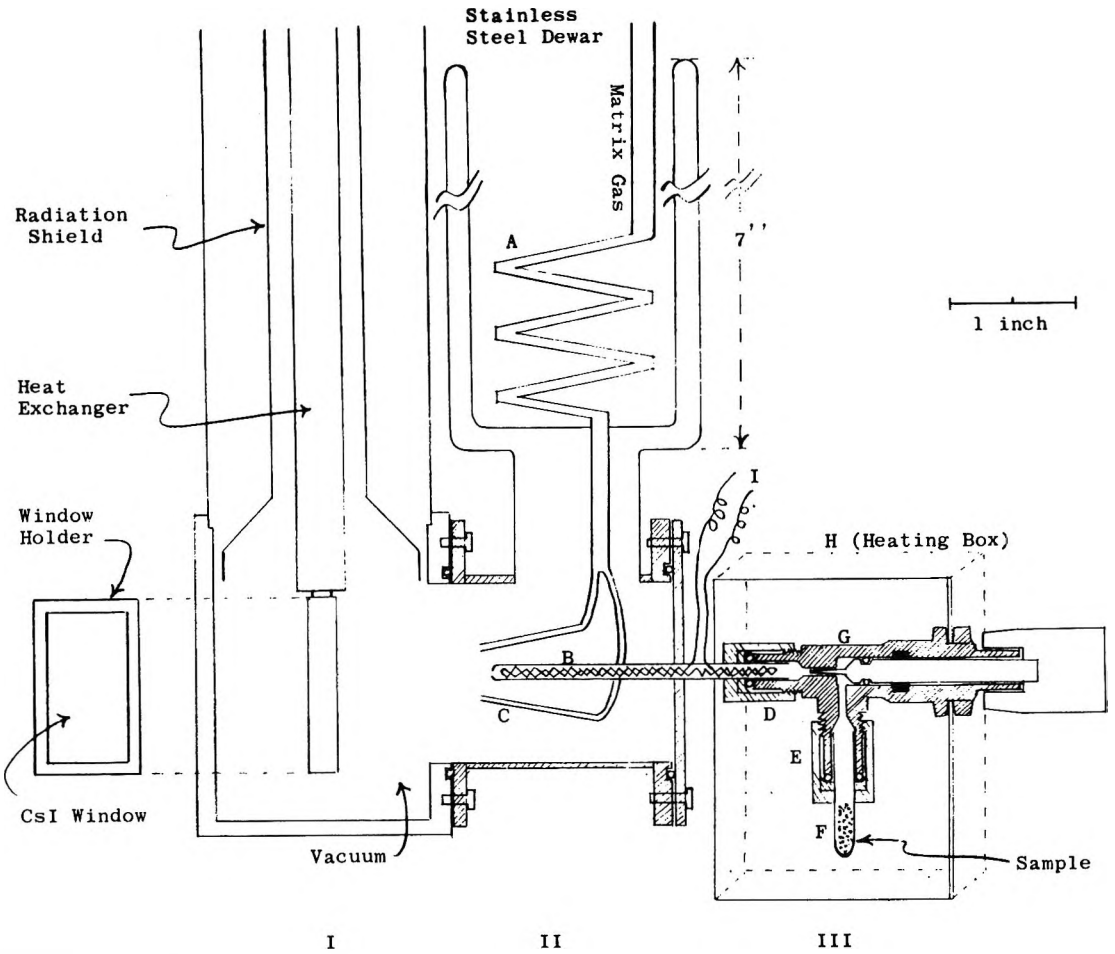


Figure 1. Construction of the matrix isolation device.

lation work.[3] They obtained the monomeric species by dilution in the gas phase. However, dilution in the gas phase is impractical for a solid sample with negligible vapor pressure at room temperature. Therefore, thermal dissociation has been used in our study. The heated vapor was allowed to pass through a hot nozzle and was deposited on the cold window simultaneously with precooled matrix gas which was deposited through two separate nozzles.

The Knudsen cell has been used by many investigators to study the unassociated species of very high-boiling inorganic compounds in a low-temperature matrix. However, it usually takes a very long deposition time, and it is very inconvenient for semiroutine analysis on organic compounds. The matrix isolation cell we designed in the course of this study can isolate the monomeric species of a hydrogen bonded organic compound very effectively in a reasonably short time and can be used for routine analysis.

## Experimental Section

The instrument as shown in Figure 1 is composed of three sections. Section I is a refrigerator (the Cryo-Tip Model AC3L 110 made by Air Products and Chemicals, Inc.). The heat exchanger can reduce the temperature of the window (CsI crystal) to 20° or 6°K. Section II is a liquid nitrogen dewar which cools the inert matrix gas during deposition. Section III in Figure 1 is the heating part for the high-boiling sample. Part B is a $^1/_8$-in. stainless steel nozzle with an inside heater (I). The high temperature of this heater in B will keep the monomeric species of the sample from reassociation before leaving the nozzle. Part G is a fine metering valve (manufactured by Nupro Co.) equipped with two Viton "O" ring seals (D and E). This metering valve and the sample in a glass tube (F) are enclosed in a copper box (H) which can be heated by the heating wire around the box H. During deposition, the metering valve (G) is heated uniformly (by H) to a temperature so that enough vapor from the sample (in F) can be generated. The flow rate of the sample in the vapor phase can be controlled by the metering valve. The heater in B is maintained at a higher temperature than H, so as to ensure disassociation of the hydrogen-bonded molecules, and also prevents any deposition of the sample in nozzle B. It is very important to keep the sampling device free from deposition for routine analyses, because otherwise any impurity from the previous sample will obscure the spectrum of the new sample.

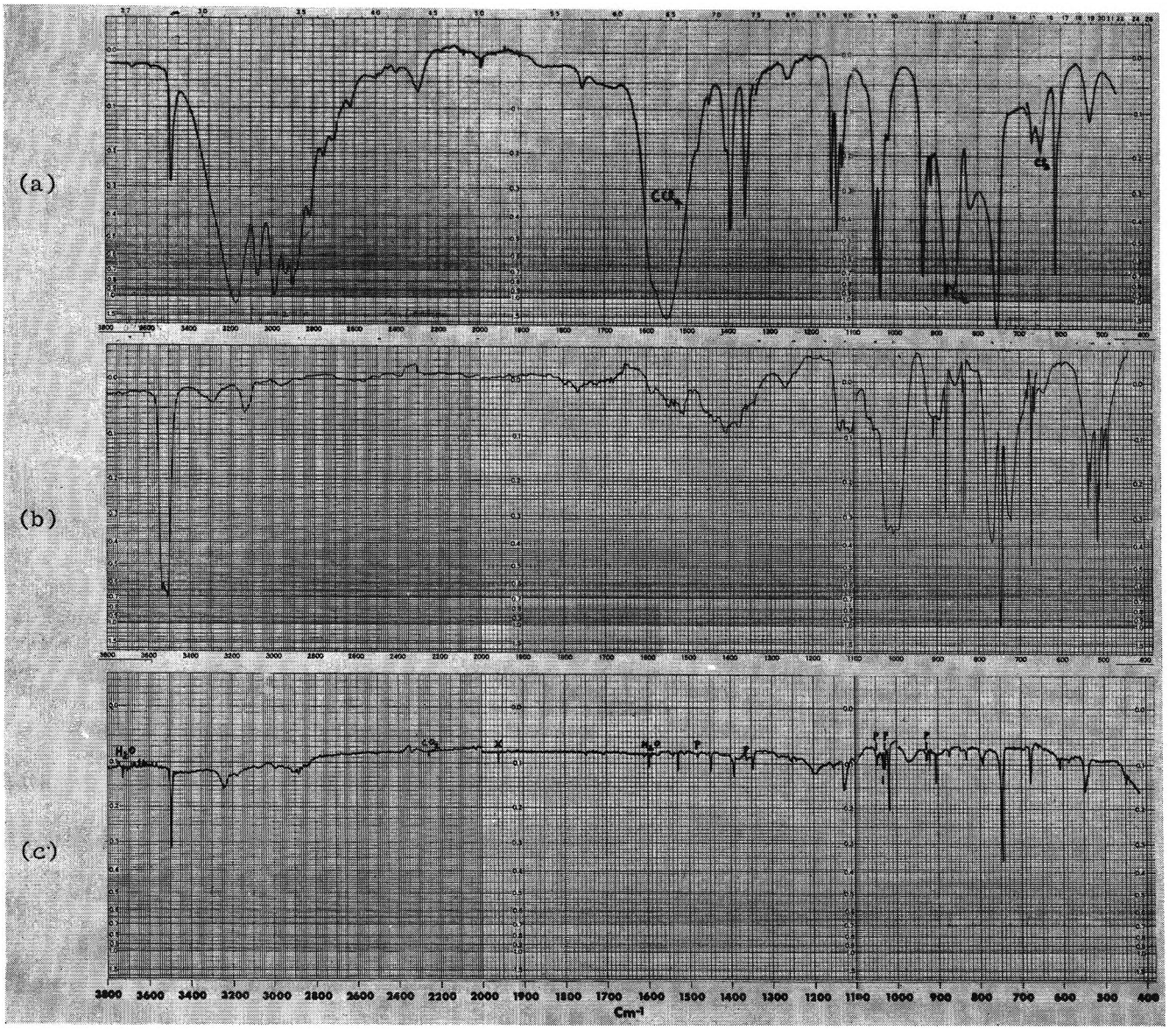


Figure 2. Infrared spectra of pyrazole: (a) in 1% $CCl_4$ and $CS_2$ solutions, 0.5-mm path length; (b) in vapor phase at 200°, 10-cm path length; (c) in argon matrix at 20°K (X: faulty spectrometer, P: associated pyrazole).

After the deposition is finished and the spectrum is recorded, the metering valve G is shut off, the heater on H is turned off, and a door on box H is opened. The glass tube F will cool faster than that of G because of the difference in heat capacity between the glass and the stainless steel. The excess sample is recondensed in F and removed from the system by opening the "O" ring seal E. Therefore, one can exchange sample without breaking the vacuum in the vacuum shroud. A heater on the tip of the heat exchanger is used to warm the cold window in a short time without upsetting the refrigerant in the main dewar; thus, the sample on the cold window can be evaporated with the matrix gas. Now the whole system is ready to isolate a new sample. The small amount of air trapped in the glass tube F will have a negligible effect on the matrix isolation. This rapid exchange of the samples is necessary for routine analysis. The total deposition time for all the spectra taken was 1 hr or less. The argon flow rate was about 13 mmol/hr. The amount of sample deposited on the window cannot be determined because the very small sample weight lost cannot be measured accurately. The flow rates of both matrix gas and the sample were controlled by needle valves and the mixing ratio was adjusted until the good monomeric spectrum was obtained. All the spectra observed in this study were recorded on either a Perkin-Elmer Model 225 spectrometer or on a Beckman Model IR-9 spectrometer.

*Pyrazole.* Pyrazole molecules have hydrogen bonds of moderate strength (mp 70°, bp 186°). Figure 2a is the infrared spectrum of pyrazole dissolved in $CCl_4$ and $CS_2$. The broad band in the region 3300–2800 $cm^{-1}$ indicates that the major portion of the molecules exist as dimers, trimers, or polymers in 1% $CCl_4$ solution.

Figure 2b is the infrared spectrum of pyrazole

vapor at 200°. Obviously, all molecules are unassociated at this temperature as indicated by the single N–H stretching absorption band at 3530 $cm^{-1}$. However, the overlapping of the broad bands in the lower frequency region, especially in the region 1600–1300 $cm^{-1}$, makes it very difficult to assign the spectrum.

Figure 2c is the infrared spectrum of unassociated pyrazole isolated in an Argon matrix at 20°K. The four sharp lines in the region 1300–1550 $cm^{-1}$, which are very diffuse in Figure 2b, result from ring vibrations.[6] The associated pyrazole bands are marked in the spectrum (Figure 2c).

The infrared spectrum of pyrazole in vapor phase has been assigned by Zecchina, *et al.*[6] Their assignment and the frequencies observed in the argon matrix in this work are listed in Table I. In the vapor phase, pyrazole has a complex band structure in the region 590 ~ 480 $cm^{-1}$. However, in the low-temperature matrix spectrum this region is considerably less complex, showing only a band at 548 $cm^{-1}$ with a shoulder at 540 $cm^{-1}$. In the vapor phase the complex band structure is assigned to the N–H out-of-plane bending vibration ($\gamma_{NH}$) and other hot bands. In the matrix spectrum, the 548/540 $cm^{-1}$ doublet is assigned to $\gamma_{NH}$ of pyrazole molecules which are trapped in slightly different matrix crystal sites, since the $\gamma_{NH}$ vibration is very sensitive to intermolecular interaction.

The in-plane N–H deformation ($\delta_{NH}$) of pyrazole is also expected to be sensitive to the environment. The 1125-$cm^{-1}$ band in the matrix spectrum has a relatively large half band width and is assigned to the $\delta_{NH}$ vibration. A similar type of band was observed in the matrix spectrum of imidazole at 1125 $cm^{-1}$ and is also assigned to the $\delta_{NH}$ vibration.

*Imidazole.* Imidazole is a strongly hydrogen-bonded compound (mp 90°, bp 256°) which is almost insoluble in $CCl_4$. In chloroform imidazole only partially dissociates into monomeric form. Figure 3b is the infrared spectrum of imidazole in the gas phase at 200°. The overlapping of the broad bands in this spectrum makes the spectrum analysis difficult even though the molecules exist in monomeric form at this temperature. Figure 3c is the infrared spectrum of the argon matrix isolated imidazole monomers at 20°K. The sample in glass tube F (Figure 1) was heated to 100°, and nozzle B was kept at 200°. The sharp absorption lines in the spectrum can be very easily recognized. (The lines marked with X are window background and grating changes.) Figure 3a is the infrared spectrum of the solid imidazole at −190°. The differences between the spectra (a) and (c) indicate the changes between associated and unassociated forms.

The complete assignment of the vibrational spectra of imidazole in the solid phase have been made by many authors,[7-9] but no complete agreement has been reached between those authors. The vapor-phase infrared spectrum of imidazole has also been assigned.[7,8] The observed frequencies of imidazole isolated in argon matrix and in the vapor phase are compared in Table I and no large difference between them was observed except the following. The in-plane N–H deformation ($\delta_{NH}$), which has not been assigned by Perchard, *et al.*,[8] is assigned to the band at 1125 $cm^{-1}$ in the matrix spectrum based on the discussion given in previous section for pyrazole. At least two sharp bands were observed at 551 and 538 $cm^{-1}$ in the matrix spectrum which we assign to $\gamma_{NH}$ split by different crystal sites. The 1412-

**Table I:** Observed Frequencies of Pyrazole and Imidazole

| | Assignment[e] | Pyrazole Matrix,[a] $cm^{-1}$ | Pyrazole Vapor,[b] $cm^{-1}$ | Imidazole Matrix,[a] $cm^{-1}$ | Imidazole Vapor,[c] $cm^{-1}$ |
|---|---|---|---|---|---|
| A′ | $\nu_{NH}$ | 3492 | 3541 | 3504 | 3518 |
| | $\nu_{CH}$ | | 3140 | | 3160 |
| | $\nu_{CH}$ | | 3074 | | 3135 |
| | $\nu_{CH}$ | | | | 3135 |
| | $\omega$ | 1538 | 1530 | 1518 | 1530 |
| | $\omega$ | 1448 | 1446 | 1480 | 1480 |
| | | | | 1412 | |
| | $\omega$ | 1392 | 1394 | 1404 | 1405 |
| | $\omega$ | 1346 | 1359 | 1325 | 1330 |
| | $\delta_{CH}$ | 1240 | 1253 | 1252 | 1260 |
| | $\delta_{NH}$ + $\omega$ | 1120 – 1130 | 1121 | 1120 ~ 1130 | 1127 |
| | $\delta_{CH}$ | 1032 | 1057 | 1074 | 1074 |
| | $\delta_{CH}$ | 1018 | 1021 | 1056 | 1055 |
| | $\Delta$ | 920 | 931 | 900 | 930[d] |
| | $\Delta$ | 905 | 910 | 892 | 890 |
| A″ | $\gamma_{CH}$ | 873 | 879 | 850 | 855[d] |
| | $\gamma_{CH}$ | 832 | 833 | 810 | 809 |
| | $\gamma_{CH}$ | 745 | 744 | 728 – 735 | 723 |
| | $\Gamma$ | 678 | 668 | 662 | 668 |
| | $\Gamma$ | 608 | 612 | 636 ~ 631 | 626 |
| | | | 536[a] | | |
| | | | 529 | | |
| | $\gamma_{NH}$ | 548 | 513 | 551 | 513 |
| | | 540 | 509 | 538 | |
| | | | 498 | | |
| | | | 488 | | |

[a] This work. [b] See ref 6. [c] See ref 8. Perchard, *et al.*, *J. Chim. Phys.*, **62**, 1344 (1965); **62**, 1334 (1965). [d] The assignment of 930 and 855 $cm^{-1}$ was reversed in ref 8. [e] A′: in-plane vibrations, $\nu$ = stretching, $\omega$ = ring stretching, $\delta$ = bending, $\Delta$ = ring bending; A″: out-of-plane vibrations, $\gamma$ = bending, $\Gamma$ = ring bending.

(6) A. Zecchina, L. Cerruti, S. Coluccia, and E. Borello, *J. Chem. Soc., B*, 1363 (1967).

(7) M. Milone and E. Borello, "Proceedings of the International Meeting Molecular Spectroscopy," Bologne Pergamon Press, Inc., Elmsford, N. Y., 1962, p 885.

(8) C. Perchard, A. Bellocq, and A. Novak, *J. Chim. Phys.*, **62**, 1344 (1965); **62**, 1334 (1965).

(9) M. Cordes, De, N. D., and J. L. Walter, *Spectrochim. Acta*, **24A**, 237 (1968).

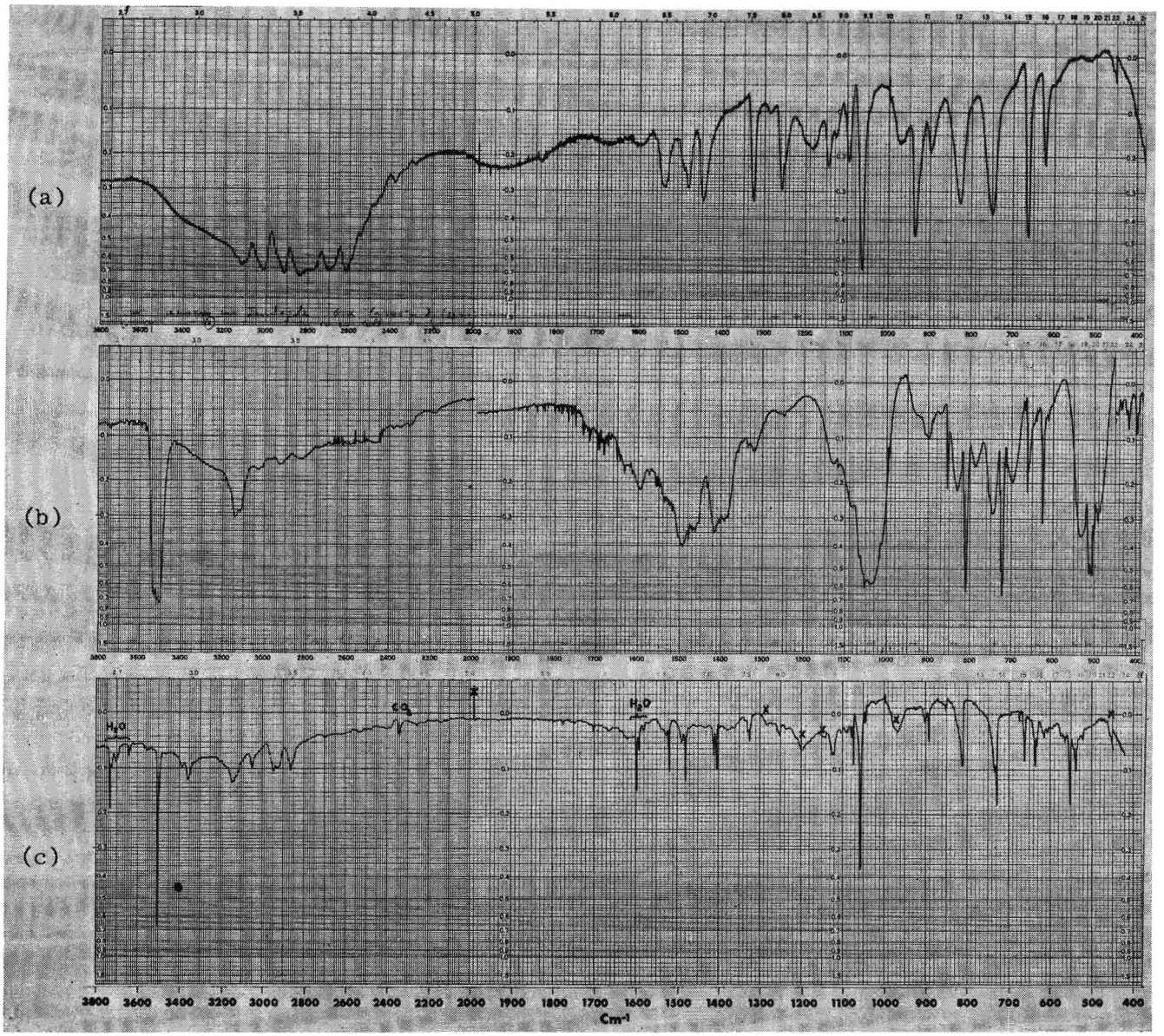


Figure 3. Infrared spectra of imidazole: (a) in solid phase at 80°K; (b) in vapor phase at 200°K; (c) in argon matrix at 20°K (X: grating changes (at 1990 and 450 $cm^{-1}$) and window background).

$cm^{-1}$ band in matrix spectrum is probably due to the combination vibration.

The pyrazole and imidazole molecules are similar in structure. Close resemblance between the infrared spectra of these two compounds was observed (Figures 2 and 3). Similar vibrational assignments have been made for pyrazole[6] and imidazole[8] (Table I) except that the 930 and 855-$cm^{-1}$ bands of imidazole in the vapor phase were assigned as $\gamma_{CH}$ (A″) and $\Delta$ (A′),[8] and in pyrazole,[6] the 931 and 879-$cm^{-1}$ bands in vapor phase were assigned as $\Delta$ (A′) and $\gamma_{CH}$ (A″), respectively. However, in our vapor phase spectrum of imidazole (Figure 3b), the 855-$cm^{-1}$ band is type C. Therefore, in imidazole, we assign the 855-$cm^{-1}$ band as $\gamma_{CH}$ (A″) and the 930 $cm^{-1}$ bands as $\Delta$ (A′). This reverse assignment for imidazole makes the data consistent with that of pyrazole.

*Dimethyl Phosphinic Acid.* Infrared spectrum of solid dimethyl phosphinic acid (Figure 4a) shows very broad bands in the region 3000–1500 $cm^{-1}$ which indicates the existing of strong intermolecular hydrogen bonding (mp 92°, bp 377°). Figure 4b is the infrared spectrum of dimethyl phosphonic acid isolated in argon matrix (sample temperature 120°, nozzle temperature 180°).

Obviously, the monomeric dimethyl phosphonic acid molecule has quite a different spectrum than that of the solid phase.

No vibrational assignment can be found in the literature for dimethyl phosphinic acid. The tentative assignment of the matrix spectrum given in Table II is obtained by comparison with vibrational frequencies of sodium dimethyl phosphinate.[10] The isolated dimethyl phosphinic acid molecule has 30 fundamental fre-

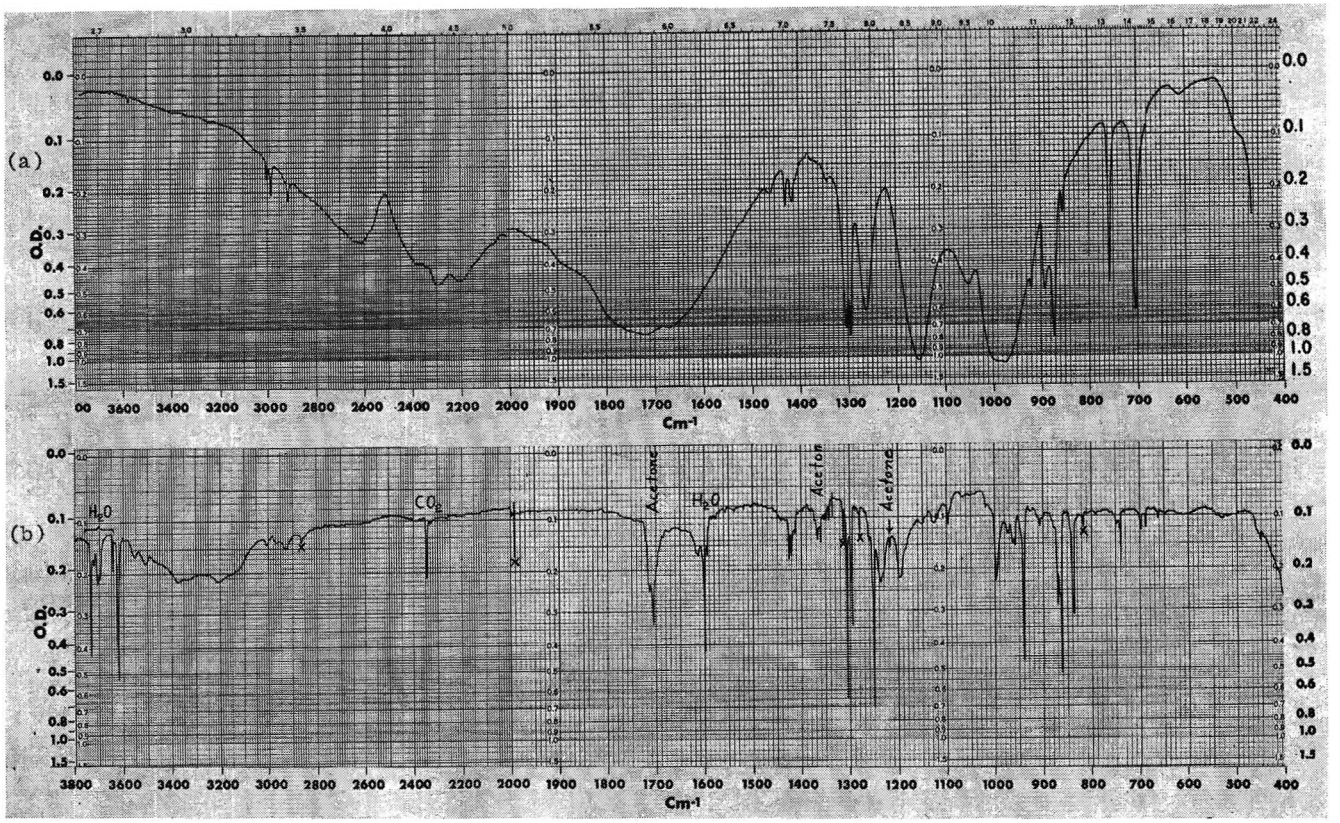


Figure 4. Infrared spectra of dimethyl phosphinic acid: (a) in fluorolube-nujol mulls; (b) in Argon matrix at 20°K (X: grating changes and other unidentified associated species).

**Table II:** Observed Frequencies of Dimethyl Phosphinic Acid

| Assignment | No. of fundamental | Obsd freq in matrix |
|---|---|---|
| $\nu_{OH}$ | 1 | 3620 |
| $\nu_{CH}$ | 6 | 2910 ~ 3010 |
| a-$\delta_{CH_3}$ | 4 | 1425, 1420, 1412 |
| s-$\delta_{CH_3}$ | 2 | 1305, 1295 |
| $\nu_{P=O}$ | 1 | 1250 |
| $\nu_{P-O}$ | 1 | 940 |
| $\rho_{CH_3}$ | 4 | 870, 862, 838, 835 |
| a-$\nu_{PC_2}$ | 1 | 740 |
| s-$\nu_{PC_2}$ | 1 | 698 |

quencies. They can be described as 18 methyl vibrations (6 stretching $\nu_{CH_3}$, 6 deformations $\delta_{DH_3}$, 4 rockings $\rho_{CH_3}$, and 2 torsions $\tau_{CH_3}$), 3 OH vibrations ($\nu_{OH}$, in-plane bending $\delta_{OH}$, and out-of-plane bending $\gamma_{OH}$), 4 skeletal stretching and 5 skeletal bending of the

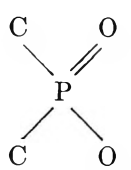


group. The frequencies of the methyl vibrations are relatively insensitive to the phase change (from solid phase to matrix isolated monomer), and most of them can be assigned by correlation (Table II). The characteristic $\nu_{OH}$ frequency is assigned to the 3620-cm$^{-1}$ band. The $\nu_{P=O}$ stretching vibration occurs at 1152 cm$^{-1}$ and the $\nu_{P-O}$ stretching vibration occurs at 985 cm$^{-1}$ in the solid phase respectively, shift, to 1250 and 940 cm$^{-1}$ in the matrix isolated phase. The large shift of the $\nu_{P=O}$ stretching vibration results from the hydrogen bonding in the solid phase. The antisymmetric and symmetric $\nu_{PC_2}$ stretching vibrations are assigned to 740 and 698-cm$^{-1}$ bands for the isolated molecules by correlation.

The in-plane OH bending ($\delta_{OH}$) vibration in the solid phase occurs at 1262 cm$^{-1}$. We would expect $\delta_{OH}$ to occur at lower frequency in the unassociated species. There are three relatively broad bands observed at 1236, 1196, and 998 cm$^{-1}$ in the matrix spectrum. One of these bands may be assigned to the $\delta_{OH}$ vibration because the $\delta_{OH}$ absorption may be broad due to the disorder effect in the matrix crystal. The other two of the three broad bands may be due to a-$\nu_{PO_2}$ and s-$\nu_{PO_2}$ absorption of the undisassociated molecules. The other unassigned bands, $\tau_{CH_3}$, $\gamma_{OH}$ and skeletal bending modes should have frequencies lower than the observed spectrum range.

(10) R. A. Nyquist, *J. Mol. Struct.*, **2**, 111 (1968).

# Nuclear Magnetic Resonance Coupling Constants to Tin in 3,3,3-Trifluoropropyltin Compounds

by Dwight E. Williams, Louis H. Toporcer, and Gary M. Ronk

*Dow Corning Corporation, Midland, Michigan 48640* *(Received January 7, 1970)*

The various nmr coupling constants between tin and hydrogen and fluorine have been determined from the heteronuclearly decoupled $^1H$ and $^{19}F$ nmr spectra of eleven 3,3,3-trifluoropropyltin compounds. These results are discussed in the light of Barfield's Alternate Molecular Orbital theory of spin coupling. The invalidity of the use of coupling constants to determine hydridization is briefly discussed. We conclude that for our data it is not necessary to invoke a "spatial mechanism" of spin coupling. The vicinal tin–hydrogen coupling constant was found to be larger than the geminal tin–hydrogen coupling constant in most instances despite reports that the opposite case is a characteristic of metal–alkyl compounds. Our data indicate that a postulated intramolecular interaction between tin and fluorine does not occur.

## I. Introduction

Recently the $^1H$ nmr spectra of organotin compounds have received great attention in the literature. The types of compounds studied have included methyltin hydrides, methyltin halides, ethyltin halides, and others.[1-6] Studies have particularly focused on the tin–hydrogen coupling constants. A peculiarity of tin–alkyl as well as of metal–alkyl compounds in general is that the vicinal metal–hydrogen coupling constant often exceeds the analogous geminal coupling constant.[1] The short-range coupling constants have been related empirically to heats of complex formation,[2] as well as to bond polarities[3] and Taft substituent constants,[4] and they have also been employed to determine tin hybridization and its variation with tin substituents.[5,6] The longer range coupling constants involving various nuclei in organometallic compounds have been used to probe the detailed geometry and conformation[7] of molecules as well as to investigate weak intermolecular interactions.[8]

We wish to report the various coupling constants we have obtained from the $^1H$ and $^{19}F$ nmr spectra of 11 3,3,3-trifluoropropyl ($PrF_3$) tin compounds. These compounds have three different types of coupling constants involving the tin nucleus (see Figure 1) and hence are especially rich in spin coupling information. We have discussed our data in the light of Barfield's alternate molecular orbital (AMO) theory of coupling constants[9] and its relevance to the question of a "spatial mechanism" of spin coupling.[10] The long-range tin–fluorine coupling constant is also of interest since we expect it would reflect a postulated donor–acceptor interaction between fluorine and tin (compounds such as trimethyltin fluoride form pentacoordinate tin chain polymers in the solid state[11]).

## II. Experimental Section

Both $^1H$ and $^{19}F$ nmr spectra were obtained at 28.5° with a Varian Associates HA-60IL spectrometer operated at 60.00 or 56.44 MHz in the frequency sweep locked mode. Heteronuclear spin decoupling at both frequencies was achieved with an Nmr Specialties Inc. SD-60B spin decoupler. Peak separations were measured by the difference between the lock and the sweep frequency. All of the tin compounds were synthesized at Dow Corning Corp., and were well characterized by standard analytical and spectroscopic techniques. The compounds were used as 50 vol % solutions in reagent grade benzene. This solvent was chosen to provide a noninterfering lock signal for the $^1H$ nmr spectra.

The heteronuclearly decoupled $^1H$ nmr spectra of the tin compounds were typical of the AA'BB' spin system. The 8% natural abundance of $^{117}Sn$ and the 9% natural abundance of $^{119}Sn$ produced two sets of tin satellites typical of the AA'BB'X spin system. An example of the resultant spectra is shown in Figure 2. The AA'BB' spectra were analyzed by the method of Pople, *et al.*,[12] and the derived parameters were subse-

(1) J. W. Emsley, J. Feeney, and L. H. Sutcliffe, "High Resolution Nuclear Magnetic Resonance Spectroscopy," Vol. 2, Pergamon Press, New York, N. Y., 1966.

(2) M. Borghini, *C. R. H. Acad. Sci., Ser. B*, **B262**, 337 (1966).

(3) L. Verdonck, G. P. Vanderkelen, and Z. Eeckhaut, *J. Organometal. Chem.*, **11**, 487 (1968).

(4) M. L. Maddox, N. Flitcroft, and H. D. Kaesz, *ibid.*, **4**, 50 (1965).

(5) E. V. VanDenBerghe and G. P. VanDerKelen, *ibid.*, **6**, 515 (1966).

(6) H. D. Kaesz and N. Flitcroft, *J. Amer. Chem. Soc.*, **85**, 1377 (1963).

(7) M. M. Kreevoy and J. F. Schaefer, *J. Organometal. Chem.*, **6**, 589 (1966).

(8) E. F. Kiefer, W. L. Waters, and D. A. Carlson, *J. Amer. Chem. Soc.*, **90**, 5127 (1968).

(9) M. Barfield, *J. Chem. Phys.*, **44**, 1836 (1966).

(10) L. Petrakis and C. H. Sederholm, *ibid.*, **35**, 1243 (1961).

(11) H. C. Clark, R. J. O'Brien, and J. Trotter, *J. Chem. Soc.*, 2332 (1964).

(12) J. A. Pople, W. G. Schneider, and H. J. Bernstein, "High-Resolution Nuclear Magnetic Resonance," McGraw-Hill Publications, New York, N. Y., 1959.

**Table I:** Nmr Parameters for 3,3,3-Trifluoropropyltin Compounds[a]

| Compound | $^2J_{H_a{}^{119}Sn}$ | $^2J_{H_b{}^{119}Sn}$ | $^4J_{F^{119}Sn}$ | $^3J_{HH}$ | $^3J_{H_bF}$ | $\tau_{H_a}$ | $\tau_{H_b}$ | $\phi_F$ |
|---|---|---|---|---|---|---|---|---|
| $(PrF_3)_4Sn$ | +55.0 | −48.4 | ~0 | 8.7 | 10.6 | 9.23 | 8.07 | 69.6 |
| $(PrF_3)_3SnMe$ | +55.4 | −43.8 | ~0 | 8.7 | 10.3 | 9.22 | 8.02 | 69.3 |
| $(PrF_3)_2SnMe_2$ | +54.0 | −42.1 | ~0 | 8.9 | 10.3 | 9.25 | 8.02 | 69.4 |
| $PrF_3SnMe_3$ | +54.0 | −41.3 | ~0 | 8.9 | 10.4 | 9.21 | 7.98 | 69.5 |
| $(PrF_3)_3SnPh$ | +57.2 | −43.8 | 1.9 | 8.8 | 10.1 | 9.01 | 8.00 | 68.9 |
| $(PrF_3)_2SnPh_2$ | +56.6 | −39.9 | 1.5 | 9.0 | 10.3 | 8.82 | 7.97 | 69.1 |
| $PrF_3SnPh_3$ | +57.5 | −36.1 | ~0 | 9.0 | 10.2 | 8.56 | 7.81 | 69.4 |
| $(PrF_3)_3SnOMe$ | +59.4 | −57.0 | 2.8 | 8.7 | 10.5 | 9.00 | 7.89 | 70.0 |
| | (59.4) | (57.1) | | | | | | |
| $(PrF_3)_3SnCl$ | +56.9 | −66.6 | 4.0 | 8.5 | 10.1 | 8.88 | 7.87 | 69.1 |
| | (57.5) | (66.3) | | | | | | |
| $(PrF_3)_2SnCl_2$ | +65.5 | −107.1 | 5.0 | 8.0 | 9.9 | 8.48 | 7.77 | 68.4 |
| | (65.9) | (107.1) | | | | | | |
| $PrF_3SnCl_3$ | +93.6 | −180.2 | 2.3 | 7.5 | 9.7 | 8.48 | 8.00 | 67.5 |
| | (93.7) | (180.7) | | | | | | |

[a] $J$ values are given in Hz; $\tau$ and $\phi$ are given in ppm referred to TMS and $CFCl_3$. $PrF_3 \equiv CF_3CH_2CH_2$; $Me \equiv CH_3$; $Ph \equiv C_6H_5$. Error limits are given in the experimental section. $H_a$ is the proton geminal to tin while $H_b$ is the vicinal proton.

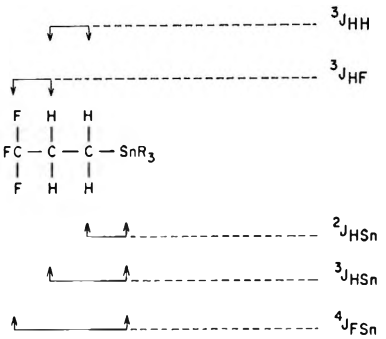


Figure 1. Schematic of $PrF_3SnR_3$ coupling constants.

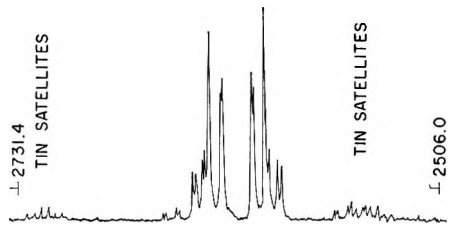


Figure 2. Heterodecoupled $^1H$ nmr spectrum of $PrF_3SnCl_3$. The center of the principal peaks is 328.4 Hz upfield from benzene.

quently used to complete the analysis of the AA'BB'X spectra by the effective chemical shift method.[13] A short computer program was written to perform the analysis. Portions of the BB' section of the spectra were too broadened by residual coupling to the fluorine to be used in the AA'BB' analysis. Similarly, the inner tin satellites were not used in the AA'BB'X analysis because of considerable broadening due to peak overlap and smaller effective chemical shift. However, there was still sufficient data redundancy for us to estimate maximum errors to be as follows: for $^2J_{HSn}$ and $^3J_{HSn}$, ±1.0 Hz (±0.5 when both sets of satellites, $^{117}Sn$ and $^{119}Sn$, were resolved); for $^4J_{FSn}$, $^3J_{HH}$, and $^3J_{HF}$, ±0.2 Hz; for $\tau$, ±0.005 ppm; for $\phi$, ±0.05 ppm. The absolute errors for $\tau$ and $\phi$ are somewhat larger than these estimates since the benzene-locking signal was used as a secondary reference for the $\tau$ values and an external capillary of $(CF_2Br)_2$ was similarly used for the $\phi$ values.

The heteronuclearly decoupled $^{19}F$ nmr spectra of these compounds showed a single sharp peak. In those compounds in which the tin–fluorine coupling constant is appreciable, an additional satellite peak is present on each side of the main peak.

## III. Results

Coupling constants and chemical shifts have been obtained for 11 trifluoropropyltin compounds and are given in Table I. The nomenclature of the coupling constants can be understood by reference to Figure 1. $J$ and $J'$ were not determined separately but rather their average value ($^3J_{HH}$) was given.[1] The values of $^2J_{H^{119}Sn}$ and $^3J_{H^{119}Sn}$ in parentheses in Table I were not experimentally determined but rather were computed from the measured $^{117}Sn$ coupling constants and the magnetogyric ratios of $^{117}Sn$ and $^{119}Sn$. The good agreement between the two sets of values demonstrates that the above error limits are pessimistic. When the parenthetical value is not given, only a single set of peaks was resolved and the $^{119}Sn$ coupling constants were calculated by assuming that the values computed from the single set of satellite peaks are equal to $(J_{^{117}Sn} + J_{^{119}Sn})/2$. The signs of $^2J_{H^{119}Sn}$ and $^3J_{H^{119}Sn}$ were assigned on the basis of analogy to similar compounds,[14] since our spectra demonstrated only that two coupling constants have opposite signs.

(13) J. A. Pople and T. Schaefer, *Mol. Phys.*, 3, 547 (1961).
(14) W. MacFarlane, *J. Chem. Soc. A*, 528 (1967).

## IV. Discussion

First we would like to discuss Barfield's theory of spin coupling[9] since it provides a useful framework within which to consider our results. After several approximations this theory predicts that the one-, two-, and three-bond coupling constants will be as follows

$$^1J_{NN'} = K[1/(1 + S)^2]$$

$$^2J_{NN'} = K[-(1 - \lambda^2)/(S(1 - S^2))]$$

$$^3J_{NN'} = K[\lambda^2 P^2_{NN'}/(1 - S^2)]$$

$$K = C\phi^2_N(0)\phi^2_{N'}(0)/\Delta E$$

In the above equation, $C$ is a known constant proportional to the magnetogyric ratios of the coupled nuclei, N and N′; $S$ and $P_{NN'}$ are the overlap integral and the bond order between s orbitals centered on the two coupled nuclei; the s-electron densities at these nuclei are $\phi^2_N(0)$ and $\phi^2_{N'}(0)$. Although the average excitation energy, $\Delta E$, can only be estimated, all other variables in these equations can be calculated by use of the variational principle including the AMO parameter, $\lambda^2$, which cannot exceed 1. However, these formulas shall be used only to provide a qualitative basis for discussion. Other formulations of the calculation of the spin coupling constant are better suited for quantitative work but not for qualitative discussion.[15]

A strong point of the AMO theory is that the signs of coupling constants of protons with other nuclei are correctly predicted. The main theoretical objection to the theory is that it is based upon a single determinant—average excitation energy approximation.[15] However, it does provide long-range spin correlation.[9] A practical objection to this theory may be that it does not permit one to use coupling constants to obtain hydridizations. However, we shall see that this "fault" corresponds to the facts. Major discrepancies occur when the AMO theory is applied to fluorine coupling constants and the approximations of the theory should be poorly suited for this case, particularly since the 2s electrons of fluorine are thought to be only weakly involved in bonding. The most satisfactory quantitative theory of spin coupling also encounters difficulties with fluorine coupling constants.[15]

Barfield's AMO theory of spin coupling is based upon the Fermi contact term in the magnetic Hamiltonian. However, it has often been supposed that a "spatial mechanism" is important in transmitting spin coupling.[10] That is, in addition to the Fermi contact term for which the s orbitals are crucial, the electron orbital and magnetic dipole terms directly involving the p orbitals may be important.[12] This mechanism was postulated to explain the fact that fluorine–fluorine[16] and fluorine–hydrogen[17] coupling constants often depend more strongly on spatial rather than on bond separation. In addition, the nonlinear relation[18] between $^2J_{H^{119}Sn}$ and $^3J_{H^{119}Sn}$ as well as the nonzero intercept in the linear relation[14] between $^1J_{^{13}C^{119}Sn}$ and $^2J_{H^{119}Sn}$ have been attributed to a "spatial mechanism."

We have observed a nonlinear relation between $^2J_{H^{119}Sn}$ and $^3J_{H^{119}Sn}$ (see Table I). In fact, the magnitudes of the two coupling constants sometimes vary in opposite directions. $^3J_{HH}$ changes little, which indicates that conformational changes which would affect $P^2_{NN'}$ are not responsible for the nonlinearity. Similar results have been observed in ethyltin derivatives in which *gauche–trans* conformational changes are not possible.[18] However, a consideration of the above AMO equations indicates that this feature of metal–hydrogen coupling constants does not require a "spatial mechanism" of spin coupling. For instance, not only may $P^2_{NN'}$ depend on other factors in addition to molecular geometry, but also both $\lambda^2$ and $\phi^2_N(0)$ as well as $\Delta E$ may be simultaneously changing, in which case $^2J$ and $^3J$ would not be linearly related even though the Fermi contact term was dominant.

Since we had originally planned to use the $^2J_{H^{119}Sn}$ values to measure the tin atom hybridization, we would like to discuss briefly why, as the above formulas indicate, this procedure should no longer be considered valid. Although coupling constants have been extensively used to measure the hybridization of coupled nuclei,[6,19] it has become increasingly clear recently that any correlation between these two quantities is coincidental. The most convincing demonstration of this for tin coupling constants was provided by MacFarlane,[14] who showed that although $^1J_{^{119}Sn^{13}C}$ and $^2J_{^{119}SnH}$ were linearly related, the correlation has a nonzero intercept in compounds of the type $(CH_3)_{4-a}SnX_a$. Several other studies of tin compounds support this contention.[3,18] In addition, theoretical studies of $^1J_{^{13}CH}$ have shown that other factors such as the effective nuclear charge[20] and the average excitation energy[21] have a more important effect on the change in coupling constant than hybridization. Recent coupling constant calculations by Pople, *et al.*,[22] on $CH_3F$ and $CH_2F_2$ when compared with experimental bond angles may be interpreted to mean that even in the absence of effective nuclear charge changes the coupling constant does not reflect the hybridization. Finally, bond angle determinations[23] and valence bond wave-

(15) J. A. Pople, J. W. McIver, Jr., and N. S. Ostlund, *J. Chem. Phys.*, **49**, 2965 (1968).

(16) S. Ng and C. H. Sederholm, *ibid.*, **40**, 2090 (1964).

(17) J. P. N. Brewer, R. Hearey, and B. A. Maples, *Chem. Commun.*, (1), 27 (1967).

(18) J. Lorberth and H. Vahrenkamp, *J. Organometal. Chem.*, 11, 111 (1968).

(19) J. N. Schoolery, *J. Chem. Phys.*, **31**, 1427 (1959).

(20) D. M. Grant and W. M. Lichtman, *J. Amer. Chem. Soc.*, **87**, 3994 (1965).

(21) N. Cyr and T. J. R. Cyr, *J. Chem. Phys.*, **47**, 3082 (1967).

(22) J. A. Pople, private communication, 1969.

(23) C. Juan and H. S. Gutowsky, *ibid.*, **37**, 2198 (1962).

function calculations[24] indicate that although the direction of the change in hybridization is correctly predicted by use of the coupling constant in many instances, the actual magnitude of the change is far smaller.

It has been said that a characteristic of metal–alkyl compounds is that the vicinal is larger than the geminal metal–hydrogen coupling constant.[1] This behavior has been observed in $^{199}$Hg, $^{207}$Tl, $^{119}$Sn, $^{29}$Si, and $^{13}$C compounds.[1] As can be seen in Table I, this is not what we have observed. The converse holds for the majority of our compounds. What we have observed is that $^3J_{H^{119}Sn}$ is much more sensitive to substituent effects than $^2J_{H^{119}Sn}$, and that $^3J_{H^{119}Sn}$ may be either smaller or in a few cases substantially larger than $^2J_{H^{119}Sn}$. Since according to the AMO equations $^3J_{NN'}$ depends upon one more variable than $^2J_{NN'}$, namely the bond order, this increased sensitivity is not unexpected. Several other theories of spin coupling have assumed that the bond order depends only upon the molecular geometry,[25,26] but this seems to be a dubious assumption to us.

The nmr data are relevant to the possibility that a fluorine atom complexes the tin to form a pentacoordinate tin chelate structure in these compounds. This type of intramolecular interaction occurs in certain organosilicon compounds in which a nitrogen atom is the coordinating ligand[27,28] and should be even more likely to occur for tin compounds since tin has a greater tendency to form extracoordinate species. Intermolecular interactions of this type are common for tin compounds; for example, trimethyltin fluoride[11] as well as cyanide,[29] forms pentacoordinate tin chain polymers in the solid state while distannoxane compounds exist as pentacoordinate tin dimers in both the solid state and in solution.[30]

Intermolecular interactions of this type do not occur for the trifluoropropyltin compounds in benzene solution except for the methoxy derivative which exists as a dimer.[31] In this case the coordinating ligand is probably the methoxy group rather than fluorine. Cryoscopic and osmometric molecular weight determinations have shown that the chloride derivatives are only weakly self-associated in benzene solution.[31] However, intramolecular interactions may well occur, as mass spectral data have indicated for the gas phase cations of these compounds.[32] However, the Mössbauer spectra of the alkyl derivatives show no measurable quadrupole splitting,[33] indicating that in those compounds which lack electronegative tin ligands the interaction does not occur. Unfortunately, the Mössbauer spectra of those compounds in which tin has electronegative ligands will display quadrupole splitting regardless of the tin coordination and these are the compounds in which fluorine should interact most strongly with tin due to d orbital contraction.[34]

If the intramolecular interaction occurs in the chloride derivatives, it is weak enough so that rapid exchange occurs between complexed and uncomplexed fluorine since we observed no multiplicity in the heteronuclearly decoupled $^{19}$F nmr spectra beyond that due to the $^{117,119}$Sn satellites. On the other hand, if the intramolecular complex forms, the tin-fluorine coupling constant should be large even if "intramolecular exchange" were rapid. We do observe an increase in $^4J_{F^{119}Sn}$ in the chloro derivatives. However, their magnitude and the fact that the methoxy and phenyl compounds also show a comparable increase still does not encourage belief in this interaction. Furthermore, the coupling constant has a maximum value at the dichloride whereas both statistical and ligand contraction of *d* orbital arguments predict a maximum at the trichloride. Hence both Mössbauer and nmr spectra of these compounds indicate that the postulated intramolecular interaction is not important in these compounds.

(24) V. S. Watts and J. H. Goldstein, *Theor. Chim. Acta*, **7**, 181 (1967).

(25) M. Karplus, *J. Chem. Phys.*, **30**, 11 (1959).

(26) H. Conroy, "Advances in Organic Chemistry," Vol. II, Interscience, New York, N. Y., 1960.

(27) F. P. Boer, J. W. Turley, and J. J. Flynn, *J. Amer. Chem. Soc.*, **90**, 5102 (1968).

(28) C. L. Frye, G. A. Vincent, and G. L. Hauschildt, *ibid.*, **88**, 2727 (1966).

(29) E. O. Schlemper and D. Britton, *Inorg. Chem.*, **5**, 507 (1966).

(30) W. J. Considine, G. A. Baum, and R. C. Jones, *J. Organometal. Chem.*, **3**, 308 (1965).

(31) D. E. Williams and L. H. Toporcer, unpublished observations.

(32) R. S. Gohlke, private communication, 1968.

(33) D. E. Williams and C. W. Kocher, *J. Chem. Phys.*, **52**, 1480 (1970).

(34) C. A. Coulson and F. A. Gianturco, *J. Chem. Soc., A*, 1618 (1968).

# The Kerr Constants of Aqueous Solutions of Glycine Peptides[1]

by W. H. Orttung and J. M. Orttung[2]

*Department of Chemistry, University of California, Riverside, California 92502* *(Received November 6, 1969)*

The Kerr constants, refractive indices, and densities of aqueous solutions of di-, tri-, and tetraglycine were measured at 25° over a range of concentrations. The optical data were determined at 436, 546, and 578 mμ. Dielectric increments for fully extended conformations were predicted using Scholte's ellipsoidal model theory. Comparison with the available data suggested that coiled conformations are important for peptides longer than diglycine. The shape and C-terminal carboxyl contributions to the optical anisotropy of diglycine were large enough to explain most of the observed Kerr constant increment, so that the intrinsic anisotropy of the peptide unit could not be deduced. The linear dependence on the number of residues observed for both the dielectric and Kerr constant increments suggested that the optical anisotropy of the peptide is approximately independent of $n$ for $n$ = 2–4.

## Introduction

The investigations described in this paper are part of a continuing effort to understand the optical anisotropy and dielectric parameters of small molecules of biological interest. In earlier studies of the aqueous solution Kerr constants and crystal refractive indices of a series of amino acids,[3,4] the form and intrinsic contributions to the optical anisotropy were estimated from the data. The crystal and solution results were self-consistent with regard to intrinsic birefringence and suggested that the ellipsoidal model estimate of the form effect in the solution environment may have been too large. The latter observation has also been reported in studies of helical polypeptides and elongated proteins.[5,6] A study of the glycine peptides is a logical extension of the amino acid investigations. Additional factors in the peptide systems are the dipole moment and optical anisotropy of the peptide unit and internal rotations between adjacent peptides and the terminal charged groups.

The dielectric properties of simple peptides have been the subject of many investigations. Eyring[7] obtained a general expression for the dipole moment of complex molecules in terms of bond (or rigid unit) contributions, and gave an explicit expression in terms of bond angles for the case of free rotation. Kuhn[8] calculated the dipole moment due to the charged ends of a flexible zwitterion polymer, taking into account attraction between the charged ends and a distance of minimum approach. Proportionality between the mean-square dipole moment and the number of polymerized units, $n$, was predicted for large values of $n$. Experimental investigations of the dielectric increments of glycine peptides[9] showed a nearly linear relationship for $n$ varying from 1 to 6. More recently, Beacham, *et al.*,[10] have studied the dielectric increments of all of the diastereoisomeric di-, tri-, and tetrapeptides of either alanine or serine. The all-L peptide had the largest dielectric increment in each case, suggesting a preference for extended conformations.

Kurland and Wilson[11] measured the magnitude and orientation of the dipole moment of formamide in the vapor phase. Brant and Flory[12] showed that dipolar interactions between neighboring peptides have an important stabilizing effect on extended conformations of nonhelical polypeptide chains. Flory and Schimmel[13] carried out detailed calculations of the mean-square dipole moments of short glycine peptides, obtaining excellent agreement with the data. Holzwarth and Backman[14] have recently included dipole–dipole electrostatic interactions in calculations on the stabilities of polyproline conformations I and II. These authors also discussed destabilizing electrostatic end effects in $\alpha$-helical conformations. Chains with fewer than seven residues have not been observed to form $\alpha$ helices.[15]

Earlier studies related to the Kerr effect of simple peptides fall into two main categories. The first in-

(1) Experimental aspects of this work were carried out in the Department of Chemistry at Stanford University and were supported in part by Grant No. G15555 from the National Science Foundation and by an institutional research grant of the American Cancer Society. Other aspects of the investigation were supported by Public Health Service Research Grant GM11683 from the Division of General Medical Sciences.

(2) Supported in part by Public Health Service Fellowship GPM-18,279 from the Division of General Medical Sciences.

(3) W. H. Orttung and J. A. Meyers, *J. Phys. Chem.*, **67**, 1911 (1963).

(4) W. H. Orttung and R. W. Armour, *ibid.*, **71**, 2846 (1967).

(5) J. Y. Cassim and E. W. Taylor, *Biophys. J.*, **5**, 531 (1965).

(6) P. J. Oriel and J. A. Schellman, *Biopolymers*, **4**, 469 (1966).

(7) H. Eyring, *Phys. Rev.*, **39**, 746 (1932).

(8) W. Kuhn, *Z. Phys. Chem.*, **A175**, 1 (1935).

(9) (a) J. Wyman, Jr., and T. L. McMeekin, *J. Amer. Chem. Soc.*, **55**, 908 (1933); (b) W. P. Connor, R. P. Clarke, and C. P. Smyth, *ibid.*, **64**, 1379 (1942).

(10) J. Beacham, V. T. Ivanov, G. W. Kenner, and R. C. Sheppard, *Chem. Commun.*, 386 (1965).

(11) R. J. Kurland and E. B. Wilson, Jr., *J. Chem. Phys.*, **27**, 585 (1957).

(12) D. A. Brant and P. J. Flory, *J. Amer. Chem. Soc.*, **87**, 2791 (1965).

(13) P. J. Flory and P. R. Schimmel, *ibid.*, **89**, 6807 (1967).

(14) G. Holzwarth and K. Backman, *Biopolymers*, **8**, 883 (1969).

(15) M. Goodman and I. Rosen, *ibid.*, **2**, 537 (1964).

cludes efforts to understand the Kerr effect of polymers, and the second deals with the optical properties of the peptide group. Theoretical studies of the Kerr effect of polymers[16-20] have the common feature of assuming additivity of bond or group polarizability tensors. Experimental studies[21] and general theoretical considerations[22] suggest that this assumption is of doubtful validity.

Aroney, Le Fevre, and Singh[23] measured the dielectric increments and Kerr constants of a series of amides in dioxane solution, and McMeekin, Groves, and Hipp[24] obtained the molar refractions for a series of simple peptides in aqueous solution. Pertinent spectroscopic investigations include vacuum ultraviolet absorption studies,[25,26] ultraviolet dichroism measurements,[27,28] and studies of the effect of polypeptide conformations on the far-ultraviolet absorption spectrum and its polarization.[29-31] Schellman and Nielsen[32] have recently considered the theory of amide spectra, and Takashima[33] has used molecular orbital theory to calculate the $\pi$-electron contribution to the peptide group optical anisotropy.

## Experimental Section

*Apparatus and Methods.* The density, refractive index, and Kerr effect apparatus and methods have been described previously.[34,35]

*Materials.* Chromatographically homogeneous samples of Mann Research Laboratories di-, tri-, and tetraglycine and California Corp. for Chemical Research diglycine were used. A sample of tetraglycine was also obtained from Nutritional Biochemicals Corp. The Mann and Calbiochem di- and triglycine were recrystallized twice from warm water and methanol. The Mann tetraglycine was used directly, and the Nutritional tetraglycine was recrystallized four times from warm water and methanol.

The resistances of the solutions at 1000 cps were measured in the Kerr cell and the specific conductivity, $\kappa$, was calculated from the relation $\kappa = d/AR = (25 \times 10^{-3})/R$, where $A$ and $d$ are the area and separation of the electrodes, and $R$ is the resistance of the solution. Values obtained for the increments $10^6(\kappa - \kappa_0)/m$, where $m$ is the molality, were 170, 440, and 1800 for di-, tri-, and tetraglycine, respectively. Comparable values reported by Wyman and McMeekin[9a] were 5200, 2900, and 70,000, respectively.

The solubility of both tetraglycine samples appeared to be 0.030–0.035 mol/l., in contrast with values of 0.06 mol/l. reported in the dielectric constant investigations[9] and 0.05 mol/l. used in titration studies.[36] A slight residue was observed in the Mann tetraglycine solutions, but the results for both samples were in agreement and were proportional to concentration, within experimental error.

## Results

*Densities.* The data are shown in Table I. The molar concentrations, $c$, and the apparent molal volumes of the solutes, $\phi_v$, were calculated in the usual way,[37]

**Table I:** Density Data at 25°

| $m$ | $c$ | $d$, g/ml | $10^5\Delta$ | $\phi_v$, ml/mol |
|---|---|---|---|---|
| | | Diglycine | | |
| 0.0 | 0.0 | 0.99707 | | |
| 0.09764 | 0.09663 | 1.00247 | +0.4 | 76.46 |
| 0.19666 | 0.19318 | 1.00781 | −0.3 | 76.72 |
| 0.30252 | 0.29479 | 1.01340 | −0.9 | 76.95 |
| 0.40775 | 0.39419 | 1.01883 | +0.3 | 77.14 |
| | | Triglycine | | |
| 0.04973 | 0.04931 | 1.00088 | +0.4 | 112.19 |
| 0.09924 | 0.09786 | 1.00460 | −0.4 | 112.50 |
| 0.14982 | 0.14691 | 1.00835 | −0.6 | 112.70 |
| 0.20066 | 0.19566 | 1.01208 | +1.0 | 112.81 |
| | | Tetraglycine | | |
| 0.00664 | 0.00661 | 0.99769 | −0.7 | 152 |
| 0.00770 | 0.00766 | 0.99780 | −0.2 | 151 |
| 0.00894 | 0.00890 | 0.99793 | +1.2 | 150 |
| 0.00996 | 0.00991 | 0.99802 | 0.0 | 151 |

(16) H. A. Stuart and A. Peterlin, *J. Polymer Sci.*, **5**, 551 (1950).

(17) R. P. Smith and E. M. Mortensen, *J. Chem. Phys.*, **35**, 714 (1961).

(18) D. A. Dows, *ibid.*, **41**, 2656 (1964).

(19) K. Nagai and T. Ishikawa, *ibid.*, **43**, 4508 (1965).

(20) P. J. Flory and R. L. Jernigan, *ibid.*, **48**, 3823 (1968).

(21) J. Powers, D. A. Keedy, and R. S. Stein, *ibid.*, **35**, 376 (1961); R. L. Rowell and R. S. Stein, *ibid.*, **47**, 2985 (1967).

(22) K. S. Pitzer, *Advan. Chem. Phys.*, **2**, 59 (1959).

(23) M. J. Aroney, R. J. W. Le Fevre, and A. N. Singh, *J. Chem. Soc.*, 3179 (1965).

(24) T. L. McMeekin, M. L. Groves, and N. J. Hipp, Advances in Chemistry Series, No. 44, American Chemical Society, Washington, D. C., 1964, p 54.

(25) H. D. Hunt and W. T. Simpson, *J. Amer. Chem. Soc.*, **75**, 4540 (1953).

(26) J. W. Preiss and R. Setlow, *J. Chem. Phys.*, **25**, 138 (1956).

(27) J. C. Ward, *Proc. Roy. Soc.*, **A228**, 205 (1955).

(28) D. L. Peterson and W. T. Simpson, *J. Amer. Chem. Soc.*, **79**, 2375 (1957).

(29) K. Rosenheck and P. Doty, *Proc. Natl. Acad. Sci. U. S.*, **47**, 1775 (1961).

(30) W. B. Gratzer, G. M. Holzwarth, and P. Doty, *ibid.*, **47**, 1785 (1961).

(31) I. Tinoco, Jr., A. Halpern, and W. T. Simpson in "Polyamino Acids, Polypeptides, and Proteins," M. A. Stahmann, Ed., The University of Wisconsin Press, Madison, Wis., 1962, p 147.

(32) J. A. Schellman and E. B. Nielsen, *J. Phys. Chem.*, **71**, 3914 (1967).

(33) S. Takashima, Abstracts, 158th National Meeting of the American Chemical Society, New York, N. Y., Sept 1969, No. BIOL 174.

(34) W. H. Orttung, *J. Phys. Chem.*, **67**, 1102 (1963).

(35) W. H. Orttung and J. A. Meyers, *ibid.*, **67**, 1905 (1963).

(36) S. Glasstone and E. F. Hammel, *J. Amer. Chem. Soc.*, **63**, 243 (1941).

(37) H. S. Harned and B. B. Owen, "The Physical Chemistry of Electrolytic Solutions," 3rd ed, Reinhold Publishing Corp., New York, N. Y., 1958.

using $d_0 = 0.997064$ and $M_2 = 132.119$, 189.171, and 246.223 for di-, tri-, and tetraglycine, respectively. The data were fitted by the expressions

$$d = 0.05587m - 0.00616m^2 + \Delta \quad (1)$$

$$d = 0.07718m - 0.0122m^2 + \Delta \quad (2)$$

$$d = 0.095m + \Delta \quad (3)$$

The deviations, $\Delta$, are shown in Table I. Densities calculated from eq 1–3 for the concentrations reported in the dielectric studies[9a] agree within experimental error. Martin, *et al.*,[38] reported a partial specific volume of 0.5907 ± 0.0015 ml/g for tetraglycine, corresponding to a partial molal volume of 145.4 ± 0.3 ml.

*Refractive Indices.* The data are shown in Table II

**Table II:** Refractive Index Data at 25°

| $m$ | $10^6\Delta n$ 436 mμ | 546 mμ | 578 mμ |
|---|---|---|---|
| | Diglycine | | |
| 0.09479 | 2443 | 2377 | 2360 |
| 0.14231 | 3644 | 3546 | 3522 |
| 0.18631 | 4758 | 4627 | 4600 |
| 0.25063 | 6352 | 6177 | 6141 |
| 0.28057 | 7094 | 6900 | 6850 |
| | Triglycine | | |
| 0.05025 | 1845 | 1788 | 1778 |
| 0.07460 | 2725 | 2647 | 2630 |
| 0.09937 | 3618 | 3512 | 3491 |
| 0.12355 | 4483 | 4349 | 4325 |
| 0.15122 | 5470 | 5308 | 5275 |
| | Tetraglycine | | |
| 0.00573 | 267 | 264 | 258 |
| 0.00844 | 404 | 388 | 382 |
| 0.00999 | 461 | 447 | 444 |
| 0.01201 | 565 | 546 | 543 |
| 0.01260 | 580 | 564 | 563 |

and were fitted to expressions of the form

$$10^6\Delta n = am + bm^2 \quad (4)$$

Values of $a$ and $b$ are shown in Table III. The precision of the data was consistent with the limiting precision of the refractometer ($\pm 3 \times 10^{-6}$ in $\Delta n$).

The Lorenz–Lorentz polarizability, $\alpha_2$, was calculated for each point and plotted *vs.* $m$, following the procedure used for the amino acid data.[3,34] The values shown in Table IV were obtained by extrapolation to $m = 0$ for di- and triglycine and by averaging over all concentrations for tetraglycine. The dispersion parameters, $f$ and $\lambda_0$, are also shown, the results for tetraglycine being only rough estimates. The values for glycine[34] are also shown for comparison. McMeekin, Groves, and Hipp[24] reported molar refractions of 29.89 and 41.33 ml for di- and triglycine at 25° and 589 mμ. Multiplication of the corresponding values from Table IV (at 578 mμ) by $4\pi N_A/3$ gives 29.84 and 43.10 ml, respectively, in satisfactory agreement with McMeekin, *et al.* It is interesting to note that $3f$ is slightly smaller than the number of outer-shell electrons in di-, tri-, and tetraglycine, while for alanine and α-aminoisobutyric acid,[3] $3f$ was slightly larger than the number of outer-shell electrons.

*Kerr Constants.* The data for $B = \Delta n/\lambda E^2$ are shown in Table V. The average molal increments and average deviations are shown in Table VI along with the earlier results for glycine.[3]

## Calculations

*Dipole Moments.* In an earlier analysis of the dielectric increments of amino acid solutions,[3] vacuum dipole moments were extracted from the data using Scholte's ellipsoidal model theory. The results were compared with the charge separation dipoles and the discrepancy was attributed to bond dipoles. In the case of peptides, the need to consider conformational flexibility makes the same approach to the problem unattractive because it would be difficult to make a rational selection of shape parameters. As an alternative approach, we have carried out the calculation in reverse by assuming fully extended *trans*-peptide conformations and estimating shape parameters, charge separation, bond dipoles, etc. to obtain predicted dielectric increments for comparison with experimental values.

The geometrical parameters chosen for planar *trans*-diglycine are shown in Figure 1. These values are based on the X-ray structure of Hughes and Moore,[39] Pauling's dimensions for the planar amide group,[40] the C–O distance in formate ion,[41] and the $-NH_3^+$ geometry from the nmr experiments of Webb and Moulton.[42] The molecular shape predicted by adding Stuart radii to the diglycine skeleton is shown in Figure 2. Similar drawings were made for tri- and tetraglycine.

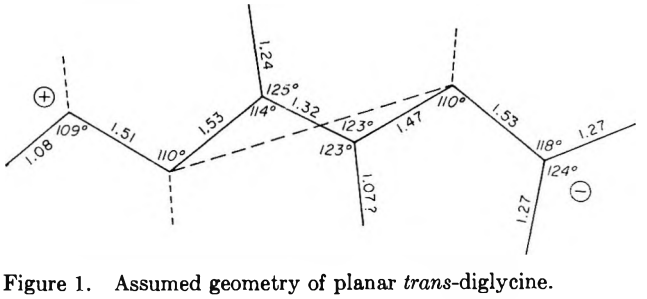


Figure 1. Assumed geometry of planar *trans*-diglycine.

(38) W. G. Martin, C. A. Winkler, and W. H. Cook, *Can. J. Chem.*, **37**, 1662 (1959).

(39) E. W. Hughes and W. J. Moore, *J. Amer. Chem. Soc.*, **71**, 2618 (1949).

(40) L. Pauling, "The Nature of the Chemical Bond," 3rd ed, Cornell University Press, Ithaca, N. Y., 1960.

(41) C. R. Noller, "Chemistry of Organic Compounds," 2nd ed, W. B. Saunders Co., Philadelphia, Pa., 1958, p 155.

(42) W. E. Webb and W. G. Moulton, *J. Chem. Phys.*, **36**, 1911 (1962).

**Table III:** Parameters for Equations Fitted to the Refractive Index Data

| | $a$ | | | $b$ | | |
|---|---|---|---|---|---|---|
| | 436 mμ | 546 mμ | 578 mμ | 436 mμ | 546 mμ | 578 mμ |
| Diglycine | 0.02599 | 0.02529 | 0.02513 | 0.00253 | 0.00251 | 0.00251 |
| Triglycine | 0.03688 | 0.03583 | 0.03563 | 0.00472 | 0.00490 | 0.00496 |
| Tetraglycine | 0.0467 | 0.0454 | 0.0449 | ... | ... | ... |

**Table IV:** Mean Polarizabilities and Dispersion Parameters

| | $10^{24}(\alpha_2)_{m=0}$ | | | $\lambda_0$, | |
|---|---|---|---|---|---|
| | 436 mμ | 546 mμ | 578 mμ | Å | $f$ |
| Glycine | 6.669 | 6.558 | 6.534 | 940 | 10.0 |
| Diglycine | 12.110 | 11.881 | 11.830 | 983 | 16.7 |
| Triglycine | 17.507 | 17.154 | 17.086 | 1012 | 22.8 |
| Tetraglycine | 23.0 | 22.5 | 22.4 | (1010) | (30) |

**Table V:** Kerr Constants at 25°

| | $10^7B$ | | |
|---|---|---|---|
| $m$ | 436 mμ | 546 mμ | 578 mμ |
| 0.0 | 3.72 | 2.89 | 2.72 |
| 0.0274 | 6.45 | 5.13 | 4.97 |
| 0.0359 | 6.94 | 5.62 | 5.75 |
| 0.0419 | 7.44 | 6.10 | 6.16 |
| 0.0532 | 9.0 | 7.3 | 7.1 |
| 0.0664 | ... | 8.7 | 8.2 |
| 0.0734 | 11.0 | 8.4 | 7.9 |
| 0.0882 | 12.9 | 10.0 | 9.6 |
| 0.1084 | 15.0 | 11.1 | 11.3 |
| | Triglycine | | |
| 0.00972 | 5.52 | 4.46 | 4.06 |
| 0.01479 | ... | 5.22 | 4.90 |
| 0.01823 | 7.08 | ... | ... |
| 0.02075 | 7.92 | 6.26 | 5.76 |
| 0.02327 | 8.00 | ... | ... |
| 0.02536 | 8.29 | 7.25 | 6.64 |
| 0.02998 | ... | 7.50 | 7.19 |
| | Tetraglycine | | |
| 0.00296 | 4.40 | 3.45 | 3.45 |
| 0.00325 | ... | 3.56 | ... |
| 0.00463 | 4.90 | 3.94 | 3.79 |
| 0.00655 | 5.66 | 4.17 | 4.32 |
| 0.00869 | 6.38 | 4.97 | ... |

**Table VI:** Kerr Constant Increments at 25°

| | $10^7(B - B_1)/m$ | | |
|---|---|---|---|
| | 436 mμ | 546 mμ | 578 mμ |
| Glycine | 19.4 ± 0.3 | 14.8 ± 0.5 | 14.8 ± 0.3 |
| Diglycine | 98 ± 5 | 80 ± 4 | 80 ± 3 |
| Triglycine | 183 ± 5 | 161 ± 5 | 147 ± 4 |
| Tetraglycine | 272 ± 30 | 211 ± 17 | 241 ± 6 |

cine and the fully extended conformations were fitted by ellipsoids whose principal diameters, $2a'$, $2b'$, and $2c'$, are shown in Table VII. The form factors $A_i$

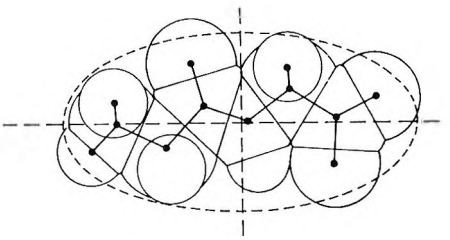

Figure 2. The shape of planar *trans*-diglycine obtained by adding Stuart radii (O, 1.22 Å; N, 1.35 Å; C, 1.45 Å; H, 0.9 Å) to the skeleton of Figure 1. The dashed line indicates the ellipsoidal parameters chosen to represent the shape.

in Table VII were estimated by the method used in the amino acid paper,[3] as were the effective dielectric constants $n_{e2}^2$, which were found to be 2.83, 2.99, and 3.13 for di-, tri-, and tetraglycine, respectively.

The vacuum dipole moments of the extended peptides were calculated as the sum of embedded charge and bond dipole contributions. The embedded charge contributions were evaluated in the manner described previously,[3] assuming the minus charge to be halfway between the carboxyl oxygens and the plus charge to be in the $H_3$ plane of the $-NH_3^+$ group. The bond dipole of the peptide group was taken as 3.71 D at 39.6° to the C–N bond.[11] The C–C and C–H bond moments were neglected, and the $-CO_2^-$ and $-C-NH_3^+$ bond moments were roughly estimated as 2 and 1 D, respectively, from the amino acid data. The bond dipole contribution was less than 10% of the embedded charge contribution for all cases considered, and the total vacuum dipole moment was predicted to be within 3° of the long axis of the ellipsoid for di-, tri-, and tetraglycine (and within 8° for glycine). The magnitudes obtained were 12.7, 25.3, 40.0, and 55.4 D for glycine–tetraglycine, respectively.

The dielectric increments were then calculated with the aid of eq 10 of the earlier paper,[3] assuming the vacuum dipole to be along the $a$ axis (or 1 axis) of the shape ellipsoid and using the data of Connor, Clarke, and Smyth[9b] where needed on the right-hand side of the equation. The predicted values of the dielectric increments, $\Delta\epsilon/m$, were 19.6, 69.3, 148.3, and 255.1 for glycine–tetraglycine. A comparison with the experimental values (22.6, 70.4, 114.5, and 165.8)[9b] is shown graphically in Figure 3. The predictions for the longer peptides are too high because the tendency of the peptides to coil has not been recognized. The

**Table VII:** Ellipsoidal Diameters and Form Factors for Extended *trans* Conformations

| | $2a'$ | $2b'$ | $2c'$ | $b'/a'$ | $c'/a'$ | $A_a$ | $A_b$ | $A_c$ |
|---|---|---|---|---|---|---|---|---|
| Glycine | 6.1 | 4.7 | 3.8 | 0.771 | 0.614 | 0.239 | 0.330 | 0.430 |
| Diglycine | 10.0 | 5.0 | 3.8 | 0.500 | 0.380 | 0.150 | 0.362 | 0.490 |
| Triglycine | 14.0 | 5.0 | 3.8 | 0.357 | 0.272 | 0.100 | 0.386 | 0.515 |
| Tetraglycine | 18.0 | 5.0 | 3.8 | 0.278 | 0.211 | 0.070 | 0.402 | 0.527 |

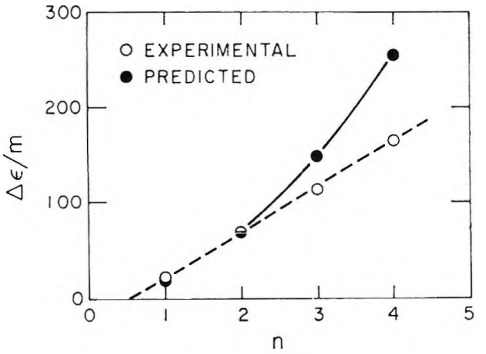


Figure 3. Experimental[9b] and predicted dielectric increments *vs.* the number of glycine residues. The predictions are for extended *trans*-peptide conformations and are calculated in the framework of the Scholte ellipsoidal cavity model theory.

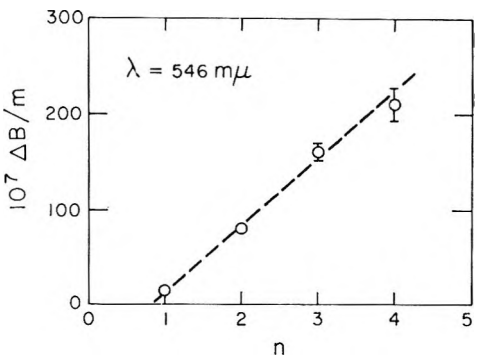


Figure 4. A plot of the experimental Kerr constant increments *vs.* the number of glycine residues at 546 mμ.

close agreement obtained for diglycine may or may not indicate that the monopeptide prefers an extended conformation. The almost linear dependence of the data on the number of residues would be predicted for long random coils but is somewhat surprising for short, relatively rigid peptides.

*Optical Anisotropies.* Since the optical anisotropy of the peptide group is unknown, it is not possible to predict the Kerr constant increment from molecular parameters. In addition, the preceding calculations suggest that it is not permissible to assume extended conformations, with the possible exception of diglycine.

As an exploratory calculation for diglycine, it is of interest to estimate the optical anisotropy, $\alpha_{11} - (1/2)(\alpha_{22} + \alpha_{33})$, by using Scholte's theory for the orienting factor and by assuming an extended conformation. The result may then be compared with estimated shape-effect carboxyl contributions to see whether the contribution of the peptide group to the optical anisotropy is likely to be important. Using eq 12 of the earlier paper[3] and the Kerr constant increment of diglycine at 546 mμ an "experimental" optical anisotropy of $1.74 \times 10^{-24}$ was obtained by the approach outlined above. The predicted contribution of the shape effect, according to eq 13 of the earlier paper,[3] was $1.8 \times 10^{-24}$ for extended *trans*-diglycine. This value is slightly greater than the total observed optical anisotropy. The contribution of the carboxyl group was estimated by assigning all of the intrinsic anisotropy of glycine to this group and then considering the effect of the carboxyl orientation within the peptide on its contribution to the optical anisotropy. Calculated values ranged from 0.60 to $-1.42 \times 10^{-24}$ for various cases. It is therefore clear that the present data cannot be used to estimate the intrinsic optical anisotropy of the peptide group unless the shape and carboxyl contributions can be more reliably calculated.

The Kerr constant increments at 546 mμ are plotted in Figure 4 to show the dependence on the number of residues. It is striking that both this plot and the plot of dielectric increments in Figure 3 are essentially linear. It must therefore be concluded that the optical anisotropy increases only very slowly, if at all, with increasing $n$, and may in fact be a slightly decreasing function of $n$ for $n > 2$.

## Discussion

Several important conclusions are suggested by the essentially qualitative analysis of the data presented above. The shape effect and C-terminal carboxyl are major contributions to the optical anisotropy of small peptides in aqueous solution. These contributions are large enough to obscure the effect of the peptide group optical anisotropy in the case of diglycine. The linear dependence of both the dielectric and Kerr constant increments on the number of residues suggests that the optical anisotropy is essentially independent of $n > 2$. Such a situation could occur if the coiling of the longer chains led to a more nearly spherical average shape. If the intrinsic optical anisotropy were small for all $n$, or if it did not increase significantly with increasing $n$, its effect would not be noticeable in comparison to the shape effect. Further progress in the analysis of these data awaits the development of an adequate theory of the shape effect.

# Water Structure in Solutions of the Sodium Salts of Some Aliphatic Acids[1,2]

by Harriet Snell and Jerome Greyson

*Rocketdyne, A Division of North American Rockwell Corporation, Canoga Park, California* *(Received December 30, 1969)*

Entropies of transfer between heavy and normal water for the sodium salts of the group of aliphatic acids from the formate to the caproate have been determined from combination of heats of transfer obtained from calorimetric measurements with free energies of transfer obtained from cell measurements. The standard heat of transfer for the process salt in heavy water to normal water was negative for sodium formate, near zero for sodium propionate and butyrate, and positive for sodium caproate. Solvent-structure influence, established from the sign and magnitude of the transfer entropies, indicated a transition from structure breaking to structure making in passing from sodium formate to sodium caproate. Increases in solute concentration lead to decreases in the absolute value of the entropy of transfer. The structure influence and the concentration dependence of the entropies of transfer of the salts have been explained in terms of the Gurney cosphere model.

## Introduction

A continuing program has been under way in this laboratory in which the nature of the structure of water and the influence of electrolytes thereon have been investigated. The approach has been thermodynamic in that it has been directed toward determination of the entropy effects associated with the transfer of ionic salts between heavy and normal water. Justification for relating transfer entropies to water structure has been presented in detail elsewhere as have the details of the experimental techniques.[3-7] Suffice it to say here that the properties of heavy and normal water are similar except to the extent to which they are structured, and the sign and magnitude of the transfer entropy can be related to structure influence.

Systems that have been studied and reported in earlier publications have included solutions of alkali halides[3,4] and alkaline earth chlorides.[5,6] In this paper, we report the results of measurements of solutions of the sodium salts of several low carbon number aliphatic acids.

## Experimental Section

*Materials.* Heavy water (99.75% $D_2O$) was obtained from the U. S. Atomic Energy Commission, Savannah River Operations Office, Aiken, S. C. All normal water solution measurements were made with $CO_2$-free conductivity water ($3.6 \times 10^{-7}$ ohm$^{-1}$ cm$^{-1}$ at 25°). For the heat of dilution measurements and for the cell measurements, all starting solutions were prepared by weight in duplicate.

All starting chemicals, except sodium caproate and sodium valerate, were reagent grade and were used without further treatment. Sodium formate, sodium acetate, sodium propionate, sodium butyrate, and sodium isobutyrate were oven dried to constant weight at 105°.

Anhydrous sodium caproate was prepared from 99% *n*-caproic acid and a 51.2% aqueous solution of sodium hydroxide in a fashion recommended by Vold.[8] The preparation was carried out in a nitrogen-filled glove bag. Caproic acid was dissolved in an equal volume of 70:30 ethanol–water, and a stoichiometric quantity of 51.2% aqueous sodium hydroxide was added. The solution was then neutralized with 0.05% aqueous sodium hydroxide to the phenolphthalein end point with the aid of filter paper, which had been treated with the indicator and dried. The latter step served to repress hydrolysis and substantially reduce the free acid content of the product. The solvent was evaporated on a hot plate. Final drying was carried out in a vacuum oven at 155°. Anhydrous sodium valerate was prepared similarly from material that chromatographic analysis showed to be 95.1% *n*-valeric acid.

*Calorimeter Measurements.* Integral heat of dilution and/or integral heat of solution measurements in normal and heavy water were made for each of the salts. Experimental procedures and the methods for calculating the heats of transfer from the resulting data have been described previously for both the integral heat of solution[5] and dilution heat[6] measurements. For the dilution measurements, the starting solutions were 2.5 aquamolal, *i.e.*, moles of salt/55.5 moles of solvent, except for the sodium caproate solution, which was 2.0 aquamolal. A single dilution heat was measured for each process and for each solution by diluting it approximately 100-fold. Dilution volumes were selected such

(1) This research was supported by the Research Division of the Office of Saline Water, U. S. Department of the Interior, under Contract No. 14-01-0001-1701.

(2) Presented in part at the 158th National Meeting of the American Chemical Society, New York, N. Y., Sept 1969.

(3) J. Greyson, *J. Phys. Chem.*, **66**, 2218 (1962).

(4) J. Greyson, *ibid.*, **71**, 2210 (1967).

(5) J. Greyson and H. Snell, *ibid.*, **73**, 3208 (1969).

(6) J. Greyson and H. Snell, *ibid.*, **73**, 4423 (1969).

(7) R. E. Kerwin, Ph.D. Thesis, University of Pittsburgh, 1964.

(8) M. J. Vold, private communication, Department of Chemistry, University of Southern California.

**Table I:** Integral Heats of Solution for Sodium Formate, Sodium Acetate, Sodium Propionate, and Sodium Butyrate in Normal and Heavy Water at 25.0°

| Solvent | Temp, °C | Final concn, aquamolality | Measd $\Delta H$,[a] kcal/mol |
|---|---|---|---|
| | | Sodium Formate | |
| $H_2O$ | 24.99 | 0.1189 | 0.266 |
| | 25.00 | 0.1217 | 0.267 |
| | 24.99 | 0.1308 | 0.268 |
| | 25.00 | 0.1336 | 0.271 |
| | 25.00 | 0.1440 | 0.272 |
| | | | $\Delta\bar{H}$ = 0.269 ± 0.003 |
| $D_2O$ | 25.00 | 0.1314 | 0.465 |
| | 25.00 | 0.1410 | 0.467 |
| | 25.00 | 0.1446 | 0.470 |
| | 25.00 | 0.1449 | 0.458 |
| | 25.00 | 0.1486 | 0.459 |
| | | | $\Delta\bar{H}$ = 0.464 ± 0.005 |
| | | Sodium Acetate | |
| $H_2O$ | 25.01 | 0.01410 | −4.012 |
| | 25.00 | 0.05610 | −3.979 |
| | 25.01 | 0.05668 | −3.967 |
| | 25.00 | 0.07693 | −3.933 |
| | | | $\Delta\bar{H}$ = −3.973 ± 0.038 |
| $D_2O$ | 25.01 | 0.02414 | −3.915 |
| | 25.00 | 0.04729 | −3.903 |
| | 25.01 | 0.05689 | −3.918 |
| | 25.01 | 0.07530 | −3.885 |
| | | | $\Delta\bar{H}$ = −3.905 ± 0.015 |
| | | Sodium Propionate | |
| $H_2O$ | 25.01 | 0.01240 | −3.044 |
| | 25.01 | 0.01246 | −3.060 |
| | 25.01 | 0.01619 | −2.990 |
| | 25.01 | 0.02706 | −3.002 |
| | 25.01 | 0.03600 | −2.979 |
| | | | $\Delta\bar{H}$ = −3.015 ± 0.016 |
| $D_2O$ | 25.01 | 0.01267 | −3.022 |
| | 25.01 | 0.01740 | −3.044 |
| | 25.01 | 0.01939 | −2.976 |
| | 25.00 | 0.02836 | −2.950 |
| | 25.01 | 0.03540 | −3.007 |
| | | | $\Delta\bar{H}$ = −2.999 ± 0.037 |
| | | Sodium Butyrate | |
| $H_2O$ | 25.00 | 0.01942 | −3.393 |
| | 25.01 | 0.03235 | −3.398 |
| | 25.01 | 0.03855 | −3.397 |
| | 25.01 | 0.05334 | −3.353 |
| | | | $\Delta\bar{H}$ = 3.385 ± 0.022 |
| $D_2O$ | 25.01 | 0.02358 | −3.394 |
| | 25.01 | 0.03430 | −3.429 |
| | 25.01 | 0.05052 | −3.386 |
| | 25.01 | 0.05719 | −3.397 |
| | | | $\Delta\bar{H}$ = −3.402 ± 0.019 |

[a] The mean values and the root-mean-square deviations are also listed.

that the final concentration was 0.02 aquamolal for all salts. As reported before,[6] the value 31 cal/mol was used to correct the heats measured for the heat effect contributed by the isotopic exchange reaction in the integral heat of dilution experiments.

*Emf–Transfer Free Energy Measurements.* The experimental apparatus and general procedure for obtaining the free energies of transfer of salts between heavy and normal water have been described elsewhere.[3,4] Potential measurements were made with the same equipment as that described in a previous publication.[4] For this work, however, a Leeds and Northrup K-4 potentiometer was used. Measurements were carried out at 25.0 ± 0.2°. The emf measurements were made in cells of the type

$$\mathrm{Ag|AgCl|NaCl}\ (a_0)\,|^+|\underset{H_2O}{\mathrm{NaR}}\ (a_\alpha)\,|^-|\underset{H_2O}{\mathrm{NaR}}\ (a_\beta)\,|^+|\underset{H_2O}{\mathrm{NaCl}}\ (a_0)\,|\mathrm{AgCl|Ag}$$

where the configuration

$$\mathrm{Ag|AgCl|NaCl}\ (a_0)\,|^+|\ \underset{H_2O}{}$$

is a cation-reversible membrane electrode reversible to sodium ion. The symbol R refers to an aliphatic acid anion, and the anion-exchange membrane, $|^-|$, permits the diffusion of anions between the solvents. It has been shown that the emf's of such cells are related to the free energy of the transfer of 1 equiv of salt from $D_2O$ at activity $a_\beta$ to $H_2O$ at activity $a_\alpha$.[3,4]

## Results and Discussion

The calorimetric data are presented in Tables I and II. Table I summarizes the integral heat of solution data, obtained for sodium formate, acetate, propionate, and butyrate. Table II includes the integral heats of dilution and the heats of transfer calculated from the measurements. The mean values of the heats and the root-mean square deviations are also given in the tables. As noted previously,[4] the standard heat of transfer for salts between heavy and normal water is defined as the difference between the values of the heats of solution in the isotopic solvents at in-

**Table II:** Integral Heats of Dilution and Heats of Transfer for Sodium Salts of Some Aliphatic Acids in Normal and Heavy Water at 25.0°

| Salt | Concn, aquamolality—Initial | Concn, aquamolality—Final | $\Delta H_{dil}^{H_2O}$, cal/mol | $\Delta H_{dil}^{D_2O}$, cal/mol | $\Delta H_{dil}$, cal/mol—$H_2O$ into $D_2O$ | $\Delta H_{dil}$, cal/mol—$D_2O$ into $H_2O$ | $\Delta H_{tr}^{\circ}$,[a] cal/mol | $\Delta H_{tr}^{0}$,[b] cal/mol |
|---|---|---|---|---|---|---|---|---|
| Sodium formate | 2.500 | 0.02500 | 0 | +83 | +209 | −121 | −121 ± 9 | −205 ± 9 |
| | | | | +85 | +214 | −107 | | −195 ± 6[c] |
| Sodium acetate | 2.500 | 0.02400 | −387 | −368 | −316 | −408 | −26 ± 18 | −65 ± 18 |
| | | | −408 | −348 | −322 | −412 | | −68 ± 42[c] |
| Sodium propionate | ... | ... | ... | ... | ... | ... | ... | −16 ± 40[c] |
| Sodium butyrate | ... | ... | ... | ... | ... | ... | ... | +17 ± 29[c] |
| Sodium isobutyrate | 2.509 | 0.02260 | −1093 | −1098 | −1134 | −1064 | +39 ± 11 | +36 ± 11 |
| | | | −1104 | −1094 | −1150 | −1071 | | |
| Sodium valerate | 2.500 | 0.02260 | −1711 | −1757 | −1747 | −1679 | +12 ± 19 | +54 ± 17 |
| | | | −1693 | −1732 | −1741 | −1678 | | |
| Sodium caproate | 2.000 | 0.01728 | −2087 | −2186 | −2153 | −2070 | −7 ± 17 | +99 ± 17 |
| | | | −2058 | −2172 | −2176 | −2075 | | |

[a] Concentrations equal initial concentrations. [b] Standard enthalpies of transfer have been assumed equal to the transfer values at the final concentrations tabulated. [c] These data were calculated from integral heat of solution measurements.

**Table III:** Heat, Emf, Free Energy, and Entropy of Transfer from $D_2O$ to $H_2O$ for the Sodium Salts of Some Aliphatic Acids at 25.0°

| Salt | Dilute soln—$\Delta H_{tr}^{0}$,[b] cal/mol | Dilute soln—Emf, mV | Dilute soln—$\Delta F_{tr}^{0}$, cal/mol | Dilute soln—$\Delta S_{tr}^{0}$, cal/mol deg | Concd soln[c] $\Delta H_{tr}$, cal/mol |
|---|---|---|---|---|---|
| Sodium formate | −205 ± 9 | −0.8 ± 0.2 | +19 | −0.75 | −121 ± 9 |
| Sodium acetate | −65 ± 18 | −1.5 ± 0.2 | +34 | −0.33 | −26 ± 18 |
| Sodium propionate | −16 ± 40[a] | −1.9 ± 0.2 | +45 | −0.20 | ... |
| Sodium butyrate | +17 ± 29[a] | −2.0 ± 0.2 | +46 | −0.097 | ... |
| Sodium isobutyrate | +36 ± 11 | ... | ... | ... | +39 ± 11 |
| Sodium valerate | +54 ± 17 | −1.7 ± 0.2 | +39 | +0.050 | +12 ± 19 |
| Sodium caproate | +99 ± 17 | −1.7 ± 0.2 | +39 | +0.20 | −7 ± 17 |

[a] These data were calculated from integral heat of solution measurements. [b] Standard enthalpies of transfer have been assumed equal to the transfer values at the final concentrations tabulated in Table II. [c] Concentrations equal to the initial values in Table II.

finite dilution. The heats of transfer listed in Table II, calculated for dilute solutions ranging in concentration from 0.01 to 0.1 aquamolal, were assumed equal to the standard heats of transfer. Justification for doing so has been given previously.[5]

The cell data are summarized in Table III along with the calorimetric data and calculations of the associated free energy and entropy changes for the transfer process. The measured emf values are the cell potentials with equal concentrations in each half-cell. The standard emf values and the associated free energies were calculated by assuming equal activity coefficients for the salts in heavy and normal water. The sign of the emf is defined such that positive values indicate a spontaneous transfer of salt from heavy to normal water. The precision of the measurements was approximately ±0.2 mV.

For the purpose of calculating entropy values, contributions to the cell emf, which have been shown to result from solvent transport through the cell membranes,[9] have been neglected. Justification for neglecting them results from a study which indicated that for anion-exchange membrane cells containing halide ions, differences in solvent contributions arising among members of the same family were second order relative to the total contributions characteristic of the family.[10] It is assumed that similar characteristics would be exhibited by the aliphatic acid anions and that solvent-transport corrections would not change the sequence of emf values shown in Table III or the resultant sequence of calculated free energies of transfer. Thus, even if the solvent correction characteristic of the family of aliphatic acid anions were large relative to the measured emf values in Table III, the net effect would be to shift the calculated entropies of transfer up or down scale but not to change the sequence as shown. However, the nonpolar moieties of the aliphatic acid anions do not

(9) J. Greyson, *J. Phys. Chem.*, 71, 259 (1967).
(10) J. Greyson, *ibid.*, 71, 4549 (1967).

solvate to any large extent,[11] and it is not expected that solvent-transport corrections would be large. Thus we conclude that the entropies as shown are correct in sequence and probably correct in value within the general limits of our experimental reproducibility.

It is to be noted that the emf values and the resulting transfer free energies for all of the salts indicate that they pass spontaneously from normal to heavy water. However, the standard heat of transfer for the process salt in heavy water into normal water is negative for sodium formate, near zero for sodium propionate and sodium butyrate, and positive for sodium caproate. Calculated entropy values follow the same general pattern as the heats, decreasing in the transfer process for the formate and increasing for the caproate.

It is also to be noted that the heat of transfer diminishes in absolute value with increased concentration. Lack of activity coefficient data prevents formal calculation of the concentration dependence of the entropy of transfer. However, a characteristic of transfer measurements between heavy and normal water solutions has been that the value of the entropy is dominated by the heat of transfer, even in concentrated solutions.[12] Dominance of the heats can be seen in Table III for the dilute solutions of formate and caproate. It seems, therefore, that it is not unreasonable to expect dominance of the heats for these salts in concentrated solutions also. Thus, the diminishing heat of transfer can be used as an indication of diminishing entropy of transfer with increasing solution concentration.

Considerable attention has recently been given to the Gurney cosphere model[13] for structural interactions in aqueous systems.[12,14,15] As will be seen, the model provides an almost ideal explanation for the results of the work reported here. The Gurney model in its simplest terms states that the solute particles in aqueous systems are surrounded by spherical shells of solvent modified in structure from that in the pure solvent. The concentration dependence of properties attributable to structural interactions results from the increasing overlap of the spherical shells with increasing concentration; *i.e.*, the concentration of cosphere solvent per mole of solute decreases with increasing solute concentration.

In the process of solution of solute to infinite dilution, the entropy per mole of salt associated with the formation of cosphere solvent could be negative or positive as determined by whether the modified structure of the shell were more or less ordered than the pure solvent. Similarly, because of the changing concentration of cosphere solvent per mole of solute, the process of dilution will give rise to an entropy change dependent on the relative ordering of pure and cosphere solvent. A structure-breaking solute would, therefore, exhibit a positive entropy change in the process of solution to infinite dilution because of the formation of disordered solvent shells about each particle. Dilution of a concentrated solution of the same solute to infinite dilution would also exhibit an increase in entropy because ordered solvent would be used to complete the disordered solvent shells, which in the concentrated solution had been completed by overlapping cospheres. The contrary, of course, would be true of structure-making solutes and, in general, the sign of the entropy change associated with both solution and dilution processes for a given solution will be the same.

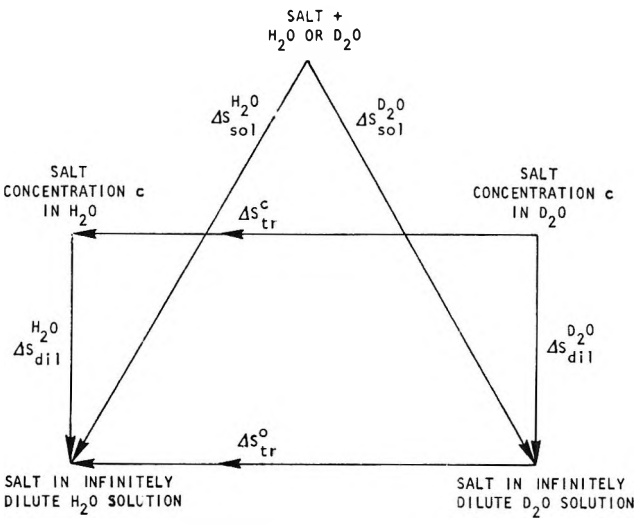


Figure 1. Process for transfer of salt from $D_2O$ to $H_2O$.

Application of the Gurney model to transfer of solute between heavy and normal water is best illustrated by reference to the processes shown in Figure 1. The entropy of transfer between the infinitely dilute solutions is given by the equation

$$\Delta S_{tr}^{0} = \Delta S_{sol}^{H_2O} - \Delta S_{sol}^{D_2O} \quad (1)$$

for the process of transfer of salt from heavy into normal water. For the same process in concentrated solution, the entropy of transfer can be expressed by the equation

$$\Delta S_{tr}^{c} = \Delta S_{dil}^{D_2O} + \Delta S_{tr}^{0} - \Delta S_{dil}^{H_2O} \quad (2)$$

Since heavy water is more structured than normal water, the entropy change associated with the solution of structure-breaking salts (*i.e.*, the formation of structure-broken cospheres) in the $D_2O$ would be more positive than the entropy associated with solution of the same species in normal water, if one can assume that cospheres for each of the solvents are equally disordered.

(11) T. L. Kavanau, "Water and Solute Water Interactions," Holden-Day, Inc., San Francisco, Calif., 1964.

(12) Y. C. Wu and H. L. Friedman, *J. Phys. Chem.*, **70**, 166 (1966).

(13) R. W. Gurney, "Ionic Processes in Solution," Dover Publications, Inc., New York, N. Y., 1962.

(14) R. H. Wood, R. A. Rooney, and J. N. Braddock, *J. Phys. Chem.*, **73**, 1673 (1969).

(15) J. E. Desnoyers, M. Arel, G. Perron, and C. Jolicoeur, *ibid.*, **73**, 3346 (1969).

Thus, from eq 1, the entropy of transfer, $\Delta S_{tr}^0$, for a structure-breaking solute is seen to be negative in passing from heavy into normal water.

In a dilution process, in which a structure breaker is in solution, the resulting increased concentration of disordered shells per mole of solute will result in a more positive entropy change in the more highly structured $D_2O$ than it will in $H_2O$. Thus, values of $\Delta S_{dil}^{D_2O}$ will also be more positive than $\Delta S_{dil}^{H_2O}$. The net result, as examination of eq 2 reveals, is that $\Delta S_{tr}^c$ is less negative than $\Delta S_{tr}^0$.

Consideration of solution and dilution processes for structure-making solutes leads to similar conclusions except that the signs are reversed. That is, structure-making solutes will give rise to shells with more structure than pure solvent. Thus, solution of a structure maker in $D_2O$ will lead to a larger reduction in entropy (more negative $\Delta S$) than solution of the same species in normal water. From eq 1, it can be seen, therefore, that $\Delta S_{tr}^0$ will be positive. Dilution processes will also lead to reduction in entropy because of the formation of more shells per mole of salt. However, the value of $\Delta S_{dil}^{D_2O}$ will be more negative than $\Delta S_{dil}^{H_2O}$ because more structure will be made in the cospheres of heavy water than in the cospheres of normal water. Thus, as can be seen from eq 2, the value of $\Delta S_{tr}^c$ will become less positive as concentration increases.

In general, then, application of the Gurney model to processes under way in transferring solutes between heavy and normal water leads to the conclusion that increases in solute concentration lead to decreases in the absolute value of the entropy of transfer, regardless of whether the solute behaves as a structure maker or breaker.

That the characteristics as described in the foregoing discussion are displayed by the aliphatic acid salts can be seen by examination of the data in Table III. In passing from sodium formate to sodium caproate, the transfer entropies in the dilute solutions pass from negative to positive values, indicating a transition from structure-breaking to structure-making influence. Such results are in accord with the prevailing view that, in proportion to their carbon number, saturated hydrocarbon moieties increase the degree of hydrogen bonding among neighboring water molecules and the apparent structuring in water. The data are also in accord with the proposed formation of shells about the solutes with structural properties progressing from less ordered to more ordered than solvent.

An noted before, the heats of transfer for the concentrated solutions, compared to those for the dilute solutions, decrease in absolute value for all the salts, except perhaps for the sodium isobutyrate. The isobutyrate displays no difference within experimental error; however, it may represent a transition entity, which is neither structure breaking nor making. The extremes, sodium formate and caproate, do display a clear decrease in absolute value of the heat of transfer with increasing concentration. If the assumption that the heats of transfer are representative of the entropy values is valid, the data are in agreement with the model presented; *i.e.*, decreases in transfer entropy are exhibited with increased concentration regardless of the structure-influencing properties of the solute.

In conclusion, it is worth noting that the concentrations of sodium valerate and caproate in the solutions used for the dilution experiments were in excess of their critical micelle concentrations.[16] Micelle formation can be looked upon as a process in which solute collects into aggregates of individual particles with solvent shells coalescing about the individual aggregates. Upon dilution, demicellization would result in the formation of shells about the individual members of the aggregates, with a corresponding reduction in entropy per mole of solute. Thus, the presence of micelles in the concentrated solutions strengthens the fit of the cosphere model to the data since the coalescence of solvent about an aggregate of individual particles is really an example of extreme cosphere overlap.

(16) E. R. B. Smith and R. A. Robinson, *Trans. Faraday Soc.*, **38**, 70 (1942).

# Activity Coefficients of Hydrochloric Acid in Some Dilute Mixed Electrolyte Solutions

by C. J. Downes[1]

*Department of Chemistry, University of Otago, Dunedin, New Zealand* *(Received December 8, 1969)*

Activity coefficients of hydrochloric acid in salt solutions have been measured at 20, 25, 30, and 35°. The added salts were tetramethylammonium chloride, tetraethylammonium chloride, barium chloride, strontium chloride, and the bolaform electrolytes ethylenediamine dihydrochloride and hexamethylenediamine dihydrochloride. Measurements were made at constant total ionic strength and Harned's rule was found to hold in all cases. The results at an ionic strength of 0.1 mol $kg^{-1}$ are discussed in terms of the Bronsted–Guggenheim specific interaction theory.

## Introduction

The variation of the activity coefficient of a single electrolyte in dilute solution, generally, can be represented by a Debye–Hückel term with the addition of a term involving a specific interaction coefficient.[2] It has been proposed[2] that activity coefficients of dilute mixed electrolyte solutions can be calculated from the properties of the single electrolytes. The interpretation[3] of Guntelberg's measurements of the activity coefficients of hydrochloric acid in alkali chloride solutions substantiates the validity of this proposal. Recently, Covington[4] measured the activity coefficients of hydrochloric acid in mixed solutions with calcium chloride and with manganous chloride. He stated that his results for the hydrochloric acid–calcium chloride system were in reasonable agreement with the predictions of the specific interaction theory.

The purpose of the present work has been to investigate mixtures of hydrochloric acid solutions containing a wide variety of added salts. The cations of the added salts cover a range of sizes, charges, and shapes.

## Theory

*Specific Interaction Theory.* Guggenheim and Turgeon[2] have presented equations describing the variation of the activity coefficients in dilute electrolyte solutions. For the mean activity coefficient of an electrolyte, having cation R and anion X, they deduce

$$\ln \gamma_{R,X} = -\alpha Z_R|Z_X|\frac{I^{1/2}}{1+I^{1/2}} + \frac{\nu_R}{\nu_R+\nu_X}2\sum_{X'}\beta_{R,X'}m_{X'} + \frac{\nu_X}{\nu_R+\nu_X}2\sum_{R'}\beta_{R',X}m_{R'} \quad (1)$$

where $\gamma$ is the mean activity coefficient, $\alpha = 1.171$ $kg^{1/2}$ $mol^{-1/2}$ for water as solvent at 25°, $Z_R$ and $Z_X$ are the charge numbers of the cation and anion, $I$ is the total ionic strength, $\nu_R$ and $\nu_X$ are the number of moles of cation and anion in one mole of electrolyte, $\beta$ is an interaction coefficient, and $m_i$ is the molality of species i. In eq 1 R′ denotes every cation and X′ denotes every anion present in the solution. If only a single electrolyte is present in the solution this formula can be simplified to

$$\ln \gamma = -\alpha Z_R|Z_X|\frac{I^{1/2}}{1+I^{1/2}} + 2\bar{\nu}\beta m \quad (2)$$

where $\bar{\nu}$ is the harmonic mean of $\nu_R$ and $\nu_X$.

The corresponding formula involving decadic logarithms is

$$\log \gamma = -AZ_R|Z_X|\frac{I^{1/2}}{1+I^{1/2}} + Bm \quad (3)$$

where

$$B = \frac{2\bar{\nu}}{2.303}\beta \quad (4)$$

*Harned's Rule.* For many mixtures of two electrolytes, at constant total ionic strength, it has been found that the logarithm of the mean activity coefficient of each electrolyte is approximately a linear function of the ionic strength fraction of the other component

$$\log \gamma_1 = \log \gamma_{1(0)} - \alpha_{12}I_2 \quad (5)$$

where the subscripts 1 and 2 refer to the two solutes and $\gamma_{1(0)}$ is the activity coefficient of component 1 in a pure solution of 1 at the same ionic strength as the total ionic strength of the mixture. For mixtures of 1 and 2,

(1) Baas Becking Geobiological Laboratory, Box 378, Canberra City, A.C.T. 2601, Australia.

(2) E. A. Guggenheim and J. C. Turgeon, *Trans. Faraday Soc.*, **51**, 747 (1955).

(3) G. N. Lewis, M. Randall, K. S. Pitzer, and L. Brewer, "Thermodynamics," 2nd ed, McGraw-Hill Publications, New York, N. Y., 1961, p 570.

(4) A. K. Covington, *J. Chem. Soc.*, 4906 (1965).

$\alpha_{12}$ is a constant for a given total ionic strength. Most of the evidence for the general approximate validity of eq 5, Harned's rule,[5] comes from measurements at high total ionic strength. The specific interaction theory predicts that Harned's rule should be followed at low ionic strengths and that the Harned rule coefficients, $\alpha_{12}$ and $\alpha_{21}$, can be expressed in terms of the specific interaction coefficients. The general expression for $\alpha_{12}$ for a mixture of two electrolytes is

$$\alpha_{12} = \frac{1}{2.303}\left[2\beta_{R1,X1}\frac{2\nu_{R1}\nu_{X1}}{\nu_{R1}+\nu_{X1}}\frac{2}{\nu_{R1}Z_{R1}^2+\nu_{X1}Z_{X1}^2} - 2\beta_{R1,X2}\frac{\nu_{R1}\nu_{X2}}{\nu_{R1}+\nu_{X1}}\frac{2}{\nu_{R2}Z_{R2}^2+\nu_{X2}Z_{X2}^2} - 2\beta_{R2,X1}\frac{\nu_{X1}\nu_{R2}}{\nu_{R1}+\nu_{X1}}\frac{2}{\nu_{R2}Z_{R2}^2+\nu_{X2}Z_{X2}^2}\right] \quad (6)$$

where the subscripts R1 and X1 refer to the cation and anion of electrolyte 1, with similar nomenclature for electrolyte 2.

In the next section the experimental results for $\alpha_{12}$, at an ionic strength of 0.1 mol $kg^{-1}$, will be compared with the values calculated by use of specific interaction coefficients (eq 6), and the validity of eq 5 as a description of the variation of the activity coefficients of hydrochloric acid in the higher ionic strength mixtures will be ascertained.

## Experimental Section

The emf's of cells such as

$$Pt|H_2(g)|HCl\ (m_1),\ MCl\ (m_2)|AgCl|Ag \quad (I)$$

were measured and the activity coefficients of hydrochloric acid in the mixtures were calculated by using eq 7. Values of 2.3026 $RT/F$ used are from the list

$$E = E^0 - \frac{2.3026RT}{F}\log m_{H^+}m_{Cl^-}\gamma_{\pm}^2 \quad (7)$$

given by Robinson and Stokes.[6] Bases for the thermal-electrolytic silver–silver chloride electrodes were formed by sealing pairs of platinum spirals in extended soda glass joints. The electrodes were aged in 0.1 $m$ NaCl which was deoxygenated by bubbling nitrogen. A day after preparation the bias potentials of a batch were usually less than $\pm 0.02$ mV on comparison with an aged reference electrode. The pair of hydrogen electrodes used in each cell was lightly coated with platinum black by the method of Hills and Ives.[7] The potentials of the cells were measured with a Pye potentiometer, Catalog No. 7565, used in conjunction with a Scalamp galvanometer, Catalog No. 7904/S and a certified Weston standard cell. The cell vessels were of conventional design[8] and the solutions, which had been deoxygenated by bubbling hydrogen, were transferred to the cell vessel without contacting the atmosphere. Purified hydrogen was bubbled through two saturators containing cell solution, and then past the platinum electrodes, at the rate of two to three bubbles per second. Values listed by Bates[9] were used to correct the emf's to a pressure of dry hydrogen of 760 mm. The depth effect correction[10] was not applied. The cells were thermostated at each temperature with variations of less than 0.01°. Certified bomb calorimeter thermometers were used to set the thermostat.

*Hydrochloric Acid.* A stock solution of hydrochloric acid was prepared from twice-distilled constant boiling acid. Analytical reagent grade acid was used to make up the constant boiling acid. Bromide content[11] was found to be less than 0.002 mol %.

*Barium Chloride and Strontium Chloride.* The BDHAR products were found to contain 0.001 mol % bromide and each was recrystallized twice from water.

*Tetramethylammonium Chloride.* A sample of the BDH salt contained about 0.1 mol % bromide. This impurity was reduced to less than 0.001 mol % by passing an aqueous solution of the salt very slowly through a bed of Amberlite IRA − 400AR grade resin in the chloride form. The eluate was carefully evaporated to near dryness and the remainder of the water removed by heating on a vacuum hot plate at 100–120° for 20 hr. The anhydrous salt was recrystallized from methanol and then dried on a vacuum hotplate for 10 hr at 130°, before determining the chloride content gravimetrically as silver chloride. *Anal.* Calcd for $(CH_3)_4NCl$: Cl, 32.33. Found: Cl, 32.30.

*Tetraethylammonium Chloride.* This salt was prepared by metathesis of the iodide which was made by refluxing equimolar amounts of BDH triethylamine and ethyl iodide, using methanol as solvent. The tetraethylammonium iodide which crystallized on cooling the solution was recrystallized from water. Conversion to the chloride was accomplished by adding a slight excess of silver chloride to a solution of the iodide in methanol. After filtering off the silver halides the methanol was removed with a rotary evaporator and the product precipitated from a chloroform solution with dry ether. The salt was found to be contaminated with significant amounts (>0.005 mol %) of bromide which was shown later to have come from the chloroform. This bromide was removed from an aqueous solution of the salt by the method used for tetramethylammonium chloride.

(5) H. S. Harned and B. B. Owen, "The Physical Chemistry of Electrolyte Solutions," 3rd ed, Reinhold Publishing Corporation, New York, N. Y., 1958, Chapter 14.

(6) R. A. Robinson and R. H. Stokes, "Electrolyte Solutions," 2nd ed, Butterworth and Co. (Publishers) Ltd., London, 1959, p 469.

(7) G. J. Hills and D. J. G. Ives in "Reference Electrodes," D. J. G. Ives and G. J. Janz, Ed., Academic Press, Inc., New York, N. Y., 1961, p 107.

(8) H. S. Harned and J. O. Morrison, *Amer. J. Sci.*, 195, 161 (1937).

(9) R. G. Bates, "Determination of pH," John Wiley and Sons, New York, N. Y., 1964, p 234.

(10) Reference 9, p 233.

(11) W. C. Somerville and A. D. Campbell, *Mikrochim. Acta*, 5–6, 991 (1963).

**Table I:** Activity Coefficients of HCl in the System HCl ($m_1$)-$(CH_3)_4NCl$ ($m_2$)-$H_2O$ at 0.1 mol $kg^{-1}$ Ionic Strength

| | | 20° | | | 25° | | | 30° | | | 35° | | |
|---|---|---|---|---|---|---|---|---|---|---|---|---|---|
| $m_1$ | $m_2$ | $E$ | $-\text{Log } \gamma_1$ | $10^5\Delta$[a] | $E$ | $-\text{Log } \gamma_1$ | $10^5\Delta$ | $E$ | $-\text{Log } \gamma_1$ | $10^5\Delta$ | $E$ | $-\text{Log } \gamma_1$ | $10^5\Delta$ |
| 0.1 | 0 | 0.35345 | 0.0976 | −34 | 0.35258 | 0.0987 | −26 | 0.35161 | 0.1002 | −22 | 0.35052 | 0.1018 | −24 |
| 0.09 | 0.01 | 0.35629 | 0.0991 | +18 | 0.35547 | 0.1003 | +7 | 0.35455 | 0.1017 | +13 | 0.35349 | 0.1032 | +11 |
| 0.07 | 0.03 | 0.36237 | 0.1031 | +21 | 0.36237 | 0.1040 | +25 | 0.36156 | 0.1054 | +12 | 0.36059 | 0.1067 | +12 |
| 0.05 | 0.05 | 0.37208 | 0.1072 | +15 | 0.37149 | 0.1081 | +3 | 0.37080 | 0.1092 | +2 | 0.36995 | 0.1102 | +13 |
| 0.03 | 0.07 | 0.38548 | 0.1115 | −12 | 0.38508 | 0.1120 | 0 | 0.38459 | 0.1129 | +2 | 0.38396 | 0.1138 | +4 |
| 0.01 | 0.09 | 0.41370 | 0.1155 | −8 | 0.41378 | 0.1160 | −12 | 0.41375 | 0.1167 | −9 | 0.41358 | 0.1175 | −15 |
| Log $\gamma_{1(0)}$ | | −0.09726 ± 0.00016 | | | −0.09844 ± 0.00013 | | | −0.09998 ± 0.00010 | | | −0.10156 ± 0.00012 | | |
| $\alpha_{12}$ | | 0.2018 ± 0.0031 | | | 0.1938 ± 0.0025 | | | 0.1848 ± 0.0019 | | | 0.1755 ± 0.0023 | | |

[a] $\Delta$ = log (exptl activity coeff) − log (value calcd by least squares).

**Table II:** Activity Coefficients of HCl in the System HCl ($m_1$)-$(C_2H_5)_4NCl$ ($m_2$)-$H_2O$ at 0.1 mol $kg^{-1}$ Ionic Strength

| | | 20° | | | 25° | | | 30° | | | 35° | | |
|---|---|---|---|---|---|---|---|---|---|---|---|---|---|
| $m_1$ | $m_2$ | $E$ | $-\text{Log } \gamma_1$ | $10^5\Delta$[a] | $E$ | $-\text{Log } \gamma_1$ | $10^5\Delta$ | $E$ | $-\text{Log } \gamma_1$ | $10^5\Delta$ | $E$ | $-\text{Log } \gamma_1$ | $10^5\Delta$ |
| 0.1 | 0 | 0.35345 | 0.0976 | +12 | 0.35258 | 0.0987 | +13 | 0.35161 | 0.1002 | +15 | 0.35052 | 0.1018 | +7 |
| 0.09 | 0.01 | 0.35637 | 0.0998 | −6 | 0.35555 | 0.1010 | −21 | 0.35462 | 0.1023 | −7 | 0.35355 | 0.1037 | −2 |
| 0.07 | 0.03 | 0.36319 | 0.1038 | −2 | 0.36244 | 0.1046 | +11 | 0.36163 | 0.1060 | −1 | 0.36066 | 0.1073 | −1 |
| 0.05 | 0.05 | 0.37216 | 0.1079 | −8 | 0.37157 | 0.1087 | −6 | 0.37089 | 0.1099 | −15 | 0.37005 | 0.1110 | −9 |
| 0.03 | 0.07 | 0.38553 | 0.1119 | −4 | 0.38514 | 0.1125 | +6 | 0.38467 | 0.1136 | −10 | 0.38404 | 0.1145 | +3 |
| 0.01 | 0.09 | 0.41374 | 0.1158 | +10 | 0.41384 | 0.1165 | −2 | 0.41379 | 0.1171 | +15 | 0.41365 | 0.1181 | +4 |
| Log $\gamma_{1(0)}$ | | −0.09772 ± 0.00006 | | | −0.09883 ± 0.00009 | | | −0.10035 ± 0.00010 | | | −0.10187 ± 0.00004 | | |
| $\alpha_{12}$ | | 0.2020 ± 0.0012 | | | 0.1961 ± 0.0018 | | | 0.1879 ± 0.0018 | | | 0.1808 ± 0.0008 | | |

[a] $\Delta$ = log (exptl activity coeff) − log (value calcd by least squares).

The tetraethylammonium chloride was recrystallized from methanol and then from an acetone–ethanol solvent; in each case the solutions were cooled with a solid carbon dioxide–alcohol mixture. The chloride content of the salt was determined gravimetrically, after drying for two 12-hr periods at 130–140° on a vacuum hotplate. *Anal.* Calcd for $(C_2H_5)_4NCl$: Cl, 21.39, Found: Cl, 21.43; bromide content <0.001 mol %.

*Ethylenediamine Dihydrochloride.* Dilute hydrochloric acid, prepared from doubly distilled acid, was slowly added to BDH ethylenediamine until the pH of the solution was about 2. The salt was recrystallized from ethanol and dried for 18 hr at 20° on a vacuum hotplate. *Anal.* Calcd for $ClNH_3(CH_2)_2NH_3Cl$: Cl, 53.26. Found: Cl, 53.05.

*Hexamethylenediamine Dihydrochloride.* An aqueous solution of BDH hexamethylenediamine was slowly neutralized with pure dilute hydrochloric acid. The solution was concentrated, until the salt started to crystallize, by evaporating[12] the water at a pressure of about 20 mm and a temperature of 45°. A slight discoloration of the salt was removed by shaking a solution of the salt in methanol with carbon black. The hexamethylenediamine dihydrochloride was recrystallized twice from methanol by cooling to the temperature of solid carbon dioxide. Before analysis, it was dried at 20° for 9 hr on a vacuum hotplate. *Anal.* Calcd for $ClNH_3(CH_2)_6NH_3Cl$: Cl, 37.49. Found: Cl, 37.45.

Stock solutions were prepared from the purified reagents and distilled water. The concentration of the solutions was determined, in triplicate, by weighing the chloride as silver chloride. The mixed solutions were made up by weight.

The concentrations of the stock solutions were known to better than ±0.02%. The error in the concentrations of the cell solutions was variable, but it is estimated that the square root of the sum of the squares of errors due to temperature fluctuation, concentration of solution, and response of the electrodes should be less than 0.04 mV. The makers guarantee the accuracy of the potentiometer to 0.1 mV, but it is likely that the difference in potential of two cells can be measured more accurately.

## Results

The measured emf's and the calculated activity coefficients are listed in Tables I to VII. The $E^0$'s used in calculating the activity coefficients by eq 7 were found by measuring the potential of cell I when the electrolyte consisted of 0.01 *m* HCl. These $E^0$s and the values assumed for the activity coefficient of 0.01 *m* HCl are listed in Table VIII. The value of the activity coefficient at 25° is that suggested by Bates, *et al.*,[13] and the

(12) D. H. Everett and B. R. W. Pinsent, *Proc. Roy. Soc.*, **A215**, 416 (1952).

**Table III:** Activity Coefficients of HCl in the System HCl ($m_1$)–BaCl ($I_2$)–$H_2O$ at 0.1 mol $kg^{-1}$ Ionic Strength

| | | 20° | | | 25° | | | 30° | | | 35° | | |
|---|---|---|---|---|---|---|---|---|---|---|---|---|---|
| $m_1$ | $I_2$ | $E$ | $-\text{Log } \gamma_1$ | $10^5\Delta$[a] | $E$ | $-\text{Log } \gamma_1$ | $10^5\Delta$ | $E$ | $-\text{Log } \gamma_1$ | $10^5\Delta$ | $E$ | $-\text{Log } \gamma_1$ | $10^5\Delta$ |
| 0.1 | 0 | 0.35345 | 0.0976 | −8 | 0.35258 | 0.0987 | +1 | 0.35161 | 0.1002 | +11 | 0.35052 | 0.1018 | +11 |
| 0.09 | 0.01 | 0.35706 | 0.0984 | +4 | 0.35626 | 0.0996 | 0 | 0.35538 | 0.1013 | −13 | 0.35434 | 0.1028 | −9 |
| 0.07 | 0.03 | 0.36544 | 0.1003 | −1 | 0.36476 | 0.1014 | −2 | 0.36401 | 0.1029 | −1 | 0.36309 | 0.1043 | +1 |
| 0.05 | 0.05 | 0.37609 | 0.1021 | −4 | 0.37560 | 0.1032 | −3 | 0.37501 | 0.1046 | 0 | 0.37428 | 0.1060 | −10 |
| 0.03 | 0.07 | 0.39130 | 0.1038 | +19 | 0.39106 | 0.1048 | +15 | 0.39072 | 0.1062 | +12 | 0.39023 | 0.1074 | +10 |
| 0.01 | 0.09 | 0.42160 | 0.1060 | −16 | 0.42186 | 0.1068 | −7 | 0.42203 | 0.1081 | −6 | 0.42202 | 0.1091 | 0 |
| Log $\gamma_{1(0)}$ | | −0.09752 ± 0.00009 | | | −0.09871 ± 0.00006 | | | −0.10031 ± 0.00007 | | | −0.10191 ± 0.00007 | | |
| $\alpha_{12}$ | | 0.0924 ± 0.0017 | | | 0.0891 ± 0.0011 | | | 0.0858 ± 0.0014 | | | 0.0798 ± 0.0013 | | |

[a] $\Delta$ = log (exptl activity coeff) − log (value calcd by least squares).

**Table IV:** Activity Coefficients of HCl in the System HCl ($m_1$)–$SrCl_2$ ($I_2$)–$H_2O$ at 0.1 mol $kg^{-1}$ Ionic Strength

| | | 20° | | | 25° | | | 30° | | | 35° | | |
|---|---|---|---|---|---|---|---|---|---|---|---|---|---|
| $m_1$ | $I_2$ | $E$ | $-\text{Log } \gamma_1$ | $10^5\Delta$[a] | $E$ | $-\text{Log } \gamma_1$ | $10^5\Delta$ | $E$ | $-\text{Log } \gamma_1$ | $10^5\Delta$ | $E$ | $-\text{Log } \gamma_1$ | $10^5\Delta$ |
| 0.1 | 0 | 0.35345 | 0.0976 | +28 | 0.35258 | 0.0987 | +37 | 0.35161 | 0.1002 | +43 | 0.35052 | 0.1018 | +37 |
| 0.09 | 0.01 | 0.35712 | 0.0989 | −24 | 0.35633 | 0.1002 | −36 | 0.35545 | 0.1019 | −52 | 0.35439 | 0.1032 | −34 |
| 0.03 | 0.07 | 0.39129 | 0.1037 | −31 | 0.39104 | 0.1047 | −23 | 0.39073 | 0.1062 | −31 | 0.39022 | 0.1073 | −30 |
| 0.01 | 0.09 | 0.42145 | 0.1047 | +27 | 0.42173 | 0.1058 | +22 | 0.42190 | 0.1070 | +40 | 0.42190 | 0.1081 | +27 |
| Log $\gamma_{1(0)}$ | | −0.09788 ± 0.00029 | | | −0.09907 ± 0.00032 | | | −0.10063 ± 0.00044 | | | −0.10217 ± 0.00034 | | |
| $\alpha_{12}$ | | 0.0788 ± 0.0051 | | | 0.0772 ± 0.0056 | | | 0.0752 ± 0.0039 | | | 0.0689 ± 0.0059 | | |

[a] $\Delta$ = log (exptl activity coeff) − log (value calcd by least squares).

**Table V:** Activity Coefficients of HCl in the System HCl ($m_1$)–$ClNH_3(CH_2)_2NH_3Cl$ ($I_2$)–$H_2O$ at 0.1 mol $kg^{-1}$ Ionic Strength

| | | 20° | | | 25° | | | 30° | | | 35° | | |
|---|---|---|---|---|---|---|---|---|---|---|---|---|---|
| $m_1$ | $I_2$ | $E$ | $-\text{Log } \gamma_1$ | $10^5\Delta$[a] | $E$ | $-\text{Log } \gamma_1$ | $10^5\Delta$ | $E$ | $-\text{Log } \gamma_1$ | $10^5\Delta$ | $E$ | $-\text{Log } \gamma_1$ | $10^5\Delta$ |
| 0.1 | 0 | 0.35345 | 0.0976 | −2 | 0.35258 | 0.0987 | +10 | 0.35161 | 0.1002 | +5 | 0.35052 | 0.1018 | −5 |
| 0.09 | 0.01 | 0.35715 | 0.0991 | +5 | 0.35636 | 0.1005 | −15 | 0.35544 | 0.1018 | −4 | 0.35440 | 0.1033 | −5 |
| 0.07 | 0.03 | 0.36569 | 0.1025 | −20 | 0.36502 | 0.1036 | −13 | 0.36426 | 0.1050 | −21 | 0.36334 | 0.1063 | −5 |
| 0.05 | 0.05 | 0.37645 | 0.1052 | +24 | 0.37596 | 0.1063 | +28 | 0.37536 | 0.1075 | +31 | 0.37465 | 0.1090 | +24 |
| 0.03 | 0.07 | 0.39186 | 0.1086 | −1 | 0.39163 | 0.1097 | 0 | 0.39129 | 0.1109 | −7 | 0.39082 | 0.1122 | +4 |
| 0.01 | 0.09 | 0.42228 | 0.1118 | −6 | 0.42258 | 0.1129 | −9 | 0.42273 | 0.1139 | −4 | 0.42280 | 0.1154 | −16 |
| Log $\gamma_{1(0)}$ | | −0.09758 ± 0.00011 | | | −0.09880 ± 0.00012 | | | −0.10025 ± 0.00013 | | | −0.10175 ± 0.00010 | | |
| $\alpha_{12}$ | | 0.1573 ± 0.0021 | | | 0.1557 ± 0.0024 | | | 0.1512 ± 0.0025 | | | 0.1499 ± 0.0019 | | |

[a] $\Delta$ = log (exptl activity coeff) − log (value calcd by least squares).

values at the other temperatures were decided upon by consideration of this value and all the values at the other temperatures listed in Table 10 of a paper by Gupta, Hills, and Ives.[14] It is likely that this procedure results in a slight loss of precision when the temperature variation of the activity coefficients is being considered. When the emf obtained in the present work, for a particular concentration of hydrochloric acid, is compared with that obtained by others considerable deviations are found, but it is obvious that any given experimenter can measure very precisely the difference in potential of two cells containing different concentrations of hydrochloric acid.

The constants, $\alpha_{12}$ and log $\gamma_{1(0)}$, of the Harned rule expression (eq 5) are listed in Tables I to VII. They were calculated by the method of least squares and the errors quoted for these constants are the standard errors obtained by this procedure.

## Discussion

*Tetraalkylammonium Chlorides.* The results show that the addition of tetraethylammonium chloride has nearly the same effect as tetramethylammonium chloride on the activity coefficient of hydrochloric acid, at least at a total ionic strength of 0.1 mol $kg^{-1}$. As a test of the specific interaction theory the $\alpha_{12}$ values may be compared with those calculated from the properties

(13) R. G. Bates, E. A. Guggenheim, H. S. Harned, D. J. G. Ives, G. J. Janz, C. B. Monk, R. A. Robinson, R. H. Stokes, and W. F. K. Wynne-Jones, *J. Chem. Phys.*, **25**, 361 (1956).

(14) S. R. Gupta, G. J. Hills, and D. J. G. Ives, *Trans. Faraday Soc.*, **59**, 1874 (1963).

**Table VI:** Activity Coefficients of HCl in the System HCl ($m_1$)-$ClNH_3(CH_2)_2NH_3Cl$ ($I_2$)-$H_2O$ at 1.0 mol $kg^{-1}$ Ionic Strength

| | | 20° | | | 25° | | | 30° | | | 35° | | |
|---|---|---|---|---|---|---|---|---|---|---|---|---|---|
| $m_1$ | $I_2$ | $E$ | $-\text{Log } \gamma_1$ | $10^5\Delta$[a] | $E$ | $-\text{Log } \gamma_1$ | $10^5\Delta$ | $E$ | $-\text{Log } \gamma_1$ | $10^5\Delta$ | $E$ | $-\text{Log } \gamma_1$ | $10^5\Delta$ |
| 1.0 | 0 | 0.23590 | 0.0871 | −39 | 0.23337 | 0.0912 | −26 | 0.23081 | 0.0960 | −30 | 0.22804 | 0.1002 | −28 |
| 0.9 | 0.1 | 0.24058 | 0.0971 | −9 | 0.23811 | 0.1010 | +2 | 0.23559 | 0.1055 | +7 | 0.23289 | 0.1096 | +4 |
| 0.7 | 0.3 | 0.25109 | 0.1173 | +30 | 0.24880 | 0.1213 | −10 | 0.24642 | 0.1254 | −7 | 0.24385 | 0.1291 | −4 |
| 0.5 | 0.5 | 0.26393 | 0.1379 | +30 | 0.26175 | 0.1410 | +37 | 0.25954 | 0.1447 | +38 | 0.25716 | 0.1482 | +30 |
| 0.3 | 0.7 | 0.28130 | 0.1582 | +59 | 0.27938 | 0.1609 | +64 | 0.27742 | 0.1643 | +54 | 0.27527 | 0.1673 | +62 |
| 0.1 | 0.9 | 0.31390 | 0.1801 | −71 | 0.31248 | 0.1824 | −68 | 0.31101 | 0.1852 | −61 | 0.30939 | 0.1880 | −64 |
| Log $\gamma_{1(0)}$ | | −0.08671 ± 0.00037 | | | −0.09094 ± 0.00035 | | | −0.09570 ± 0.00032 | | | −0.09992 ± 0.00033 | | |
| $\alpha_{12}$ | | 0.1030 ± 0.0007 | | | 0.1009 ± 0.0007 | | | 0.0988 ± 0.0006 | | | 0.0972 ± 0.0006 | | |

[a] $\Delta$ = log (exptl activity coeff) − log (value calcd by least squares).

**Table VII:** Activity Coefficients of HCl in the System HCl ($m_1$)-$ClNH_3(CH_2)_6NH_3Cl$ ($I_2$)-$H_2O$ at 0.1 mol $kg^{-1}$ Ionic Strength

| | | 20° | | | 25° | | | 30° | | | 35° | | |
|---|---|---|---|---|---|---|---|---|---|---|---|---|---|
| $m_1$ | $I_2$ | $E$ | $-\text{Log } \gamma_1$ | $10^5\Delta$[a] | $E$ | $-\text{Log } \gamma_1$ | $10^5\Delta$ | $E$ | $-\text{Log } \gamma_1$ | $10^5\Delta$ | $E$ | $-\text{Log } \gamma_1$ | $10^5\Delta$ |
| 0.1 | 0 | 0.35345 | 0.0976 | −24 | 0.35258 | 0.0987 | −8 | 0.35161 | 0.1002 | −4 | 0.35052 | 0.1018 | −12 |
| 0.09 | 0.01 | 0.35710 | 0.0987 | +1 | 0.35630 | 0.1000 | −5 | 0.35539 | 0.1014 | +3 | 0.35434 | 0.1028 | +10 |
| 0.07 | 0.03 | 0.36555 | 0.1012 | +22 | 0.36490 | 0.1026 | +1 | 0.36414 | 0.1040 | −2 | 0.36323 | 0.1054 | −6 |
| 0.05 | 0.05 | 0.37630 | 0.1039 | +23 | 0.37581 | 0.1050 | +27 | 0.37523 | 0.1064 | +13 | 0.37447 | 0.1076 | +18 |
| 0.03 | 0.07 | 0.39166 | 0.1069 | −6 | 0.39143 | 0.1080 | −7 | 0.39108 | 0.1092 | −12 | 0.39058 | 0.1103 | −8 |
| 0.01 | 0.09 | 0.42204 | 0.1097 | −15 | 0.42231 | 0.1107 | −11 | 0.42245 | 0.1116 | +3 | 0.42247 | 0.1127 | −4 |
| Log $\gamma_{1(0)}$ | | −0.09736 ± 0.00014 | | | −0.09862 ± 0.00011 | | | −0.10016 ± 0.00006 | | | −0.10168 ± 0.00009 | | |
| $\alpha_{12}$ | | 0.1355 ± 0.0028 | | | 0.1330 ± 0.0020 | | | 0.1275 ± 0.0012 | | | 0.1220 ± 0.0017 | | |

[a] $\Delta$ = log (exptl activity coeff) − log (value calcd by least squares).

**Table VIII:** Potentials of Cell Containing 0.01 $m$ HCl and Standard Potentials of Ag-AgCl Electrode

| Temp, °C | Corr emf | $\gamma$ | $E^0$, abs V |
|---|---|---|---|
| 20 | 0.46347 | 0.905 | 0.22577 |
| 25 | 0.46440 | 0.904 | 0.22258 |
| 30 | 0.46519 | 0.903 | 0.21926 |
| 35 | 0.46583 | 0.902 | 0.21579 |

of the single electrolytes. It appears that the only free energy data available for tetramethyl and tetraethylammonium chloride at 25° are the isopiestic results of Lindenbaum and Boyd.[15] They list smoothed values of the osmotic coefficient $\phi$, at round molalities. The values of $\phi$ at 0.1 mol $kg^{-1}$ can be used with the osmotic coefficient of hydrochloric acid at the same concentration, to calculate $\alpha_{12}$ using the equation

$$\alpha_{12} = \frac{\phi_1 - \phi_2}{2.303m} \quad (8)$$

which is eq 34-32 given by Pitzer and Brewer.[3] The osmotic coefficients used and the experimental and calculated values of $\alpha_{12}$ are given in Table IX. The agreement between calculated and experimental $\alpha_{12}$ values does not appear to be close enough to confirm the Bronsted-Guggenheim theory for these systems. For agreement, the osmotic coefficients of the quaternary ammonium chlorides would need to be about 0.900 at 0.1 mol $kg^{-1}$. However, the osmotic coefficients listed by Lindenbaum and Boyd for these two salts at 0.1 mol $kg^{-1}$ are extrapolated values obtained from results at higher concentrations and are therefore subject to correction when experimental data for dilute solutions become available. Some idea of the uncertainty involved in the extrapolation may be gained by comparing their estimated value of 0.910 for tetramethylammonium bromide at 0.1 mol $kg^{-1}$ with Levien's[16] experimental result of 0.8981 at the same concentration. Therefore, it would seem that the specific interaction theory may predict the correct value of $\alpha_{12}$, but confirmation will have to wait till more accurate values for the osmotic

**Table IX:** Osmotic Coefficients of Added Salts and the Harned Coefficient $\alpha_{12}$ at 25°

| Electrolyte | $\phi$, 0.1 $m$ | $\alpha_{12}$ calcd | $\alpha_{12}$ exptl |
|---|---|---|---|
| $(CH_3)_4NCl$ | 0.914[a] | 0.126 | 0.194 |
| $(C_2H_5)_4NCl$ | 0.913[a] | 0.130 | 0.196 |
| HCl | 0.943[b] | | |

[a] From ref 15. [b] From ref 6, p 483.

(15) S. Lindenbaum and G. E. Boyd, *J. Phys. Chem.*, **68**, 911 (1964).
(16) B. J. Levien, *Aust. J. Chem.*, **18**, 1161 (1965).

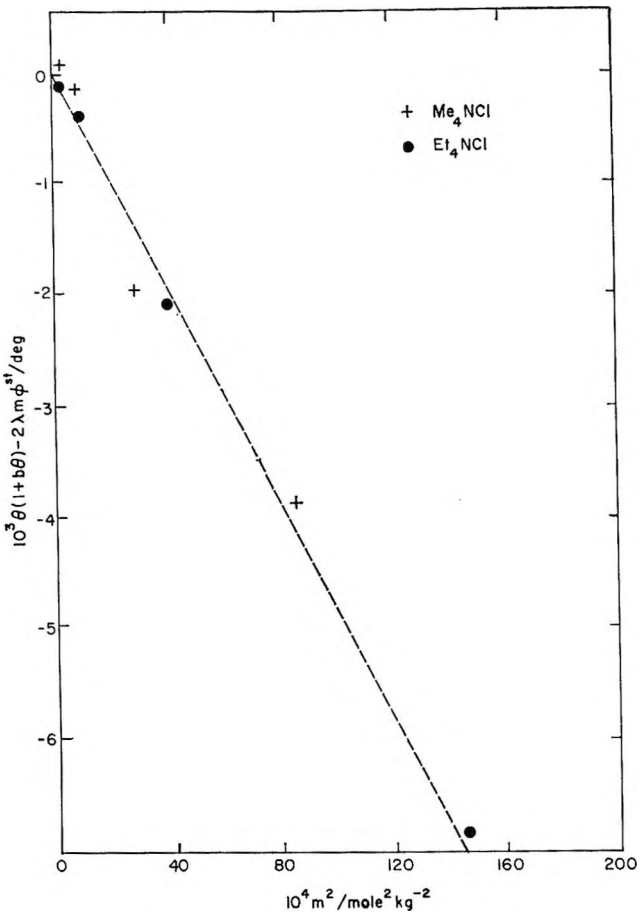


Figure 1. Results obtained by treating Lange's[17] freezing point measurements for $Me_4NCl$ and $Et_4NCl$ by the method of Guggenheim and Turgeon.[2]

coefficients of the two quaternary ammonium chlorides in dilute solutions are available.

Lange[17] has measured the freezing point depressions of aqueous solutions of many quaternary ammonium halides. His results for tetramethylammonium chloride and tetraethylammonium chloride can be treated by the method used by Guggenheim and Turgeon[2] in their analysis of freezing point data to give specific interaction coefficients for these salts. They derive an equation

$$\theta(1 + b\theta) - (\nu_+ + \nu_-)\lambda m\phi^{st} = 2\nu_+\nu_-\beta\lambda m^2 \quad (9)$$

where the cryoscopic constants $\lambda$ and $b$ have the values $\lambda = 1.860$ deg mol$^{-1}$ kg, $b = 4.8 \times 10^{-4}$ deg$^{-1}$, and $\theta$ is the freezing point depression. They define $\phi^{st} = 1 - {}^1/_3\alpha Z_+Z_-I^{1/2}\sigma(I^{1/2})$ where $\sigma$ is the function

$$\sigma(y) = \frac{3}{y^3}\left[1 + y - \frac{1}{1+y} - 2\ln(1+y)\right] \quad (10)$$

this corresponds to assuming $\log \gamma^{st} = AZ_+Z_-I^{1/2}/1 + I^{1/2}$. If the left-hand side of eq 9 is plotted against $m^2$ the interaction coefficient $\beta$ may be evaluated. The results of these calculations are shown in Figure 1 and, as there are few points at the higher concentrations, the values of $\beta$ at the two highest concentrations for each salt were evaluated directly and are listed in Table X. If the mean of each of these pairs is used and $\beta_{H,Cl}$ is taken[2] to be 0.27 mol$^{-1}$ kg, then $\alpha_{12}$ can be calculated from eq 6. These values of $\alpha_{12}$ are compared with the experimental values in Table XI. Considering the 25° difference in the temperature, the correlation is satisfactory though the temperature coefficient of $\alpha_{12}$, if it remains constant, suggests that $\alpha_{12}$ for both mixtures would be about 0.235 at 0°, in which case $\beta_{R_4N,Cl}$ must be about $-0.29$ mol$^{-1}$ kg if the specific interaction theory is correct. Unfortunately, Lange's results must be treated with caution as Brown and Prue[18] have shown that his measurements of the freezing point depression of aqueous potassium chloride solutions are not very accurate.

**Table X:** Interaction Coefficients for Quaternary Ammonium Salts at 0°

| Salt | Molality | $\beta^a$ |
|---|---|---|
| $(CH_3)_4NCl$ | 0.05342 | −0.19 |
| $(CH_3)_4NCl$ | 0.0924 | −0.12 |
| $(C_2H_5)_4NCl$ | 0.06302 | −0.14 |
| $(C_2H_5)_4NCl$ | 0.1209 | −0.13 |

[a] Calculated using data in ref 17.

**Table XI:** Harned Coefficients for HCl–$R_4NCl$–$H_2O$ Systems at 25°

| Added salt | $\alpha_{12}$ calcd | $\alpha_{12}$ exptl |
|---|---|---|
| $(CH_3)_4NCl$ | 0.23 | 0.194 |
| $(C_2H_5)_4NCl$ | 0.18 | 0.196 |

*Alkaline Earth Chlorides.* The variation of the activity coefficient of hydrochloric acid in mixtures with barium chloride and with strontium chloride, at a constant total ionic strength of 0.1 mol kg$^{-1}$, is listed in Tables III and IV and it is evident from the $\Delta$ values that hydrochloric acid follows Harned's rule in the HCl–$BaCl_2$–$H_2O$ system, and probably does so in the HCl–$SrCl_2$–$H_2O$ system, though in this case there are insufficient experimental points to be sure.

The results at 25° are compared in Table XII with Smith's[19] results for the HCl–$MgCl_2$–$H_2O$ system and with Covington's[4] results for the HCl–$CaCl_2$–$H_2O$ system. From the list given by Guggenheim and Stokes,[20] the order of the activity coefficients of the pure

(17) J. Lange, *Z. Phys. Chem., Abt A*, **168**, 147 (1934).

(18) P. G. M. Brown and J. E. Prue, *Proc. Roy. Soc.*, **A232**, 320 (1955).

(19) R. F. Smith, Ph.D. Thesis, University of Otago, 1962, unpublished.

(20) E. A. Guggenheim and R. H. Stokes, *Trans. Faraday Soc.*, **54**, 1646 (1958).

**Table XII:** Activity, Interaction, and Harned Coefficients for HCl–Alkaline Earth Chloride–$H_2O$ Systems at 25°

| Salt | Log $\gamma$ at 0.03 $m$ | $B_{M,Cl}$ | $\alpha_{12}$ calcd | $\alpha_{12}$ exptl |
|---|---|---|---|---|
| $MgCl_2$ | −0.2072 | 1.11 ± 0.06[d] | 0.017 ± 0.008 | 0.0521[a] |
| $CaCl_2$ | −0.2109 | 1.00 ± 0.06[d] | 0.031 ± 0.008 | 0.0506 ± 0.0043[b] |
| $SrCl_2$ | −0.2112 | 0.99 ± 0.06[d] | 0.032 ± 0.008 | 0.0772 ± 0.0056[c] |
| $BaCl_2$ | −0.2132 | 0.93 ± 0.06[d] | 0.040 ± 0.008 | 0.0891 ± 0.0011[c] |

[a] Data from ref 19 with standard error approximately the same as for $BaCl_2$. [b] Data from ref 4. [c] Present work. [d] Calculated from data in ref 20.

salts at 0.1 mol $kg^{-1}$ is $MgCl_2 > CaCl_2 > SrCl_2 > BaCl_2$. Apart from the possible inversion of $MgCl_2$ and $CaCl_2$, the magnitude of the effect of these salts on the activity coefficient of HCl is in the reverse order—the salt with the lowest activity coefficient decreases the activity coefficient of HCl by the greatest amount. An analogous relationship has been found with mixtures of hydrochloric acid and the alkali chlorides.[21]

The validity of the specific interaction theory for these mixtures of 1:1 and 2:1 valency type electrolytes at 25° can be tested by comparing the experimental Harned coefficients $\alpha_{12}$ with the values calculated (using eq 6) from the properties of the single electrolytes. The value assumed[2] for $B_{H,Cl}$ is 0.234 $mol^{-1}$ kg and the specific interaction coefficients for the alkaline earth chlorides can be calculated by substituting values for the activity coefficients at 0.03 $m$ in eq 4. The parameters given by Guggenheim and Stokes[20] were used to calculate these activity coefficients. They are therefore wholly dependent, except for calcium chloride, on the results of isopiestic measurements at concentrations of 0.1 $m$ and above. The alkaline earth chloride specific interaction coefficients and the calculated $\alpha_{12}$ values are listed in Table XII. The errors calculated for $B$ and $\alpha_{12}$ assume that log $\gamma$ for the added salt is known within ±0.002 and that the error in $B_{H,Cl}$ can be neglected.

These results show that the specific interaction theory is probably consistent with the result for the HCl–$CaCl_2$–$H_2O$ system but not for the others. It must be remembered in making these tests that the deviations to be expected are not large. Indeed, the difference between the calculated and experimental activity coefficient of a trace of HCl in 0.03 $m$ $BaCl_2$ corresponds to a difference in emf of about 0.5 mV. However, it is believed that such deviations are outside experimental error.

The value of $\alpha_{12}$ (experimental) listed in Table XII for HCl–$CaCl_2$–$H_2O$ mixtures was calculated from Covington's measurements[4] noting that values of log $\gamma_{HCl(CaCl_2)}$ − log $\gamma_{HCl(0)}$ in Table 1 of his paper should be negative (this alteration changes the slope of the line of Figure 1 of his paper), and that his expression for $\ln\gamma_{HCl(MCl_2)}$ is incorrect. He gives (eq 3 of ref 3)

$$\ln \gamma_{HCl(MCl_2)} - \ln \gamma_{HCl(0)} = (\beta_{H,Cl} - {}^1/_3\beta_{M,Cl})xI + {}^1/_3\beta_{M,Cl}I - \beta_{H,Cl}I$$

where $m_{H^+} = xI$ and $m_{Ca^{2+}} = {}^1/_3(1 - x)I$. This should be

$$\ln \gamma_{HCl(MCl_2)} - \ln \gamma_{HCl(0)} = ({}^4/_3\beta_{H,Cl} - {}^1/_3\beta_{M,Cl})xI + {}^1/_3\beta_{M,Cl}I - {}^4/_3\beta_{H,Cl}I$$

The incorrect expression is consistent with taking $m_{Cl^-} = I$ whereas it should be $m_{Cl^-} = xI + {}^2/_3(1 - x)I$. With these corrections we find

$$\alpha_{12} = \frac{1}{2.303}({}^4/_3\beta_{H,Cl} - {}^1/_3\beta_{Ca,Cl}) \qquad (11)$$

(which is in accord with eq 6) compared with Covington's equation

$$\alpha_{12} = \frac{1}{2.303}(\beta_{H,Cl} - {}^1/_3\beta_{Ca,Cl})$$

and, assuming as did Covington that $B_{H,Cl} = 0.22$ $mol^{-1}$ kg, $B_{Ca,Cl} = 0.77$ $mol^{-1}$ kg compared with Covington's calculation of $B_{Ca,Cl} = 0.55$ $mol^{-1}$ kg.

*Bolaform Electrolytes.* By measuring the acid dissociation of diammonium ions, Everett and Pinsent[12] were able to state that the distance over which an ion exerts a significant influence on the solvent structure is roughly 5 Å, since when two unit positive charges are 5 Å apart their zones of influence overlap very considerably, while at a separation of 10 Å this effect has almost disappeared. Catalin atomic models suggest an intercharge distance of 9 Å for the hexamethylenediammonium ion and 4.5 Å for the ethylenediammonium ion though these lengths are dependent, especially for the longer chain, on the configuration given to the linkages. The value quoted for the hexamethylenediammonium ion is for the chain fully extended. It was thought possible that these ions, because of the separation of their charges, might not behave as +2 ions with regard to their contribution to the ionic strength and that Harned's rule might not be valid for these systems.

From the results at an ionic strength of 0.1 mol $kg^{-1}$ listed in Tables V and VII it is clear that the variation of the activity coefficient of hydrochloric acid in the mixtures follows Harned's rule closely and that the ethylenediamine and hexamethylenediamine bolions decrease the activity coefficient of hydrochloric acid to a

(21) Reference 5, p 594.

greater extent than do the alkaline earth cations. The results listed in Table VI for the hydrochloric acid–ethylenediamine dihydrochloride system show that, even at an ionic strength of 1.0 mol $kg^{-1}$, the activity coefficient of hydrochloric acid has a linear variation at constant total ionic strength though the deviations are larger. The effects sought at these comparatively low concentrations might become apparent at higher ionic strengths as Bonner, Rushing, and Torres[22] have reported that the bolaform electrolyte, ethanedisulfonic acid, behaves similarly to other 1:2 electrolytes in dilute solutions, while in concentrated solutions its behavior approaches that of a solution of a 1:1 electrolyte of twice the molality. The behavior of the diammonium ions may be more complicated than some other bolions which are rigid as the intercharge distance may be concentration dependent. As Bower and Robinson[23] have shown that the linear variation of activity coefficients is not restricted to constant ionic strength, but is also applicable at total ionic concentration for some mixtures, the interpretation of results at high ionic strength in terms of ionic models is unlikely to be simple.

## Conclusions

On consideration of the results obtained in this and other work it appears that the specific interaction theory gives a valid description of the behavior of many dilute mixed solutions of strong 1:1 electrolytes. There is reasonable evidence to suggest that this theory is approximate for mixtures containing multiply charged ions. The Harned rule has been shown to apply to hydrochloric acid in some dilute mixed solutions containing bolaform electrolytes.

*Acknowledgment.* I wish to thank Professors M. H. Panckhurst and H. N. Parton for their assistance. This research was carried out during the tenure of a Research Fund Fellowship awarded by the New Zealand University Grants Committee.

(22) O. D. Bonner, C. Rushing, and A. L. Torres, *J. Phys. Chem.*, **72**, 4290 (1968).

(23) R. A. Robinson and V. E. Bower, *J. Res. Nat. Bur. Stand.*, **A69**, 19 (1965).

# Coalescence of Synthetic Latices. Surface Energy through Differential Calorimetry

**by T. G. Mahr**

*Film Research Laboratory, Experimental Station, E. I. du Pont de Nemours and Company, Wilmington, Delaware 19898* *(Received August 4, 1969)*

Surface energy of amorphous, synthetic latices was measured by employing differential thermal analytical methods. Latices consisting of polystyrene and various polyvinylidene chloride type copolymers were freeze-dried and specific surfaces, measured by electron microscopy and gas adsorption, were correlated. From quantitative evaluation of the sintering curves the following conclusions were reached. 1. Coalescence of latices proceeds in the absence of water. 2. From thermal analytical measurements surface tension can be calculated, if the specific surface is known. 3. The technique is generally applicable to measure surface energy, sintering, and film formation of amorphous systems of high specific surface.

## Introduction

The term "synthetic latex" refers to colloidal suspensions of synthetic polymers prepared by emulsion or suspension polymerization.[1] With different compositions and varied preparation conditions, they can be made into a variety of colloidal dispersions with spherical particles having different sizes, size distributions, and second-order (glass) transition temperatures. From the theoretical point of view they are a suitable model system for observing viscous flow, sintering, and surface phenomena. As will be discussed, conclusions can be applied to disperse systems in general containing amorphous particles.

Many recent papers deal with the sintering of synthetic latices.[2-5] One theory attributes the major

(1) F. A. Bovey, *et al.*, "Emulsion Polymerization," Interscience Publishers, New York, N. Y., 1955, p 3.

(2) D. P. Seetz, *J. Appl. Polym. Sci.*, **9**, 3759 (1965).

**Table I:** Synthetic Latices

| No. | Polymer | Part. size diam, $\mu$ | $T_g$ or mp, °C | Specific gravity, g/cm³ | Theor sp surface, m²/g | |
|---|---|---|---|---|---|---|
| 1 | Polystyrene[a] I | 0.109 | ~100.0 | 1.05[e] | 52.0 | Monodisperse, solids: 10% std dev in diam, 0.0027 $\mu$, no. meas 318, run no. LS-1044E |
| 2 | Polystyrene[a] II | 0.126 | ~100.0 | 1.05[e] | 45.0 | Monodisperse, solids: 10% stn dev in diam, 0.0043 $\mu$, no. meas 328, run no. LS-052A |
| 3 | Polystyrene[a] III | 0.234 | ~100.0 | 1.05[e] | 23.0 | Monodisperse, solids: 10% stn dev in diam, 0.0026 $\mu$, no. meas 245, run no. LS-1047E |
| 4 | 77%[b] vinylidene chloride by weight (Saran I)[c](6) | ~0.0370 | ~32.0 | 1.60[d] | ~90.0 | Polydisperse |
| 5 | 93%[b] vinylidene chloride by weight (Saran II)[c,f] | ~0.0750 | ~160.0 | ... | ~40.0 | Polydisperse |

[a] Bioproducts Dept., The Dow Co., Midland, Mich. [b] Film Dept., Du Pont Co., Wilmington, Del. [c] Trade Mark of the Dow Chemical Co. [d] By analytical ultracentrifugation, electron microscopy and furnished with polystyrene samples by the Dow Chemical Co. [e] H. W. McCormick, *J. Colloid Sci.*, **19**, 179 (1964). [f] ASTM D883.

driving force in the sintering of latices (and for that matter, any material of high specific surface in the presence of a liquid) to capillary pressure,[4] and subsequent authors have accepted as fact that the evaporation of the liquid dispersion media and sintering (I use the term sintering instead of coalescence for phenomenological reasons) are not only concurrent events but energetically interrelated. Experiments supporting this theory fail to separate and examine independently the two phenomena.

This study attempted to separate sintering from evaporation of the dispersion media both in time and for the energy balance. The present paper examines sintering of latex particles by measuring the disappearance of their large specific surface. The basic method applied is differential thermal analysis. In a following article the sintering of latices in the presence of water will be discussed.

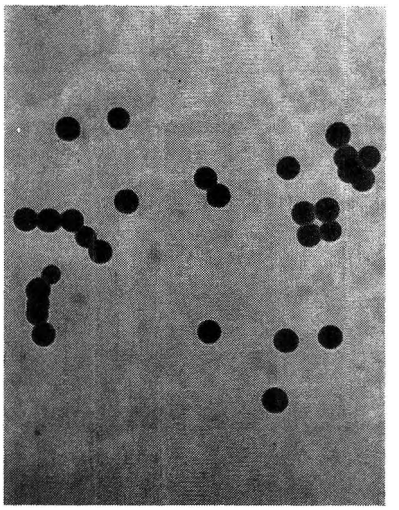

Figure 1. Electromicrograph of Dow monodisperse polystyrene latex, about 110,000×; average particle size diameter 0.109 $\mu$.

## Experimental Section

*Materials.* For this study chemical composition, molecular weight, branching, etc., of the macromolecules which form the particulates are important only to the extent that they determine certain physical and surface characteristics of the system. Among these are second-order (glass) transition temperature and crystallinity.

Properties of the dispersions used in this study are given in Table I. The Dow polystyrene samples (I–III in Table I) form a series of well-defined amorphous, synthetic latices, containing spherical particles of uniform diameter within a given latex (Figure 1). The theoretical specific surfaces were calculated using the particle diameters and specific gravities.

*Methods of Sample Preparations and Measurement.* *1. Lyophilization (Freeze-Drying).* (All samples were dialyzed exhaustively for removal of surfactants and ionic impurities.) In this method, the water is quickly frozen and the ice is sublimed at low temperatures and under vacuum. In freeze-drying the latex particles are locked into position and should not migrate. It is not always feasible to preserve the original particulate structure by this method. In the process of freezing, various structures of ice develop with accompanying pressures which affect the particle size of the latex before the ice even starts to sublime. Our materials, being in a quasi-glassy state, tend to form junctions between the particles on drying with a reduction in the

(3) J. W. Vanderhoff, *et al.*, *J. Macromol. Chem.*, 1, 361 (1966).
(4) G. L. Brown, *J. Polym. Sci.*, 22, 423 (1956).
(5) P. K. Issacs, *J. Macromol. Chem.*, 1, 163 (1965).

specific surface. Freezing was done in a thermostat at $-10°$,[6] and this temperature was maintained during sublimation. The solids content of the latices did not exceed 10% polymer by weight. The ice was sublimed into a trap immersed in a trichloroethylene–Dry Ice mixture. The pressure in the system at the end of the procedure was <0.005 Torr.

*2. Measurement of Specific Surface of Lyophilized Latices.* We wanted to follow latex sintering by thermal changes in the system arising from surface disappearance. Therefore, we had to be sure that prior to measurement the latices possessed a significant fraction of the original specific surface. This was determined by electron microscopy (Figure 2) and by nitrogen adsorption, using the Perkin-Elmer 212C Sorptometer. In the Dow polystyrene samples and Saran II the total original surface was preserved as measured by nitrogen adsorption. Electron micrographs showed virtually no junctions between particles. Saran I partially sintered during lyophilization (Table II and Figure 3).

**Table II:** Correlations between Theoretical and Surface Areas Determined by Sorptometry

| Polymer[a] | Specific surface area, $m^2/g$ — Theor | Measd |
|---|---|---|
| Polystyrene I | 52.0 | 51.4 |
| Polystyrene II | 45.0 | 46.9 |
| Polystyrene III | 23.0 | 23.9 |
| Saran I | ~90.0 | ~18.0 |
| Saran II | ~40.0 | ~40.0 |

[a] See Table I.

*3. Particle Size Determination.* Sedimentation velocities were measured with the Beckman Spinco Model E analytical ultracentrifuge. Because of their size and spherical shape the displacement by diffusion of the latex particles is negligible, and the sedimentation coefficient can be related to particle diameter by means of Stoke's law

$$d = \frac{2(\rho_0\eta_0 S_0)}{2(\rho_1 - S_0)} \qquad (1)$$

where $S_0$ = sedimentation coefficient, $\eta_0$ = viscosity of dispersion medium at run temperature, $\rho_1$ = density of polymer at run temperature, $\rho_0$ = density of dispersion medium at run temperature.

*4. Thermal Analysis. a. General.* All thermal measurements were made with the Du Pont 900 differential thermal analyzer and the 900 350 plug-in module calorimeter cell. The calibration coefficient was determined with the six-metal method. The basic equation for the calorimeter cell using the Du Pont 900 X-Y plotter is (Instruction Manual, p II–5).

$$\Delta h(\text{mcal/mg}) = \frac{EA\Delta T_s T_s}{Ma} \qquad (2)$$

where $\Delta h$ is the specific enthalpy change in cal/g, $E$ is the calibration coefficient, cal/deg min, $A$ is the

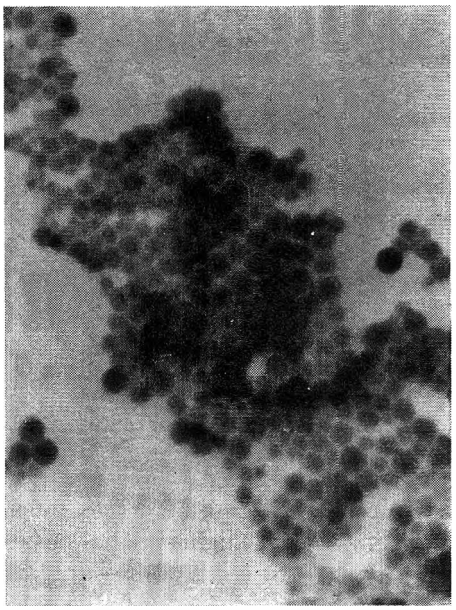

Figure 2. Electromicrograph of No. 5 Saran II latex (Table I) after lyophilization, about 110,000×; average particle size diameter 0.075 μ.

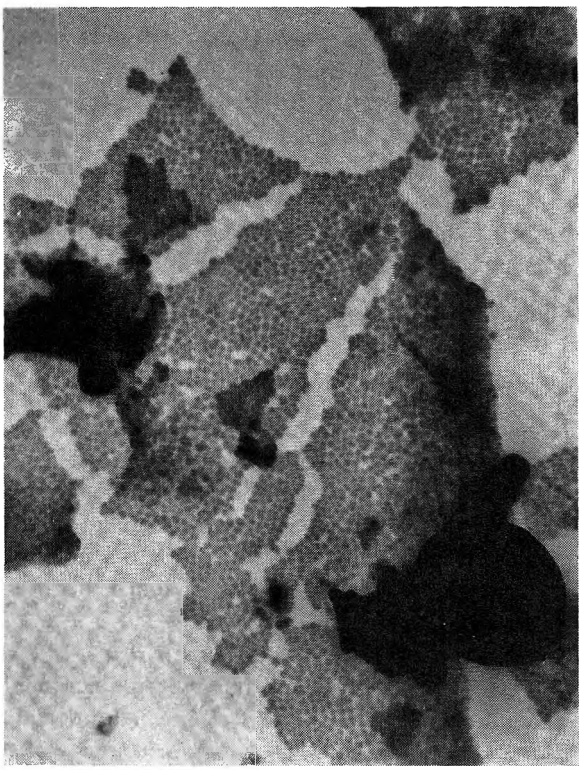

Figure 3. Electromicrograph of No. 4 Saran I latex (Table I) after lyophilization, about 60,000×; average particle size diameter 0.038 μ.

(6) S. Murou and F. Nomura, *Kogyo Kagaka Zasshi*, **68**, 1800 (1965).

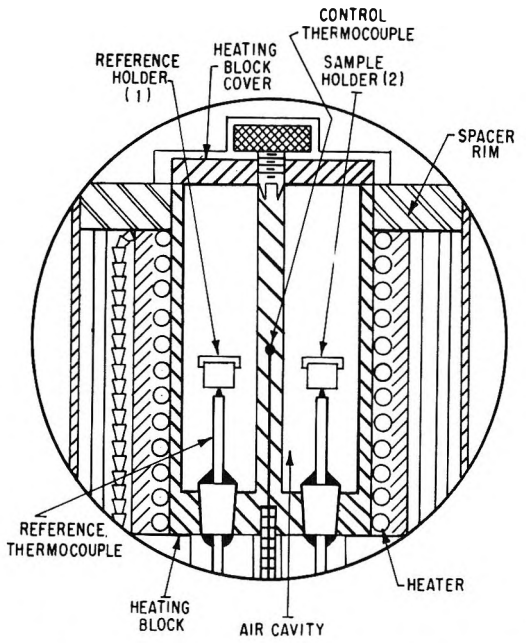


Figure 4. Du Pont 900–350 plug-in module calorimetric cell.

peak area, in.$^2$, $\Delta T_s$ is the $Y$-axis sensitivity setting, deg/in., $T_s$ is the $X$-axis sensitivity setting, deg/in., $M$ is the sample mass, g, $a$ is the heating rate, deg/min.

*b. Calorimetric Compensation Method.* A simple modification of the differential calorimetric method is proposed here to distinguish between reversible and irreversible changes which occurred in the system during thermal analysis. This method, which we term the calorimetric compensation method (CCM), is based on the reversibility of the systems heat capacity, heat conductivity and second-order (glass) transition. (This is "exactly" true only in amorphous material.)

To visualize this method, see Figure 1, which illustrates the calorimeter cell (Figure 4). It is equipped with two holders (or cups) (1) and (2). Holder (1) is the reference holder and (2) is the sample holder.

From the lyophilized latex being measured, two samples identical in weight (to ~2%) are measured into two "liners" supplied with the calorimetric cell. (These liners are constructed so that weight difference between them is less than 0.1 mg.) The analysis is performed in consecutive steps, A, B, and C. It is recommended that the instrument settings (program) be kept constant during all three steps.

*Step A.* A premeasured dried latex sample is placed in the sample holder (2), and a usual run is performed. This must be terminated before the cell temperature reaches the decomposition temperature of the material.

*Step B.* After the calorimeter cell is cooled to the original starting temperature, the sample is carefully transferred from sample holder (2) to reference holder (1). Now, a second premeasured (and not yet heated) sample is placed in the sample holder (2). We repeat

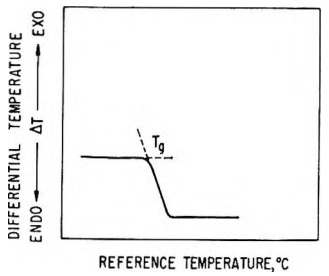


Figure 5. Idea. dta diagram of a second-order (glass) transition.

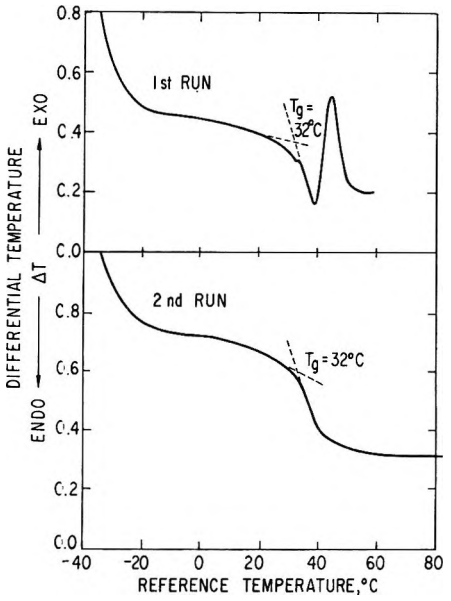


Figure 6. Dta diagram of lyophilized No. 4 Saran I latex.

the thermal run as in step A, with samples in both holders. The sample in the reference holder (1) will show the reversible thermal changes, whereas the fresh sample in the sample holder (2) will show both reversible and irreversible changes. We assume the only irreversible change is the disappearance of the specific surface or sintering (coalescence, film formation) of the latices.

*Step C. Control Step.* After the cell is cooled once more, the test run is performed without touching the two samples. In this test, both samples will undergo only the reversible changes, they should balance each other, and the resultant thermogram should be a regular base line for the instrument.

## Results

Results of our measurements are in Figures 5–10. Figure 5 shows a second-order (glass) transition for the "ideal" case in a dta diagram. (We used both dta and calorimetric modes. The two do not differ fundamentally. We used dta for depicting a change qualitatively and then made quantitative determinations by a calorimetric method.) It should make no difference if we go from low to high temperature or in

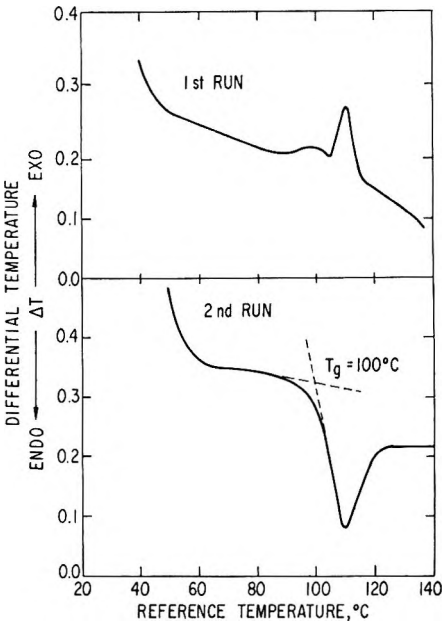


Figure 7. Differential calorimetric diagram of lyophilized No. 1 Dow monodisperse polystyrene I latex, average particle size diameter 0.109 $\mu$.

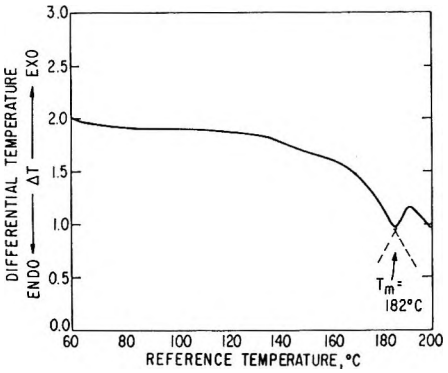


Figure 8. Dta diagram of No. 5 Saran II lyophilized latex.

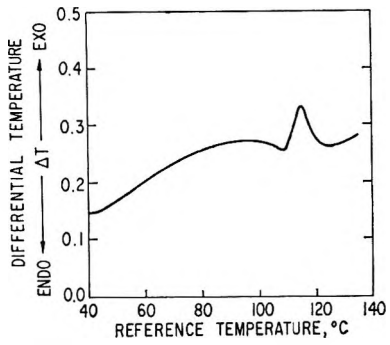


Figure 9. Calorimetric compensation method, step A of No. 1 Dow monodisperse polystyrene I lyophilized latex.

reverse. Figure 6 shows the actual dta curve of a lyophilized No. 4 type latex. (See Table I.) Although this is a very "soft" latex ($T_g$ ~32°), some surface was still preserved prior to the dta measurement. Figure

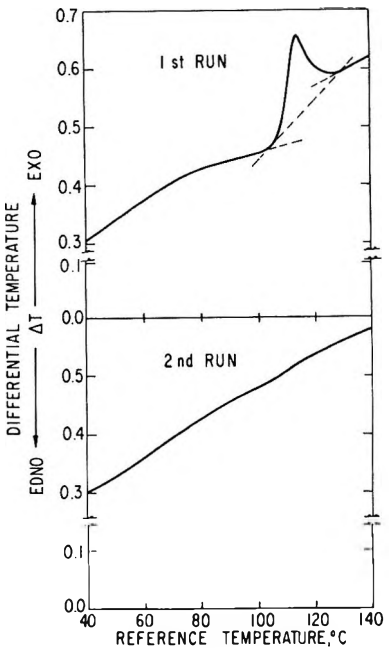


Figure 10. Calorimetric compensation method of No. 1 Dow monodisperse polystyrene I lyophilized latex: step B, first run; step C, second run.

7 is a similar dta curve for the Dow monodisperse polystyrene latex with particle size of 0.109 $\mu$. In this sample, the theoretical surface was preserved in the freeze-drying operation. Figure 8 is the special case of latex No. 5, a Saran II which is crystalline. Figure 9 illustrates a scan in the calorimetric mode for latex No. 1. This figure is the quantitative equivalent of Figure 7. We can thus assign a caloric value to the area under the maximum. Figure 10 illustrates the use of the calorimetric compensation technique applied to latex No. 1.

*Calculations.* For the calorimetric compensation mode (holds strictly only for purely amorphous material) we assume that the only energy change involves the loss of surface and thus

$$F_1 - F_2 = \Delta F = \gamma_0 \Delta S \qquad (3)$$

where $F_1$ is the free energy of the material already sintered (in reference holder); $F_2$ is the free energy of the fresh material of identical weight (in the sample holder). $\gamma_0$ is the surface tension and $\Delta S$ is the change in the total area in cm$^2$.

If we further assume that the original surface area of the lyophilized latices practically disappeared in the sintering process then the surface enthalpy

$$U^s \text{ (erg cm}^{-2}) = \frac{(4.184 \times 10^6)\Delta h}{Ms} = \frac{\Delta H}{\Delta S} \qquad (4)$$

where $s$ is the specific surface in m$^2$/g as determined by electron microscopy and nitrogen adsorption.

The results are shown in Table III. Division by $\Delta S$, using eq 3 and 4, gives eq 5. If 0.06 dyn cm$^{-1}$

**Table III:** Surface Energy Calculations from the Calorimetric Compensation Method (CCM) Lyophilized Synthetic Latices

| Sample | Spec surf, $m^2/g$ meas | Sample wt, $T_g$ | Area under curve, in.$^2$ | Calcd eq, cal/g | $10^7$ ergs | Surf energy $U^s$, erg/cm$^2$ | Temp[a] of $T_g$ | Remarks |
|---|---|---|---|---|---|---|---|---|
| Polystyrene I | 51.4 | 13.0 | 0.667 | 0.563 | 2.36 | 45.9 | 106.0 | |
| | | 14.6 | 0.776 | 0.574 | 2.40 | 46.7 | 106.0 | |
| | | 13.9 | 0.746 | 0.578 | 2.42 | 47.1 | 106.0 | |
| Polystyrene II | 46.9 | 14.8 | 0.666 | 0.486 | 2.04 | 43.6 | 106.0 | |
| Polystyrene III | 23.9 | 16.0 | 0.303 | 0.205 | 0.86 | 36.0 | 106.0 | |
| Saran I | 18.7 | 17.1 | 0.647 | 0.372 | 1.56 | 83.4 | 39.0 | Surface only partly preserved |
| Saran II | 44.6 | 16.9 | 1.300 | 0.954 | 4.00 | 89.6 | 190.0 | Dec around 190° |

[a] The second-order glass transition temperatures were measured by differential thermal analysis.

$$\gamma_0 = U^s + T\left(\frac{\partial \gamma_0}{\partial T}\right)_{n,P} \qquad (5)$$

$\mathrm{deg}^{-1}$ is substituted for $-\mathrm{d}\gamma/\mathrm{d}T$,[7] good agreement with surface tension data of polymers is obtained (see Table IV).

**Table IV:** Intrinsic Viscosity and Number Average Molecular Weight of the Polymers in the Dow Monodisperse Polystyrene Latices No. 1, 2, and 3

| | Intrinsic viscosity, $[\eta]$, dl/g[a] | Particle size, $\mu$ | $\bar{M}_n$[b] | $\gamma_0$, 25°, dyn/cm |
|---|---|---|---|---|
| Dow polystyrene | 0.78 | 0.109 | 84,600 | 27 |
| | 1.11 | 0.126 | 147,800 | 24 |
| | 1.70 | 0.234 | 159,900 | 17 |

[a] $[\eta]$, dl/g in toluene at 30°, graph attached. [b] $\bar{M}_n$ is in toluene at 36° in stabin shell automatic osmometer.

## Discussion

Before discussing the experimental results, I emphasize that the consideration in regard to the CCM method is quantitatively true only when the system is amorphous and the only change taking place is the loss of surface. The particular case of crystalline materials will be treated later.

The second runs illustrated in Figures 6 and 7 closely resemble the idealized trace for the identification of $T_g$ (Figure 5) and the determined values correlate with data from other experiments. The only difference between the first and second runs is the sintering which follows the second-order transition. This sintering is associated with the disappearance of the high specific surface and the area under the maximum is assigned to the disappearance of surface energy.

The calorimetric compensation method (CCM) aims to eliminate interference from the superposition of the transition and surface effects by compensating for the transition. (The maximum curves, due to surface effects superimposed on the sigmoid shape $T_g$ transition curves in the dta diagrams, can result in an apparent reduction of size and shift of the locus erroneous observations found in the dta literature, where the materials measured had a high specific surface (>10 $m^2/g$).)[7] Sequences A, B, and C are illustrated in Figures 9 and 10. Figure 9 is a regular calorimetric diagram of a Dow polystyrene sample (No. 1) with particle size 0.109 $\mu$ (step A). The first run (step B) in Figure 10 shows the same peak with the CCM. The dotted line marks the "base line" chosen for calculations. The second run is step C, the controlling step, and illustrates that the two samples are well compensated. The surface energies in Table III were calculated from areas obtained from curves similar to that shown in Figure 10. From literature values[8,9] for the critical surface tension of polystyrene and its temperature dependence[10,11] we can calculate the polystyrene surface tension between 26 and 31 dyn/cm at 106°. This is to be compared with our measurements of 27, 24, and 17 dyn/cm for the same temperature, ~106°. This agreement supports the identity of the irreversible measurable energy with the loss of surface area at sintering. It follows that sintering and film formation can take place in the dry (lyophilized) latex in the total absence of water. The total surface energy of the solid polymer at that temperature can be calculated from calorimetric data, if we know the specific surface from other measurements.

There is one more problem to be discussed with regard to the surface tensions calculated for the three polystyrene samples. The values 27, 24, and 17 dyn/cm (106°) differ by more than experimental error. Intrinsic viscosities and number-average molecular weights for the constituent macromolecules of the

(7) See, *e.g.*, W. J. Smothers and Yao Chiang, "Handbook of D.T.A.," Chemistry Publishing Co., New York, N. Y., 1966, Figure 3:6, p 54 and Table 3:2, p 55.

(8) A. H. Ellison and W. A. Zisman, *J. Phys. Chem.*, **58**, 503 (1954).

(9) N. L. Jarvis, R. B. Fox, and W. A. Zisman, Advances in Chemistry Series, 43, American Chemical Society, Washington, D. C., 1964, p 317.

(10) R. F. Roe, *Proc. Nat. Acad. Sci. U. S.* **56**, 819 (1966).

(11) R. F. Roe, *J. Phys. Chem.*, **69**, 2809 (1965).

latices (Table IV) show a marked increase in molecular weight as the particle size increases. Tentatively, the decline of air–solid surface tension of latices seems to be associated with the increase in average molecular weight of the polymer chains forming the particles.

For No. 4 Saran I latex ($T_g \sim 32°$) only a part of the original specific surface is maintained during lyophilization. Using the determined surface of the lyophilized latex the calculated total surface energy is high (80 dyn/cm at 40°), and reproducibility is poor. It is possible this composition crystallizes above the $T_g$ and shows excess heat evolution.

Number 5 Type Saran II latex has a high degree of crystallinity as determined by X-ray diffraction measurements. Its film formation under ordinary circumstances is poor and the contours of the individual latex particles on the electromicrographs of deposited films is clearly distinguishable. In agreement with this neither the CCM nor the dta counterpart shows signs of change up to ~180° where a well-defined maximum occurs. The interpretation of this is cloudy since the material starts to decompose around this temperature. The energies measured, therefore, can be the combined effect of surface loss, melting, and decomposition.

The dta and CCM methods, described here, are a sensitive analytical tool for observing sintering and film formation of colloidal materials.

*Acknowledgments.* I would like to express my thanks to Dr. F. P. Gay of Du Pont, Film Department, Experimental Station, and to Professor W. H. Stockmayer for help and encouragement.

# Hydrogenation of Ethylene over Exploded Palladium Wire

**by Charles P. Nash and Ronald L. Musselman**

*Department of Chemistry, University of California, Davis, California 95616* *(Received October 27, 1969)*

Metal dispersions produced by exploding palladium wire in argon near atmospheric pressure catalyze the hydrogenation of ethylene at room temperature. The fastest reaction follows a Rideal mechanism with hydrogen as the adsorbed species. The kinetic data also suggest that ethylene adsorbed on these surfaces may be hydrogenated, but at a relatively slow rate.

## Introduction

In recent years a few reports have appeared documenting attempts to utilize the metal dispersions produced when a wire is exploded in a gaseous atmosphere. Karioris, Fish, and Royster[1,2] have established that under the proper conditions an aerosol of spherical metal particles having diameters of a few hundred angstroms may be produced by this method. Nash and De Sieno[3] have shown that in some particularly favorable cases the infrared spectra of molecules absorbed on these surfaces may be recorded.

A recent paper by Thomson and Webb[4] reports that nickel, palladium, and platinum, when exploded in argon, failed to catalyze the hydrogenation of ethylene, whereas palladium wires exploded in hydrogen atmospheres gave catalytically active surfaces. Because of the possible mechanistic implications of this result, we have undertaken a reexamination of the catalytic activity of palladium exploded in an argon atmosphere.

## Experimental Section

*Materials.* The 0.25-mm diameter palladium wire used in these experiments was obtained from the Metals and Controls subsidiary of Texas Instruments, Attleboro, Mass. The argon (purity > 99.99%) and ethylene (CP grade) were supplied by the Matheson Co. The argon was used without further treatment while the ethylene was distilled three times by trap-to-trap transfer methods and stored frozen in a liquid nitrogen trap. The mass spectrum of the ethylene prepared in this manner showed a trace of contamination by butane, with no other impurities. The hydrogen (minimum 99.99%, from Liquid Carbonic Co) was passed through a liquid nitrogen trap packed with glass beads. No impurity could be detected in its final mass spectrum.

*Reaction Vessel.* The wires were exploded and the catalytic reactions were studied in a chamber consisting of three parts. The uppermost part was an inverted 160-mm desiccator bottom with the flange polished smooth

(1) F. G. Karioris, B. R. Fish, and G. W. Royster, "Exploding Wires," Vol. 2, W. G. Chace and H. K. Moore, Ed., Plenum Publishing Corp., New York, N. Y., 1962, p 299.

(2) F. G. Karioris and B. R. Fish, *J. Colloid Sci.*, **17**, 155 (1962).

(3) C. P. Nash and R. P. De Sieno, *J. Phys. Chem.*, **69**, 2139 (1965).

(4) S. J. Thomson and G. Webb, *Chem. Commun.*, 473 (1965).

with cerium oxide. The center part was made from a 20 cm diameter × 3.7 cm thick Pyrex telescope blank. A 12-cm diameter hole was cut in the center of the blank. Electrodes fashioned from 12-mm steel bolt stock were installed in diametrically opposed holes drilled through the edges of the disk. The electrodes were sealed into the disk by filling the entire channel with epoxy resin and using Viton O rings between the nuts and the glass on both ends of the bolt stock, further to ensure vacuum tightness. When a wire was fastened between the two electrodes across the hole in the disk its length measured 11 cm. The plane faces of the disk were polished smooth and flat with cerium oxide.

The bottom part of the chamber was constructed entirely of heavy-wall Pyrex tubing. One end of a 10-cm length of 15-cm o.d. tubing was flanged and polished in a fashion identical with the lip of a desiccator. The other end was joined with a gradual taper to a 20-cm length of 8-cm o.d. tubing, the bottom end of which terminated in a hemispherical dome. Near the bottom of the 8-cm section, across its diameter, flanged holes were provided to accept two sodium chloride windows. The windows themselves were made from salt plates secured with epoxy resin to Lucite disks in which O-ring grooves had been machined to match the flanges on the openings into the chamber. The salt plates and the grooves were both on the same side of the plastic disk. Thus the windows were supported inside the chamber and were forced against the backing disk by the shock wave from the explosion. When the windows were on the outside of the disk they were invariably blown off, usually through failure of the salt itself rather than the adhesive joint.

Two Viton O rings were used to provide vacuum seals when the three sections of the chamber were assembled in sandwich fashion. Clamping rings and bolts were used to secure the sections together, and the bolts were tightened continually as the chamber was evacuated and the O rings were compressed. Viton O rings and clamping plates also secured the windows to the chamber. The chamber was connected to the vacuum system by a 10-mm Teflon stopcock, also fitted with Viton O rings, mounted near the top of the 15-cm o.d. section just below the electrode disk. The chamber was isolated from the remainder of the vacuum system by a Dry Ice–acetone trap. When the chamber was properly assembled it was capable of maintaining a vacuum of at least $10^{-4}$ Torr for at least a week. The volume of the entire chamber assembly was 6 l.

*Experimental Procedure.* Preliminary experiments quickly established that palladium exploded in argon gave catalytically active materials for which reaction times were typically a few minutes. We therefore have used the infrared spectrum of the product ethane to monitor the course of the reaction. A typical experimental sequence involved the installation of a wire weighing 70 mg in the chamber, after which it was outgassed by heating it electrically at a dull red glow *in vacuo* for at least 4 hr. The chamber was filled with 700 Torr of argon, and the wire was exploded with a 28-$\mu$F condenser bank charged to 11 kV.

The resulting aerosol was allowed to settle for at least 2 hr, at the end of which a heavy, soot-like deposit was found, principally in three places: on the hemispherical bottom, on the tapering section of the wall, and on top of the electrode disk. Thus there are roughly three well-separated zones in which the catalytic reaction occurs in our "static" system.

After the aerosol had been deposited, the chamber was evacuated for about 6 hr at a pressure below $10^{-4}$ Torr. One of the reactant gases was then introduced into the chamber at a known pressure. The other gas was stored in a 1 l. side-bulb, branching off from the main stopcock, at a known overpressure such that when the main stopcock was opened for 10–15 sec and then closed again, pressure equalization would yield the desired composition of reactant gases in the chamber. Experiments in which ethane was pulsed into a chamber filled with hydrogen showed that within 10 sec pressures were equalized and homogeneous mixing was obtained.

The chamber was mounted in the sample beam of a Beckman IR-12 infrared spectrophotometer set to monitor the absorbance of the ethane peak at 2881.5 $cm^{-1}$ as a function of time. The usual rate of chart-drive was 1.8 in./min. The spectrophotometer was adjusted to read zero absorbance, the main stopcock was cracked briefly, and the desired reaction ensued immediately.

The monitor peak of ethane at 2881.5 $cm^{-1}$ was shown in separate calibration experiments to span the absorbance range 0–1 when the ethane pressure in the chamber ranged from 0 to 77 Torr, irrespective of the partial pressure of hydrogen which was present.

The raw data for any experiment comprised a plot of the absorbance (pressure) of ethane *vs.* time. Instantaneous rates of reaction were obtained by constructing tangents to the curve by the usual mirror method. The instantaneous compositions could be calculated from the known stoichiometry of the hydrogenation reaction, which mass spectrometer analysis showed to be the only process occurring in the system.

## Results

The first result of these experiments, of a purely qualitative nature, is the observation that, irrespective of the order of addition of the reactant gases, palladium exploded in 700 Torr of argon produces a functioning catalyst for the hydrogenation of ethylene. This result contrasts sharply with that of Thomson and Webb, who reported the system to be inactive.

A freshly prepared dispersion gave a catalyst which displayed extremely high, but erratic, activity. After six or seven runs on a given preparation, however,

the surface stabilized and thereafter consistently reproducible behavior was obtained. Laidler and Townshend[5] have noted a similar effect with nickel films.

A series of ten experiments with the most active stable surface which we obtained served to establish the nature of the dominant mechanism for reaction mixtures in which hydrogen, in excess, was introduced into the reaction vessel first. When the data gathered over the course of each of these reactions was plotted in first order fashion, *i.e.*, −log (fraction of ethylene remaining) *vs.* time, consistently good straight lines were obtained to over 90% conversion. The slopes of these lines, however, showed slight but real increases as the initial hydrogen:ethylene ratio was increased. For example, a series for which the initial ethylene pressures were all 20 Torr and the initial hydrogen pressures were 60, 120, and 240 Torr, gave apparent first-order rate constants of 1.1, 1.6, and 1.8 $min^{-1}$, respectively.

When the data were plotted as log rate *vs.* log ethylene pressure, good straight lines were obtained with slopes in the range 1.0–1.3. By taking vertical sections through these curves it was possible to construct a new family of curves depicting reaction rate *vs.* hydrogen pressure, the ethylene pressure being a constant on each curve. Figure 1 shows this family of constructs. While the data for the various ethylene isobars show considerable scatter, the drawn curves provide a reasonable fit to the points. The four curves have been drawn in accordance with a first-order ethylene dependence. The inclined straight lines in Figure 1, whose slopes are the same as the several apparent first-order rate constants, join the points obtained from any single run. With few exceptions, the data points scatter from the drawn curves in a systematic fashion. Those points from runs for which the initial ethylene pressure was high lie below the average curve, while those for which the initial pressure of ethylene was low lie above it.

Since our mechanistic conclusions for this surface will be based on Figure 1, which was constructed from a number of discrete experiments, it is essential to demonstrate both the stability of the "seasoned" surface and to show that it is instantaneously responsive to the changing conditions in the gas phase. Fulfillment of the stability condition was assured by periodic check runs using a standard mixture. The responsive character was demonstrated in a series of four experiments in which premixed samples of 80 Torr of $H_2$ + 40 Torr of ethylene was allowed to react in the chamber until half the ethylene was hydrogenated. In two experiments the hydrogen pressure was then suddenly increased from 60 Torr to 120 Torr with a pulse from a side storage bulb. In two other experiments 60 Torr of helium rather than hydrogen was injected. In either case the system was subjected to an appreciable disturbance, the relaxation time of which is nonnegligible and indeterminate. Thus the apparent rates of ethane production measured immediately after the

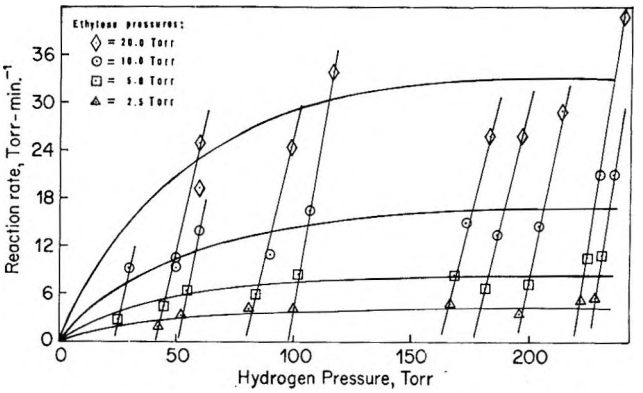


Figure 1. The hydrogen dependence of the rate of production of ethane. The ethylene dependence is first order.

injection of the two different gases were not quite those which one would have expected on the basis of the 20 Torr ethylene isobar in Figure 1 for hydrogen pressures of 60 and 120 Torr. The *difference* in the apparent rates, however, was nearly the 7 Torr/min value which this isobar yields for those hydrogen pressures. As the reactions proceeded, both the rates and the rate differences tended to conform to the predictions of Figure 1. As further substantiation of the stability of the surface, all four of the runs superimposed up to the time of gas injection and each like pair superimposed thereafter.

In contrast to the fairly straightforward kinetic behavior found in runs over a catalyst having high intrinsic activity, studies of a preparation whose activity was, for no obvious reason, only about half as great, gave very complex results. When pseudo-first-order plots were made for reaction mixtures having 120 Torr of hydrogen plus 11, 22, 41, and 75 Torr of ethylene, rate constants of 2.6, 1.2, 0.7, and 0.4 $min^{-1}$ were obtained. That is, the apparent rate constants are nearly inversely proportional to the initial ethylene pressure. Qualitatively identical behavior was found for mixtures in which the ethylene was introduced first, but the magnitude of the rate constants was diminished by ~15%.

When the data from a number of these same runs was plotted as log rate *vs.* log ethylene, the "apparent order" in ethylene changed continuously from ~1.5 at the beginning of the reaction to ~0.5 near the end.

## Discussion

We shall discuss the kinetic results in terms of the three principal mechanisms which have been proposed for this kind of process.[6] In the so-called Rideal Type I mechanism, reaction occurs between an ethylene ad-

(5) K. J. Laidler and R. E. Townshend, *Trans. Faraday Soc.*, **57**, 1590 (1961).

(6) K. J. Laidler, "Chemical Kinetics," 2nd ed. McGraw-Hill Publications, New York, N. Y., 1965.

sorbed on the surface and hydrogen from the gas phase. The rate law for this process has the form

$$\text{Rate} = \frac{K[H_2][C_2H_4]}{1 + L[C_2H_4]} \quad (1)$$

where $K$ is a measure of the intrinsic activity of the catalyst, $L$ is the ratio of the rate constants for the adsorption and desorption of ethylene, and the bracketed quantities are pressures of the species in the gas phase.

In the alternative Rideal Type II mechanism, adsorbed hydrogen molecules react with gaseous ethylene in accordance with the rate law

$$\text{Rate} = \frac{A[H_2][C_2H_4]}{1 + B[H_2]} \quad (2)$$

The third mechanism, that of Langmuir and Hinshelwood, describes the reaction between adsorbed hydrogen molecules and adsorbed ethylene. The rate law is

$$\text{Rate} = \frac{D[H_2][C_2H_4]}{\{1 + B[H_2] + L[C_2H_4]\}^2} \quad (3)$$

The single mechanism which fits nearly all the facts depicted in Figure 1, and the discussion preceding it, is the Rideal Type II. The drawn curves in this figure were calculated from eq 2 using the parameters $A = 4.1 \times 10^{-2}$ Torr$^{-1}$ min$^{-1}$, $B = 2.1 \times 10^{-2}$ Torr$^{-1}$.

By taking the total derivative of eq 2 and using the known stoichiometry of the reaction to equate $d[C_2H_4] = d[H_2]$, one may write

$$\frac{d(\text{Rate})}{d[C_2H_4]} = \frac{([H_2] + [C_2H_4])\text{Rate}}{[H_2][C_2H_4]} - \frac{B(\text{Rate})}{1 + B[H_2]} \quad (4)$$

or

$$\frac{d \log (\text{Rate})}{d \log [C_2H_4]} = 1 + [C_2H_4]\left(\frac{1}{[H_2]} - \frac{B}{1 + B[H_2]}\right) \quad (5)$$

Equation 4 may be used to calculate values of the slopes of the lines through the points from any given run in Figure 1 with the result that for the values of $A$ and $B$ just cited, the value of $d(\text{Rate})/d[C_2H_4]$ varies within any run by at most 10% from beginning to end. Thus semilog plots of the time dependence of the ethylene pressure will be decently linear even though the hydrogen pressure is continuously changing. Equation 4 also yields, in agreement with experiment, the gradual increase in the slopes of the lines as the average hydrogen pressure increases. To a considerable extent the linearity of the semilog first-order plots is a numerical artifact. A different surface, for which the value of $A$ was only $1.5 \times 10^{-2}$ Torr$^{-1}$ min$^{-1}$, gave plots in which the apparent first-order rate constant decreased by a factor of 2 over the course of the reaction.

Although the most active surfaces are adequately described by a mechanism in which hydrogen is the adsorbed reactive species, other mechanisms involving adsorbed ethylene must also be possible, and indeed are quite important on the least active surfaces. Equation 5 embodies the functional form of the log (Rate) *vs.* log $[C_2H_4]$ plots to be expected for surfaces on which only the Rideal Type II mechanism is operating. From this equation one might reasonably expect apparent orders in ethylene which are between 1.0 and 1.3, but never less than 1.0. This prediction is contradicted by the behavior cited for the inactive surfaces, on which fractional orders were commonly observed toward the end of the reaction.

Neither a pure Rideal Type I nor a pure Langmuir–Hinshelwood mechanism reproduces this trend. Total differentiation of eq 1 and 3 gives

$$\frac{d \log (\text{Rate})}{d \log [C_2H_4]} = 1 + [C_2H_4]\left(\frac{1}{[H_2]} - \frac{L}{1 + L[C_2H_4]}\right) \quad (6)$$

$$\frac{d \log (\text{Rate})}{d \log [C_2H_4]} = 1 + [C_2H_4]\left(\frac{1}{[H_2]} - \frac{2(B + L)}{1 + B[H_2] + L[C_2H_4]}\right) \quad (7)$$

respectively. Both of these equations allow fractional order in ethylene but neither permits a given run to change from >1 to <1 as it proceeds. In eq 7, for example, the deviation from apparent order unity is obtained by comparing the terms

$$1 + B[H_2] + L[C_2H_4] \text{ vs. } 2(B + L)[H_2] \quad (8)$$

which may be rearranged to

$$\left[\frac{1 + B\{[H_2] - [C_2H_4]\}}{(B + L)} - \{[H_2] - [C_2H_4]\}\right] \text{ vs. } [H_2] \quad (9)$$

The combination of terms on the left in eq 9 is an invariant over the course of the reaction, while $[H_2]$ continuously decreases. Thus if a reaction begins with order >1 it remains so, although it is theoretically possible for the order of an *L–H* reaction to cross one from lower to higher. The amount of the variation is, of course, moderated by the continuously decreasing factor $[C_2H_4]$ as well, so that in the limit all three types of reactions should become apparently first order in ethylene on a log–log plot.

The data on inactive surfaces suggests that there is a large percentage of sites on which ethylene is strongly adsorbed, and from which it is removed only slowly by reaction. In qualitative terms, as it slowly comes off and is replaced by hydrogen, the faster R-II reaction becomes progressively more important and a log–log plot of gross rate *vs.* ethylene pressure curves away from the ethylene axis. On the active surfaces the

fraction of sites "immobilized" by ethylene is much smaller, although the systematic scatter in Figure 1 suggests that some ethylene adsorption is occurring.

The rate law which we find for the hydrogenation of ethylene on an active surface is in disagreement with the results of Bond, *et al.*,[7] who studied the same reaction over alumina-supported palladium at −18° and found, over essentially the same pressure range spanned by our experiments, approximately a first-order dependence on hydrogen pressure and an accurately zero-order dependence on ethylene pressure. These authors discuss their results in terms of various alternative reactions of adsorbed ethylene or ethyl radicals, whereas adsorbed hydrogen is significantly more reactive than adsorbed ethylene in the present instance. Bond, *et al.*,[7] cite no actual rate data so there is no way to compare the intrinsic activities of the two catalysts, but it is possible that the activation energies for reactions of adsorbed hydrogen or ethylene are so different that qualitatively different behavior would be found at two temperatures nearly 50° apart. It may also be, of course, that the two catalysts, made in very different ways, would give different results under any or all conditions. In particular, the explosively produced catalysts might contain trace contamination from the electrodes which could account for some of the irreproducibility we have described.

The failure of Thomson and Webb[4] to produce an active surface in their argon experiments might possibly stem from the fact that their explosions, carried out in 200 Torr of argon, were very inefficient with respect to aerosol production; *i.e.*, they presumably had only very small surface areas. The incoherent films they describe are consistent with a large fraction of the energy having been expended in the peripheral arcs which are known to occur when wires are exploded in argon at pressures below $\sim^1/_4$ atm.[8,9] Why active surfaces were produced when a hydrogen atmosphere was used we are at a loss to explain.

*Acknowledgment.* This work was supported by the U. S. Atomic Energy Commission through the Lawrence Radiation Laboratory, Livermore, Calif.

(7) G. C. Bond, J. J. Philipson, P. B. Wells, and J. M. Winter bottom, *Trans. Faraday Soc.*, 62, 443 (1966).

(8) F. D. Bennett and D. D. Shear in ref 1, p 181.

(9) T. Korneff, J. L. Bohn, and F. H. Nadig in "Exploding Wires," Vol. 1, W. G. Chace and H. K. Moore, Ed., Plenum Publishing Corp., New York, N. Y., 1959, p 104.

# Heat Capacity and Thermodynamic Properties of [2.2]Paracyclophane. The Mechanism of the 50°K Transition[1]

**by John T. S. Andrews and Edgar F. Westrum, Jr.[2]**

*Department of Chemistry, University of Michigan, Ann Arbor, Michigan 48104* *(Received October 14, 1969)*

The heat capacity of [2.2]paracyclophane, $C_{16}H_{16}$, has been measured by adiabatic calorimetry from 10 to 350°K. The 298°K values of the heat capacity, entropy, and enthalpy and Gibbs functions are 60.31, 63.50, 30.74 and −32.76 cal/(mol deg), respectively. The heat capacity is smooth and normal except near 50°K, where a rounded maximum indicates a transition ($T_{max}$ = 55.5°K, $\Delta S$ = 1 ± 0.5 cal/(mol deg), $\Delta H$ = 51 cal/mol. A possible explanation of the transition in terms of the twisting of the molecular structure is advanced; this explanation is consistent with the thermodynamic functions and the observed shape of the transition.

## Introduction

The macrocyclic hydrocarbon [2.2]paracyclophane ($C_{16}H_{16}$, di-*p*-xylylene) was first reported by Brown[3,4] among the polymerization products of *p*-xylene, and the direct synthesis using high-dilution ring-closure techniques was independently reported by Cram.[5] Brown[4] used X-ray techniques to ascertain the structure of his product and showed that it was akin to that of a bivalve mollusc, two benzene rings being held parallel one over the other, and fastened together by

(1) This work was supported in part by the Division of Research of the United States Atomic Energy Commission and was presented at the 157th National Meeting of the American Chemical Society, Minneapolis, Minn., 1969.

(2) To whom correspondence concerning this work should be addressed.

(3) C. J. Brown and A. C. Farthing, *Nature*, 164, 915 (1949).

dual two-carbon bridges attached at the *para* positions. This structure was subsequently confirmed through X-ray determinations by Lonsdale and her coworkers[6] and by Bekoe and Trueblood.[7]

The molecule is of interest to a thermochemist in two major respects. First, it is very compact and symmetric; such are the attributes of "plastic crystals" in which significant molecular motion is apparent below the melting point. Second, the molecule is highly strained, as may be ascertained from the molecular structure; not only are the benzene rings "dished," but the carbon–carbon bonds in the middle of the bridges are elongated. Despite these relieving measures, the benzene rings still approach within 3.1 Å, much less than the van der Waals distance of about 3.4 Å. Boyd[8] has measured the energy of combustion of this material and calculates a strain energy of 31 kcal $mol^{-1}$. He goes further and assigns this energy among the different contributions to the strain: 15 kcal $mol^{-1}$ to the deformation of the aromatic rings, 5 to the stretching of the bridging carbon–carbon bonds, and 4 to the eclipsing of the hydrogens on the bridging carbons.

The strained molecular structure is apparently stabilized by the crystal lattice, as [2.2]paracyclophane is remarkably stable up to the elevated melting point of 280°. The melt polymerizes rapidly.

Measurement of the thermal properties of this material would be expected to show if it were "plastic" and would throw light on the relationship between structure and thermophysical properties in such a strained molecule.

## Experimental Section

The sample of [2.2]paracyclophane was obtained from Hi Laboratories, Whitmore Lake, Michigan. It was purified by a series of six consecutive vacuum sublimations, after which the material had a snowy white appearance and contained no involatile impurities. During the course of the sublimation, great care was taken that the temperature did not rise above 140°. At higher temperatures the material polymerizes readily in a vacuum. The final calorimetric sample consisted of small, regular crystals which melted at 280° when heated rapidly in a sealed tube.

The sample was loaded directly into a gold-plated copper calorimeter equipped with a gold-gasketted screw seal (calorimeter laboratory designation W-37, tare weight including closure 34.575 g, internal volume 32.45 $cm^3$). Helium gas (0.000186 g) was sealed within the calorimeter to assist in thermal equilibration. The calorimetric mass of the sample was 20.453 *in vacuo;* a density of 1.229 g $cm^{-3}$ was used for the vacuum correction.[6]

The heat capacity of the loaded calorimeter was measured in the Mark III vacuum cryostat[9] by the quasi-adiabatic technique[10] which employs intermittent heating. Voltages were measured with the aid of a Leeds and Northrup White microvolt potentiometer and a galvanometer equipped with a 5-m optical path. With this apparatus, voltages may be determined with a precision of a few hundredths of a microvolt. The temperature of the calorimeter was measured with a capsule-type platinum resistance thermometer ($R_{273}$ = 25 ohms) which was inserted into a well reentrant to the calorimeter. To assist in the maintenance of adiabatic conditions, the calorimeter was entirely surrounded by an adiabatic shield and the temperature of the shield was controlled in three segments by electronic three-action controllers driven by thermocouples. All measurements of mass, voltage, time, resistance, and temperature were referred to calibrations performed by the National Bureau of Standards.

The heat capacity results were corrected for "curvature" occasioned by the use of finite temperature differences, and were also corrected for the heat capacity of the empty calorimeter and thermometer–heater assembly (which was measured in a separate series of experiments). Slight corrections were also made for the (small) differences in gaseous helium and thermal conduction (Apiezon T) grease present in the calorimetric mass when the heat capacity of the calorimeter (filled and empty) was measured.

## Results and Discussion

The experimental heat capacity measurements, corrected as noted above, are presented on a molal basis in Table I. ($C_{16}H_{16}$ = 208.31, 1961 atomic weights).[11] They are illustrated in Figure 1, where it may be seen that the shape of the curve follows the usual sigmate curve, save for the region about 50°K where a rounded peak may be seen. The determinations in Table I are presented in chronological order, and the temperature differences employed in each determination may be estimated as the difference between the mean temperature of adjacent determinations. The results are presented in terms of the defined thermochemical calorie (=4.184 J) and an ice point of 273.15°K. The heat capacity measurements have been

(4) C. J. Brown, *J. Chem. Soc.*, 3265 (1953).

(5) D. J. Cram and H. Steinberg, *J. Amer. Chem. Soc.*, **73**, 5691 (1951).

(6) K. Lonsdale, H. J. Milledge, and K. V. K. Rao, *Proc. Roy. Soc.*, **A255**, 82 (1960).

(7) D. A. Bekoe and K. N. Trueblood, Paper J-12, Abstracts of the Annual Meeting of the American Crystallographic Association, at Bozman, Mont., July 1964.

(8) R. H. Boyd, *Tetrahedron*, **22**, 119 (1966).

(9) H. G. Carlson, Ph.D. Thesis, The University of Michigan, Ann Arbor, Mich., 1964. U. S. Atomic Energy Commission Report TID-15153 (1962).

(10) E. F. Westrum, Jr., G. T. Furukawa, and J. P. McCullough in "Experimental Thermodynamics," Vol. 1, J. P. McCullough and D. W. Scott, Ed., Butterworth and Co. (Publishers) Ltd., London, 1968.

(11) A. E. Cameron and E. Wichers, *J. Amer. Chem. Soc.*, **84**, 4175 (1962).

**Table I:** Experimental Heat Capacity of [2.2]Paracyclophane[a]

| Temp, °K | $C_p$/cal deg$^{-1}$ mol$^{-1}$ | Temp, °K | $C_p$/cal deg$^{-1}$ mol$^{-1}$ | Temp, °K | $C_p$/cal deg$^{-1}$ mol$^{-1}$ |
|---|---|---|---|---|---|
| Series I | | 338.17 | 69.37 | 72.23 | 17.43 |
| | | 346.47 | 70.83 | 81.46 | 18.83 |
| 170.56 | 33.70 | Series III | | 90.18 | 20.20 |
| 178.75 | 35.31 | | | 99.11 | 21.49 |
| 187.80 | 37.04 | 10.73 | 1.087 | 108.20 | 22.92 |
| 197.58 | 38.99 | 11.04 | 1.377 | 117.91 | 24.51 |
| 207.93 | 40.91 | 11.76 | 1.636 | 128.04 | 26.25 |
| 217.88 | 43.02 | 12.78 | 1.924 | 137.62 | 27.86 |
| 227.92 | 45.11 | 13.99 | 2.397 | 146.86 | 29.46 |
| 238.05 | 47.27 | 15.69 | 3.064 | 156.15 | 31.09 |
| 247.87 | 49.32 | 17.62 | 3.570 | 165.51 | 32.80 |
| 257.60 | 51.46 | 19.87 | 4.843 | 174.85 | 45.54 |
| 267.13 | 53.46 | 22.71 | 6.006 | 184.27 | 36.30 |
| 276.67 | 55.60 | 25.77 | 7.255 | Series IV | |
| 286.10 | 57.66 | 29.02 | 8.583 | | |
| 295.50 | 59.89 | 32.23 | 9.689 | 42.01 | 13.200 |
| 305.02 | 61.83 | 35.44 | 10.877 | 44.25 | 14.219 |
| 314.49 | 63.95 | 39.03 | 12.104 | 46.93 | 15.63 |
| Series II | | 43.25 | 13.836 | 50.89 | 16.40 |
| | | 48.27 | 16.16 | 56.15 | 16.97 |
| 313.53 | 63.75 | 54.08 | 17.01 | 61.83 | 16.52 |
| 321.67 | 65.52 | 60.76 | 16.74 | 67.42 | 16.78 |
| 329.89 | 67.44 | 63.30 | 16.54 | | |

[a] Throughout this paper the defined thermochemical calorie (=4.184 J), an ice point of 273.15°K, and a molecular weight of 208.31 are employed.

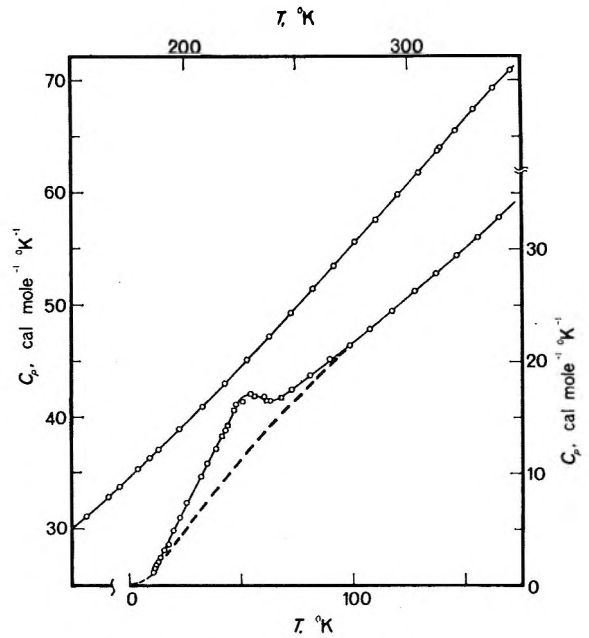


Figure 1. Heat capacity of [2.2]paracyclophane.

Integrated to obtain the thermodynamic functions given in Table II. Save for the region about 50°K, the measurements were least-squares fitted by a polynomial in reduced temperature, using algorithms developed in this laboratory. Analytic expansion and integration of the polynomial gave the values of Table II. The integration of the heat capacity through the anomalous region about 50°K was accomplished by direct numerical methods using a large scale plot. The resulting thermodynamic functions are considered to be characterized by a precision of a few tenths of 1% near 50°K, and by about 0.01% above this temperature.

**Table II:** Thermodynamic Functions of [2.2]Paracyclophane[a]

| Temp, °K | $C_p$/cal deg$^{-1}$ mol$^{-1}$ | $S°$/cal deg$^{-1}$ mol$^{-1}$ | $(H° - H°_0)$/ cal mol$^{-1}$ | $-(G° - H°_0)/T$/ cal deg$^{-1}$ mol$^{-1}$ |
|---|---|---|---|---|
| | | Crystal II | | |
| 10 | 0.88 | 0.33 | 2.5 | 0.08 |
| 20 | 4.90 | 2.15 | 31.1 | 0.60 |
| | | Transition Region | | |
| 30 | 8.93 | 4.91 | 100.5 | 1.56 |
| 40 | 12.44 | 7.97 | 207.5 | 2.78 |
| 50 | 16.56 | 11.21 | 353.4 | 4.14 |
| 60 | 16.81 | 14.29 | 522.5 | 5.58 |
| | | Crystal I | | |
| 70 | 17.13 | 16.86 | 689.6 | 7.01 |
| 80 | 18.59 | 19.24 | 868.1 | 8.39 |
| 90 | 20.13 | 19.24 | 1061.6 | 9.73 |
| 100 | 21.68 | 23.72 | 1270.7 | 11.02 |
| 110 | 23.25 | 25.86 | 1495.3 | 12.27 |
| 120 | 24.86 | 27.95 | 1736 | 13.49 |
| 130 | 26.51 | 30.01 | 1993 | 14.68 |
| 140 | 28.23 | 32.04 | 2266 | 15.85 |
| 150 | 30.00 | 34.04 | 2557 | 17.00 |
| 160 | 31.81 | 36.04 | 2866 | 18.12 |
| 170 | 33.66 | 38.02 | 3194 | 19.24 |
| 180 | 35.54 | 40.00 | 3539 | 20.33 |
| 190 | 37.46 | 41.97 | 3904 | 21.42 |
| 200 | 39.39 | 43.94 | 4289 | 22.50 |
| 210 | 41.38 | 45.91 | 4692 | 23.53 |
| 220 | 43.41 | 47.88 | 5116 | 24.63 |
| 230 | 45.50 | 49.86 | 5561 | 25.68 |
| 240 | 47.65 | 51.84 | 6026 | 26.73 |
| 250 | 49.81 | 53.83 | 6514 | 27.77 |
| 260 | 52.00 | 55.82 | 7023 | 28.81 |
| 270 | 54.19 | 57.83 | 7554 | 29.85 |
| 273.15 | 54.87 | 58.46 | 7725 | 30.18 |
| 280 | 56.36 | 59.84 | 8106 | 30.89 |
| 290 | 58.53 | 61.85 | 8681 | 31.92 |
| 298.15 | 60.31 | 63.50 | 9165 | 32.76 |
| 300 | 60.71 | 63.87 | 9277 | 32.95 |
| 310 | 62.93 | 65.90 | 9895 | 33.98 |
| 320 | 65.21 | 67.93 | 10536 | 35.01 |
| 330 | 67.51 | 69.98 | 11200 | 36.04 |
| 340 | 69.68 | 72.03 | 11886 | 37.06 |
| 350 | 71.31 | 74.07 | 12591 | 38.10 |

[a] Throughout this paper the defined thermochemical calorie (=4.184 J), an ice point of 273.15°K, and a molecular weight of 208.31 are employed.

**Table III:** Enthalpy and Entropy of Transition of [2.2]Paracyclophane[a]

| Series, designation | No. of detns | $T_1$/°K | $T_2$/°K | $(H_{T_2} - H_{T_1})$/ cal mol$^{-1}$ | $(H_{70} - H_{25})$/ cal mol$^{-1}$ | | $(S_{70} - S_{25})$/ cal mol$^{-1}$ °K$^{-1}$ |
|---|---|---|---|---|---|---|---|
| I | 5 | 37.12 | 64.33 | 423.01 | | 606.5 | |
| II | 7 | 40.96 | 70.11 | 469.80 | | 604.2 | |
| | | | | | Av | 605.4 | |
| | | | | | Smooth curve | (606.3) | 12.55 |
| | | | | | Lattice contribution | 555.5 | 11.52 |
| | | | | | $\Delta_t H$ | 51 | |
| | | | | | | $\Delta_t S$ | $1.0 \pm 0.5$ |

[a] Throughout this paper the defined thermochemical calorie (=4.184 J), an ice point of 273.15°K, and a molecular weight of 208.31 are employed. $T_{max}$/°K = 55.5.

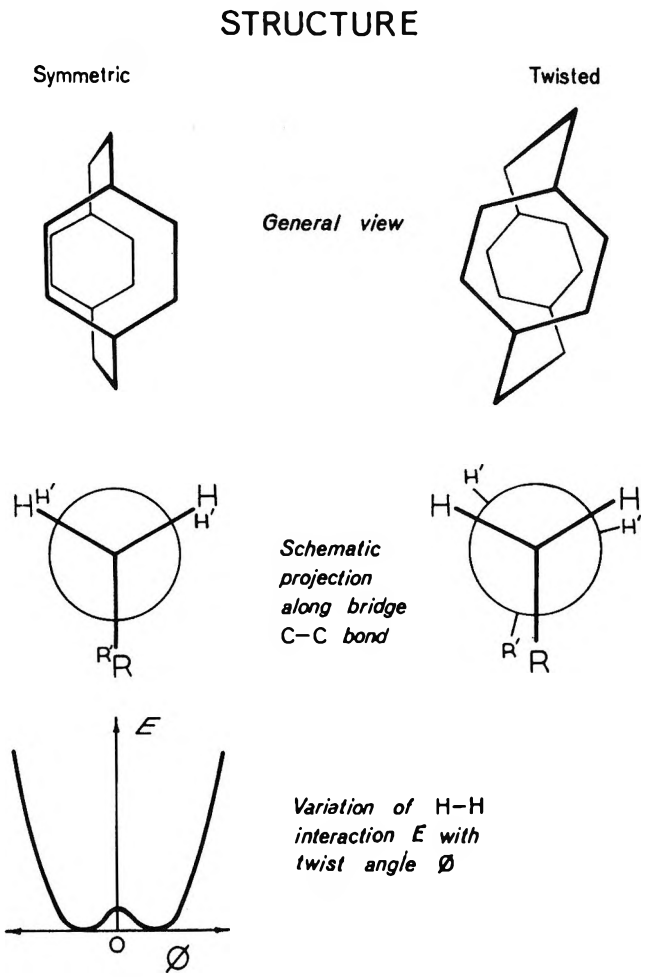


Figure 2. Proposed symmetric and twist structures of [2.2]paracyclophane.

In order that the thermodynamic functions associated with the process which occasions the anomaly may be evaluated, it is first necessary to define the "normal" or lattice behavior through this region. The anomaly was so far down on the steep portion of the heat capacity curve that it was not possible to define normal behavior by linear extrapolation. Attempts to fit the heat capacity above and below the transition by semitheoretical expressions (Debye or Einstein terms) failed, as insufficient information concerning the molecular vibrations[12] was available to calculate the internal heat capacity of the molecule and so, by difference, the lattice terms. Under these conditions we have postulated a lattice heat capacity through the transition region which is indicated in Figure 1. Numerical quadrature of this curve yielded the thermodynamic increments associated with the lattice in the transition region. The thermodynamics of the transition process were then calculated (Table III). The large uncertainties assigned to these values are primarily due to the uncertainty in the lattice heat capacity.

The measured entropy increment for this transition ($1 \pm 0.5$ cal mol$^{-1}$ deg$^{-1}$) is almost that of a twofold randomizing process ($R \ln 2 = 1.38$ cal mol$^{-1}$ deg$^{-1}$). In the absence of definitive structural information throughout the transition region, we can do no more than suggest a possible explanation.

The molecular symmetry of [2.2]paracyclophane is *mmm*. The portion of the strain of this configuration due to the eclipsed interactions of the hydrogen atoms on the bridging carbons (to which cause Boyd[8] ascribed 4 kcal mol$^{-1}$ of strain energy) may be relieved if the molecule twists slightly to either side of the symmetric form. This twisting and the resulting hydrogen interactions are illustrated in Figure 2. The symmetric position represents a configuration of high energy with a shallow potential well on each side. At temperatures around 300°K, the molecule behaves as though this twisting were a vibrational mode and the observed X-ray structure is determined by the time average over this vibration (*i.e.*, the *mmm* structure). At low temperatures, this mode may not be excited sufficiently for the molecule to surmount the intervening barrier and each molecule will remain in one or other of the twist forms. We suggest that the transition occurs when this twisting mode is sufficiently excited for the molecule to pass from one twist form to the other. Two high-temperature configurations in equilibrium are

(12) V. Schettino, M. P. Marzocchi, and G. Sbrana, *J. Mol. Struct.*, 2, 39 (1968).

thus attained from a single low-temperature configuration and the disordering aspect of the transition process will be characterized by an entropy change of $R$ ln 2. Since there is no energy difference between forms, either might, of course, exist exclusively in a separate crystal.

The shape of the excess heat capacity through the transition has features common to both Schottky (rounded maximum) and λ (the slopes above and below the transition) anomalies. λ anomalies arise where the disordering phenomenon is cooperative, Schottky anomalies where it is not (for a more complete discussion see Fowler).[13] The shape of this transition in [2.2]-paracyclophane suggests, therefore, that it is characterized by a weakly cooperative disordering phenomenon. The proposed molecular twisting would affect only nearest neighbors and so the transition shape is not inconsistent with the proposed mechanism. In the absence of definitive physical evidence this mechanism cannot be regarded as other than tentative. Nmr and ir spectroscopy throughout the transition region might well indicate the truth of the matter, and X-ray structural information as a function of temperature would be of great interest.

*Acknowledgments.* The authors are grateful for the support of the United States Atomic Energy Commission throughout this research. They also thank Mrs. Suong-Sik Kim for her help with the calculations.

(13) R. H. Fowler, "Statistical Mechanics," Cambridge University Press, Cambridge, 1936, p 807.

# Photoelectric Effects in Solid Electrolyte Materials

**by John H. Kennedy**

*Chemistry Department, University of California, Santa Barbara, California 93106*

**and Emil Boodman**

*Bissett-Berman Corporation, Santa Monica, California* *(Received September 22, 1969)*

The photoelectric responses of silver sulfide bromide, $Ag_3SBr$, and silver sulfide iodide, $Ag_3SI$, have been observed as a function of wavelength. A fast initial photocurrent is followed by a lower steady-state current. From the amount of silver deposited coulometrically during light exposure, the photocurrent was shown to be predominantly ionic in nature. The results are ascribed to a photoreaction with sulfide ions, producing silver ion photocurrent.

## Introduction

Photoelectric effects with solid silver halides have been studied by several investigators both in polycrystalline material[1,2] and single crystal material.[3] As part of our studies on electrochemical properties of solid electrolyte materials, we have examined the effect of light impinging upon an electrolyte surface coated with a partially transparent gold electrode. The solid electrolytes studied were primarily $Ag_3SBr$ and $Ag_3SI$, but results are compared with those from similar experiments carried out with AgBr, AgI, $Ag_2S$, and $RbAg_4I_5$. Silver sulfide halides could have interesting photoreaction behavior as well as electrochemical behavior, since they are well defined compounds, but may demonstrate properties related to the parent compounds AgBr, AgI, and $Ag_2S$. Electrical conductivity has been shown to be almost entirely ionic, unlike $Ag_2S$, yet orders of magnitude higher than the corresponding silver halides.[4-6] It will be shown that photoelectric properties are also significantly different from the parent compounds.

Photoreactions of AgBr and $Ag_2S$ have been described by slightly different mechanisms, but in essence the net result is the same. Tan and Trautweiler[3] view the initial reaction in AgBr to be the production of an electron–hole pair with the holes being trapped near the point of creation by reaction with AgBr to form $Br^0$ and silver ion interstitials. The more mobile photoelectrons diffuse into the bulk material and eventually become trapped by reaction with a silver ion interstitial

(1) S. E. Sheppard, W. Vanselow, and V. C. Hall, *J. Phys. Chem.*, **33**, 311, 1403 (1929).

(2) W. Cooper, *J. Phys. Chem.*, **66**, 857 (1962).

(3) Y. T. Tan and F. Trautweiler, *J. Appl. Phys.*, **40**, 66 (1969).

(4) V. Reuter and K. Hardel, *Naturwissenschaften*, **48**, 161 (1961).

(5) T. Takahashi and O. Yamamoto, *Electrochim. Acta*, **11**, 779 (1966).

(6) J. H. Kennedy and F. Chen, *J. Electrochem. Soc.*, **116**, 207 (1969).

to form $Ag^0$. The net reaction is the formation of bromine atoms near the surface, silver atoms in the bulk, and a net flow of silver ion interstitials from the surface into the bulk material. Photoresponse begins at wavelengths below 500 nm.

For silver sulfide, Scholz postulated that photons eject electrons directly from sulfide ion donors to form $S^0$ near the surface.[7] The photoelectrons migrate into the bulk and combine with an acceptor such as interstitial silver ions to form silver atoms. The surface would build up an excess of silver ions, and these would migrate in the form of silver ion interstitials into the bulk. As can be seen, the net reaction would be analogous to the AgBr reaction. However, Ichimescu and Suciu report a photoconductivity maximum at 1050 nm[8] which is much lower in energy compared to the AgBr reaction.

## Experimental Section

*Materials.* $Ag_3SBr$ and $Ag_3SI$ were prepared by the method described previously[6] using analytical reagent grade silver salts. Silver and gold electrodes, with the exception of the gold minigrid screen, were prepared from 99.99% pure powders. The minigrid screen was a 45% transparent electro-formed grid made by Buckbee–Mears and consisted of 1000 lines/in.

*Photoelectric Cells.* Pellet-type cells were prepared by compressing powders with a Perkin-Elmer KBr pellet die. The silver or gold electrodes were formed from micron-sized powders pressed at 1000 psi. While the silver pellet was in the press, the powdered electrolyte was placed into the die cavity and tamped in place. The gold minigrid was placed on the tamped electrolyte powder and the entire assembly, silver pellet, electrolyte, and gold minigrid, was brought to a full applied pressure of 24,000 psi. The completed pellet measured 13.5 mm diameter by approximately 0.80 mm thickness. The photoresponse electrode was the gold minigrid, while the solid silver or solid gold electrodes were counterelectrodes. The pellets had a resistance of 5–10 ohms as measured with a 1 kHz signal. Electrical contact to the pellet was made by using gold-plated beryllium–copper lead springs.

*Photoconductivity Measurements.* A potential was applied between the gold grid and counterelectrode with the grid being positive. After allowing the current to reach a steady-state value, the grid electrode was exposed to light from either a Honeywell Prox-o-lite xenon flash tube or a Bausch and Lomb Nicholas microscope illuminator, Model 31-33-56, for continuous illumination. For wavelength studies, a Bausch and Lomb monochromator was incorporated between source and photocell. The source for wavelength studies was a Sylvania Sungun Lamp (FAW) with a temperature of 6200°K and 27,000 candle power at the beam center. Data given are uncorrected for spectral output. Since spectral output for the particular lamp used was not measured, data given are uncorrected for spectral output. The lamp type has a spectral peak energy *ca.* 500 nm and drops off rapidly above 1000 nm. Correction of the data would enhance the near-infrared peaks with some shift toward higher wavelength. Photocurrent response was recorded on an Electro Instruments Model 520 X-Y Plotter.

By using open-circuit conditions in place of an applied voltage, photovoltaic response was also measured with the same instrumentation.

*Coulometry Measurements.* Pellets of $Ag_3SBr$ sandwiched between a gold grid electrode and a gold counterelectrode were fabricated, and the gold counterelectrode was then split to form a three-electrode system. The third electrode acted primarily as an auxiliary, but as it became silver plated, this electrode could also be considered a silver reference electrode. The other solid gold electrode, designated electrode two, was used to collect silver during the experiments, which was then determined coulometrically. The grid, electrode one, was the photoresponsive electrode.

First, electrodes one and two were brought to a positive potential *vs.* electrode three, an operation called "anodic clearing." Following the "clearing" operation, electrode one was held at a positive potential *vs.* electrode two, while electrode three was disconnected. Blank runs were carried out in the dark, but normally this step was with the grid electrode exposed to light. After a period of time of 2–10 min, electrode two was "read-out" coulometrically at a constant current *vs.* electrode three. When silver was completely stripped from electrode two, the potential rose sharply, and the current was automatically stopped when electrode two was +0.500 V *vs.* electrode three. This operation was the same as that used for solid electrolyte coulometers.[6,9] Coulombs of charge were determined from the constant current and time for this read-out and was compared with the coulombs of charge during the light exposure period calculated from the area under the current–time curve.

## Results and Discussion

Photoresponse was observed with $Ag_3SBr$ pellets when the transparent gold electrode was exposed to flashes from a xenon tube 2 in. away. With 250 mV applied between the electrodes (transparent gold electrode positive), peak currents of 22 $\mu$A were recorded. The current decreased as the strobe distance increased, but the peak current appeared saturated for distances less than 2 in.

When continuous illumination was used, two effects were noted. An inital peak current was reached in

(7) A. Scholz, *Ann. Phys.* (Leipzig), 19, 175 (1956).

(8) A. Ichimescu and P. Suciu, *Rev. Roum. Phys.*, 12, 917 (1967).

(9) J. H. Kennedy, F. Chen, and A. Clifton, *J. Electrochem. Soc.*, 115, 918 (1968).

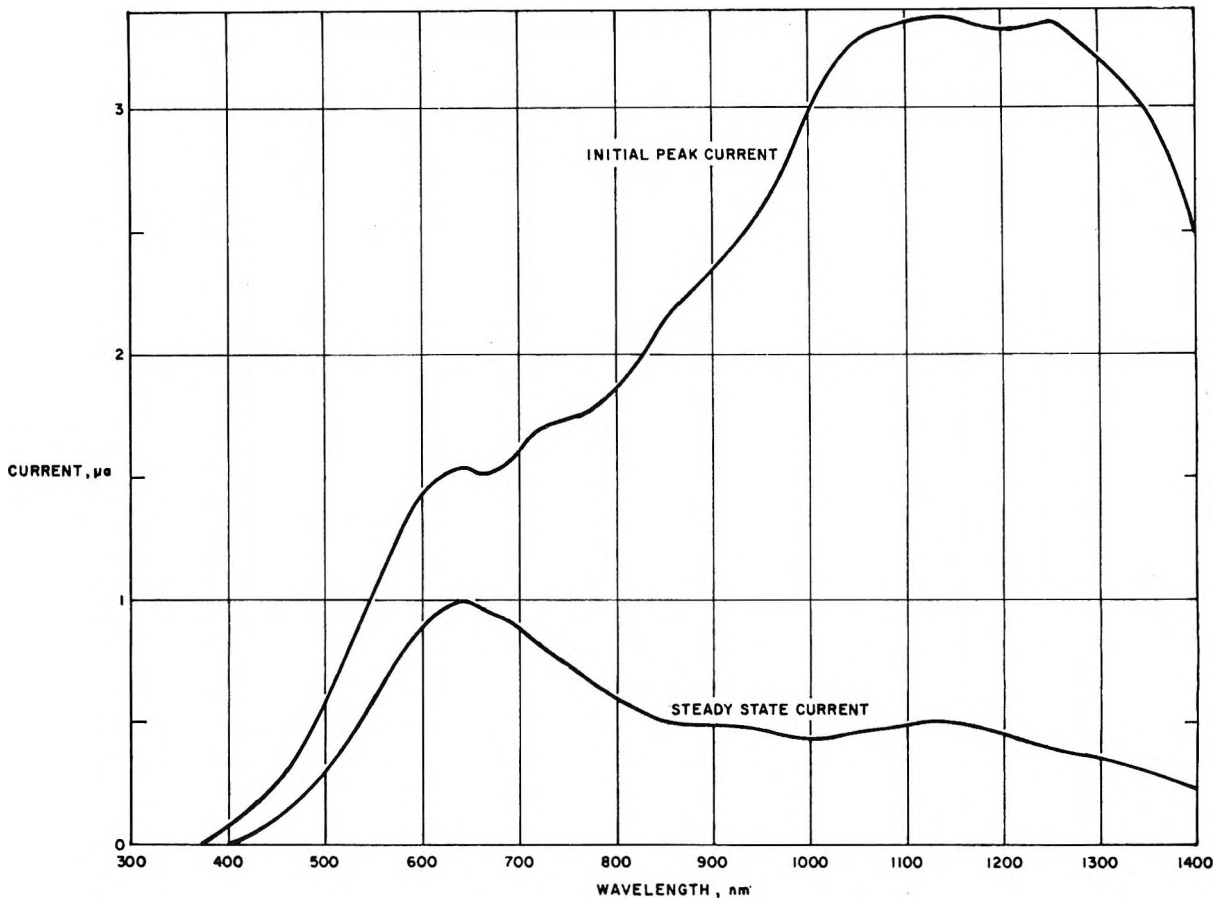


Figure 1. Photoconductivity of $Ag_3SBr$. Applied voltage 50 mV, circuit resistance 100 ohms, illuminated by Sylvania FAW 6200°K color temperature lamp.

less than 100 msec which then decayed to a lower steady-state value. Differences between the peak current and steady-state current varied with material and wavelength; the results are shown in Figures 1 and 2. Current was also a function of applied voltage, as can be seen in Figure 3, with the highest currents being observed with 50–100 mV applied voltage. The difference between peak and steady-state current was much more pronounced with $Ag_3SI$ than $Ag_3SBr$. Steady-state currents for $Ag_3SBr$ in the visible region were 50–75% as great as the initial peak currents, but were only about 10% of peak currents in the near-ir, similar to $Ag_3SI$ behavior. Except for some of the visible wavelength steady-state currents, $Ag_3SBr$ showed lower photocurrents than $Ag_3SI$.

In addition to a current response with an applied voltage, these electrolytes exhibited a voltage output under open circuit conditions of 10–15 mV for $Ag_3SBr$ at 1200 nm. The transparent gold electrode became negative with respect to its potential prior to illumination, but in most cases was still positive with respect to the counterelectrode. Open-circuit dark potential varied with the previous history of the pellets, but the response from dark to light was highly reproducible. Under continuous direct daylight illumination the voltages could exceed 30 mV. However, recovery time to the previous dark condition took several minutes.

Similar experiments using pellets of AgBr, AgI, and $Ag_2S$ showed no detectable response. Although these materials are known to be photoresponsive, only $Ag_3SI$ and $Ag_3SBr$ with high ionic conductivity exhibited photoconductivity under the conditions used. Experiments with $RbAg_4I_5$, which has even higher ionic conductivity,[10] showed some response at lower wavelengths but not the high peaks around 1000 nm which can be attributed to the presence of sulfide.

A three-electrode system was designed to investigate the nature of the photocurrent, *i.e.*, ionic and/or electronic contributions. In this cell, photocurrent flowed between the positive gold minigrid electrode and a pure gold counterelectrode. Ionic current would plate silver on the gold counterelectrode which could then be stripped coulometrically. The technique was the same as that used for studying solid electrolyte coulometry.[6,9] The clearing operations to ensure a pure gold surface at the beginning of light exposure are described in the experimental section. Results in Table I show that the photocurrent is indeed ionic in nature. It may be pointed out that this technique

(10) B. B. Owens and G. R. Argue, *Science*, **157**, 308 (1967).

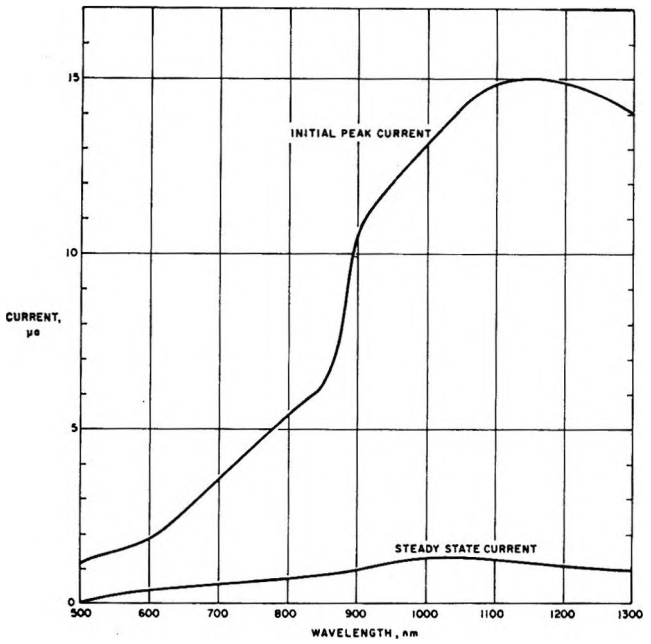


Figure 2. Photoconductivity of $Ag_3SI$. Applied voltage 75 mV, circuit resistance 100 ohms, illuminated by Sylvania FAW 6200°K color temperature lamp.

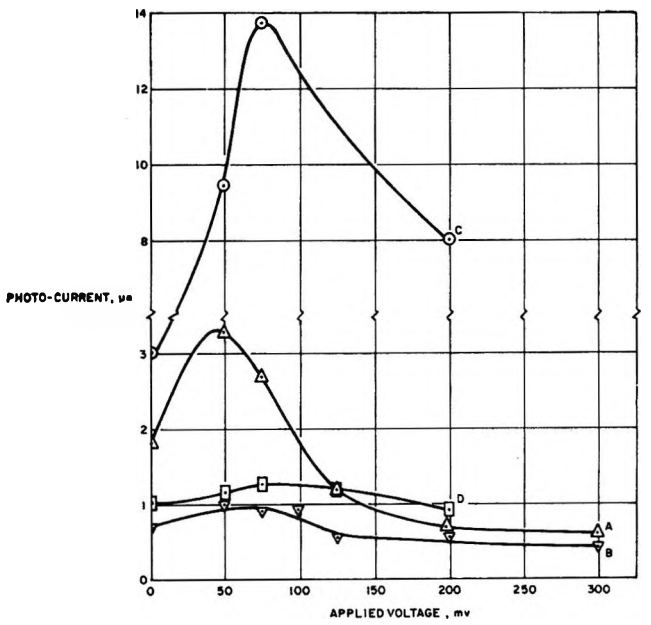


Figure 3. Photocurrent dependence on applied voltage: A, $Ag_3SBr$ peak current at 1100 nm; B, $Ag_3SBr$ steady state current at 650 nm; C, $Ag_3SI$ peak current at 1100 nm; D, $Ag_3SI$ steady state current at 650 nm.

may be useful for measuring light signals with storage of the information in the form of plated silver which can be read out by anodic stripping at a later time.

Based on these results, the following mechanism is postulated. Photons produce photoelectrons by reaction with sulfide ions near the gold minigrid electrode and making it become more negative at open circuit. When held positive, the minigrid electrode collects

**Table I:** Integration of Photocurrent Results of $Ag_3SBr$

| Photocurrent | | | | |
|---|---|---|---|---|
| Duration, sec | Peak current, μA | Charge, mC | Silver plated, mC | Diff, %[a] |
| 450 | 50 | 15.6 | 17.8 | +14 |
| 360 | 90 | 23.7 | 23.2 | −2 |
| 500 | 60 | 18.8 | 17.2 | −9 |
| 400 | 60 | 18.0 | 20.2 | +12 |
| 300 | 45 | 10.0 | 11.4 | +11 |
| 330 | 80 | 21.4 | 21.6 | +1 |
| 300 | 48 | 11.0 | 13.3[b] | +21 |

[a] Positive difference assigned for more silver found than charge calculated by integrating photocurrent. [b] Silver stripped 2.5 hr after exposure, showing storage capability. From ref 6, Figure 10 it is seen that a positive error is expected after storage, amounting to about 1.5 mC. If this correction is included, the silver-plated value becomes 11.8 and the difference is +7%.

the electrons which then flow through the electrical circuit to the counterelectrode. In previous studies, the light-exposed surface was not kept positive, which allowed the photoelectrons to diffuse into the bulk material. The applied voltage dependence, shown in Figure 3, suggests that photoionization occurs more readily as the local Fermi level at the minigrid is raised (less positive voltage), but that the existence of at least some positive potential aids the electrode collection process. Sulfide ions at the electrode surface would be especially active and account for the initial peak currents shown in Figure 1 and 2. The lower steady-state currents, on the other hand, are supported by migration of electrons produced away from the electrode surface toward the positive electrode.

At the counterelectrode, silver ions migrating to the cathode are reduced to silver metal. Since a buildup of excess silver ions would occur at the anode as sulfide ions are oxidized to sulfur, there would be a net flow of silver ions from anode to cathode which is the same as that postulated in the previous photovoltaic studies with AgBr or $Ag_2S$. Since the photoelectrons are collected by the positive gold electrode, the photocurrent is ionic in nature. The process depends on fast migration of silver ions and helps to account for the high response of $Ag_3SBr$ and $Ag_3SI$ compared to AgBr, AgI, or $Ag_2S$. For compounds of low conductivity, the rate-controlling step could actually be the migration of silver ions since the migration of photoelectrons toward the anode mentioned above would also depend on a cooperative migration of charge carriers in the electrolyte to preserve charge balance. However, the high conductivity of $Ag_3SBr$ and $Ag_3SI$ should be ample to support the low photocurrents observed.

The wavelength dependence suggests that the photoreaction is primarily due to reaction with sulfide. The peak response at 1100–1200 nm is close to the 1050-nm peak reported for $Ag_2S$. It must be remembered that

$Ag_3SX$ does not contain $Ag_2S$ as such, but does contain sulfide ions surrounded by silver ions as does $Ag_2S$. A shift in the maximum would not be surprising since the sulfide ion environment is somewhat different. The additional small peak found for $Ag_3SBr$ between 600 and 700 nm may be a contribution from a photoreaction involving bromide or possibly a second ionization of sulfur ions. The maximum response for AgBr films was recently reported to be 365 nm,[11] the same as AgI.[11] However, some response has been observed close to 500 nm for AgBr[3] and may be shifted to higher wavelength by the change in environment. Photoreaction with iodide appears to be absent although there was some response in the visible region which could include a contribution from such a reaction.

In conclusion, the photoreaction appears to be primarily with sulfide, but the ionic current which flows is supported by the facile migration of silver ions present in $Ag_3SX$ compounds.

*Acknowledgment.* The authors thank Mr. Currie of Bissett-Berman Corp. for carrying out many of the experiments described.

(11) B. U. Barshchevskii, *Fiz. Tverd. Tela*, **10**, 3689 (1968).

# Activity Coefficients of Solutions from the Intensity Ratio of Rayleigh to Brillouin Scattering[1]

**by Louis Fishman and Raymond D. Mountain**

*Institute for Basic Standards, National Bureau of Standards, Washington, D. C. 20234* *(Received December 29, 1969)*

The ratio of the intensity of Rayleigh to Brillouin scattered light for a binary mixture with internal degrees of freedom is determined by calculating the frequency spectrum of fluctuations in concentration, temperature, and pressure. Thermodynamic fluctuation theory and linearized hydrodynamic equations, modified to include the internal degrees of freedom through a frequency-dependent volume viscosity, are employed in the calculation. The intensity ratio is of interest as it may be used to determine activity coefficients. A method of doing so when the system contains internal degrees of freedom is described.

## Introduction

Miller has pointed out how light scattering experiments, in which the Rayleigh and Brillouin components of the scattered light are resolved, may be used to determine the activity coefficients of binary solutions.[2a] The ratio $J$ of the intensity of the Rayleigh to the Brillouin scattered light was found from thermodynamic fluctuation theory[2b] to be

$$\frac{J}{k_BT} = \frac{(\partial\epsilon/\partial c)^2_{p,T}/(\partial\mu/\partial c)_{p,T} + (\partial\epsilon/\partial T)^2_{p,c}T_o/C_p}{\rho_o/\beta_s[(\partial\epsilon/\partial_p)_{T,c} + (T_o\alpha_T/\rho_oC_p)(\partial\epsilon/\partial T)_{p,c}]^2} \quad (1)$$

Here $k_BT$ is Boltzmann's constant times the absolute temperature, $\epsilon$ is the dielectric constant (measured at optical frequencies), $\mu$ is the chemical potential, and c is the concentration as defined by Landau and Lifshitz,[3] $C_p$ is the specific heat at constant pressure, $\rho$ is the density, $p$ is the pressure, $\beta_s$ is the adiabatic compressibility, and $\alpha_T$ is the isothermal expansion coefficient of the mixture. The subscript o indicates an equilibrium quantity. The appropriateness of this result was confirmed by a dynamical calculation made by Deutch and one of the authors.[4]

In a subsequent paper, Miller and Lee reported measurements of the intensity ratio for several dilute solutions.[5] It is not possible to apply eq 1 directly to most of these measurements as several of the solvents chosen exhibit internal degrees of freedom (thermal relaxation or structural relaxation). In recognition of this situation, Miller and Lee heuristically developed a modified

(1) Contribution of the National Bureau of Standards, not subject to copyright.

(2) (a) G. A. Miller, *J. Phys. Chem.*, **71**, 2305 (1967); (b) L. D. Landau and E. M. Lifshitz, "Statistical Physics," Addison-Wesley Publishing Co., Inc., Reading, Mass., 1958, Chapter 12.

(3) L. D. Landau and E. M. Lifshitz, "Fluid Mechanics," Addison-Wesley Publishing Co., Inc., Reading, Mass., 1959, Chapter 6. For 1 g of solution $\mu = \mu_1/m_1 - \mu_2/m_2$ where $\mu_1$ and $\mu_2$ are the chemical potentials and $m_1$ and $m_2$ are the masses of the two species. If $n_1$ is the number of particles of substance one in 1 g then $c = n_1m_1$.

(4) R. D. Mountain and J. M. Deutch, *J. Chem. Phys.*, **50**, 1103 (1969).

(5) G. A. Miller and C. S. Lee, *J. Phys. Chem.*, **72**, 4644 (1968).

expression for $J$ which takes the effects of the internal degrees of freedom into account for dilute solutions. It has been shown for a one-component fluid that internal degrees of freedom can lead to substantial departures from the thermodynamic fluctuation theory prediction for the intensity ratio of the Rayleigh to the Brillouin scattered light.[6-9] In these cases it is frequently necessary to employ a dynamical calculation of the spectrum of the scattered light to obtain a reliable estimate of the intensity ratio. In this paper we describe such a calculation for a binary mixture, with internal degrees of freedom.

The principal result of this calculation is contained in eq 14. This is a generalization of the intensity ratio expression, eq 1, to the case where the internal degrees of freedom may be described in terms of a frequency dependent volume viscosity which exhibits a single relaxation time. This form for the viscosity is frequently employed to describe thermal relaxation. A more complex form is usually employed to describe structural relaxation in detail.[10] Even so, the single relaxation time expression for the intensity ratio may be usefully used to characterize such processes in an approximate way. We shall find that Miller and Lee's extension of eq 1 for dilute solutions with internal modes is reasonable for the case of thermal relaxation but not generally applicable for the case of structural relaxation. Our result differs from Miller and Lee's expression for the intensity ratio. The quantities appearing in eq 14 apply to the binary mixture itself whereas Miller and Lee use pure solvent quantities and extrapolate to the dilute solution quantities.

## Calculation

The intensity of the light scattered by thermodynamic fluctuations is given by[11]

$$I(k,\omega) = I_0[Nk_0^4/32\pi^3R^2][\sin^2\Phi]S(k,\omega) \quad (2)$$

where $k$ is the change in the wave vector and $\omega$ is the change in the angular frequency of the light resulting from the scattering; $R$ is the distance from the scattering volume to the point of observation; $\Phi$ is the angle between the electric vector of the plane polarized incident light of intensity $I_0$ and $R$. The relationship between the magnitude of $k$ and the magnitude of $k_0$, the wave vector of the incident light, is, when $\Phi = \pi/2$

$$k = 2nk_0 \sin \theta/2 \quad (3)$$

Here $n$ is the index of refraction and $\theta$ is the scattering angle. The generalized structure factor $S(k,\omega)$ is the space and time Fourier transform of the correlation function for fluctuations in the dielectric constant of the fluid

$$S(k,\omega) = 2Re \int_0^\infty dt \int dr dr' \langle \delta\epsilon(r + r',t)\delta\epsilon(0,0)\rangle \exp[i(k\cdot r - \omega t)] \quad (4)$$

The fluctuations in the dielectric constant are related to fluctuations in the local thermodynamic quantities pressure, concentration, and temperature by

$$\delta\epsilon(r,t) = \left(\frac{\partial\epsilon}{\partial p}\right)_{c,T} \delta p(r,t) + \left(\frac{\partial\epsilon}{\partial c}\right)_{p,T} \delta c(r,t) + \left(\frac{\partial\epsilon}{\partial T}\right)_{p,c} \delta T(r,t) \quad (5)$$

The calculation proceeds along the same lines as those described in ref 4. The dynamics of the fluctuations in pressure, concentration, and temperature are characterized by linearized hydrodynamic equations for a binary solution.[12] The Navier–Stokes equation is modified so that the volume viscosity, assumed to be constant in ref 4, is now assumed to have a part which relaxes by a single relaxation time mechanism. These linearized equations of motion are the continuity eq 6, the divergence of the Navier–Stokes eq 7, the

$$\frac{\partial\rho}{\partial t} + \rho_0 \operatorname{div} v = 0 \quad (6)$$

$$\frac{\partial \operatorname{div} v}{\partial t} = -\frac{1}{\rho_0}\nabla^2 p + b_0\nabla^2 \operatorname{div} v + (c_\infty^2 - c_0^2)\int_0^t e^{-t'/\tau}\nabla^2 \operatorname{div} v(t - t')\, dt' \quad (7)$$

diffusion eq 8, and the energy transport eq 9. In these

$$\frac{\partial c}{\partial t} = D[\nabla^2 c + (k_T/T_0)\nabla^2 T + (k_p/p_0)\nabla^2 p] \quad (8)$$

$$\rho_0 C_p \frac{\partial T}{\partial t} - \rho_0 k_T \left(\frac{\partial\mu}{\partial c}\right)_{p,T}\frac{\partial c}{\partial t} + \rho_0 T_0 \left(\frac{\partial S}{\partial c}\right)_{T,c}\frac{\partial p}{\partial t} = \kappa\nabla^2 T \quad (9)$$

equations $\rho$ is the density, $b_0$ is the frequency independent part of the kinematic viscosity, $c_\infty$ and $c_0$ are the infinite- and zero-frequency sound velocities, $\tau$ is the single relaxation time for the internal degree of freedom, $D$ is the binary diffusion coefficient, $k_T$ is the thermal diffusion ratio, $\kappa$ is the thermal conductivity, and $k_p$ is the thermodynamic quantity

$$k_p = -\frac{(p_0/\rho_0)^2(\partial\rho/\partial c)_{p,T}}{(\partial\mu/\partial c)_{p,T}} \quad (10)$$

(6) R. D. Mountain, *J. Res. Nat. Bur. Stand.*, **70A**, 207 (1966).

(7) C. J. Montrose, V. A. Solovyev, and T. A. Litovitz, *J. Acoust. Soc. Amer.*, **43**, 117 (1968).

(8) A. B. Bhatia and E. Tong, *Phys. Rev.*, **173**, 231 (1968).

(9) W. H. Nichols and E. F. Carome, *J. Chem. Phys.*, **49**, 1000 (1968).

(10) K. F. Herzfeld and T. A. Litovitz, "Absorption and Dispersion of Ultrasonic Waves," Academic Press, New York, N. Y., 1959.

(11) L. D. Landau and E. M. Lifshitz, "Electrodynamics of Continuous Media," Addison-Wesley Publishing Co., Inc., Reading, Mass., 1960, Chapter 14.

(12) These equations are developed in ref 3.

This set of four equations in five unknowns is closed by assuming local thermodynamic equilibrium exists between the density and the pressure, the temperature, and the concentration, that is

$$\delta\rho = \left(\frac{\partial\rho}{\partial p}\right)_{T,c}\delta p + \left(\frac{\partial\rho}{\partial T}\right)_{p,c}\delta T + \left(\frac{\partial\rho}{\partial c}\right)_{p,T}\delta c \quad (11)$$

is used to replace $\delta\rho$ in eq 6. These equations are then solved using the Fourier–Laplace transforms to obtain an expression for the spectrum of light scattered by the fluctuations.

The Fourier–Laplace transforms of eq 6–9 and 11 are taken to obtain linear algebraic equations for the transformed quantities $\hat{c}(k,z)$, $ik\hat{v}(k,z)$, $\hat{p}(k,z)$, and $\hat{T}(k,z)$ where

$$c(k,z) = \int_0^\infty dt \int_v dr e^{ik\cdot r - zt} c(r,t)$$

These equations are solved in terms of initial values; *e.g.*, $c(k, t = 0)$. The structure factor $S(k,\omega)$ is then constructed using eq 4 and 5. Thermodynamic fluctuation theoy[2,4] is employed to evaluate the equilibrium averages indicated by the angular brackets $\langle \ldots \rangle$.

The result of these calculations is

$$S(k,\omega) = \left(\frac{\partial\epsilon}{\partial c}\right)^2_{p,T}\frac{k_B T_o}{(\partial\mu/\partial c)_{p,T}}\left\{\frac{2Dk^2}{(Dk^2)^2+\omega^2} + \right.$$

$$\frac{(c_\infty k\tau)^2 - (vk\tau)^2 + (c_o/v)^4 - (c_o/v)^2}{(vk\tau)^2 + (c_o/v)^4}\frac{2c_o^2/v^2\tau}{(c_o^2/v^2\tau)^2+\omega^2} +$$

$$\frac{(c_o/v)^2(1 - c_o^2/v^2) + (vk\tau)^2(1 - c_\infty^2/v^2)}{(vk\tau)^2 + (c_o/v)^4} \times$$

$$\left[\frac{\Gamma_B}{\Gamma_B^2 + (\omega - vk)^2} + \frac{\Gamma_B}{\Gamma_B^2 + (\omega + vk)^2}\right] +$$

$$\frac{vk\tau(1 - c_o^2/v^2)^2}{(vk\tau)^2 + (c_o/v)^4}\left[\frac{vk + \omega}{\Gamma_B^2 + (vk+\omega)^2} + \right.$$

$$\left.\left.\frac{vk - \omega}{\Gamma_B^2 + (vk-\omega)^2}\right]\right\} + \left[\left(\frac{\partial\epsilon}{\partial p}\right)_{T,c} + \right.$$

$$\left.\frac{T_o\alpha_T}{\rho_o C_p}\left(\frac{\partial\epsilon}{\partial T}\right)_{p,c}\right]^2\frac{k_B T_o^2}{C_p}\left\{\frac{2\chi k^2}{(\chi k^2)^2+\omega^2} + \right.$$

$$\frac{(c_o/v)^4 - (c_o/v)^2 + (c_\infty k\tau)^2 - (vk\tau)^2}{(vk\tau)^2 + (c_o/v)^4}\frac{2c_o^2/v^2\tau}{(c_o^2/v^2\tau)^2+\omega^2} +$$

$$\frac{c_o^2/v^2(1 - c_o^2/v^2) + (vk\tau)^2 - (c_\infty k\tau)^2}{(vk\tau)^2 + (c_o/v)^4} \times$$

$$\left[\frac{\Gamma_B}{\Gamma_B^2 + (\omega - vk)^2} + \frac{\Gamma_B}{\Gamma_B^2 + (\omega + vk)^2}\right] +$$

$$\frac{vk\tau[c_o^2/v^2(1 - c_\infty^2/v^2) - (1 - c_o^2/v^2)]}{(vk\tau)^2 + (c_o/v)^4} \times$$

$$\left.\left[\frac{vk + \omega}{\Gamma_B^2 + (vk+\omega)^2} + \frac{vk - \omega}{\Gamma_B^2 + (vk-\omega)^2}\right]\right\} +$$

$$\left(\frac{\partial\epsilon}{\partial p}\right)^2_{c,T}\frac{k_B T\rho_o}{\beta_s}\left\{\frac{(c_\infty k\tau)^2 - (c_o k\tau)^2 + (c_o/v)^4 - (c_o/v)^2}{(vk\tau)^2 + (c_o/v)^4} \times \right.$$

$$\frac{2c_o^2/v^2\tau}{(c_o^2/v^2\tau)^2 + (\omega^2)} +$$

$$\frac{(vk\tau)^2 - (c_\infty k\tau)^2 + (c_o k\tau)^2 + (c_o/v)^2}{(vk\tau)^2 + (c_o/v)^4} \times$$

$$\left[\frac{\Gamma_B}{\Gamma_B^2 + (\omega - vk)^2} + \frac{\Gamma_B}{\Gamma_B^2 + (\omega + vk)^2}\right] +$$

$$\frac{vk\tau[(c_o/v)^2 - (c_\infty/v)^2(c_o/v)^2 + (c_o/v)^4 - 1]}{(vk\tau)^2 + (c_o/v)^4} \times$$

$$\left.\left[\frac{vk + \omega}{\Gamma_B^2 + (vk+\omega)^2} + \frac{vk - \omega}{\Gamma_B^2 + (vk-\omega)^2}\right]\right\} \quad (12)$$

The quantities $v$ and $\Gamma_B$ are the velocity and absorption coefficient for the propagating decay modes. They are obtained by solving the dispersion equation for the system. For the case under discussion the dispersion equation for the propagating modes is

$$-i\omega^3\tau - \omega^2 + i\omega c_\infty^2 k^2\tau + c_o^2 k^2 = 0 \quad (13)$$

The quantity $\chi$ is the thermal diffusivity $\kappa/\rho_o C_p$. This result is an approximation to the formally exact solution of the problem. In obtaining this expression we make the reasonable assumptions $b_o k^2/c_o k \ll 1$, $\chi k^2/c_o k \ll 1$ and $b_o k^2\tau \ll 1$ for all values of $k$. These are the same assumptions used in ref 6. Also we have assumed $D \ll \chi$.

Equation 12 reduces to the result of ref 4 when $\tau = 0$. The coupling of the concentration fluctuations to the propagating modes comes about because $\tau$ is not small. While we can assume the nonrelaxing viscosity term satisfies $b_o k^2/c_o k \ll 1$ we cannot make such an assumption for the relaxing term since

$$(c_\infty^2 - c_o^2)k^2\tau/(1 + i\omega\tau)$$

is comparable to $c_o k$ and must be taken into account. By doing so, we arrive at eq 12.

## Discussion

As we are principally concerned with the intensity ratio let us restrict our discussion to the intensity associated with the individual terms. For purposes of this discussion we shall assign the Lorentzian term having a width $(c_o^2/v^2\tau)$ to the central component. This is reasonable since this term is significant only when $vk\tau \gtrsim 1$ so that the Brillouin frequency is greater than the width of this term. With this definition of the central component the intensity ratio $J(k)$ of the Rayleigh to the Brillouin components is

$$J(k) = \frac{J(0)[1 + A(k)] + B(k)}{1 - B(k) - J(0)A(k)} \quad (14)$$

Here $J(0)$ is Miller's result given in eq 1. The quantities $A(k)$ and $B(k)$ are

$$A(k) = \frac{(c_\infty^2 - v^2)k^2\tau^2 + (c_0/v)^4 - (c_0/v)^2}{(vk\tau)^2 + (c_0/v)^4} \quad (15)$$

$$B(k) = \frac{(c_\infty^2 - c_0^2)k^2\tau^2 + (c_0/v)^4 - (c_0/v)^2}{(vk\tau)^2 + (c_0/v)^4} \quad (16)$$

These functions have the properties that as $k \to 0$, $A(k) = B(k) = 0$ and that as $k \to \infty$, $A(k) = 0$ and $B(k) = 1 - (c_0/c_\infty)^2$. This means that as $k \to 0$ $(vk\tau \ll 1)$ $J(k) \to J(0)$ as it must. Also as $k \to \infty$ $(vk\tau \gg 1)$

$$J \to \frac{c_\infty^2}{c_0^2} J(0) - 1 + \frac{c_\infty^2}{c_0^2} \quad (17)$$

The wave vector dependent quantities $v(k)$, $A(k)$, and $B(k)$ have been computed for a system with properties similar to those of $CCl_4$ ($c_0 = 10^3$ m/sec, $c_\infty = 1.15 \times 10^3$ m/sec, $n = 1.5$, and $\tau = 5 \times 10^{-11}$ sec). The functions $A(k)$ and $B(k)$ are displayed in Figure 1, for this system as a function of wave vector. The scattering angle $\theta$ is indicated on the top of Figure 1 to illustrate the relation between scattering angle and wave vector. (Values $n = 1.5$ and $\lambda_0 = 6328$ Å were used to determine $\theta$ in eq 3.) The wave vector dependent velocity $v(k)$ is displayed in Figure 2.

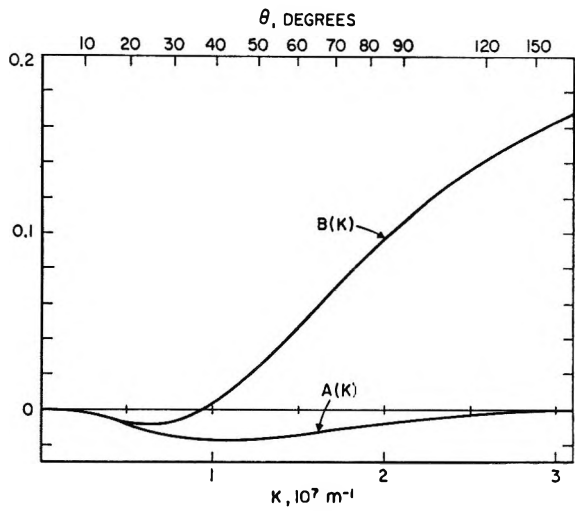


Figure 1. $A(k)$ and $B(k)$ as a function of $k$ (and of $\theta$) for a system with parameters; $c_0 = 10^3$ m/sec, $c_\infty = 1.15$ m/sec, $n = 1.5$, and $\tau = 5 \times 10^{-11}$ sec, the scattering angles correspond to red light ($\lambda_0$ 6328 Å).

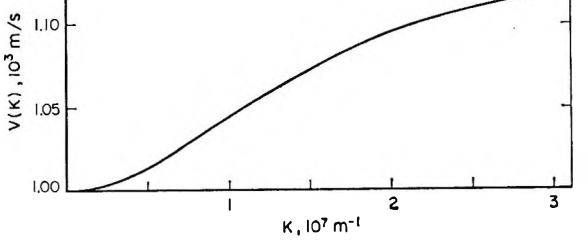


Figure 2. Wave vector dependent velocity $v(k)$ as a function of $k$ for a system with parameters; $c_0 = 10^3$ m/sec, $c_\infty = 1.15$ m/sec, and $\tau = 5 \times 10^{-11}$ sec.

It would appear that $A(k)$ is a relatively unimportant term. The term $B(k)$ is quite important for all but the small scattering angles. For $\theta = 90°$, $B(k) \approx 0.1$ and therefore can make an important contribution to the intensity ratio.

How does this relate to the work of Miller and Lee? They propose to extract activity coefficients for dilute solutions from measured values of $J(k)$ (with $k$ fixed) through the use of an expression with the form

$$J = A + BKRTx_1/(\partial\mu_2/\partial x_2)_{p,T} \quad (18)$$

Here $A$, $B$, and $K$ are quantities to be determined by other experiments and $R$ is the gas constant. The subscript 1 refers to the solvent and the subscript 2 refers to the solute. Thus $x_1$ is the mole fraction of solvent and $\mu_2$ is the chemical potential of the solute. Once this is done the activity coefficient is to be determined from the concentration dependence of $(\partial\mu_2/\partial x_2)_{p,T}$.

It would appear that the success of Miller and Lee's formulation depends crucially on whether or not the quantities $c_\infty$, $c_0$, and $\tau$ depend significantly on the concentration. In addition, those authors assume that the temperature and pressure fluctuation terms may be equated to the corresponding terms for the pure solvent. In this way eq 18 differs from our result, eq 14, since all quantities in our expression refer to the solution.

In the case of thermal relaxation these assumptions appear to hold for dilute solutions. As reported in ref 5, eq 18 was found to be an acceptable representation for the intensity ratio data. This is reasonable as the function $B(k)$ should not depend strongly on concentration for dilute solutions.

For systems undergoing structural relaxation the relaxation parameters $c_\infty$, $c_0$, and $\tau$ are usually quite sensitive to the concentration. This will seriously complicate the process of determining activity coefficients from intensity ratio measurements made at one scattering angle.

It is still possible to use this method if measurements are made as a function of wave vector $k$ as well as of concentration. If the scattering angle is small enough $(vk\tau \ll 1)$, one may use eq 1 to describe the intensity ratio. If this is not feasible, measurements made at several scattering angles may be used to determine $B(k)$ and $J(O)$ jointly. Once $J(O)$ is known, one proceeds as before. Although this procedure requires measurements for several scattering angles, there is still much to recommend it as a means of obtaining activity coefficients. The principal one is that only relative intensity measurements are required. This is a considerable simplification over traditional light scattering methods which require accurate intensity measurements.

For systems undergoing structural relaxation, the single relaxation time formulation employed here will not be adequate and a more involved expression for the frequency dependence of the kinematic viscosity should be used in the calculations. This is a straightforward calculation which we do not discuss here.

# The Transient Electric Birefringence of Rigid Macromolecules in Solution under the Action of a Rectangular Pulse and a Reversing Pulse

**by Mitsuhiro Matsumoto, Hiroshi Watanabe, and Koshiro Yoshioka**

*Department of Chemistry, College of General Education, University of Tokyo, Meguroku, Tokyo, Japan*
*(Received December 2, 1969)*

The diffusion equation describing the rotational diffusion of axially symmetric rigid macromolecules in solution placed in an electric field is solved by the use of the perturbation method, and equations for the rise of the birefringence under the action of a rectangular electrical pulse and for the birefringence in a rapidly reversed electric field are derived from the angular distribution function thus obtained. Calculations are performed up to the fourth-order perturbation in the general case and up to the sixth-order perturbation in the case of pure permanent dipole orientation. The extent of applicability of the Benoit theory for the rise birefringence and the Tinoco–Yamaoka theory for the reverse birefringence is discussed. Further, the effect of polydispersity is considered. It is shown that the rise, reverse, and decay curves are related by a simple equation even for a polydisperse system.

## Introduction

When a rectangular electrical pulse is applied to a macromolecular solution, the birefringence produced changes with time; it rises, reaches a steady state, if the pulse duration is sufficiently long, and then decays.[1,2] This pulse technique has been successfully used for investigating the electrical and hydrodynamical properties of rigid macromolecules in solution.[3] Benoit[1] has developed a theory for the rise and decay of the electric birefringence. He considered an ellipsoid of revolution with a permanent dipole moment along the symmetry axis as a model for the macromolecule and solved the diffusion equation which describes the rotational diffusion of rigid macromolecules in an electric field by expanding the angular distribution function in a series of Legendre functions. He obtained an expression for the rise of the birefringence which is valid at low fields and showed that the mechanism of electrical orientation can be elucidated from the rise curve. Tinoco[4] has extended Benoit's theory to include the effect of a transverse component of the permanent dipole moment. He also considered the contribution of the fluctuating dipole moment due to proton migration to the rise of the birefringence. O'Konski, Yoshioka, and Orttung[5] have obtained equations for the rise of the birefringence at infinitely high field strength in the cases of pure permanent dipole orientation and pure induced dipole orientation, following the treatment of Schwarz,[6] who pointed out that the effect of rotational diffusion can be neglected at infinitely high field strength. Nishinari and Yoshioka[7] have proposed a theory for the rise of the birefringence which holds for arbitrary field strength in the initial stage. They showed that it is possible to determine the permanent dipole moment and the anisotropy of electrical polarizability separately from measurements of the rise of the birefringence at high fields.

O'Konski and Haltner[8] have introduced the reversing-pulse technique in birefringence measurements; a square pulse is applied to a macromolecular solution, and, after the steady-state birefringence is achieved, the field is rapidly reversed in sign. This technique is very

(1) H. Benoit, *Ann. Phys.*, **6**, 561 (1951).

(2) C. T. O'Konski and B. H. Zimm, *Science*, **111**, 113 (1950).

(3) For a review, see K. Yoshioka and H. Watanabe in "Physical Principles and Techniques of Protein Chemistry, Part A," S. J. Leach, Ed., Academic Press, Inc., New York, N. Y., 1969, p 335.

(4) I. Tinoco, Jr., *J. Amer. Chem. Soc.*, **77**, 4486 (1955).

(5) C. T. O'Konski, K. Yoshioka, and W. H. Orttung, *J. Phys. Chem.*, **63**, 1558 (1959).

(6) G. Schwarz, *Z. Phys.*, **145**, 563 (1956).

(7) K. Nishinari and K. Yoshioka, *Kolloid-Z. Z. Polym.*, **235**, 1189 (1969).

(8) C. T. O'Konski and A. J. Haltner, *J. Amer. Chem. Soc.*, **79**, 5634 (1957).

useful for investigating the mechanisms of electrical orientation. Tinoco and Yamaoka[9] have derived equations for the birefringence under the action of a reversing pulse and plotted them for various values of the electrical parameters of the macromolecule. Their equations are valid at low fields.

In this paper we derive equations for the rise and reverse birefringences which hold even for higher fields. The angular distribution function of rigid macromolecules in an electric field is obtained by solving the diffusion equation by the use of the perturbation method. Calculations are performed up to the fourth-order perturbation in the general case and up to the sixth-order perturbation in the case of pure permanent dipole orientation. The results are also presented in graphs. The extent of applicability of the Benoit theory for the rise of the birefringence and the Tinoco–Yamaoka theory for the reverse birefringence is discussed. Further, the effect of polydispersity on the rise and reverse birefringence is considered, and a simple equation relating the rise, reverse, and decay curves which hold even for a polydisperse system is obtained.

## Theory

The time dependence of the birefringence for a dilute solution of rigid macromolecules under the action of a rectangular pulse and a reversing pulse will be considered. We assume that the macromolecule has a common axis of symmetry for its electrical, optical, and hydrodynamic properties and the permanent dipole moment is along this axis. When an electric field is applied to the solution, a torque is exerted on the macromolecule and the angular distribution function of orientation changes with time. The angular distribution function $f(\theta, t)$, which depends on time $t$ and the angle $\theta$ between the symmetry axis of the macromolecule and the field direction, should satisfy the diffusion equation

$$\frac{\partial f}{\partial t} = \Theta\nabla^2 f - \operatorname{div}\left(f\frac{M}{\zeta}\right) \tag{1}$$

where $\Theta$ is the rotational diffusion constant for rotation about the transverse axis, $M$ is the torque, $\zeta$ is the rotational frictional coefficient, and the symbol $\nabla^2$ is the Laplacian operator. On introducing Einstein's relation $\Theta = kT/\zeta$, where $k$ is the Boltzmann constant and $T$ is the absolute temperature, eq 1 becomes

$$\frac{1}{\Theta}\frac{\partial f}{\partial t} = \nabla^2 f - \frac{1}{kT}\operatorname{div}(fM) \tag{2}$$

In the present model the torque is given by

$$M = -\mu' E \sin\theta - (\alpha_1 - \alpha_2)E^2 \sin\theta\cos\theta \tag{3}$$

where $E$ is the field strength, $\mu'$ is the apparent permanent dipole moment in solution, and $\alpha_1$ and $\alpha_2$ are the excess electrical polarizabilities along the symmetry and transverse axes, respectively. Introducing the notations

$$u = \cos\theta \tag{4}$$

$$\beta = (\mu'/kT)E = bE \tag{5a}$$

and

$$\gamma = [(\alpha_1 - \alpha_2)/2kT]E^2 = cE^2 \tag{5b}$$

we obtain from eq 2 and 3

$$\frac{\partial}{\partial u}\left\{(1-u^2)\frac{\partial f}{\partial u} - (1-u^2)\times (\beta + 2\gamma u)f\right\} = \frac{1}{\Theta}\frac{\partial f}{\partial t} \tag{6}$$

To solve this partial differential equation we attempt to separate variables by the substitution

$$f(u, t) = g(t)h(u) \tag{7}$$

Introducing this into eq 6 and dividing by $g(t)h(u)$, we obtain

$$\frac{1}{h}\frac{\mathrm{d}}{\mathrm{d}u}\left\{(1-u^2)\frac{\mathrm{d}h}{\mathrm{d}u} - (1-u^2)\times (\beta + 2\gamma u)h\right\} = \frac{1}{\Theta}\frac{1}{g}\frac{\mathrm{d}g}{\mathrm{d}t} \tag{8}$$

The right side of eq 8 is a function of $t$ alone and the left side is a function of $u$ alone. Hence the value of the quantity to which each side is equal must be a constant, which we call $-\lambda$. Equation 8 can then be written as two differential equations, namely

$$\frac{1}{\Theta}\frac{\mathrm{d}g}{\mathrm{d}t} = -\lambda g \tag{9}$$

and

$$\frac{\mathrm{d}}{\mathrm{d}u}\left\{(1-u^2)\frac{\mathrm{d}h}{\mathrm{d}u} - (1-u^2)\times (\beta + 2\gamma u)h\right\} + \lambda h = 0 \tag{10}$$

The equation for $g(t)$ can be integrated at once to give

$$g(t) = (\text{constant})\exp(-\lambda\Theta t) \tag{11}$$

whereas the equation for $h(u)$ cannot be analytically integrated in general. However, eq 10 is transformed into the self-adjoint form by multiplying it by $\exp(-\beta u - \gamma u^2)$, namely

$$\frac{\mathrm{d}}{\mathrm{d}u}\left\{(1-u^2)\exp(-\beta u - \gamma u^2)\frac{\mathrm{d}h}{\mathrm{d}u}\right\} + (6\gamma u^2 + 2\beta u - 2\gamma)\exp(-\beta u - \gamma u^2)h + \lambda\exp(-\beta u - \gamma u^2)h = 0 \tag{12}$$

(9) I. Tinoco, Jr., and K. Yamaoka, *J. Phys. Chem.*, **63**, 423 (1959).

This equation is a kind of the Liouville equation with two singular points at $u = 1$ and $u = -1$. Denoting the solution by $h_n$ for $\lambda = \lambda_n$ and by $h_m$ for $\lambda = \lambda_m$, we multiply the equation for $h_n$ by $h_m$ and the equation for $h_m$ by $h_n$ and subtract the one from the other. Integrating the resulting equation from $-1$ to 1, we obtain the relation

$$(\lambda_n - \lambda_m)\int_{-1}^{1} h_n h_m \exp(-\beta u - \gamma u^2)\, du = 0 \quad (13)$$

as long as $h_n$ and $h_m$ are finite at $u = 1$ and $u = -1$. Equation 13 indicates that $h_n \exp\{-(\beta u + \gamma u^2)/2\}$ and $h_m \exp\{-(\beta u + \gamma u^2)/2\}$ are mutually orthogonal and that $\lambda_n$ and $\lambda_m$ are the eigenvalues. Making the substitution

$$y_n(u) = h_n(u) \exp\{-(\beta u + \gamma u^2)/2\} \quad (14)$$

into eq 10 and referring to eq 5a and 5b, we find that $y_n$ must satisfy the equation

$$\frac{d}{du}\left\{(1 - u^2)\frac{dy_n}{du}\right\} + \left[buE + \left\{\left(\frac{b^2}{4} + 3c\right)u^2 - \left(\frac{b^2}{4} + c\right)\right\}E^2 + bc(u^3 - u)E^3 + c^2(u^4 - u^2)E^4\right]y_n + \lambda_n y_n = 0 \quad (15)$$

In the limit as $E \to 0$, eq 15 reduces to

$$\frac{d}{du}\left\{(1 - u^2)\frac{dy_n}{du}\right\} + \lambda_n y_n = 0 \quad (16)$$

For the solution of this equation to be finite in the range $-1 \leqq u \leqq 1$, $\lambda_n = n(n + 1)$ with $n = 0, 1, 2, \ldots$. The function $y_n$ corresponding to $\lambda_n$ is the Legendre function of degree $n$, $P_n(u)$.

We can obtain an approximate solution of eq 15 by the use of the perturbation method. Let us expand the eigenvalue $\lambda_n$ and the eigenfunction $y_n$ in terms of $E$

$$\lambda_n = n(n + 1) + \alpha_n E + \beta_n E^2 + \gamma_n E^3 + \delta_n E^4 + \ldots \quad (17)$$

$$y_n(u) = P_n(u) + a_n(u)E + b_n(u)E^2 + c_n(u)E^3 + d_n(u)E^4 + \ldots \quad (18)$$

Introducing eq 17 and 18 in eq 15 and equating the terms of $E$, $E^2$, $E^3$, and $E^4$ to zero, we obtain a set of differential equations

$$\frac{d}{du}\left\{(1 - u^2)\frac{da_n}{du}\right\} + (bu + \alpha_n)P_n + n(n + 1)a_n = 0 \quad (19a)$$

$$\frac{d}{du}\left\{(1 - u^2)\frac{db_n}{du}\right\} + \left\{\left(\frac{b^2}{4} + 3c\right)u^2 - \left(\frac{b^2}{4} + c\right) + \beta_n\right\}P_n + (bu + \alpha_n)a_n + n(n + 1)b_n = 0 \quad (19b)$$

$$\frac{d}{du}\left\{(1 - u^2)\frac{dc_n}{du}\right\} + \{bc(u^3 - u) + \gamma_n\}P_n + \left\{\left(\frac{b^2}{4} + 3c\right)u^2 - \left(\frac{b^2}{4} + c\right) + \beta_n\right\}a_n + (bu + \alpha_n)b_n + n(n + 1)c_n = 0 \quad (19c)$$

$$\frac{d}{du}\left\{(1 - u^2)\frac{dd_n}{du}\right\} + \{c^2(u^4 - u^2) + \delta_n\}P_n + \{bc(u^3 - u) + \gamma_n\}a_n + \left\{\left(\frac{b^2}{4} + 3c\right)u^2 - \left(\frac{b^2}{4} + c\right) + \beta_n\right\}b_n + (bu + \alpha_n)c_n + n(n + 1)d_n = 0 \quad (19d)$$

These equations are solved by expanding $a_n(u)$, $b_n(u)$, $c_n(u)$, and $d_n(u)$ in terms of Legendre functions. The coefficients of expansion are subject to the condition

$$\int_{-1}^{1} {y_n}^2\, du = \frac{2}{2n + 1} \quad (20)$$

In this work we retained all terms up to $E^4$. It is to be noted that $\alpha_n = \gamma_n = 0$.

Thus, the general solution of eq 6 is given by

$$f(u, t) = \sum_{n=0}^{\infty} A_n h_n \exp(-\lambda_n \Theta t) = \sum_{n=0}^{\infty} A_n y_n \exp\{(\beta u + \gamma u^2)/2\} \exp(-\lambda_n \Theta t) \quad (21)$$

where $A_n$'s are constants. For the rise process, $A_n$'s are determined so as to satisfy the initial condition

$$f(u, 0) = \sum_{n=0}^{\infty} A_n h_n = \sum_{n=0}^{\infty} A_n y_n \exp\{(\beta u + \gamma u^2)/2\} = \frac{1}{4\pi} \quad (22)$$

From eq 22 and the orthogonality of $y_n$ we obtain

$$A_n = \frac{2n + 1}{8\pi}\int_{-1}^{1} y_n \exp\{-(\beta u + \gamma u^2)/2\}\, du \quad (23)$$

The solution of eq 10 for $\lambda = 0$ gives $h_0$, and it is found that

$$f(u, \infty) = A_0 h_0 = \frac{\exp(\beta u + \gamma u^2)}{2\pi\int_{-1}^{1} \exp(\beta u + \gamma u^2)\, du} \quad (24)$$

For a reversing pulse, the angular distribution function is obtained by replacing $E$ by $-E$ ($\beta$ by $-\beta$) in the preceding treatment and applying the initial condition

$$f(u, 0) = \sum_{n=0}^{\infty} A_n h_n = \frac{\exp(\beta u + \gamma u^2)}{2\pi\int_{-1}^{1} \exp(\beta u + \gamma u^2)\, du} \quad (25)$$

It is found that

$$f(u, \infty) = A_0 h_0 = \frac{\exp(-\beta u + \gamma u^2)}{2\pi \int_{-1}^{1} \exp(-\beta u + \gamma u^2)\, du} \quad (26)$$

*Birefringence.* The electric birefringence is given by[10]

$$\Delta n = \frac{2\pi c(g_1 - g_2)}{n\rho} 2\pi \int_{-1}^{1} \frac{3u^2 - 1}{2} f(u, t)\, du \quad (27)$$

where $c$ is the concentration in grams per cubic centimeter, $\rho$ is the density of the solute, $n$ is the refractive index of the solution, and $g_1 - g_2$ is the optical anisotropy factor. Substituting eq 21 into eq 27 and expanding the exponential functions up to the terms of $E^4$, we can perform the integration. The final result for the rise of the normalized birefringence, $\Delta(t)$, is

$$\Delta(t) \equiv \frac{\Delta n(t)}{\Delta n(\infty)} = 1 - \frac{X_1}{X_0} \exp(-\lambda_1 \Theta t) + \frac{X_2}{X_0} \exp(-\lambda_2 \Theta t) - \frac{X_3}{X_0} \exp(-\lambda_3 \Theta t) \quad (28)$$

where $\Delta n(t)$ is the birefringence at time $t$, $\Delta n(\infty)$ is the birefringence for $t \to \infty$, *i.e.*, the steady-state birefringence, and $\lambda_1$, $\lambda_2$, $\lambda_3$, $X_0$, $X_1$, $X_2$, and $X_3$, are functions of $\beta$ and $\gamma$

$$\lambda_1 = 2 + \beta^2/5 - 4\gamma/5 \quad (29a)$$

$$\lambda_2 = 6 + \beta^2/7 - 4\gamma/7 \quad (29b)$$

$$\lambda_3 = 12 + 2\beta^2/15 - 8\gamma/15 \quad (29c)$$

$$X_0 = \beta^2 + 2\gamma - \frac{2}{21}(\beta^4 - 2\beta^2\gamma - 2\gamma^2) \quad (30a)$$

$$X_1 = \frac{3}{2}\beta^2 - \frac{3}{350}(9\beta^4 - \beta^2\gamma) \quad (30b)$$

$$X_2 = \frac{1}{2}(\beta^2 - 4\gamma) + \frac{1}{42}(\beta^4 - 11\beta^2\gamma - 8\gamma^2) \quad (30c)$$

$$X_3 = \frac{1}{175}(\beta^4 - 14\beta^2\gamma) \quad (30d)$$

The normalized birefringence in a rapidly reversed electric field is given by

$$\Delta(t) = 1 - \frac{X_1'}{X_0'} \exp(-\lambda_1 \Theta t) + \frac{X_2'}{X_0'} \exp(-\lambda_2 \Theta t) - \frac{X_3'}{X_0'} \exp(-\lambda_3 \Theta t) \quad (31)$$

where $\lambda_1$, $\lambda_2$, and $\lambda_3$ are the same as expressed by eq 29, and

$$X_0' = \beta^2 + 2\gamma + \frac{1}{14}(\beta^4 + 12\beta^2\gamma + 12\gamma^2) \quad (32a)$$

$$X_1' = 3\beta^2 + \frac{3}{175}(26\beta^4 + 71\beta^2\gamma) \quad (32b)$$

$$X_2' = 3\beta^2 + \frac{1}{7}(4\beta^4 + 9\beta^2\gamma) \quad (32c)$$

$$X_3' = \frac{2}{175}(11\beta^4 + 6\beta^2\gamma) \quad (32d)$$

At limiting low fields, the equation for the rise of the birefringence reduces to

$$\Delta(t) = 1 - \frac{3\beta^2}{2(\beta^2 + 2\gamma)} \exp(-2\Theta t) + \frac{\beta^2 - 4\gamma}{2(\beta^2 + 2\gamma)} \exp(-6\Theta t) \quad (33)$$

and the equation for the birefringence in a rapidly reversed field reduces to

$$\Delta(t) = 1 - \frac{3\beta^2}{\beta^2 + 2\gamma} \exp(-2\Theta t) + \frac{3\beta^2}{\beta^2 + 2\gamma} \exp(-6\Theta t) \quad (34)$$

These equations coincide with those of Benoit[1] and Tinoco and Yamaoka.[9] In these cases the normalized birefringence *vs.* $\Theta t$ curves are solely determined by

$$r \equiv \beta^2/2\gamma = b^2/2c = \mu'^2/(\alpha_1 - \alpha_2)kT \quad (35)$$

independent of the field strength.

In the special case of pure permanent dipole orientation we performed the calculation of the birefringence up to the terms in $E^6$ (sixth-order perturbation). For the rise of the birefringence, we have

$$\Delta(t) = 1 - \frac{1}{X_0}\left(\frac{3}{2}\beta^2 - \frac{27}{350}\beta^4 + \frac{49}{5000}\beta^6\right) \times \exp\left\{-\left(2 + \frac{1}{5}\beta^2 - \frac{1}{3500}\beta^4\right)\Theta t\right\} + \frac{1}{X_0}\left(\frac{1}{2}\beta^2 + \frac{1}{42}\beta^4 - \frac{65}{172{,}872}\beta^6\right) \exp\left\{-\left(6 + \frac{1}{7}\beta^2 - \frac{1}{4116}\beta^4\right)\Theta t\right\} - \frac{1}{X_0}\left(\frac{1}{175}\beta^4 + \frac{19}{157{,}500}\beta^6\right) \exp\left\{-\left(12 + \frac{2}{15}\beta^2 + \frac{19}{222{,}750}\beta^4\right)\Theta t\right\} + \frac{1}{X_0}\left(\frac{1}{48{,}020}\beta^6\right) \exp\left\{-\left(20 + \frac{10}{77}\beta^2 + \frac{37{,}913}{427{,}314{,}888}\beta^4\right)\Theta t\right\} \quad (36)$$

where

$$X_0 = \beta^2 - \frac{2}{21}\beta^4 + \frac{1}{105}\beta^6$$

(10) A. Peterlin and H. A. Stuart, *Z. Phys.*, 112, 129 (1939).

For the birefringence in a rapidly reversed field, we have

$$\Delta(t) = 1 - \frac{1}{X_0'}\left(3\beta^2 + \frac{78}{175}\beta^4 + \frac{269}{8750}\beta^6\right) \times \exp\left\{-\left(2 + \frac{1}{5}\beta^2 - \frac{1}{3500}\beta^4\right)\Theta t\right\} + \frac{1}{X_0'}\left(3\beta^2 + \frac{4}{7}\beta^4 + \frac{659}{14,406}\beta^6\right) \exp\left\{-\left(6 + \frac{1}{7}\beta^2 - \frac{1}{4116}\beta^4\right) \times \Theta t\right\} - \frac{1}{X_0'}\left(\frac{22}{175}\beta^4 + \frac{443}{26,250}\beta^6\right) \exp\left\{-\left(12 + \frac{2}{15}\beta^2 + \frac{19}{222,750}\beta^4\right)\Theta t\right\} + \frac{1}{X_0'}\left(\frac{9}{4802}\beta^6\right) \times \exp\left\{-\left(20 + \frac{10}{77}\beta^2 + \frac{37,913}{427,314,888}\beta^4\right)\Theta t\right\} \quad (37)$$

where

$$X_0' = \beta^2 + \frac{1}{14}\beta^4 + \frac{1}{504}\beta^6$$

*Polydispersity.* For a polydisperse system, the rise or buildup of the birefringence at limiting low fields is given by

$$\Delta_B(t) = 1 - \frac{3\sum_i c_i\beta_i^2 \exp(-2\Theta_i t)}{2\sum_i c_i(\beta_i^2 + 2\gamma_i)} + \frac{\sum_i c_i(\beta_i^2 - 4\gamma_i) \exp(-6\Theta_i t)}{2\sum_i c_i(\beta_i^2 + 2\gamma_i)} \quad (38)$$

instead of eq 33, if it is assumed that all components have the same density and the same optical anisotropy factor. This assumption will hold for helical polypeptides, for instance. On the other hand, the decay of the birefringence is given by

$$\Delta_D(t) = \frac{\sum_i c_i(\beta_i^2 + 2\gamma_i) \exp(-6\Theta_i t)}{\sum_i c_i(\beta_i^2 + 2\gamma_i)} = \Delta_D^P(t) + \Delta_D^I(t) \quad (39)$$

where $\Delta_D^P(t)$ and $\Delta_D^I(t)$ are defined by

$$\Delta_D^P(t) = \frac{\sum_i c_i\beta_i^2 \exp(-6\Theta_i t)}{\sum_i c_i(\beta_i^2 + 2\gamma_i)} \quad (40a)$$

$$\Delta_D^I(t) = \frac{\sum_i c_i(2\gamma_i) \exp(-6\Theta_i t)}{\sum_i c_i(\beta_i^2 + 2\gamma_i)} \quad (40b)$$

Substituting eq 40a and 40b into eq 38, we obtain

$$\Delta_B(t) = 1 - \frac{3}{2}\Delta_D^P(t/3) + \frac{1}{2}\Delta_D^P(t) - \Delta_D^I(t) \quad (41)$$

The birefringence in a rapidly reversed field for a polydisperse system is given by

$$\Delta_R(t) = 1 - \frac{3\sum_i c_i\beta_i^2 \exp(-2\Theta_i t)}{\sum_i c_i(\beta_i^2 + 2\gamma_i)} + \frac{3\sum_i c_i\beta_i^2 \exp(-6\Theta_i t)}{\sum_i c_i(\beta_i^2 + 2\gamma_i)} \quad (42)$$

instead of eq 34. From eq 42 and 40a we obtain

$$\Delta_R(t) = 1 - 3\Delta_D^P(t/3) + 3\Delta_D^P(t) \quad (43)$$

In the case of pure permanent dipole orientation, eq 41 and 43 reduce to

$$\Delta_B(t) = 1 - \frac{3}{2}\Delta_D(t/3) + \frac{1}{2}\Delta_D(t) \quad (44)$$

and

$$\Delta_R(t) = 1 - 3\Delta_D(t/3) + 3\Delta_D(t) \quad (45)$$

respectively. On the other hand, in the case of pure induced dipole orientation, we have

$$\Delta_B(t) = 1 - \Delta_D(t) \quad (46)$$

and

$$\Delta_R(t) = 1 \quad (47)$$

Thus, in these special cases, the rise and reverse curves can be obtained from the decay curve even for a polydisperse system, as long as the interactions between macromolecules are negligible.

In general, $\Delta_B(t)$, $\Delta_R(t)$, and $\Delta_D(t)$ are related by a simple equation. Namely, from eq 39, 41, and 43, we obtain

$$2\Delta_B(t) - \Delta_R(t) = 1 - 2\Delta_D(t) \quad (48)$$

## Results and Discussion

Equation 28 for the rise of the normalized birefringence is plotted for various values of $\beta^2$ and $\gamma$ in Figures 1 and 2. The broken curves in these figures indicate the normalized rise curves at limiting low fields (Benoit's equation, eq 33). When the ratio $r$ $(=\beta^2/2\gamma)$ is positive and small (*e.g.*, $r = 0.75$), a negative deviation from Benoit's equation is noticed at higher fields. On the other hand, when $r$ is positive and large (*e.g.*, $r = 2.5$), a positive deviation is noticed. When $r$ is negative, the deviation from Benoit's equation is more pronounced than in the case of $r \geqq 0$, as shown in Figure 2. In order to express the deviation quantitatively, the values of $\Delta(t)/[\Delta(t)]_{E\to 0}$ for $\Theta t = 0.5$ and 1 are given in Table I.

Equation 31 for the normalized birefringence in a rapidly reversed field is plotted for various values of $\beta^2$ and $\gamma$ in Figures 3 and 4. The broken curves in these figures indicate the normalized reverse curves at

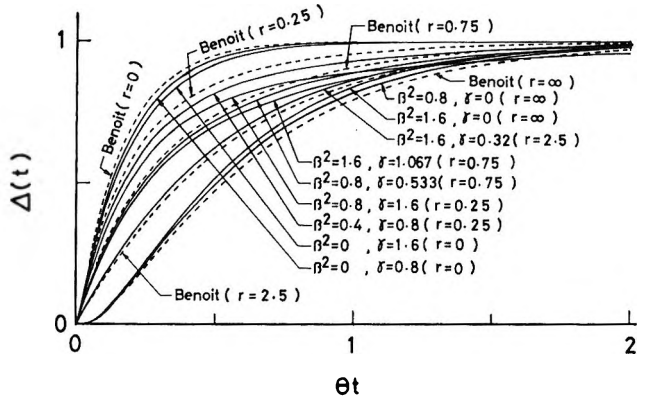


Figure 1. Normalized rise birefringence plotted *vs.* $\theta t$ for various values of $\beta^2$ and $\gamma(\geqq 0)$.

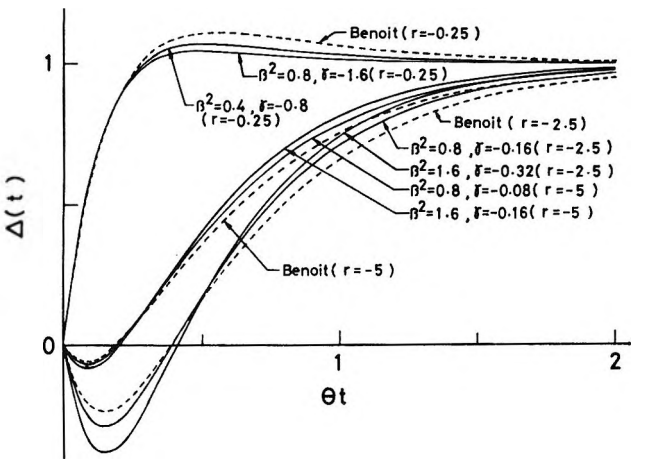


Figure 2. Normalized rise birefringence plotted *vs.* $\theta t$ for various values of $\beta^2$ and $\gamma(< 0)$.

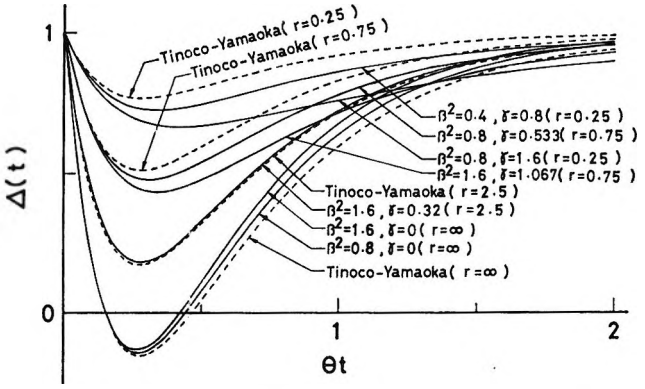


Figure 3. Normalized reverse birefringence plotted *vs.* $\theta t$ for various values of $\beta^2$ and $\gamma(\geqq 0)$.

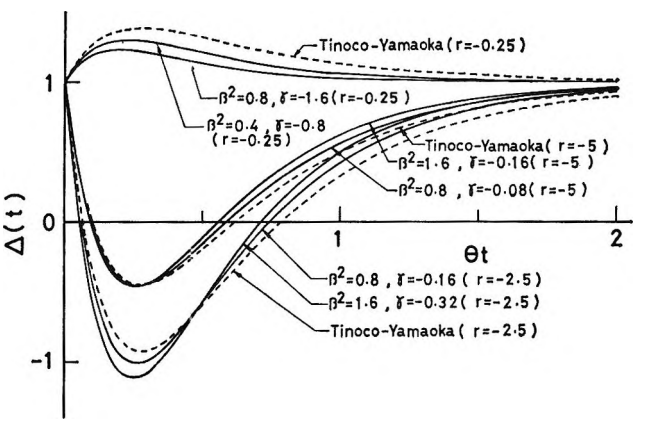


Figure 4. Normalized reverse birefringence plotted *vs.* $\theta t$ for various values of $\beta^2$ and $\gamma(<0)$.

**Table I:** Deviation from Benoit's Equation for Various Values of $\beta^2$ and $\gamma$

| $r$ | $\beta^2$ | $\gamma$ | $\Delta(t)/[\Delta(t)]_{E\to 0}$ for $\theta t$ = 0.5 | $\Delta(t)/[\Delta(t)]_{E\to 0}$ for $\theta t$ = 1 |
|---|---|---|---|---|
| 0 | 0 | 0.8 | 0.986 | 0.998 |
| | 0 | 1.6 | 0.970 | 0.996 |
| 0.25 | 0.4 | 0.8 | 0.962 | 0.974 |
| | 0.8 | 1.6 | 0.915 | 0.932 |
| 0.75 | 0.8 | 0.533 | 0.975 | 0.979 |
| | 1.6 | 1.067 | 0.948 | 0.955 |
| 2.5 | 0.8 | 0.16 | 1.016 | 1.007 |
| | 1.6 | 0.32 | 1.033 | 1.014 |
| ∞ | 0.8 | 0 | 1.052 | 1.029 |
| | 1.6 | 0 | 1.097 | 1.054 |
| −0.25 | 0.4 | −0.8 | 0.966 | 0.969 |
| | 0.8 | −1.6 | 0.943 | 0.954 |
| −2.5 | 0.8 | −0.16 | 1.093 | 1.070 |
| | 1.6 | −0.32 | 0.983 | 1.115 |
| −5 | 0.8 | −0.08 | 1.079 | 1.046 |
| | 1.6 | −0.16 | 1.134 | 1.083 |

**Table II:** Deviation from the Tinoco–Yamaoka Equation for Various Values of $\beta^2$ and $\gamma$

| $r$ | $\beta^2$ | $\gamma$ | $[1-\Delta(t)]/[1-\Delta(t)]_{E\to 0}$ for $\theta t$ = 0.24 | $\Delta(t)/[\Delta(t)]_{E\to 0}$ for $\theta t$ = 1 |
|---|---|---|---|---|
| 0.25 | 0.4 | 0.8 | 1.130 | 0.938 |
| | 0.8 | 1.6 | 1.297 | 0.830 |
| 0.75 | 0.8 | 0.533 | 1.049 | 0.940 |
| | 1.6 | 1.067 | 1.112 | 0.861 |
| 2.5 | 0.8 | 0.16 | 0.998 | 1.004 |
| | 1.6 | 0.32 | 0.994 | 1.011 |
| ∞ | 0.8 | 0 | 0.997 | 1.066 |
| | 1.6 | 0 | 0.988 | 1.130 |
| −0.25 | 0.4 | −0.8 | 0.787 | 0.938 |
| | 0.8 | −1.6 | 0.596 | 0.907 |
| −2.5 | 0.8 | −0.16 | 1.050 | 1.269 |
| | 1.6 | −0.32 | 1.110 | 1.491 |
| −5 | 0.8 | −0.08 | 1.011 | 1.127 |
| | 1.6 | −0.16 | 1.017 | 1.243 |

limiting low fields (the Tinoco–Yamaoka equation, eq 34). The values of $[1-\Delta(t)]/[1-\Delta(t)]_{E\to 0}$ for $\theta t = 0.24$ and $\Delta(t)/[\Delta(t)]_{E\to 0}$ for $\theta t = 1$ are presented in Table II. These values show the deviation from the Tinoco–Yamaoka equation at higher fields.

In the special case of pure permanent dipole orientation ($\gamma = 0$), we compare the results of calculations for

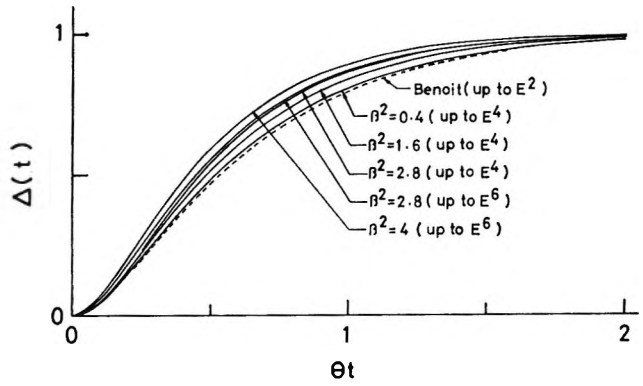


Figure 5. Normalized rise birefringence plotted *vs.* $\theta t$ in the case of pure permanent dipole orientation ($\gamma = 0$), according to eq 33 (Benoit's equation, up to $E^2$ terms), eq 28 (up to $E^4$ terms), and eq 36 (up to $E^6$ terms).

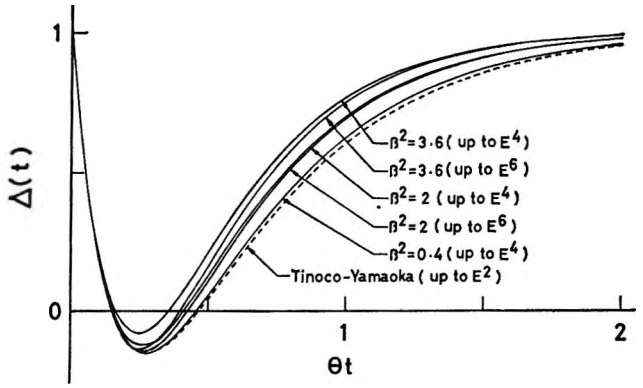


Figure 6. Normalized reverse birefringence plotted *vs.* $\theta t$ in the case of pure permanent dipole orientation ($\gamma = 0$), according to eq 34 (Tinoco-Yamaoka's equation, up to $E^2$ terms), eq 31 (up to $E^4$ terms), and eq 37 (up to $E^6$ terms).

the rise birefringence according to eq 33 (Benoit's equation, up to $E^2$ terms), eq 28 (up to $E^4$ terms), and eq 36 (up to $E^6$ terms) in Figure 5. When $\beta^2 < 0.4$, we can use Benoit's equation without significant error. If $\mu' = 2 \times 10^3$ D and $T = 300°$K, for example, the field strength corresponding to $\beta^2 = 0.4$ is calculated to be $3.9 \times 10^3$ V/cm. When $\beta^2$ is larger than 0.4, but smaller than 2.8, we should utilize eq 28. For $\beta^2 > 2.8$, we must turn to eq 36.

The results of calculations for the reverse birefringence according to eq 34 (the Tinoco–Yamaoka equation, up to $E^2$ terms), eq 31 (up to $E^4$ terms), and eq 37 (up to $E^6$ terms) in the case of pure permanent dipole orientation are compared in Figure 6. We can roughly say that the Tinoco–Yamaoka equation holds for $\beta^2 < 0.4$ and eq 31 holds for $\beta^2 < 2$.

Finally we wish to discuss the effect of polydispersity on the initial slopes of the normalized rise and reverse curves at limiting low fields. For a monodisperse system, the initial slope of the normalized rise curve is equal to $6\,\Theta/(r+1)$ and that of the normalized reverse curve is equal to $-12r\Theta/(r+1)$. For a polydisperse system, the initial slope of the rise curve is obtained from eq 38 as

$$\left(\frac{d\Delta_B(t)}{dt}\right)_{t\to 0} = \frac{6}{r^*+1}\frac{\sum_i c_i\gamma_i\Theta_i}{\sum_i c_i\gamma_i} \tag{49}$$

and the initial slope of the reverse curve is obtained from eq 42 as

$$\left(\frac{d\Delta_R(t)}{dt}\right)_{t\to 0} = -\frac{12r^*}{r^*+1}\frac{\sum_i c_i\beta_i^2\Theta_i}{\sum_i c_i\beta_i^2} \tag{50}$$

where $r^*$ is defined by the relation

$$r^* = \frac{\sum_i c_i\beta_i^2}{\sum_i c_i(2\gamma_i)} = \frac{\text{weight average of } \beta^2}{\text{weight average of } 2\gamma} \tag{51}$$

Further, from eq 49 and 50 we obtain

$$\left(\frac{d\Delta_R(t)}{dt}\right)_{t\to 0}\Big/\left(\frac{d\Delta_B(t)}{dt}\right)_{t\to 0} = -\frac{\sum_i c_i\Theta_i\beta_i^2}{\sum_i c_i\Theta_i\gamma_i} \tag{52}$$

This ratio reduces to $-\beta^2/\gamma$ ($=-2r$) for a monodisperse system. Although the right side of eq 52 represents the ratio of some complicated average of $\beta^2$ to that of $\gamma$, unlike $r^*$, it is useful because it can be directly obtained from experiments.

*Acknowledgment.* This work was supported in part by research grants from the Ministry of Education of Japan, to which the authors wish to express their gratitude.

# Molecular Orbital Study of the Electronic Structure and Spectrum of Hexahydro-1,3,5-trinitro-s-triazine

by Malcolm K. Orloff, Patricia A. Mullen, and Francis C. Rauch

*Central Research Division, American Cyanamid Company, Stamford, Connecticut 06904* *(Received December 19, 1969)*

Molecular orbital calculations (CNDO) have been utilized in a study of the electronic structure and ultraviolet absorption spectrum of hexahydro-1,3,5-trinitro-s-triazine (RDX). The vacuum uv absorption spectrum of RDX in acetonitrile has been measured from 3600 to 1840 Å. Prominent absorption maxima are observed at 2360 Å ($\epsilon$ 11,000 $M^{-1}$ cm$^{-1}$) and at 1955 Å ($\epsilon$ 16,400 $M^{-1}$ cm$^{-1}$). These bands are assigned as $\pi \rightarrow \pi^*$ transitions localized on the nitro groups on the basis of the MO calculations.

## I. Introduction

The title compound (RDX) has been the subject of continued interest because of its use as a secondary explosive.[1-3] In conjunction with present efforts in these laboratories to study the mechanism of decomposition of this material, we have carried out all valence-electron molecular orbital calculations on four different conformations of RDX in order to obtain information concerning the electronic structure and spectrum of the molecule. The atomic charge densities, overlap populations, and total ground-state energies have been obtained for these conformers and the results have been related to experimental observations. We have also measured the vacuum uv spectrum of RDX in the region from 3600 to 1840 Å and assigned the observed transitions with the aid of the MO calculations.

## II. Experimental Section

Pure RDX was supplied by Dr. B. Suryanarayana of the Explosives Laboratory, Picatinny Arsenal, Dover, N. J. This material was purified from military grade RDX (Holston Defense Corp.) by recrystallization from $\gamma$-butyrolactone, to remove most of the octahydro-1,3,5,7-tetranitro-s-tetrazine (HMX) impurity, followed by three recrystallizations from aqueous acetone. The purified RDX was supplied to us under ethanol. Before use the RDX was filtered and dried for 16 hr at 60° under vacuum. The melting point of the final material was found to be 204.5–205° dec as measured on a calibrated microscope hot stage. A purity of greater than 99.5% was determined by a chromatographic analysis using the procedure of Rowe.[4] This material was stored in the dark and dried by the procedure given above prior to this spectral investigation.

The absorption spectrum of RDX in Eastman spectrograde acetonitrile was measured from 3600 to 2000 Å using a Cary Model 14R spectrophotometer and from 2400 to 1840 Å using a Jarrell-Ash normal-incidence vacuum spectrometer. The vacuum ultraviolet instrumentation and slit width have been described previously.[5] The cells employed in this investigation were of fused quartz with path lengths of 0.1 and 2 cm and of stainless steel with $MgF_2$ windows (2 mm thick—Harshaw Chemical Co.) and path length of 0.078 cm. The concentrations of RDX solutions were between $9.1 \times 10^{-3}$ and $4.0 \times 10^{-3}$ $M$.

Two to four determinations of absorbance were recorded every 10 Å over the spectral region 1840–3600 Å and the data presented as molar extinction coefficient ($\epsilon$) in units of $M^{-1}$ cm$^{-1}$ *vs.* wave number in kK (cm$^{-1}$ $\times$ 10$^3$). The variation in $\epsilon$ was less than $\pm 5\%$.

## III. Calculations

The MO method used in this study is the CNDO/2 treatment developed by Pople and coworkers.[6] In this semiempirical treatment, all the valence electrons in a molecule are taken into account explicitly, so that in the case of RDX there are 84 electrons distributed among 66 atomic orbitals. For the calculation of ground-state properties, we have used the MO parameters suggested by Pople and Segal;[6] therefore, the only input data necessary to perform the calculations are the coordinates of the atoms in the molecule.

The positional coordinates of the carbon, nitrogen, and oxygen atoms for RDX in the crystalline phase have been determined by X-ray diffraction.[7] The

(1) A. J. B. Robertson, *Trans. Faraday Soc.*, **45**, 85 (1949).

(2) B. Suryanarayana, R. J. Graybush, and J. R. Autera, *Chem. Ind.* (London), 2177 (1967).

(3) F. C. Rauch and A. J. Fanelli, *J. Phys. Chem.*, **73**, 1604 (1969).

(4) M. L. Rowe, *J. Gas Chromatogr.*, **4**, 531 (1967).

(5) P. A. Mullen and M. K. Orloff, *J. Mol. Spectrosc.*, **30**, 140 (1969).

(6) J. A. Pople, D. P. Santry, and G. A. Segal, *J. Chem. Phys.*, **43**, S 129 (1965); J. A. Pople and G. A. Segal, *ibid.*, **43**, S 136 (1965); **44**, 3289 (1966).

(7) P. M. Harris, "An Investigation of the Crystalline Structure of Aromatic Trinitro- and Related Compounds," Ohio State University Research Foundation AFOSR-TR-59-165.

molecule was found to be in a chair conformation with two of the N–N bonds (1.41 Å) almost parallel to one another and roughly perpendicular to the "average plane" of the ring atoms, whereas the third N–N bond (1.36 Å) was found to be in a direction lying in this "plane."[7] No information appears to be available on the precise structure of RDX in the liquid or vapor phase.

In this theoretical study, we performed MO calculations on the RDX molecule in the following four conformations.[8] (1) The chair form corresponding to the experimentally determined structure of RDX in a crystalline state.[7] (2) An idealized chair form in which the three $C_2N$–$NO_2$ groups are (individually) planar as found for crystalline HMX and a threefold molecular symmetry is assumed; bond lengths and angles are average values taken from RDX[7] and HMX.[9] (3) A chair form identical with (2) above, except the three $NO_2$ groups are rotated 90° about each N–N bond. (4) A boat conformer derived from (2) above with carbon and nitrogen atoms placed bow and stern.

## IV. Results and Discussion

*1. Ground State.* The theoretically calculated electronic charge distribution is essentially the same for each of the four conformations of RDX studied. In Table I we list the calculated atomic charge densities found for conformer 2, which is the most convenient to report because of the threefold symmetry (see Figure 1 for the numbering of the atoms in the molecule). A point of interest here is the relatively high positive charge ($q$ = +0.21) on the carbon atoms and the negative charge ($q$ = −0.33) on the oxygen atoms. This result is consistent with the proposed mechanism for the decomposition of RDX (in the liquid phase) which involves either intra- or intermolecular carbon–oxygen interaction.[1-3] It is also consistent with the short intermolecular C···O contact distance of 3.21 Å in crystalline RDX, which we have calculated from the X-ray diffraction data in ref 7. This short contact distance compared to the 3.4 Å obtained from the sum of van der Waals radii implies a strong attractive force between the carbon and oxygen atoms. As in the case of crystalline HMX,[9] the C···O contact is not in line with any C–H bond direction, and is therefore not a "hydrogen bond."

**Table I:** Calculated Atomic Charge Densities in RDX

| Atom[a] | Charge | Atom[a] | Charge |
|---|---|---|---|
| 1 | −0.170 | 4 | 0.212 |
| 2 | 0.573 | 5 | 0.047 |
| 3 | −0.329 | 6 | −0.005 |

[a] See Figure 1 for the numbering of the atoms in RDX conformer 2.

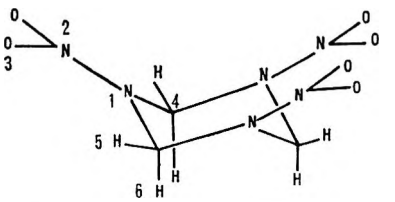

Figure 1. Numbering of the atoms in RDX (conformer 2).

Although the electronic charge densities are the same in the four RDX conformers studied, the calculated dipole moments are quite different because of geometrical considerations. The calculated dipole moments for conformers 1, 2, 3, and 4 are 7.76, 4.96, 4.45, and 1.08 D, respectively. The value for the dipole moment of nitramine in dioxane is 3.75 D;[10] however, we are not aware of any experimental value for the dipole moment of RDX itself.

The calculated overlap populations were also found to be insensitive to conformational changes and, as in the case of charge densities, we may consider the results obtained for conformer 2. Overlap populations obtained from MO calculations may be used to estimate bond energies by establishing a curve of overlap population *vs.* bond energy for molecules containing the atom pair under study.[11] In order to obtain such a calibration curve for the N–N bond, calculations were performed on $N_2H_4$, $N_2H_2$, and $N_2$. The resultant overlap populations, along with the experimental bond energies, are presented in Table

**Table II:** Calculated Overlap Populations and Observed Bond Energies for Compounds Containing N–N Bonds

| Molecule | N–N bond overlap pop. | N–N bond energy, kcal/mol |
|---|---|---|
| $N_2H_4$ | 0.55[a] | 60[c] |
| $N_2H_2$ | 0.91[a] | 109[d] |
| $N_2$ | 1.33[a] | 225[c] |
| RDX | 0.62[b] | 66[e] |

[a] MO calculations were carried out on molecules built from standard bond lengths and angles given in J. A. Pople and M. Gordon, *J. Amer. Chem. Soc.*, **89**, 4253 (1967). [b] Conformer 2. [c] T. L. Cottrell, "The Strengths of Chemical Bonds," 2nd ed, Butterworths and Co. (Publishers) Ltd., London, 1958, p 278. [d] "JANAF Thermochemical Tables," Dow Chemical Co., Midland, Mich., 1965. [e] Extrapolated from curve of overlap population *vs.* bond energy for $N_2H_4$, $N_2H_2$, and $N_2$ molecules.

(8) The $x$, $y$, $z$ positional coordinates of the atoms in the RDX conformers, which were used in the calculations, are available from the authors upon request.

(9) P. F. Eliand and R. Pepinsky, *Z. Kristallogr. Kristallgeometrie Kristallphys. Kristallchem.*, **106**, 273 (1955).

(10) E. C. E. Hunter and J. R. Partington, *J. Chem. Soc.*, 309 (1933).

(11) J. J. Kaufman, "Theoretical and Quantum Chemistry of N, O, F Compounds," ARPA Contract No. DA-31-124-ARO-D-203, Final Report, p 122.

II. A value of 66 kcal/mol is obtained for the energy of the N–N bond in RDX from the calibration curve. A bond energy of this magnitude correlates reasonably well with the limited kinetic data obtained in these laboratories on the gas-phase decomposition of RDX in which the rate-controlling step is the homolytic rupture of the N–N bond.[3] The calculated value of the overlap population for the N–N bond in RDX indicates that this bond possesses some double-bond character. The overlap population for the C–N bond in RDX is found to be equal to that (0.67) calculated for the model single-bond compound $H_3C-NH_2$ and a bond energy of 80 kcal/mol[12] is therefore estimated for the C–N bond in RDX.

The theoretically calculated total energies of RDX vary with conformation and the results are shown in Table III. It is the difference between the calculated energies and not their absolute values which is of significance in this work. Moreover, the more negative energies correspond to more stable conformations. The results of the MO calculations in RDX indicate that the structure observed in the crystal (conformation 1) is energetically less favorable than either conformation 2 or 4 by 7 kcal/mol. It should be noted, however, that the quantum mechanical calculations are carried out on the isolated molecule and thus the theoretical results should be compared with measurements made on the molecule in the gas phase. In general, significant changes in conformation may be brought about by packing forces in the crystal which are absent in the gas and liquid. Such a phenomenon has been observed for molecules such as diboron tetrachloride (which is eclipsed in the crystal and staggered in the vapor)[13] and biphenyl (in which the two phenyl rings are nearly planar in the crystal and progressively more skewed in the liquid and vapor).[14] In the case of crystalline RDX, it is reasonable that the additional forces due to crystal packing account for more than 7 kcal/mol. Therefore, the calculations predict that the conformation of RDX in the liquid and vapor has a higher degree of symmetry than that observed in the crystal. The ground-state calculations indicate that the boat and chair 2 conformers are equally stable and, therefore, equally probable. We will return to this point later in conjunction with the calculated electronic spectrum.

**Table III:** Calculated Total Energy of RDX Conformers

| Conformer[a] | *E*, kcal/mol |
|---|---|
| 1 | −129,951 |
| 2 | −129,958 |
| 3 | −129,927 |
| 4 | −129,958 |

[a] See section III for description of conformers.

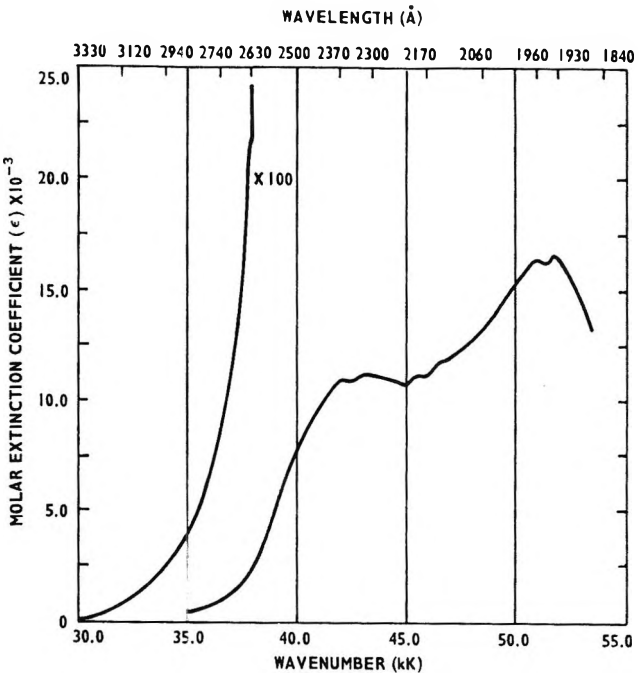


Figure 2. Vacuum ultraviolet absorption spectrum of RDX in acetonitrile.

From a consideration of the results in Table III for conformers 2 and 3, a rotational energy barrier of approximately 10 kcal/mol ($^1/_3[-129{,}927 - (-129{,}958)]$) is predicted for the rotation of an $NO_2$ group about the N–N bond in RDX. Additional calculations on intermediate angles of twist were not attempted due to the large computational times involved for a molecule of this size.

*2. Excited States.* The absorption spectrum of RDX in acetonitrile is shown in Figure 2 as molar extinction coefficient $\epsilon$ *vs.* wave number. Two distinct absorption bands are seen at 2360 Å ($\epsilon$ 11,000 $M^{-1}$ cm$^{-1}$) and at 1955 Å ($\epsilon$ 16,400 $M^{-1}$ cm$^{-1}$) with weak vibrational structure superimposed on each band. The 2360-Å band is less distinct and the spectrum is similar to that reported by Jones and Thorn[15] when the data are plotted as log $\epsilon$ *vs.* wave number. The spectrum reported by Jones and Thorn was not extended far enough into the uv to observe the second band maximum. Stals, Barraclough, and Buchanan[16] have reported the absorption spectrum of RDX in

(12) T. L. Cottrell, "The Strengths of Chemical Bonds," 2nd ed, Butterworths and Co. (Publications) Ltd., London, 1958, p 274.

(13) E. B. Moore, Jr., *J. Chem. Phys.*, **43**, 503 (1965).

(14) H. Suzuki, "Electronic Absorption Spectra and Geometry of Organic Molecules," Academic Press, Inc., New York, N. Y., Chapter 12.

(15) R. N. Jones and G. D. Thorn, *Can. J. Res.*, **278**, 828 (1949).

(16) J. Stals, C. G. Barraclough, and A. S. Buchanan, *Trans. Faraday Soc.*, **65**, 904 (1969).

acetonitrile and several other solvents. Our results agree with those of Stals, *et al.*, on the energy of the longer wavelength maximum at about 2360 Å; the location of the higher energy band at 1955 Å was made possible through the use of the vacuum uv instrumentation.

The CNDO/2 method cannot be used successfully to study electronic spectral transitions unless the theory is modified in some way. In this study, we have used the modifications introduced by Del Bene and Jaffé[17] including configuration interaction due to the 25 lowest singly excited states to calculate the absorption spectrum of RDX in conformations 2 and 4. The calculated spectral transition energies are almost identical for conformers 2 and 4 indicating that the nitramino groups are effectively insulated and are not conjugated with the ring. The only difference in the two calculated spectra is the ratio of the oscillator strengths, $f$, of the two strong transitions. This ratio is 0.7 for conformer 2 and 1.0 for conformer 4. Inasmuch as the ratio of observed extinction coefficients is 0.67, the results suggest that the chair conformer 2 is the one actually found in solution or in the gas phase and accordingly we report the results calculated for that conformer along with the experimental values in Table IV. Although the calculated energies are only in fair agreement with experiment, the pattern of $f$ values makes the assignments of the transitions straightforward. From an analysis of the MO wavefunctions, the two prominent absorption bands observed at 2360 and 1955 Å are assigned as absorptions arising primarily from $\pi \rightarrow \pi^*$ transitions localized on the nitro groups. In addition, we conclude that there are weak $n \rightarrow \pi^*$ absorption bands buried in the 2360-Å band which result from promotion of the nonbonding electrons on the oxygen atoms.

**Table IV:** Calculated and Observed Spectral Transitions in RDX

| Calcd[a] | | | Obsd | |
|---|---|---|---|---|
| λ, Å | $f$ | Type[b] | λ, Å | $\epsilon$, $M^{-1}$ cm$^{-1}$ |
| 2165 | 0.006 | $n \rightarrow \pi^*$ | 2740 | 900 |
| 1997 | 0.005 | $n \rightarrow \pi^*$ | | |
| 1970 | 0.16 | $n \rightarrow \pi^*$[c] | 2640 | 2,100 |
| 1969 | 0.01 | $\pi \rightarrow \pi^*$ | | |
| 1903 | 0.79 | $\pi \rightarrow \pi^*$ | 2360 | 11,000 |
| 1896 | 1.13 | $\pi \rightarrow \pi^*$ | 1955 | 16,400 |

[a] Calculated for conformer 2. [b] The assignment shown in this column represents the leading term in the configuration interaction wave function. [c] Although this transition is predominantly $n \rightarrow \pi^*$, there is a 12% contribution from a $\pi \rightarrow \pi^*$ intramolecular charge transfer (nitramino N to the $NO_2$ group) which enhances the $f$ value.

In conclusion it should be noted that Stals, Barraclough, and Buchanan carried out VESCF CI calculations on N,N-dimethyl nitramine and extended their results to the excited states of RDX.[16] Our MO calculations on RDX confirm the validity of their approach to the interpretation of the spectrum and support their assignments with a minor exception. We assign the first excited singlet state of RDX to an n, $\pi^*$ transition rather than to an n, $\sigma^*$ state; although, as pointed out by Stals, *et al.*, the $\pi$, n, and $\sigma$ orbitals are intimately mixed in nitramino type molecules. The assignment of the lowest excited singlet state as an n, $\pi^*$ state (as opposed to a $\pi$, $\pi^*$ state) is consistent with the failure to observe fluorescence from RDX.[16]

*Acknowledgment.* This research was supported by Picatinny Arsenal, U. S. Army Munitions Command.

(17) J. Del Bene and H. H. Jaffé, *J. Chem. Phys.*, 48, 4050 (1968).

# A Trajectory Study of Phosphorus-32 Recoil in Sodium Phosphates

by Don L. Bunker and Gregg Van Volkenburgh

*Department of Chemistry, University of California, Irvine, California* *(Received January 23, 1970)*

We made a classical trajectory study of the recoil of $^{32}P$, from $^{31}P$ $(n,\gamma)^{32}P$, in several kinds of sodium phosphate crystal. The chemical effects of this have been extensively studied, but the results are inconclusive. Our calculations strongly suggest that in anhydrous crystals, the primary process is the ejection of either P or P + O (or P + OH, in sodium hydrogen phosphates) from the crystal cage. These fragments traverse only a few neighboring sites before becoming bound. When there is water of hydration, escape of P is severely impeded. It either remains in its original cage or comes to rest in an adjoining one. Preservation of a P–O bond during the recoil process is extremely unlikely.

## Introduction

When the nuclear reaction $^{31}P$ $(n,\gamma)^{32}P$ is carried out by irradiation of crystalline orthophosphates with neutrons, many different phosphorus oxyanions are formed. Analysis of the dissolved crystal after irradiation has shown the presence of orthophosphite, hypophosphate, hypophosphite, isohypophosphate, diphosphite, pyrophosphate, tripolyphosphate, and more complicated polymeric forms. These must arise from the recoil of $^{32}P$ on emission of one or more $\gamma$ rays of the several high energies that are possible.

Contradictory suggestions have been made about the immediate result of this recoil. It has been proposed that almost none[1] and that almost all[2] of the $^{32}P$ escapes its original lattice cage. Intermediate views include half O, half P ejection[3] and that P, O, and $PO_2$ are the principal ejected fragments.[4] Changes in the results when hydrated crystals are irradiated have been used[2] to support the view that recoil out of the cage is important. The present state of understanding of this area of recoil chemistry is not very satisfactory.

Our study had two purposes. One was to obtain insight into the nature of the $^{32}P$ recoil process. The other was to introduce trajectory methods into condensed-phase problems. For the gas phase, trajectory studies have been used as an aid to understanding reaction dynamics for some time. Systems of up to 6 atoms[5] have been investigated. A solid-state calculation of radiation damage exists[6] in which there were 500 atoms (of Cu) but no molecular interactions, so that simpler computation procedures could be used than are required in a chemical study. We needed a chemically interesting problem of complexity intermediate between these two kinds of calculation. The $^{32}P$ recoils in sodium phosphate crystals provided an ideal choice.

## The Method and the Model

We obtained the trajectories of the atoms by solving Hamilton's equations in cartesian coordinates

$$dp_{x_i}/dt = -\partial H/\partial x_i; \qquad dx_i/dt = \partial H/\partial p_{x_i} \quad (1)$$

with corresponding expressions for $y$ and $z$, and using

$$p_{x_i} = m_i(dx_i/dt), \text{ etc.} \quad (2)$$

$$T = {}^1/_2 \sum_{i=1}^{N} (p_{x_i}^2 + p_{y_i}^2 + p_{z_i}^2)/m_i;$$

$$T + U = H \quad (3)$$

in which $U$ is the potential energy. The number of atoms $N$ was either 5 or 9. The methods of numerical solution were standard ones.[7]

The starting conditions were chosen to correspond to a randomly oriented P velocity vector, with a fixed magnitude calculated from a prescribed $\gamma$-ray energy. All other atoms were initially at rest. Trajectories were ordinarily terminated if it was determined, from its position and kinetic energy relative to the other atoms, that P had escaped its cage. The complete program for doing all this was written in optimized assembly language for a Digital Equipment Corp. PDP-10. Single precision (27 bit floating fraction, with rounding) was adequate, and several recoils per minute could be simulated.

We used 3 general classes of model in order to compare recoil behavior in increasingly complex surroundings. These will be called the *free*, *bound*, and *hydrated* models of the orthophosphate ion. For each of these we also provided the option of replacing one

(1) T. R. Sato, P. A. Sellers, and H. H. Strain, *J. Inorg. Nucl. Chem.*, 11, 84 (1969); see also *Chem. Eff. Nucl. Transform., Proc. Symp.*, 1, 503 (1961).

(2) L. Lindner and G. Harbottle, *J. Inorg. Nucl. Chem.*, 15, 386 (1960); see also *Chem. Eff. Nucl. Transform., Proc. Symp.*, 1, 485 (1961).

(3) W. F. Libby, *J. Amer. Chem. Soc.*, 62, 1930 (1940).

(4) V. C. Anselmo, Thesis, University of Kansas, 1961 (University Microfilms, Ann Arbor, Mich.).

(5) D. L. Bunker and M. D. Pattengill, *Chem. Phys. Lett.*, 4, 315 (1969).

(6) J. B. Gibson, A. N. Goland, M. Milgram, and G. H. Vineyard, *Phys. Rev.*, 120, 1229 (1960).

(7) The Runge–Kutta–Gill method was used to start the integrations: S. Gill, *Proc. Cambridge Phil. Soc.*, 47, 96 (1951). The faster but not self-starting Adams–Moulton integration was then applied: *e.g.*, J. B. Scarborough, "Numerical Mathematical Analysis," Johns Hopkins Press, Baltimore, Md., 1962, pp 318–325.

or two of the O by OH, so that the series $Na_3PO_4$, $Na_2HPO_4$, $NaH_2PO_4$ could be studied.

*Free* phosphate was, in effect, a gaseous ion. It had 4 O arrayed in a regular tetrahedron about P, each one bound to it by a Morse potential. The O repelled one another by virtue of parabolically rising repulsion functions which began at prescribed values of the O–O distances. The possibility of $O_2$ formation was omitted, and it was later verified that objectionably small O–O distances did not occur in the trajectories. The potential energy for this model was

$$U = \sum_{i=1}^{4} D[1 - \exp(-\beta(r_i - r_0))]^2 + U_{12} + U_{13} + U_{14} + U_{23} + U_{24} + U_{34} \quad (4)$$

where

$$U_{ij} = k(s_{ij} - s_0)^2 \quad (5a)$$

if $s_{ij} < s_0$ or

$$U_{ij} = 0 \quad (5b)$$

in all other cases. The P–O distances are $r_i$, the O–O distances are $s_{ij}$. These are easily expressed in cartesian coordinates for the purposes of eq 3. The estimated[8] value of $D$ was 100 kcal. Spectroscopy[9] gives 1.54 Å for $r_0$ and 2.13 $Å^{-1}$ for $\beta$. The repulsion parameters, whose values are not very critical, were arbitrarily $k$ = 332 kcal/Å and $s_0$ = 1.2 Å. With this $k$ there is 118 kcal of repulsion at $s_{ij}$ = 0.6 Å. Since we are uncertain of how the charges in the fragmented ion are distributed, we have adopted these simplified interactions. The results do not seem unduly sensitive to this.

*Bound* phosphate represents the anhydrous sodium phosphate lattice, with the unit cell simplified to a cube. In this model alternating corners of the cube were used as fixed anchor points, to which the O were bound. This involved adding to the $U$ of eq 4 the additional Morse terms

$$\sum_{i=1}^{4} D'[1 - \exp(-\beta'(r_i' - r_0'))]^2 \quad (6)$$

in which $r_i'$ are O–anchor distances. From the known density of the $Na_3PO_4$ crystal, $r_0'$ = 2.57 Å. To make our simplified lattice electrically neutral, we would need to associate 6 elementary positive charges with each anchor point and $^3/_4$ electron charge with each O. The electrostatic interaction energy for each O–anchor bond, calculated on this basis, is 580 kcal. This is not an unreasonable value for such a quantity, and was used for $D'$. The unknown $\beta'$ was arbitrarily set equal to $\beta$.

For this model we tested the sensitivity of the results to the assumed values of the parameters. The most critical assumptions are probably those about $D$ and $D'$. We tried a variant model ($D$ = 125, $D'$ = 435). As will be shown, no qualitative differences arose when we did this.

*Hydrated* phosphate was limited by computer economics to the fictitious form $Na_3PO_4 \cdot 4H_2O$. The 4 $H_2O$ were each single particles of mass 18 amu, symmetrically introduced above the tetrahedral faces of the $PO_4$ ion at a distance of 2.83 Å from P. The additional repulsions, to be added to eq 4 and 6, are

$$\sum_{i=1}^{4} k_p(\rho_i - \rho_0)^2 + \sum_{i,j} k(s_{ij}' - s_0)^2 \quad (7)$$

These are of the same form as in eq 5, including the cutoff feature. The P–$H_2O$ distances are $\rho_i$; $\rho_0$ = 2.5 $Å^2$; $k_p$ is such that there is $8 \times 10^3$ kcal of repulsion energy at $\rho_i$ = 1.25 Å. The sum over $i,j$ gives the O–$H_2O$ repulsions. There are 12 of these. Each $H_2O$ interacts with the 3O at the corners of the nearby tetrahedral face. The fourth O interaction for each $H_2O$ and the inter-$H_2O$ repulsions may be omitted. We let $k$ and $s_0$ have the same values as in eq 5. None of these parameter values is very critical, since in any event we will surely obtain a valid lower limit to the complexity of $Na_3PO_4 \cdot 12H_2O$.

For the hydrogen phosphates, there are the following changes, arising from different charge distributions and unit cell volumes. In $Na_2HPO_4$, $D'$ = 296, $r_0'$ = 2.99. In $NaH_2PO_4$, $D'$ = 126, $r_0'$ = 2.64. In these cases we take OH as a single particle of mass 17 amu, and we delete the potential term between it and the corresponding anchor point. The unit cell remains cubical.

## Results and Discussion

The most immediately interesting data are the distributions of fragment types that escape the recoil site. These are presented in Tables I and II for all the cases that were studied. Actual numbers of computed events are shown; the uncertainty will be roughly ± the square root of each figure. The four $\gamma$-ray energies[10] that were used sample the $^{32}P$ recoil spectrum in a representative way. This spectrum has four intense transitions, of which we used 6.79 MeV (the highest of the four), 3.90, and 2.10 (the lowest). These occur with relative probability 10:14:13 and together make up 44% of all transitions. The very weak 7.85-MeV emission is 0.09 MeV below the maximum observed; the only transition lower than 2.10 MeV is a weak one at 1.60. A rough estimate of the probable combined results for the full range of transition ener-

(8) By Pauling's rule (electronegativity formula), 85 kcal; from Pauling's bond length–bond order and Johnston's bond energy–bond order ("BEBO") formulas, 99 kcal, using the known bond length; by comparison with known P–O bond strengths, perhaps 120 kcal.

(9) D. W. J. Cruickshank and E. A. Robinson, *Spectrochim. Acta*, 22, 557 (1966).

(10) The corresponding P velocities are 7.95, 6.87, 3.95, and 2.12 × $10^8$ cm $sec^{-1}$. The P kinetic energies are 2.44 × $10^4$, 1.82 × $10^4$, 6.00 × $10^3$, and 1.74 × $10^3$ kcal.

**Table I:** Fragment Distribution in $^{32}P$ Recoils, Anhydrous Cases

| Model | γ energy, MeV | No. of events with ejection of: P only | P + O | P + OH | P + O + OH |
|---|---|---|---|---|---|
| Free $PO_4^{3-}$ | 7.85 | 62 | 38 | ... | ... |
| | 3.90 | 16 | 84 | ... | ... |
| Bound $PO_4^{3-}$ | 6.79 | 70 | 30 | ... | ... |
| | 3.90 | 62 | 38 | ... | ... |
| | 2.10 | 81 | 19 | ... | ... |
| Variant of bound $PO_4^{3-}$ | 6.79 | 68 | 32 | ... | ... |
| | 3.90 | 63 | 37 | ... | ... |
| | 2.10 | 60 | 40 | ... | ... |
| Bound $HPO_4^{2-}$ | 6.79 | 61 | 30 | 9 | 0 |
| | 3.90 | 54 | 34 | 12 | 0 |
| | 2.10 | 48 | 35 | 15 | 2 |
| Bound $H_2PO_4^-$ | 6.79 | 46 | 25 | 29 | 0 |
| | 3.90 | 41 | 33 | 26 | 0 |
| | 2.10 | 33 | 27 | 28 | 4[a] |

[a] Also 3(P + 2OH), 2(P + 2O), 1 each OH, 2OH, and (O + OH).

gies can be obtained by adding the numbers in the tables.

A striking result is that *P–O bonds are almost never carried away* from the recoil site.[11] The sole mild exception to this rule is the messy situation that developed at the lowest energy in $NaH_2PO_4 \cdot 4H_2O$. In free phosphate, if P recoils in a direction where there is no O, it escapes; if there is an O, it too is carried away. The chemical bonds might as well not be present. When P is moving fastest, it is most likely to escape alone, as would be expected. Adding the anchor points, in the bound model, makes O more difficult to dislodge but does not change the character of the recoil process.

The hydrogen phosphates produce (non-P) fragments in amounts intermediate between what was observed for free and bound phosphate, which is reasonable. The ratios between (P + O) and (P + OH) ejection are in proportion to the numbers of O and OH, which again indicates that the initial recoil direction largely determines the outcome. A very feeble exception to this, for anhydrous crystals, occurs at the lowest energy for $H_2PO_4^-$, where there are a few complex trajectories leading in four cases to retention of P.

This effect is magnified, however, when the $4H_2O$ are present. The increasing clutter of the unit cell leads to more complicated trajectories, even at high energies. (Note the substantial number of cases in which more than two fragments were ejected.) At low energies the retention of P has become very appreciable, and might even be the dominant feature if we were able to put in all 12 waters of hydration.

These observations suggest that most of the penetrating power of the P is exhausted in the process of its escape from its original cage. To discuss this more fully, we need the energy spectra of the ejected fragments. Our data on this are too extensive for full presentation, so we have displayed selected examples in

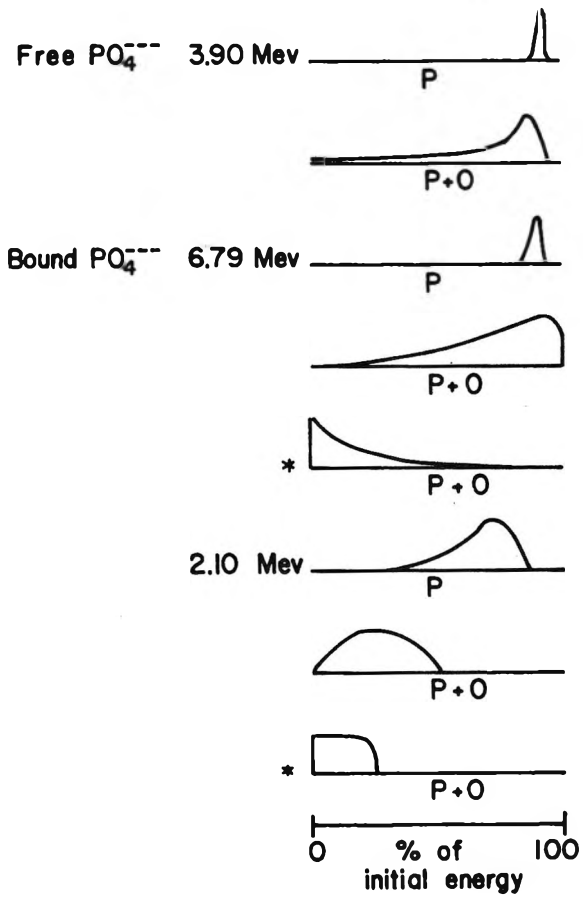


Figure 1. Smoothed energy spectra, on a scale of 0 to 100% of original recoil energy, of ejected fragments in anhydrous crystals. The energies are for P atoms, unless marked (*) for O atoms. The type of ejection process is listed under each spectrum. Vertical units are arbitrary.

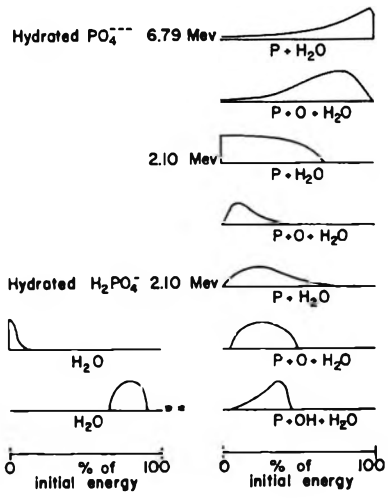


Figure 2. Same as in Figure 1, but for hydrated crystals. The spectrum marked (**) is for $H_2O$.

(11) The parameters of the variant model of anhydrous $Na_3PO_4$ were chosen to provide the maximum opportunity for preservation of the P–O bond.

**Table II:** Fragment Distribution in $^{32}P$ Recoils, Hydrated Cases

| Model | γ energy, MeV | No. of events with ejection of: P only | $H_2O$ only | P + O | P + $H_2O$ | P + O + $H_2O$ | O + $H_2O$ | P + OH | P + OH + $H_2O$ |
|---|---|---|---|---|---|---|---|---|---|
| $PO_4^{3-}(H_2O)_4$ | 6.79 | 3 | 0 | 3 | 67 | 27 | 0 | ... | ... |
| | 3.90 | 1 | 0 | 1 | 60 | 38 | 0 | ... | ... |
| | 2.10 | 0 | 22 | 1 | 58 | 11 | 8 | ... | ... |
| $H_2PO_4^-(H_2O)_4$ | 6.79 | 1 | 0 | 4 | 53 | 15 | 0 | 4 | 23 |
| | 3.90 | 0 | 2 | 0 | 38 | 31 | 0 | 1 | 28 |
| | 2.10 | 0 | 16 | 2 | 17 | 10 | 3 | 1 | 12[a] |

[a] Also PO + 2 (non-P) fragments, 3; POH + 1 or 2 (non-P) fragments, 11; $P(OH)_2$ + 1 or 2 (non-P) fragments, 8; P + 3 fragments, 2; assorted (non-P) fragments not listed above, 17.

Figures 1 and 2. (We have omitted intermediate energies, cases in which OH behaves like O, and minor ejection modes.) In the hydrated crystals, Figure 2, the degradation of the initial P energy is very apparent; the P will probably be unable to escape the next cage it enters. Even in the anhydrous cases the energy loss is not negligible. Most P leave their original sites, but very many must become entangled with the O in the neighboring cells and stopped.

We have, then, the following description of the P recoil process. At first P behaves as if it were a free particle, without chemical bonds. It moves until it hits something, and in this first encounter the chemical nature of the struck object is relatively unimportant. The chance of P escaping its original lattice cell depends mostly on the number of things there are for it to hit. In an anhydrous crystal it is likely to get away, in our fictitious tetrahydrate escape is considerably harder, and in real dodecahydrated $Na_3PO_4$ it must be very difficult indeed. A large fraction of the P energy is lost at every encounter, especially at low recoil energies. The final bonding of P to the crystal occurs within a very few cell lengths (in hydrated crystals, one at most) of its original site. These chemical bonds are very seldom the same ones the P had before its recoil. Nevertheless, the individual ions recovered from the final solution must be largely made of atoms that were near neighbors in the crystal before it was irradiated.

We might therefore speculate, on the basis of our results for anhydrous crystals, that oxygen-poor monomeric ions (such as orthophosphite and hypophosphite) arise from P + O ejection followed by reflection of P back to its original site by the surrounding lattice. We might also suppose that dimeric species represent migration of P to the next lattice cage and that polymeric species such as tripolyphosphate require traversal of more than one neighboring P site. Hydration of the crystal would then tend to suppress polymeric forms and encourage monomeric ones, as the experimental results apparently show.[2]

## Conclusions

Our findings most nearly support the original suggestion of Libby[3] that P and O are the most important fragments ejected from the lattice unit where the recoil occurred. In hydrated crystals at least one $H_2O$ is also displaced. Retention of P is only important at low energies in hydrated crystals, and P–O bonds rarely survive the P recoil. Nevertheless, the region of disruption of the crystal is relatively small; only a few unit cells are involved.

We also conclude that trajectory studies of condensed-phase chemical dynamics are both feasible and useful.

*Acknowledgments.* We are highly indebted to F. S. Rowland for arousing our interest in this problem. The project was supported by the National Science Foundation, whom we thank. We acknowledge the valuable assistance of Barbara Jacobson in the data processing phase of the work.

# The Structure and Properties of Acid Sites in a Mixed-Oxide System. I. Synthesis and Infrared Characterization

by K. H. Bourne, F. R. Cannings,[1] and R. C. Pitkethly

*The British Petroleum Company Limited, BP Research Center, Chertsey Road, Sunbury-on-Thames, Middlesex, England*
*(Received August 19, 1969)*

By synthesizing materials containing aluminum atoms in different environments in a silica matrix, an attempt has been made to separate and characterize two discrete acid site structures likely to coexist in commercial silica–aluminas. The two structures are aluminum atoms incorporated (a) onto a silica gel surface and (b) into a silica gel lattice. This paper describes the preparation of the materials and their characterization by infrared spectroscopy. A study has been made of the dehydration and dehydroxylation of the two materials and of concurrent changes in acidity as measured by pyridine adsorption. With the aluminum-on-silica species, the interconversion of Brønsted and Lewis acid sites has been demonstrated: each Brønsted acid site gives rise to a Lewis site on dehydration. The aluminum-in-silica species was shown to contain only Brønsted acid sites after dehydration.

## Introduction

Because of its use as a catalyst for a wide variety of chemical conversion processes, silica–alumina has attracted a great deal of attention from research workers over many years. Since its preparation involves a cohydrolysis to form the mixed oxides, the constituents of silica–alumina are likely to be present in every possible degree of intermixing, from regions where perfect alternation of silica and alumina occurs in the oxide lattice to regions where bulk silica or alumina are found. Say and Rase[2] have demonstrated the existence of alumina aggregates in such a material. It is a logical extension of this argument to point out that not all the catalytically active sites in silica–alumina are likely to be of the same type and that, in the extreme case, there may be as many types of active site as there are possible aluminum environments.

In an attempt to study the relationship between catalytic activity and structures in this complex material several workers have investigated the nature of its surface by studying the bonding of amines to the surface using infrared techniques.[3-5] Parry[3a] and Basila, *et al.*,[3b] have successfully used pyridine to differentiate between Brønsted and Lewis acid sites on silica–alumina. The superiority of this amine over ammonia is not in doubt: the former gives rise to sharp absorption bands in the region 1400–1660 $cm^{-1}$, and those arising from a pyridinium ion (pyridine plus Brønsted acid site) are readily distinguishable from those of coordinated pyridine (pyridine plus Lewis acid site). Adsorbed ammonia gives broad, poorly defined bands. Further, because of its strongly basic character, ammonia combines with even the weakest acid site and behaves nonselectively; silica gel will retain an appreciable quantity of ammonia after evacuation at elevated temperatures.[6]

However, because of the complex nature of silica–alumina, the infrared absorption and the catalytic activity studies must have measured the average effects of a large number of different, active, acidic species. In recent work, we have prepared novel materials, resembling silica–alumina, in which the active sites may reasonably be considered to be of discrete types, and have compared their physical and chemical properties using infrared, chemisorption, and hydrocarbon cracking techniques. These materials are of two kinds. In one, aluminum atoms are placed onto a silica surface (designated aluminum-on-silica) and in the other they are buried within the silica (aluminum-in-silica). In each case we believe that the aluminum atoms have only oxygen and silicon atoms as their near neighbors in the oxide lattice and that, as such, they are discrete, potential catalytic sites.

This paper describes the preparation of the materials and their characterization by infrared spectroscopy and other techniques. A further paper will report on the differentiation of the chemical properties of the materials by benzene chemisorption and *t*-butylbenzene cracking studies.

## Experimental Section

(*a*) *Materials.* The water used throughout this work was deionized (resistivity > 1.5 megohms/cm) and

(1) Communications arising from the paper should be addressed to this coauthor.

(2) G. R. Say and H. F. Rase, *Ind. Eng. Chem., Prod. Res. Develop.*, 250, Sept (1966).

(3) (a) E. P. Parry, *J. Catal.*, **2**, 371 (1963); (b) M. R. Basila, T. R. Kantner, and K. H. Rhee, *J. Phys. Chem.*, **68**, 3197 (1964).

(4) M. R. Basila and T. R. Kantner, *ibid.*, **70**, 1681 (1966).

(5) M. R. Basila and K. H. Rhee, Abstracts, 145th National Meeting of the American Chemical Society, New York, N. Y., Sept 1963, Paper 26-I.

(6) G. Bliznakov and R. Polikarova, *J. Catal.*, **5**, 18 (1966).

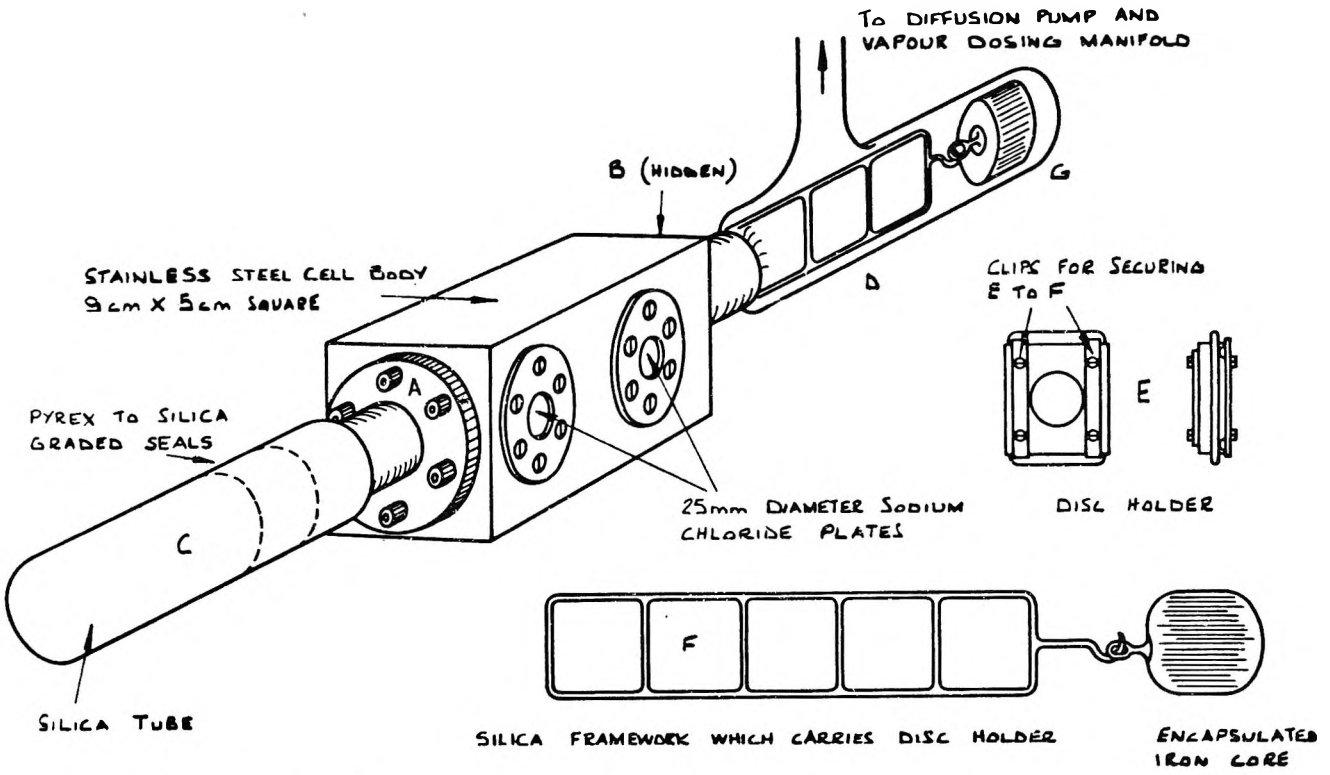


Figure 1. Infrared cell and disk holder.

all chemicals were of Analar grade. Pyridine was degassed and dried over 5A molecular sieve.

Sorbosil U30 silica gel of 72–100 mesh particle size, supplied by Messrs. Joseph Crosfield, Warrington, Lancs, was extracted with 0.1 *N* hydrochloric acid to remove traces of sodium and iron. It was then washed with water in a Soxhlet apparatus for 8 hr and dried at 110° for 24 hr. All aluminum-on-silica preparations were derived from this parent material by contacting it with aqueous solutions of aluminum sulfate hexadecahydrate. The amount of aluminum taken up by the gel may be increased by increasing the concentration of the sulfate solution, by repeating the treatment with fresh solution, or by percolating the solution through a bed of the gel. The incorporation of ions onto a gel surface by such techniques has been described by Maatman and coworkers[7] as ion exchange. Following such a percolation procedure with 0.1 *M* aluminum sulfate solution, the gel was exhaustively extracted with water to remove surplus salt and dried overnight at 110°. Its aluminum content was 1.3% by weight.

Two samples of aluminum-in-silica were made by stirring for 16 hr, a mixture of tetraethylorthosilicate (Monsanto Chemicals, London) with twice its volume of hydrochloric acid, at pH 2. Sufficient aluminum sulfate was dissolved in this mixture to give an aluminum content of 0.5 or 1 wt % on the silica. Ammonia solution (2 *N*) was then stirred rapidly into the mix until it gelled, at pH 6. The hydrogel was separated, reslurried with 10 volumes of water, filtered off, dried for 2 hr at 110°, and at 350° for 4 hr. The calcined gel was transferred to a glass column where dilute nitric acid (1 *N*) was run over it at a rate of 2 vol/vol hr, until the eluate was free of aluminum, as measured spectrophotometrically at 386 mμ using 8-hydroxyquinoline as an indicator. The acid washing procedure lasted 7 days, after which the treated gel was exhaustively extracted with water and dried overnight at 110°. The aluminum contents of these silicas were 0.045 and 0.15 wt %.

The number of strongly protonic centers on both preparations was estimated by exchange with saturated sodium bicarbonate solution, followed by water washing. The final sodium content was regarded as a direct measure of the number of acid centers.

(*b*) *Sample Preparation.* Self-supporting 13-mm diameter disks of silica, aluminum-on-silica (1.3 wt % aluminum), and aluminum-in-silica (0.045 wt % aluminum) were formed by pressing the oxide powder at 9000 kg/cm² in a conventional KBr die. Suitably sized powders were produced by prolonged grinding in a large agate pestle and mortar. Unless stated otherwise, approximately 11 mg of sample was used for each disk.

(*c*) *Infrared Cell.* The cell is shown in Figure 1. The body was machined from a 9 × 5 × 5 cm³ stainless steel block, recesses being cut to accommodate 4 O-rings

(7) D. L. Dugger, J. H. Stanton, B. N. Irby, B. L. McConnell, W. W. Cummings, and R. W. Maatman, *J. Phys. Chem.*, **68**, 757 (1964).

and 25 mm diameter by 3 mm thick circular rock salt plates. These windows were held in place with bolted rings. Flanges A and B were sealed with aluminum gaskets. The horizontal side arm C, constructed from a 1-in. Kovar-to-Pyrex seal, was graded through glass seals to a quartz finger. This could be surrounded by a thermostatically controlled 500-W furnace rated to 800°.

The disk was mounted vertically in a stainless-steel holder, E, which clipped onto the silica framework, F. The latter could be moved through grooves in the cell body, back and forth along the side arm, C, by the action of a Pyrex-encapsulated iron core, G, and external magnet. After calcining in the quartz section of the tube, the disk was withdrawn and reproducibly positioned in the analytical beam of the infrared spectrometer. The cell was part of a vacuum manifold connected to conventional, commerically available equipment, capable of maintaining a limiting dynamic pressure of *ca.* $2 \times 10^{-6}$ Torr. Pyridine and water vapor were introduced through greaseless diaphragm stopcocks attached to the manifold. Details of the various dosing operations are given at relevant places in the text.

(*d*) *Spectra.* Spectra were recorded on a Grubb-Parsons GS 2, double-beam infrared grating spectrometer, range 2–15 $\mu$m (5000 to 660 $cm^{-1}$). The manufacturer's specification of a limiting resolution of $\pm 1$ $cm^{-1}$ is more realistically assessed at $\pm 3$ $cm^{-1}$ under the conditions of this work. Attenuation of the reference beam, with an adjustable comb, was frequently necessary to compensate for the energy lost in light scattering by the disk. All spectra were run ostensibly at room temperature but this assumption neglects the heating effect of the infrared beam. Absorbances were calculated from band heights.

## Results and Discussion

(*a*) *Sodium Treatment of Aluminum–Silicas.* When various aluminum-on and aluminum-in-silicas were contacted with sodium bicarbonate solution, carbon dioxide was evolved and sodium incorporated onto the gel. Not all this sodium could be leached from the gel by exhaustive water extraction; neither silica nor alumina shows this ability to retain sodium ions. The data in Table I show that each aluminum atom retained one sodium ion (or "half" a divalent ion); this, in turn, suggests that each behaved as a discrete protonically acidic species, whether or not the aluminum was buried within the silica structure (the analytical errors at the lowest Al contents are relatively high).

Washing with 0.1 *N* hydrochloric acid readily removed all the aluminum from the aluminum-on-silica. This behavior immediately distinguishes it from aluminum-in-silica and indicates that all the aluminum is at the silica surface in the former material.

(*b*) *Water on Silica Gel and Aluminum-on-Silica.*

**Table I:** Analysis of Variously Treated Aluminium Silicas

| Host material | Al, % wt | Na[a] guest, % wt | Other guest ions,[b] % wt | Guest ion/Al atom ratio |
|---|---|---|---|---|
| Al-on-silica | 0.16 | 0.14 | ... | 1.0 |
| | 0.70 | 0.63 | ... | 1.1 |
| | 1.36 | 1.24 | ... | 1.1 |
| | 1.20 | ... | 1.30 Ni | 0.5 |
| | 0.28 | ... | 0.15 Mg | 0.6 |
| Al-in-silica | 0.15 | 0.20 | ... | 1.6 |

[a] Treatment with sodium bicarbonate. [b] Treatment with the respective metal sulfates.

Few differences appeared in the infrared spectra of disks of the parent silica and of aluminum-on-silica on dehydration and dehydroxylation at temperatures up to 600° in a vacuum, although the latter retained water rather more strongly. The 1630-$cm^{-1}$ band, assignable to water deformation, was small and stayed sensibly constant on pumping the silica at temperatures in the range 25–600°, but with aluminum-on-silica a decrease in absorbance was observed down to a value close to that found for the silica. The band was never completely removed; it seems likely that the residue can be attributed to an SiO overtone[8] rather than to water trapped by capillary collapse on disk formation[9], since the two samples approached a similar final state following different dehydration patterns.

In the hydroxyl stretching region, dehydration gave rise to the anticipated sharpening of the broad 3-$\mu$m band with the emergence, at treatments above 500°, of a peak at 3744 $cm^{-1}$ assignable to isolated silanol groups.[9-11] Bands at 3795, 3737, and 3698 $cm^{-1}$, assigned by Peri[11] to Al–OH stretch, did not appear at any degree of dehydration of the aluminum-on-silica up to treatment temperatures of 600°. Failure to discern such bands was probably due to the low concentration of aluminum in the sample and to the fact that any such OH groups would necessarily interact with other hydroxyl groups in their vicinity. They would then merely contribute to the broad 3-$\mu$m band.

Table II shows results of a study of the relative rehydration properties of silica and aluminum-on-silica samples. The absorbance of the 1630-$cm^{-1}$ band was utilized to estimate molecular water contents. After a preliminary 1 hr evacuation at 25°, spectra were obtained from 6.5-mg disks of silica and aluminum-on-silica. The disks were then calcined at the temperature indicated, cooled, dosed with water vapor, and again pumped for 1 hr at 25°.

(8) H. A. Benesi and A. C. Jones, *J. Phys. Chem.*, **63**, 179 (1959).
(9) F. H. Hambleton, J. A. Hockey, and J. A. G. Taylor, *Nature*, **208**, 138 (1965).
(10) R. S. McDonald, *J. Phys. Chem.*, **62**, 1168 (1956).
(11) J. B. Peri, *ibid.*, **70**, 2937 (1966).

**Table II:** Absorbance of 1630-cm$^{-1}$ Band

| Treatment of disk | Silica | Al-on-silica |
|---|---|---|
| Evacuation 1 hr at 25° | 0.049 | 0.074 |
| Evacuation 1 hr at 350° | 0.044 | 0.071 |
| Water added at 25° | 0.255[a] | 0.516[a] |
| Evacuation 1 hr at 25° | 0.047 | 0.086 |
| Evacuation 1 hr at 500° | 0.045 | 0.058 |
| Water added at 25° | 0.162[a] | 0.417[a] |
| Evacuation 1 hr at 25° | 0.050 | 0.094 |
| Evacuation 1 hr at 600° | 0.050 | 0.057 |
| Water added at 25° | 0.299[a] | 0.271[a] |
| Evacuation 1 hr at 25° | 0.049 | 0.091 |

[a] Variations caused by differences in the amount of water added.

The ascending thermal treatments had no effect on the 1630-cm$^{-1}$ band of silica and consequently the amount of molecular water retained by this sample at all stages must be regarded as zero. With aluminum-on-silica the variations in band intensity suggest that dehydration produces sites which are subsequently able to chemisorb water strongly. These sites are probably Lewis acid centers formed from Brønsted sites according to the following scheme.

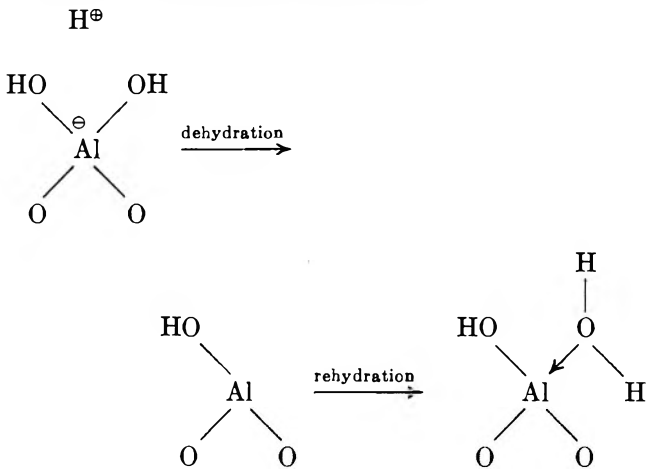


This subject is further discussed in a later section of the paper. The data also indicate that some molecular water is very strongly adsorbed by aluminum-on-silica, since evacuation at 350° does not completely remove it from the surface.

(c) *Spectra of Adsorbed Pyridine.* Parry[3a] and Basila, *et al.*,[3b] have defined the solid acid sites on commercial silica–alumina surfaces in terms of the infrared spectra of adsorbed pyridine in the region 1660–1400 cm$^{-1}$. By calibration against synthesized standards, the spectra obtained in the current work have been used to classify the types of site effecting adsorption as Lewis (LPy) Brønsted (BPy) or surface hydroxyl (HPy). Table III lists the assignments of the different bands; the 19 b modes have been used to distinguish between different types of adsorbed pyridine.[12,13]

**Table III:** Pyridine Assignments in the Range 1660–1400 cm$^{-1}$

| Type | Py,[a] cm$^{-1}$ | HPy,[b] cm$^{-1}$ | BPy,[c] cm$^{-1}$ | LPy,[d] cm$^{-1}$ |
|---|---|---|---|---|
| Mode[e] 8a | 1582 | 1614 | 1639 | 1617 |
| 8b | ... | 1593 | 1613 | ... |
| 19a | 1483 | 1490 | 1489 | 1495 |
| 19b | 1440 | 1438 | 1539 | 1451 |

[a] A dilute solution in chloroform. [b] Taken from Sidorov.[12] [c] From synthesized pyridinium hydrochloride. [d] From synthesized pyridine–aluminum chloride. [e] Designations taken from Turkevitch.[13]

The assignments are in accord with those in the work of Gill, *et al.*, and of Cook[14] on LPy and BPy complexes.

It can be seen that the pyridinium ion alone produced a band in the vicinity of 1540 cm$^{-1}$ and the appearance of this band in the spectrum of a disk is taken as indication of the presence of Brønsted acidity. Coordinately bonded or Lewis pyridine generated a unique band at 1451 cm$^{-1}$ where the pyridinium ion does not absorb. Pyridine itself gives a band at 1440 cm$^{-1}$.

(d) *Pyridine Adsorbed on Silica Gel.* Figure 2b shows the spectrum of pyridine adsorbed onto the parent silica, pretreated by evacuation at 400° for 1 hr. Addition of water did not significantly change the spectrum. Evacuation for 10 min at room temperature removed all the bands ascribable to physisorbed pyridine and those remaining, at 1599 and 1447 cm$^{-1}$ (spectrum c), are assignable to hydrogen bonded pyridine. These were lost on pumping for 24 hr at 25°. All bands attributable to adsorbed pyridine were rapidly removed by pumping a dosed sample at 100°. The lack of a band at 1546 cm$^{-1}$ implies the absence of BPy and the 1447-cm$^{-1}$ band is at too low a frequency to be attributed to LPy. The pyridine is only weakly retained and adsorption occurs on or adjacent to hydroxyl groups. The effect was observed on hydroxyl stretch intensity at 3700–3740 cm$^{-1}$. The preferential location for attachment seems to be weakly H-bonded OH groups. Isolated hydroxyl groups were not affected at low pyridine concentrations. These results are in general agreement with those of Parry.[2]

(e) *Acid Sites on Aluminum-on-Silica.* Evacuation for 1 hr at 400° of a disk of aluminum-on-silica (1.3 wt % aluminum), that had previously been contacted with pyridine vapor at room temperature, produced the spectrum shown in Figure 3a. The bands at 1624, 1496, 1462 (shoulder), and 1456 cm$^{-1}$ are typical of very firmly held LPy, and demonstrate the strength of the adsorption sites. The splitting in the

(12) A. N. Sidorov, *Opt. Spektrosk.*, **8**, 806 (1960).

(13) C. H. Kline and J. Turkevitch, *J. Chem. Phys.*, **12**, 300 (1944).

(14) N. S. Gill, R. H. Nuttall, D. E. Scaife, and D. W. A. Sharp, *J. Inorg. Nucl. Chem.*, **18**, 79 (1961); D. Cook, *Can. J. Chem.*, **39**, 2009 (1961).

lowest energy band indicates the presence of two distinct forms of Lewis acid center.[15]

On addition of water vapor (spectrum b), the 1456-$cm^{-1}$ peak shrank and revealed a very small band at 1446 $cm^{-1}$, arising from HPy. The 19a mode at 1496 $cm^{-1}$ was converted to absorption at 1490 $cm^{-1}$, and a broad band appeared at 1547 $cm^{-1}$. All these observations are consistent with the generation of BPy at the expense of LPy. The variation in the intensity of the 19a mode is shown in Figure 3 and the shift from 1496 $cm^{-1}$ to 1490 $cm^{-1}$ is easily detected. This change in the frequency has not been reported previously; it was very apparent in this work.

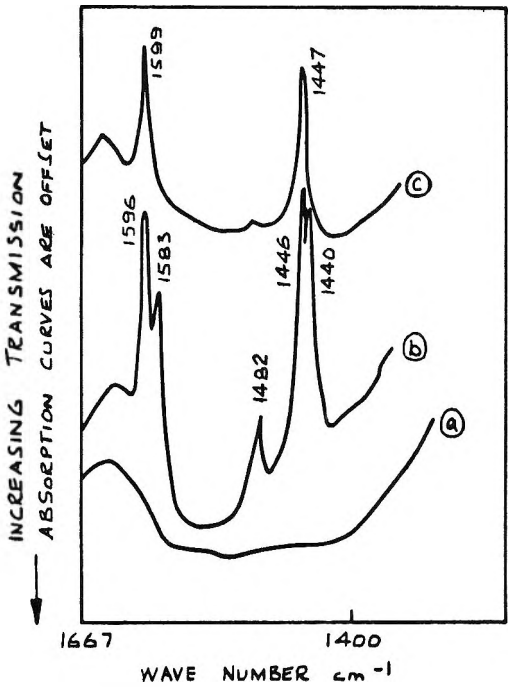


Figure 2. The infrared spectra of pyridine on silica (transmission *vs.* $cm^{-1}$): a, silica evacuated for 1 hr at 400°; b, pyridine added; c, evacuated for 10 min at 25°.

When more water together with pyridine was added (spectrum c), the absorbances of the bands at 1490 and 1547 $cm^{-1}$ changed minimally from 0.248 to 0.248, and 0.056 to 0.054, respectively. Those of the band at 1446 $cm^{-1}$ increased from 0.010 to 0.193. It is difficult, therefore, to believe that the band at 1490 $cm^{-1}$ contains more than a very small contribution from HPy. This view is supported by the spectra of pyridine on silica, displaying bands only at 1599 and 1447 $cm^{-1}$. Evacuation for the times given produced a reduction, then elimination, of HPy after pumping for 1 hr. The increase in Lewis acidity during this process can be followed in Figure 3. Finally, the spectrum reverts to (a) after 1 hr evacuation at 400°. We conclude that conversion of these Lewis acid sites to Brønsted is reversible and depends on the combination of water with the surface. This statement is consistent

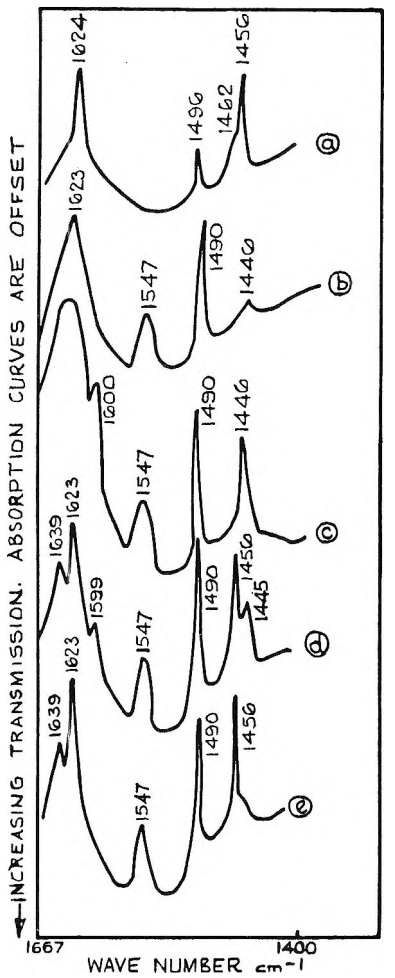


Figure 3. The infrared spectra of pyridine on aluminum-on-silica: a, disk dosed with pyridine at 25° then evacuated for 1 hr at 400°; b, water vapor admitted at 25°; c, more water vapor plus some pyridine admitted at 25°; d, disk evacuated for 10 min at 25°; e, disk evacuated 1 hr at 25°.

with the simple representation of an acid-center of aluminum-on-silica, given on a preceding page.

Pyridine must slightly modify the stability of the sites and probably facilitates the removal of $H_2O$. The generation of BPy occurs whether pyridine or water is added first to a dehydrated aluminum-on-silica. This implies that the water molecule can react with a center that is obstructed by pyridine. Pyridine is the stronger base and generally remains after a calcination which detaches chemisorbed water molecules from the surface, but some sites can lose pyridine before water, as will be explained later.

Figure 4 shows results from a more extensive examination of the interrelationship of Lewis and Brønsted acidities. A disk of the aluminum-on-silica, was successively evacuated for 1 hr at $T_X$° (referred to as treatment X), dosed with pyridine, dosed with water vapor, and then evacuated again for 1 hr at 25° (the

(15) F. R. Cannings, *J. Phys. Chem.*, **72**, 4691 (1968).

**Table IV:** Total Acidity of One Disk of Aluminum-on-Silica, Based on the LPy Scale of Measurement (Arbitrary Units) after Each Cycle Y Treatment

| | Evacuation temp, °C (*i.e.*, treatment X) | | | | | | |
|---|---|---|---|---|---|---|---|
| | 25 | 200 | 300 | 400 | 500 | 600 | 700 |
| BPy ($A_{1547}$) | 0.072 | 0.075 | 0.047 | 0.048 | 0.046 | 0.030 | 0.030 |
| BPy converted to LPy scale | 0.189 | 0.194 | 0.123 | 0.124 | 0.120 | 0.078 | 0.078 |
| LPy | 0.151 | 0.154 | 0.217 | 0.233 | 0.228 | 0.236 | 0.141 |
| Total acidity on LPy scale | 0.340 | 0.348 | 0.340 | 0.357 | 0.348 | 0.314 | 0.219 |

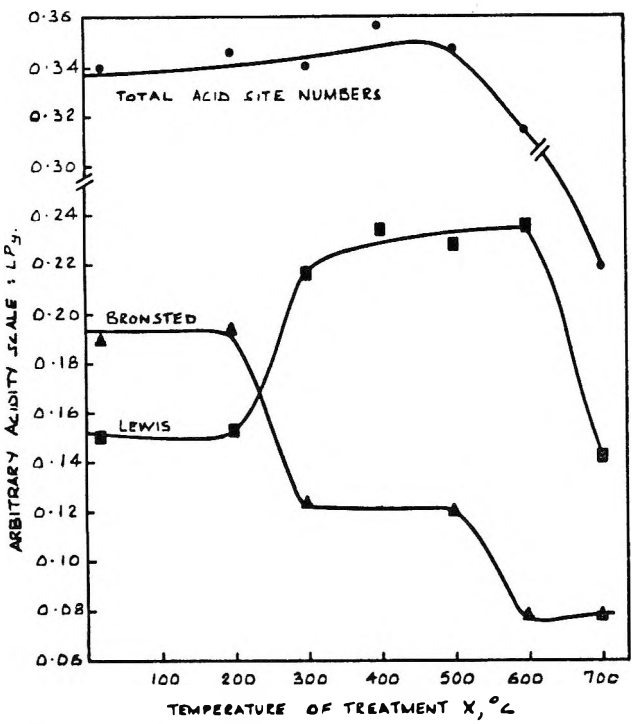


Figure 4. Relative numbers of coexisting acid sites and total acidity of 1.3 wt % aluminum-on-silica after cycle Y, against temperature of evacuation in treatment X.

complete treatment is known as cycle Y). The temperature, $T_X°$, of treatment X was increased from 25 to 200° and then in increments of 100° until 700° was reached, while the procedure for the rest of cycle Y remained unchanged.

Spectra were run at the stages shown in Table IV.

It was possible, from the work on water dosing alone, to establish the numerical relationship between the absorption coefficients of the 1547 (BPy) and 1456 (LPy) $cm^{-1}$ bands. The assumption was made that water converted all LPy remaining on the sample after evacuation at 400° to BPy. This is justified, to a first approximation, by the appearance of spectra a and b of Figure 3. The relevant absorbances, calculated from peak heights, are 0.049 and 0.128, and the conversion factor

$$\frac{A_{1456}}{A_{1547}} = 2.61$$

is obtained.

On this basis Table IV was compiled, showing the total acidity (here absorbance and acidity are equated), on the LPy scale, of aluminum-on-silica and the results are plotted in Figure 4. This exercise illustrates the conservation of recoverable acid site numbers. They remain sensibly constant after calcinations up to 500°.

At 600° there is an irreversible loss of 10% of the total acidity, and the Brønsted acid sites suffer depletion. The more severe calcination temperature of 700° probably altered the oxide lattice. In all these measurements, HPy existed only in trace quantities.

In one additional experiment, after evacuation at 600°, dosing and subsequent room temperature evacuation, the disk stood for 70 hr in a pyridine–water vapor atmosphere. The absorbances of the acid site bands then became (after the standard 25° evacuation) BPy 0.062; LPy 0.146. Total acidity remained at 0.31, but there was a considerable conversion of LPy to BPy, when compared with the corresponding values in Table IV. This evidence suggests that a slow process of rehydroxylation occurs on some of the aluminum atoms and those involved may well be the sites which previously have been observed to strongly chemisorb molecular water. The relative proportions of the two acid site types depend on the immediate history of the sample. Referring to those regions of Figure 4 where plateaux occur, after 100° evacuation, 5 Brønsted to 4 Lewis sites exist. The ratio changes to 1 Brønsted to 2 Lewis after 400° evacuation.

The amount of pyridine retained by the disk after treatment X at temperatures up to 700°, is plotted in Figure 5. BPy disappeared above 300°, whereas some LPy remained at 700°.

There is some empirical evidence to suggest that the elimination of the 1547-$cm^{-1}$ vibration is not solely due to the loss of water from Brønsted acid sites. On readmission of dry pyridine after the evacuation, a small quantity of BPy is found, when the temperature of evacuation does not exceed 500°. This did not occur during 600° determinations, so the likelihood of some water accompanying the pyridine dose is disproved.

The results from a separate series of experiments in which the sequence of operations for cycle Y was followed, except that all water dosing was omitted, are shown in Figure 6. The constancy of acid site numbers is maintained to 500°.

**Table V:** Absorbances of Pyridine on a Partially Sodium Exchanged Aluminum-on-Silica[a]

| Treatment | Wave number 1624 cm$^{-1}$ LPy | 1598 cm$^{-1}$ HPy | 1546 cm$^{-1}$ BPy | 1493 cm$^{-1}$ ... | 1456 cm$^{-1}$ LPy | 1445 cm$^{-1}$ HPy |
|---|---|---|---|---|---|---|
| Disk evacuated 1 hr at 25°; dosed with pyridine and water and evacuated for 1 hr at 25° | 0.048 | 0.045 | 0.047 | 0.135 | 0.070 | 0.086 |
| Evacuated 1 hr at 300° | 0.074 | ... | ... | 0.034 | 0.082 | ... |
| Dosed with pyridine and water and evacuated for 1 hr at 25° | 0.092 | 0.075 | 0.020 | 0.058 | 0.115 | 0.135 |
| Evacuated 1 hr at 600° | Nil | | | | | |
| Dosed with pyridine and water and evacuated for 1 hr at 25° | 0.063 | 0.088 | 0.012 | 0.053 | 0.070 | 0.189 |

[a] Using 0.71 wt % Na; using 1.3 wt % Al.

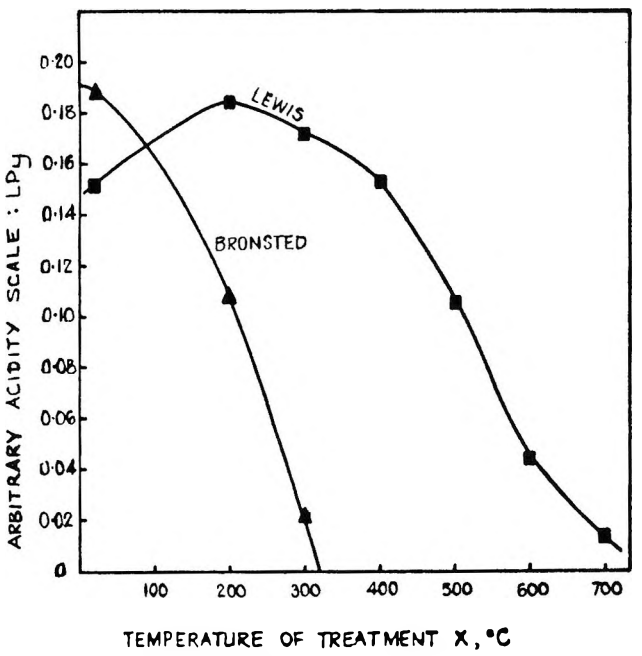


Figure 5. Relative numbers of coexisting acid sites detected on 1.3 wt % aluminum-on-silica after treatment X, against temperature of treatment X.

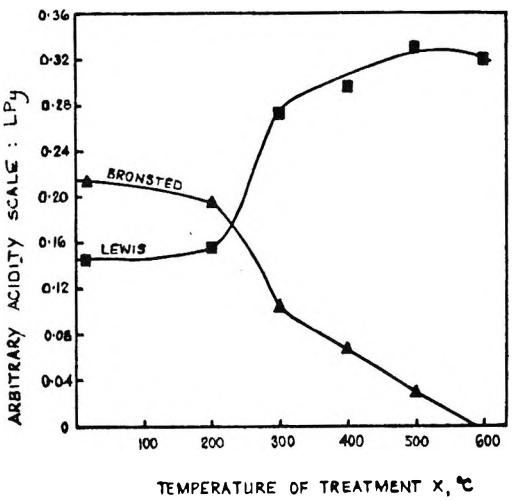


Figure 6. Relative numbers of coexisting acid sites on 1.3 wt % aluminum-on-silica after cycle Y, but omitting all water dosing, against temperature of evacuation for treatment X.

(*f*) *Sodium Exchanged Aluminum-on-Silica.* Examination of an aluminum-on-silica disk, partly exchanged with sodium, Na = 0.71 wt %, Al = 1.3 wt % (fully exchanged would be 1.1 wt % sodium), produced spectra summarized in Table V. LPy and BPy contents are quite high, reflecting the lack of sodium neutralization of some of the acid sites. The ratio LPy/BPy after 300° evacuation, pyridine and water dosing and evacuation at room temperature, is similar for this material and the parent aluminum-on-silica, again indicating that the two forms of acid are located at the same center.

The self-consistency of the overall method is demonstrated by a simple calculation. After cycle Y at 300°, BPy absorbance is 0.047 (Table IV) for the parent aluminum-on-silica. Taking into account the weights of material used for the disk (11 mg for the aluminum-on-silica parent, 13 mg for the sodium exchanged sample) and the neutralization by sodium, on a one sodium atom for one aluminum atom basis, the absorbance of the partly exchanged disk can be predicted thus

$$A_{1546} = 0.047 \times \frac{13}{11} \times \frac{1.1 - 0.71}{1.1} = 0.021$$

This value is in excellent agreement with that found in practice (Table V). Apart from supporting the technique, the validity of the calculation shows either that all the Brønsted sites detected on the aluminum-on-silica are of equal strength (on the assumption that the stronger acid sites would exchange preferentially with sodium bicarbonate) or that all Brønsted sites are strong enough to retain pyridine to the completion of cycle Y. The latter is the more likely explanation, confirming that pyridine is a very satisfactory selective base for solid acid site investigation.

Another feature of the spectra of partly sodium exchanged aluminum-on-silica is the increase of the 1445-cm$^{-1}$ band with increased temperature of treatment X

(columns 3 and 7 of Table V). This absorption probably arises from pyridine associated with the sodium ion, rather than pure HPy. Sodium obviously modifies the behavior of the acid site, and healing modifies the effect of the sodium. This change may be the initial step in the formation of new, weaker Brønsted acid sites, a subject referred to by Flockhart and Pink.[16] The change is accompanied by a decrease in BPy concentration.

*Acid Sites on Aluminum-in-Silica.* Whereas with aluminum-on-silica brief washing with a dilute mineral acid removes all aluminum from the gel, aluminum-in-silica contains a residue of aluminum that cannot be leached out by acid. The aluminum is believed to be buried within the silica lattice, bonded *via* oxygen atoms to four silica atoms and to carry a proton thus

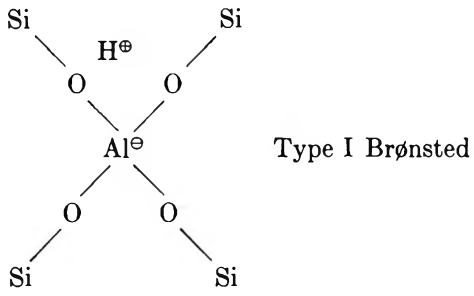


Type I Brønsted

Evacuation and heating should not so readily remove protons from this material, because of lack of neighboring hydroxyl groups. The center should behave as a permanent Brønsted acid.

A 25 mg disk gave spectra, after dosing and pumping at 25°, showing the presence of HPy and BPy, with the former predominating. Evacuation at 200° eliminated all the HPy, and some BPy was lost without a concomitant increase in LPy. Evacuation at 270° removed all pyridine.

A similar treatment of a disk of 0.16% wt aluminum-on-silica (*i.e.*, of comparable aluminum content) produced a spectrum, after evacuation at 270°, that contained the bands of both LPy and BPy. Therefore, it is unlikely that with the former material, the generation of Lewis acid structures from Brønsted has escaped notice, particularly when one considers the relative extinction coefficients of the two bands.

The bonding of pyridine to the site appears weaker than in the case of aluminum-on-silica and this must be due to the different environment of the aluminum. The results are consistent with the structure as originally envisaged, one that precludes the facile formation of Lewis acidity and provides a source of heat stable protons.

Pyridine dosing of disks of aluminum-in-silica that had previously been calcined at 400 and 500° initially produced only HPy. On standing, BPy slowly developed; the formation of BPy was accelerated by the addition of water vapor. No LPy was detected.

The likelihood of free unhydrated protons in the solid oxide is regarded by Hall and coworkers[17] as doubtful. They demonstrated that on deammination of $NH_4$ zeolite, the liberated protons attached themselves to, and opened, Al–O–Si bridges and formed hydroxyl groups. It could be that with aluminum-in-silica a buried proton is sufficiently stabilized by the proximity of the oxygen lattice to remain intact. In the hydrated state it becomes available at the surface of the oxide, to undergo ion exchange or form BPy with adsorbed pyridine.

Evidence of hydrogen ion migration in zeolites has been recorded[18] and the same mechanism would explain these observations. The migration is probably enhanced by a basic adsorbate.

*The Structures of the Acid Sites.* Any theory we propose to explain the observed interchange of acid types has to include the formation of two distinct Lewis acid centers, corresponding to the major absorption of LPy at 1455 $cm^{-1}$ and the shoulder found at 1462 $cm^{-1}$. The frequency of the latter indicates that it is the stronger electrophilic site.

We believe that the geometry of the predominant site produced by aluminum exchange with a fully hydroxylated silica, can be represented by a two-bond attachment to the silica lattice. The aluminum assumes tetrahedral coordination and carries two hydroxyl groups and a formal negative charge that is balanced by an exchangeable proton.

Additional evidence for this aluminum environment has been obtained from the reaction of carbon tetrachloride with a fully sodium exchanged 1.3 wt % aluminum-on-silica. Substitution of the hydroxyls located on the aluminum occurs, and the chlorine to aluminum ratio found is 2 to 1. (The technique has been described.[19])

The reactions of this type of site that occur on calcination can be represented by the following scheme.

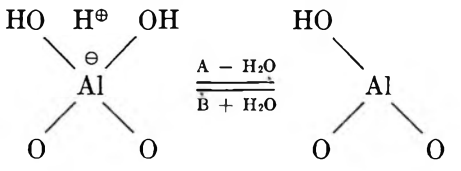


Type II Brønsted 1546 $cm^{-1}$

Type IV Lewis 1455 $cm^{-1}$

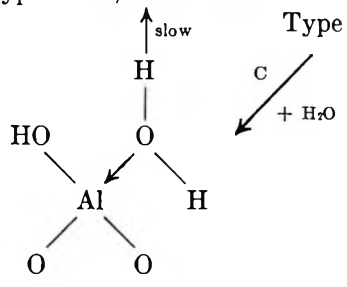


Type IVa Lewis 1455 $cm^{-1}$

(16) B. D. Flockhart and R. C. Pink, *J. Catal.*, **4**, 90 (1965).

The route followed on rehydration can be either B or C. The latter corresponds to the slow recovery of Brønsted acidity (BPy), observed when the sample was contacted with a pyridine–water mixture for 70 hr. The appropriate 19b vibration of adsorbed pyridine is also shown. The existence of Type IVa sites explains the presence of molecular water detected after rehydration of calcined specimens. It should be added that coordination of water, leading to slow regeneration of Brønsted sites, may also occur on the Type VI site (see below). The Type IV site is a Lewis acid producing a pyridine band at 1455 $cm^{-1}$.

In addition we consider that a second type of aluminum site, in much lower concentration, is formed during the aluminum sulfate exchange process. This only appears at favorable surface environments and the site closely resembles those found on zeolite,[17] involving three Al–O–Si linkages. This site can behave either as a Lewis or Brønsted acid, depending on the degree of ionization of a nearby silanol group.

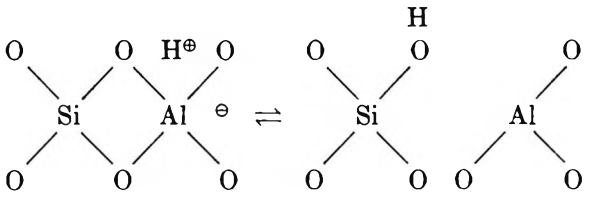

Type III Brønsted 1546 $cm^{-1}$

Type V Lewis 1455 $cm^{-1}$

The presence of Type III sites would explain the Brønsted acidity found even after evacuation at 500°. A slight decrease of the isolated hydroxyl band intensity detected after pyridine dosing and evacuation is confirmatory evidence.

A condensation reaction between two Type V species, as suggested by Stamires and Turkevich[20] to account for radical ion forming electron traps, could generate a stronger Lewis acid

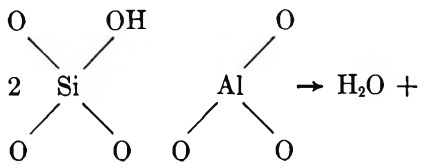

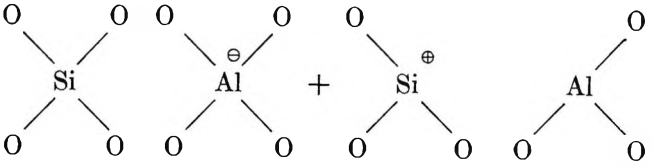

Type VI Lewis 1462 $cm^{-1}$

In a previous study of mordenite,[15] Type VI sites were believed to be responsible for the 1462-$cm^{-1}$ band of adsorbed pyridine. Their structure leads one to expect them to be stronger acids than Type IV sites and the shift in frequency of the adsorbed pyridine is consistent with this.

The probable ratio of Type II to Type III in the fully hydrated state is not known but is likely to be greater than 10:1. The apparent loss in acid site numbers at 600° may be partially due to the formation of Type VI.

## Summary

The data have established that aluminum-in-silica behaves differently from aluminum-on-silica on dehydration, and an explanation, in terms of structural changes, has been offered.

Reaction of aqueous aluminum sulfate with the surface of silica gel produces two types of Brønsted acid site in which aluminum is bonded to the surface through two or four oxygen bridges (Types II and III, respectively). Both can dehydrate to Lewis acid sites (Types IV and VI). A third type of Brønsted site exists (Type I) with aluminum completely enclosed in the silica lattice by four oxygen bridges, as in aluminum-in-silica, and is resistant to dehydration.

The Lewis acid sites of Type VI are present only in small numbers and are similar to those found in much higher concentration in mordenite.

*Acknowledgment.* Permission to publish this paper has been given by The British Petroleum Company Limited.

(17) J. B. Uytterhoeven, L. G. Christner, and W. K. Hall, *J. Phys. Chem.*, **69**, 2117 (1965).

(18) J. W. Ward, *ibid.*, **73**, 2086 (1969).

(19) British Patent Application No. 35490/68.

(20) D. N. Stamires and J. Turkevich, *J. Amer. Chem. Soc.*, **86**, 749, 757 (1964).

# Carbonate Radical in Flash Photolysis and Pulse Radiolysis of Aqueous Carbonate Solutions

by David Behar, Gideon Czapski, and Itzhak Duchovny

*Department of Physical Chemistry, Hebrew University, Jerusalem, Israel* *(Received October 7, 1969)*

The carbonate radical, $CO_3^-$, may be generated by the reaction of carbonate or bicarbonate ions with hydroxyl radicals. The flash photolysis of hydrogen peroxide solutions and the pulse radiolysis of water are utilized as sources of hydroxyl radicals from which it is found that the basic form of the hydroxyl radical, $O^-$, contributes little to the production of $CO_3^-$, even up to pH 14. Reactions of $CO_3^-$ with hydrogen peroxide ($k = 8 \times 10^5\ M^{-1}\ sec^{-1}$) and with $HO_2^-$ ($k = 5.6 \times 10^7\ M^{-1}\ sec^{-1}$) are observed. The carbonate radical and the perhydroxyl radical ion, $O_2^-$, are formed in equimolar concentrations in the flash photolysis of oxygen-saturated carbonate solutions, and from this, the extinction coefficient of $O_2^-$ is found to be $1850 \pm 200\ M^{-1}\ cm^{-1}$ by comparison with the better known extinction coefficient of $CO_3^-$. The product of the reaction $CO_3^- + O_2^-$ is assumed to be $CO_5^{2-}$ having a half-life time of several seconds and $\epsilon_{CO_5^{2-}}^{2600} = 410\ M^{-1}\ cm^{-1}$.

## Introduction

The carbonate radical ion, produced in pulse radiolysis of aqueous solutions, is assumed to be formed according to the reactions[1-5]

$$OH + CO_3^{2-} \longrightarrow CO_3^- + OH^- \qquad (1a)$$

In highly alkaline solutions, $O^-$ is assumed to react with carbonate to give the same radical,[5] according to

$$O^- + CO_3^{2-} \xrightarrow{H_2O} CO_3^- + 2OH^- \qquad (1b)$$

At relatively low pH's, reaction 1a may be replaced by

$$OH + HCO_3^- \longrightarrow CO_3^- + H_2O \qquad (1c)$$

The spectrum of the radical was obtained[4,5] with a maximum absorption at 6000 Å. The same spectrum was found when the radical was produced by flash photolysis of carbonate solutions[6] according to

$$CO_3^{2-} \xrightarrow{h\nu} CO_3^- + e_{aq}^- \qquad (2)$$

The decay of $CO_3^-$ in oxygen-free solutions is found to be second order, according to one of the following reactions[5]

$$CO_3^- + CO_3^- \longrightarrow CO_2 + CO_4^{2-} \qquad (3a)$$

or

$$CO_3^- + CO_3^- \xrightarrow{H_2O} 2CO_2 + HO_2^- + OH^- \qquad (3b)$$

In flash photolysis and pulse radiolysis of $O_2$-saturated carbonate solutions, $CO_3^-$ and $O_2^-$ are produced. In these systems, $CO_3^-$ decays mainly in the reaction

$$CO_3^- + O_2^- \longrightarrow \text{products} \qquad (4)$$

The rate constant of this reaction is a subject of disagreement in the literature.[6,7] We studied the reactivity of OH and $O^-$ toward $CO_3^{2-}$, as well as that of $CO_3^-$ toward $H_2O_2$ as a function of pH. The reaction of $CO_3^-$ with $O_2^-$ and the extinction coefficient of $O_2^-$ were also studied.

## Experimental Section

*Materials.* $NaHCO_3$ and $Na_2CO_3$ (Baker) and NaOH (Merck) were of analytical grade and were used without further purification. Hydrogen peroxide (B-DH) was purified by irradiation, followed by distillation collecting the middle fraction only. This procedure was twice repeated. All water used was triply distilled.

*Sample Preparation.* Solutions were saturated with $N_2$ or $O_2$ in syringes. The solutions were introduced from syringes into the irradiation cell, through A5 ground joints. The details of this method have been described previously.[8]

*Analytical Methods.* The concentration of the hydrogen peroxide was determined by titration with potassium permanganate. The proper concentrations were made by dilution, a few seconds before the flash, so that the thermal decomposition of $H_2O_2$ could be ignored.

*Apparatus.* Samples were irradiated in Spectrosil cells. The cell for flash photolysis was 5 cm long and 1.4 cm i.d. Details of the flash photolysis assembly have been described previously.[8] Some solutions

(1) S. Gordon, E. J. Hart, M. S. Matheson, J. Rabani, and J. K. Thomas, *J. Amer. Chem. Soc.*, **85**, 1375 (1963).

(2) G. E. Adams and J. W. Boag, *Proc. Chem. Soc.*, 112 (1964).

(3) G. E. Adams, J. W. Boag, and B. D. Michael, *Trans. Faraday Soc.*, **61**, 1417 (1965).

(4) G. E. Adams, J. W. Boag, and B. D. Michael, *ibid.*, **61**, 1674 (1965).

(5) J. L. Weeks and J. Rabani, *J. Phys. Chem.*, **70**, 2100 (1966).

(6) E. Hayon and J. J. McGarvey, *ibid.*, **71**, 1472 (1967).

(7) G. E. Adams, J. W. Boag, and B. D. Michael, *Proc. Roy. Soc., A*, **289**, 321 (1965).

(8) D. Behar and G. Czapski, *Isr. J. Chem.*, **6**, 43 (1968).

were irradiated by pulse radiolysis in a 4-cm cell, with light passing thrice through the cell; details of this technique will appear elsewhere.[9] Pulses (200 mA) of 5-MeV electrons with pulse duration of about 1 $\mu$sec were used.

## Results and Discussion

The hydroxyl radical was produced in flash photolysis of hydrogen peroxide solutions

$$H_2O_2 \xrightarrow{h\nu} 2OH \qquad (5)$$

and produces $CO_3^-$ by some combination of reactions 1a, 1b, and 1c. In the presence of hydrogen peroxide, another reaction of the hydroxyl radical is

$$\text{"OH"} + \text{"}H_2O_2\text{"} \longrightarrow \text{"}HO_2\text{"} + H_2O \qquad (6)$$

As all experiments were carried out at pH >8, $HO_2$ was totally ionized and present as $O_2^-$.[10] "OH" and "$H_2O_2$" may be present in their dissociated or undissociated forms (depending on the pH of the solution).

In order to work under conditions in which reaction 6 can be ignored in comparison to reactions 1a and 1b, we redetermined the rate constant of "OH" with $CO_3^{2-}$ as a function of pH.

*The Reactivity of "OH" with $CO_3^{2-}$.* The reaction of "OH" with $CO_3^{2-}$ was measured in pulse radiolysis of carbonate solution saturated with $N_2O$ at pH 11–14.8. The formation of $CO_3^-$ was followed at 6000 Å and found to be of first order. The pseudo-first-order rate constant $k_{obsd}$ was determined at each pH for 4–5 different concentrations of $CO_3^{2-}$ (at pH 14.8 for one $CO_3^{2-}$ concentration.) The second-order rate constant was determined as the slope of the line of $k_{obsd}$ *vs.* carbonate concentration. The results are given in Table I.

**Table I:** Dependence of $k_{\text{"OH"}+CO_3^{2-}}$ as Function of $[OH^-]$

| $[OH^-]$, $M$ | $k$, $M^{-1}$ sec$^{-1}$ |
|---|---|
| 5.9 | $1.1 \times 10^6$ |
| 1.2 | $2.5 \times 10^6$ |
| 0.1 | $4.8 \times 10^7$ |
| $10^{-3}$ | $3.65 \times 10^8$ |

The value of the rate constant at pH 11 is that of $k_{1a}$ which is in good agreement with earlier determinations ($3 \times 10^8$ $M^{-1}$ sec$^{-1}$,[11] $2 \times 10^8$ $M^{-1}$ sec$^{-1}$,[3] $4.2 \times 10^8$ $M^{-1}$ sec$^{-1}$.[5]

The rate of $k_{1b}$ was given as $4.4 \times 10^7$ $M^{-1}$ sec$^{-1}$,[12] $<10^7$ $M^{-1}$ sec$^{-1}$.[5] Our determination (Table I) shows that most of the reactivity of "OH" even up to pH 14 could be due to the small fraction of the undissociated hydroxyl radical. If $O^-$ reacts with $CO_3^{2-}$ at all, we find $k_{1b} \leq 5 \times 10^5$ $M^{-1}$ sec$^{-1}$ which is smaller by about two orders of magnitude as compared to earlier determinations.

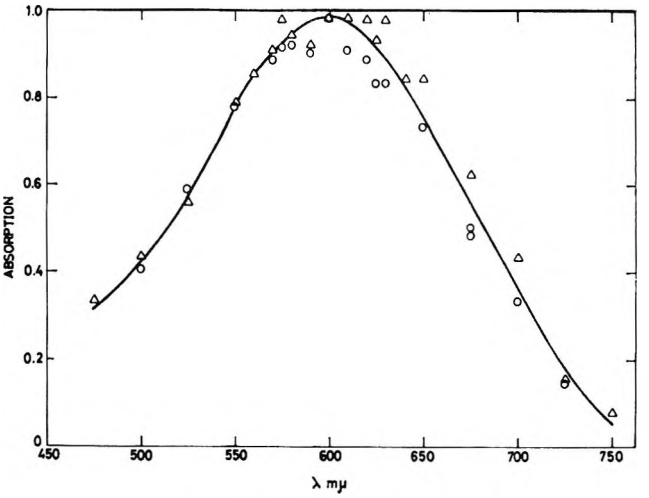


Figure 1. Spectrum of $CO^{3-}$ radical formed in flash photolysis of $N_2$-saturated solution of $H_2O_2$ with $Na_2CO_3$ or $NaHCO_3$: Δ, $2 \times 10^{-4}$ $M$ $H_2O_2$ + 1 $M$ $Na_2CO_3$, pH 13; O, $10^{-3}$ $M$ $H_2O_2$ + 1 $M$ $NaHCO_3$, pH 8.

In the flash photolysis experiments, even at the highest pH (pH 14) the ratio $[CO_3^{2-}]/[HO_2^-]$ was 2500 or greater, the value of $k_{\text{"OH"}+CO_3^{2-}}$ from Table I is $2.5 \times 10^6$ $M^{-1}$ sec$^{-1}$, and $k_{6b} = 5 \times 10^8$ $M^{-1}$ sec$^{-1}$,[8]

$$OH + H_2O_2 \longrightarrow HO_2 + H_2O \qquad (6a)$$

$$O^- + HO_2^- \longrightarrow O_2^- + OH^- \qquad (6b)$$

so the ratio $k_{\text{"OH"}+CO_3^{2-}}[CO_3^{2-}]/k_{6b}[HO_2^-]$ is 12.5. In most experiments the ratio was much higher as both, $[H_2O_2]$ was smaller and the pH was lower. It is clear that under these conditions, reactions 6a and 6b do not occur to any appreciable extent and that any $O_2^-$ formed through reaction 6 would be negligible.

*Spectrum of $CO_3^-$.* The shape of the absorption spectrum of the carbonate radical was determined in flash photolysis of $H_2O_2$, in the presence of $NaHCO_3$ or $Na_2CO_3$, at pH 8 and 13, respectively.

The spectra are identical within experimental error at these pH's (Figure 1). There is no evidence that two forms of the $CO_3^-$ radical might exist in the pH range 8–13, due to any acid–base equilibrium. This is in accordance with the pH independence of the recombination rate constant of the carbonate radical, apart from the effect of the ionic strength.[5]

Earlier determinations of the absorption spectrum[5,6] agree with ours, having the absorption maximum at

(9) Internal Report of the Accelerator Laboratory, Hebrew University, Jerusalem, Israel.

(10) G. Czapski and L. M. Dorfman, *J. Phys. Chem.*, 68, 1169 (1964).

(11) J. K. Thomas, *Trans. Faraday Soc.*, 61, 702 (1965).

(12) M. Anbar and P. Neta, *Intr. J. Appl. Radiat. Isotop.*, 18, 493 (1967). Unpublished data of D. M. Brown.

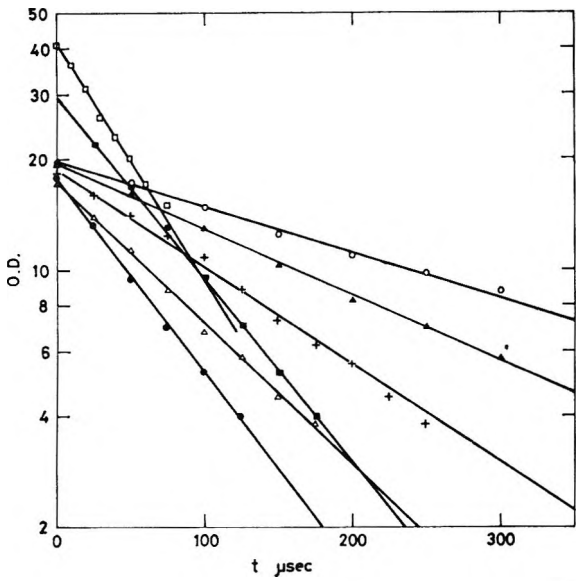


Figure 2. Typical decay curves of $CO_3^-$ followed at 6000 Å, in flash photolysis of $N_2$-saturated solution of $H_2O_2$ and 1 $M$ $Na_2CO_3$, at pH 11.2: ○, 0.11 m$M$ $H_2O_2$; ▲, 0.17 m$M$ $H_2O_2$; ×, 0.22 m$M$ $H_2O_2$; △, 0.33 m$M$ $H_2O_2$; ■, 0.44 m$M$ $H_2O_2$; ●, 0.55 m$M$ $H_2O_2$; □, 0.66 m$M$ $H_2O_2$.

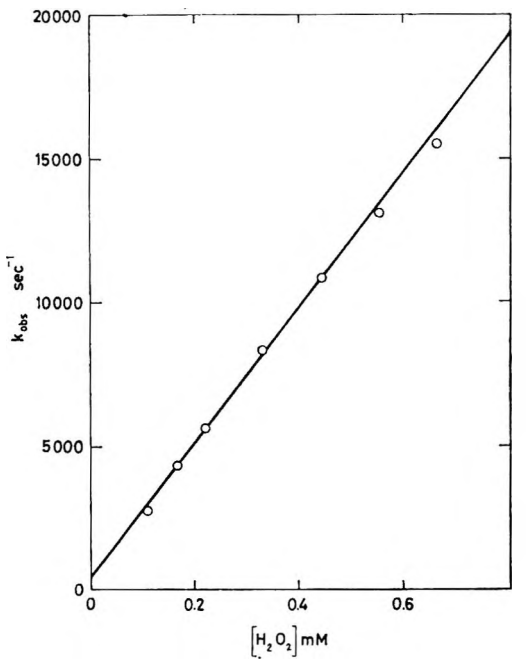


Figure 3. The dependence of the pseudo-first-order rate constant of the reaction of $CO_3^-$ with $H_2O_2$, on $[H_2O_2]$. (Values of $k_{obsd}$ are obtained from Figure 2.)

6000 Å. We did not, however, determine the absolute value of the extinction coefficient ($\epsilon_{6000}$ = 1860 cm$^{-1}$ $M^{-1}$, found by Weeks and Rabani).[5]

*The Reaction of $CO_3^-$ with $H_2O_2$.* The decay of the $CO_3^-$ absorption was followed at 6000 Å in the flash photolysis of $H_2O_2$ in solutions containing 1 mol/l. of $CO_3^{2-}$ and $HCO_3^-$. The decay was first order in both $CO_3^-$ and $H_2O_2$ and followed the rate equation

$$-\frac{d(CO_3^-)}{dt} = k_8(\text{"}H_2O_2\text{"})(CO_3^-) \qquad (7)$$

where ("$H_2O_2$") = ($H_2O_2$) + ($HO_2^-$). Equation 7 leads us to assume the existence of reaction 8. As the

$$CO_3^- + \text{"}H_2O_2\text{"} \longrightarrow \text{products} \qquad (8)$$

"$H_2O_2$" concentration was much higher than that of $CO_3^-$, a first-order decay of $CO_3^-$ was to be expected. First-order plots, at various $H_2O_2$ concentrations, are given in Figure 2; the pseudo-first-order rate constants $k_{obsd}$ were calculated from these. The $k_{obsd}$ values thus obtained were then plotted as a function of $H_2O_2$ concentration (Figure 3) and $k_8$ was calculated.

Reaction 8 explains the deviations from the second-order plots of the $CO_3^-$ recombination kinetics, found by Weeks and Rabani.[5] (They found that the second-order decay was too fast as the reaction proceeds.) If recombination of $CO_3^-$ produces $H_2O_2$, (reaction 3b), the decay of $CO_3^-$ would be self-catalytic.

The second-order rate constant $k_8$ is found to be pH dependent. Figure 4 shows the variation of $k_8$ as a function of pH. Such a behavior is typical of a system where one (or both) of the reactants have two forms which are in acid–base equilibrium and which react with different rates. However, the possibility that the carbonate radical is in an acid–base equilibrium

$$H^+ + CO_3^- \rightleftharpoons HCO_3$$

in the pH region studied can be ruled out because of the following reasons: (a) the pH independence of the recombination rate constant of the $CO_3^-$ radical;[5] (b) the identical spectra of the radical when measured at pH 8 and 13; (c) the dissociation constant of the second hydrogen of carbonic acid is 4.4 × 10$^{-11}$ (p$K$ = 10.36). The p$K$ of the radical would be ex-

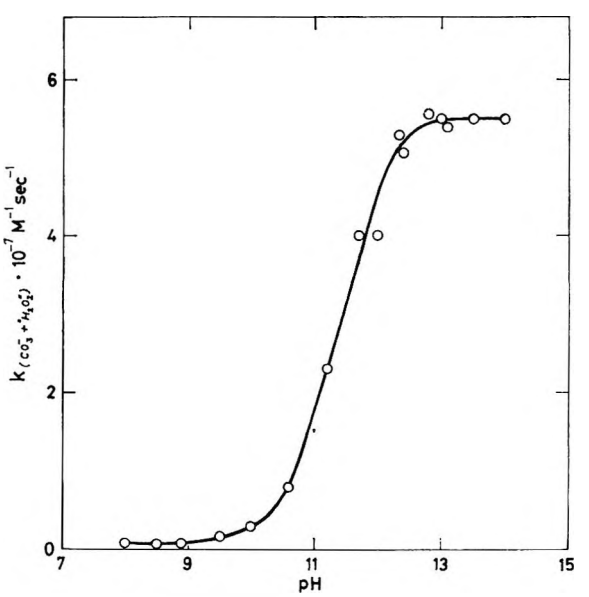


Figure 4. $k_{(CO_3^- + \text{"}H_2O_2\text{"})}$ as a function of pH.

pected to be lower than this (similar behavior is seen in the cases of $H_2O_2$:$HO_2$[10,13,14] and ROH:RO[15]).

As $CO_3^-$ is probably not responsible for the change of $k_8$ with pH, one comes to the conclusion that the equilibrium $H_2O_2 \rightleftarrows H^+ + HO_2^-$ is the cause of the pH dependence of $k_8$.

We suggest that the following mechanism governs the disappearance of the carbonate radical in reaction with hydrogen peroxide

$$CO_3^- + H_2O_2 \longrightarrow \text{products} \qquad (9)$$

$$CO_3^- + HO_2^- \longrightarrow \text{products} \qquad (9a)$$

$$H_2O_2 \rightleftarrows H^+ + HO_2^- \qquad K$$

where $K$ is the dissociation constant of $H_2O_2$. Thus

$$\frac{-d(CO_3^-)}{dt} = k_9(CO_3^-)(H_2O_2) + k_{9a}(CO_3^-)(HO_2^-)$$

If ("$H_2O_2$") = $(H_2O_2) + (HO_2^-)$ the decay rate will be

$$\frac{-d[CO_3^-]}{dt} = \frac{k_9 + k_{9a}\dfrac{K}{[H^+]}}{1 + \dfrac{K}{[H^+]}}[\text{"}H_2O_2\text{"}][CO_3^-]$$

with

$$k_{obsd} = \frac{k_9 + k_{9a}\dfrac{K}{[H^+]}}{1 + \dfrac{K}{[H^+]}} \qquad (10)$$

Rearranging eq 10, one obtains

$$\frac{K}{[H^+]} = \frac{k_{obsd} - k_9}{k_{9a} - k_{obsd}}$$

or

$$pH = pK + \log \frac{k_{obsd} - k_9}{k_{9a} - k_{obsd}} \qquad (11)$$

where $K$ is the equilibrium constant at the measured ionic strength. With a correction made for the ionic strength,[14] eq 11 can be expressed as

$$pH = pK_0 + \log \frac{k_{obsd} - k_9}{k_{9a} - k_{obsd}} - \frac{A\sqrt{\mu}}{1 + \sqrt{\mu}} \qquad (12)$$

where $A = 0.5$, $\mu$ is the ionic strength, and $K_0$ is the equilibrium constant at zero ionic strength. A plot of pH *vs.* log $(k_{obsd} - k_9/k_{9a} - k_{obsd}) - (A\sqrt{\mu}/1 + \sqrt{\mu})$ should yield a straight line, with intercept equal to $pK_0$. When taking the plateau values of $k_{obsd}$ as given in Figure 4 ($k_9 = 8 \times 10^5\ M^{-1}\ sec^{-1}$, and $k_{9a} = 5.6 \times 10^7\ M^{-1}\ sec^{-1}$) and using eq 12, we did obtain a straight line which is shown in Figure 5, and from which we derived the value of $pK_0 = 11.7 \pm 0.2$. This value agrees very well with that of 11.85 ± 0.1 obtained by Jortner and Stein[14] at 19°, and of 11.76 ± 0.02 obtained by Evans and Uri[16] at 20°. The possible ionic strength

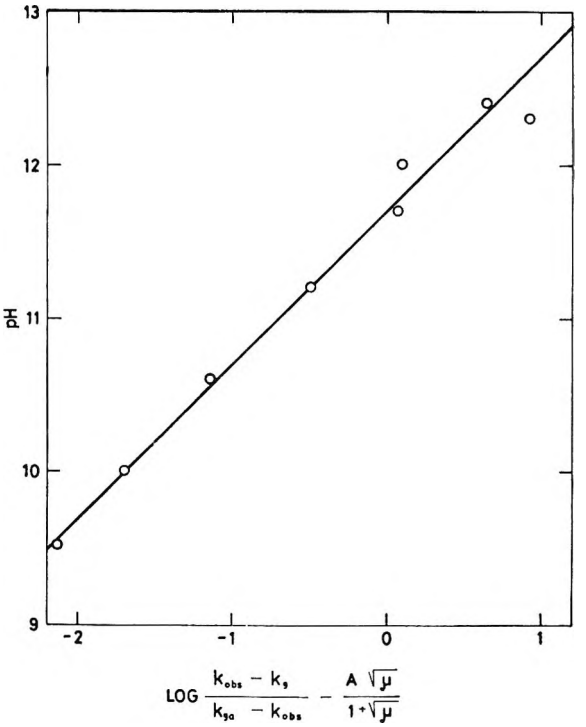


Figure 5. The dependence of pH on a function of $k_{obsd}$ and $\mu$.

dependence of $k_{9a}$ was neglected as $\mu$ was almost constant, and about 3 in all experiments.

*The Reaction $CO_3^- + O_2^-$.* As we wanted to follow the reaction which takes place between the carbonate radical and the hydroperoxy radical, we flash photolyzed a 0.2 $M$ $Na_2CO_3$ solution saturated with oxygen. The primary photolytic process is probably

$$CO_3^{2-} \xrightarrow{h\nu} CO_3^- + e_{aq}^- \qquad (2)$$

followed by

$$e_{aq}^- + O_2 \longrightarrow O_2^- \qquad (13)$$

There are practically equal concentrations of $CO_3^-$ and $O_2^-$ at the end of the flash. In addition to reaction 2, some of the hydroxide ions may be photolyzed

$$OH^- \xrightarrow{h\nu} OH + e_{aq}^- \qquad (14)$$

This would have no effect on our assumption of equimolar concentrations of $O_2^-$ and $CO_3^-$, as $e_{aq}^-$ will yield $O_2^-$ and OH will form with carbonate $CO_3^-$. We found the absorption to decay at 6000 Å in a second-order process, but at 2600 Å the absorption had two decay modes: second order in the millisecond range and a first-order one with a half lifetime of about 2 sec. This slow decay is similar to that of $O_2^-$ in the alkaline region. If $O_2^-$ and $CO_3^-$ concentrations

(13) H. A. Schwarz, *J. Phys. Chem.*, **66**, 255 (1962).

(14) J. Jortner and G. Stein, *Bull. Res. Counc. Isr., A*, **6**, 239 (1957).

(15) K. D. Asmus, A. Henglein, A. Wigger, and G. Beck, *Ber. Bunsenges. Phys. Chem.*, **70**, 756 (1966).

(16) M. G. Evans and N. Uri, *Trans. Faraday Soc.*, **45**, 224 (1949).

are equal, then it is not very probable that any excess of $O_2^-$ will be left at the end of the second-order decay, as the reaction of $CO_3^-$ with $O_2^-$ is much faster than those of $O_2^- + O_2^-$ and $CO_3^- + CO_3^-$ at the same pH.

In order to make sure that the long-lived intermediate was not the $O_2^-$, we pulse-radiolized a 0.2 $M$ solution of carbonate containing $O_2$ and $N_2O$, in which the initial ratio after the pulse of $CO_3^-$ to $O_2^-$ amounted to 3.8.

We found that this long-lived intermediate exists even in this solution, and the ratio $D_0^{2600}/D_\infty^{2600}$ remained 4 in the presence, and absence, of $N_2O$, which is inconsistent with its identification as excess of $O_2^-$. ($D_0^{2600}$ is the initial absorption at 2600 Å and $D_\infty^{2600}$ is the absorption taken 5 msec after the pulse, where the fast decay is over and no appreciable decay of the long-lived product occurs.) Thus, the formation of a new intermediate is suggested which might be the $CO_5^{2-}$ (the recombination product of $CO_3^- + O_2^-$) and which decomposes most probably in a first-order process to $CO_3^{2-} + O_2$. From the initial absorption of $O_2^-$ at 2600 Å, taking $\epsilon_{O_2^-}^{2600} = 1850\ M^{-1}\ cm^{-1}$, we determined $\epsilon_{CO_5^{2-}}^{2600} = (410 \pm 40)\ M^{-1}\ cm^{-1}$.

A similar behavior was observed by Hayon[17] in flash photolysis of aerated phosphate solutions where $O_2^-$ and $H_2PO_4$ (or $HPO_4^-$) were produced simultaneously and, after the $O_2^-$ decayed, a long-lived intermediate was observed with a maximum absorption around 2600 Å.

$\epsilon_{O_2^-}^{2600}$ was determined from the results of the flash photolysis of oxygenated carbonate solutions, where equimolar concentrations of $CO_3^-$ and $O_2^-$ are formed. $\epsilon_{O_2^-}^{2600}$ was calculated from the initial absorptions of $O_2^-$ and $CO_3^-$ at 2600 Å and that of $CO_3^-$ at 6000 Å, taking $\epsilon_{CO_3^-}^{6000} = 1860\ M^{-1}\ cm^{-1}$ [5] and $\epsilon_{CO_3^-}^{2600} = 200\ M^{-1}\ cm^{-1}$.[5] We obtained $\epsilon_{O_2^-}^{2600} = (1850 \pm 200)\ M^{-1}\ cm^{-1}$. This value is compared with other determinations in Table II.[7,10,18-21]

The decays of $O_2^-$ and $CO_3^-$ at 2600 Å and 6000 Å in the flash photolysis of $O_2$-saturated $CO_3^{2-}$ solutions was found to be second order. At 2600 Å $1/(D^{2600} - D_\infty^{2600})$ was plotted as a function of time and the slope of the line was taken as $k_4/l(\epsilon_{O_2^-}^{2600} + \epsilon_{CO_3^-}^{2600} - \epsilon_{CO_5^{2-}}^{2600})$. Using the extinction coefficients of $O_2^-$, $CO_3^-$, and $CO_5^{2-}$ at 2600 Å and that of $CO_3^-$ at 6000 Å (1850, 200, 410, and 1860 $M^{-1}\ cm^{-1}$, respectively), we obtained at both wavelengths the same rate constant for the reaction

$$CO_3^- + O_2^- \longrightarrow \text{products} \qquad (4)$$

$k_4 = (4 \pm 1) \times 10^8\ M^{-1}\ sec^{-1}$ in comparison with $1.5 \times 10^9\ M^{-1}\ sec^{-1}$ reported by Adams, *et al.*,[7] and $1.4 \times 10^8\ M^{-1}\ sec^{-1}$ (the value $1.4 \times 10^8\ M^{-1}\ sec^{-1}$ was calculated assuming $\epsilon_{O_2^-}^{2600} = 900\ M^{-1}\ cm^{-1}$, taking the value of $\epsilon_{O_2^-}^{2600} = 1850\ M^{-1}\ cm^{-1}$ found by us one arrives at $k_4 = 2.8 \times 10^8\ M^{-1}\ sec^{-1}$) by Hayon and McGarvey.[6]

**Table II:** The Extinction Coefficient of $O_2^-$

| λ, Å | $\epsilon_{O_2^-}$, $M^{-1}\ cm^{-1}$ | Ref |
|---|---|---|
| 2540 | 1900 | 18 |
| 2600 | 870[a] | 10 |
| 2600 | 1220 | 7 |
| 2600 neutral pH | 1000 | 19 |
| 2600 alkaline pH | 1100–2000 | 19 |
| 2600 | 1675 | 20 |
| 2600 | 1700 | 21 |
| 2600 | 1850 | This work |

[a] This value is not accurate as no correction was made for the absorption of the OH radical.

*Acknowledgment.* We gratefully acknowledge the support of this research by the U. S. Atomic Energy Commission under Contract AT(30-1)-3753.

(17) J. Robert Huber and E. Hayon, *J. Phys. Chem.*, **72**, 3820 (1968).

(18) J. H. Baxendale, *Radiat. Res.*, **17**, 312 (1962).

(19) J. Rabani, Advances in Chemistry Series, No. 81, American Chemical Society, Washington, D. C., 1968, p 131.

(20) J. Rabani and S. O. Nielsen, *J. Phys. Chem.*, **73**, 3736 (1969).

(21) D. Behar, G. Czapski, L. M. Dorfman, J. Rabani, and H. A. Schwarz, to be published.

# Translational Frictional Coefficients of Molecules in Aqueous Solution

**by Hisashi Uedaira and Hatsuho Uedaira**

*Research Institute for Polymers and Textiles, 4 Sawatari, Kanagawaku, Yokohama, Japan* *(Received October 2, 1969)*

Diffusion coefficients for aqueous fructose and β-cyclodextrin solutions at 25° were measured by the Rayleigh interference method. The translational frictional coefficients of sucrose, raffinose, and β-cyclodextrin were calculated, being based on the limiting diffusion coefficients of fructose and glucose. The frictional coefficients of oligopeptides and dicarboxylic ions were also calculated. If the effect of the local viscosity around a molecule of solute is corrected, the agreement between the calculated and observed frictional coefficients is very good.

## Introduction

The diffusion coefficients of small molecules in aqueous solutions at infinite dilution are, in principle, calculable from the Stokes–Einstein relation. The Stokes radius of the solute has been regarded as a measure of hydration and departure from strictly spherical shape.[1] For small molecules of arbitrary structure, it is hardly practical to compare the theoretical translational frictional coefficient with the experimental value. In a previous report,[2] we calculated the frictional coefficient of maltose in aqueous solution by the shell model,[3] also correcting for the effect of the local viscosity of water around the molecules of maltose. The agreement between the calculated and observed values was good. This method can be applied to a molecule or ion of arbitrary structure.

In the present paper, we report the diffusion coefficients for fructose and β-cyclodextrin in aqueous solutions at 25°. The translational frictional coefficients of β-cyclodextrin, oligosaccharides, oligopeptides, and divalent carboxylic ions at infinite dilution are calculated and compared with the experimental values.

## Experimental Section

*Samples.* Fructose (DIFCO Co.) was recrystallized twice from water–ethanol solution. Purified β-cyclodextrin was kindly supplied by Dr. S. Tomita of Government Industrial Research Institute. [His kindness is greatly appreciated.] All solutions were prepared by weight, using deionized water as the solvent.

*Diffusion Measurements.* The diffusion experiments were performed at 25 ± 0.01° using a Spinco Model H diffusion apparatus as a Rayleigh interferometer. Kodak Type M glass photographic plates (4 in. × 5 in.) were used. The concentration difference of the solution on both sides of the diffusion boundary was adjusted so that the total number of Rayleigh fringes became 50 or 60. The procedure was then the same as that previously described.[2]

## Results

The mean concentration in each diffusion experiment and the corresponding observed value of the diffusion coefficient for the fructose solution are given in Table I. The corresponding data for β-cyclodextrin are given in Table II. To represent the experimental diffusion coefficients the method of least squares was used to obtain the expressions

**Table I:** Diffusion Coefficients of Fructose in Water at 25°

| | c, wt % | | | | |
|---|---|---|---|---|---|
| | 0.22924 | 0.94981 | 1.51603 | 2.00038 | 2.52132 |
| $10^6D$, cm²/sec | 6.981 | 6.930 | 6.880 | 6.837 | 6.798 |

**Table II:** Diffusion Coefficients of β-Cyclodextrin in Water at 25°

| | c, wt % | | | | |
|---|---|---|---|---|---|
| | 0.23137 | 0.50177 | 1.02443 | 1.52376 | 1.93773 |
| $10^6D$, cm²/sec | 3.307 | 3.284 | 3.239 | 3.190 | 3.148 |

$$D \times 10^6 = 7.002 - 0.0813c \qquad c < 3 \text{ wt \%} \quad (1)$$

for the fructose solution, and

$$D \times 10^6 = 3.332 - 0.0938c \qquad c < 2 \text{ wt \%} \quad (2)$$

for the β-cyclodextrin solution, with an average deviation of ±0.06%.

## Discussion

Recently, Bloomfield, Dalton, and Van Holde,[3] using the shell model, proposed the following expression for the translational frictional coefficient of any macromolecule that can be visualized to be composed of $n$ spherical subunits.

(1) H. J. V. Tyrell, "Diffusion and Heat Flow in Liquids," Butterworths and Co. (Publishers) Ltd., London, 1961, Chapter 7.

(2) H. Uedaira and H. Uedaira, *Bull. Chem. Soc. Jap.*, **42**, 2140 (1969).

(3) V. Bloomfield, W. D. Dalton, and K. E. Van Holde, *Biopolymers*, **5**, 135 (1967).

$$f = \frac{6\pi\eta_0\left(\sum_{s=1}^{n} r_s^2\right)^2}{\sum_{s=1}^{n} r_s^3 + \sum_{s=1}^{n}\sum_{l=1}^{n}{}' r_s^2 r_l^2 \langle R_{ls}^{-1}\rangle} \quad (3)$$

Here $R_{ls}$ is the distance between centers of two spherical shells of radius $r_l$ and $r_s$, and $\eta_0$ is the viscosity of the solvent. If all of the subunits are identical, eq 3 reduces to the Kirkwood equation.[4]

The translational frictional coefficients of homologous molecules in aqueous solution can be calculated from eq 3, if a correction for the local viscosity around a solute molecule is made. In the following, we calculate the frictional coefficients of molecules made up of identical submolecules and also of those made up of submolecules of different size.

(*a*) *Frictional Coefficients of Molecules Composed of Identical Submolecules.* The frictional coefficients, $f_2$ and $f_3$, of dimer and linear trimer can be calculated from eq 3 to be

$$f_2 = 1.33(6\pi\eta r_a) \quad (4)$$

$$f_3 = 1.59(6\pi\eta r_a) \quad (5)$$

where $r_a$ is the radius of the submolecule and $\eta$ is the viscosity of water. These relations are obtained from eq 8 and 9, putting $k$ equal to 1.

The assumption that the solvent is a continuum in the derivation of the Stokes relation and eq 3 implies that the dimensions of the diffusing particles are large in comparison with those of the solvent molecules. This assumption does not hold in the case of a small molecule, and its frictional coefficient is affected by the structure of solvent. The water structure around a molecule in aqueous solution is different from that of bulk water. For example, it is known from nmr spectroscopy[5] that the time of reorientation of a water molecule around molecules such as inorganic, organic ions, and alcohols is different from that of a water molecule in pure water.

A water molecule close to a solute molecule constantly exchanges its site with other neighboring water molecules. The translational motion of a molecule with tightly bound water molecules in aqueous solution is strongly inhibited,[6,7] and the motion is affected by the interaction between water and solute. This mechanism is supported by nmr.[5] Therefore, a molecule in motion in water encounters a different structure from that of pure water, and so the local viscosity of water around the molecule is different from that of pure water. For small molecules, this effect cannot be neglected. The water structure around a submolecule and the molecule composed of a number of submolecules in aqueous solution is regarded as identical, provided that the submolecules are all the same. Therefore, the ratio of the translational frictional coefficients of the molecule and its submolecule is independent of the water structure. Thus, we obtain $f_2/f_1 = 1.33$ for dimer, and $f_3/f_1 = 1.59$ for trimer from eq 4 and 5, where $f_1 = 6\pi\eta r_a$. In diffusion of a small molecule, $f_1$ should be expressed strictly by $a\pi\eta r_a$,[8-10] but this is not important in the calculation of the ratio of the frictional coefficients.

The diffusion coefficient is inversely proportional to the frictional coefficient. Therefore, if the limiting diffusion coefficients of the molecule and submolecule are determined from the experiments, the ratio of the experimental values of the frictional coefficients is obtained. The results for diglycine, triglycine, succinic, and adipinic ions are listed in Table III. The submolecules which are used in the calculations of the ratios of the frictional coefficients are listed in the second column of Table III. The limiting diffusion coefficients of the molecules and submolecules are given in the third and fourth columns. For carboxylic anions, the limiting mobilities are given in the corresponding columns. The values of the ratios of the experimental and calculated frictional coefficients are given in the sixth and seventh columns, respectively. For the carboxylic ions, the experimental frictional coefficients were calculated from the limiting mobilities. Agreement between the calculated and observed values is very good.

Now, as an example of a more complex molecule, we calculate the frictional coefficient of $\beta$-cyclodextrin. As $\beta$-cyclodextrin is a macrocyclic nonreducing D-glucosyl polymer containing seven residues bonded by $\alpha$ links, we can regard this molecule as a pearl necklace consisting of seven identical spheres. The translational frictional coefficient $f_{CD}$ of this molecule can be calculated from eq 3. As shown in Figure 1, the centers of the glucose units form a regular heptagon. We can calculate each value of $R_{ls}$ in eq 3 by $r_G$ and the value of the interior angle of the regular heptagon (128°3′). We obtain the expression

$$f_{CD} = 2.33(6\pi\eta r_G) \quad (6)$$

where $r_G$ is the radius of glucose. We have $f_{CD}/f_1 = 2.33$ from eq 6, where $f_1$ is the frictional coefficient of

(4) J. G. Kirkwood, *J. Polym. Sci.*, 12, 1 (1954).

(5) H. G. Herz and M. D. Zeidler, *Ber. Bunsenges. Phys. Chem.*, 68, 821 (1964).

(6) O. Ya. Samoilov, "Struktura Vodn'kh Rastvorov Elektrolitov i Gidrataziya Ionov," Akademy Nauk, Moscow, 1957, Chapter 5.

(7) H. Uedaira and H. Uedaira, *Zh. Fiz. Khim.*, 42, 3042 (1968).

(8) S. Glasstone, K. J. Laidler, and H. Eyring, "The Theory of Rate Processes," McGraw-Hill Publications, New York, N. Y., 1941, Chapter 9.

(9) The deviation from Stokes law also can be caused by failure of the nonslip boundary condition. A slip of a water molecule may occur on the surface of a nonpolar molecule. On the other hand, water molecules around the nonpolar molecule form an ice-like structure[10] and become less mobile than in pure water.[5,7] Thus the local viscosity of water around the molecule is different from that of pure water. Whether the nonslip boundary condition holds or does not hold, the effect of local viscosity exists in solution for an associating solvent.

(10) H. S. Frank and M. W. Evans, *J. Phys. Chem.*, 13, 507 (1945).

**Table III:** Translational Frictional Coefficients of Oligosaccharides, Oligopeptides, and Dicarboxylic Ions at 25° in Water

| Molecules | Sub-molecules | $10^6 D_0$, cm²/sec | $10^6 D_{01}$, cm²/sec | $k$ | $(f/f_1)_{exptl}$ | $(f/f_1)_{calcd}$ |
|---|---|---|---|---|---|---|
| β-Cyclodextrin | Glucose | 3.332 | 6.75[a] | | 2.03 | 2.05 |
| Sucrose | Glucose | 5.23[a] | 6.75[a] | 0.962 | 1.29 | 1.30 |
| | Fructose | | 7.002 | 1.037 | 1.34 | 1.36 |
| Raffinose | Glucose | 4.359[b] | 6.75[a] | 0.962 | 1.55 | 1.56 |
| | Fructose | | 7.002 | 1.037 | 1.60 | 1.61 |
| Diglycine | Glycine | 7.909[c] | 10.554[c] | | 1.33 | 1.33 |
| Triglycine | Glycine | 6.652[c] | 10.554[c] | | 1.59 | 1.59 |
| Glycylalanine | Alanine | 7.221[c] | 9.097[c] | 0.862 | 1.26 | 1.26 |
| | Glycine | | 10.554[c] | 1.160 | 1.46 | 1.45 |
| $(CH_2COO)_2^{2-}$ | $CH_3COO^-$ | 60.65[d] | 40.89[d] | | 1.35 | 1.33 |
| $(C_2H_4COO)_2^{2-}$ | $C_2H_5COO^-$ | 52.58[d] | 35.82[d] | | 1.36 | 1.33 |

[a] Reference 11. [b] P. J. Dunlop, *J. Phys. Chem.*, **60**, 1464 (1956). [c] T. Shedlovsky, Ed., "Electrochemistry in Biology and Medicine," John Wiley and Sons, New York, N. Y., 1955, Chapter 12. [d] The units are cm²/ohm equiv: J. D'Ans, A. Eucken, G. Joos, and W. A. Roth, Ed., "Landolt-Börnstein Tabellen," Vol. 2, 6th ed, 7 Part II, Springer-Verlag, Berlin, 1960.

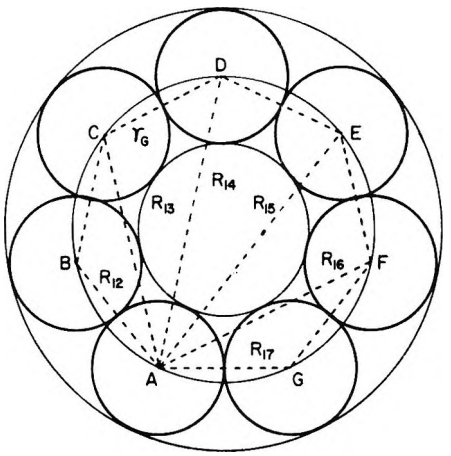


Figure 1. Model of β-cyclodextrin.

glucose. The limiting diffusion coefficient of β-cyclodextrin is $3.332 \times 10^{-6}$ cm²/sec from eq 2. The limiting diffusion coefficient of glucose in aqueous solution at 25° obtained by Gladden and Dole[11] is $6.75 \times 10^{-6}$ cm²/sec. The ratio of the experimental frictional coefficient of β-cyclodextrin to that of glucose is

$$f_{CD}/f_1 = D_{0G}/D_{0CD} = 2.03$$

The calculated value is larger than the experimental value.

The molecule of β-cyclodextrin can also be regarded as a ring consisting of seven glucose molecules, instead of the above necklace model (see Figure 1). Tchen[12] calculated the translational frictional tensor of the ring molecule, and the following expression for the frictional coefficient was obtained by Zwanzig[13]

$$f = 36\pi\eta L/11 \log (L/r) \qquad (7)$$

where $L$ is the length of the ring. For β-cyclodextrin, the value of $L$ calculated from Figure 1 is equal to $14.47r_G$. Therefore, we have $f_{CD}/f_1 = 2.05$. The agreement between this value and the experimental value is satisfactory. The ring model also agrees with the molecular model.[14]

(*b*) *Frictional Coefficients of Molecules Composed of Different Submolecules.* The frictional coefficient of a molecule which consists of two submolecules of radii $r_a$ and $r_b$ can be calculated from eq 3, and is found to be

$$f_2 = \frac{6\pi\eta r_a(1 + k^2)^2(1 + k)}{1 + k + 2k^2 + k^3 + k^4} \qquad (8)$$

where $k = r_b/r_a$.

The frictional coefficient of a molecule which consists of two submolecules of radius $r_a$ and a submolecule of radius $r_b$ (see Figure 2) is given by the following expression

$$f_3 = \frac{6\pi\eta r_a(2 + k^2)^2(1 + k)(2 + k)}{(2 + k^3)(1 + k)(2 + k) + 2 + 3k + 7k^2 + 4k^3} \qquad (9)$$

where $k = r_b/r_a$. In the calculation of eq 9, it was assumed that the centers of the three submolecules were on a straight line and that the submolecule of radius $r_b$ was located at an end of the molecule.

The experimental value of the ratio of the frictional coefficient for sucrose to that of glucose is given in the third line of Table III. The calculated value of the corresponding ratio is given in the same line. Let $r_a$ and $r_b$ be the radii of glucose and fructose, respectively.

(11) J. K. Gladden and M. Dole, *J. Amer. Chem. Soc.*, **75**, 3900 (1953).

(12) Chan-Mou Tchen, *J. Appl. Phys.*, **25**, 463 (1954).

(13) R. Zwanzig, *J. Chem. Phys.*, **45**, 1858 (1966). He pointed out that the Kirkwood eq 4 is not exact, and showed that the correct result obtained from eq 8 was smaller than the incorrect one by the factor 11/12.

(14) R. L. Whistler and E. F. Paschell, Ed., "Starch: Chemistry and Technology," Vol. 1, Academic Press, Inc., New York, N. Y., 1965, Chapter 9.

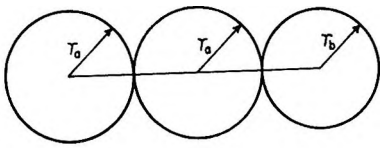


Figure 2. Model of raffinose.

As the radius of a molecule is inversely proportional to its diffusion coefficient, the value of $k$ is determined from the ratio of the limiting diffusion coefficients of the submolecules. The limiting diffusion coefficient of fructose in water is $7.002 \times 10^{-6}$ cm$^2$/sec from eq 1 and that of glucose is $6.75 \times 10^{-6}$ cm$^2$/sec. Hence $k = 0.962$.

Similarly, the ratio of the frictional coefficient for sucrose to that of fructose is obtained. In this case, the value of $k$ in eq 8 is 1.037 and $r_a$ must be substituted by $r_b$. The experimental and calculated values are given in the fourth line of Table III.

The values of the ratios of the frictional coefficients for raffinose to that of its submolecules are given in the fifth and sixth lines of Table III. In the calculation of the frictional coefficient for raffinose, the radius of galactose was taken to be the same as that of glucose.

The values of the ratios of the frictional coefficients for glycylalanine to that of its submolecules are given in the ninth and tenth lines of Table III.

In all cases, the agreement between the observed and calculated values is very good. Thus, the frictional coefficient of a molecule with any structure can be accurately calculated, relative to the frictional coefficients of its constituent submolecules. The absolute calculation of the frictional coefficient requires a correction for the effect of local viscosity, particularly important for an associating solvent.

*Acknowledgment.* The authors thank Dr. K. Tsuda in our Institute for helpful discussion.

# Thermodynamic Properties of Associated Solutions.

# I. Mixtures of the Type A + B + $AB_2$

**by Alexander Apelblat**

*Israel Atomic Energy Commission, Nuclear Research Center, Negev, Beer-Sheva, Israel* *(Received October 8, 1969)*

The theory of ideal associated solutions of the type A + B + $AB_2$ has been investigated in detail. The chemical equilibrium, the activity coefficients, the excess thermodynamic functions, and the standard reaction parameters were considered. Special attention was directed towards the evaluation of the boiling and condensation temperature curves for these solutions and the conditions necessary for the occurrence of an azeotrope. The theoretical predictions for the A + B + $AB_2$ model were compared with experimental data for binary methanol–propionic acid systems.

## Introduction

Deviations from the ideal behavior in the systems containing components capable to form intermolecular hydrogen bonds are frequently explained by the formation of relatively stable configurations (associates) between like molecules (self-association) or unlike molecules (complexing). The general theory of the ideal associated solutions (effect of different sizes and shapes of complexes is neglected) is given by Prigogine and Defay[1] and Hildebrand and Scott.[2] Kehiaian and coworkers[3] treated in detail the mixtures of the type A + B + AB, A + $A_r$ + B and the Mecke–Kempter type of association, A + $A_2$ + $A_3$ + ... $A_r$ + B. The work of Saroléa-Mathot[4] on A + B + AB and McGlashan and Rastogi,[5] Rastogi and Girdhar[6] on A + B + AB + $AB_2$ type of association are worth noting. A number of theoretical and experimental investigations[7-14] concern the binary systems containing alcohols.

(1) I. Prigogine and R. Defay, "Chemical Thermodynamics," John Wiley and Sons, New York, N. Y., 1965.

(2) J. H. Hildebrand and R. L. Scott, "The Solubility of Nonelectrolytes," 3rd ed, Dover Publications, Inc., New York, N. Y., 1964.

(3) H. Kehiaian and A. Treszczanowicz, *Bull. Soc. Chim. Fr.*, 1561 (1969). In this paper there is an extensive list of Kehiaian's works.

(4) L. Saroléa-Mathot, *Trans. Faraday Soc.*, **49**, 8 (1953).

(5) M. L. McGlashan and R. P. Rastogi, *ibid.*, **54**, 496 (1958).

(6) R. P. Rastogi and H. L. Girdhar, *Proc. Nat. Instit. Sci., India*, **A28**, 470 (1962).

(7) J. A. Barker, *J. Chem. Phys.*, **20**, 1526 (1952).

However, the alcohol–carboxylic acid solutions were only rarely investigated.[15,16]

Izmailov[17] summarized a number of Russian works where dilute solutions of carboxylic acids in alcohols were investigated. From molecular weights, determined by the freezing point depression method, using benzene as the cryoscopic medium and from the infrared measurements, he concluded that in a solution rich in alcohol (the mole fraction of the acid was less than 0.1) only the $AB_2$ complex is formed (A, acetic acid; B, methyl, ethyl, and butyl alcohols). The stretching frequency of the H-bonded carboxyl group ($\nu_{CO\cdots H}$ = 1707 $cm^{-1}$) occurs only in the infrared spectrum. It is assumed that it belongs to the following complex

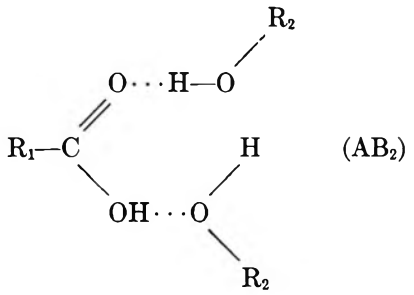

($AB_2$)

The additional bands appear when the concentration of the acid increases. The first band is attributed to the monomeric frequency of the acetic acid, $\nu_{CO}$ = 1745 $cm^{-1}$, and the second (as the acidity increases), with the dimetric acetic acid, $\nu$ = 1660 $cm^{-1}$; *i.e.*, the formation of the following AB and $A_2$ complexes is postulated[17]

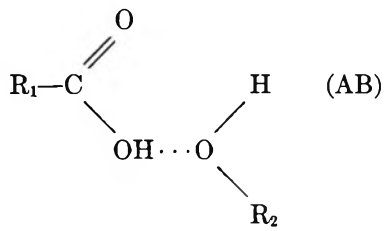

(AB)

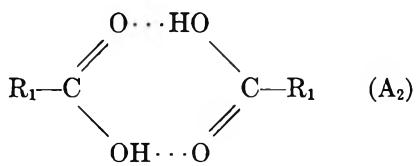

($A_2$)

From the cryoscopic measurements at ~6° in benzene, the equilibrium constants for $AB_2$ formation were estimated to be $10^3$–$10^4$ $m^{-2}$ for carboxylic and halogen–carboxylic acids with methyl and butyl alcohols.[17]

Gas chromatographic measurements performed in our laboratory for the solutions of alkylphosphoric acids in polar solvents[18] (methanol, acetone, chloroform and water) resulted in increased interest in the complex formation of $AB_2$ or $AB_j$, $j \geq 1$. Also the results of molecular weight measurements, obtained from vapor pressure osmometry for uranyl nitrate and thorium nitrate solutions in tributyl phosphate,[19] have been interpreted by assuming the formation of $AB_2$ and $AB_2 + AB_3$ complexes, respectively (A, denotes $UO_2(NO_3)_2$, and $Th(NO_3)_4$, and B is tributyl phosphate).

The present paper gives some aspects of the theory of associated solutions of the type A + B + $AB_2$. There is a possibility of simultaneous formation of number complexes in the carboxylic acid–alcohol solutions. However it is more convenient to consider the formation of one complex only. As pointed out above, the deviations from ideality in alcohol-rich solutions can be explained by the formation of $AB_2$. The situation is more complex when AB, $AB_2$, and $A_2$ are formed. These will be dealt with in a succeeding paper.

## Chemical Equilibrium

Consider a solution of the molecular species A and B. The solution contains the complex $AB_2$ resulting from the association reaction $A + 2B \rightleftharpoons AB_2$. The mole fractions actually present in the mixture of, A, B, and $AB_2$ ($x_A$, $x_B$, and $x_{AB_2} \equiv \xi$) are related to the stoichiometric mole fraction $x$ of the nominal component A in the following way.

$$x_A = x(1 + 2\xi) - \xi$$
$$x_B = 1 - x(1 + 2\xi) \qquad (1)$$

The equilibrium constant of the association reaction is given by

$$K = \frac{x_{AB_2}}{x_A x_B^2} \qquad (2)$$

or using (1).

$$4x^2(1 - 2x)\xi^3 + 4x(-1 + 3x - 3x^2)\xi^2 + [1/K + (1 - x)(1 - 3x + 6x^2)]\xi - x(1 - x)^2 = 0 \qquad (3)$$

The third-order equation for $\xi$ (3) was solved, treating $K$ as parameter, $\xi = f(K|x)$. The results of the cal-

(8) J. A. Barker and F. Smith, *J. Chem. Phys.*, **22**, 375 (1954).
(9) H. Renon and J. M. Prausnitz, *Chem. Eng. Sci.*, **22**, 299 (1967).
(10) I. A. Wiehe and E. B. Bagley, *Ind. Eng. Chem. Fundam.*, **6**, 209 (1967).
(11) I. Nemesh, N. N. Ugarova, and O. Dobish, *Russ. J. Phys. Chem.*, **41**, 554 (1967).
(12) R. W. Haskell, H. B. Hollinger, and H. C. Van Ness, *J. Phys. Chem.*, **72**, 4534 (1968).
(13) E. Hála, J. Pick, V. Fried, and O. Vilim, "Vapor-liquid Equilibrium," 2nd ed, Pergamon Press, Inc., Oxford, 1967.
(14) E. Hála, I. Wichterle, J. Polák, and T. Boublik, "Vapor-Liquid Equilibrium Data at Normal Pressures," Pergamon Press, Oxford, 1968.
(15) A. Rius, J. K. Otero, and A. Macarron, *Chem. Eng. Sci.*, **10**, 105 (1959).
(16) N. G. Krokhin, *Russ. J. Phys. Chem.*, **41**, 340 (1967).
(17) N. A. Izmailov, "Electrochemistry of Solutions," 2nd ed, Izd. Khimya, Moscow, 1966, pp 275–284, 563–564.
(18) A. Apelblat, *J. Inorg. Nucl. Chem.*, **31**, 483 (1969).
(19) A. Apelblat and A. Hornik, *Israel J. Chem.*, **7**, 45 (1969).

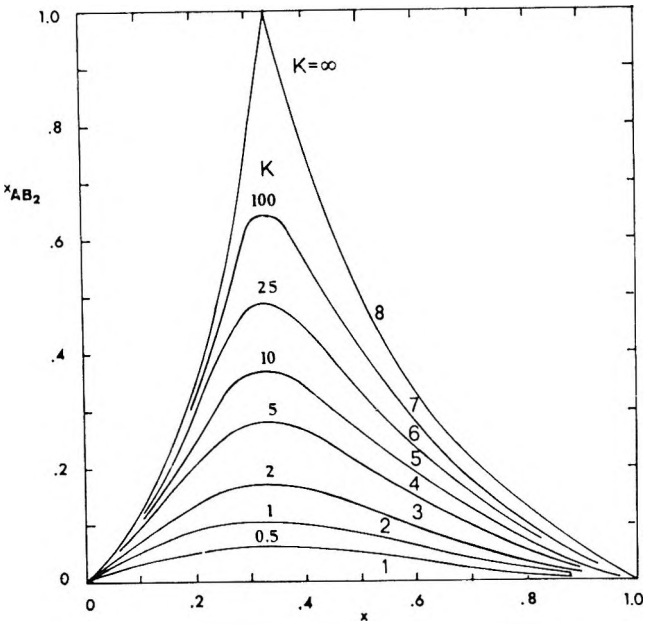


Figure 1. Mole fraction of $x_{AB_2}$ *vs.* the stoichiometric mole fraction $x$ of the nominal component A for various values of the association constant $K$.

culations are presented in Figure 1. Equation 3 has two trivial solutions for $x = 0$ and $x = 1$, where $\xi = 0$. For $x = {}^1/_2$ eq 3 is reduced to the equation of the second order, which has the solution $\xi = {}^1/_2 + 1/K\ (1 - \sqrt{1 + K})$. The derivative of $\xi$ with respect to $x$ is

$$\frac{\partial \xi}{\partial x} = \frac{\begin{array}{r}2(3x - 1)[4x\xi^3 + 2(3x - 1)\xi^2 + \\ (3x - 2)\xi] + 1 - 4x + 3x^2\end{array}}{\begin{array}{r}12x^2(1 - 2x)\xi^2 + 8x(-1 + 3x - 3x^2)\xi + \\ 1/K + (1 - x)(1 - 3x + 6x^2)\end{array}} \quad (4)$$

In the limit

$$\lim_{\substack{x\to 0\\(\xi\to 0)}} \left(\frac{\partial \xi}{\partial x}\right) = \lim_{\substack{\xi\to 0\\(x\to 0)}} \left(\frac{\xi}{x}\right) = \frac{K}{1 + K} \quad (5)$$

$$\lim_{\substack{x\to 1\\(\xi\to 0)}} \left(\frac{\partial \xi}{\partial x}\right) = 0$$

Equating $(\partial\xi/\partial x)$ to zero one obtains that the maximum concentration of $AB_2$ appears for $x = {}^1/_3$, *i.e.*, for any $K$, the value of $\xi_{max}$ is given by the solution of the equation

$$\xi_{max}^3 - 3\xi_{max}^2 + 3\left(\frac{9}{4K} + 1\right)\xi_{max} - 1 = 0 \quad (6)$$

and from (6)

$$\xi_{max} = 1 + \frac{3}{2}\left[-\left(\frac{1 + D}{K}\right)^{1/3} + \left(-\frac{1 - D}{K}\right)^{1/3}\right]$$

$$D \equiv \left(\frac{1 + K}{K}\right)^{1/2} \quad (7)$$

As expected, $\xi_{max}$ tends to unity for $K \to \infty$.

## The Excess Thermodynamic Functions

From the fact that the chemical potentials of the nominal components in an associated mixture are equal to the chemical potentials of the monomer molecules,[1] the excess Gibbs energy of mixing can be written in the form

$$G^E = RT\,[x \ln (x/x_A) + (1 - x) \ln (x_B/(1 - x))] \quad (8)$$

this is a particular case of the Prigogine equation.[1] Using eq 1, the activity coefficients of the nominal components A and B, $\gamma_1 = x_A/x$ and $\gamma_2 = x_B/(1 - x)$, are

$$\gamma_1 = 1 + 2\xi - \xi/x$$

$$\gamma_2 = 1 - \frac{2\xi x}{1 - x} \quad (9)$$

Since $x_B \leq 1 - x$, it follows that $\gamma_2$ is lower than unity. This is also true for $\gamma_1$ when $x < {}^1/_2$. In the limit

$$\lim_{x\to 0} \gamma_1 = 1/(K + 1) = \gamma_1^\infty, \lim_{x\to 1} \gamma_1 = 1$$

$$\lim_{x\to 0} \gamma_2 = 1, \lim_{x\to 1} \gamma_2 = 1 \quad (10)$$

The extremal values of the activity coefficients appear for $x = {}^2/_3$ and $\gamma_1 = \gamma_2$ for $x = {}^1/_3$ (Figure 2). The activities $a_1 = P_1/P_A^\circ$ and $a_2 = P_2/P_B^\circ$ for the association of the type A + B + $AB_2$ are shown in Figure 3.

Calculating the derivative of $G^E$ with respect to $x$ (for constant $T$, $P$) and using the Gibbs–Duhem relationship, one obtains

$$\left(\frac{\partial G^E}{\partial x}\right) = RT \ln \gamma_1/\gamma_2 \quad (11)$$

$$g_1^E = \lim_{x\to 0}\left(\frac{\partial G^E}{\partial x}\right) = RT \ln \gamma_1^\infty \quad (12)$$

$$g_2^E = 0$$

$(\partial G^E/\partial x)$ equals zero when $\gamma_1 = \gamma_2$, *i.e.*, for $x = {}^1/_3$ the excess free energy of mixing $G^E$ (which is always negative) has a minimum. The function $-G^E/RT = f(K|x)$ is presented in Figure 4.

The excess enthalpy of mixing for the associated mixture of the type A + B + $AB_2$ is given by

$$H^E = \Delta H^\circ \frac{\xi}{1 + 2\xi} \quad (13)$$

where the standard reaction enthalpy, $\Delta H^\circ = h_{AB_2}^\circ - h_A^\circ - 2h_B^\circ$ contains the molar enthalpies of the molecular species $AB_2$, A, and B, respectively. Since

$$\left(\frac{\partial H^E}{\partial x}\right) = \Delta H^\circ \frac{\left(\frac{\partial \xi}{\partial x}\right)}{(1 + 2\xi)^2} \quad (14)$$

It follows from eq 4 that the extreme of $H^E$ appears for

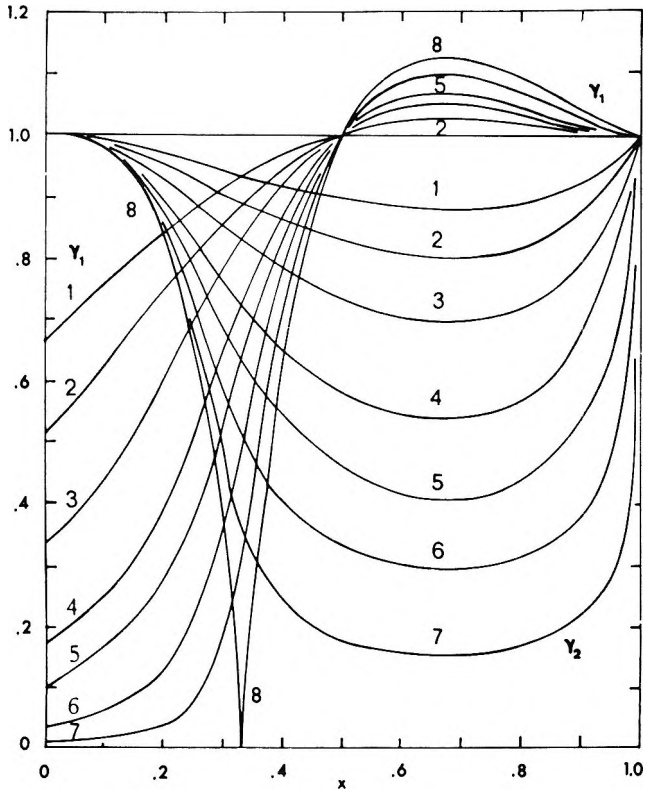


Figure 2. Activity coefficients $\gamma_1$ and $\gamma_2$ as functions of the stoichiometric mole fraction $x$ for various $K$. Notation as in Figure 1.

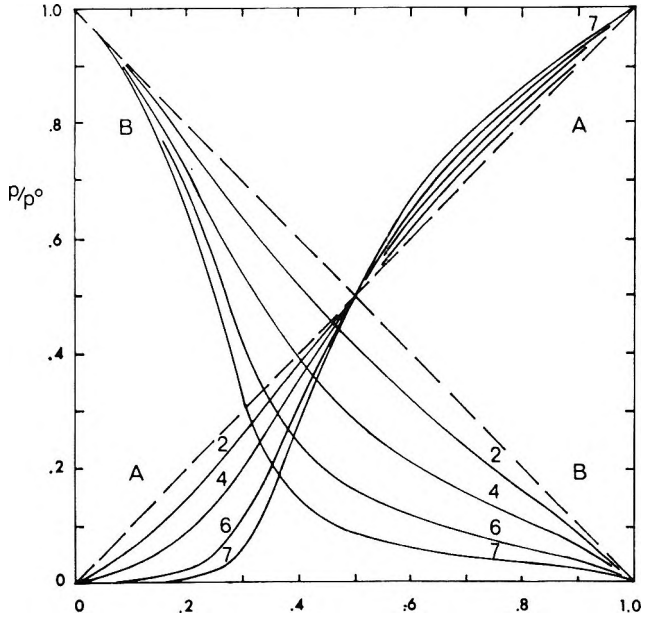


Figure 3. Activities of the nominal components A and B as functions of the stoichiometric mole fraction $x$ for various $K$. Notation as in Figure 1.

$x = 1/3$. The excess enthalpy of mixing $H^E$ always has the same sign as $\Delta H°$, because usually $\Delta H° < 0$, $H^E$ is also negative. The excess enthalpy of mixing at infinite dilution is

$$h_1^E = \lim_{x \to 0} \left( \frac{\partial H^E}{\partial x} \right) = \frac{\Delta H° K}{1 + K}$$

$$h_1^E = -RT^2 \left( \frac{\partial \ln \gamma_1^\infty}{T} \right) \qquad (15)$$

when $\xi_{max} \to 1$, $(K \to \infty)$, then $H^E \to 0$, *i.e.*, as expected, the heat of mixing of undissociated $AB_2$ is zero. The function $H^E/\Delta H° = f(K|x)$ is given in Figure 5.

Using eq 8, 9, and 13, the excess entropy of mixing is

$$S^E = \frac{\Delta H°}{T} \frac{\xi}{(1 + 2\xi)} - R\left[ x \ln \left( 1 + 2\xi - \frac{\xi}{x} \right) + (1 - x) \ln \left( 1 - \frac{2x\xi}{1 - x} \right) \right] \qquad (16)$$

and taking into account that $\Delta G° = -RT \ln K$, the standard entropy of the association reaction can be calculated from

$$\Delta S° = R\left[ \ln K + T \left( \frac{\partial \ln K}{\partial T} \right)_P \right] \qquad (17)$$

The standard reaction entropy $\Delta S°$, is related to the loss of orientations of the molecules A and B when the complex is formed.[1] Each molecule A or B can be oriented in $\eta$ ways with respect to the neighboring molecules, while in the complex, one orientation of A and B is so favorable that it always occurs. The value of $\eta$ is of the same order of magnitude as the number of the

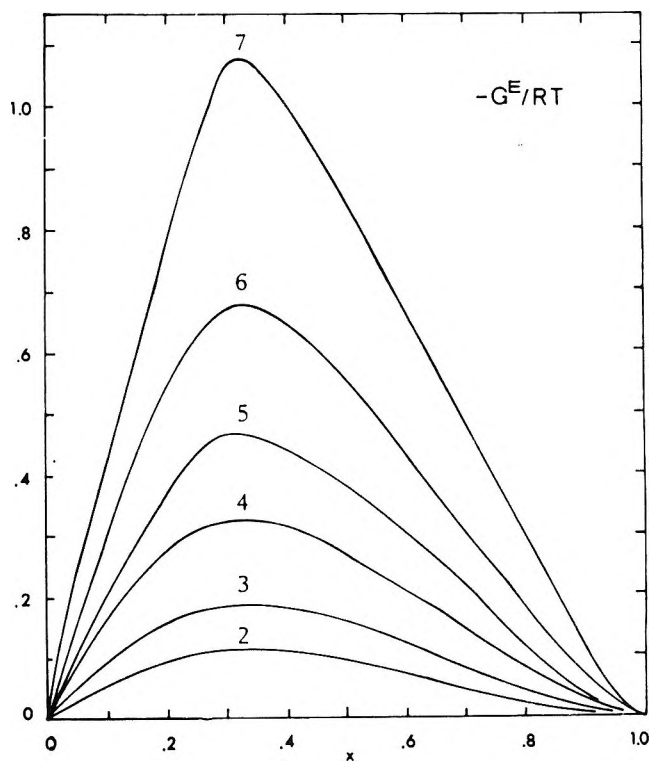


Figure 4. Normalized excess Gibbs energy of mixing $-G^E/RT$ as a function of the stoichiometric mole fraction $x$ for various $K$. Notation as in Figure 1.

nearest neighbors $z$. These conclusions are based on Saroléa-Mathot[4] investigations for AB complexes and Rastogi and Girdhar[6] for AB + $AB_2$ mixtures. Similarly, from the lattice model of associated solutions one obtains

$$\Delta S^\circ = -3R \ln \eta \tag{18}$$

*i.e.*, $\Delta S^\circ$ is always negative. Since $\eta$ is related to $\Delta H^\circ$ by

$$K = \eta^{-3} \exp\left(-\frac{\Delta H^\circ}{RT}\right) \tag{19}$$

therefore $S^E$ in eq 16 is the difference between two terms which are always negative. Their absolute value determines the sign of $S^E$, *i.e.*, $S^E$ can acquire any positive or negative value. For small values of $K$ (in this case $\gamma_1 - 1 \ll 1$ and $\gamma_2 - 1 \ll 1$) one obtains by expanding the logarithms in eq 16 that $S^E/R \simeq ((\Delta H^\circ/RT) + 1)\xi$, and the excess entropy is then positive for $K\eta^3 < 1$.

The excess volume $V^E$ (Figure 5) is given by

$$V^E = \Delta V^\circ \frac{\xi}{1 + 2\xi} \qquad V^\circ \equiv (v_{AB_2}^\circ - v_A^\circ - 2v_B^\circ) \tag{20}$$

and the excess heat capacity $C_P^E$ is

$$C_P^E = \left\{\frac{\Delta C_P^\circ \xi}{1 + 2\xi} + R\left(\frac{\Delta H^\circ \xi}{1 + 2\xi}\right)^2 \times \frac{[1 - x(1 + 2\xi)]}{x[K(1 - x(1 + 2\xi))^3 - 4\xi^2]}\right\} \tag{21}$$

$$\Delta C_P^\circ \equiv (c_{AB_2}^\circ - c_A^\circ - 2c_B^\circ)$$

$V^E$ and $C_P^E$ were derived similarly as other excess thermodynamic functions.

## Boiling and Condensation Curves for the Ideal Associated Solutions of the Type A + B + $AB_2$

We shall now evaluate a liquid–vapor diagram at constant pressure. Assuming that in the temperature interval under consideration the latent heats of the components A and B (denoted by 1 and 2) are independent of temperature and that vapor phase is a perfect gas mixture, we have[1]

$$y = \frac{\gamma_1(\gamma_2 e^{\lambda_2} - 1)}{\gamma_2 e^{\lambda_1 + \lambda_2} - \gamma_1} \qquad x = \frac{e^{\lambda_1}(\gamma_2 e^{\lambda_2} - 1)}{\gamma_2 e^{\lambda_1 + \lambda_2} - \gamma_1} \tag{22}$$

where the stoichiometric mole fraction of A in a liquid phase is denoted by $x$ and in a vapor phase by $y$ and

$$\lambda_1 = \frac{\Delta_e h_1^\circ}{RT_1^\circ}\left(\frac{T_1^\circ}{T} - 1\right) \qquad \lambda_2 = \frac{\Delta_e h_2^\circ}{RT_2^\circ}\left(1 - \frac{T_2^\circ}{T}\right) \tag{23}$$

where $\Delta_e h^\circ$ is the heat of evaporation of the pure liquid component and $T^\circ$ its boiling point. For the case where both phases are ideal, eq 22 are reduced to van Laar relationships.[1] The condensation and boiling point curves are given in eq 22 in implicit form because the activity coefficients are dependent on the equilibrium constant $K$ and the equilibrium constant depends on temperature (eq 3 and 9).

We shall now introduce the relative volatility $\alpha(x, T)$ defined by

$$\alpha(x,T) \equiv \frac{\frac{y}{1 - y}}{\frac{x}{1 - x}} \tag{24}$$

then for the ideal case ($\gamma_1 = \gamma_2 = 1$) one has from eq 22

$$\alpha_0(T) = \exp[-(\lambda_1 + \lambda_2)] \tag{25}$$

or

$$RT \ln \alpha_0(T) = \left[(\Delta_e h_2^\circ - \Delta_e h_1^\circ) + T\left(\frac{\Delta_e h_1^\circ}{T_1^\circ} - \frac{\Delta_e h_2^\circ}{T_2^\circ}\right)\right] \tag{26}$$

For $\Delta_e h_1^\circ \simeq \Delta_e h_2^\circ = \Delta_e h^\circ$ (*i.e.*, for isotopes, isomers) $\alpha_0$ is nearly independent of temperature

$$\ln \alpha_0 = \left[\left(\frac{\Delta_e h^\circ}{R}\right)\frac{T_2^\circ - T_1^\circ}{T_1^\circ T_2^\circ}\right] \tag{27}$$

Using eq 22, 24, and 25 one obtains

$$\alpha(x,T) = \frac{\gamma_1}{\gamma_2}\alpha_0(T) \tag{28}$$

Introducing the derivative of $G^E$ with respect to $x$ from (11) into (29) one obtains

$$\left(\frac{\partial G^E}{\partial x}\right) = RT \ln \frac{\alpha(x,T)}{\alpha_0(T)} = RT \ln\left[\left(\frac{1 - x}{x}\right)\frac{x(1 + 2\xi) - \xi}{1 - x(1 + 2\xi)}\right] \tag{29}$$

The additional term $-\frac{H^E}{RT^2}\left(\frac{dT}{dx}\right)$ is small and is omitted in (29). In the limit, from (10) and (12)

$$\alpha(x \to 0, T) = \frac{\alpha_0(T)}{1 + K} \qquad \alpha\begin{pmatrix} x \to 1/3, & T \\ x \to 1, & T \end{pmatrix} = \alpha_0(T) \tag{30}$$

*i.e.*, $\alpha(x, T)/\alpha_0(T) \leq 1$ for $x \leq 1/3$ and $\alpha(x, T)/\alpha_0(T) > 1$ for $x > 1/2$. Using eq 24, 28, and 9, the vapor–liquid equilibrium curve has the form

$$y = \frac{\alpha_0(T)[x(1 + 2\xi) - \xi]}{1 - \xi + [\alpha_0(T) - 1][x(1 + 2\xi) - \xi]} \tag{31}$$

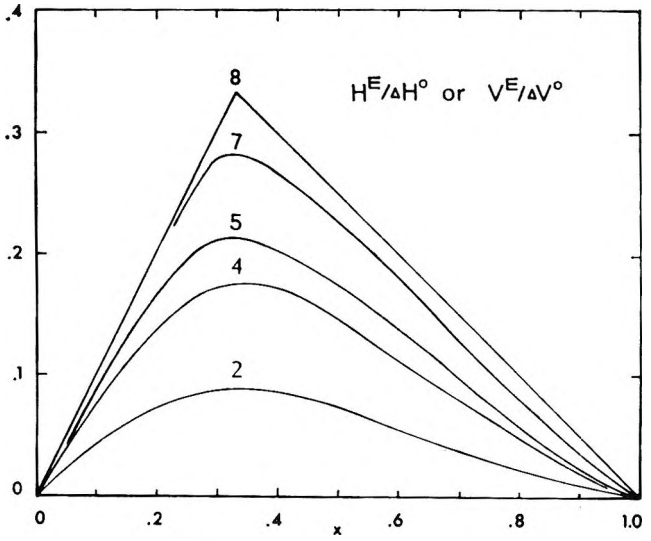


Figure 5. Normalized enthalpy of mixing $H^E/\Delta H°$ and excess volume $V^E/\Delta V°$ as functions of the stoichiometric mole fraction $x$ for various $K$. Notation as in Figure 1.

or

$$y = \frac{\alpha_0(T)x_A}{1 - \xi + [\alpha_0(T) - 1]x_A} \tag{32}$$

where $x_A$ and $\xi$ are given in eq 1, 2, and 3. For $\xi \to 0$, the ideal equilibrium curve is

$$y = \frac{\alpha_0 x}{1 + (\alpha_0 - 1)x} \tag{33}$$

Expanding the exponents in eq 22 (this is possible because usually $T \sim T°$, $\lambda \simeq \Delta_e h°/R(T°)^2(T° - T) \simeq 4 \times 10^{-2}$) one obtains the first approximation for the boiling temperature curve at constant pressure

$$T \simeq \left[\frac{\lambda_2°T_2° + x(1 + 2\xi)(\lambda_1°T_1° - \lambda_2°T_2°)}{\lambda_2° + x(1 + 2\xi)(\lambda_1° - \lambda_2°)}\right] \tag{34}$$

$$\lambda_i° \equiv \frac{\Delta_e h_i°}{RT_i°} \qquad i = 1, 2$$

$$T \simeq T_1°\left[\frac{1 - x_B\left(1 - \frac{\lambda_2°T_2°}{\lambda_1°T_1°}\right)}{1 - x_B\left(1 - \frac{\lambda_2°}{\lambda_1°}\right)}\right] \tag{35}$$

Calculating $T$ from eq 34 or 35 for given $x$ and $K(T)$ (*i.e.*, for a given $\xi$, eq 3) and introducing $T$ into the first equation in (22), one obtains the condensation temperature curve. For a given isobaric vapor–liquid equilibrium, the constant $K(T)$ can be evaluated from eq 30 or from the data at $x = {}^1/_2$; *i.e.*, from the data

$$K(T) = \frac{\left[1 - \left(\frac{\alpha_0(T)}{\alpha({}^1/_2, T)}\right)\right]}{\left[\frac{\alpha_0(T)}{2\alpha({}^1/_2, T)}\right]^2} \tag{36}$$

$y - x - T$, $\alpha_0(T)$, the values of $K$ at different temperatures can be derived

$$\begin{aligned} x &= 0, & \frac{\alpha}{\alpha_0} &= \frac{1}{1 + K} < 1, & K &\neq 0 \\ x &= {}^1/_3, & \frac{\alpha}{\alpha_0} &= 1 \\ x &= {}^1/_2, & \frac{\alpha}{\alpha_0} &= \frac{K}{2(\sqrt{K + 1} - 1)} > 1 \\ x &= 1, & \frac{\alpha}{\alpha_0} &= 1 \end{aligned} \tag{37}$$

or for any $x$, by using eq 2, 9, and 28.

From eq 22 and 28 one obtains the conditions which are necessary for the occurrence of the azeotrope ($y = x$, $\alpha(x,T) = 1$); eq 38 can be written in the form of (39)

$$\begin{aligned} \gamma_1^{AZ} &= e^{\lambda_1^{AZ}} \\ \gamma_2^{AZ}e^{\lambda_2^{AZ}} &= 1 \end{aligned} \tag{38}$$

$$\frac{T_i°}{T_{AZ}} = \left[1 + \frac{\ln \gamma_i^{AZ}}{\lambda_i°}\right] \qquad i = 1, 2 \tag{39}$$

or excluding $T_{AZ}$

$$\lambda_2°T_2° \ln \gamma_1^{AZ} - \lambda_1°T_1° \ln \gamma_2^{AZ} = \lambda_1°\lambda_2°(T_1° - T_2°) \tag{40}$$

If both liquids obey the Trouton law ($\lambda_1° = \lambda_2° = \lambda°$) then

$$\ln [(\gamma_1^{AZ})^{T_2°}(\gamma_2^{AZ})^{T_1°}] = \lambda°(T_1° - T_2°) \tag{41}$$

From the fact that for an association of the type $AB_2$, the activity coefficients are $\gamma_1 < 1$ and $\gamma_2 < 1$ for $x < {}^1/_2$ (Figure 2, eq 9) and $\gamma_1 \geq 1$ and $\gamma_2 < 1$ for $x \geq {}^1/_2$, one has, according to eq 39, $T_{AZ} > T_1°$ and $T_{AZ} > T_2°$ for $x < {}^1/_2$ and $T_{AZ} < T_1°$ and $T_{AZ} > T_2°$ for $x > {}^1/_2$. The last inequalities for $x > {}^1/_2$ cannot be satisfied simultaneously. Therefore the azeotrope for $x > {}^1/_2$ does not appear. An exception is a double azeotrope. From the first inequalities one obtains that the negative azeotrope which corresponds to a maximum in $T$ and a minimum in $P$ can occur only for $x < {}^1/_2$. In this case the increase in temperature will cause a decrease of the mole fraction of the component having the higher evaporation heat[1] and the condensation temperature curve is always convex.[20] In spite of the fact that the alcohol–carboxylic acid systems cannot be considered as "pure" $AB_2$ systems, the results of the Rius, *et al.*,[15] and of Krokhin[16] are not contradictory to the conclusion reached here. The system 1-butanol (2)–acetic acid (1) at 706 mm forms an azeotrope with the azeotropic temperature $T_{AZ} = 393.43°K$. The mole fraction of the acid is $x = 0.482$ and the boiling points are $T_1° =$

(20) W. Malesinski, "Azeotropy and Other Theoretical Problems of Vapor-Liquid Equilibrium," Interscience Publishers, New York, N. Y., 1965.

387.73°K and $T_2°$ = 388.93°K for acetic acid and 1-butanol, respectively. In the isopentyl alcohol (2)–acetic acid (1) system[16] the azeotropic mixtures are formed at 760 mm for $T_{AZ}$ = 406.13°K ($T_1°$ = 391.23°K, $T_2°$ = 403.88°K, and $x$ = 0.22) and at 20 mm, $T_{AZ}$ = 327.63°K ($T_1°$ = 303.13°K, $T_2°$ = 324.29°K, and $x$ = 0.25). The systems mentioned above are consistent with $x_{AZ} < 1/2$ and $T_{AZ} > T_1°, T_2°$.

For the systems with known $x_{AZ}$, $T_{AZ}$, the value of $\xi_{AZ}$ can be calculated from eq 39.

$$\xi_{AZ} = \left[\frac{x_{AZ}}{1 - 2x_{AZ}}(1 - e^{\lambda_1 AZ})\right] \simeq \left[\frac{x_{AZ}}{1 - 2x_{AZ}}\lambda_1°\left(\frac{T_1°}{T_{AZ}} - 1\right)\right] \quad (42)$$

and using eq 1, 2, and 42, the value of $K$ can be found.

The equilibrium constant $K$ can be also evaluated by taking into consideration that at the azeotropic point, under isobaric conditions

$$P = P_{AZ} = P_1°\gamma_1 = P_2°\gamma_2 \quad (43)$$

and therefore

$$\xi_{AZ} = \frac{x_{AZ}}{1 - 2x_{AZ}}\left(1 - \frac{P}{P_1°}\right) = \frac{1 - x_{AZ}}{2x_{AZ}}\left(1 - \frac{P}{P_2°}\right) \quad (44)$$

where $P_1°$ and $P_2°$ are the vapor pressure of the pure components at the azeotropic temperature $T_{AZ}$.

The identification and analysis of the associated solutions is based on experimental data and on theoretical predictions (*e.g.*, for the A + B + $AB_2$ mixture, the composition of a mixture with extremal value of heat of mixing is $x = 1/3$, where for the A + B + AB mixture it is $x = 1/2$). Complete description of the system is possible if the value of $K(T)$ and the standard thermodynamic functions are known. A number of experimental techniques usually serve for determination of equilibrium constants.[21] We shall now consider two of the less frequently used methods, gas chromatography and determination of the total vapor pressure. The equilibrium constant $K(T)$ and the standard thermodynamic properties can be evaluated from gas chromatographic measurements[18] by using eq 10, 15, and 17.

For a mixture of the type A + B + $AB_2$, the total pressure determined at constant temperature is

$$P = P_1°x\gamma_1 + P_2°(1 - x)\gamma_2 = P_1°x_A + P_2°x_B \quad (45)$$

In eq 45 the pressure contribution of the $AB_2$ complex is neglected. The excess pressure $\Delta P^{ex}$, defined as the difference between the pressure calculated from the Raoult law and the total measured vapor pressure, is

$$\Delta P^{ex} = P_1°(x - x_A) + P_2°(1 - x - x_B) \quad (46)$$

or using $x_A$ and $x_B$ from eq 1

$$\xi = \frac{\Delta P^{ex}}{P_1°(1 - 2x) + P_2°2x} \quad (47)$$

For $x = 1/2$, one has $\xi = \Delta P^{ex}/P_2°$, and the equilibrium constant is

$$K = \frac{2\left(\frac{\Delta P^{ex}}{P_2°}\right)}{\left(\frac{1}{2} - \frac{\Delta P^{ex}}{P_2°}\right)^2} \quad (48)$$

The usefulness of eq 48 is illustrated here by presenting the total vapor pressure in the propionic acid (1)–methanol (2) system at 25.03°, measured by us. According to (48) one obtains from the determined $\Delta P^{ex}$ = 6.70 mm at $x = 1/2$ and from $P_1°$ = 4.24 mm and $P_2°$ = 127.81 mm that $K$ = 0.523. Using this value of $K$, the total vapor pressure was calculated by using eq 1, 2, and 45. Figure 6 illustrates the agreement between the calculated and the measured values of $P$, especially in the concentration region rich in alcohol. Obviously, at higher concentration of propionic acid the effect of the acid dimerization cannot be neglected.

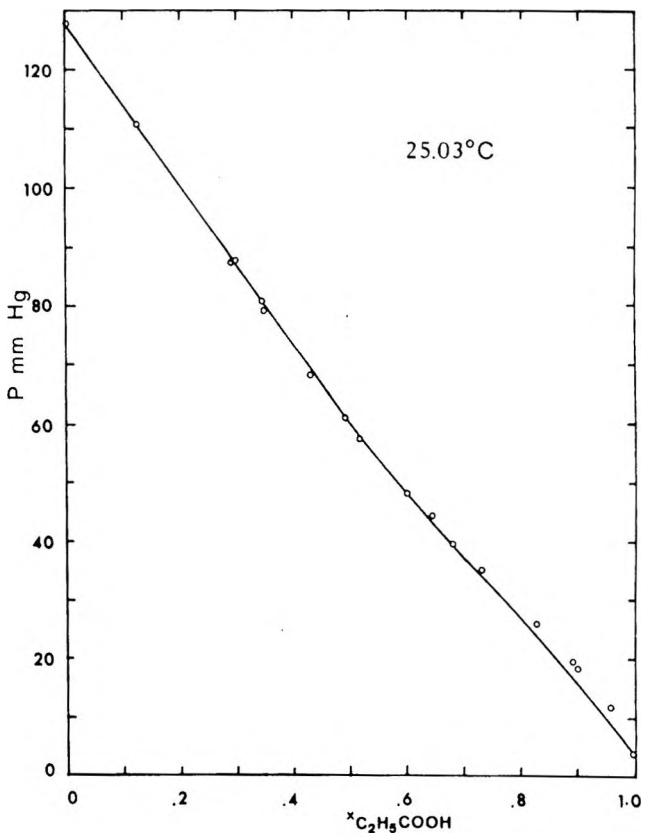


Figure 6. Total vapor pressure of the methanol–propionic acid system at 25.03°. The circles are experimental points; the line was calculated for the A + B + $AB_2$ model with $K$ = 0.523, according to eq 1, 2, and 45.

(21) F. J. C. Rossotti and H. Rossotti, "The Determination of Stability Constants," McGraw-Hill Publications, New York, N. Y., 1961.

# NOTES

## Analysis of the Proton Magnetic Resonance Spectrum of Cyclopropene

by Joseph B. Lambert,[1a] Andrew P. Jovanovich,[1b] and Wallace L. Oliver, Jr.[1c]

*Department of Chemistry and Materials Research Center, Northwestern University, Evanston, Illinois 60201*
*(Received January 2, 1970)*

The magnitude of the vicinal coupling between protons on a double bond in cyclic alkenes is critically dependent on ring size.[2] The spectrum of the extreme member of this series, cyclopropene I, never has been fully analyzed,[3] and in particular the alkenic coupling ($J_{12}$), which is of theoretical and practical

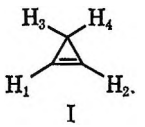


I

importance, has not been determined. 3,3-Dimethylcyclopropene has served as a substitute in some studies.[4a] Although $J_{12}$ is obscured in this system by a long-range coupling to the methyl protons,[2] a value of about 1.4 Hz was determined by a decoupling experiment.[4a]

Consequently, we have prepared the parent hydrocarbon[4b] and examined its proton spectrum at 90 MHz on the Bruker HFX-10 spectrometer.[5] Cyclopropene presents a classic first-order $A_2X_2$ spectrum (Figure 1). To measure the coupling $J_{12}$ between the equivalent nuclei, the $^{13}C$ satellite of the vinylic proton spectrum must be examined. The downfield half of the satellite spectrum consists of a doublet of triplets (Figure 2); the triplet splitting corresponds to $J_{13}$ and the doublet splitting to $J_{12}$. The magnitude of $J_{12}$ was found to be 1.3 Hz; the experimental method did

**Table I:** Nmr Parameters for Cyclopropene

| $\delta_1 = \delta_2 =$ 7.06 ppm | $\delta_3 = \delta_4 =$ 0.93 ppm |
|---|---|
| $\lvert J_{12}\rvert$ = 1.3 Hz | $\lvert J_{13}\rvert$ = 1.75 Hz |
| $J_{^{13}C\text{-}H}$ = +226 Hz | $J_{34}$ = (indeterminate, assumed to be −12.00 Hz) |

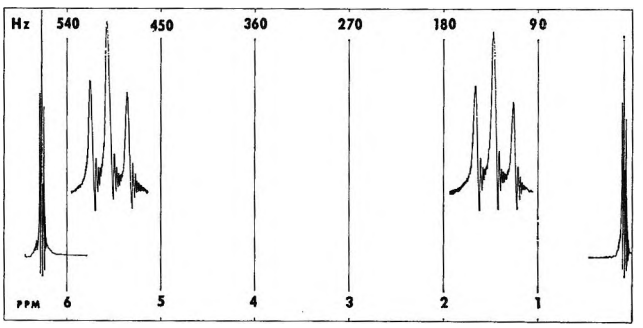


Figure 1. The 90-MHz proton spectrum of neat cyclopropene. The scale is marked at 10 Hz/cm, with the blow-up expanded by a factor of 10. The distance between each component of the triplet is 1.75 Hz.

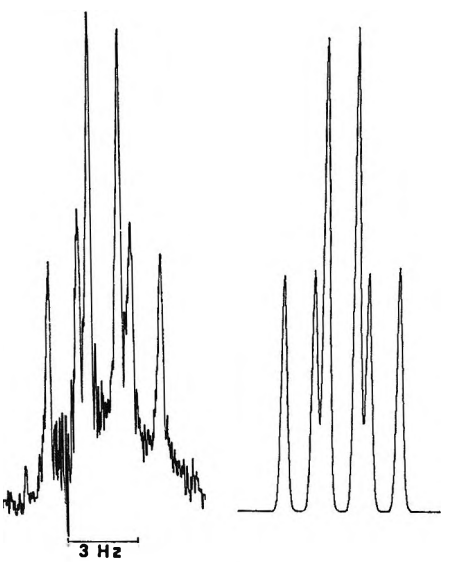


Figure 2. The downfield $^{13}C$-satellite spectrum of the alkenic protons of cyclopropene, observed (left) and calculated (right).

(1) (a) Alfred P. Sloan Foundation Fellow, 1968–1970. This work was supported by the National Science Foundation (Grant GP-9257) and by the Advanced Research Projects Agency of the Department of Defense through the Northwestern University Materials Research Center; (b) NDEA Fellow, 1967–1969; (c) National Science Foundation Trainee, 1966–1967; National Institutes of Health Predoctoral Fellow, 1968–1970.

(2) O. L. Chapman, *J. Amer. Chem. Soc.*, **85**, 2014 (1963); G. V. Smith and H. Kriloff, *ibid.*, **85**, 2016 (1963); P. Laszlo and P. von R. Schleyer, *ibid.*, **85**, 2017 (1963); S. Borčić and J. D. Roberts, *ibid.*, **87**, 1056 (1965); E. A. Hill and J. D. Roberts, *ibid.*, **89**, 2047 (1967).

(3) K. B. Wiberg and B. J. Nist, *ibid.*, **83**, 1226 (1961).

(4) (a) G. L. Closs, *Proc. Chem. Soc. London*, 152 (1962); *Advan. Alicyclic. Chem.*, 1, 76 (1966); (b) G. L. Closs and K. D. Krantz, *J. Org. Chem.*, **31**, 638 (1966).

(5) We thank the National Science Foundation for an equipment grant that made the purchase of this instrument possible. Neat cyclopropene was examined at −60°. The details of preparation may be found in the doctoral dissertation of A. P. Jovanovich, Northwestern University, 1969.

not permit a sign determination. The derived spectral data are collected in Table I and are illustrated in part in the calculated spectrum of Figure 2.

The chemical shifts and the allylic coupling ($J_{13}$) have been reported and discussed previously.[3] The magnitude of $J_{12}$ (1.3 Hz) continues the downward trend of the higher cycloalkenes ($C_6$, 8.8; $C_5$, 5.1; $C_4$, 2.85 Hz);[2] it may be the smallest vicinal coupling measured between protons with 0° dihedral angle in a hydrocarbon.[6,7] The magnitude of $J_{^{13}C-H}$ (226 Hz) indicates that the alkenic bond to hydrogen possesses about 45% s character.[8] With these measurements, the lower cycloalkene series is now complete.

(6) M. Karplus, *J. Amer. Chem. Soc.*, **85**, 2870 (1963).

(7) Even in cyclopropenone, $J_{12}$ (3 Hz) is larger, *cf.* R. Breslow and G. Ryan, *ibid.*, **89**, 3073 (1967).

(8) N. Muller and D. E. Pritchard, *J. Chem. Phys.*, **31**, 768 (1959); J. N. Shoolery, *ibid.*, **31**, 1427 (1959).

## Effects of Deuteration and Heavy Atom Additives on the Scintillation Lifetime of *p*-Terphenyl in Benzene at 22°

by R. M. Lambrecht, T. M. Kelly, and J. A. Merrigan

*Research Laboratories, Eastman Kodak Company, Rochester, New York 14650* *(Received January 28, 1970)*

Addition of iodo- and bromobenzenes to a scintillator solution of *p*-terphenyl in benzene quenches the scintillation intensity as a function of the concentration of the additives. The quenching of the intensity is governed by Stern–Volmer kinetics and proper treatment of the data yields the Stern–Volmer quenching constants.[1-3] By using a single photon timing spectrometer with subnanosecond resolution, we have examined the variations in scintillation lifetimes as altered by selected heavy atom additives and found that lifetime measurements can be used to determine Stern–Volmer quenching constants. Quenching of the scintillation lifetimes of perprotonated *p*-terphenyl and deuterated *p*-terphenyl-$D_{14}$ as a function of concentration of fluoro-, chloro-, bromo-, and iodobenzene and bromocyclohexane are presented. The results support the hypothesis that these additives affect the luminescence of *p*-terphenyl in benzene solvent by interfering with energy transfer from the solvent to the fluor.

### Experimental Section

Scintillation lifetimes ($1.44 \times T_{1/2}$) were measured by the fast-slow coincidence method of start-stop timing coupled with single-photon detection.[4,5] By this method the rise and decay of scintillation intensity is determined by measuring the distribution of time intervals between the beginning of the scintillation and detection of a single photon. Since the probability of single photon detection is proportional to the scintillation intensity, the number of detections *vs.* the time of detection outlines the variation of intensity with time. The mean rise and decay times were resolved by a computer least-squares iterative fit to the data of two exponential functions representing the rise and decay of the scintillation intensity. A second eximer decay was not evident for 2.5 decades down from the peak intensity. The region of 7 to 70% of the peak was used for exponential fit of the data.

The scintillation decay spectrometer was constructed from ORTEC and LeCroy Research Systems NIM components with RCA-8575 photomultipliers. Twenty $\mu$Ci of $^{65}Zn$ was used as a source of 1.12 MeV $\gamma$ rays to stimulate scintillation. The "start" of a scintillation was established by collecting a sizable fraction of the fluorescence photons on a photomultiplier. The scintillation was filtered to achieve single-photon detection on a separate "stop" photomultiplier. The time between start and stop was measured by an ORTEC 437 time-to-pulse-height converter and stored on a RIDL 400 channel analyzer. The resolution of the spectrometer was measured by the Čerenkov radiator method[6,7] using $^{60}Co$ as a source of coincident $\gamma$ rays. The instrumental response function was symmetrical with a full width at half maximum of 1.0 nsec and an equivalent lifetime of the slope less than 0.2 nsec. This system is described in detail elsewhere.[8]

The scintillation decay time for NATON-136 from 7–70% of the peak intensity was measured at 1.9 ± 0.1 nsec in agreement[7] with 1.87 ± 0.1 nsec. When the NATON-136 spectrum was separated into two decay components the values were 1.6 and 8 nsec compared with recently reported values of 1.6 and 10 nsec.[6]

Eastman Grade benzene, halobenzenes, and *p*-terphenyl were used in the scintillators. Deuterated *p*-terphenyl-$D_{14}$, 98% atomic purity, was used as received from Mallinckrodt Nuclear Corp. The liquid scintillators were prepared in the presence of air[9] and placed in a 1-in. right cylinder quartz container

(1) J. L. Kropp and M. Burton, *J. Chem. Phys.*, **37**, 1742 (1962).

(2) J. B. Birks and S. Georghiou, *Proc. Phys. Soc., London (At. Mol. Phys.)*, **1**, 958 (1968).

(3) J. B. Birks, S. Georghiou, and I. H. Munro, *ibid.*, **1**, 266 (1968).

(4) L. M. Bollinger and G. E. Thomas, *Rev. Sci. Instrum.*, **32**, 1044 (1961).

(5) Y. Koechlin and A. Raviart, *Nucl. Instr. Methods*, **29**, 45 (1964).

(6) F. J. Lynch, *I.E.E.E. Trans. Nucl. Sci.*, **NS-15**, 102 (1968).

(7) (a) J. Kirkbride, E. C. Yates, and D. G. Crandall, *Nucl. Instr. Methods*, **52**, 293 (1967); (b) E. C. Yates and D. G. Crandall, *I.E.E.E. Trans. Nucl. Sci.*, **NS-13**, 153 (1966).

(8) R. M. Lambrecht, T. M. Kelly, and J. A. Merrigan, submitted for publication in *Chem. Instrum.*

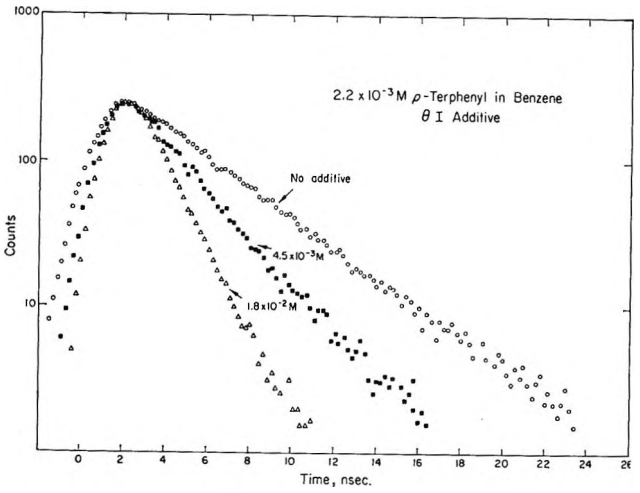


Figure 1. Scintillation decay spectra of $2.2 \times 10^{-3}$ *M* *p*-terphenyl in benzene as a function of iodobenzene addition.

which was optically coupled to the start photomultiplier. All measurements were made at 22°.

## Results and Discussion

Deuteration is known to alter the phosphorescence lifetimes of many aromatic hydrocarbons.[10] The measured fluorescence lifetimes have been studied less, but in some specific cases the lifetimes have increased owing to deuteration of the fluor.[11-13] Laposa, *et al.*,[11] found no difference in the fluorescence lifetimes of deuterated and protonated *p*-terphenyl in a rigid medium (77°K) of ethyl ether, isopentane, and ethyl alcohol, concluding that the $S_1$–$S_0$ radiationless transitions were unimportant. We found no effect of deuteration on the scintillation decay spectra of $2.2 \times 10^{-3}$ *M* *p*-terphenyl-$H_{14}$ or $D_{14}$ in liquid benzene. Both the rise and decay times were identical within experimental error as were the heavy atom additive effects.

The effect of adding iodobenzene to a $2.2 \times 10^{-3}$ *M* solution of *p*-terphenyl in benzene is illustrated in Figure 1. The spectra are centered at the peak to show clearly that both the rates of rise and decay of luminescence intensity were increased by the additive. Similar but less pronounced effects were observed with additions of bromobenzene and chlorobenzene. Fluorobenzene had no effect. The aliphatic bromocyclohexane had a small quenching effect but much less than bromobenzene. The lifetime quenching effects of these heavy atom additives as a function of concentration are shown in Table I. By observing the size of the scintillation pulse from the start photomultiplier, we found that the scintillation intensity also decreased as the concentration of additive was increased.

The scintillation rise time may be expected to be related to energy transfer from the solvent (benzene) to the solute (*p*-terphenyl), whereas the decay time would be related to the decay of the excited singlet

**Table I:** Scintillation Rise and Decay Times in Benzene Solution[a] of $2.2 \times 10^{-3}$ *M* *p*-Terphenyl-$H_{14}$ and -$D_{14}$[b] as a Function of Additives at 22°

| Additive | *M* | $\tau_{rise}$, nsec[c] | $\tau_{decay}$, nsec[d] |
|---|---|---|---|
| None[b] | | 1.0 | 4.7 |
| $C_6H_5I$ | $1.80 \times 10^{-3}$ | 0.90 | 3.7 |
| | $4.49 \times 10^{-3}$ | 0.85 | 2.8 |
| | $8.98 \times 10^{-3}$ | 0.77 | 2.1 |
| | $1.35 \times 10^{-2}$ | 0.62 | 1.7 |
| | $1.80 \times 10^{-2}$ | 0.56 | 1.6 |
| | $2.25 \times 10^{-2}$ | 0.59 | 1.5 |
| | $2.69 \times 10^{-2}$ | 0.53 | 1.5 |
| $C_6H_5Br$ | $4.77 \times 10^{-3}$ | 0.95 | 3.5 |
| | $9.55 \times 10^{-3}$ | 0.88 | 2.7 |
| | $2.86 \times 10^{-2}$ | 0.79 | 2.1 |
| | $4.77 \times 10^{-2}$ | 0.70 | 1.9 |
| $C_6H_5Cl$ | $8.88 \times 10^{-3}$ | 0.98 | 3.9 |
| | $1.78 \times 10^{-2}$ | 0.95 | 3.6 |
| | $3.56 \times 10^{-2}$ | 0.92 | 3.1 |
| | $5.30 \times 10^{-2}$ | 0.84 | 2.8 |
| | $7.99 \times 10^{-2}$ | 0.60 | 2.3 |
| $C_6H_5F$ | $1.07 \times 10^{0}$ | 0.99 | 4.6 |
| $C_6H_{11}Br$ | $2.45 \times 10^{-2}$ | 1.0 | 4.5 |
| | $4.89 \times 10^{-2}$ | 1.0 | 4.3 |
| | $1.30 \times 10^{-1}$ | 1.0 | 3.9 |
| | $4.24 \times 10^{-1}$ | 0.98 | 3.4 |

[a] Liquid scintillators were prepared in the presence of air. Degassed samples had 15–20% longer decay times. [b] Perdeuterated and perprotonated samples gave the same scintillation spectra within experimental errors. [c] Rise times were calculated from a single exponential fit of the data from 7 to 70% of the peak. Experimental error, ±0.1 nsec. [d] Decay times were calculated from a single exponential fit from 70 to 7% of the peak. Experimental error, ±0.1 nsec.

state of *p*-terphenyl.[6,14] However, the scintillation decay time may be dictated by the energy transfer process if it is slower than the fluorescence lifetime of *p*-terphenyl. The decay time of the donor species in pure benzene is of the order of $10^{-8}$ sec,[15] and the fluorescence lifetime of benzene has been reported as 27 nsec.[13] Therefore, one would expect the energy transfer from benzene to *p*-terphenyl to be the controlling rate process for the scintillation. Hence, the heavy atom additive

(9) Kropp and Burton[1] have shown that oxygen and added quenchers are in simple competition in *p*-terphenyl (6.1 m*M*) in benzene and do not interact with each other. Hence the mode of heavy atom additive quenching is not affected by the presence of air.

(10) See the examples and their references: (a) J. W. Rabalais, H. J. Maria, and S. P. McGlynn, *J. Chem. Phys.*, **51**, 2259 (1969); (b) T. D. Gierke, R. J. Watts, and S. J. Strickler, *ibid.*, **50**, 5425 (1969); (c) M. R. Wright, R. P. Frosch, and G. W. Robinson, *ibid.*, **33**, 934 (1960).

(11) J. D. Laposa, E. C. Lin, and R. E. Kellogg, *ibid.*, **42**, 3025 (1965).

(12) N. J. Turro and R. Engel, *J. Amer. Chem. Soc.*, **90**, 2989 (1968).

(13) W. P. Hellman, *J. Chem. Phys.*, **51**, 354 (1969).

(14) F. J. Lynch, "Organic Scintillators," D. L. Horrocks, Ed., Gordon and Breach Science Publishers, Inc., New York, N. Y., 1968, p 293.

(15) H. Dreeskamp and M. Burton, *Z. Elektrochem.*, **64**, 165 (1960).

effect of quenching the scintillation decay time may be caused by quenching of the excited state of benzene.

For energy to be transferred efficiently from the excited benzene donor to an acceptor, the absorption spectrum of the acceptor must overlap the fluorescence spectrum of the donor.[16] Although relative extinction coefficients and related parameters have considerable bearing, if one compares the absorption spectra of the additives studied with the fluorescence emission spectrum of benzene, the overlap increases with increasing scintillation quenching from fluorobenzene to iodobenzene.[17,18] There is no significant overlap of the absorption spectra of the additives with the fluorescence emission spectrum of *p*-terphenyl.

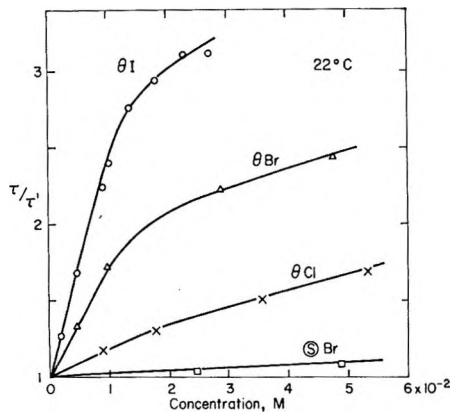


Figure 2. Heavy atom quenching effects in $2.2 \times 10^{-3}$ *M* *p*-terphenyl in benzene as a function of concentration of additives.

If, as it appears, the additive interactions with the transfer of excitation energy to the fluor are more important than their deexcitation interactions with the excited fluor and this energy transfer controls the scintillation decay time, one may use the scintillation decay times to determine values of the additive quenching constants. Stern–Volmer kinetics generally describe the luminescence behavior in solvents of low viscosity such as benzene.[1-3,19] Hence, the equation $\tau/\tau' = 1 + \gamma_s[A]$ may be used to describe the quenching of the lifetime by an additive, where $\tau$ is the lifetime without additive, $\tau'$ is the lifetime in the presence of an additive at concentration [A], and $\gamma_s$ is the quenching constant. The manner in which iodo-, bromo-, and chlorobenzene, and bromocyclohexane additives quench the energy transfer is depicted in Figure 2. The analysis over the linear regions of the curves at low concentrations indicates the values of $\gamma_s$ are 140 $M^{-1}$, 70 $M^{-1}$, 18 $M^{-1}$, and 2 $M^{-1}$, respectively. The downward deviation from a linear Stern–Volmer plot at higher concentrations gives confirming evidence that interactions of the additives with the solvent or in transferring energy to the fluor are more important than deexcitation interactions with the excited fluor.[1]

Absorption and fluorescence spectra of the constituents and combinations of the constituents in the scintillators were compared. There was no indication of any additional species such as a charge-transfer complex. Thus, the results support the hypothesis that the heavy atom additives quench energy transfer from benzene to *p*-terphenyl by spin–orbit coupling between benzene and the additives.

(16) T. Forster, "Fluoreszenz Organischer Verbindungen," Vandenhoeck and Ruprecht, Gottingen, Germany, 1951.

(17) I. B. Berlman, "Handbook of Fluorescence Spectra of Aromatic Molecules," Academic Press, Inc., New York, N. Y., 1965.

(18) American Petroleum Institute, "Ultraviolet Spectral Data," Agricultural and Mechanical College of Texas, 1959.

(19) J. Yguerabide and M. Burton, *J. Chem. Phys.*, **37**, 1757 (1962).

## Solid State Photochemical Rearrangement of o-Nitrobenzylideneaniline

by E. Hadjoudis[1a] and E. Hayon

*Pioneering Research Laboratory, U. S. Army Natick Laboratories, Natick, Massachusetts 01760* *(Received November 17, 1969)*

The photochemical rearrangement of *o*-nitrobenzaldehyde to *o*-nitrosobenzoic acid in both the solid state and in solution was first discovered by Ciamician and Silber.[1b] An analogous photo-induced isomeric change was found[2] on irradiation of *o*-nitrobenzylideneaniline in benzene solution, resulting in the formation of *o*-nitrosobenzanilide, mp 171°.

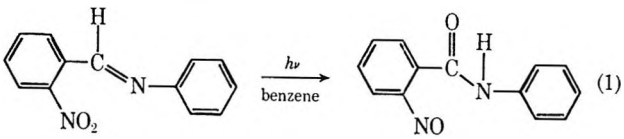

(1)

Crystalline *o*-nitrobenzylideneaniline (ONB) has been reported[3] to change into a permanent deeper colored dimorphic variety under the influence of actinic light, with a melting point 2° lower than that of the starting compound (mp 69.5°). On melting, the dimorphic variety was reported[3] to revert back to its original form.

This note will present evidence that ONB undergoes the photochemical rearrangement (1) in the crystalline state, and will clarify the nature and stability of the so-called dimorphic variety. Powdered yellow crystals of ONB were irradiated in a thin layer under a high-pressure mercury lamp (cut-off filter at 320 nm). The

(1) (a) Visiting Scientist from the Nuclear Research Center "Democritos," Athens, Greece; (b) G. Ciamician and P. Silber, *Ber. Deut. Chem. Ges.*, **34**, 2040 (1901).

(2) F. Sachs and R. Kempf, *ibid.*, **35**, 2704 (1902).

(3) A. Senier and R. Clarke, *J. Chem. Soc.*, **105**, 1917 (1914).

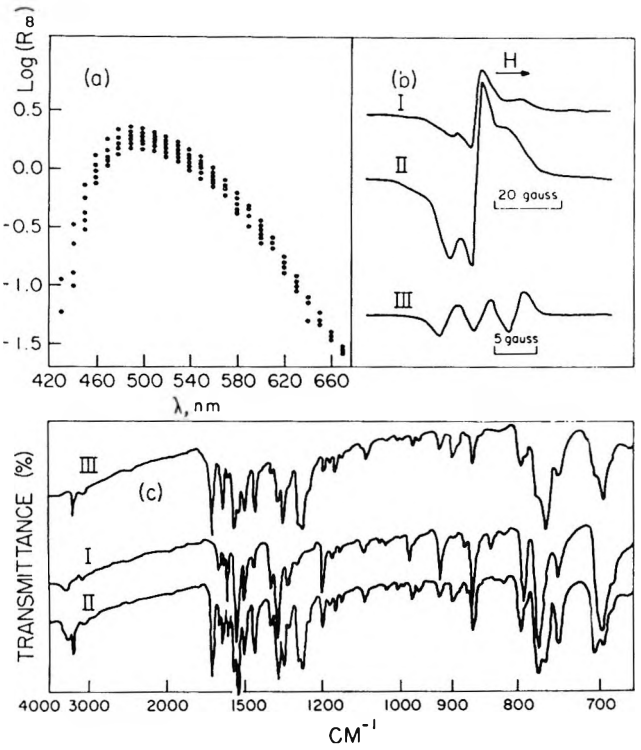


Figure 1. (a) Reflectance spectra produced on illumination for 1.5 hr of *o*-nitrobenzylideneaniline with light of $\lambda > 320$ nm: top points taken immediately after exposure, and succeeding spectra taken after standing in darkness for 8, 21, 48, 64, and 140 days, respectively. (b) Esr spectra of radicals produced on photolysis of *o*-nitrobenzylideneaniline: I, orange-red crystalline form, II, deep yellow crystalline form, III, in heptane solution ($\sim 5 \times 10^{-3}$ *M*). (c) Ir solid spectra of *o*-nitrobenzylideneaniline mp 69.5°, I; after 85 hr exposures to light, mp 120–140°, II; and of *o*-nitrosobenzanilide, mp 171°, III.

yellow color turns to orange-red and this color persists for many hours until, after about 20 hr illumination, a sudden change takes place and the orange-red color turns to a deep yellow: deep yellow spots first appear on the surface of the orange-red powder from which the new color spreads around and covers all the material in a matter of minutes, like a phase transformation under illumination. These photo-induced changes were followed using reflectance spectroscopy, esr, and ir spectroscopy.

The reflectance spectrum (using a Zeiss spectrophotometer PMQ11 with reflectance attachment) of the orange-red color is shown in Figure 1a, using the unexposed ONB as the reflectance standard and the Kubelka-Munk equation to derive[4] the spectrum, $\lambda_{max} \sim 490$ nm. The fading of the orange-red color with time is also shown (Figure 1a), and the kinetics was found to follow a first-order process with $k \sim 2.5 \times 10^{-6}$ min$^{-1}$. The infrared solid spectra of ONB, of ONB after 85 hr photolysis (deep yellow form), and of *o*-nitrosobenzanilide (prepared from the photolysis of ONB in benzene, extracted product has a mp 171°) are shown in Figure 1c. The esr spectra of radicals produced[5] on irradiation of ONB are shown in Figure 1b.

The experimental results obtained indicate that (a) the intensity of the new ir bands and the melting of the solid increase with time of irradiation. The similarity of the ir spectrum with that of *o*-nitrosobenzanilide confirms the existence of the photochemical rearrangement according to reaction 1; (b) contrary to earlier work,[3] the unphotolyzed ONB, the orange-red, and the deep-yellow forms of ONB all produce after melting a similar ir spectrum, but different from the nonmelted unphotolyzed ONB crystal; (c) in the flash photolysis[6] of ONB in heptane solutions a transient with $\lambda_{max} \sim 460$ nm is observed which is somewhat similar to the reflectance spectrum and is assigned to the quinoid form

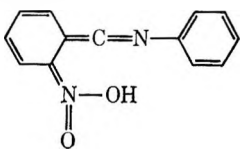


the precursor of *o*-nitrosobenzanilide. However, since the ir bands of the nitroso compound are observed in both the orange-red and deep-yellow forms, it would appear that the orange-red color is not associated with the quinoid form of ONB; (d) furthermore, the similarity of the esr spectra of both the orange-red and deep-yellow forms would indicate that the radical is not connected with the orange-red color and is probably the result of a simultaneous photochemical process.

(4) G. Kortum, M. Kortum-Seiler, and S. D. Bailey, *J. Phys. Chem.*, 66, 2439 (1962).

(5) We thank Dr. M. Arick for measuring the esr spectra.

(6) E. Hadjoudis and E. Hayon, in preparation.

## Activity Coefficients in Mixed Solutions. Prediction of Harned Coefficients from Ionic Entropies

by J. V. Leyendekkers

*Division of Fisheries and Oceanography, CSIRO, Sydney 2230, Australia* *(Received November 25, 1969)*

The Harned equations

$$\log \gamma_1/\gamma_1^0 = -\alpha_{12} I_2 \quad (1)$$

$$\log \gamma_2/\gamma_2^0 = -\alpha_{21} I_1 \quad (2)$$

apply to a large number of two-electrolyte systems.[1] Preliminary analysis of available data indicates that for a system of two electrolytes i and j with a common anion the coefficients can be estimated simply from the relationship (eq 3)

**Table I:** Conventional Ionic Entropies at 25° Computed Relative to $\bar{S}°_{H^+} = 0$ in the Hypothetical Standard State of 1 g-ion/kg of Water[1b]

| | Code | | | | | | | | | | | |
|---|---|---|---|---|---|---|---|---|---|---|---|---|
| | 1 | 2 | 3 | 4 | 5 | 6 | 7 | 8 | 9 | 10 | 11 | |
| Ion | $H^+$ | $Li^+$ | $Na^+$ | $K^+$ | $Cs^+$ | $Mg^{2+}$ | $Ca^{2+}$ | $Sr^{2+}$ | $Ba^{2+}$ | $Al^{3+}$ | $Ce^{3+}$ | $Cl^-$ |
| $\bar{S}°_i$, cal deg$^{-1}$ mol$^{-1}$ | 0 | 3.4 | 14.4 | 24.5 | 31.8 | −28.2 | −13.2 | −9.4 | 3 | −74.9 | −38.3[a] | 13.2 |

[a] Calculated from eq 4.

**Table II:** Experimental Values of Harned Coefficients at 25°

| $I$, $m$ | System 1 | System 2 | $\alpha_{12}$ | $\alpha_{21}$ | $I$, $m$ | System 1 | System 2 | $\alpha_{12}$ | $\alpha_{21}$ |
|---|---|---|---|---|---|---|---|---|---|
| 2 | HCl | LiCl | 0.005[1c] | | 2.0 | KCl | CsCl | 0.013[5b] | −0.009[5b] |
| | HCl | NaCl | 0.031 | | | KCl | $CaCl_2$[a] | −0.016[5j] | |
| | HCl | KCl | 0.0575 | | | KCl | $BaCl_2$ | −0.002[5k] | |
| | HCl | CsCl | 0.099 | | 0.1 | NaCl | $CaCl_2$ | 0.069[5l] | |
| | HCl | $SrCl_2$ | 0.058 | | 0.2 | NaCl | $CaCl_2$ | 0.036 | |
| | HCl | $BaCl_2$ | 0.0653[1c]–0.0617[5m] | | 0.5 | NaCl | $CaCl_2$ | 0.011 | |
| | HCl | $AlCl_3$ | 0.063 | | 0.7 | NaCl | KCl | 0.024[5c] | |
| | HCl | $CeCl_3$ | 0.0908 | | | NaCl | CsCl | 0.051[5d] | |
| | LiCl | NaCl | 0.031[5a] | −0.037[5a] | | NaCl | $MgCl_2$ | −0.019[5e,f] | |
| | LiCl | KCl | 0.067 | −0.032 | | NaCl | $CaCl_2$ | −0.01[5g] | |
| | LiCl | CsCl | 0.111[5b] | −0.016[5b] | | NaCl | $BaCl_2$ | 0.0082[5i] | |
| | NaCl | KCl | 0.0230[5c] | −0.0084[5c] | 6 | NaCl | LiCl | −0.033[5a] | 0.042[5a] |
| | NaCl | CsCl | 0.044[5d] | −0.008[5d] | | NaCl | KCl | 0.025[5c] | |
| | NaCl | $MgCl_2$ | −0.013[5e,f] | | | NaCl | CsCl | 0.0437[5d] | −0.0033[5d] |
| | NaCl | $CaCl_2$ | −0.005[5g,h] | | | NaCl | $MgCl_2$ | −0.009[5f] | |
| | NaCl | $BaCl_2$ | 0.0111[5i] | | | NaCl | $CaCl_2$ | 0.0015[5g,h] | |

[a] Estimated from graph, ref 5j. This system does not obey Harned's rule.

$$\alpha_{ij} = a + b\bar{S}°_{ij} \quad (3)$$

where $a$ and $b$ are parameters characteristic of a given electrolyte at a given ionic strength, $I$. $\bar{S}°_{ij}$ is a function of the conventional ionic entropies, which have been computed from experimental data for a large number of ions.[1b] These entropies can be estimated from the empirical relationship[1c,2]

$$\bar{S}° = {}^3/_2R \ln W + 37 - 270|z|/r^2 \quad (4)$$

where $R$ is the gas constant, $W$ the atomic weight, $|z|$ the absolute value of the valency, and $r$ the effective radius of the ion in solution (taken as 1.0 Å more than the crystal radius for anions and 2.0 Å more for cations).

While $\bar{S}°_{ij}$ is an empirically derived function, its form was suggested by the theory of Friedman[3] and general thermodynamic considerations, the original idea being initiated by a paper of Wood, *et al.*, on enthalpies of mixing.[4] The simplest possible function was adopted, the weighted sum of the conventional entropies of the three ionic species in the mixture. The weights were chosen with the restriction that all possible pairs of ions contribute for a charge-asymmetric system whereas for a charge-symmetric system only cation–cation pair terms are nonzero. The ionic charges were considered the most appropriate quantities to use for the weights, and a suitable entropy function was found to be

$$\bar{S}°_{ij} = Z_1\bar{S}°_1 + Z_2\bar{S}°_2 + Z_3\bar{S}°_3 \quad (5)$$

the suffixes 1, 2, and 3 refer to the ions $i^+$, $j^+$, $j^-$, respectively, and

$$Z_1 = (3z_1 - z_3)(z_2 - z_1)/4(z_3 - z_1)$$

$$Z_2 = 1/z_2^2$$

$$Z_3 = 3(z_1 - z_3)(z_2 - z_1)/z_1^2(z_2 - z_3)$$

$z$ being the charge on the ion, *e.g.*, for the system NaCl–$CaCl_2$, $z_1 = +1$, $z_2 = +2$ and $z_3 = -1$, $Z_1 = -{}^1/_2$, $Z_2 = {}^1/_4$, and $Z_3 = 2$, so that

(1) (a) R. A. Robinson and R. H. Stokes, "Electrolyte Solutions," 2nd ed, Butterworth, London, 1959; (b) G. N. Lewis and M. Randall, revised by K. S. Pitzer and L. Brewer, "Thermodynamics," 2nd ed, McGraw, New York, N. Y., 1961, p 400; (c) See ref 1b, p 523; (d) H. S. Harned and B. B. Owen, "The Physical Chemistry of Electrolytic Solutions," 3rd ed, Reinhold, New York, N. Y., 1963.

(2) R. E. Powell and W. M. Latimer, *J. Chem. Phys.*, 19, 1139 (1951).

(3) H. L. Friedman, "Ionic Solution Theory," Interscience, New York, N. Y., 1962, eq 18.36.

(4) R. H. Wood, J. D. Patton, and M. Ghamkhar, *J. Phys. Chem.*, 73, 346 (1969).

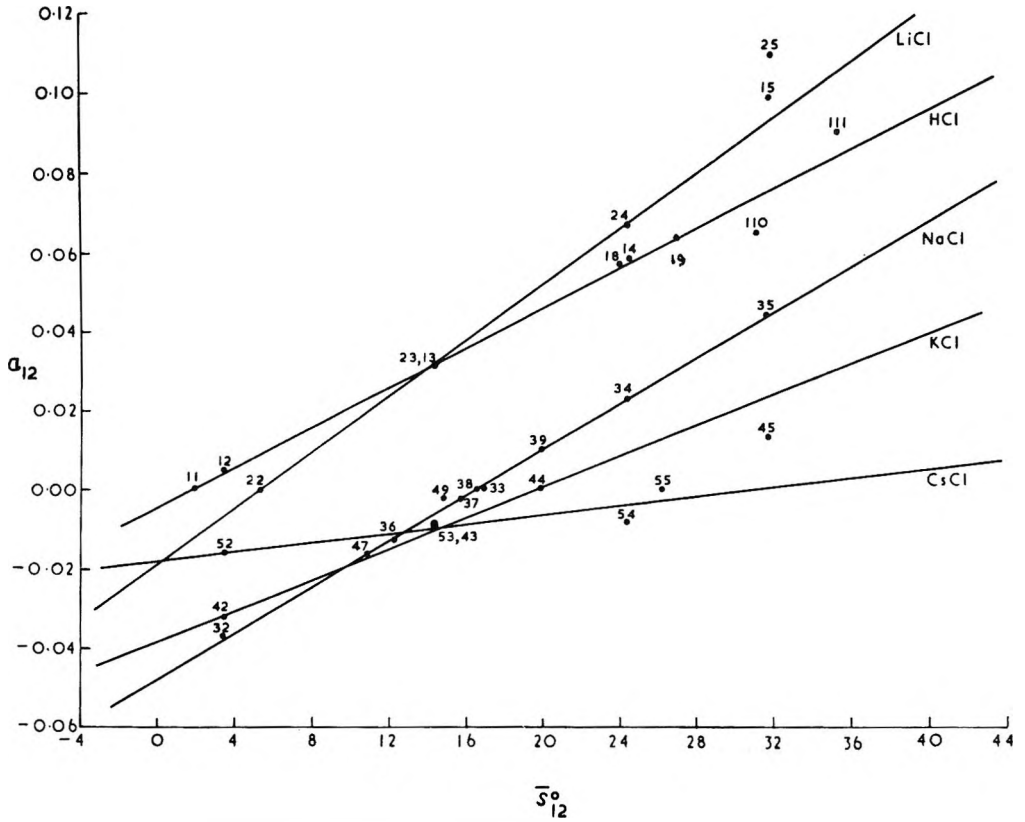


Figure 1. Harned coefficients (Table II) of five electrolytes *vs.* the ionic entropies to give the H lines characteristic of the electrolyte at $I = 2$, and at 25°. The number pairs ij refer to the electrolytes i and j as per the cation coding (Table I); *e.g.*, 39 represents the system NaCl-$BaCl_2$.

$$\bar{S}^\circ_{NaCl(CaCl_2)} = -{}^1/_2\bar{S}^\circ_{Na^+} + {}^1/_4\bar{S}^\circ_{Ca^{2+}} + 2\bar{S}^\circ_{Cl^-}$$

and for HCl–$AlCl_3$

$$\bar{S}^\circ_{HCl(AlCl_3)} = 3\bar{S}^\circ_{Cl^-} + {}^1/_9\bar{S}^\circ_{Al^{3+}}$$

since $\bar{S}^\circ_{H^+} = 0$

Values of $\bar{S}^\circ_{ij}$ have been computed for five electrolytes (the chlorides of H, Li, Na, K, and Cs) to cover a wide range of chloride systems. The entropies are listed in Table I. For the system HCl–$CeCl_3$, $\bar{S}^\circ_{Ce^{3+}}$ was computed from eq 4. $\bar{S}_{ij}{}^\circ$ values were then plotted against the experimental values of the Harned coefficients (Table II[5]) for the respective electrolyte. Figure 1 shows the results for $I = 2$. The effect of any added chloride on a particular electrolyte is neatly summarized by the characteristic line (the H line) of the electrolyte at the given ionic strength. The deviations from the line indicate a deficiency in the simple entropy functions, although eq 1 and 2 might not apply and experimental errors could also contribute. The relationships should, however, prove useful since only the ionic entropies, which are usually readily available or can be estimated from eq 4, and d(log $\gamma_{ij}$) for a few "interfering" cations are required to construct the H line. The Harned coefficients for the electrolyte with any other chloride can then be predicted with reasonable accuracy from this line. At least, this is what the preliminary results suggest and extension to other more complicated systems seems feasible.[6] An important advantage is that information on the single electrolyte is not required for the prediction of the Harned coefficients; frequently it is only the change of the activity coefficient with solution composition that is required rather than its absolute value.

The point on the H line representing the limiting case of the single electrolyte solution might be expected to have the coordinates ($\bar{S}^\circ_{i^+}$,0). However, this is not the case and it is necessary to apply a correction to the standard-state entropy. This shift in the coordinate is interpreted as arising from solvent modification by i, the

(5) (a) R. A. Robinson and C. K. Lim, *Trans. Faraday Soc.*, **49**, 1144 (1953); (b) R. M. Rush and R. A. Robinson, *J. Tenn. Acad. Sci.*, **43**, 22 (1968); (c) R. A. Robinson, *J. Phys. Chem.*, **65**, 662 (1961); (d) R. A. Robinson, *J. Amer. Chem. Soc.*, **74**, 6035 (1952); (e) Y. C. Wu, R. M. Rush, and G. Scatchard, *J. Phys. Chem.*, **72**, 4048 (1968); (f) R. F. Platford, *ibid.*, 4053 (1968); (g) R. A. Robinson and V. E. Bower, *J. Res. Nat. Bur. Stand., Sect A*, **70**, 313 (1966); (h) R. D. Lanier, *J. Phys. Chem.*, **69**, 3992 (1965); (i) R. A. Robinson and V. E. Bower, *J. Res. Nat. Bur. Stand., Sect A*, **69**, 19 (1965); (j) R. A. Robinson and A. K. Covington, *ibid.*, **72**, 239 (1968); (k) R. A. Robinson and V. E. Bower, *ibid.*, **69**, 439 (1965); (l) E. W. Moore and J. W. Ross, *J. Appl. Physiol.*, **20**, 1332 (1965); (m) H. S. Harned and R. A. Robinson, "Multicomponent Electrolyte Solutions," Pergamon, London, 1968, p 66.

(6) (a) C. M. Criss, R. P. Held, and E. Luksha, *J. Phys. Chem.*, **72**, 2970 (1968); (b) F. Franks and D. S. Reid, *ibid.*, **73**, 3152 (1969). Extension to mixed solvents seems feasible too in view of the work of these authors.

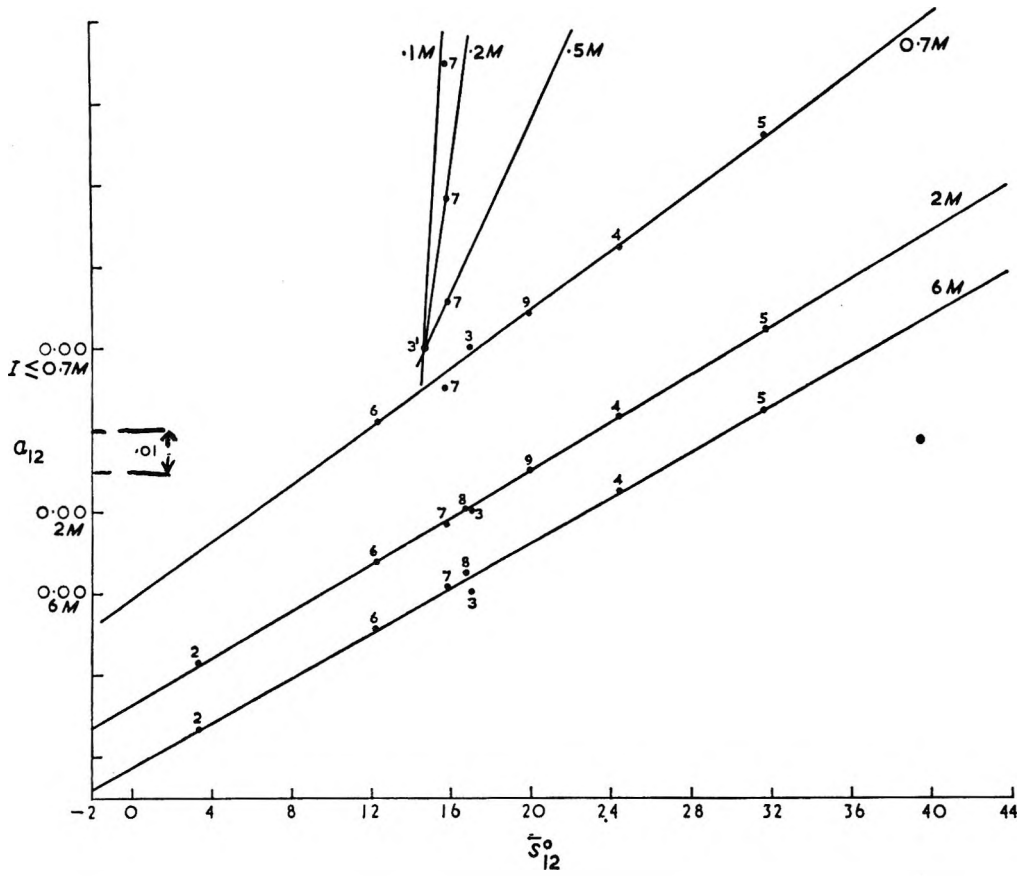


Figure 2. The H lines of NaCl for different ionic strengths. The lines have been spaced out for clarity as indicated by the respective zero ordinate. The temperature is 25°. The numbers represent the added cation chloride as coded in Table I.

water structure is altered and hence there is a change in the entropy of solution of all the j electrolytes. Below a certain ionic strength (say 0.5 $M$) this effect would probably be small. A reasonably accurate prediction of $\bar{S}^\circ_{ii}$ would be useful when only one or two experimental points are available; hence I have chosen what seems an appropriate variable, the "structure-breaking entropy," $\Delta\bar{S}^{st}$, defined by Frank and Evans,[7,8] (Table III), and a simple linear form to derive the equation

**Table III:** Values of the "Structure-Breaking Entropy"[1a]

| | Ion | | | | | |
|---|---|---|---|---|---|---|
| | $Li^+$ | $H^+$ | $Na^+$ | $K^+$ | $Cs^+$ | $Cl^-$ |
| $\Delta\bar{S}^{st}$ | −1.1 | 0 | +4 | +12.0 | +15.7 | +10.2 |

$$\bar{S}^\circ_{ii} = \bar{S}^\circ_{i+} - c(\Delta\bar{S}^{st}_{i-} + \Delta\bar{S}^{st}_{i+}) \qquad (6)$$

where $c$, for the data used here, has a value of 0.2 and is negative for structure makers ($Li^+$, $H^+$, $Na^+$) and positive for structure breakers ($K^+$, $Cs^+$).

Figure 2 illustrates the effect of changing ionic strength on the slope of the H lines of sodium chloride. The 0.7 $M$ line should be of particular interest in the oceanographic field. The lines at $I < 0.7$ $M$ have been derived from only one experimental system since, as far as I know, there are no other suitable data available. In addition, the assumption that $\bar{S}^\circ_{ii} = \bar{S}^\circ_{i+}$ was made. If these lines represent the true situation then it appears that at very low ionic strengths the Harned coefficients become either very small (*e.g.*, for the chlorides of Mg, Li, and H) or very large (*e.g.*, for the chlorides of Ca, Ba, K, Cs, etc.).

The basic function of the H lines is expected to be simple prediction of the Harned coefficients, and because of the form of the eq 3 and 4 it is hoped that the theory can be extended to systems at other temperatures and pressures and to investigations of single ion activity coefficients in mixed solutions. However, the relationship of the Harned coefficients to other important thermodynamic quantities such as the free energy should extend the usefulness of the H lines, especially when the underlying theory is worked out.

Finally, it is emphasized that the conclusions reached here are only introductory[9] the main aim being to bring the relationships to general attention and stimulate

(7) H. S. Frank and M. W. Evans, *J. Chem. Phys.*, **13**, 507 (1945).

(8) See ref 1a, p 16.

(9) (a) Data for 2:1/2:1 electrolyte systems are very few but these electrolytes also have characteristic H lines. Data are given by: (b) Souheng Wu, Ph.D. Thesis, University of Kansas, University Microfilms, Inc., Ann Arbor, Mich., 1965; (c) R. A. Robinson and V. E. Bower, *J. Res. Nat. Bur. Stand., Sect. A*, **70**, 305 (1966).

interest in mixed electrolyte solutions. Many more data are needed to test the general applicability of the relationships in lieu of any rigorous theoretical basis. The data are very incomplete even for 1:1 electrolyte systems; measurements (made during the 1930's) on the well-quoted HCl–alkali halide systems being still limited to only one of the components, *viz.* HCl.

## Physical Adsorption of Vapors on Ice. III. Argon, Nitrogen, and Carbon Monoxide

by N. K. Nair and Arthur W. Adamson

*Department of Chemistry, University of Southern California, Los Angeles, California 90007* *(Received November 25, 1969)*

Previous investigations in this laboratory have shown that ice powder acts as a low-energy adsorbent toward nitrogen at 77°K,[1] as do also a number of other molecular solids.[2] These last results appeared to set a rather low maximum to the level of dispersion interaction between small molecules in an adsorbent–adsorbate situation. There remained the possibility, however, especially in the case of ice, that classical electrostatic interactions were still making a major contribution through the presence of surface dipoles. The purpose of the present study was to examine this possibility through the use of a series of cryoscopically similar but electrically different adsorbates. Thus carbon monoxide possesses both dipole and quadrupole moments, nitrogen only the latter, and argon neither.

The ice sample was prepared by directing a fine spray of superheated steam into liquid nitrogen[3] and were not allowed to warm beyond liquid oxygen temperature. The adsorption measurements and related procedures were essentially as previously described.[1-3] The gases were supplied by the Matheson Co., with minimum purity specifications of greater than 99.99%.

A set of adsorption isotherms is shown in Figure 1. There was no hysteresis and the samples were surface stable to repeated adsorption–desorption experiments. For example, the original 77.3°K nitrogen isotherm was duplicated following the 90.1°K carbon monoxide isotherm. The BET equation was well obeyed and gave $v_m$ values of 7.8 ($N_2$), 6.9 (Ar), and 8.4 (CO) in $cm^3$ (STP)/g. Further, the characteristic isotherm[4,5] plots were closely superimposable for $P/P_0 > 0.35$: they gave $v_m$ values of 6.7 (Ar) and 8.0 (CO) relative to closely 7.8 $cm^3$ (STP)/g for nitrogen, assuming the three adsorbates have the same molecular density in the multilayer region. However, argon may not be able to pack so closely as do the other two adsorbates, since the specific surface areas obtained were ($m^2$/g): 33.8 ($N_2$), 25.6 (Ar), 36.1 (CO). These were calculated

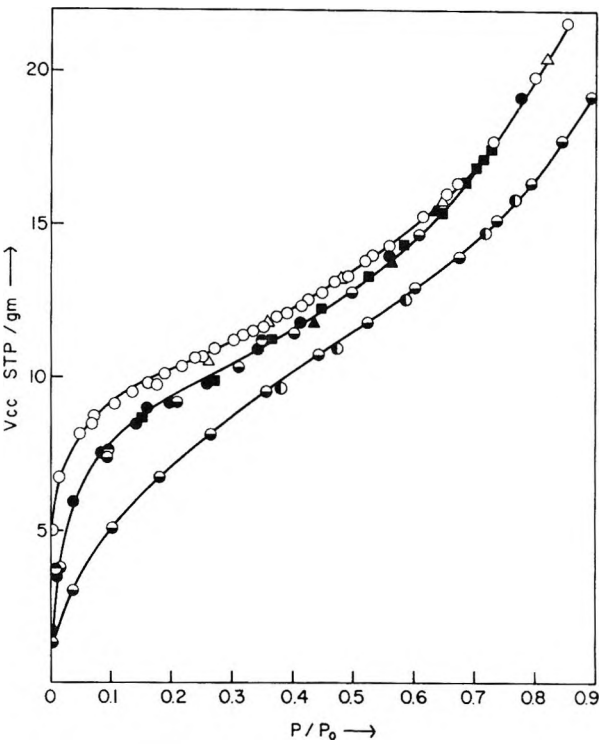


Figure 1. Adsorption isotherms for nitrogen, argon, and carbon monoxide on ice at 77°K. Nitrogen: ●, adsorption; ▲, desorption; ■, adsorption following 90.1°K nitrogen isotherm; ◓, adsorption following 90.1°K argon isotherm; ◒, adsorption following 90.1°K carbon monoxide isotherm. Argon: ◑, adsorption; ◐, desorption. Carbon monoxide: ○, adsorption; △, desorption.

using the BET $v_m$ values and equivalent spherical cross sections (based on the adsorbate liquid densities) of 16.2 ($N_2$), 13.8 (Ar), and 16.0 (CO) Å$^2$.

Of more direct interest to the purpose of the investigation is the relative behavior in the submonolayer region. Figure 2 shows the variations with surface coverage of the isosteric heats and partial molar entropies of adsorption, as determined from pairs of isotherms at 77.3 and 90.1°K, both relative to the gas phase at 1 atm. The plots for nitrogen are very similar to those previously reported for nonannealed ice.[1] Also the $q_{st}$ plots are reasonably consistent with the average heats of adsorption as given by BET c values of 85 ($N_2$), 17 (Ar), and 183 (CO).

In comparing the behavior of the three adsorbates it is instructive to consider their physical properties, summarized in Table I. First, the $q_{st}$ plots for nitrogen and argon show the former to interact slightly more strongly than the latter, as would be expected from the 6%

(1) A. W. Adamson, L. M. Dormant, and M. Oren, *J. Colloid Interface Sci.*, **25**, 206 (1967).

(2) L. M. Dormant and A. W. Adamson, *ibid.*, **28**, 459 (1968).

(3) M. Oren and A. W. Adamson, Preprints of the 43rd National Colloid Symposium, Cleveland, Ohio, 1969.

(4) A. W. Adamson, "The Physical Chemistry of Surfaces," 2nd ed, Interscience Publishers, New York, N. Y., 1967, p 604.

(5) C. Pierce, *J. Phys. Chem.*, **72**, 3673 (1968).

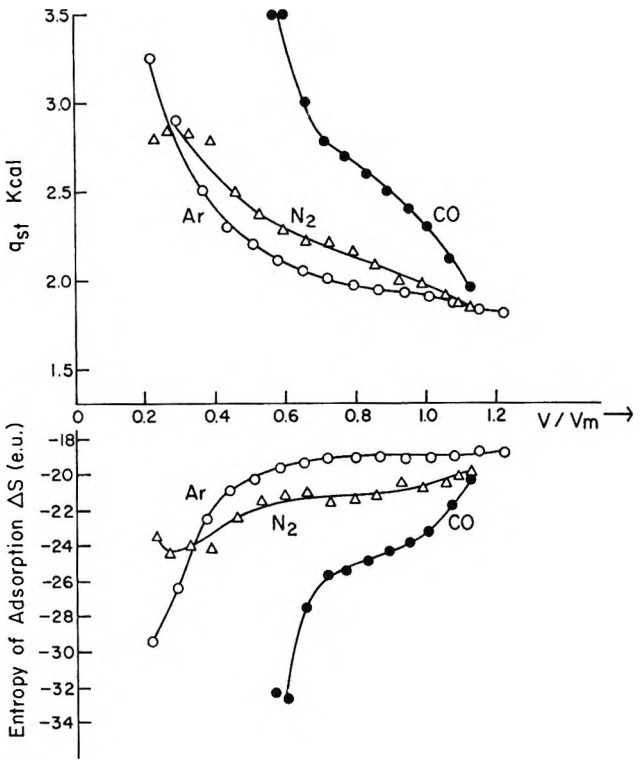


Figure 2. Top: isosteric heats of adsorption relative to gas phase. Bottom: partial molar adsorption entropies, as given by $-T\Delta S = q_{st} + RT \ln P$.

**Table I:** Physical Properties of Argon, Nitrogen, and Carbon Monoxide Species

| | $10^{-24}\alpha$,[a] cm³ | $\mu$,[b] D | $10^{-26}Q$,[b] esu cm² | $Q_v$,[c] kcal/mol |
|---|---|---|---|---|
| Ar | 1.63 | ... | ... | 1.55 |
| $N_2$ | 1.73 | ... | −1.4 | 1.33 |
| CO | 1.94 | 0.11 | 0.4 | 1.44 |

[a] From Landolt-Börnstein, "Zahlenwerte und Functionen," Vol. 1, Springer-Verlag, Berlin, 1951, Part 3, p 510 ff. [b] A. E. M. Keijzers, J. J. van Aarsten, and W. Prins, *J. Amer. Chem. Soc.*, **90**, 3107 (1968). [c] "International Critical Tables," McGraw-Hill Book Co., New York, N. Y., 1933; "Selected Values of Chemical Thermodynamic Properties," National Bureau of Standards Circular 500, U. S. Government Printing Office, Washington, D. C., 1952; D. K. Stull and G. C. Sinke, Advances in Chemistry Series, No. 18, American Chemical Society, Washington, D. C., 1956.

greater polarizability for nitrogen, assuming dispersion interactions only. That is, were a strong permanent surface electric field (and field gradient) present, then oriented adsorption of the nitrogen through interaction with its quadrupole moment should have led to a much increased adsorption energy. A similar experimental observation was made by Beebe and coworkers[6] in the case of Spheron 6, as contrasted with the difference of some 2 kcal/mol between the heats of adsorption of nitrogen and of argon on rutile.[7] Nitrogen quadrupole interaction was invoked in this last case.

However, the quadrupole axis is that of the molecule, and for such interaction to occur with a surface field, the adsorbed nitrogen should tend toward a surface-perpendicular orientation, at the expense of dispersion and polarization interactions. If the surface electric field is small, the surface parallel configuration might be preferred, in which case little or no contribution from the quadrupole moment would be expected.

The same reasoning applies to carbon monoxide since, judging from the $v_m$ value, the molecular orientation is the same as for nitrogen, that is, surface parallel, yet the heat of adsorption is now significantly larger. Similar behavior was found for *n*-hexane on ice[3] (above −35°); in this case it seemed clear that surface restructuring accompanied adsorption. As noted earlier,[1] the inertness of ice toward nitrogen suggests that the surface hydrogen atoms form bent hydrogen bonds between oxygens, thereby reducing the surface dipole field otherwise expected. We suggest that even the small dipole moment of carbon monoxide is sufficient to make favorable its insertion into this surface hydrogen-bonding structure. Certainly, the quite negative adsorption entropy suggests that the surface binding is rigid.

In summary, ice surface appears, on the one hand, not to have appreciable intrinsic electric fields. On the other hand, it seems capable of specific structure-sensitive interactions with all but the most nonpolar molecules.

*Acknowledgment.* This investigation was supported in part by a grant from the Air Force Office of Scientific Research (AROSR-1007-66).

(6) R. A. Beebe, J. Biscoe, W. R. Smith, and C. B. Wendell, *J. Amer. Chem. Soc.*, 69, 95 (1947).

(7) L. E. Drain and J. E. Morrison, *Trans. Faraday Soc.*, 49, 654 (1953).

## Opposite Effect of Urea and Some of Its Derivatives on Water Structure

by G. Barone, E. Rizzo, and V. Vitagliano[1]

*Istituto Chimico, Università di Napoli, Via Mezzocannone 4, 80134 Naples, Italy* *(Received December 16, 1969)*

The effect of urea on the structure of water has been the subject of contrasting opinions in recent years. The interest on this argument is mainly connected with the denaturing properties of urea on proteins and with the interpretation of denaturation processes. Some authors[2] suggested that urea might enter the

(1) This work has been carried out with the financial support of the Italian CNR.

(2) M. Abu-Hamidiyah, *J. Phys. Chem.*, 69, 2720 (1965).

water "clusters" and substitute some water molecules without appreciable steric effects. This fact should stabilize, somehow, the water structure. On the other hand, the thermodynamic properties of aqueous urea[3] and some urea derivative[4,5] solutions can be interpreted in terms of a monomer–dimer equilibrium which does not account for structuring properties of these compounds. Ultrasonic absorption and velocity in aqueous urea solutions,[6] some viscosity[7] and thermal[8] data have even shown that urea acts as a structure breaker. This fact is in agreement with a recent statistical analysis.[9] A wide discussion of the problem of water structure[10] may be found in a recent review by Eisenberg and Kauzmann.[11]

This problem has been approached by several authors through ir spectroscopy. An interesting method of studying water solutions has been suggested by Worley and Klotz,[12] who found that the ir differential spectra of dilute $H_2O$ in $D_2O$ show some well-defined absorption bands which can be attributed to the stretching of the free –OH (1416 m$\mu$) and to that of –OH interested in a hydrogen bond (1525, 1556, 1666 m$\mu$). By increasing temperature, the extinction coefficient at 1416 m$\mu$ increases, while those of the other bands decrease. A well-defined isosbestic point at 1468 m$\mu$ can be seen. The equilibrium between free and associated (–OH) in water can be studied by following the spectrum changes in this region as a function of temperature.

These authors used only the 1416 and 1556-m$\mu$ bands; they introduced a definition of "structural temperature"[13,14] of a ternary solution ($H_2O$ + $D_2O$ + solute) at a given temperature, as the temperature at which a binary ($H_2O$ + $D_2O$) mixture—with the same $H_2O$–$D_2O$ composition—has the same absorption ratio

$$R = A_{1556}/A_{1416} \qquad (1)$$

The enthalpy of the H-bond formation can be evaluated from the ratios (1) at different temperatures through eq 2

$$\log R = -\frac{\Delta H_f^\circ}{4.576}\frac{1}{T} + \text{constant} \qquad (2)$$

In a recent note from our laboratory[15] a good agreement between structural temperature values from conductivity data of KCl in hexamethylenetetramine–water solutions and Worley and Klotz ir structural temperature values has been obtained. We have applied here their technique[12] to study the effect of urea and urea derivatives on the water structure and we have found that, while urea acts as a water-breaking agent, all its derivatives act, to different extent, as water structuring agents.

## Experimental Section

Urea and monomethylurea (MMU) (C. Erba products), N,N′-dimethylurea (NN′ DMU), N,N′-diethylurea (NN′DEU), and N,N-diethylurea (NNDEU) (Fluka products) were purified by several crystallizations from ethanol (Urea and MMU) and water–ethanol mixtures.

Tetramethylurea (TMU) (Merck product) was vacuum distilled in nitrogen atmosphere and stored in a freezer. Urea and NH-containing derivatives have been deuterated by adding small amounts of $D_2O$ to a weighted amount of the compound and drying under vacuum, assuming statistical partition.[16] The $D_2O$ addition was repeated several times until the spectrum of urea solutions in $D_2O$ was identical with that of pure $D_2O$ in the 1350–1650-m$\mu$ region.[17]

Urea–$D_2O$ reference solutions and urea–($D_2O$ + 5.7% $H_2O$) running solutions were made by weight, at the same urea molar fraction. In the following, however, data have been reported as molality of ureas, where the molality is computed with respect to the $D_2O$ reference solutions. The ir differential spectra have been recorded with a Beckman DK2 spectrophotometer for each solution at several temperatures. Urea and its derivatives containing N–D groups show an ir spectrum with an additional band in the 1460–1480-m$\mu$ region which can be attributed to the partial substitution of deuterium with hydrogen in the ($D_2O$ + 5.7% $H_2O$) solutions. This band, although disturbing the isosbestic point position, does not affect appreciably the spectrum region around 1416 and 1556 m$\mu$.

## Results

In Figure 1 the "structural temperatures" of all examined solutions are given as a function of the urea molality at the experimental temperature of 25°. While urea has structural temperatures higher than

(3) R. H. Stokes, *J. Phys. Chem.*, **69**, 4012 (1965).

(4) V. Crescenzi, F. Quadrifoglio, and V. Vitagliano, *Ric. Sci.*, **37**, 529 (1967).

(5) O. D. Bonner and W. H. Breazeale, *J. Chem. Eng. Data*, 10, 325 (1965).

(6) D. V. Beauregard and R. E. Barrett, *J. Chem. Phys.*, **49**, 5241 (1968).

(7) G. A. Vidulich, J. R. Andrade, P. B. Blanchette, and T. J. Gilligan, *ibid.*, **73**, 1621 (1969).

(8) V. I. Khamova A. M. Ponomareva, and K. P. Mishchenko, *Russ. J. Phys. Chem.*, **40**, 748 (1966).

(9) H. S. Frank and F. Franks, *J. Chem. Phys.*, **48**, 4746 (1968).

(10) G. Nemethy and H. A. Sheraga, *ibid.*, **36**, 3382 (1962).

(11) D. Eisenberg and W. Kauzmann, "The Structure and Properties of Water," Clarendon Press, Oxford, 1969.

(12) J. D. Worley and I. M. Klotz, *J. Chem. Phys.*, **45**, 2868 (1966).

(13) J. D. Bernal and R. H. Fowler, *ibid.*, **1**, 515 (1933); *Usp. Fiz. Nauk*, **14**, 586 (1934).

(14) R. A. Robinson and R. H. Stokes, "Electrolyte Solutions," Butterworths and Co. (Publications) Ltd., London, 1959, p 309.

(15) G. Barone, V. Crescenzi, and V. Vitagliano, *J. Phys. Chem.*, **72**, 2588 (1968).

(16) A. E. Brodsky, *Trans. Faraday Soc.*, **33**, 1180 (1937).

(17) New bands appear in the 1650–1750-m$\mu$ region for the $D_2O$ solutions, which have been attributed to the overtones of the C–D stretching, due to a partial deuteration of the $CH_3$ and $CH_2$ activated by the neighbor carbonyl groups.[16]

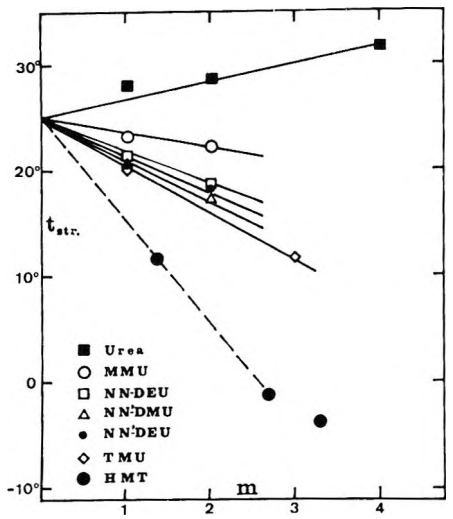


Figure 1. Structural temperatures of urea–water solutions as a function of molality. ●, HMT data of hexamethylenetetramine–water solutions taken from ref 15.

the experimental one, showing a small breaking effect on the water structure, all its derivatives act as light structuring agents, the efficiency being in the order MMU < NNDEU < NN'DMU ≃ NN'DEU < TMU. This sequence is significative since it follows the increasing amount of hydrophobic substituents.

It is interesting to note the inversion between the NN'DMU and the NNDEU that can be attributed to the fact that two ethyl groups bound to the same nitrogen atom may interact with each other and require less organized water to be solvated than two methyl groups bound to different nitrogen atoms. The effect of the ureas on the enthalpy of H-bond formation, computed through eq 2, has also been estimated and the results seem to agree with the structuring efficiency order previously given, the data reported below (Table I) are only indicative.

**Table I:** $D_2O$–$H_2O$ Mixtures[a]

| Compd | $d\Delta H_f°/dm$, (kcal/mol of OH)/(mol of solute/1000 g of $D_2O$) |
|---|---|
| Urea | 0.10 ± 0.03 |
| MMU | −0.05 ± 0.02 |
| NNDEU | −0.13 ± 0.05 |
| NN'DMU | −0.13 ± 0.05 |
| NN'DEU | −0.13 ± 0.05 |
| TMU | −0.23 ± 0.05 |

[a] $\Delta H_f°$ = −2.33 ± 0.05 kcal/mol

In connection with the opposite effect on water structure of urea and of its derivatives, we like to remember that solubility in water of hydrocarbons and nonpolar solutes as well as critical micelle concentration of surfactants is increased both by structure-breaker substances, such as urea or guanidinium salts[18–21] and by structure-maker ones, such as methylurea or hexamethylenetetramine,[22] so that both classes of compounds must weaken the hydrophobic effect, even through a different mechanism.

Protein denaturation by urea cannot be ascribed only to its effect on water structure, and specific interactions of the amino groups with the peptide chain must be taken in account; it is significative on this respect to remember the effect of urea and its derivatives on the solutions of some molecules containing several peptide links. A salting-in effect is observed which decreases by increasing the number of substituents to the amino hydrogens and which parallels decreasing denaturating power.[23] On the other hand, the increasing efficiency as denaturing agents of tetralkylammonium salts by increasing their structuring power shows the existence of a water structure effect on protein denaturation.[24] Work is in progress in our laboratory to evaluate the relative weight of both effects on the conformational stability of some proteins.

(18) D. B. Wethlaufer, S. K. Malik, L. Stoller, and R. L. Coffin, *J. Amer. Chem. Soc.*, **86**, 508 (1964).
(19) W. Bruning and A. Holtzer, *ibid.*, **83**, 4865 (1961).
(20) P. Mukerjee and A. Ray, *J. Phys. Chem.*, **67**, 190 (1963).
(21) M. J. Schick, *ibid.*, **68**, 3585 (1964).
(22) G. Barone, V. Crescenzi, A. M. Liquori, and F. Quadrifoglio, *ibid.*, **71**, 984 (1967).
(23) D. R. Robinson and W. P. Jencks, *J. Amer. Chem. Soc.*, **87**, 2462 (1965).
(24) P. H. Von Hippel and K. I. Wong, *J. Biol. Chem.*, **240**, 3905 (1965).

## Nuclear Magnetic Resonance of Aqueous Solutions of Sodium Perrhenate

by R. A. Dwek, Z. Luz, and M. Shporer

*Isotope Department, Weizmann Institute of Science, Rehovot, Israel* (*Received December 29, 1969*)

In the present note we report nmr measurements on aqueous solutions of $NaReO_4$. The nmr spectrum of the two magnetic rhenium isotopes was recorded using the broad line method at a field of ~14 kG. The following values for $1/T_2$ (in $sec^{-1}$) were obtained for a 0.8 $M$ solution at room temperature: $^{185}Re$, 4.5 × $10^4$; $^{187}Re$, 4.25 × $10^4$. These values are exceedingly large and may only arise from quadrupolar relaxation. Broadening due to chemical exchange can be ruled out since an unlikely large chemical shift between the exchanging rhenium species would have to be assumed; moreover, from the decrease of the Re line width with

temperature (measured between 25 and 93°) an activation energy of 3.4 kcal/mol has been calculated. This value is consistent with a rotational tumbling process but is too low for a chemical exchange reaction. Also the widths of the two Re isotopes are proportional to the square of their quadrupolar moments as expected if the relaxation is governed by quadrupolar interaction. On the other hand, the possibility that the relaxation is *via* interaction with paramagnetic impurities is excluded because they would affect the $^{17}O$ and $^{1}H$ resonances of $ReO_4^-$ and solvent water contrary to the experimental observations.

From the Re nmr line width the Re quadrupolar interaction (QI) constant can be calculated using the equation[1]

$$\frac{1}{T_2} = \frac{3}{125}\left(\frac{e^2qQ}{h}\right)^2\tau \qquad (1)$$

where cylindrical symmetry of the QI tensor is assumed. If we assume that the relaxation is due to rotational tumbling, $\tau$ is the tumbling time of the complex and may be calculated from Debye's relation: $\tau = (4\pi a^3\eta/3kT) = 1.2 \times 10^{-11}$ sec (where the radius $a$ is taken[2,3] as 2.3 Å). From this value and the experimental result for $1/T_2$ the QI constant of $^{187}Re$ is calculated to be $(e^2qQ/h) \simeq 60$ Mhz. This value is about one-third of the value found by Rogers and Rao in solid $KReO_4$.[4]

The question now arises as to the origin of the Re QI in the $ReO_4^-$ solution, *i.e.*, whether it is due to ion pairing, solvation effects, or to an intrinsic distortion of the $ReO_4^-$ ion. To test these possibilities the following observations were made. (a) The Re nmr line width was found to be independent of the $NaReO_4$ concentration within the range 0.25 *M* to 1.2 *M*. (b) Addition of up to 2 *M* NaCl to a 1 *M* aqueous solution of $NaReO_4$ had no effect on the observed Re nmr line width. (c) The line width was independent of pH in the range pH 1–13. (d) $Na^+$ longitudinal relaxation times were measured at a field of 7 kG using the pulse method. The results for $1/T_1$ in a 1 *M* solution of $NaReO_4$ and NaCl were 27 $sec^{-1}$ and 20 $sec^{-1}$, respectively. (e) The $^{17}O$ nmr spectrum in a 1 *M* $NaReO_4$ solution (containing ~10 atom % $^{17}O$) consisted of the bulk water line and only one additional line shifted to low field by 579 ppm (*cf.* Figgis, *et al.*[5]). The widths of the peaks were: $1/T_2(H_2O) = 160$ $sec^{-1}$ and $1/T_2(Re^{17}O_4) = 210$ $sec^{-1}$, and the ratio of the integrated intensities of the two signals was consistent with having four oxygen atoms per $NaReO_4$ molecule in the solution.

These results indicate that ion pairing is not responsible for the QI, for if this were the case the broadening of the Re would depend on the concentration of the electrolytes, or if ion pairing were complete, even in the most dilute solution, the sodium relaxation time would have been significantly affected too. (The difference in $1/T_1$ of Na between the NaCl and $NaReO_4$ solutions is of the order commonly observed in aqueous solutions of sodium salts.)[6] It seems quite certain that there is no permanent distortion from tetrahedral symmetry of the $ReO_4^-$ ion in solution. This conclusion rests on ir, Raman, and uv and visible studies.[7-11] It is, however, possible that the QI arises from loosely bound solvent molecules having a very short lifetime in the solvation shell. These complexes may be thought of as "collision complexes" which cause an instantaneous distortion of the tetrahedron. If this is so, then the correlation time to be used in eq 1 might well be shorter than $10^{-11}$ sec and the result for $e^2Qq/h$ (which in this model is the root mean square value of the QI) correspondingly higher. A similar interpretation was previously offered for the quadrupolar relaxation of Mn in aqueous solution of $MnO_4^-$.[12] There it was found that $1/T_1(Mn) \simeq 20$ $sec^{-1}$. If the relaxation mechanism of the central atoms in both $XO_4^-$ ions were analogous, one would expect the ratio of their relaxation rate to be as the square of the quadrupole interaction in compounds of similar structure. Examination of quadrupole resonance data shows this ratio to be around 100,[13] and in at least one case about 1000.[14] (These values are considerably larger than the ratio of the square of the quadrupole moments, apparently due to the greater electronic polarization of Re relative to Mn.) The ratios of the $1/T_1$'s is, however, ~2000 which is significantly higher.

*Acknowledgment.* R. A. D. is indebted to the Royal Society for a travel grant to Israel and to the Weizmann Institute for hospitality during the summer of 1969.

(1) A. Abragam, "The Principles of Nuclear Magnetism," Oxford University Press, Oxford, 1960, Chapter VIII.

(2) The value 2.3 Å was taken as the sum of the Re–O distance[4] (1.7 Å) and the oxygen ionic radius (0.6 Å).

(3) J. C. Marrow, *Acta Cryst.*, **13**, 443 (1960).

(4) M. T. Rogers and K. V. S. Rama Rao, *J. Chem. Phys.*, **44**, 1229 (1968).

(5) B. N. Figgis, R. G. Kidd, and R. S. Nyholm, *Proc. Roy. Soc., Ser. A*, **269**, 468 (1962).

(6) M. Eisenstadt and H. L. Friedman, *J. Chem. Phys.*, **44**, 1407 (1962).

(7) L. A. Woodward and H. L. Roberts, *Trans. Faraday Soc.*, **52**, 615 (1956); L. A. Woodward, *ibid.*, **54**, 1271 (1958).

(8) H. H. Classen and A. J. Zielen, *J. Chem. Phys.*, **22**, 707 (1954).

(9) R. H. Busey and O. L. Keller, Jr., *ibid.*, **41**, 215 (1961).

(10) E. J. Wells, A. D. Jordan, D. S. Alderdice, and I. G. Ross, *Aust. J. Chem.*, **20**, 2315 (1967).

(11) G. E. Boyd, *J. Chem. Educ.*, **36**, 3 (1959).

(12) M. Broze and Z. Luz, *J. Phys. Chem.*, **73**, 1600 (1969).

(13) A. N. Nesmeyanov, G. K. Semin, E. V. Bryuchova, T. A. Babushkina, K. N. Anisimov, N. E. Kolobova, and Yu. V. Makarov, *Tetrahedron Lett.*, **37**, 3987 (1968).

(14) E. A. C. Lucken, "XIVth Colloque Ampere, Ljubljana, 1966," R. Blinc, Ed., North-Holland Publishing Company, Amsterdam, 1967, p 1121; S. Segel and R. Barnus, *Phys. Rev.*, **107**, 638 (1957).

## On the Competition between Unimolecular Dissociation and Ion–Molecule Reaction of *cis*-2-Butene Molecular Ions

by Stephen J. Wisniewski, Roger P. Clow, and Jean H. Futrell[1a,b]

*Department of Chemistry, University of Utah, Salt Lake City, Utah 84112* *(Received December 29, 1969)*

A number of recent papers have been concerned with ion–molecule reactions of unsaturated compounds.[2-5] A frequent observation for these systems is an apparent inhibition period before a substantial amount of reaction of the molecular ion is reflected through a decrease in the intensity of that ion; occasionally, there is even an increase in the intensity of the ion such that it goes through a maximum as a function of pressure of the neutral species in the mass spectrometer ion source.[2c,4a] Generally, it has been possible to account for these features by invoking an essentially charge exchange reaction of certain fragment ions from these systems with the neutral molecule. In some cases it has been demonstrated unequivocally through studies involving a tandem mass spectrometer that this is the correct interpretation.[2] One recent report of ion–molecule reactions in the isomeric butenes[2c] demonstrated, however, that the initial increase of the parent ion, $C_4H_8^+$, in *cis*-2-butene is much greater than could be accounted for by charge exchange. Both *cis*- and *trans*-2-butene reflect a very large increase in intensity of the parent ion; in the *cis* isomer, it increases by about 17% of total ionization. This behavior is illustrated in Figure 1, which shows the dependence of ion intensity for the major ions of *cis*-butene on pressure in the ion source as observed in a high-pressure time-of-flight mass spectrometer.[2c]

These workers postulated that the initial increase in parent *cis*-2-butene occurred *via* collisional stabilization of excited parent ions, reflecting the competition between the primary decomposition reaction

$$C_4H_8^{+\prime\prime} \longrightarrow \text{fragments} \qquad (1)$$

and collisional stabilization of vibronically excited molecular ions

$$C_4H_8^{+\prime\prime} + C_4H_8 \longrightarrow C_4H_8^{+\prime} + C_4H_8 \qquad (2)$$

It is likely that this effect is particularly pronounced for the *cis*-2-butene molecular ion because the cross section for subsequent ion–molecule reactions consuming $C_4H_8^+$ is somewhat lower than for molecular ions from the other butene isomers.

Figure 1 illustrates the pressure dependence of the major ions, as observed in the high-pressure mass spectrometer. The observation for the butene isomers of intense metastable ions[2c] and theoretical considerations[6] both suggest that long-lived vibronically excited states are anticipated as a general feature for unsaturated systems. If this explanation is correct, however, it implies relatively specialized conditions for the competition to be observed in the case of the *cis* isomer and not for other butenes. Specifically, it calls for a fairly close match between the rates of the unimolecular

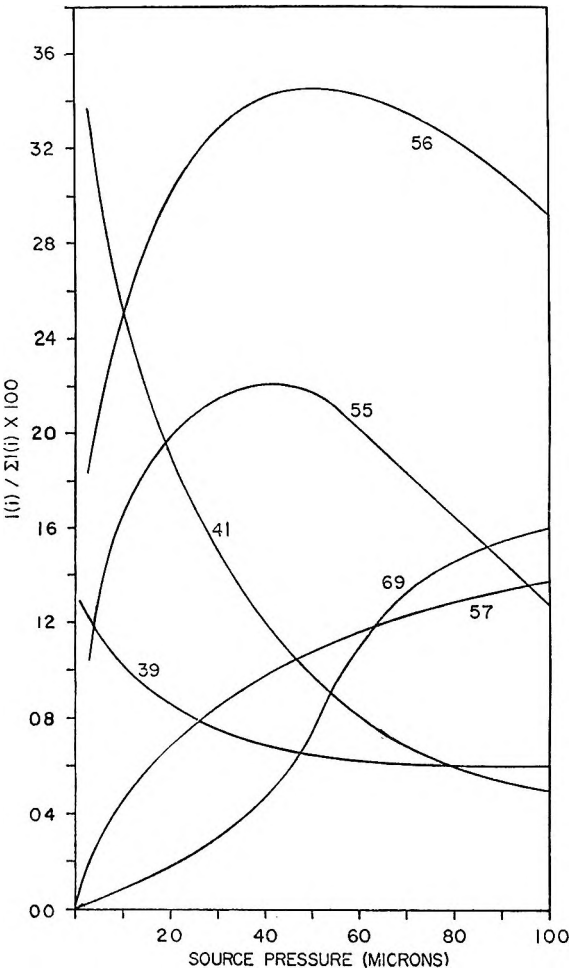


Figure 1. Pressure dependence of major ions in the mass spectrum of *cis*-2-butene. High-pressure study in conventional mass spectrometer, data of ref 2c.

(1) (a) Alfred P. Sloan Fellow, 1968–1970. (b) This investigation was supported in part by a Public Health Service Research Career Development Award, 1 KO4 GM42390-01 GMK, from the National Institute of General Medical Sciences.

(2) (a) J. H. Futrell and T. O. Tiernan, *J. Phys. Chem.*, **72**, 158 (1968); (b) T. O. Tiernan and J. H. Futrell, *ibid.*, **72**, 3080 (1968); (c) F. P. Abramson and J. H. Futrell, *ibid.*, **72**, 1994 (1968); (d) B. M. Hughes, T. O. Tiernan, and J. H. Futrell, *ibid.*, **73**, 829 (1969).

(3) A. G. Harrison, *Can. J. Chem.*, **41**, 236 (1962); A. A. Herod and A. G. Harrison, *J. Phys. Chem.*, **73**, 3189 (1969); J. J. Myher and A. G. Harrison, *Can. J. Chem.*, **46**, 101 (1968); J. J. Myher and A. G. Harrison, *J. Phys. Chem.*, **72**, 1905 (1968).

(4) (a) V. Aquilanti, A. Galli, A. Giardini-Guidoni, and G. G. Volpi, *Trans. Faraday Soc.*, **63**, 926 (1967); (b) S. Wexler, A. Lifshitz, and A. Quattrochi, Advances in Chemistry Series, No. 58, American Chemical Society, Washington, D. C., 1966, p 193.

(5) J. L. Beauchamp, L. R. Andrews, and J. D. Baldeschwieler, *J. Amer. Chem. Soc.*, **89**, 4569 (1967).

(6) M. Vestal, personal communication.

dissociation (reaction 1) and the collision frequency of the stabilization reaction 2 under the conditions of the experiment illustrated in Figure 1. Consequently, one would not expect that the same type of behavior—observed in at least two high pressure mass spectrometer experiments—would also maintain, if one could change the time scale of the apparatus significantly.

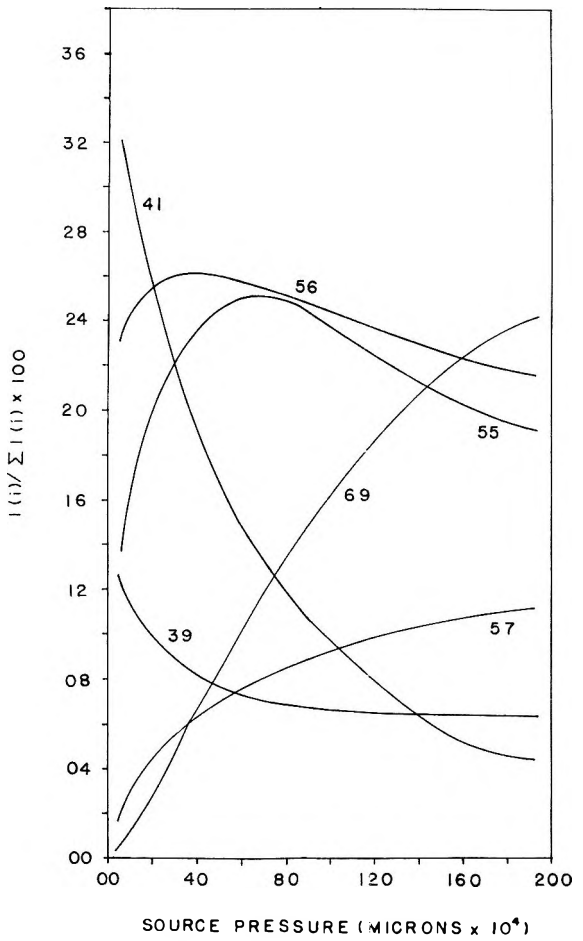


Figure 2. Pressure dependence of major ions in the mass spectrum of *cis*-2-butene. Ion cyclotron resonance study.

A new technique for the study of ion–molecule reactions, ion cyclotron resonance,[7] is characterized by a very different time scale from conventional mass spectrometer ion sources. Typically, ion lifetimes in an ion cyclotron resonance experiment range from 1 to several msec, while ion source residence times for conventional instruments vary from less than 1 μsec to perhaps 10 μsec. Thus, if the lifetime of the ionic species undergoing reaction is a significant variable, one would anticipate both qualitative and quantitative differences in the ion–molecule reaction chemistry, as studied by ion cyclotron resonance and by conventional magnetic or time-of-flight mass spectrometry. That this is indeed the case is reflected by Figure 2, which displays the dependence of the same major ion species in the *cis*-2-butene system on pressure in an ion cyclotron resonance experiment.

The pressure scale in the ion cyclotron resonance experiment is of course very different from that in the conventional high-pressure experiment because of the very different ion residence time in the apparatus. The key feature of the present results is that the collision frequency is lower by about two orders of magnitude, so that the ensemble of molecular ion states with lifetimes in the neighborhood of 1 μsec have all decayed before stabilizing collisions can occur. In the above reaction scheme, reaction 1 should compete much more effectively with reaction 2 in an ICR experiment. Therefore, one would anticipate that the parent ion intensity would increase by a much smaller amount than in a conventional ion–molecule reaction study. That this is the case is amply demonstrated by Figure 2. Here the behavior is qualitatively the same as those of the other butenes in the conventional experiments,[2c] and the extent of collisional stabilization in eq 2 is so much reduced that it is not detectable in the present results.

These experiments were run in an ion cyclotron resonance apparatus, which has been described previously[8] using source, reaction zone, and analyzer drift fields of 0.76, 0.38, and 0.16 V/cm, respectively. The total ion current was maintained at $1.5 \times 10^{-13}$ A to minimize complications of space charge, and the intensities of the observed ions were corrected for mass dependence of power absorption[9] and for the change in ion residence time as the spectrum is developed by sweeping magnetically. Rate constants deduced from a semi-log plot of the data of Figure 2 are in agreement within a factor of 3 of rates deduced by Abramson and Futrell.[2c]

We therefore conclude that the postulated competition between unimolecular dissociation and subsequent reaction is indeed the proper explanation for the substantial increase in parent-ion intensity noted previously for *cis*-2-butene. We believe that this is the first example which has shown explicitly the effects of lifetime of a reactive ion and, hence, the significance of collision frequency in an ion–molecule reaction experiment. Now that the ion cyclotron resonance method is being used extensively for the study of these reactions, we think it likely that a number of additional examples will be found.

*Acknowledgment.* This research was supported by the Aerospace Research Laboratories, Contract F33-615-68-C-1022. Their assistance is greatfully acknowledged.

(7) J. D. Baldeschwieler, *Science*, **159**, 263 (1968).

(8) R. P. Clow and J. H. Futrell, *Int. J. of Mass Spectrom. Ion Phys.*, in press.

(9) P. Llewellyn, K. R. Jennings, and J. H. Futrell, to be published.

## The Electron Spin Resonance Spectra of the Dibenzo[b,f]thiepin Sulfoxide and Thioxanthone Sulfoxide Anion Radicals

by A. Trifunac and E. T. Kaiser[1]

*Searle Chemistry Laboratory, University of Chicago, Chicago, Illinois 60637* *(Received January 7, 1970)*

The anion radicals of thioxanthone sulfoxide and dibenzo[b,f]thiepin sulfoxide have now been prepared in 1,2-dimethoxyethane solution by potassium metal reduction. The esr spectra of the radicals were recorded and proton coupling constants were assigned by examining the esr spectra of anion radicals formed from several methyl-substituted derivatives of the sulfoxides.

The esr spectra of the anion radicals of thioxanthone, thioxanthone sulfone, and dibenzo[b,f]thiepin have been reported and discussed.[2-7] In the case of the thioxanthone system attention was focused[3,4,6] on the influence of changes in the oxidation state of sulfur on the magnitude of the proton coupling constants measured from the esr spectra of the radicals. Considerable information is now available on the comparison of radicals formed from aromatic sulfides and aromatic sulfones,[6] but few aromatic sulfoxide anion radicals have been studied in the past largely because suitable syntheses for the appropriate sulfoxides had not been developed. The sulfoxide of thioxanthone was described recently[8] so we were encouraged to embark on an investigation of the preparation and characterization of the corresponding anion radical as well as that of dibenzo[b,f]thiepin sulfoxide.

### Experimental Section

Radicals were prepared by potassium metal reduction in 1,2-dimethoxyethane (DME) solutions using the usual high-vacuum techniques.[9] Esr spectra were recorded at −50° since radicals were found to decompose at higher temperatures. A Varian Model V4500 spectrometer equipped with a 9-in. magnet and Fieldial control was used for these measurements.

*Preparation of Compounds.* Thioxanthone was obtained from Aldrich and was used without further purification. 4-Methyl-, 1,4-dimethyl-, and 2,4-dimethylthioxanthone were prepared by the method of Marsden and Smiles.[10] The preparation of the dibenzothiepins used as precursors to obtain the corresponding sulfoxides has been described.[7] The sulfoxides were all prepared by the oxidation of the sulfides with iodosobenzene diacetate by the method of Castrillon and Szmant,[8] and they were purified by chromatography on silica gel and recrystallization from methanol or ethanol. Satisfactory analyses and mass spectra were obtained for the sulfoxides.

### Results and Discussion

The structures of thioxanthone sulfoxide and dibenzo[b,f]thiepin sulfoxide are shown in formulas I and II, respectively, together with the appropriate numbering of the ring positions.

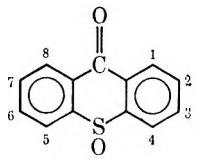

I

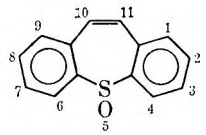

II

The esr spectrum of the anion radical of thioxanthone sulfoxide prepared by potassium metal reduction in 1,2-dimethoxyethane solvent is shown in Figure 1. Table I lists the coupling constants measured from this spectrum. The assignment of proton coupling constants was done by examining the esr spectra of anion radicals prepared from 4-methyl-, 2,4-dimethyl-, and 1,4-dimethylthioxanthone sulfoxide. The assignment is based on the fact that $Q_{CH_3}$ is about equal to $Q_H$ for most aromatic systems. Thus the width of the esr spectrum of a methyl-labeled aromatic anion radical is approximately equal to the width of the parent radical plus twice the coupling constant at the position of methyl substitution. The measured widths for the spectra of the methyl-substituted anion radicals are given in Table II along with those expected on the basis of our assignments.

**Table I:** Coupling Constants from the Epr Spectrum of the Thioxanthone Sulfoxide Anion Radical

| Position | $A_H$ (K metal), G |
|---|---|
| 1 | 2.06 |
| 2 | 0.92 |
| 3 | 2.44 |
| 4 | 0.69 |
| Metal | 0.11 |

(1) Fellow of the Alfred P. Sloan Foundation.

(2) G. Vincow, *J. Chem. Phys.*, **37**, 2484 (1962).

(3) E. T. Kaiser and D. H. Eargle, Jr., *J. Amer. Chem. Soc.*, **89**, 1821 (1963).

(4) M. M. Urberg and E. T. Kaiser, *ibid.*, **89**, 5179 (1967).

(5) M. M. Urberg and C. Tempas, *ibid.*, **90**, 5477 (1968).

(6) M. M. Urberg and E. T. Kaiser, an article in "Radical Ions," E. T. Kaiser and L. Kevan, Ed., Wiley-Interscience, New York, N. Y., 1968, p 301.

(7) M. M. Urberg and E. T. Kaiser, *J. Amer. Chem. Soc.*, **89**, 5931 (1967).

(8) J. P. A. Castrillon and H. H. Szmant, *ibid.*, **89**, 976 (1967).

(9) The technique employed has been described by M. M. Urberg, Ph.D. Thesis, University of Chicago (1967).

(10) E. G. Marsden and S. Smiles, *J. Chem. Soc.*, 1353 (1911).

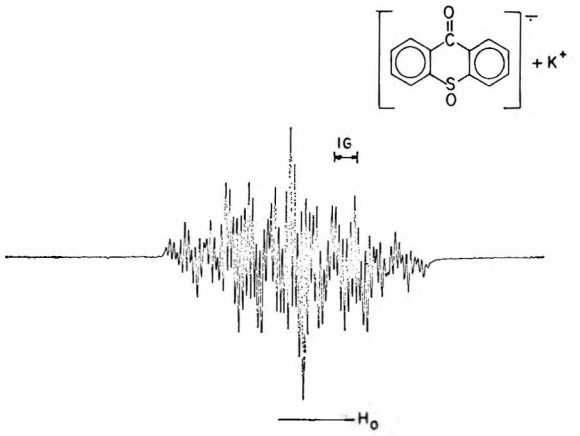


Figure 1.

**Table II:** Widths in Gauss of Epr Spectra of the Anion Radicals of Methyl-Substituted Thioxanthone Sulfoxides

| Compound | Measured | Expected |
|---|---|---|
| Thioxanthone sulfoxide | 12.2 | |
| 4-Methyl- | 12.9 | 13.6 |
| 2,4-Dimethyl- | 15.3 | 15.5 |
| 1,4-Dimethyl- | 15.85 | 17.7 |

As in the cases of the thioxanthone and thioxanthone sulfone anion radicals,[4] the coupling constants for the 1 and 3 portions of the aromatic rings are large relative to those for the 2 and 4 positions. It is interesting that the total width of the spectrum of the thioxanthone sulfoxide radical (Table II) is somewhat less than that observed previously for the sulfone species (13.6 G).[4] A possible qualitative interpretation of this observation might be that the sulfoxide group withdraws unpaired electron density from the outer aromatic rings of the thioxanthone system to at least as great an extent as the sulfone group does.[11] The esr spectra of the anion radicals obtained from the methyl-substituted compounds were not sufficiently resolved to permit their detailed analysis.

The esr spectrum of the anion radical prepared by potassium metal reduction of dibenzo[*b*,*f*]thiepin sulfoxide is shown in Figure 2. Table III lists the coupling constants measured from this spectrum. The assignment of the coupling constants was based on an examination of the esr spectra of the anion radicals prepared from 1,4-dimethyl-, 2,4-dimethyl-, and 10,11-dimethyldibenzo[*b*,*f*]thiepin sulfoxide. The widths of the spectra of these radicals are given in Table IV.

**Table III:** Proton Coupling Constants for the Anion Radical of Dibenzo[*b*,*f*]thiepin Sulfoxide

| Position | $A_H$ (K metal), G |
|---|---|
| 1 | 0.95 |
| 2 | 0.14 |
| 3 | 3.52 |
| 4 | 0.71 |
| 10 | 3.52 |

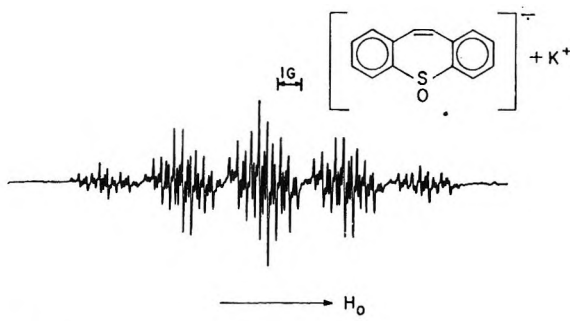


Figure 2.

**Table IV:** Widths of the Epr Spectra of Substituted Dibenzo[*b*,*f*]thiepin Sulfoxide Anion Radicals

| Compound | Spectral width, G — Measd | Exptd |
|---|---|---|
| Dibenzo[*b*,*f*]thiepin sulfoxide | 17.6 | |
| 1,4-Dimethyl-substituted sulfoxide | 22.0 | 21.0 |
| 2,4-Dimethyl-substituted sulfoxide | 19.1 | 19.4 |
| 10,11-Dimethyl-substituted sulfoxide | 24.8 | 31.8 |

The spectra of the 1,4-dimethyl-DBTP and 2,4-dimethyl-DBTP sulfoxide radicals were not well resolved but their total widths were in satisfactory agreement with those expected. The spectrum of the radical from 10,11-dimethyl-DBTP sulfoxide was extremely similar to that found earlier for the anion radical of the corresponding sulfide.[7] Only five groups of lines could be seen for 10,11-dimethyl-DBTP sulfoxide anion radical under the usual conditions of measurement employed. A total of seven groups of lines could be seen at a drastically increased signal level, but we were unable to observe all nine groups of lines which would be expected on the basis of our assignments. For this reason the total width of the spectrum which we measured (Table IV) was considerably less than that expected. The portion of the spectrum we observed for the sulfoxide radical was well resolved, however.

As can be seen from Table IV, the total expected width for the DBTP-sulfoxide radical (17.6 G) is significantly reduced compared to that for the sulfide radical (20.6 G).[7] This observation could be interpreted as an indication that in the dibenzo[*b*,*f*]thiepin system the sulfoxide group is more effective than the sulfide group in withdrawing electron spin density from the outer aromatic rings. As in the case of the

(11) We intend to explore further the validity of this possible interpretation of our findings.

anion radical of dibenzo[*b*,*f*]thiepin,[7] the spin density in the sulfoxide radical at the aromatic ring position *para* to the sulfur atom (position 2) is small. Thus, conjugation through the sulfoxide bridge appears to be much weaker than conjugation through the vinyl residue.

*Acknowledgments.* We gratefully acknowledge the support of the National Science Foundation.

## Energy Transfer Reactions of $N_2(A^3\Sigma_u^+)$. II. Quenching and Emission by Oxygen and Nitrogen Atoms

by J. A. Meyer, D. W. Setser, and D. H. Stedman

*Chemistry Department, Kansas State University, Manhattan, Kansas 66502* *(Received January 26, 1970)*

One of the major processes for removal of $N_2(A^3\Sigma_u^+)$ in active nitrogen involves reaction with ground state nitrogen atoms.[1-3] Young[2] obtained a rate of $3 \times 10^{13}$ cm$^3$ mol$^{-1}$ sec$^{-1}$ from measurements of the decay time of $N_2(A^3\Sigma_u^+)$ in the presence of $N(^4S)$, and Wray[4] obtained a similar value from shock tube studies. Thrush[5] has suggested a value which is a factor of 10 less and, most recently, Weinreb and Mannella[6] deduced an upper limit $3 \times 10^{11}$ cm$^3$ mol$^{-1}$ sec$^{-1}$ for $N_2(A^3\Sigma_u^+)$ in high vibrational levels. None of these studies, however, has been concerned with the disposition of the high exothermicity (6.17 eV from $N_2(A^3\Sigma_u^+, v = 0)$ to $N_2(X^1\Sigma_g^+, v = 0)$ of this process. This energy may go into excitation of the $N(^2P(3.57$ eV), $^2D(2.38$ eV)) states and/or vibrational excitation of $N_2(X^1\Sigma_g^+)$. We have found definite evidence that some of the released energy goes into excitation of the $N(^2P)$ state by directly observing $N(^2P \rightarrow {}^4S)$ emission ($\tau = 12$ sec) at 3466 Å. This reaction may be an excitation source for 3466 Å emission in the aurora. We previously showed that $N_2(A^3\Sigma_u^+)$ reacts with $O(^3P)$ to give excitation of $O(^1S)$ emission ($\tau = 0.8$ sec) at 5577 Å.

### Experimental Section

Our system employed a double-discharge flow apparatus in which a flow of $N_2(A^3\Sigma_u^+)$ molecules and a flow of nitrogen atoms were brought together just upstream of a quartz window. This window formed the front end of a 10 cm long reaction cell (22-mm i.d. quartz). For our pumping speeds the time for the gas to flow through this 10-cm reaction vessel was 4 msec. Spectroscopic observations of the $N_2(A^3\Sigma_u^+ - X^1\Sigma_g^-)$ and $N(^2P - {}^4S)$ transitions were made along the 10-cm path length. Several reaction vessels were used in attempts to enhance mixing and increase emission intensities; the same general behavior reported below was found for all vessels. The $N_2(A^3\Sigma_u^+)$ molecules were generated in one discharge-flow system using collisions of argon metastable atoms ($^3P_{0,2}$) and molecular nitrogen;[7-10] the concentration was $10^9$–$10^{10}$ molecules/cm$^3$ which was sufficient for direct monitoring of the forbidden $N_2(A^3\Sigma_u^+ \rightarrow X^1\Sigma_g^+)$ Vegard–Kaplan emission by viewing the flow tube end-on. The Ar* + $N_2$ system is a "clean" source,[9,10] of $N_2(A^3\Sigma_u^+)$; *i.e.*, it is free from other reactive species such as nitrogen atoms. This source gives almost equal concentrations of the 0 and 1 vibrational levels[10] which permits study of the role of vibrational excitation in the reactions of $N_2(A^3\Sigma_u^+)$. The second discharge-flow system was a flow of pure nitrogen or a flow of nitrogen in an argon carrier through a microwave discharge. The concentration of nitrogen atoms was measured using the nitric oxide titration technique and by monitoring the nitrogen first positive bands of the Lewis–Rayleigh afterglow[11] with a bare photomultiplier tube which viewed across the reaction vessel. The concentration of nitrogen atoms was varied by altering the discharge power in pure nitrogen or by altering the flow of molecular nitrogen into the argon carrier at constant discharge power. Spectroscopic observations were made with a 0.75 *m* Jarrell–Ash Czerny–Turner scanning spectrometer equipped with an EMI 9558Q photomultiplier and a PAR phase sensitive amplification system. Use of maximum sensitivity and largest slit widths was necessary to measure the very weak $N(^2P \rightarrow {}^4S)$, $\tau = 12$ sec,[12] and $N_2(^3\Sigma_u^+ - X^1\Sigma_g^+)$ emissions, $\tau = 2.1$ sec.[13,14]

(1) R. A. Young, *Can. J. Chem.*, **44**, 1171 (1966).

(2) R. A. Young and G. St. John, *J. Chem. Phys.*, **48**, 895 (1968).

(3) C. H. Dugan, *J. Chem. Phys.*, **47**, 1512 (1967).

(4) K. L. Wray, *ibid.*, **44**, 623 (1966).

(5) B. A. Thrush, *ibid.*, **47**, 3691 (1967).

(6) M. Weinreb and G. G. Mannella, *ibid.*, **50**, 3129 (1969).

(7) J. A. Meyer, D. H. Stedman, and D. W. Setser, *Astrophys. J.*, **157**, 1023 (1969). A spectrum of the Vegard–Kaplan emission obtained from our apparatus is shown in this reference. See text for improved values of rate constants for O and $O_2$ with $N_2(A)$ previously reported by this reference.

(8) D. H. Stedman, J. A. Meyer, and D. W. Setser, *J. Chem. Phys.*, **48**, 4320 (1968).

(9) D. H. Stedman and D. W. Setser, *Chem. Phys. Lett.*, **2**, 542 (1968); *J. Chem. Phys.*, **50**, 2256 (1969).

(10) D. W. Setser, D. H. Stedman, and J. A. Coxon, *ibid.*, in press.

(11) A. Wright and C. A. Winkler, "Active Nitrogen," Academic Press, Inc., New York, N. Y., 1968.

(12) R. H. Garstang, "Aurora and Airglow," Pergamon Press, New York, N. Y., 1956, p 324.

(13) D. E. Shemansky and N. P. Carleton, *J. Chem. Phys.*, **51**, 682 (1969).

(14) D. E. Shemansky, *ibid.*, **51**, 689 (1969).

## Results and Discussion

No nitrogen atom emission was detected in the mixing region when either discharge was turned off. However, with both discharge-flow systems operating, $N(^2P \rightarrow {}^4S)$ emission at 3466 Å was observed. This emission intensity for constant [N] was studied as a function of $N_2(A^3\Sigma_u^+)$ concentration by simply varying the discharge current in the $N_2(A^3\Sigma_u^+)$ source over a small current range. The intensity of the (0, 6) and (1, 9) bands from the $N_2$ Vegard–Kaplan emission served as a measure of the concentration of $N_2(A^3\Sigma_u^+)$. Typical results of such an experiment are shown in Figure 1, and a linear correlation is evident. The $N(^2P \rightarrow {}^4S)$ emission at 3466 Å was also studied as a function of [N] at constant $[N_2(A^3\Sigma_u^+)]$ and a linear correlation existed as shown in Figure 2. The linearity of the

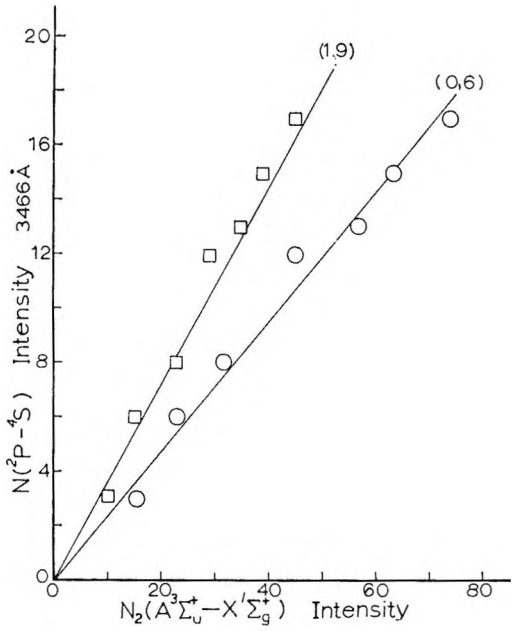


Figure 1. Variation of the intensity of the $N(^2P–{}^4S)$ transition with $N_2(A^3\Sigma_u^+)$ concentration at a constant [N]; the total pressure is 3.2 Torr. The (1, 9), □, and (0, 6), ○, bands were used to monitor the concentration of $N_2(A^3\Sigma_u^+)$. The intensities from both emissions are in arbitrary units.

figure extends to $[N] = 1 \times 10^{13}$ atoms/cm³ in an argon carrier gas. Experiments with molecular nitrogen as the N atom carrier showed deviation from linearity at approximately the same [N]. These data provide conclusive evidence for reaction 1.

$$N_2(A^3\Sigma_u^+, v = 0, 1) + N(^4S) \longrightarrow N_2(X^1\Sigma_g^+) + N(^2P) \quad (1)$$

The relative quenching behavior of the $v' = 0$ and 1 levels of $N_2(A^3\Sigma_u^+)$ was studied by observing the decline in intensity of the (0, 6) and (1, 9) Vegard–Kaplan bands as a function of [N]; both levels behaved approximately in the same way, although the $v = 1$ level may have a 10% higher rate constant. No emission from the $N(^2D)$ state ($N(^2D–{}^4S)$, $\tau = 26$ hr)[12] was observed; our detection system is not adequate for detecting the $N(^2P \rightarrow {}^2D)$ line at 10,400 Å. This transition also is weak and would be obscured by $N_2$ first positive bands.[11] The rate constant for quenching of $N_2(A^3\Sigma_u^+)$ by N atoms was estimated in two ways.

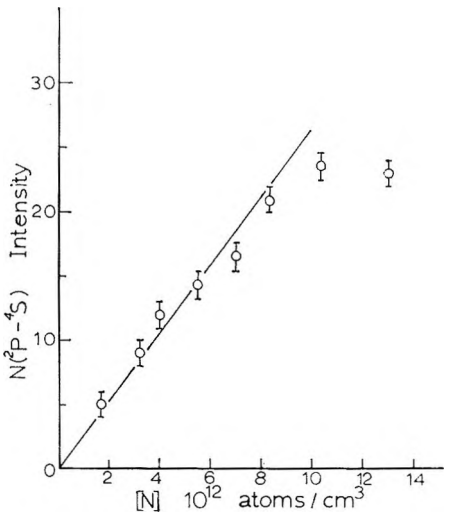


Figure 2. Variation of the intensity of the $N(^2P–{}^4S)$ transition with [N] at a constant *initial* concentration of $N_2(A^3\Sigma_u^+)$, total pressure = 4.3 Torr. The emission was viewed along the reaction vessel; the deviation from linearity probably arises from significant quenching of $N_2(A^3\Sigma_u^+)$, thereby causing $[N_2(A^3\Sigma_u)^+]$ to decline.

The quenching of nitrogen atoms was compared to molecular oxygen by increasing [N] until 30% quenching of $N_2(A)$ emission was obtained; this degree of quenching then was matched by adding $O_2$, and $k_1$ was found from $k_1[N] = k_{O_2}[O_2]$ at the same degree of quenching. Using a value[15] for $k_{O_2}$ of $3.6 \times 10^{12}$ cm³ mol⁻¹ sec⁻¹ gives $k_1 = 3.1 \times 10^{13}$ cm³ mol⁻¹ sec⁻¹. The second method employed Hg as a monitor[9] of $N_2(A^3\Sigma_u^+)$ concentration. Mercury was added to the

(15) (a) J. A. Meyer and D. W. Setser, unpublished work. Steady-state measurements of $N_2(A^3\Sigma_u^+)$ reactions in active nitrogen (see ref 9) have been done; the quenching rate for $O_2$ was $4.6 \times 10^{12}$ cm³ mol⁻¹ sec⁻¹. (b) R. A. Young, G. Black, and T. G. Slanger, *J. Chem. Phys.*, **50**, 303 (1969). This investigation used the vacuum uv photolysis of $N_2O$ as a source of $N_2(A^3\Sigma_u^+)$ and found $k_{O_2} = 2.3 \times 10^{12}$ cm³ mol⁻¹ sec⁻¹. (c) We also measured $k_{O_2}$ directly by the mercury technique in the present double discharge study and found $k_{O_2} = 3.6 \times 10^{12}$ cm³ mol⁻¹ sec⁻¹. Quenching measurements indicate the $N_2(A^3\Sigma_u^+)$ $v = 1$ level reacts 1.3 times more rapidly than the $v = 0$ level with $O_2$. This $k_{O_2}$ is for an equal mixture of $v = 0$ and 1; the values listed in (a) and (b) are for an unknown mixture of vibrational states. Adding NO downstream to the products from $N_2(A) + O_2$ gave strong air afterglow (O + NO) emission. Therefore, a significant fraction of $O_2$ quenching leads to formation of oxygen atoms.

flowing gas until the intensity of the $Hg(^3P_1-^1S_0)$ transition at 2537 Å was sufficient to be observed (perpendicular to the reaction vessel) 6 cm downstream from the point of mixing. This small quantity of Hg did not cause quenching of Vegard–Kaplan emission. The variation of the 2537-Å mercury emission with [N] was monitored 6 cm downstream from the point of mixing. The intensity fitted a first-order decay plot; combining the slope with the known flow velocity gave a rate constant of $2.6 \times 10^{13}$ cm$^3$ mol$^{-1}$ sec$^{-1}$. Our measurements thus confirm Young's and Wray's value of $3 \times 10^{13}$ cc mol$^{-1}$ sec$^{-1}$ for the quenching of $N_2(A)$ by $N(^4S)$ rather than the lower values proposed by others.[5,6]

Results similar to those depicted in Figures 1 and 2 previously have been reported[7] for excitation of the $O(^1S-^1D)$ emission at 5577 Å by $N_2(A^3\Sigma_u^+, v = 0,1)$. That work was repeated in the present apparatus and reaction 2 was confirmed. The $N_2(A^3\Sigma_u^+)$ $v = 0$ and 1 levels reacted at nearly the same rate, as was found

$$N_2(A^3\Sigma_u^+, v = 0, 1) + O(^3P) \longrightarrow N_2(X^1\Sigma_g^+) + O(^1S) \quad (2)$$

for reaction 1. Absolute intensity measurements previously were made[16] for this case and $4 \pm 2$ $N_2(A^3\Sigma_u^+)$ molecules gave one 5577-Å proton.[16] We suggested that collisions with the wall and reactive impurities remove $O(^1S)$ and that reaction 2 is a significant and perhaps the main channel in the overall quenching of $N_2(A^3\Sigma_u^+)$ by oxygen atoms. The rate constant for overall quenching by oxygen atoms was remeasured by comparison with $O_2$, and $k_2/k_{O_2} = 3$–4 was confirmed. Using a better estimate[15c] for $k_{O_2}$ gives $k_2 = 1.3 \times 10^{13}$ cm$^3$ mol$^{-1}$ sec$^{-1}$.

The $N(^2P-^4S)$ line is only very weakly present at low pressures in the Lewis–Rayleigh[11] afterglow, but at higher pressures (20–760 Torr) Noxon[17] observed this emission with an "ozonizer type" discharge through pure nitrogen. He also observed $N_2$ Vegard–Kaplan emission but discarded the possibility of $N_2(A^3\Sigma_u^+)$ exciting $N(^2P)$ with the argument that the $[N_2(A^3\Sigma_u^+)$ was too small to account for the $N(^2P-^4S)$ intensity. Campbell and Thrush,[18] however, reconsidered Noxon's data and suggested reaction 1 followed by fast quenching of $N(^2P)$ by $N(^4S)$, reaction 3. If this is the case,

$$N(^2P) + N(^4S) \longrightarrow N(^4S) + N(^4S) \text{ or } N(^2D) \quad (3)$$

at sufficiently high [N] the $N(^2P-^4S)$ emission should be independent of [N]: $I(3466) = (k_1[N_2(A)][N])/k_3[N] + \tau^{-1}[N(^2P)] + k(\text{wall}))$. The data of Figure 2, however, show a linear increase of $I(3466)$ with [N] at constant $[N_2(A^3\Sigma_u^+)]$. For the maximum [N] of $1.6 \times 10^{-11}$ mol cm$^{-3}$ for which the plot is linear, $k_3$ must be less than $1 \times 10^9$ cm$^3$ mol$^{-1}$ sec$^{-1}$ in order that the first term of the denominator be 0.20 of the second. The role of wall removal is unknown but it may be the dominant step; then our experiments only set a limit to $k_3$ based upon the competition between $k_3[N]$ and $k(\text{wall})$.

The $N(^2P-^4S)$ line is absent from spectra of the airglow as is $N_2$ Vegard–Kaplan emission; however, both of these emissions are present in the spectra of the aurora,[19] as is the 5577-Å oxygen line. It is evident, therefore, that $N(^2P-^4S)$ emission at 3466 Å is present in systems where both $N(^4S)$ and $N_2(A^3\Sigma_u^+)$ occur and our data show that reaction 1 may be one source of this emission. Very recently, Weinreb and Mannella[20] suggested that the products from a microwave discharge in $O_2$ (probably excited $O_2$ molecules) induce a collisional crossing from high vibrational levels of $N_2(A^3\Sigma_u^+)$, formed by N atom recombination at metallic surfaces, into $N_2(B^3\pi_g)$. In view of the relatively rapid vibrational relaxation[10] of $N_2(A^3\Sigma_u^+)$ molecules by $N_2$ to levels $v = 0$ and 1 and of the fast removal of $N_2(A^3\Sigma_u^+)$ by $O_2$,[15c] N, and O directly demonstrated by our work, an alternative explanation of this phenomenon should be considered.

The question arises whether reaction 1 is an energy transfer step or an atom exchange reaction and whether reaction 1 is the only reaction channel for N atom quenching of $N_2(A^3\Sigma_u^+)$. A direct answer will require $^{15}N$ labeling experiments. A linear correlation diagram shows that $N_3$ states formed from $N(^4S) + N_2(A^3\Sigma_u^+)$ do not correlate with states from $N(^2P) + N_2(X^1\Sigma_g^+)$. Nonlinear $N_3$ states (at present unknown)[21] would make such a correlation possible. The $N(^4S) + N_2(A^3\Sigma_u^+)$ linear states may correlate with $N(^4S) + N_2(X^1\Sigma_g^+)$ or with $N(^2D) + N_2(X^1\Sigma_g^+)$; however, unknown $\Sigma^-$ states of $N_3$ are needed. At the present time an energy transfer collision is the most attractive mechanism for reaction 1.

*Acknowledgments.* This work was supported by the National Air Pollution Control Administration Consumer Protection and Environmental Health Service, Public Health Service, Grant AP-00391.

(16) Use of the new radiative lifetime[13,14] (2.1 sec) for $N_2(A^3\Sigma_u^+)$ rather than the old 12 sec$^{-1}$ value changes our previous measurement of $20 \pm 10$ $N_2(A)$ molecules per $O(^1S)$ photon to that quoted in the text. (The $O(^1S)$ lifetime is ~1 sec so the number of measured $O(^1S)$ photons is equivalent to the number of $O(^1S)$ atoms).

(17) J. F. Noxon, *J. Chem. Phys.*, **36**, 926 (1962).

(18) L. M. Campbell and B. A. Thrush, *Trans. Faraday Soc.*, **65**, 32 (1969).

(19) J. W. Chamberlain, "Physics of the Aurora and Airglow," Academic Press, Inc., New York, N. Y., 1961.

(20) M. P. Weinreb and G. G. Mannella, *J. Chem. Phys.*, **51**, 4973 (1969).

(21) G. Herzberg, "Electronic Spectra of Polyatomic Molecules," Van Nostrand-Reinhold Co., Inc., Princeton, N. J., 1966, p 593.

# A Reference Solution for Electrical Conductance Measurements to 800° and 12,000 Bars. Aqueous 0.01 Demal Potassium Chloride

by Arvin S. Quist, William L. Marshall,

*Reactor Chemistry Division, Oak Ridge National Laboratory,*[1] *Oak Ridge, Tennessee 37830*

E. U. Franck, and W. von Osten

*Institut für Physikalische Chemie und Elektrochemie der Universität, 75 Karlsruhe, West Germany* *(Received January 22, 1970)*

In recent years there has been much interest in the behavior of aqueous electrolyte solutions at high temperatures and pressures.[2] Experimental investigations of the properties of water and aqueous solutions have been greatly facilitated by the availability of new alloys that retain excellent mechanical strength at temperatures to 800° and above. Consequently, many measurements have been made on aqueous systems at supercritical temperatures and pressures. Since one of the simplest and most direct methods of investigating the behavior of ions in solution is the measurement of the electrical conductances of the solutions, several of these researches have been concerned with the measurement of this property. In view of the interest in conductance measurements at high temperatures and pressures, it seems desirable to establish a "reference" solution to permit direct comparison of the results obtained in different laboratories. Establishing reliable conductivity values for such a solution at these high temperatures and pressures would also allow direct experimental determination of cell constants under these conditions.

A 0.01 demal KCl solution (defined as 0.745263 g KCl/1000 g solution[3]) appears to be an appropriate choice as the reference solution for conductance measurements at high temperatures and pressures. This solution has been used for many years as a standard solution for cell constant determinations near 25° and atmospheric pressure.[3] Since aqueous KCl is both stable and a relatively strong electrolyte at supercritical temperatures and pressures, this solution would also appear to be suitable for use as a reference solution at these high temperatures and pressures. In recent years many conductance measurements have been made on either 0.01 demal or 0.01 *m* KCl solutions at temperatures to 1000° and at pressures to 12,000 bars. These measurements have been performed in the authors' laboratories over a period of years using several different designs of conductance cells and pressure vessels. Table I summarizes the ranges of temperature and pressure for the different sets of measurements from our laboratories. The literature references are included; these also contain descriptions of the conductance cells and experimental techniques.

**Table I:** Summary of Electrical Conductance Measurements on 0.01 Demal (or 0.01 Molal) Aqueous KCl Solutions at Elevated Temperatures and Pressures

| Investigators | Temp range, °C | Max pressure, bars |
|---|---|---|
| Franck[a] | 250–750 | 2,500 |
| Hensel and Franck[b] | 45–130 | 8,000 |
| Franck, Hartmann, and Hensel[c] | 45–220 | 8,000 |
| Ritzert and Franck[d] | 200–750 | 6,000 |
| Mangold and Franck[e] | 300–1000 | 12,000 |
| Renkert[f] | 200–350 | 8,000 |
| von Osten[g] | 200–400 | 8,000 |
| Quist and Marshall[h] | 0–800 | 4,000 |

[a] E. U. Franck, *Z. Phys. Chem.* (Frankfurt am Main), **8**, 92 (1956). [b] F. Hensel and E. U. Franck, *Z. Naturforsch.*, **19a**, 127 (1963). [c] E. U. Franck, D. Hartmann, and F. Hensel, *Discuss. Faraday Soc.*, **39**, 200 (1965). [d] G. Ritzert and E. U. Franck, *Ber. Bunsenges. Phys. Chem.*, **72**, 798 (1968). [e] K. Mangold and E. U. Franck, *ibid.*, **73**, 21 (1969). [f] H. Renkert, Diplomarbeit, Karlsruhe, 1965. [g] W. von Osten, Diplomarbeit, Karlsruhe, 1966. [h] A. S. Quist and W. L. Marshall, *J. Phys. Chem.*, **73**, 978 (1969), plus additional unreported measurements totaling 55 separate runs.

The experimental measurements were generally made at many different pressures at a constant temperature. Values of specific conductances at integral pressures, at the experimental temperatures, were obtained by interpolation. Some of the studies listed in Table I were carried out using 0.01 *m* rather than 0.01 demal solutions. However, minor corrections were applied so that the specific conductances could be correlated as based on 0.01 demal KCl solutions.

The measurements on KCl solutions from the sources listed in Table I were combined by plotting isobaric specific conductances *vs.* temperature and drawing a smooth curve through these data points.[4] Smoothed values for the specific conductances of 0.01 demal KCl solutions are presented in Table II at pressures from

(1) Operated by Union Carbide Corp. under contract with the U. S. Atomic Energy Commission.

(2) See, for example (*a*) E. U. Franck, *Endeavour*, **27**, 55 (1968); (b) J. W. Cobble, *Science*, **152**, 1479 (1966); (c) W. L. Marshall, *Rev. Pure Appl. Chem.*, **18**, 167 (1968).

(3) G. Jones and B. C. Bradshaw, *J. Amer. Chem. Soc.*, **55**, 1780 (1933).

(4) The earliest values of Franck (Table I, reference *a*) were omitted in this comparison because the uncertainty in these reported values was significantly larger than for those in the other references listed in Table I.

**Table II:** Specific Conductances ($ohm^{-1}$ $cm^{-1}$) × $10^5$ of 0.01 Demal KCl Solution at Integral Temperatures and Pressures

| Pressure, bars | Temp, °C | | | | | | | | | | | |
|---|---|---|---|---|---|---|---|---|---|---|---|---|
| | 100 | 150 | 200 | 250 | 300 | 350 | 400 | 450 | 500 | 600 | 700 | 800 |
| 1,000 | 368 | 498 | 599 | 663 | 689 | 685 | 650 | 578 | 460 | 125 | ... | ... |
| 2,000 | 364 | 491 | 593 | 659 | 698 | 707 | 701 | 679 | 643 | 516 | 336 | 116 |
| 3,000 | 358 | 483 | 585 | 651 | 695 | 715 | 718 | 709 | 689 | 625 | 528 | 405 |
| 4,000 | 351 | 481 | 574 | 640 | 687 | 712 | 723 | 724 | 714 | 670 | 610 | 526 |
| 6,000 | 338 | 466 | 555 | 617 | 665 | 699 | 722 | 733 | 732 | 707 | 672 | 628 |
| 8,000 | 326 | 446 | 536 | 598 | 645 | 679 | 703 | 716 | 721 | 711 | 692 | 664 |
| 10,000 | ... | ... | ... | ... | 625 | 665 | 690 | 707 | 711 | 709 | 694 | 675 |
| 12,000 | ... | ... | ... | ... | 601 | 644 | 674 | 694 | 704 | 703 | 688 | 673 |

1000 to 12,000 bars and at temperatures from 100 to 800°. These data are presented in graphical form in Figure 1, where specific conductances are plotted as a function of temperature at pressures from 1000 to 12,000 bars.

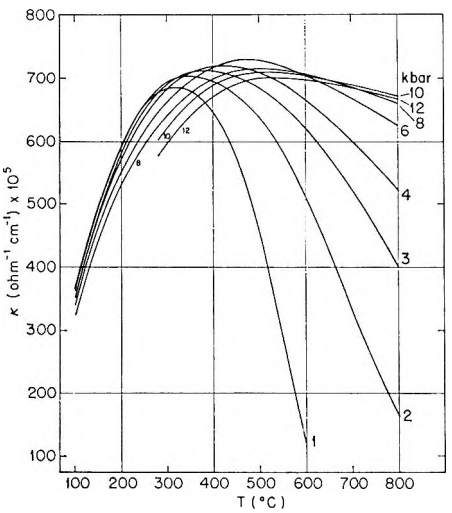


Figure 1. Specific conductances of 0.01 demal KCl solutions at integral temperatures and pressures.

In general, the results from Oak Ridge and Karlsruhe were in excellent agreement. Up to temperatures of 300° the scatter of the two sets of data about a smooth curve drawn through the combined results was generally less than 1%. Above 500° there was somewhat more scatter, but even so the differences in the two sets of data were usually less than 1% except at low pressures where the absolute values of the conductance had decreased considerably. The greatest differences between the Oak Ridge and Karlsruhe values were at temperatures near 400° at 1000 bars. Under these conditions the Oak Ridge data were up to 5% higher than the Karlsruhe results. The difference decreased with increasing pressure until at 4000 bars at 400° it was only about 1.5%.

Estimated uncertainties associated with the specific conductances reported in Table II tend to increase with increasing pressure and temperature. The probable uncertainty of about 0.5% at 100° and 1000 bars increased to approximately 1% at 8000 bars at this temperature. At higher temperatures the uncertainty was estimated to be near 1–1.5% at low pressures but in the region 10,000 to 12,000 bars it had increased to 3–4% at 800°. The uncertainty was greatest under conditions of temperature and pressure where the absolute value of the conductance was relatively low. For example, at 800° and 2000 bars the uncertainty may be as large as 5%.

**Table III:** Specific Conductances of Aqueous 0.01 *m* KCl Solutions at Saturation Vapor Pressures at Temperatures to 306°

| Temp, °C | Pressure, bars | Specific conductance, $ohm^{-1}$ $cm^{-1}$ × $10^5$ | Temp, °C | Pressure, bars | Specific conductance, $ohm^{-1}$ $cm^{-1}$ × $10^5$ |
|---|---|---|---|---|---|
| 25 | 1 | 140.9[a] | 200 | 15.6 | 603[b] |
| | | | | | 605[d] |
| 50 | 1 | 212[b] | | | |
| | | | 218 | 22.3 | 630[c] |
| 100 | 1 | 358[b] | | | |
| | | 362[c] | 225 | 25.5 | 635[b] |
| | | | | | 637[d] |
| 150 | 4.8 | 496[b] | | | |
| | | 496[d] | 281 | 65.2 | 668[c] |
| 156 | 5.6 | 512[c] | 306 | 93.4 | 654[c] |

[a] Calculated from the equation of J. E. Lind, Jr., J. J. Zwolenik, and R. M. Fuoss, *J. Amer. Chem. Soc.*, **81**, 1557 (1959). [b] A. J. Ellis, *J. Chem. Soc.*, 2299 (1963). [c] A. A. Noyes, *et al.*, "The Electrical Conductivity of Aqueous Solutions," Publication No. 63, Carnegie Institution of Washington, Washington, D. C., 1907; A. A. Noyes, *et al.*, *J. Amer. Chem. Soc.*, **30**, 335 (1908). [d] Interpolated by Ellis[b] from Noyes' data.[c]

In general, the apparatus at our laboratories were not designed to give conductances along the liquid–vapor curve which were as accurate as those previously reported by other investigators. Thus the values reported in Table III for specific conductances of 0.01

*m* KCl to 306° at saturation vapor pressures are those of earlier researchers but have been included here for completeness.

These specific conductances of KCl presented in Tables II and III are believed to represent the best values presently available for high temperatures and pressures. It is hoped that they will be useful in establishing the reliability of other conductance apparatus and in obtaining cell constants at high temperatures and pressures.

# COMMUNICATIONS TO THE EDITOR

## Dielectric Constants of Alcoholic–Water Mixtures at Low Temperature

*Sir:* In 1932, Akerlöf[1] published experimental values for $\epsilon$, the dielectric constants of hydro–alcoholic solvents, as a function of temperature between 0 and +60°. He obtained the following relation: $\log \epsilon = a - bT$. Freed and Bielski[2] showed that it is possible to dissolve proteins at low temperature ($T < 0°$) in such solvents, without denaturation, providing the extrapolated value of $\epsilon$ is approximately that of water at room temperature ($\epsilon \simeq 80$). We have further developed the use of this technique in our laboratory.[3,4] In view of the great importance of $\epsilon$, we decided to check experimentally the extrapolation of Akerlöf's law to low temperature. Using a classic method for obtaining dielectric constants[5] we measured capacity of a cylindrical condenser by means of General Radio 716 C bridge with 300 kHz for frequency. The low-temperature control device has already been described.[6]

By this method we have studied different methanol–water mixtures, methanol–ethanol–water (55:25:20, v/v) and ethylene glycol–water (50:50 v/v). The

**Table I:** Dielectric Constants of Alcoholic–Water Mixtures as a Function of the Temperature

| Mixtures | Temp, °C +20 | +10 | 0 | −10 | −20 | −30 | −40 | −50 | −60 | −70 | −80 | −90 | −100 |
|---|---|---|---|---|---|---|---|---|---|---|---|---|---|
| Methanol | 33.6 | 35.4 | 37.9 | 40.6 | 42.7 | 45.4 | 48.3 | 51.3 | 54.6 | 58.0 | 62.0 | 66.5 | |
| Methanol–water 80%–20% | 43.7 | 46.4 | 49.5 | 52.3 | 55.4 | 58.6 | 61.9 | 65.7 | 69.3 | 73.5 | 77.8 | 82.8 | 88.4 |
| Methanol–water 70%–30% | 46.3 | 49.4 | 53.0 | 56.6 | 60.1 | 63.5 | 66.8 | 70.9 | 74.9 | 79.2 | 83.5 | 88.7 | 94.0 |
| Methanol–water 60%–40% | 55.1 | 58.7 | 62.5 | 66.0 | 70.5 | 73.8 | 78.2 | 82.2 | 86.7 | 92.05 | 97.5 | 103.8 | |
| Methanol–water 50%–50% | 60.3 | 64.0 | 67.8 | 71.2 | 75.5 | 79.2 | 83.9 | 87.9 | 92.5 | | | | |
| Methanol–water 40%–60% | 63.8 | 67.7 | 71.9 | 75.6 | 79.5 | 83.5 | 87.9 | | | | | | |
| Water | 80.4 | 84.2 | 88.1 | | | | | | | | | | |
| Methanol–ethanol–water 55%–25%–20% | 43.0 | 45.7 | 48.6 | 51.2 | 54.6 | 57.9 | 61.4 | 65.3 | 69.0 | 73.5 | 78.3 | 83.7 | 89.7 |
| Ethylene glycol–water 50%–50% | 64.5 | 68.4 | 72.4 | 76.5 | 80.7 | 85.0 | 89.3 | 94.0 | 98.8 | | | | |

**Table II:** Coefficients $a$ and $b$ of Akerlöf's Law: $\log \epsilon = a - bT$, Where $T$ is the Temperature in °C

| | Mixtures: Methanol | Methanol–water 80%–20% | Methanol–water 70%–30% | Methanol–water 60%–40% | Methanol–water 50%–50% | Methanol–water 40%–60% | Water | Methanol–ethanol–water 55%–25%–20% | Ethylene glycol–water 50%–50% |
|---|---|---|---|---|---|---|---|---|---|
| $a$ | 1.580 | 1.695 | 1.730 | 1.790 | 1.830 | 1.855 | 1.945 | 1.680 | 1.860 |
| $b \times 10^3$ | 2.65 | 2.50 | 2.45 | 2.50 | 2.30 | 2.20 | 2.00 | 2.65 | 2.65 |

(1) G. Akerlöf, *J. Amer. Chem. Soc.*, **54**, 4125 (1932).

(2) B. Bielski and S. Freed, *Biochim. Biophys. Acta.*, **89**, 314 (1964).

(3) T. Shiga, M. Layani, and P. Douzou, *Bull. Soc. Chim. Biol.*, **49**, 507 (1967).

(4) R. Banerjee, P. Douzou, and A. Lombard, *Nature*, **217**, 23 (1968).

(5) A. R. Von Hippel, "Dielectric Materials and Applications," Wiley, New York, N. Y., 1954.

(6) G. Hui Bon Hoa, and C. Balny, *J. Chim. Phys.*, **66**, 1528 (1969).

values obtained are shown in Table I. Our results confirm the extrapolation of Akerlöf's law to low temperature and the constants $a$ and $b$ are shown in Table II. These results thereby permit the exact determination of the temperature of dissolution of a protein in such solvents with the least chance of denaturation.

*Acknowledgments.* The measurement cell was built with the advice of Mrs. Sixou and Danzas of Institut d'Electronique d'Orsay (France).

INSTITUT DE BIOLOGIE PHYSICO-CHIMIQUE F. TRAVERS
75—PARIS, FRANCE P. DOUZOU

RECEIVED JANUARY 20, 1970